



FRIEDRICH-SCHILLER- UNIVERSITÄT JENA

Modification of polyampholytic poly(dehydroalanine) – strategies and utilization in hybrid nanomaterials applied as smart dispersants, sensors and in photocatalysis

Dissertation

(kumulativ)

zur Erlangung des akademischen Grades

doctor rerum naturalium (Dr. rer. nat.)

vorgelegt dem Rat der Chemisch-Geowissenschaftlichen Fakultät der

Friedrich-Schiller-Universität Jena

von M. Sc. Johannes Bernhard Max

geboren am 08.01.1992 in Bad Mergentheim

Gutachter:

1. Prof. Dr. Felix Helmut Schacher, Jena (Friedrich-Schiller-Universität Jena)
2. Prof. Dr. Thomas Heinze, Jena (Friedrich-Schiller-Universität Jena)
3. Prof. Dr.-Ing. Markus Gallei, Saarbrücken (Universität des Saarlandes)

Tag der öffentlichen Verteidigung: 10.11.2021

Table of content

1. Introduction	1
1.1 Polyampholytes – definition, properties and synthesis	3
1.2 Smart, double hydrophilic polymers	11
1.3 Organic/inorganic hybrid materials.....	15
1.3.1 Polymeric hybrid materials	18
1.3.2 Polyelectrolyte-based hybrid materials in catalytic hydrogen evolution	19
1.3.3 Polyelectrolyte-based hybrid materials in sensing applications.....	21
1.4 Objective of this thesis	25
2. Synthetic routes towards PDha-based copolymers	29
2.1 Novel routes towards double hydrophilic PEG- <i>b</i> -PDha block copolymers....	29
2.2 PDha-based graft copolymers – preparation and solution properties.....	38
3. PDha-based graft copolymer based hybrid materials and applications	58
3.1 Smart amphiphilic dispersants	58
3.2 pH-controlled synthesis of AgAu nanoalloys	61
3.3 Triple-responsive smart sensors	69
3.4 Soft matrices in light-driven hydrogen evolution	73
4. Summary	86
5. Zusammenfassung.....	91
References	97
List of abbreviations.....	110
Publication list	113
Acknowledgements / Danksagung	115
Declaration of authorship / Selbständigkeitserklärung.....	118
Documentation of authorship.....	119
Publication P1 – P7	124

1. Introduction

1. Introduction

Parts of this chapter have been published in **P7**) A. Nabiyan, J. B. Max, F. H. Schacher, Double Hydrophilic Copolymers – Synthetic Approaches, Architectural Variety, and Application Fields, Chem. Soc. Rev., **2022**, DOI: 10.1039/D1CS00086A.

Today, we encounter polymers in almost every part of our daily life. They provide solutions to the emerging issues in our modern society such as nutrition, energy or health.^{1,2} Functional polymers, in particular polyelectrolytes, are receiving growing interest in modern and more advanced applications in aqueous environments.³ Polyelectrolytes, which cover polyampholytes and polyzwitterions, are macromolecules bearing ionizable groups in each repeat unit.⁴⁻⁶ Due to their charges, these materials are not only responsive towards external stimuli such as ionic strength or pH,⁷ but also interact with oppositely charged ions or small molecules,^{8,9} surfaces,^{10,11} or other polymeric materials.^{12,13}

Polyelectrolytes are of great importance in a wide range of applications where they act as flocculants and coagulants,^{14,15} super absorbers,¹⁶ or dispersing agents. Consequently, polyelectrolytes are found in many materials and processes that are relevant to industry and our daily lives.^{3,5} They are used in pharmaceuticals, cosmetics, biomedicine, waste-water treatment, biomedicine, and in the food and paper industry.^{13,15} Beyond this, polyelectrolytes are also applied in more specialty or advanced applications including surface coatings,^{17,18} as selective layers in membranes,^{19,20} antimicrobial active materials,²¹ metal ion sensing,^{8,22} in the recycling and separation of proteins and/or metal ions from different media,²³⁻²⁶ as well as in drug delivery and tissue engineering²⁷ or catalysis.²⁸ Especially in these relatively modern fields, the demand for tailor-made and multifunctional polyelectrolyte based materials is steadily increasing. In this respect, different approaches allow the design and preparation of well-defined polymeric substances that meet the requirements of a desired application precisely. One such approach is the synthesis and polymerization of novel monomers that afford polymers with unique properties owing to their specific functional groups such as common anionic or cationic moieties, *e.g.* sodium styrene sulfonate, acrylic acid, diallyl dimethyl ammonium chloride and 2-(dimethylamino)ethyl methacrylate,²⁹ or well-known zwitterionic monomers, *e.g.* (acrylamido) ammonium sulfonates.³⁰ By carefully selecting the right monomer(s), it is possible to introduce a variety of functional groups to control the properties of the polymer for a desired application. Such novel charged polymers can be accessed through controlled polymerization and using appropriate protecting groups.³¹⁻³⁵ In this manner, amphiphilic charge-bearing fragments can also be prepared providing a straight-forward approach to so

1. Introduction

called hydrophobic polyelectrolytes or polysoaps.^{36,37} There is even more potential to fine-tune the properties of a material for a specific application by the preparation of copolymers, such that even contrary properties and ‘philicities/phobicities’ may be combined. This provides us with an ample, which is furthered by the development of controlled polymerization and post-polymerization modification techniques. Therefore, the linkage of a multitude of functional segments is possible with various architectures, from linear, block, graft to star copolymers.³⁸ Concerning polyelectrolytes, particularly double hydrophilic block copolymers (DHBCs), exhibiting two water-soluble segments, and amphiphilic copolymers consisting of a hydrophobic and a hydrophilic entity, play an important role in advanced applications, due to their diverse properties, self-assembly or stimuli-responsive behavior.^{36, 39-41} Nevertheless, the direct copolymerization of distinct monomers can also give tailored random polyelectrolytes, although they might be less defined.⁴² Beyond the structural and architectural design of polyelectrolytes towards desired properties and functions, these macromolecules may be further combined with inorganic compounds to obtain high performance hybrid materials. Organic/inorganic hybrid materials are a very old class of materials, also found in nature, which combine the distinct characteristics of each material. In this way, it is possible to merge the magnetic or electrochemical properties of inorganic materials with the hydrophilic/hydrophobic balance or chemical properties of an organic compound. It is for this reason that the preparation of organic/inorganic hybrid materials remains an emerging field. Tuning the composition and interaction between the individual components on a molecular level lends tailor-made materials that often show synergistic effects.⁴³⁻⁴⁶ Within these materials, polyelectrolytes fulfill the role of dispersants,^{9, 11, 12, 47} stabilizers,^{48, 49} templates and matrices.^{50, 51} Such materials are very attractive and promising candidates in a wide range of applications in various fields including biomedicine or catalysis, due to their biocompatibility, improved stability, water solubility and complexing ability.⁵¹⁻⁵⁴

Considering the above-mentioned aspects, the design of well-defined polyelectrolyte materials for special applications remains of fundamental research interest. However, these synthetic demands can be tackled using our broad toolbox encompassing organic synthesis, controlled polymerization techniques,⁵⁵ and novel strategies to prepare inorganic/organic hybrid materials on a nanoscale. Construction of the desired materials starts with the choice of suitable monomers and their polymerization,^{56, 57} followed potentially by post-polymerization modification,⁵⁸ and the incorporation of inorganic compounds from molecular precursors or readily prepared building blocks.^{59,60} Here, polyzwitterions and polyampholytes are gaining increasing research interest since they often mimick biomacromolecules, and are highly

1. Introduction

hydrophilic and tolerant towards increasing ionic strength, when compared to simple polyanions or polycations.^{30, 56, 61} Moreover, a pH-dependent overall charge is observed for many monomers, and the oppositely charged moieties can interact with both positively- and negatively-charged compounds.^{30, 56, 61} The synthesis, properties and application of polyampholytes will be outlined in the following chapter.

1.1 Polyampholytes – definition, properties and synthesis

Definition and concepts

Polyelectrolytes are polymers bearing either positive (polycations) or negative charges (polyanions), and are typically water-soluble.⁴⁻⁶ Polyampholytes, as a subclass of polyelectrolytes, exhibit oppositely charged moieties or ionizable groups (randomly) within the polymer backbone or in the side-chain. Polyzwitterions, on the other hand, feature both groups within the same monomer unit with varying charge distribution possible.^{4-6, 56} A crucial difference between polyampholytes and polyzwitterions is that polyampholytes predominantly bear an overall net-charge and behave like a polyzwitterion within a narrow pH window. In contrast, polyzwitterions usually consist of permanently charged monomer units and therefore possess an overall neutral charge. In contrast, typical polyelectrolytes feature only one type of charge and as depicted in **Figure 1**.^{4-6, 56} Polyelectrolytes can be further classified as strong or weak. Strong polyelectrolytes are characterized by a constant charge, while the overall charge of weak polyelectrolytes varies due to protonation or deprotonation of the corresponding functional groups.²⁹ Here, the elucidation of polyampholytes will also include its related subclass polyzwitterions.

1. Introduction

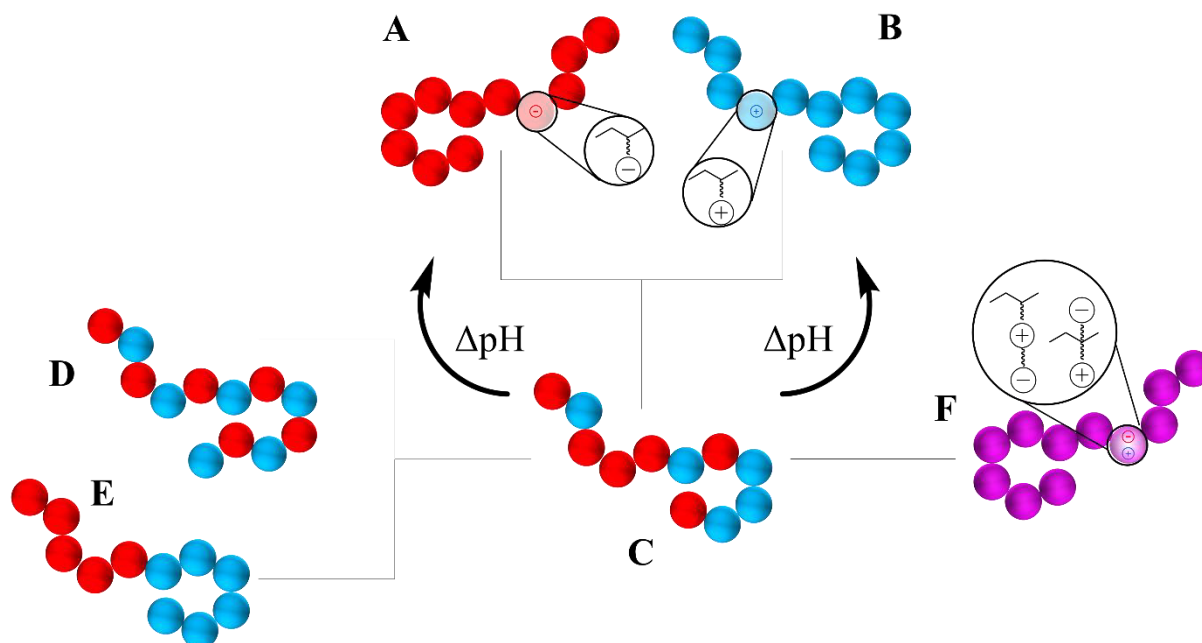


Figure 1. Schematic depiction of polyelectrolytes according to class: polyanions (A) and polycations (B), polyampholytes (C), which is further divided into polyzwitterions with an overall neutral charge (D) and block polyampholytes (E). Polyzwitterions contain two opposite charges within the same monomer unit, realized by different structural entities (F). Weak polyzwitterions / polyampholytes can be reversibly transformed into either a polyanion or polycation by changing the pH value.^{29, 56, 62}

Regarding different anionic and cationic monomers and their distribution within the polymer, polyampholytes can be referred to as ‘annealed’ if they contain ionizable moieties, ‘quenched’ if the charge is constant independent of the pH value and ‘zwitterionic’ if the number of monomers with opposing charge is equal.^{62, 63} The number of charged moieties and their distribution plays a crucial role concerning the polymers’ properties. For example, block polyampholytes, also referred to zwitterionic diblock copolymers, exhibit distinct properties, such as the formation of micelles at a certain pH value.⁶⁴⁻⁶⁶ Some polymers are at the interface between polyampholytes and polyzwitterions. They exhibit ‘zwitterionic behavior’ only in a certain pH window. Due to protonation/deprotonation of weak acidic or basic groups within the same monomer unit, a charge equilibrium is found and both charges are not necessarily found at the same time.^{32, 67} An example is poly(dehydroalanine) (PDha), featuring amino and carboxylic acid groups in each monomer unit leading to a zwitterionic window between a pH of 10.5 and 6.5.³²

Solution behavior

The outstanding properties of polyampholytes arise from their (tunable) charged moieties, determining the chemical and physical properties. In general, the solubility of polyampholytes is affected by the pH, as well as the ionic strength, which affect the intra- and intermolecular interactions. When polyampholytes have an excess of either positive or negative charges, i.e.,

1. Introduction

when they are not at the point of charge neutrality, their so-called isoelectric point (IEP), they behave like polyelectrolytes. For some polymers, this leads to strong intramolecular forces and a loss of water-solubility. On the other hand, these interactions can be disrupted by the addition of salts, that interact with the oppositely charged functional groups. This is contrary to the behavior of polyelectrolytes, and this behavior is called the ‘anti-polyelectrolyte effect’.^{57, 63, 68} These modes of attraction and repulsion were studied by E. A. Bekturov *et al.*, using an exemplarily polyampholyte, nearly equimolar poly(methacrylic acid)-*block*-poly(1-methyl-4-vinylpyridinium chloride) (PMAA-*b*-4VPCl). The dissolution and precipitation behavior in dependence of the pH value and ionic strength is illustrated in **Figure 2**.^{57, 69}

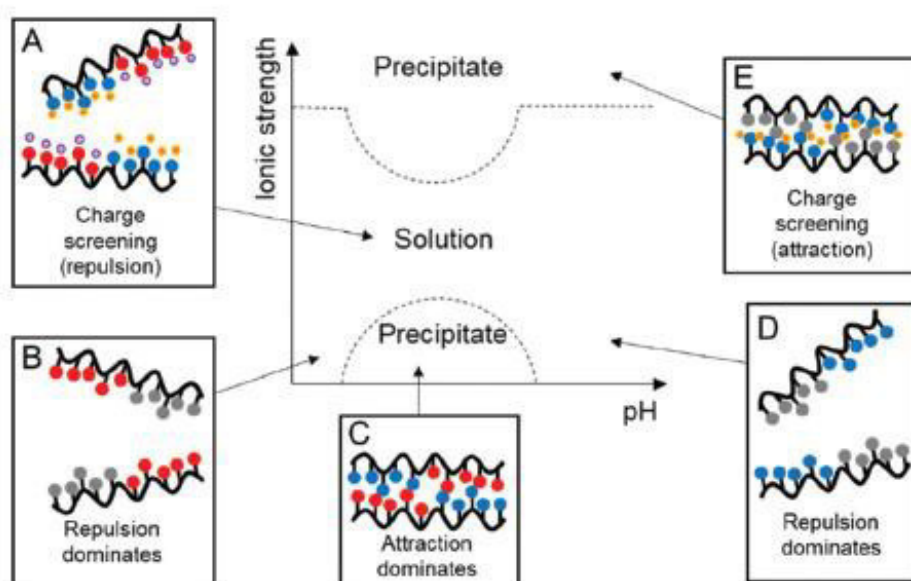


Figure 2. Illustration of the intermolecular attraction and repulsion of PMAA-*b*-4VPCl in response of the pH and ionic strength. Here, the moieties exhibit the following colours: cationic = red, anionic = blue, neutralized = grey, yellow and purple = K⁺ / Cl⁻. Reproduced from Chem Soc Rev, **2019**, 48, 757, with permission of the Royal Society of Chemistry.⁵⁷

In addition, the behavior of polyampholytes in the presence of charged surfaces, proteins, polyelectrolytes and metal cations is of particular interest regarding theoretical studies, as well as for applications (**Figure 3**).^{70, 71} Hereby, the interaction of polyampholytes with polyelectrolytes or proteins could be seen as a special case of interpolyelectrolyte complexes (IPEC) being the result of electrostatic attraction between a polyanion and a polycation.^{29, 62} Adsorption processes of polyampholytes onto surfaces play a key role in many technological applications, *e.g.* as stabilizers or modifiers. Thus, theoretical calculations support the understanding of the corresponding mechanisms.⁷²⁻⁷⁴ In general, three absorption regimes have been uncovered, where the polymer chain adopt different conformations. First, a Gaussian conformation could be assumed where the chains move freely in the solution. In the second

1. Introduction

regime, the chain size decreases with increasing surface charge density and they stretch along the surface. In the so-called pancake regime, moieties that are oppositely charged to the surface stay close to the surface within a certain length, while residues with the same charge as the surface form loops and dangle into solution.^{57, 70, 73} It is worth noting that many modified polyampholytes exist, each revealing unique properties by combining the above described characteristics with the corresponding properties of the modifier. Hydrophobically modified polyelectrolytes or polysoaps are a good example; they self-assemble in solution due to the interplay of hydrophobic and ionic interactions.⁷⁵

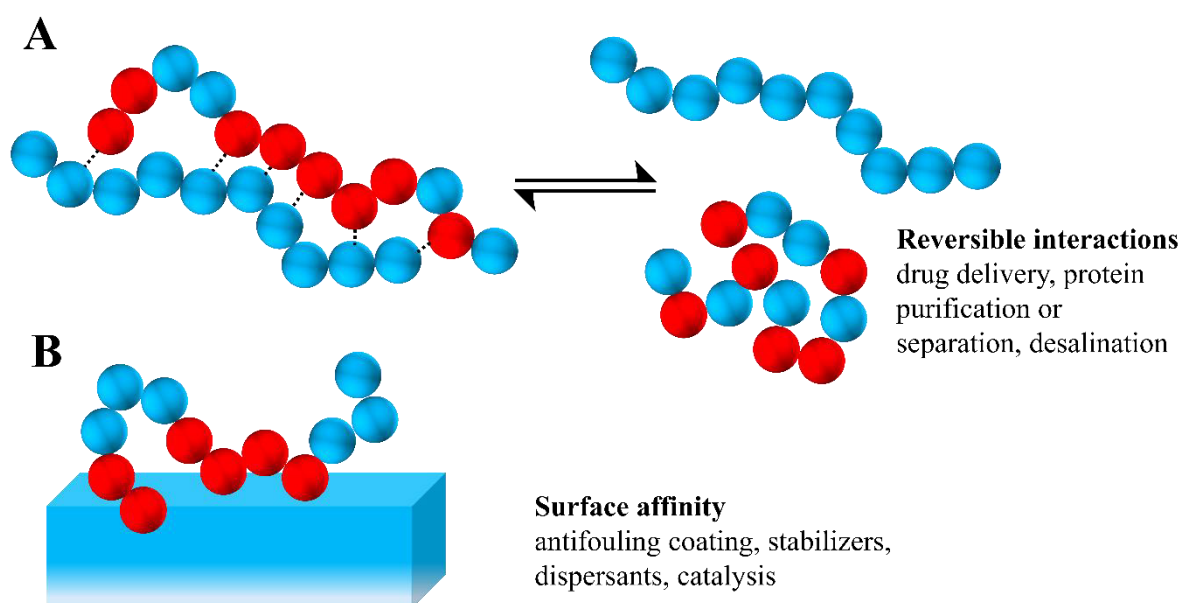


Figure 3. Illustration of the interaction of a polyampholyte with a polycation or a positively charged surfaces with their potential applications. IPEC of a polyampholyte and a polycation and its disruption close to the IEP by changing the pH-value (A). Polyampholytes can additionally interact with oppositely charged surfaces (B).^{57, 70, 76}

Synthesis and application

The versatile applications of polyampholytes rely on their above-described properties and solution behavior: high water-solubility, response to stimuli and their reversible interaction with many different compounds and surfaces.^{7, 70} Furthermore, the diversity of available polyampholytes is vast, and the preparation of tailor-made materials for each specific application is conceivable. Corresponding design aspects are summarized in **Table 1** and **Figure 4** shows some typical structures of polyampholytes.

1. Introduction

Table 1. Possible design aspects for the preparation of tailor-made polyampholytes and the options to realize this.

Design aspects	Options
Molecular composition ⁶²	Choice of monomers (weak or strong acid / base; zwitterionic) Monomer ratio
Molecular structure ^{7, 56}	Charge distribution (alternating, gradient, random, block) Location of charge (<i>e.g.</i> side-chain, backbone) Polymer architectures (linear, graft, block, star, 3D)
Non-ionic building blocks ⁷⁵	Hydrophobic: amphiphilic copolymer; hydrophilic: double hydrophilic Corresponding moieties in side-chain, segmented, backbone, ...

In respect of charged moieties, the binding of metal ions could be exploited in metal recovery, desalination or catalysis and the interaction with proteins in protein purification or separation as outlined by S. E. Kudaibergenov and A. Ciferri.⁷⁰ Moreover, synthetic or natural polyampholytes act as effective dispersants, stabilizers, flocculants or antifouling coatings,^{54, 77-79} and are also found in sensors,⁸⁰⁻⁸² or smart catalysis.^{83, 84} However, biotechnology and biomedicine are one of the most emerging fields of applications for polyampholytes with a special emphasis on hydrogels. Their most recent and future role is particularly seen in tissue engineering and delivery systems.^{63, 85, 86}

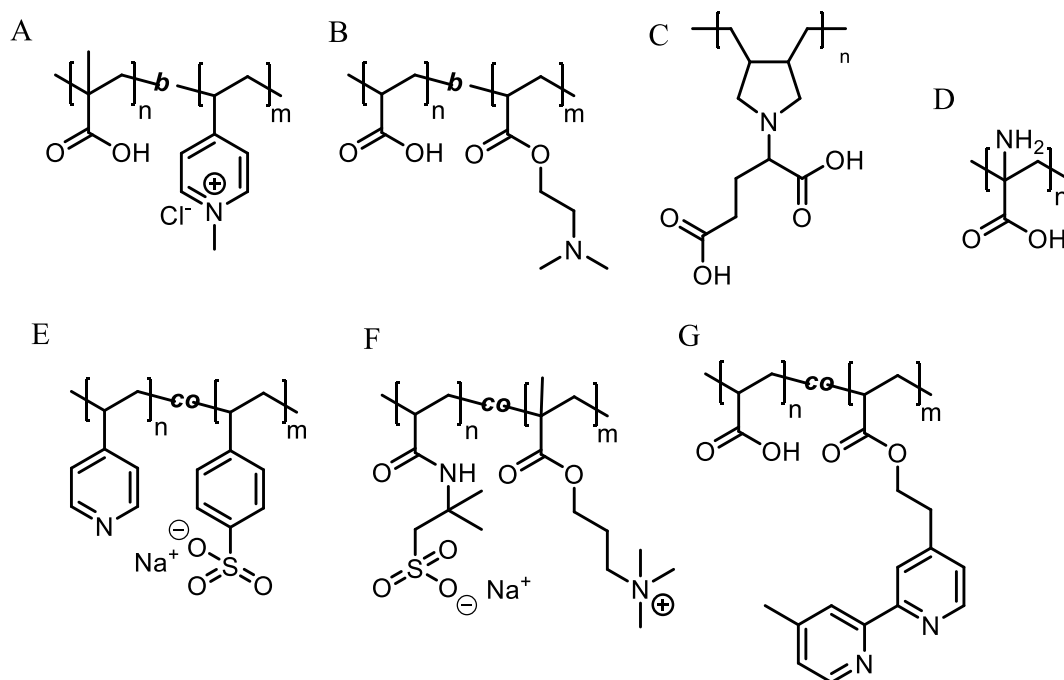


Figure 4. Typical polyampholyte structures, including block polyampholytes (A: PMAA-*b*-4VPCl,⁶⁹ B: poly(2-(dimethylamino)ethyl methacrylate)-*b*-poly(acrylic acid) (PDMAEMA-*b*-PAA)⁸⁷, homopolymers (C: poly(*N,N*-diallylglutamate)⁸⁸, D: PDha),³² and random copolymers (E: poly(styrene sulfonic acid-*co*-4-vinylpyridine),⁸⁹ F: poly(2-acrylamido-2-methyl-1-propanesulfonic acid-*co*-[3-(methacryloylamino)propyl]trimethylammonium chloride),⁹⁰ G: poly(acrylic acid)-*co*-(2-(4-(4'-methyl-2,2'-bipyridyl) ethylacrylate))).⁹¹

1. Introduction

In general, polyampholytes are designed by combining monomers that are also used in polyanions or polycations. The choice of monomers is as diverse as the possible distribution of the charged moieties and various copolymers, which benefits from a huge progress in synthetic strategies. Further, tailored polyampholytes can be synthesized, such as amphiphilic or double hydrophilic (segmented copolymers). Different polymerization techniques (typically ionic or radical) and post-polymerization modifications can be used, and in case of functional monomers, which may not be compatible with polymerization conditions, often the use of protected precursors is necessary.⁵⁷ Typical examples of polyampholytes include random copolymers, derived from free radical polymerization such as poly(styrene sulfonic acid-*co*-vinyl pyridine),⁸⁹ and block polyampholytes, *e.g.* poly(sodium methacrylate)-*b*-poly(dimethyl amino ethyl methacrylate) synthesized *via* sequential anionic living polymerization,⁹² poly(2-(1-imidazolyl)ethyl methacrylate)-*block*-poly(tetrahydro pyranyl methacrylate) *via* group transfer polymerization⁹³ and poly(4-vinylbenzyl (trimethylphosphonium) chloride)-*block*-poly(4-vinylbenzoic acid) obtained through controlled reversible addition-fragmentation chain-transfer (RAFT) polymerization.⁹⁴ In addition to the above mentioned techniques,⁵⁷ zwitterionic polymers may also be prepared via step growth polymerization,⁹⁵ ring opening metathesis polymerization,⁹⁶⁻⁹⁹ polyaddition/polycondensation,^{100, 101} as well as coupling reactions.¹⁰² Since significant advancements in controlled radical polymerization techniques marked by the advent of atom transfer radical polymerization (ATRP) by M. Sawamoto and J.-S. Wang and K. Matyjaszewski in 1995,^{103, 104} nitroxide-mediated polymerization (NMP) first described in a patent in 1985,¹⁰⁵ and RAFT by E. Rizzardo in 1998,¹⁰⁶ it is now possible to polymerize a large number of vinyl monomers. In contrast to conventional radical polymerization, corresponding polymers are characterized by low molecular weight distributions and defined molar masses. Besides the construction of complex polymer architectures, *e.g.* star, block, graft, branched or dendritic (co)polymers, it is also feasible to perform end-functionalization.¹⁰⁷ These strategies achieve control by reducing the concentration of active radical species [P•], which are prone to irreversible transfer and termination reactions, allowing a linear increase in the degree of polymerization with conversion. This could be realized by the addition of a stable radical X•, which reversibly couples with the growing chain P• ('active species') to a labile or 'dormant' P-X species. During the polymerization process the stable radical will be released in multiple steps and P• can again react with monomers M, which don't initiate with X• itself.^{3, 55} The corresponding process, which is similar for conventional NMP and ATRP, is schematically depicted in **Figure 5**. By introducing a second monomer, *e.g.* M₂ to M₁, block copolymers are formed.

1. Introduction

In ATRP, a catalytic system is used based on a transition metal (M_t^m) halide complex (**Figure 5 B**) with an alkyl halide initiator. During the polymerization process the oxidation state of M_t^m is reversibly changing, shifting between the dormant P_n-X and the active $P_n\cdot/X-M_t^m/L$ species.^{55, 107, 108} Since the invention of traditional ATRP, various ATRP-type processes have arisen to further improve this method, *e.g.* Activator ReGenerated by Electron Transfer (ARGET) and activators generated by electron transfer (AGET) allow the use of Cu(II) species and to reduce the amount of catalyst, or single-electron-transfer living polymerization (SET-LRP) using Cu(0) for a more stable handling of reagents.^{108, 109} The versatility of ATRP gives access to many different polyampholytes (or their precursors) and architectures, such as poly(2-(dimethylamino)ethyl methacrylate)-*block*-poly(acrylic acid) di-block copolymers,⁸⁷ poly(methacrylic acid-*co*-*N,N*-diethylaminoethyl methacrylate) brushes,¹¹⁰ poly(2-vinylpyridine-*co*-acrylic acid) statistical copolymers,¹¹¹ and poly(2-(2-bromoisobutyryloxy)ethyl methacrylate)-*graft*-poly((methacrylic acid)-*stat*-(2-(dimethylamino)ethyl methacrylate) densely graft copolymers.¹¹² Further, zwitterionic monomers were polymerized with a defined endgroup,¹¹³ and amphiphilic or double hydrophilic copolymers with a polyampholytic segment could be synthesized.^{34, 114}

NMP was originally performed at high temperatures (>125 °C) and relatively long reaction times (24-72 h) using nitroxides as control agents, *e.g.* one of the earliest examples 2,2,6,6-tetramethyl-1-piperidinyloxy (TEMPO, **Figure 5 C**) However, great breakthroughs have since been made with the development of novel nitroxide reagents, enabling reaction temperatures as low as 70 °C and the polymerization of more demanding monomers. Unimolecular initiators, such as BlocBuilder® have also been developed that release both an nitroxide controlling group and an alkyl radical initiator upon heating, combining two functionalities in a single reagent. Besides, the transfer of nitroxide end groups into other functional groups are thoroughly studied.¹¹⁵⁻¹¹⁷ The mechanism of NMP is mainly based on the ‘persistent radical effect’, which describes the preferred coupling of a reactive radical with a stable radical, instead of the coupling of two reactive radicals.¹¹⁶ Since NMP reveals control over a broad spectrum of monomers and is tolerant to many functional moieties, including amines, alcohols or ionic ones (sulfonic acid, ammonium, carboxylic acid), a lot of homopolymers and block copolymers can be accessed *via* this route.^{115, 116} In this manner, precursors of polyampholytic poly(styrene)-*block*-poly((acrylic acid)-*co*-(2-(4-(4'-methyl-2,2'-bipyridyl))-ethylacrylate)) or PDha were successfully synthesized *via* NMP in a well-controlled way.^{32, 91}

1. Introduction

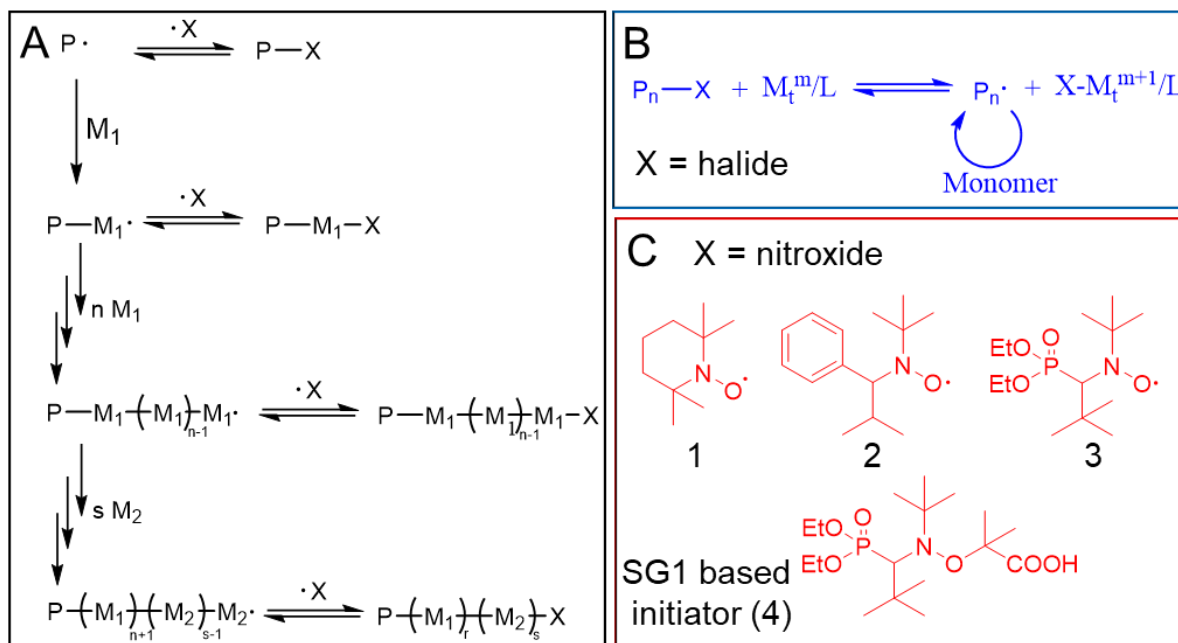


Figure 5. General schematic depiction of controlled radical polymerization processes and possible formation of a linear block copolymer after adding a second monomer (A). The mechanism of ATRP is based on the utilization of a transition metal complex (M_t^m = metal cation, L = ligand) and halides (B). Common nitroxides in NMP are 2,2,6,6-tetramethyl-1-piperidinyloxy (TEMPO, 1), 2,2,5-trimethyl-4-phenyl-3-azahexane-N-oxyl (TIPNO, 2) and 4-(diethoxyphosphinyl)-2,2,5,5-tetramethyl-3-azahexane-N-oxyl (SG1, 3). An unimolecular NMP system, such as BlocBuilder® (4), forms both the initiator and the stable nitroxide upon heating.^{3, 55, 108, 116}

In addition to advanced polymerization techniques, post-polymerization modification reactions are an important tool to prepare tailor-made polymeric materials. Subsequent modification of a polymer allows its properties to be fine-tuned and provides access to copolymers or to polyampholytes from protected precursors. One possible route is the conversion of monomers bearing suitable reactive handles that can undergo a number of chemical transformations, *e.g.*, addition, substitution, elimination and isomerization.^{58, 118} Amino moieties, which are found in many polyelectrolytes are especially useful reactive handles and have been exploited in aza-Michael addition and the ring-opening of epoxides, as exemplarily shown in **Figure 6**. In this respect, for example side-chain amino acids have been functionalized with various acryl amides and acrylic acids as Michael-acceptors.¹¹⁹ In another example, poly(ethylene imine) (PEI) has been used for the post-polymerization modification with acrylic acid and epoxyalkanes to obtain amphoteric polymeric surfactants.^{120, 121} Further polyzwitterions can be obtained from a prepared polymer by the addition of zwitterionic modifiers,¹²² or protection chemistry can be applied. Here, monomers with protected functional groups may be chosen, which are stable to polymerization conditions, when their deprotected and more reactive groups would not be suitable. For example, amines can be protected with a *tert*-butyloxy carbonyl group (boc) or carboxylic acids with esters, to enable (controlled) radical polymerizations.^{34, 123} Further, the post-polymerization modification of the endgroups, *e.g.* click chemistry, is a substantial way to obtain block copolymers and other advanced architectures in general.¹²⁴ In this way, a number

1. Introduction

of novel materials can be accessed: polyampholyte-based hydrogels,¹²⁵ or polyelectrolytes featuring a functional endgroup that can be also chemically grafted onto surfaces for an efficient immobilization.¹²⁶

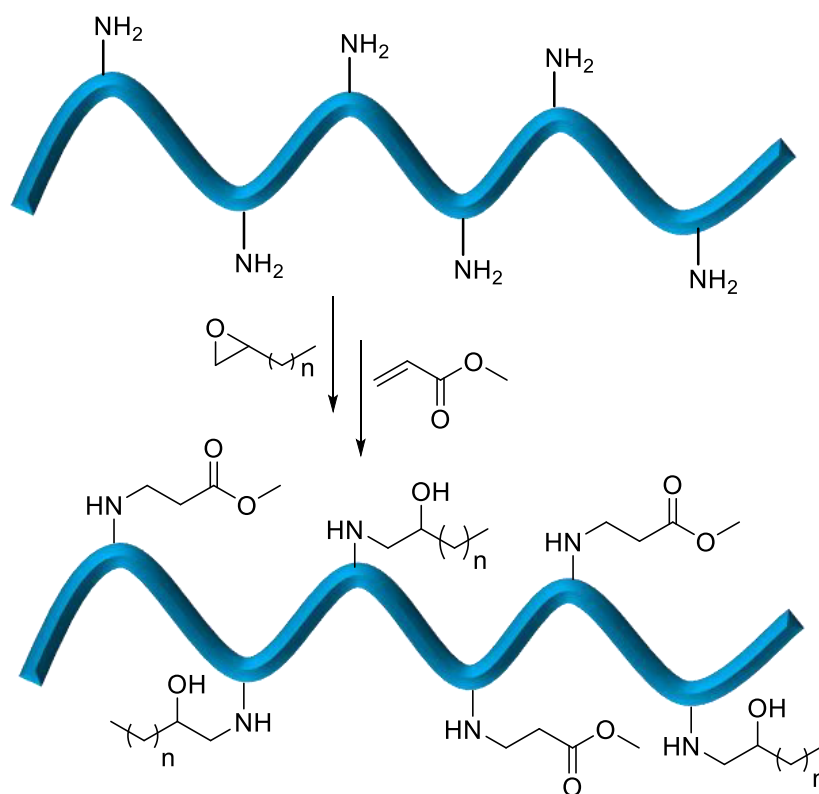


Figure 6. Schematic representation of the subsequent post-polymerization reaction of an amino group containing polymer with an epoxide and a Michael acceptor (acrylic acid methyl ester) reported by H. Hidaka and M. Moriya.^{120, 121}

The above described possibility to prepare and tune polyelectrolytes, *e.g.* by controlled radical polymerization (CRP) or post-polymerization modification techniques gives well-defined polymer materials for desired applications. Due to their responsive behavior and the interaction with various compounds, polyelectrolytes are important for the preparation of polymeric ‘smart’ materials. These materials are particularly interesting due to their potential applications, *e.g.*, as coating materials, to solve recent issues in the field of sensing, catalysis, surface engineering or biomedicine.¹²⁷ The ‘smart’ or stimuli-responsive polymers with emphasis of polyelectrolyte building blocks will now be discussed.

1.2 Smart, double hydrophilic polymers

Macromolecules showing a certain physical effect or function in solution are defined as functional polymers. As a special case, smart polymers are stimuli-responsive and react to their environment by undergoing conformational or chemical changes, which lead to a variation in their physical properties. This response can even be detected on a macroscopic scale and is further translated to a given function, such as the release of a cargo or the generation of a

1. Introduction

signal.^{3, 127, 128} External stimuli could be light,¹²⁹ pH value,¹³⁰ temperature,¹³¹ the presence of ions or the ionic strength,^{132, 133} a magnetic field,¹³⁴ or mechanical stress,¹³⁵ as depicted in **Figure 7**. Moreover, multi stimuli-responses may be found within one polymer by the combination of the corresponding monomers, *e.g.* a thermo-, pH- and metal ion-responsive copolymer.¹³⁶ Accomplishing various functions and exhibiting an efficient transduction mechanisms, this material class is promising for a growing number of important applications, *e.g.* sensors, smart coatings, catalysis or drug-delivery.¹²⁷

Smart polymeric segments are often found in double hydrophilic block copolymers (DHBCs), which are polymers that consist of two water-soluble blocks. One segment is usually responsible for maintaining water-solubility, while the other one reveals smart properties, leading to interesting aggregation behaviors.^{41, 137} The solvating block is often poly(ethylene oxide) (PEO), poly(vinyl alcohol) (PVA), or poly(2-ethyl-2-oxazoline) (PEtOx) while the functional block is often carries stimuli-responsive moieties that respond to temperature,¹³⁸⁻¹⁴⁰ pH value,^{141, 142} ionic strength,^{143, 144} irradiation with light¹⁴⁵ or the presence of redox-active compounds.¹⁴⁶ Defined nanostructures are formed by either self-assembly upon exposure to these triggers by the aggregation of the functional segment,^{137, 147} or due to the different hydrophilicities of each block in pure water.^{148, 149} It is even possible to link two stimuli-responsive segments. One segment may aggregate preferentially in solution while the other one is still promoting the overall solubility depending on the trigger applied.¹⁵⁰ In this respect, a terpolymer consisting of poly(oligo(ethylene glycol) methacrylate) as the thermo-sensitive block and a statistical, polyampholytic poly((diethylamino)ethyl methacrylate)-*co*-(methacrylic acid)) segment, shows reverse micellar formation. The individual segments shift between being the core or the corona dependent on the surrounding pH and temperature.¹⁵⁰

1. Introduction

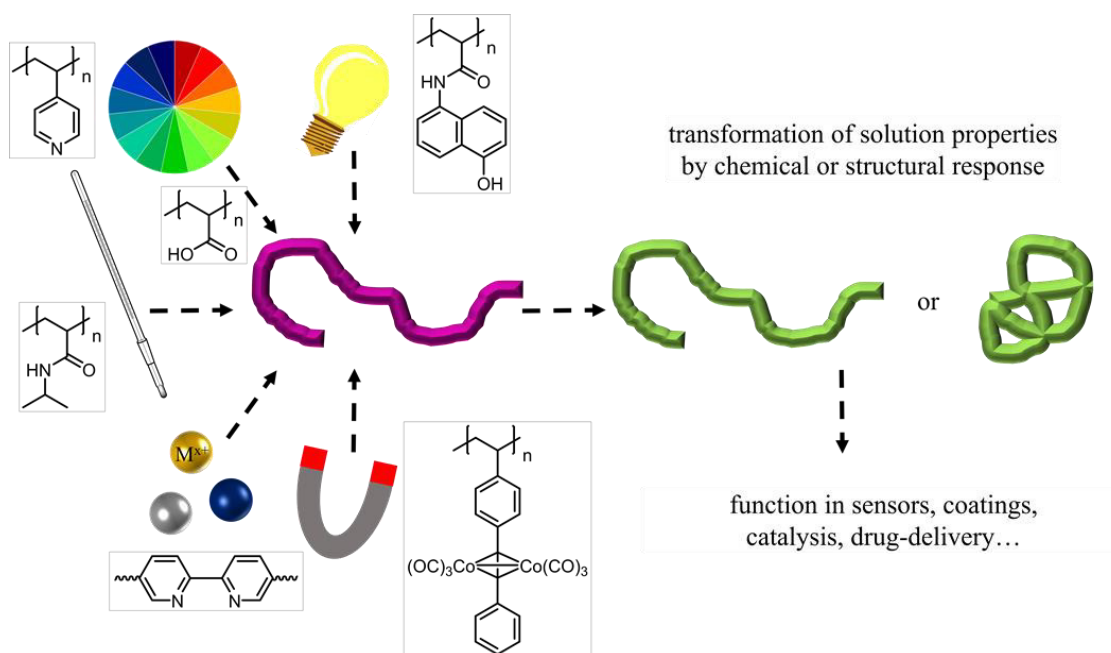


Figure 7. Depiction of a smart polymer and possible functional moieties that can be incorporated to enable a response to different external stimuli: light, pH, temperature, metal ions and a magnetic field.^{129-132, 134} As a result, the solution properties change upon exposure to a specific stimuli to fulfill a certain function.¹²⁷

DHBCs based on a pH- and metal ion responsive poly(2-acrylamido glycolic acid) (PAGA) linked to a solvating poly(*N*-acryloyl morpholine) or PEO segment are a good example for the exceptional solution and aggregation behavior of this polymer class. Such polymers form defined nanoobjects upon the addition of divalent metal cations due to the complexation with the PAGA block. Furthermore, the size and shape were dependent on the amount and type of cation added. Besides, block copolymers with poly(2-*iso*-propyl-2-oxazoline) (PiPrOx) additionally exhibit a thermo-response and the ability to crystallize. Hereby, it was possible to tune the cloud point temperature (T_{CP}) between 30 and 68°C through either changing the copolymer composition or by the complexation of metal ions. However, heating at 65°C for 6 h lead to crystallization of the PiPrOx segment. This enables advanced nano-structures to be accessed, such as spherical micelles, worms or fibers (**Figure 8**).^{143, 151} PiPrOx-*b*-PAGA assemblies were also investigated as suitable nanoreactor for the formation of CdS nanoparticles (NPs) for hydrogen evolution.⁵¹ The formation of micellar structures can be achieved by such unimolecular systems, but also by polyion complexes of a pair of oppositely charged double hydrophilic copolymers (DHCs).^{152, 153} This may be realized by the utilization of PEO-*b*-poly(L-lysine) and PEO-*b*-poly(α , β -aspartic acid), forming micelles with a IPEC core and a hydrophilic PEO shell, which could be applied in drug-delivery systems.³⁹

1. Introduction

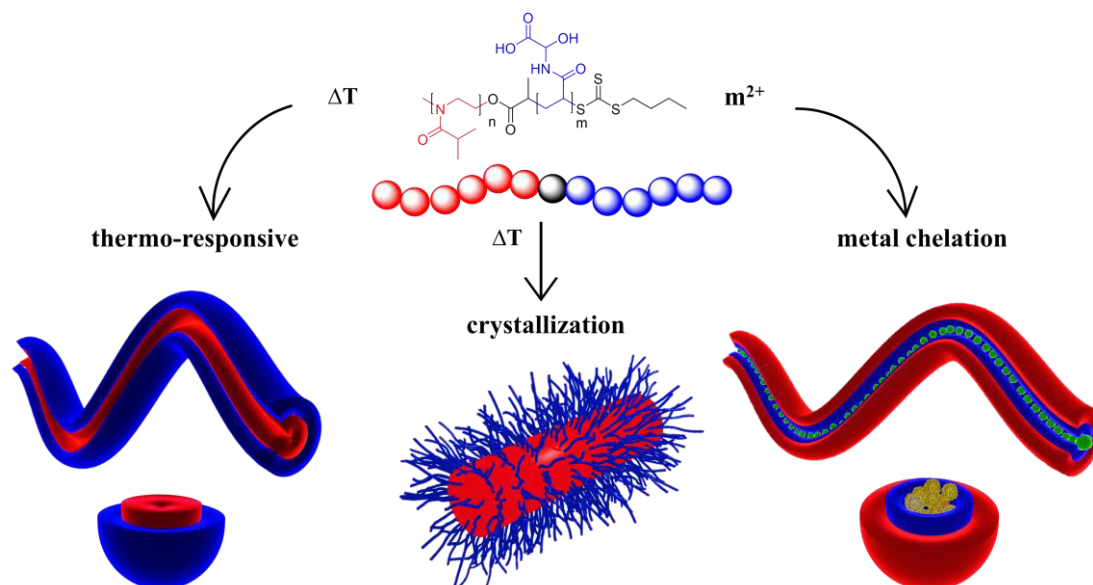


Figure 8. Structure of smart, double hydrophilic $PiPrOx-b-PAGA$ and the formation of nano-assemblies through the addition of metal cations or heating. Reprinted from *Macromolecules*, **2020**, 53, 5056-5067. Copyright 2020 of American Chemical Society.¹⁵¹

Although most examples of DHCs focus on linear block copolymers, other architectures including graft, hyperbranched, toothbrush- or star-like polymers have also been reported. They differ in their synthetic complexity and solution properties, but are also often less defined, reveal more complex aggregation behavior and chain-end effects.^{36, 147, 154, 155} Regarding these topologies, star-like macromolecules may already form unimolecular 3D structures,¹⁵⁶ or the unimolecular core-shell structures of multiarm hyperbranched polymers reveal a higher stability compared to the assemblies of linear block copolymers.¹⁵⁷ In the case of densely grafted comb-like copolymers the self-organization may be potentiated and could render them as outstanding templates.¹⁵⁸ Stars, especially, exhibit lower solution viscosities and stronger stimuli-response and interactions due to a higher density of functional groups.¹⁵⁹ Star-like double hydrophilic block copolymers have been successfully synthesized *via* cationic ring-opening polymerization, click reactions, ATRP and SET-LRP.¹⁶⁰⁻¹⁶⁴ For poly(4-vinyl pyridine)-*b*-PAA multi-arm DHCs, a pH-dependent morphology and hydrodynamic radii have been observed.¹⁶² A three-armed star-shaped terpolymer consisting of poly(*N*-isopropylacrylamide) PNIPAAm (thermo-responsive), PDMAEMA (thermo- and pH-responsive) and poly(*N*-vinylpyrrolidone) (biocompatible) segments, displays pH- and temperature-dependent assembly in solution.¹⁶⁰ Moreover, double hydrophilic block copolymers containing a hyperbranched segment have also been reported. PEO-*hyperbranched*-poly(glycerol) (PEO-*hb*-PG) was successfully synthesized and the modified polymers prepared by S. Lee *et al.* were used for pH-controlled drug release. Hereby, the branched segment features a high water-solubility and density of functional endgroups

1. Introduction

increasing potential loading capacities.^{165, 166} In another approach hyperbranched DHCs based on a positively charged hyperbranched poly(amidoamine) (HPAMAM) core (by a Michael addition reaction) and poly(ethylene glycol) (PEG) monomethyl ether (MPEG) arms linked by acylhydrazone bonds (HPAMAM-*g*-MPEG), were prepared to use as nanoreactors for the formation of CdS quantum dots.¹⁵⁷ Exhibiting a rather uncommon architecture, toothbrush-like DHCs consisting of PNIPAAm-*block*-poly(oligo(ethylene glycol) monomethyl ether methacrylate) (PNIPAAm-*b*-POEGMA) with pendant ethylene oxide side-chains have been synthesized *via* RAFT, self-assembling into vesicles and micelles.¹⁶⁷ Concerning graft copolymers, there exist three general synthetic pathways: grafting-through, grafting-onto and grafting-from.¹⁵⁵ Graft-copolymers show interesting properties due to their compact and confined structure, strong chain-end effects and complex aggregation behaviors, *e.g.* the formation of worm-like micelles.^{154, 155, 168, 169} Double hydrophilic graft copolymers were synthesized using a grafting-onto approach *via* amidation to obtain polyacetal-*graft*-PEG copolymers,¹⁷⁰ or PAA-*g*-PEG using PEG-NH₂ as a reactive handle.¹⁷¹ In a similar way PNIPAAm-*g*-PEG was synthesized from a functionalized backbone,¹⁷² while the polymer can be also be derived *via* a grafting through method from PEG macromonomers and NIPAAm.¹⁷³ Furthermore, the controlled radical polymerization techniques and/or their (sequential) combinations provide access to double hydrophilic graft copolymers *via* grafting-from, which is the most common method reported in the literature.^{154, 168, 169, 174-176} In this respect, for example a double zwitterionic graft copolymer has been synthesized, starting from carboxylated poly(*L*-lysine), which was transferred into a macro chain transfer agent and been chain extended with a sulfobetaine. The corresponding macromolecules were used to suppress protein aggregation and for protein release.¹⁷⁶ In addition, graft copolymers were found to be suitable templates for inorganic nanomaterials, and such materials are referred to hybrid materials.^{169, 177} The combination of polymers and inorganic compounds has become an important research field since the last decades, where new and interesting properties and functions can be obtained that otherwise can't be reached using any single component.⁵⁹

1.3 Organic/inorganic hybrid materials

Hybrid materials are defined as a mixture of two or more different components in a small dimension complementing each other to obtain a single entity with new or enhanced properties. The dimension can be > 1 μm for composites or < 1 nm for molecular composites, nanomaterials (1-100 nm) also belong to this material class.^{178, 179} Although organic/inorganic hybrid materials were already being used thousands of years ago in ancient Greece or China, as well as in the Maya culture in the form of hybrid clays or pigments, research in this field is developing rapidly

1. Introduction

as it can be seen in the number of patents and publications in the last few years.^{45, 60, 179, 180} Since the extensive interfacial interaction between the corresponding components plays a crucial role in the resulting material properties, this may be seen as one of the main challenges in the design of hybrid materials. In this respect, hybrid materials may be further divided into two classes: *Class 1* covers hybrids with relatively weak interactions including van der Waals forces, hydrogen bonds, ionic bonds or π - π stacking. These physical interactions mainly arise from the functional groups present. *Class 2* encompasses covalent or ionocovalent bonds, and the utilization of compatibilizers is often necessary to achieve this strong chemical interaction.^{43,}

181

Regarding the versatility of inorganic or organic components, almost endless combinations of materials are possible. Therefore, in case of a suitable interaction and synergistic behavior, new or often unknown properties and multifunctional materials might be obtained and the modulation of the materials characteristics can be achieved by an intelligent construction.^{182, 183} Common organic and inorganic components and their beneficial properties are summarized in **Table 2**. Organic materials are often used as the matrix being rather soft and flexible. While the inorganic compounds are often used as fillers and add, *e.g.*, enhanced stability, thermal, magnetic or electrical properties, to the resulting hybrid material.^{45, 46} Although most examples consider these typical organic and inorganic compounds, carbon nanomaterials, *e.g.* carbon nanotubes or fibers, are extensively used in hybrid materials due to their electrical, thermal, sorptive, mechanical and catalytic properties.¹⁸⁴

Table 2. List of organic and inorganic components and their beneficial properties, summarized by S. H. Mir *et al.* and M. S. Saveleva *et al.*^{45, 46}

Component	Examples	Beneficial properties
Organic	Polymers (<i>e.g.</i> , hydrogels, copolymers, particles), synthetic molecules, organic biological compounds (<i>e.g.</i> , lipids, enzymes, proteins, microorganisms, bacteria)	Flexibility, elasticity, hydrophilic/hydrophobic balance, reactivity, suitable and processable matrices or network modifier
Inorganic	Minerals, clays, metals, semiconductors, carbon, ceramics	High electrical and thermal conductivity, enhanced absorption, thermal stability, mechanical strength, magnetic or redox properties

Regarding the diversity of individual components and their properties, the appropriate choice of components and their interplay could be seen as the decisive challenge in this research field. In general, the preparation of hybrid materials could be seen as a '*LEGO* © approach' starting from relatively simple building blocks.¹⁸² However, different kinds of actions must be considered upon mixing the property or function of the compounds when designing desired

1. Introduction

systems. Hereby, the averaging, supplementation, addition, collaboration and creation of functions may occur.¹⁷⁸ The construction of hybrid materials can be divided into three synthetic pathways: the *in situ* formation from molecular precursors (**A**), a building block approach (**B**), and a template-assisted synthesis (**C**).⁶⁰

Route **A** is mainly based on sol-gel, hydro- or solvothermal methods or the use of bridged precursors resulting in three-dimensional organic/inorganic networks. Therefore, organically functionalized metal alkoxides or halides, as well as organosilanes, are used as typical precursors.^{60, 179} In this respect, polymeric networks containing inorganic clusters can be obtained.¹⁸⁵

In route **B**, readily prepared building blocks are mixed together. An obvious advantage of this route is that the corresponding components can be synthesized in a controlled way and characterized separately before mixing. Besides, no significant structural change will occur during hybrid material formation and prediction of the resulting properties is easier. Blending of the material components can be realized in the melt, powder or in solution state.^{43, 182} In solution, the organic compound is dissolved in a suitable solvent and inorganic compound dispersed *via* ultrasonication in it. In this way, for example polymer-coated metal oxide nanoparticles were prepared.⁵⁴

Route **C** could be seen as an interplay between route **A** and **B**, when one of the components is formed within a defined template.^{60, 179} This especially supports the formation of hierarchical or macroporous structures which is often realized by organic matrices such as synthetic polymers, surfactants or biomaterials.¹⁸⁶ Self-assembling block copolymers are particularly suitable templates,¹⁸⁷ and in this case, the above discussed double hydrophilic copolymers are used in the controlled formation of inorganic nanoparticles from metal salts or in biomineralization.^{51, 188}

In the last decades, an increasing number of hybrid materials are being found in our daily lives and are indispensable for many commercial applications, as depicted in **Figure 9**. This is not surprising regarding recent advances in synthetic strategies and the possibility to obtain tailor-made functions and properties by this material class. These innovative materials are found for example in micro-optics and -electronics, batteries, membranes, construction, insulation, coatings, packaging, cosmetics, and medicine as outlined in reviews from C. Sanchez and coworkers.^{60, 180, 181} Among the mentioned applications of hybrid materials, sensing and photocatalytic hydrogen evolution are gaining great interest, facing current medical¹⁸⁹ and environmental issues.^{51, 190} Synthetic polymers, including functional polyelectrolytes and

1. Introduction

polyampholytes, are suitable in this context as soft and hard matrices as outlined in the following chapter.



Figure 9. Commercial applications of hybrid materials in our modern society. Reprinted from *Adv. Funct. Mater.* **2018**, 28, 1704158, with permission of WILEY-VCH Verlag GmbH & Co. KGaA, Weinheim.¹⁸⁰

1.3.1 Polymeric hybrid materials

With their diverse functional groups, tailor-made structures and properties, structure-directing synthetic polymers are suitable building blocks in the construction of hybrid materials. The macromolecules can both support the preparation of nanostructured inorganic composites, such as NPs or mesoporous structures or act as stabilizers to embed inorganic moieties in coatings, or matrices. The polymeric templates can either be preserved to enclose the synthesized inorganic compound in films and solutions, or be removed by thermal or chemical extraction processes in order to obtain the pure inorganic materials.^{59, 186, 191, 192} For example ‘hard’ hybrid materials are often prepared using polymeric templates, for example mesoporous structures of aluminosilicates, titanium and niobium oxides with high crystallinity can be obtained by the use of block copolymers, *e.g.* amphiphilic poly(isoprene)-*block*-PEO (PI-*b*-PEO), where the inorganic compounds were enriched in the hydrophilic segment.^{193, 194} Moreover, covalent attachment by grafting the polymer to the surface of an inorganic NP facilitates the construction of well-defined superstructures such as films with hexagonally ordered silica cores. As an example, the surface of silica NPs was modified with an ATRP initiator in order to grow poly(styrene) (PS) chains from the surface to form a well-defined organic matrix.¹⁹⁵

‘Soft’ hybrid materials, on the other hand, are generally found under aqueous conditions. Consequently, water-soluble polymers and hydrogels are the main focus in this research field. Especially the ionic interaction of polyelectrolyte based materials with oppositely charged

1. Introduction

metal salts,⁸ or nanoparticle surfaces¹¹ renders them ideal templates for the growth and/or stabilization of inorganic compounds by the formation of strong polyion-complexes.^{177, 188, 196} The inorganic materials can be either entrapped in 3D networks, like for hydrogels, in polymer membranes, within nano-assemblies, *e.g.*, micelles, polymer monolayers or multilayers. In this respect, well-defined metal NPs can be prepared within polyelectrolytic hydrogels for application in catalysis, as reported by J. Song *et al.*¹⁹⁷ Membranes consisting of amphiphilic block copolymers were prepared and used in the immobilization of polyoxymethylates exploiting the electrostatic interaction with the hydrophilic segment.¹⁹⁸ Poly(acrylamide) has been used as a polymeric coating for the controlled growth of Au, Ag and their alloy nanoparticles from the corresponding ions in solution.¹⁹⁹ Further, polymer multilayers from a polycation and a polyanion have been used as nanoreactors for the synthesis of either Au or Ag NPs.^{200, 201} Regarding the field of DHBCs, the mechanism of metal ion complexation and subsequent reduction is of special interest, since the core is stabilized by the hydrophilic shell leading to the formation of uniform and controlled inorganic NPs.^{51, 202, 203} Hereby, the organized DHBCs fulfill also the role of nanoreactors.^{51, 164, 204} This mechanism and its advantage over the use of small ligands or molecules is shown in **Figure 10** for PEO-*b*-PAA for the formation of stable Au NPs.²⁰⁵ B. P. Bastakoti *et al.* went a step further and used both segments to interact with inorganic moieties. They attached silica in a sol-gel process within the shell around the Ag nanoparticle/polymer hybrid in the core and obtained Ag@SiO₂ nanoparticles after calcination at 500 °C.²⁰²

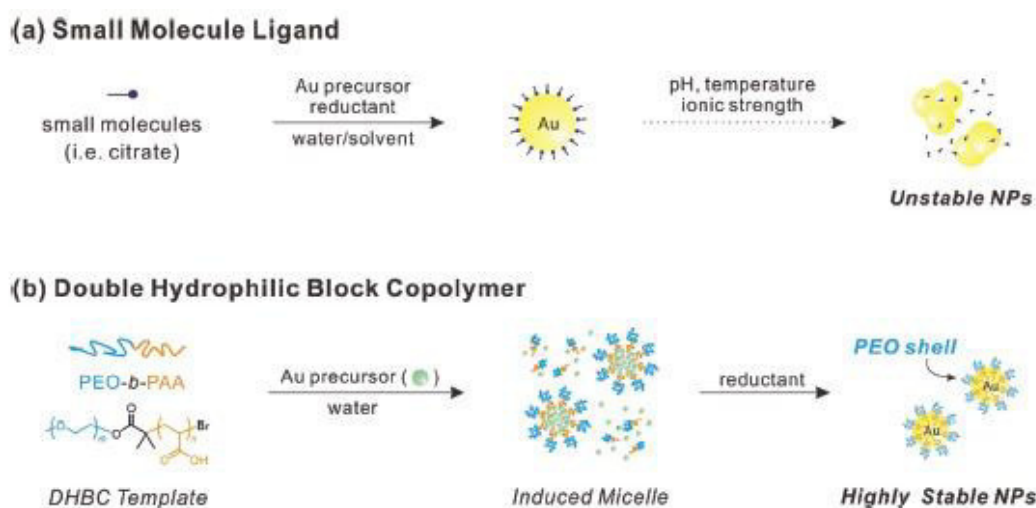


Figure 10. Double hydrophilic block copolymer templated synthesis of Au NPs in comparison to the utilization of small molecules. Reproduced from *Polym. Chem.* **2017**, 8, 4528–4537, with permission of the Royal Society of Chemistry.²⁰⁵

1.3.2 Polyelectrolyte-based hybrid materials in catalytic hydrogen evolution

The production, storage and distribution of hydrogen is key to promote sustainable and clean energy in the 21st century,²⁰⁶ and photocatalytic water-splitting exploiting solar-energy is a

1. Introduction

substantial part of it.²⁰⁷ Regarding photocatalytic hydrogen evolution, embedding catalysts in a polymer matrix was found to promote photocatalytic hydrogen evolution. This approach additionally benefits from a molecular tuneability and the variety of polymeric building blocks.^{51, 208, 209} Moreover, the efficiency of photocatalytic systems may be further enhanced using multi-component hybrid materials that contain a catalyst (*e.g.*, metal or metal oxide NPs)²¹⁰ as well as a photosensitizer,²¹¹ co-catalysts²¹¹ or electron relays.²¹² Hereby, the use of a suitable framework is crucial to connect, direct, assemble or stabilize each component and this can be realized by tailor-made polymers.^{51, 209, 213} Regarding catalysis in general, polymer nanoreactors, *e.g.* micelles, stars, hydrophobic pockets or capsules, are gaining more and more attention for creating stable conditions, defined (pseudohomogenous) environments and preventing side-reactions.^{156, 214} However, until now, only a few examples have focussed on polyelectrolyte-based systems in catalytic hydrogen evolution, although they perform in aqueous environments and are able to interact with different catalysts or sensitizers through electrostatic interactions. Numerous approaches have been reported in the literature providing different types of polyelectrolytes, forming covalent or physical assemblies, as depicted in **Figure 11**. A. M. Beiler *et al.* grafted poly(vinyl pyridine) covalently to a visible-light absorbing gallium phosphide semiconductor, which they then used to assemble cobalt centers of porphyrins to this polymeric coating. Afterwards, this hybrid material was used for the photoelectrosynthetic hydrogen evolution under solar illumination.²¹⁵ I. Romanenko *et al.* prepared nanoporous membranes by the self-assembly of amphiphilic poly(styrene-*co*-isoprene)-*block*-PDMAEMA (P(S-*co*-I)-*b*-PDMAEMA) as a soft matter matrix. In the next step, a molecular inorganic catalyst $[\text{Mo}_3\text{S}_{13}]^{2-}$ and photosensitizer $[\text{Ru}(\text{bpy})_3]^{2+}$ were immobilized onto the electrolytic block and the visible light-driven hydrogen evolution was tested.²⁰⁹ Polyelectrolytic hydrogels, as covalently linked 3D scaffolds, were also used as templates by A. S. Weingarten *et al.* (a supramolecular hydrogel),²¹⁶ and H. Sai *et al.* (a covalently crosslinked hydrogel).²¹⁷ Both molecular inorganic catalysts, as well as perylene monoimide chromophores, as supramolecular light harvesting assemblies, were entrapped and the efficient production of hydrogen was proven. A. Nabiyan *et al.* constructed micellar nanoreactors from a DHBC exhibiting a PAGA segment for an enhanced photocatalytic hydrogen evolution. First, Cd^{2+} cations were complexed within a metal chelating core and afterwards reacted to CdS nanocrystals. These hybrid materials clearly outperformed pristine CdS in solution with respect to photocatalytic water splitting.⁵¹ Recently, highly water-soluble conjugated polyelectrolytes, as water-soluble organic semiconductors, have been applied as hybrid materials for efficient photocatalytic hydrogen evolution. Their design is versatile (side-

1. Introduction

chains, counter ions, backbone...), and in addition to excellent interface modification and light-harvesting capabilities, solubility they can interact with co-catalysts.^{218, 219} Z. Hu *et al.* used cationic and anionic modified conjugated polymers to synthesize Pt NPs and they applied this hybrid materials in hydrogen evolution.²¹⁸ Although not considered photocatalytically active, a layer-by-layer assembly was used as a simple and cheap approach to construct polyelectrolyte based hybrid materials for the hydrogen evolution reaction (HER). Therefore, Pt NPs capped with poly(diallyl dimethyl ammonium chloride) were alternately deposited with poly(styrene sulfonate) or PEI to obtain films with a high level of electrochemical connection among the Pt nanoparticles allowing electrocatalytic hydrogen evolution dependent on the number of layers.²²⁰ As outlined in this chapter, polyelectrolyte-based hybrid materials have great potential in photocatalytic hydrogen evolution. However, the facile design and preparation of stable matrices to combine multifunctional compounds remains challenging. Besides, the utilization of polyampholytes featuring both positively and negatively charged moieties could be advantageous compared to ‘simple’ polyelectrolytes.

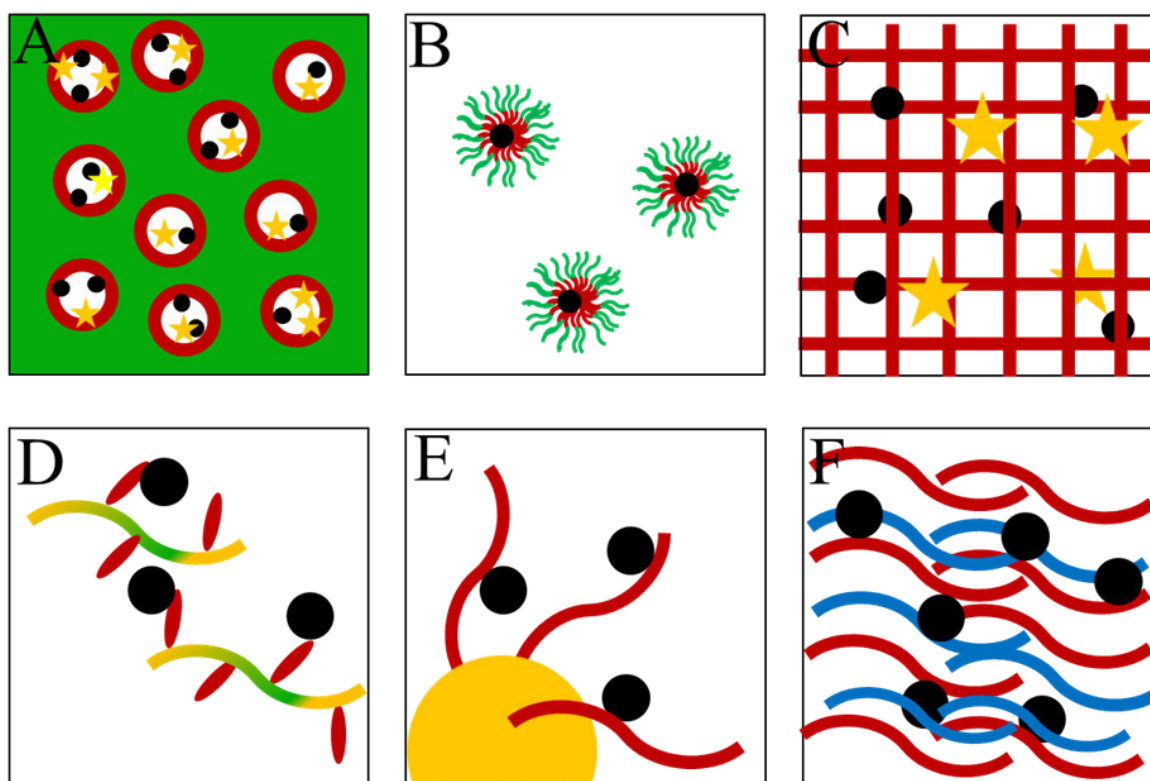


Figure 11. Hybrid materials used for catalytic hydrogen evolution based on polyelectrolytes, where the polymers form different soft matrices: A = nanoporous membranes,²⁰⁹ B = micelles,⁵¹ C = hydrogels,^{216, 217} D = nano-assemblies,²¹⁸ E = covalently grafted coatings,²¹⁵ F = layer-by-layer.²²⁰ Blue and red: polyelectrolytic building block; green: polymeric non-ionic building block; black: inorganic, molecular or nanosized catalyst; yellow: photosensitizer, chromophore, semiconducting material.

1.3.3 Polyelectrolyte-based hybrid materials in sensing applications

Another emerging application field for polymeric hybrid materials are chemical or biological sensors promoted by great advances in nanotechnology. Here, the stimuli-responsive polymers

1. Introduction

described in the previous chapter are particularly interesting candidates, creating readout signals in response to external triggers.²²¹⁻²²⁴ Similar to the polymers in HER, the polymers usually fulfill the role of functional templates, linkers, or act as the sensing element. The synergistic effects attained in such responsive hybrid materials have been comprehensively detailed in several reviews.²²¹⁻²²⁴ As an example, a fluorochromic sensor based on dynamic Eu–iminodiacetate coordination within a poly(*N,N*-dimethylacrylamide) hydrogel was prepared, responding to five different stimuli: pH, temperature, metal ions, sonication, and force (**Figure 12**). Hereby, the dissociation and formation of the complex is visualized as a fluorescent ON/OFF switch and the corresponding, multi-stimuli responsive hybrid material shows great promise as a biological sensor.²²⁵

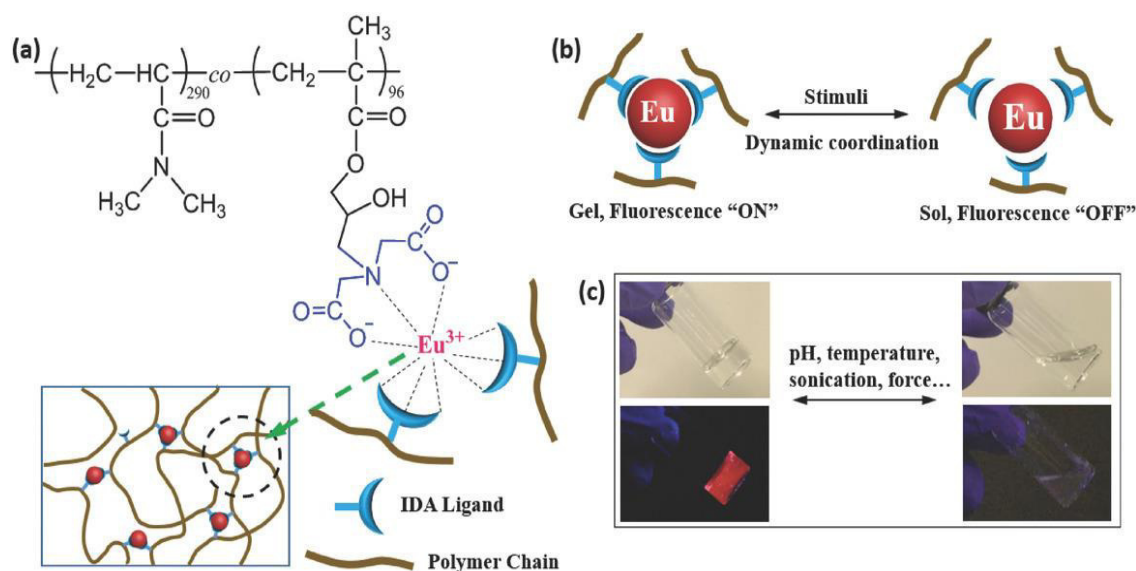


Figure 12. Fluorescent sensor based on a polymer/ Eu^{3+} hybrid material responding to pH, temperature, sonication, force or metal ions. Reprinted from *Advanced Materials*, **2018**, 30, 1706526, with permission of WILEY-VCH Verlag GmbH & Co. KGaA, Weinheim.²²⁵

Again, the use of systems based on polyelectrolyte and their copolymers may be beneficial due to their water-solubility, multi-response and favorable interactions with many inorganic materials and various analytes, such as biomolecules or ions.⁷⁰ With respect to the soft polymer matrices these systems can be further categorized in 3D networks, (*e.g.*, (micro)gels or hydrogels) or polymer modified surfaces, including coatings and core-shell materials. The versatility of the building blocks that can be used, as well as the types of sensors that have been prepared are outlined in **Table 3** and divided into cross linked polymeric scaffolds and polymer-modified surfaces (coatings).

1. Introduction

Table 3. Selected polyelectrolyte-based hybrid materials found in sensing applications.

Polyelectrolytic building block	Inorganic component ¹	Sensing of...	Reference
Polyelectrolyte-based 3D scaffolds			
Crosslinked poly(methacrylic acid)	Au NP and [Ru(bpy) ₃] ²⁺	melamine	J. Cai <i>et al.</i> ²²⁶
Poly[(<i>N</i> -isopropyl acrylamide)- <i>co</i> -(acrylic acid)] micro gel	Ag NP	H ₂ O ₂ Cr ⁶⁺	T. Shu <i>et al.</i> ²²⁷ X. Shen <i>et al.</i> ²²⁸
Alginate gels	Cu nanoclusters and CaCO ₃	glucose	S. Gou <i>et al.</i> ²²⁹
Acrylic acid copolymers hydrogels	Al ₂ O ₃ NP	pH, mechanical stress	W. Lu <i>et al.</i> ²³⁰
Poly(4-vinylphenylboronic acid- <i>co</i> -2-(dimethylamino)ethyl acrylate) gel	Ag NP	glucose	W. Wu <i>et al.</i> ²³¹
polyelectrolyte-modified surfaces			
Poly(<i>N</i> -(3-amidino)-aniline) coating	Au NP	CO ₂	Y. Ma <i>et al.</i> ²³²
Poly(aniline)	Au nanorods	electrical potential pH	J.-W. Jeon <i>et al.</i> ²³³
poly(methyl acrylate) coating	CdTe quantum dot	cysteine	M.-R. Chao <i>et al.</i> ²³⁴
2-Methacryloyloxyethyl]dimethylpropylammonium bromide copolymers	silica	humidity	C.-W. Lee <i>et al.</i> ^{235, 236}
PDMAEMA brushes	mesoporous silica	pH and T	F. Chen <i>et al.</i> ²³⁷
Polysulfonate	silica surfaces Eur ³⁺	tetracyclines	A. Motorina <i>et al.</i> ²³⁸
PAA	graphene oxide	pH	K. Paek <i>et al.</i> ²³⁹
Poly(2-vinylpyridine)	quantum dots		
Poly(diallyldimethyl ammonium chloride) coating	graphene, Au NP	H ₂ O ₂	Y. Fang <i>et al.</i> ²⁴⁰
Conjugated polyelectrolytes	carbon nanotubes	glucose	X. Pang <i>et al.</i> ^{241, 242}
Poly(butadiene)- <i>b</i> -PDMAEMA dispersan	multi-walled carbon nanotube (MWCNT)	drugs	Shumyantseva <i>et al.</i> ⁵²
Poly(<i>n</i> -butylmethacrylate)- <i>b</i> -PDMAEMA	MWCNT	DNA	L. Sigolaeva <i>et al.</i> ⁵³ V. V.
Poly(butadiene)- <i>b</i> -PDMAEMA dispersant	MWCNT	myoglobin	Shumyantseva <i>et al.</i> ²⁴³
Carboxy and ammonium modified cellulose	Au NP	cysteine, Hg ²⁺	J. You <i>et al.</i> ⁸²

¹including carbon nanomaterials

The applied hybrid materials translate the triggers and analytes into optical or electrical signals that are measured *via* well-known analytical techniques such as fluorescence,²³¹ ultraviolet-visible (UV-vis) spectroscopy,²³² luminescence,²²⁶ amperometry,²²⁶ or cyclic voltammetry.²⁴³ In this respect, small inorganic or organic molecules,^{226, 229} metal ions,²²⁸ humidity,^{235, 236} physical sizes,²³⁰ and biomolecules⁵³ can be detected. Especially in the last case, carbon nanomaterials are an emerging class of sensing materials due to their beneficial electrical and electrochemical properties, in addition to the great potential of polyelectrolyte/graphene-based

1. Introduction

hybrid materials for biosensing as summarized in a review by D. Priftis.²⁴⁴ Being highly hydrophobic materials, *e.g.*, carbon nanotubes (CNTs), amphiphilic polyelectrolytes were found to be suitable dispersants. In this case, the hydrophobic segment physically interacts with the hydrophobic carbon nanomaterial while the polyelectrolyte segment ensures water solubility and can further interact with various analytes.^{52, 53, 243}

The discussed examples in **Table 3** focus almost exclusively either on polyanionic or polycationic building blocks and the utilization of polyampholytic hybrid materials in sensing applications remains scarce. Nevertheless, use of polyampholytes in sensing applications could be beneficial due to the existence of both positive and negative charges, enabling the interaction with more than one analyte, their pH-sensitivity, high water-solubility and salt-stability.⁸²

1. Introduction

1.4 Objective of this thesis

The application of functional polymers in water, probably presenting important medium on earth, is an emerging field that has become an important part of our daily life, such as their use as super-absorbents or as additives in detergents or paper coatings.^{3, 245} Within this polymer class, polyampholytes, polyzwitterions and stimuli-responsive (double hydrophilic) macromolecules are receiving the most research attention due to their functions, versatility and performance in aqueous environments.^{41, 57, 70, 127} As a result, polyampholytes are seeing a broad field of application from dispersants, stabilizers, flocculants or antifouling coatings,^{54, 77-79} and are also found in sensors,⁸⁰⁻⁸² or smart catalysis.^{83, 84} Going one step further, the design of hybrid materials by mixing organic (*e.g.* synthetic polymers) and inorganic compounds together profits from synergistic effects, enabling contrary characteristics to be coupled into one material with unprecedented properties for novel (industrial) applications. They promise access to high performance systems, with the control over their chemical and physical properties.^{43, 46, 246} The significant progress in the field of nanotechnology over the past decades, including advanced preparation techniques and analytics, enabled the design and construction of hybrid materials. This led to a tremendous increase in hybrid material research. Using a building block and template-assisted approach, it is relatively simple to design and construct tailor-made hybrid materials for specific applications.^{60, 181, 246} The design starts with choosing suitable monomers and polymerization techniques as highlighted for polyampholytes and polyzwitterions in **Table 1, Chapter 1.1**,^{56, 57} and potentially followed by post-polymerization modification reactions.⁵⁸ Afterwards inorganic compounds can be added, where the polymers predominantly act as a matrix.^{59, 186} As a result, the combination of polyelectrolytes, especially polyampholytes, with inorganic nanomaterials will give access to unprecedented hybrids (**Chapter 1.3**). Applications that demand multi-functional materials will be targeted, such as photocatalysis,⁵¹ or sensing,⁸² to face the energy,¹⁹⁰ environmental and medical^{189, 247} issues of the 21st century. Until now, most systems are based on a multitude of individual polyelectrolytes and material combinations, as exemplarily outlined in **Table 3** for sensing applications. Therefore, it is challenging to simply reproduce, compare, and assess these hybrid materials. From this perspective, the introduction of a universal library based on a single, multifunctional polyelectrolyte seems to be beneficial and corresponding approaches will be presented within this work.

PDha featuring both amino and carboxylic moieties is a promising polyampholyte, which has been almost exclusively investigated in the working group of F. H. Schacher over the last decade (**Figure 13**).^{9, 32, 34, 54, 76, 114, 123, 248-250} It is characterized by a very high charge density, which makes charge-dependent effects very strong. Owing to the presence of weakly basic and

1. Introduction

acidic groups, the overall charge can be tuned by changing the environmental pH value, to obtain a polyanion or polycation, while the polymer behaves like a polyzwitterion in a moderate pH range (pH between 10.5 and 6.5).³² This renders PDha an interesting material for tailor-made (and reversible) interactions as already shown with polyelectrolytes, model dyes, or bovine serum albumin or nanoparticles. Other benefits of PDha are its biocompatibility, its dual pH- and ion-responsive behavior, and the presence of reactive groups that can be modified if desired. Hence, its introduction in polyelectrolyte-based hybrid materials, as well as the application in biomedicine, detergents, waste-water treatment or catalysis is foreseen. PDha is synthesized in two steps, starting from the polymerization of *tert*-butoxycarbonylaminomethylacrylate and subsequent deprotection of the of *tert*-butoxycarbonyl (boc) group and methyl ester. So far free radical, ATRP and NMP techniques have proven to be suitable for this demanding and highly reactive monomer. Until now, the number of PDha copolymers (PDha-*b*-PS and PDha-*b*-PAA)¹¹⁴ and hybrid materials (PDha@iron oxide)⁵⁴ reported remains limited. This may, in part, be due to its strong intra- and intermolecular interactions at a pH < 7, limiting its solubility range and applicability.

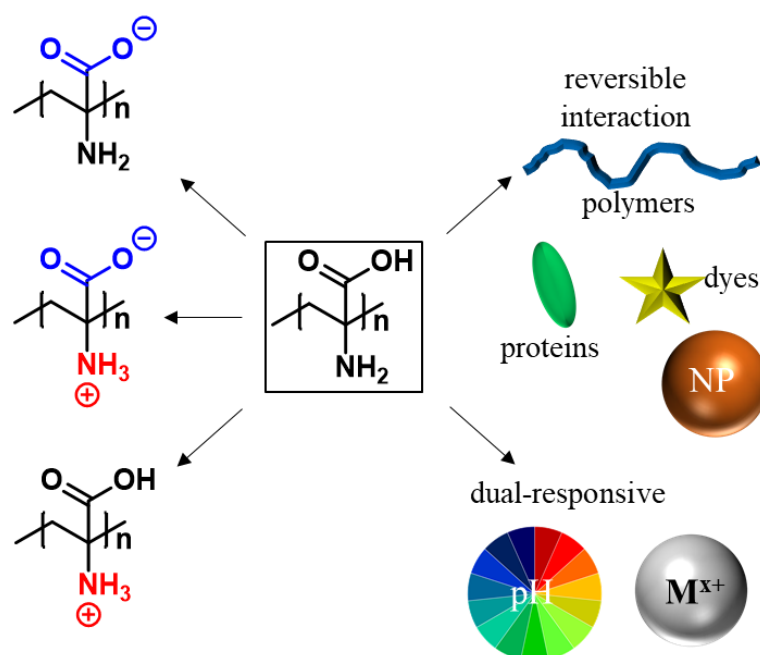


Figure 13. Chemical structure of PDha and its possible charged states depending on the pH (left). Its structure-property relationships lead to a dual-stimuli responsive behavior and allows reversible interactions with polymers, dyes, proteins, and NPs.

In this respect, the aim of this thesis is to fine-tune PDha by the establishment of a diverse copolymer library, which is necessary to overcome this obstacle and to design tailor-made polyampholytes with defined properties based on an extremely promising macromolecule (**Figure 14**). As previously outlined, the combination of corresponding polymers with inorganic or carbon nanomaterials is the key to functional materials exploiting each individual

1. Introduction

characteristic and synergistic effects, which may even exhibit unpredictable properties. As it is well-known that polymers are highly suitable matrix materials for hybrid materials,^{59, 179, 186} the use of PDha as a template will be uncovered in **Chapter 3**. Therefore, it may be combined with future nanomaterials, such as CNTs, Ag or Au NPs, TiO₂ etc., as a functional coating or stabilizer allowing their application in sensing, catalysis and more.

To achieve these goals, novel PDha copolymers were first prepared, as it will be discussed in **Chapter 2**. While ATRP and NMP appear to be suitable polymerization techniques, they had to be optimized to obtain well-defined PDha homopolymers.^{32, 34} ATRP was then used to synthesize novel dual-responsive PDha-*b*-PEG linear block copolymers *via* block extension of end-functionalized PEG macroinitiators, and compared to an alternative synthetic route using click-chemistry, which has yet to be reported for PDha. These polymers are potentially dual-responsive to pH and ions and form core-shell micelles in solution. Moreover, a novel approach was developed exploiting amino moieties as reactive handles for post-polymerization modification reactions. Among others, Michael addition reactions and the ring-opening of epoxides were discussed as versatile tools to modify reactive polymer backbones, resulting in tailor-made functional polymers.^{58, 118} These reactions can be exploited to introduce a broad variety of side-chains to PDha *via* a facile reaction in water. Therefore, a wide choice of potential Michael-acceptors and epoxides, which are mostly commercially available, were introduced in a 'lego-like' approach. Each modifier as a building block may add desired properties to PDha depending on the planned application, in particular the following features: lipophilicity (alkyl, fluoro alkyl, aromatic side-chains), hydrophilicity /dual charge (PEG, ionic side-chains), stimuli-response (NIPAAm).

After characterization of their structure, solution properties and stimuli-responsive behavior, these polyampholytes are combined with nanomaterials either by a building-block approach using ultrasonication or by exploiting the polymer as a smart template for the defined growth of NPs, as it is shown in **Chapter 3**. The focus is especially on metal and metal oxide NPs, such as Au / Ag NPs or TiO₂ nanoparticles due to their electrical, optical and catalytic properties,²⁵¹⁻²⁵³ as well as CNTs²⁵⁴ revealing, *e.g.*, outstanding conductivity and stability. Hence, these materials are important building blocks in many applications if combined with a suitable matrix. The synthesized polymers are then applied in sensing and in photocatalytic HER, which is highlighted in **Chapter 3.3** and **3.4**. While the potential of polyelectrolyte based hybrid materials has been shown to be promising in the sensing of a many different analytes (**Table 3, Chapter 1.3.3**) their sensitivity as well as applicability, must still be improved in order to expand their use in commercial applications. So far, there are limited examples where

1. Introduction

polyelectrolytes have been applied in photocatalytic HER, as outlined in **Chapter 1.3.2**, despite their high water-solubility, charge, and their ability to interact with a multitude of compounds, which may be advantageous in catalytic systems.⁸⁴ However, examples focus predominantly on polycations or polyanions, and polyampholyte-based materials have not been thoroughly developed. Hence, PDha-based copolymers should be tested as suitable matrices for photocatalytic systems.

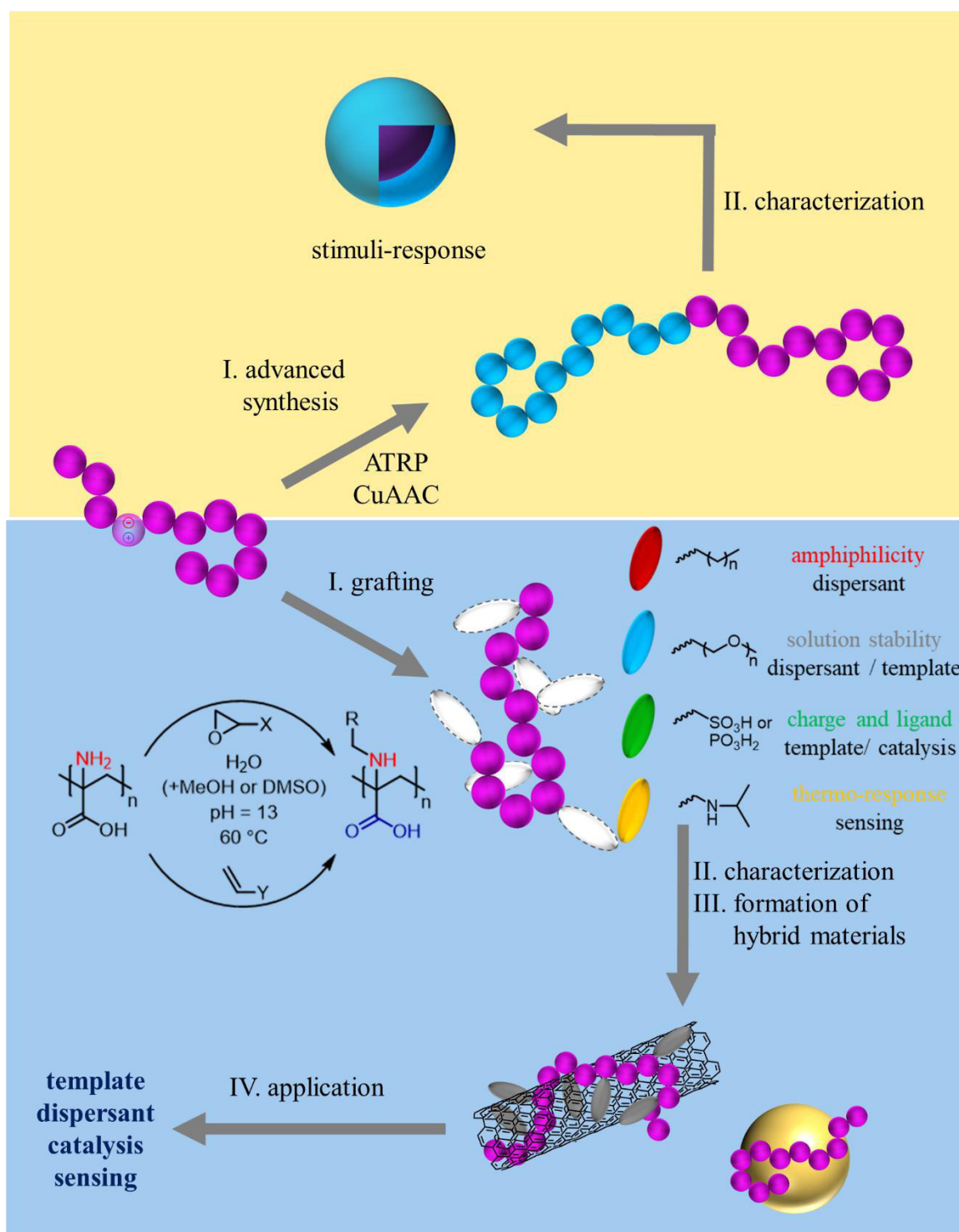


Figure 14. Routes towards a PDha-based copolymer library and hybrid materials with tailor-made properties and functions.

2. Synthetic routes towards PDha-based copolymers

PDha is a pH-responsive polyampholyte displaying an interesting solution behavior with a tunable charge and aggregation behavior due its carboxylic and amino moieties. It was found to be a promising candidate for water-based hybrid materials with reversible release mechanisms and potential applications in biomedicine or waste-water treatment.^{9, 32, 47, 76, 248} However, modifications of PDha could overcome its current limitations and further improve its properties. First, it reveals limited solubility at pH < 7,³² or upon the addition of metal cations. Second, tailored interactions, *e.g.*, hydrophobic or covalent ones, are needed in order to prepare hybrid materials with carbon nanomaterials or inorganic compounds. By modifying PDha, either through the synthesis of block copolymers or post-polymerization reactions, tailor-made polyampholytic building blocks will be obtained. Here, special attention is given to suitable controlled polymerization techniques. Until now, there exist two PDha-based block copolymers: amphiphilic PS-*b*-PDha and double hydrophilic PAA-*b*-PDha, which form self-assemblies in solution.^{34, 114} This could be extended by a DHBC containing a non-ionic segment, for example PEO, which is well known for its biocompatibility and high hydrophilicity.²⁵⁵ Moreover, alternative architectures based on PDha copolymers should be explored, which can further influence the properties and function of the polymer.²⁵⁶

2.1 Novel routes towards double hydrophilic PEG-*b*-PDha block copolymers

Parts of this chapter have been published in **P2**) Johannes B. Max, Peter J. Mons, Jessica C. Tom, and Felix H. Schacher, *Macromol. Chem. Phys.*, **2020**, *221*, 1900383.

Over the last decades DHBCs have become an emerging polymer class, due to their wide field of applications ranging from catalysis,^{51, 257, 258} magnetic resonance imaging (MRI) contrast agents,²⁵⁹ capillary coatings,²⁶⁰ sensors²⁶¹ drug-delivery or gene transfer systems,^{142, 262, 263} to biomineralization.^{188, 264} DHBCs, consisting of a solubility promoting segment and a functional one reveal unique solution properties in water.^{40, 41} Upon experiencing a response to external stimuli, *e.g.*, temperature,¹⁵¹ pH²⁶⁵ or metal ions,¹⁴³ one of the segments aggregates while the other one stabilizes the resulting nanostructured object. Polyelectrolytes, including polyampholytes and -zwitterions, exhibit outstanding characteristics, including the interaction with metal ions proteins or other oppositely charged moieties.^{29, 70} From this perspective, they are promising candidates for the charged segments in DHBCs.³⁹ In this respect, utilization of biocompatible PDha,⁵⁴ which exhibits a pH-dependent charge for catch and release mechanisms and interacts with various compounds,^{9, 54, 76, 248} could be highly sophisticated materials for the applications from catalysis to drug-delivery systems. The PDha homopolymer is derived starting from the polymerization of captodative *tert*-butoxy carbonylaminomethyl acrylate

2. Synthetic routes towards PDha-based copolymers

(*t*BAMA). For this, free radical polymerization (FRP), NMP and ATRP have been explored. NMP and ATRP in particular, provide some polymerization control over the highly reactive monomer ($\mathcal{D} < 1.2$ possible). Afterwards, the orthogonal methyl ester and boc groups were cleaved under basic (LiOH, 21-45 eq per monomer unit) and acidic conditions (trifluoroacetic acid (TFA), 10-26 eq per monomer unit) to yield the $-NH_2$ and $-COOH$ moieties.^{32, 34} Similarly, PAA-*b*-PDha was synthesized in multiple steps. First, a poly(*n*-butyl acrylate) (P*n*BA) macroinitiator was chain extended with *t*BAMA *via* ATRP to obtain the protected P*n*BA-*b*-P*t*BAMA block copolymers. Afterwards, the protecting groups were removed as described above.^{34, 114} Although the corresponding PEO-*b*-P*t*BAMA was also obtained *via* ATRP,³⁴ a major drawback of this route was the harsh reaction conditions required needed to obtain PEO-*b*-PDha. As a result, PEO-*b*-PDha connected by a hydrolysable ester linkage, could not be obtained *via* this route. Hence, alternative approaches (**Figure 15**) were investigated to obtain this promising DHBC based on more stable amide moieties. Nevertheless, compared to the typically used ester-based initiators, the corresponding amides suffer from abundant termination reactions as well as lower initiation efficiencies compared to corresponding esters.²⁶⁶⁻²⁶⁸ Route A, depicted in **Figure 15**, is the copper-catalyzed azide-alkyne cycloaddition (CuAAC), linking azide functionalized PEO and alkyne-functionalized P*t*BAMA, obtained from a unimolecular amide initiator.¹²⁴ Route B starts from an amide end-functionalized PEO macroinitiator, and is followed by chain-extension *via* ‘advanced’ ATRP techniques (aqueous solvent mixtures and single-electron transfer living radical polymerization (SET-LRP)).

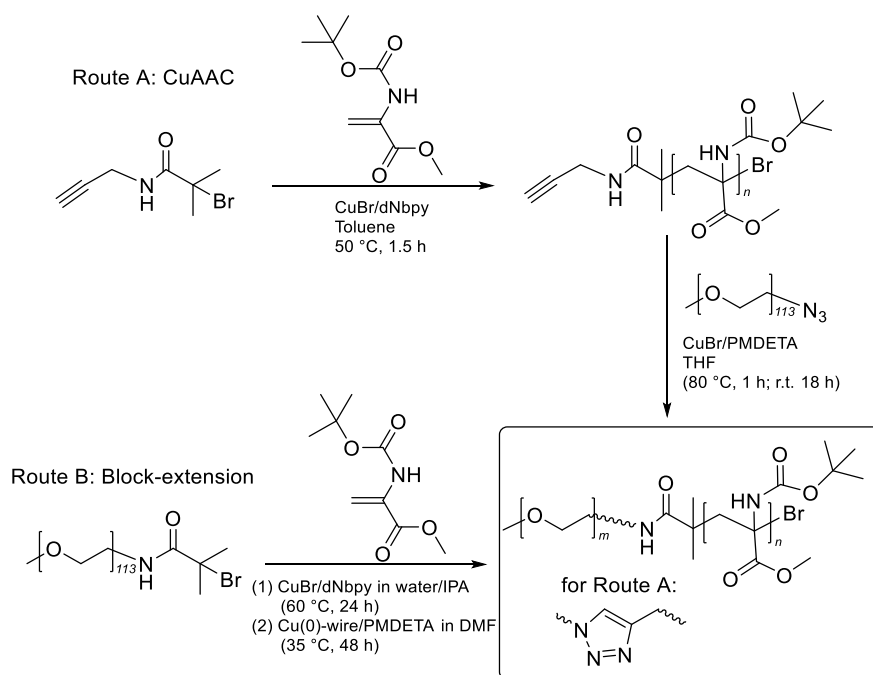


Figure 15. Synthetic pathways to PEO-*b*-P*t*BAMA as precursor to PEO-*b*-PDha. Route A: CuAAC, Route B: Chain extension *via* ATRP / SET-LRP. Reprinted from Macromol. Chem. Phys., **2020**, 221, 1900383, with permission of WILEY-VCH Verlag GmbH & Co. KGaA, Weinheim.

2. Synthetic routes towards PDha-based copolymers

After comparison of both routes, the block copolymers were deprotected and the obtained PEO-*b*-PDha investigated in respect of its solution properties, which will be discussed in the following section.

Route A: PEO-*b*-PtBAMA synthesized by the click reaction of end-functionalized blocks

CuAAC is used to covalently link two polymeric segments, one containing an alkyne moiety, and the other an azide.¹²⁴ In this respect, PEO-N₃ was synthesized as described in the literature from commercially available PEO-OH (44 or 113 repeat units),²⁶⁹ while PtBAMA-alkyne was synthesized *via* ATRP. As discussed above, an amide-based initiator exhibiting an alkyne moiety (2-bromo-2-methylpropionamide, (BMP)) was used. It should be noted that ATRP techniques are rather challenging for the CRP of *t*BAMA as a result of copper complexation by the nitrogen species, its high reactivity and steric effects and especially higher molecular weights were not achieved in a controlled way, yet.³⁴ The previously described ATRP of *t*BAMA employed methyl α -bromoisobutyrate (MeBib) as initiator, however it was not possible to directly transfer the reaction conditions to BMP. This highlights the general drawbacks of amide-based initiators such as abundant termination reactions and low initiation efficiency,²⁶⁶⁻²⁶⁸ and the polymerization was found to proceed faster. However, after adjusting various reaction parameters (T, amount of solvent, CuX species (CuBr vs CuCl), reaction time) suitable conditions were found. The results are summarized in **Table 4**. For the subsequent preparation of block copolymers *via* click chemistry, PtBAMA-alkyne with an M_n of 12700 g/mol and $D = 1.45$ (CuBr/dNbpy catalytic system, 2.0 h, THF SEC), corresponding to approximately 85 repeat units, was chosen. CuAAC was performed in accordance to literature procedures,²⁷⁰ and a clear shift of the SEC traces towards lower elution volumes proved the successful click reaction. Besides, ¹H- and ¹³C nuclear magnetic resonance (NMR) spectroscopy further supported the successful click reaction, showing signals originating from both blocks (**Figure 16**). Hereby, PEO₄₄-*b*-PtBAMA₈₅ and PEO₁₁₃-*b*-PtBAMA₈₅ exhibiting different PEO chain lengths have been obtained (**Table 4**). However, the significant differences in the apparent M_n of 22,000 and 32,000 g/mol may be ascribed to the removal of low molecular weight block copolymers during the washing step and/or different hydrodynamic radii for each individual block and the linked copolymer measured by SEC. The tailing observed in the SEC traces could also hint to the presence of small amounts of unreacted PtBAMA-alkyne.

2. Synthetic routes towards PDha-based copolymers

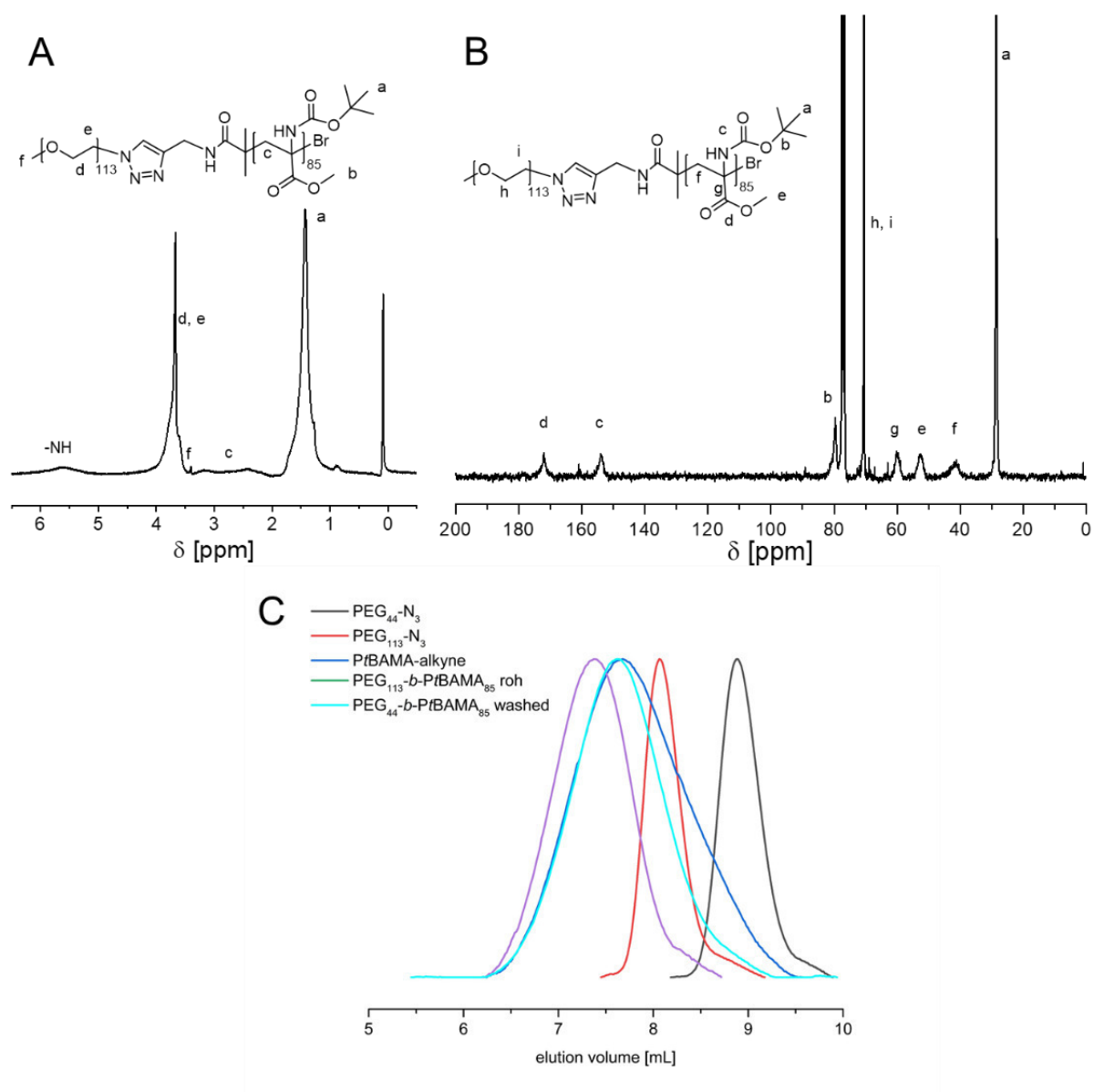


Figure 16. Characterization of the *PtBAMA-b*-PEG block copolymers obtained *via* click chemistry: ^1H - (A) and ^{13}C -NMR spectra in CDCl_3 (B), as well as the corresponding SEC traces in CHCl_3 (C). Adapted from *Macromol. Chem. Phys.*, **2020**, 221, 1900383, with permission of WILEY-VCH Verlag GmbH & Co. KGaA, Weinheim.

Route B: Block extension of an amide end-functionalized PEO macroinitiator (PEO₁₁₃-amide)

Route B may be considered a more straight-forward approach starting from a macroinitiator instead of two separately prepared polymer blocks. Here, a PEO₁₁₃-amide macroinitiator was used, instead of the already describe ester based one. Similarly to the above described *PtBAMA*-alkyne, the reported ATRP reaction conditions were hardly transferable, and the degree of polymerization (DP) was limited to 15 monomer units of *tBAMA*.³⁴ Hence, ‘advanced’ ATRP techniques were tested. Although SET-LRP has not yet been tested for *tBAMA*, SET-LRP is known to be more tolerant towards oxygen, inhibitors, polar and non-polar solvents, promotes fast reaction times and is conducted under ambient temperature.²⁷¹ On

2. Synthetic routes towards PDha-based copolymers

the other hand, aqueous ATRP may be favorable for the hydrophilic PEO₁₁₃-amide, as PEO has been block extended with DMAEMA in a water/*iso*-propanol (*i*PrOH) solvent mixture.²⁷² The optimized reaction conditions and characterized by SEC of the obtained block copolymers are summarized in **Table 4**. Both techniques gave PEO-*b*-PtBAMA with narrow molecular weight distributions of $\mathcal{D} = 1.03$ to 1.42. SET-LRP was performed at relatively low temperatures (35 °C) and the attachment of up to 46 monomer units was possible ($M_n = 13,900$ g/mol, $\mathcal{D} = 1.42$). Targeting lower molecular weights (8,200 g/mol) by using a shorter copper(0) wire, gave significantly lower \mathcal{D} of 1.06. Here, the monomer conversion was relatively low (18 % after 24 h) and a plateau was found after a linear increase in the DP, as commonly observed for a controlled polymerization (**Figure 17**). The low conversion hints towards reaching an equilibrium favoring the dormant species and the low \mathcal{D} indicates the existence of living chain ends rather than termination reactions.

Table 4: Summary of the reaction conditions used to synthesize PtBAMA-alkyne and PEO-*b*-PtBAMA, and the corresponding SEC characterization. Adapted from Macromol. Chem. Phys., **2020**, 221, 1900383, with permission of WILEY-VCH Verlag GmbH & Co. KGaA, Weinheim.

Route A	Cu(I)X (eq.)	Solvent (wt%)	T [°C]	t [h]	M_n [g/mol]	\mathcal{D}
PtBAMA-alkyne ₅₀ ^a	CuBr (1)	toluene (10)	50	1.5	10,000 ^d	1.45
PtBAMA-alkyne ₄₄ ^a	CuCl (2)	toluene (10)			8,800 ^d	1.38
PEO ₁₁₃ - <i>b</i> -PtBAMA ₈₅	-	THF (90)	80	1	32,000 ^f	1.42
PEO ₄₄ - <i>b</i> -PtBAMA ₈₅	-	THF (90)	21	18	22,200 ^f	1.55
Route B						
PEO ₁₁₃ - <i>b</i> -PtBAMA ₄₆ ^b	Cu(0) (5 cm)	DMF (33)	35	24	13,900 ^e	1.42
PEO ₁₁₃ - <i>b</i> -PtBAMA ₂₃ ^b	Cu(0) (2.5 cm)	DMF (33)			8,200 ^e	1.06
PEO ₁₁₃ - <i>b</i> -PtBAMA ₁₀ ^c	CuBr (1.5)	H ₂ O/DMF (1/1) (80)	50	24	5,200 ^e	1.03
PEO ₁₁₃ - <i>b</i> -PtBAMA ₃₉ ^c	CuBr (1.5)	H ₂ O/ <i>i</i> PrOH (1/1) (80)			5,800 ^e	1.10

[M]:[I]:[ligand (L)] = ^a100:1:1, L = dNbpy; ^b100:1:1.5, L = *N,N,N',N'',N''*-Pentamethyldiethylene triamine (PMDETA); ^c100:1.5:1.5, L = dNbpy; THF SEC (^dPS/ ^ePMMA calibration), ^fCHCl₃/triethylamine/*iso*-propanol [94/2/4], PS calibration.

Aqueous ATRP was tested for the PEO₁₁₃-amide, presuming a high solubility of the macroinitiator in water. Hereby, both water/*N,N*-dimethylformamide (DMF) and water/*i*PrOH (1/1, v/v) mixtures were tested, using a dNbpy/CuBr catalytic system. For both solvent mixtures tested low \mathcal{D} of 1.03 (water/DMF) and 1.10 (water/*i*PrOH) were found after a reaction time of 24 h, respectively and the addition of up to 39 monomer units. SEC traces revealed a shift in the elution volume as expected, and a small shoulder visible for PEO₁₁₃-*b*-PtBAMA₃₉ could be

2. Synthetic routes towards PDha-based copolymers

the result of chain-chain coupling or the formation of loose aggregates of the amphiphilic polymer.

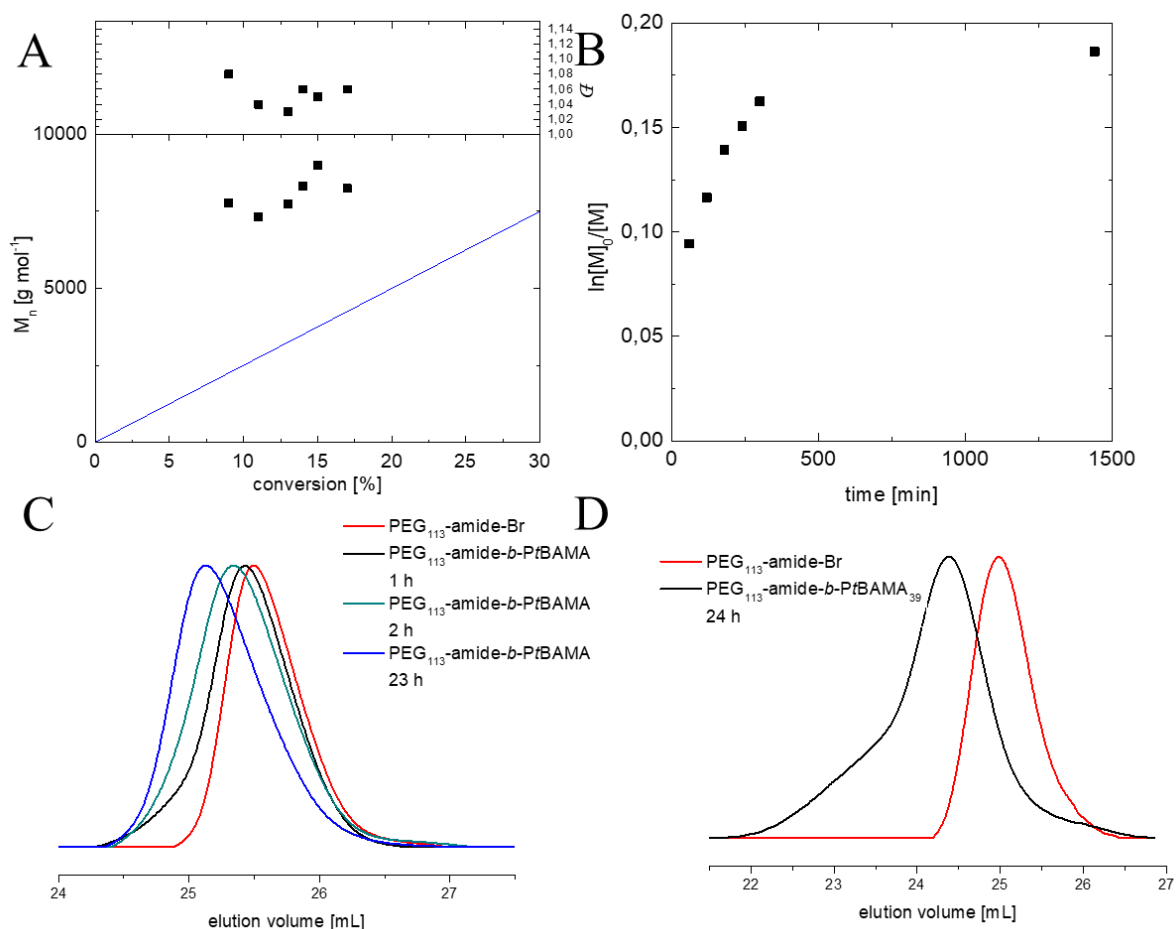


Figure 17. Investigation of the formation of PEO-*b*-PtBAMA by block extension (Route B). SET-LRP kinetic studies (A and B) (tBAMA:ligand:macroinitiator = 100:0.1:1, copper(0) wire length = 2.5 cm, $[M]_0 = 0.0248$ mmol in 1.25 mL, $T = 35$ °C). SEC traces of the aqueous ATRPs in water/DMF (C) after different time intervals, and in water/*iso*-propanol (D). The conversion was determined from $^1\text{H-NMR}$ spectroscopy and the M_n obtained by SEC. SEC traces were measured in THF (PMMA calibration). Adapted from *Macromol. Chem. Phys.*, **2020**, 221, 1900383, with permission of WILEY-VCH Verlag GmbH & Co. KGaA, Weinheim.

In direct comparison, Route B benefits from one reaction step less than Route A and results in narrow dispersities < 1.10 were reached. However, the main limitation of Route B is the relatively low conversions obtained, which results in short PtBAMA segments with a maximum of 46 repeat units under the described conditions. On the other hand, the click reaction allows the incorporation of longer PtBAMA segments, up to 85 repeating units, but with broader dispersities ($\bar{D} = 1.45$). Besides, Route A also allows the characterization of each individually synthesized polymer and an upscaling (~ 1 g) was feasible. From these results, the use of CuAAc was chosen as the best route to prepare the desired DHBCs from PEO₁₁₃-*b*-PtBAMA₈₅ and PEO₄₄-*b*-PtBAMA₈₅.

2. Synthetic routes towards PDha-based copolymers

Deprotection of *PtBAMA* homo- and copolymers is achieved under successive basic and acidic conditions to completely remove the boc and methyl ester moieties.^{32, 114} For the deprotection of the *PEO-*b*-PtBAMA* block copolymers, the protocol for the preparation of *PS-*b*-PDha* and *PAA-*b*-PDha* was adjusted (**Figure 18**),¹¹⁴ and the reaction time dramatically reduced to 15 min for each step in order to conserve the amide junction between both segments.

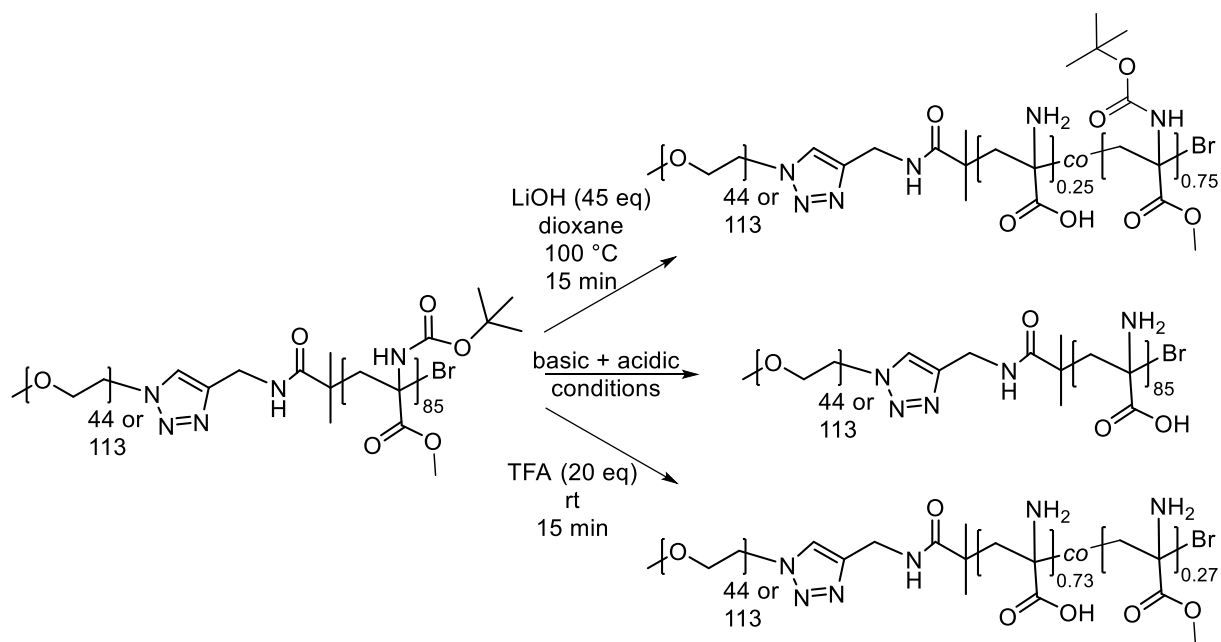


Figure 18. The deprotection of *PEO-*b*-PtBAMA* to prepare *PEO-*b*-P(tBAA_{0.75}-*co*-Dha_{0.25})* under basic conditions, *PEO-*b*-P(AMA_{0.27}-*co*-PDha_{0.73})* by the utilization of TFA, and *PEO-*b*-PDha* by successive basic and acidic deprotection. Adapted from *Macromol. Chem. Phys.*, **2020**, 221, 1900383, with permission of WILEY-VCH Verlag GmbH & Co. KGaA, Weinheim.

Each individual step resulted in the simultaneous removal of the orthogonal protecting group with 75 % remaining boc and 27 % remaining methyl ester, respectively, as determined by ¹H-NMR spectroscopy. However, treating *PEO-*b*-PtBAMA* first with basic and then acidic conditions yielded the *PEO₄₄-*b*-PDha₈₅* and *PEO₁₁₃-*b*-PDha₈₅* double hydrophilic copolymers, as proven by ¹H-NMR spectroscopy (**Figure 19 A**), where only the PDha -CH₂- backbone signals and the protons of the PEO segment were visible. It should be noted that the block copolymer containing the shorter PEO block, could also be completely deprotected in a single step, if the reaction time under basic conditions was increased to 5 h, without cleavage of the amide linkage. The DHBCs were then investigated *via* SEC in dimethylsulfoxide (DMSO) and water (**Figure 19 B, C and D**). A monomodal distribution was observed in case of *PEO₄₄-*b*-PDha₈₅*. However, a small shoulder at higher elution in the water SEC was observed for *PEO₁₁₃-*b*-PDha₈₅*, close to the solvent signal, without any evidence of cleaved PEO segments. A second distribution was observed for *PEO₁₁₃-*b*-PDha₈₅*, which may result from the formation of loose

2. Synthetic routes towards PDha-based copolymers

aggregates from the assembly of the zwitterionic PDha blocks in aqueous solution, as a bimodal distribution was not found by SEC in DMSO.

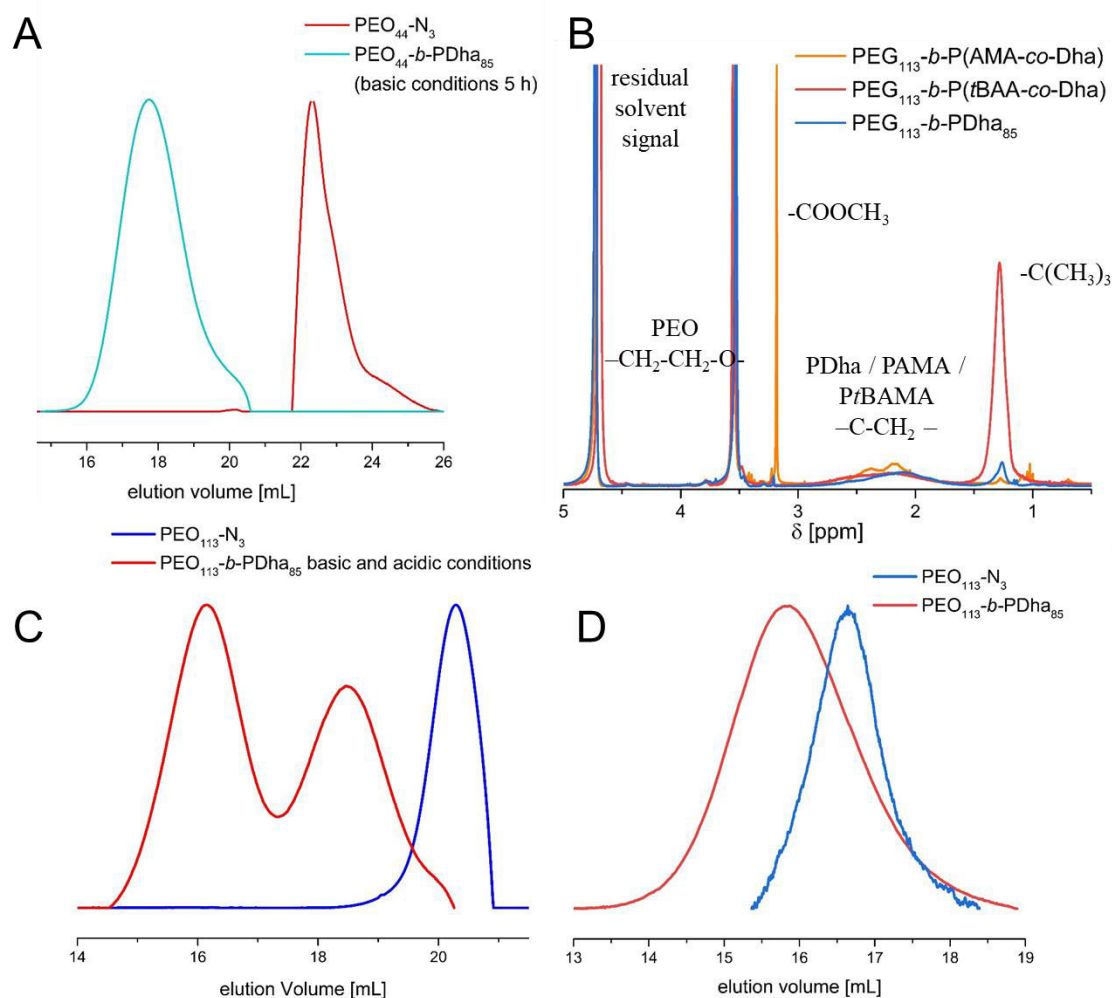


Figure 19. Analytics for deprotected PEO-*b*-PtBAMA. A: SEC elution traces of PEO₄₄-*b*-PDha₈₅ and PEO₄₄-N₃ in water. B: ¹H-NMR spectra (D₂O, 300 MHz) PEO-*b*-P(tBAA_{0.75}-*co*-Dha_{0.25}) after basic deprotection, PEO-*b*-P/AMA_{0.27}-*co*-PDha_{0.73}) after acidic conditions and PEO-*b*-PDha by successive basic and acidic deprotection. C: SEC elution traces of PEO₁₁₃-*b*-PDha₈₅ and PEO₁₁₃-N₃ in water and in DMSO (D). Adapted from Macromol. Chem. Phys., **2020**, 221, 1900383, with permission of WILEY-VCH Verlag GmbH & Co. KGaA, Weinheim.

The solution behavior under aqueous conditions was exemplarily studied using PEO₁₁₃-*b*-PDha₈₅. As compared to the PDha homopolymer, which is insoluble under acidic conditions,³² the solubility was enhanced as the DHBC was soluble over a broader pH range (4-14). This may result from the PEO segment, which is well known to enhance the hydrophilicity.²⁵⁵ Further, the ζ -potential was measured in order to determine the overall charge of the DHBC (**Figure 20 A**). PDha is found to be polyzwitterionic in a pH range of 10.5 to 6.5,³² revealing a tunable charge dependent on the pH. PEO₁₁₃-*b*-PDha₈₅ behaves like a polyanion at a pH ≥ 5 due to the deprotonated carboxylic groups. The IEP occurs at a pH of approximately 5 (0 mV), before becoming positively charged at pH < 4 (+ 1 mV), where the polymer exhibits an overall positive charge due to the protonation of the amino moieties and -COOH groups. In order to

2. Synthetic routes towards PDha-based copolymers

investigate the potential pH- and metal ion responsive behavior, the hydrodynamic radii (R_H) of PEO₁₁₃-*b*-PDha₈₅ where measured at different pH values and after the addition of Cu²⁺ ions *via* dynamic light scattering (DLS) (**Figure 20 B and C**). While at a basic pH of 9, unimers were found ($R_H = 4$), under neutral and acidic conditions the R_H increased to a maximum of 23 nm at pH 4. This observation can be explained by the aggregation of carboxylate moieties after protonation, leading to strong interactions due to the formation of hydrogen bonds. Similar self-assembly behavior at pH < 4.5 has been described in the literature for DHBCs containing a PAA segment.^{138, 273} In addition, polyelectrolytic segments can aggregate by the chelation of metal cations to form micellar structures in solution.^{143, 151} Accordingly, after the addition of CuSO₄ to a PEO₁₁₃-*b*-PDha₈₅ at pH = 9, a main distribution with a hydrodynamic radius of 40 nm was found. This could be the result of the successful Cu²⁺ complexation by the polyampholytic PDha segment, leading to the formation of nanoobjects comprising a PDha/Cu²⁺ core and a PEO corona.

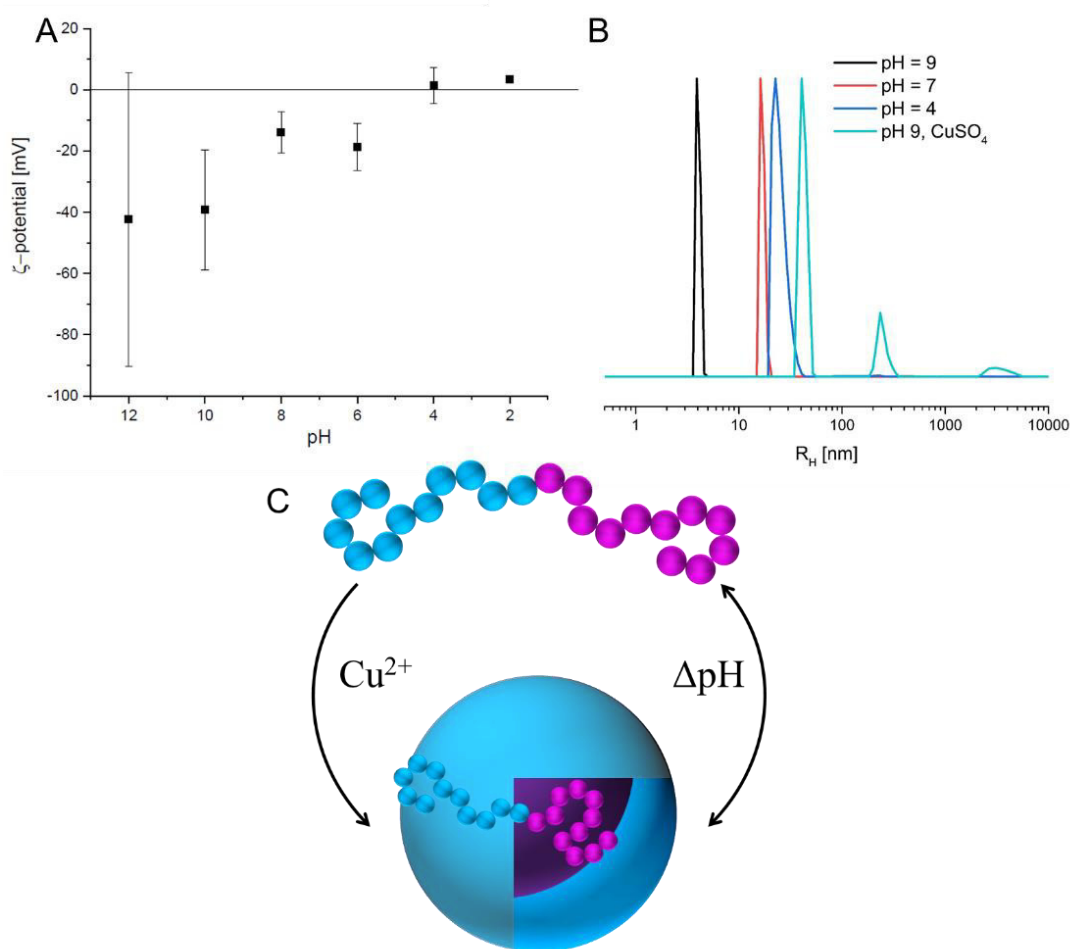


Figure 14. Investigation of the solution properties of PEO₁₁₃-*b*-PDha₈₅ measuring its ζ -potential in dependence of the pH (A) and its hydrodynamic radii from DLS at different pH-values and upon the addition of Cu²⁺ (B). Depiction of the potential pH- and metal ion induced formation of micellar nanostructures by DHBCs (C), where either complexation of cations or hydrogen bonding at low pH induce the self-assembly of the polyelectrolytic segments.^{138, 143} Adapted from *Macromol. Chem. Phys.*, **2020**, 221, 1900383, with permission of WILEY-VCH Verlag GmbH & Co. KGaA, Weinheim.

2. Synthetic routes towards PDha-based copolymers

In summary, novel double hydrophilic PEO-*b*-PDha block copolymers were successfully prepared and characterized. PEO-*b*-PtBAMA, featuring an amide junction, is more stable towards hydrolysis compared to its ester counterpart,³⁴ which was synthesized *via* two novel synthetic routes in a controlled manner: the coupling of two segments by CuAAC, and the block extension via SET-LRP and aqueous ATRP. These methods could be further applied in the synthesis of other well-defined PtBAMA homopolymers or copolymers. Afterwards, the PtBAMA block was deprotected to give PDha, without cleavage of the linked PtBAMA and PEO segments under the harsh acidic and basic conditions due to the more stable amide linkage. The solution properties of the obtained PEO-*b*-PDha was first investigated and in addition to a pH dependent charge, a pH- and metal ion- responsive aggregation behavior was observed. The self-assembly behavior can be explained by the formation of hydrogen bonds and the complexation of cations by the PDha segment as compared to literature.^{138, 143} Hence, future work will focus on the herein described PEO-*b*-PDha as a promising candidate the application in catalysis, cargo-carrying systems, biomineralization, or nanoreactors.

2.2 PDha-based graft copolymers – preparation and solution properties

Parts of this chapter have been published in **P1**) J. B. Max, D. V. Pergushov, L. Sigolaeva, and F. H. Schacher, *Polym. Chem.*, **2019**, *10*, 3006, **P3**) J. B. Max, K. Kowalczyk, M. Köhler, C. Neumann, F. Pielenz, L. V. Sigolaeva, D. V. Pergushov, A. Turchanin, F. Langenhorst, and F. H. Schacher, *Macromolecules.*, **2020**, *53*, 4511-4523, **P4**) Johannes B. Max, Afshin Nabiyan, Jonas Eichhorn, and Felix H. Schacher, *Macromol. Rapid Commun.*, **2021**, *42*, 2000671, **P5**) Afshin Nabiyan, Johannes B. Max, Christof Neumann, Magdalena Heiland, Andrey Turchanin, Carsten Streb, and F. H. Schacher, *Chem. Eur. J.*, **2021**, *27*, 1-7, **P6**) A. Nabiyan, J. B. Max, M. Micheel, J. Eichhorn, M. Wächtler, M. Schulz, C. Neumann, B. Dietzek, A. Turchanin and F. H. Schacher, *Polyampholytic graft copolymers: A platform to combine sensitizers and catalysts, in preparation*, **P7**) A. Nabiyan, J. B. Max, F. H. Schacher, *Double Hydrophilic Copolymers – Synthetic Approaches, Architectural Variety, and Application Fields*, *Chem. Soc. Rev.*, **2022**, DOI: 10.1039/D1CS00086A.

Dual-responsive PDha-based copolymers are foreseen to be interesting candidates for many potential applications. The amphiphilic and double hydrophilic block copolymers were synthesized from PtBAMA precursors, which were in turn obtained *via* ATRP techniques or the combination of ATRP and click chemistry as described in the previous chapter.^{34, 114} Although these pathways yield well-defined copolymers, their synthesis is still challenging: inert reaction conditions, scalability, limited degrees of polymerization as well as solubility issues of the resulting PDha-based block copolymers under strong acidic conditions (pH < 4).

2. Synthetic routes towards PDha-based copolymers

For this, it is necessary to find alternative strategies to overcome these challenges and to obtain tailor-made PDha-based materials. Alternative polymer topologies apart from block copolymers should also be explored, *e.g.*, star shaped, branched or graft, since the polymer architecture significantly determines the polymer properties.²⁵⁶ Graft copolymers, combine the characteristics of the backbone and side-chains, and are distinguished by their compact and confined structure, dominant chain-end effects and rather complex self-assembly behavior.^{154, 155, 168, 169} In general, they are derived *via* three grafting approaches: grafting-from, grafting-through and grafting-onto.¹⁵⁵ The grafting-onto approach can be considered a post-polymerization modification and is a versatile platform for the functionalization of previously prepared reactive macromolecules.⁵⁸ In this way, the polymer properties can be tuned by controlling the density and type of the modifier and even ‘contrary’ philicities can be combined in a single material.^{36, 38} Among others, nucleophilic amino moieties are found to be suitable reactive handles that can undergo, for example, aza-Michael additions or the ring-opening of epoxides, allowing the attachment of short side-chains to adjust the polarity or functionality.^{120, 121} There exist a number of highly reactive modifiers that are commercially available.

In this respect, PDha is a promising polyampholytic backbone for the creation of a graft copolymer library, with tailor-made solution properties, as schematically shown in **Figure 21**. Depending on the nature of the side-chain, different applications can be envisioned from sensing, photocatalysis, templates and dispersants. This straight-forward route promises easy access to a wide range of graft copolymers based on the same backbone without loss of its functionality or properties *via* a simple reaction in aqueous conditions. The synthesis and characterization of the graft copolymers will be described in this chapter.

2. Synthetic routes towards PDha-based copolymers

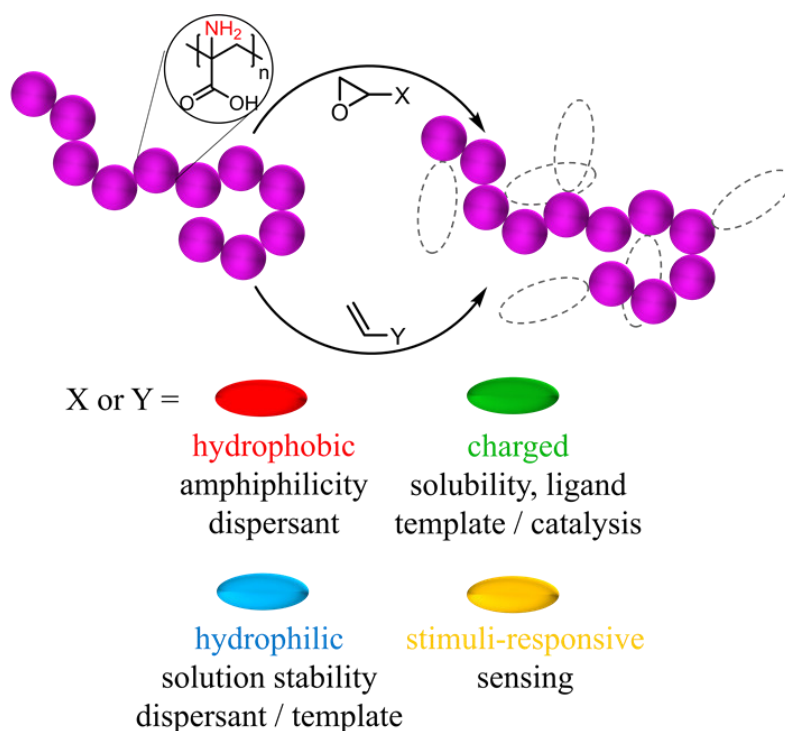


Figure 21. Preparation of PDha-based graft copolymers *via* post-polymerization modifications (ring opening of epoxides or aza-Michael additions). The side-chains can be of hydrophobic, hydrophilic, charged or stimuli-responsive in nature, expanding the possible range of applications that can be accessed.

Synthesis and characterization of PDha-based graft copolymers

PDha homopolymer was used for the preparation of the polyampholytic graft copolymers by the attachment of various side-chains in post-polymerization modification reactions. The reactive backbone was first obtained in two steps: the synthesis of *Pt*BAMA from *t*BAMA and the subsequent deprotection to poly(aminomethylacrylate-*co*-Dha) (P(AMA-*co*-Dha)). Therefore, *Pt*BAMA was synthesized *via* free and controlled radical polymerization techniques, similar to earlier reports (**Figure 22**).^{32, 34, 54} In general, an M_n between 10,000 and 15,000 g/mol or between 50 and 75 repeating units, was targeted. For the free radical polymerization trimethylbenzoyl diphenylphosphine oxide (TPO) was used as the UV-photoinitiator and the reaction was performed in 1,4-dioxane (50 wt.%) to yield *Pt*BAMA with an M_n of 14,400 g/mol and a D of 5.66. Although this polymerization method gives a high yield of up to 88 % from the amount of monomer used within 10 min, the molecular weight distribution is broad and not reproducible. Since ATRP is synthetically demanding and residual copper salts need to be removed from the final product, NMP was explored as an alternative CRP method. The reaction conditions were investigated regarding temperature, solvent and monomer concentration. In addition to BlocBuilder as a unimolecular initiator and nitroxide, an excess of the nitroxide radical itself (SG1) was added, enhancing the control over the polymerization by shifting the equilibrium to the dormant species. The most promising conditions were found to be

2. Synthetic routes towards PDha-based copolymers

[monomer]:[BlocBuilder]:[SG1] = [40]:[1]:[0.65], 66 wt% dioxane, T = 80 °C, and a reaction time of 15 min. These conditions resulted in a number average molecular weight of 11,100 g/mol and a relatively narrow distribution of 1.89. Afterwards, the boc protective groups of the so obtained P*t*BAMA homopolymers were removed using 40 eq. of TFA per repeating unit (1 h, 50 °C). While under these conditions 80 – 91 % of the methyl ester group were cleaved, and the remaining portion was removed during the post-polymerization modification reactions under basic conditions towards the polyampholytic PDha backbone.

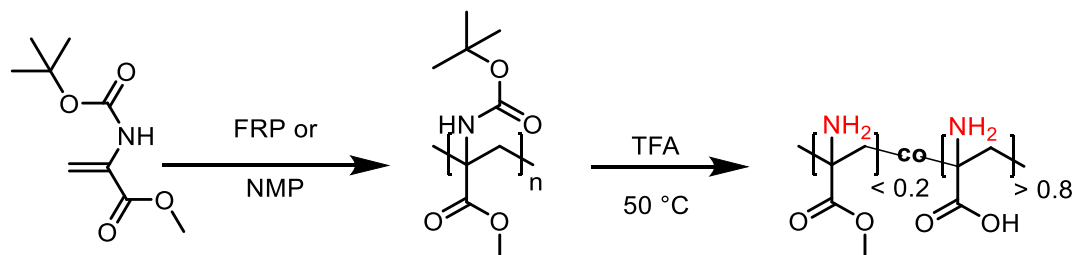


Figure 22. Synthesis of P(AMA-*co*-Dha) starting from *t*BAMA as the precursor for PDha-based graft copolymers.

For the post-polymerization of P(AMA-*co*-Dha) containing free, nucleophilic amino moieties, two convenient routes were explored. The first one is the Michael addition reaction of electrophilic vinyl compounds,¹¹⁹ and the other one the ring opening of epoxides.^{274, 275} Both polar and non-polar modifiers featuring an epoxide or a Michael acceptor functional group were chosen, in order to cover a broad range of resulting polymer properties. The side-chains should render different philicities,³⁸ such as fluorophilic, lipophilic or hydrophilic to cover a broad range of properties and functionalities. In this respect, rather hydrophobic modifiers feature alkyl (epoxyoctane, EOOct; PEG glycidyl lauryl ether, PEG LGE), aromatic (benzyl glycidyl ether, BGE) or fluoro-alkyl moieties (nonafluoropentaoxirane, NFPO). The resulting graft copolymers are amphiphilic and may be related to polysoaps being interesting candidates for surfactants, emulsifier or catalysis.³⁶ On the other hand, the hydrophilic entities consist of ionic/ionizable (2-acryl amido-2-methylpropane sulfonic acid, AMPS; carboxylic acid, COOH; *N*-butyl-*N*-(2-phosphonoethyl)acrylamide (*N*-propyl phosphonic acid acryl amide), PhA) PEG or low molecular weight, polar moieties (acrylonitrile, ACN; NIPAAm). As ionic and/or ionizable grafts, especially phosphonic acid and sulfonic acid can enhance the solubility significantly and can facilitate proton transfer, they are potentially advantageous in photocatalytic hydrogen evolution.^{276, 277} Furthermore, phosphonic acid groups are well-known to be strong ligand groups.^{278, 279} Double hydrophilic graft copolymers (DHGC) based on PEG can reveal a high solubility, while the functional backbone can interact with metal ions or NPs. Hence, such materials have great potential, and may be suitable as templates and

2. Synthetic routes towards PDha-based copolymers

nanoreactors.^{177, 203, 280} While PNIPAAm is a famous example for a thermo-responsive polymer,²⁸¹ to the best of our knowledge molecular NIPAAm as side-chain has not been investigated in respect of a thermo-response, yet. By combining NIPAAm with the pH- and metal ion-responsive PDha backbone, the resulting triple-responsive graft copolymers could potentially be implemented as sensors.¹³⁶ In general, all the utilized modifiers are commercially available, except for PhA, which was synthesized according to a literature protocol.²⁸²

A general synthetic strategy was developed for the corresponding modifiers, which may be slightly adjusted depending on the solubility and reactivity of the modifier (**Figure 23**). Since P(AMA-*co*-Dha) is insoluble in common organic solvents except dimethyl sulfoxide (DMSO), the reactions were carried out in basic water at 60 or 70 °C. A pH value of 13 was chosen, to increase the nucleophilicity of the amino moieties, and a relatively low polymer concentration (6.66 g/L) was found to be suitable to prevent precipitation during reaction. For non-polar, water-insoluble modifiers, methanol (MeOH) or DMSO in different ratios was added, to obtain homogenous reaction mixtures. Usually, an excess of the epoxide or Michael acceptor was used for two reasons: to promote high conversions, and to prevent the consumption of these reactants by potential side-reactions under basic conditions, *e.g.*, the ring opening of epoxides. Still, the unreacted low-molecular weight substances can be easily removed *via* dialysis or washing steps. It should be noted that there exist limitations in the choice of modifier regarding the reaction conditions. First, any functional groups present should survive harsh basic conditions (pH 13), which are necessary to modify the P(AMA-*co*-Dha), and hence, the attachment of isocyanates as reactive handles, for example, can be excluded. Therefore, more stable acrylamides were used instead of hydrolysable acryl esters. Finally, the reactivity of the modifiers must be considered under the relatively low reaction temperatures used. For examples, (meth)acrylamides were found to be less reactive compared to acrylamides due to their higher electron density and steric hindrance. In this respect, PAA, a di-substituted amide, was also found to be less reactive than the other Michael acceptors due to a reduced electron withdrawing effect. The synthesized copolymers are denoted PDha-*g*-M_Y where M is the added modifier, and Y is the determined degree of functionalization (DoF). The abbreviations are also shown in **Figure 23**. The successful modification and presence of the introduced side-chains were then confirmed *via* SEC, fourier-transform infrared FT-IR and NMR spectroscopy (¹H, ¹³C, ¹⁹F, ³¹P), as well as by elemental analysis. The resulting graft copolymer library is shown in **Figure 23** and the polymers and their solubility in different solvents summarized in **Table 5**. It should be noted, that PDha-*g*-ACN was not stable under the described conditions, and partially

2. Synthetic routes towards PDha-based copolymers

hydrolyzed *in situ* (~80 %) to the corresponding PDha-g-CA, as confirmed *via* potentiometric titration and FT-IR spectroscopy.

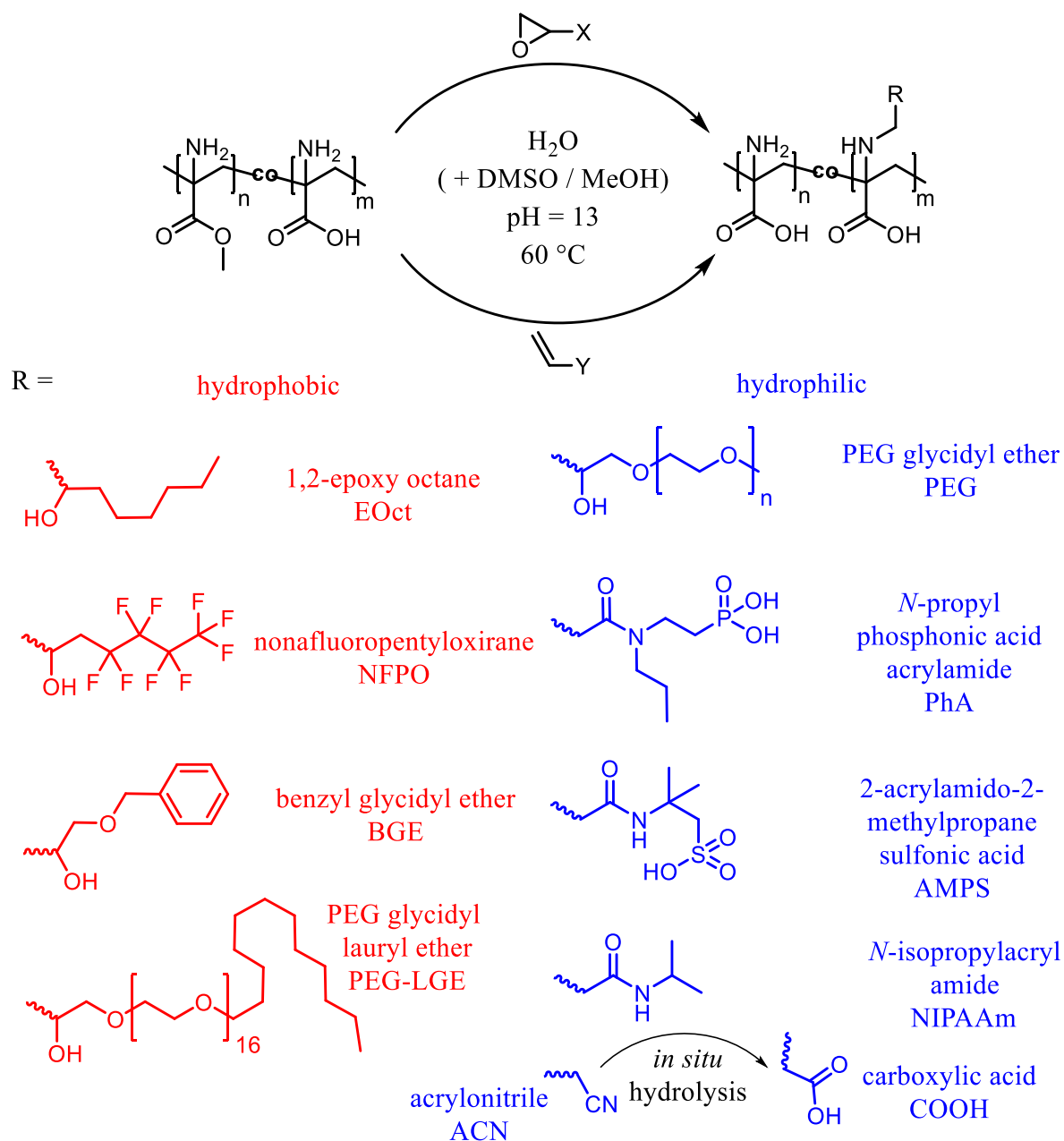


Figure 23. Graft copolymer library based on PDha obtained by the post-polymerization modification of P(AMA-*co*-Dha) with either hydrophobic (red) or hydrophilic (blue) side-chains.

Regarding the complementary polar and non-polar modifiers, both the reaction conditions as well as the resulting solubility differed significantly. For the non-polar grafts, choosing a suitable solvent mixture was crucial, and the utilization of an organic co-solvent was necessary. The polar grafts were attached in pure water, except for PhA, which seems to be rather amphiphilic. The chemical composition of the graft copolymers was elucidated *via* NMR and IR-spectroscopy, as exemplarily shown for PDha-g-NIPAAm (**Figure 24 A and B**). Here, both the side-chains and the backbone were visible, while the presence of any remaining modifier

2. Synthetic routes towards PDha-based copolymers

was excluded. Furthermore, SEC measurements (**Figure 24 C**) proved that the synthesis was successful, as the graft copolymers reveal a monomodal molecular weight distribution and a clear shift in the elution volume. This indicates that no significant side reactions occurred, and that the uniform functionalization of the PDha chains was realized.

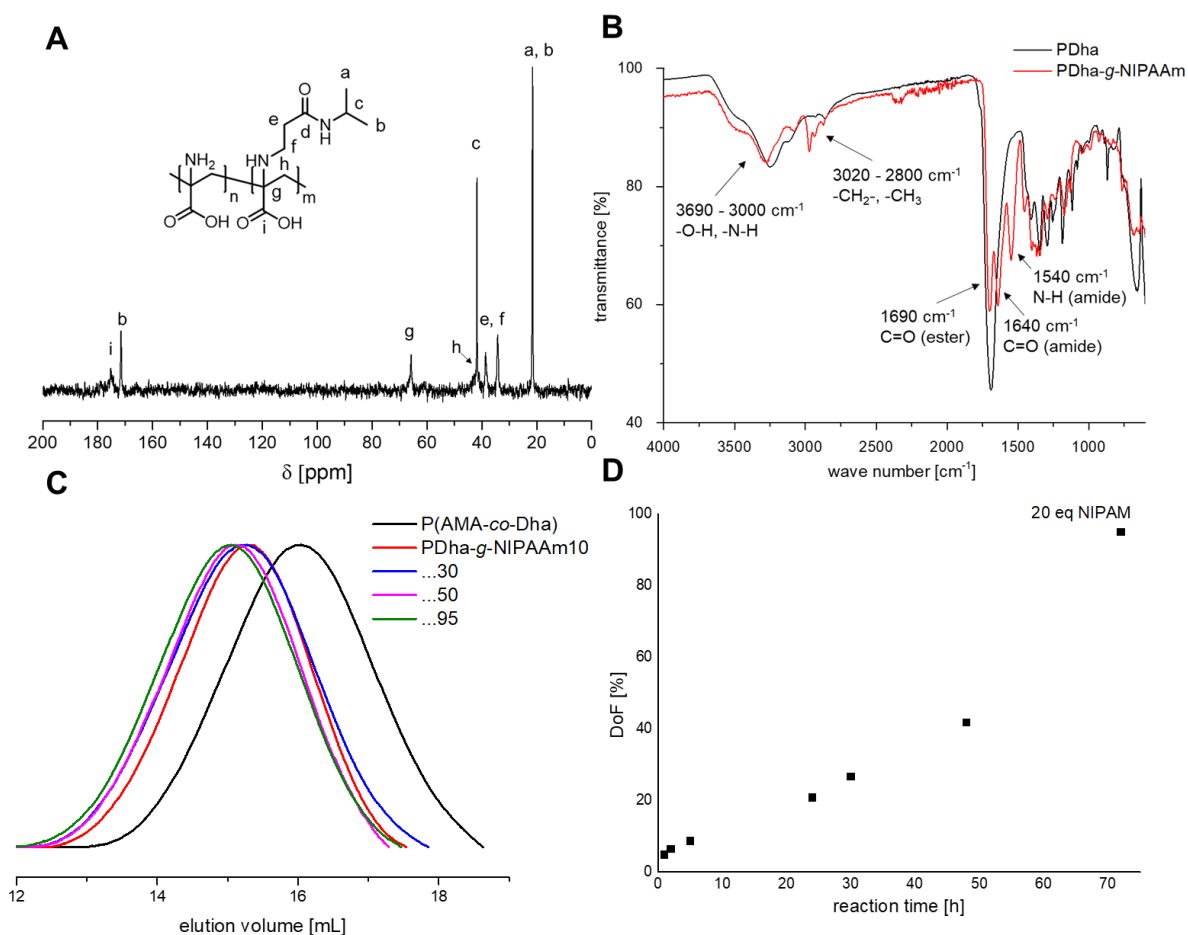


Figure 24. Characterization of the prepared PDha-g-NIPAAm *via* ¹H-NMR spectroscopy (A), FT-IR spectroscopy (B) and SEC (in DMSO) (C) of the synthesized graft copolymers with different DoF. Kinetic investigation *via* ¹H-NMR spectroscopy revealed a linear increase of the DoF with reaction time (D). Adapted from Macromol. Rapid Commun., **2021**, *42*, 2000671, with permission of WILEY-VCH Verlag GmbH & Co. KGaA, Weinheim.

The DoF, which correlates with the grafting density, was found to be an important parameter determining the resulting polymer properties and was determined *via* ¹H-NMR spectroscopy, whereby the -CH₂- protons of the repeating units were integrated and compared to the integral of the new side-chain protons. However, in case of water-insoluble graft copolymers (PDha-g-NFPO and PDha-g-PEG-LGE), elemental analysis (EA) was also used for the calculation of the DoF, where a change in the ratio between nitrogen and carbon is observed in comparison to PDha to the addition of alkyl chains. The DoF itself was tuned by the concentration of the modifier and the reaction time. In respect of PDha-g-NIPAAm, the grafting process showed a linear increase in the DoF with time (**Figure 24 D**). Hence, the number of side-chains can be

2. Synthetic routes towards PDha-based copolymers

precisely adjusted. The maximum DoF attained for the different modifiers in this work are shown in **Table 5**. This was achieved by extending the reaction time up to 10 d and using 20 eq modifier per monomer unit. The values vary between 33 and 135 %, which means that the amino moieties may in principle react two-fold. While short side-chains result in rather high DoF, due to the steric hindrance, the DoF of bulky or long side-chains is significantly lower, *e.g.*, BGE or PEG, and not all of the amino groups were accessible.

Table 5: Summary of the synthesized PDha-based graft copolymers in this work.

Modifier	Co-solvent	Maximum DoF ^a [%]	DMF	Solubility ^c			Structural characterization
				DMSO	H ₂ O ^c	MeOH	
-		0	-	+	pH > 7 ^d	-	¹ H-, ¹³ C-NMR, FT-IR
EOct	MeOH	70	+	+	pH > 7 ^d	-	¹ H-, ¹³ C-NMR, SEC
NFPO	MeOH	65 ^b	+	+	-	-	¹ H-, ¹⁹ F-NMR, solid state ¹³ C-NMR, FT-IR, SEC, EA
BGE	MeOH	50	+	+	pH > 7 ^d	-	¹ H-, ¹³ C-NMR, SEC
PEG-LGE	none	33 ^b	+	+/-	-	-	¹ H-NMR, solid state ¹³ C-NMR, FT-IR, SEC, EA
PEG 1,000 g/mol	none	50	+	+	+	+	¹ H-NMR, solid state ¹³ C-NMR, FT-IR, SEC
PhA	DMSO	66	+	+	+	+/-	¹ H-, ¹³ C-NMR, ³¹ P-NMR, FT-IR, SEC
AMPS	none	65	+	+	+	-	¹ H-, ¹³ C-NMR, FT-IR, EA, SEC
NIPAAm	none	95	+	+	+	+	¹ H-, ¹³ C-NMR, FT-IR, SEC
ACN	none	135	+	+	pH > 4 ^d	-	¹ H-, ¹³ C-NMR, FT-IR, SEC
COOH	none	135	+	+	pH > 4 ^d	-	¹ H-, ¹³ C-NMR, FT-IR, SEC

Reaction conditions: water (pH 13, KOH), T_{reaction} = 60 °C (except for PhA 70 °C), t_{ret} 48 h to 10 d. ^a Calculated from ¹H-NMR spectroscopy; ^b calculated from EA; ^c as a function of the DoF and the employed modifier: + \triangleq well soluble, clear solution; +/- \triangleq poor soluble (by heating), turbid solution, partial precipitation after time, - \triangleq insoluble (also upon heating); ^d dissolution at pH 12, before slowly titrating with HCl (0.1 M).

The solubility in different solvents of the prepared polymers was investigated (**Table 5**). It turned out, that the solubility of the graft copolymers is not only influenced by the type of modifier but also strongly depends on the DoF. While P(AMA-*co*-Dha) dissolves exclusively in water (pH > 7) or DMSO, the graft copolymers showed a different behavior. The graft copolymers were additionally soluble in DMF and a clear difference between the polar and non-polar side-chains was observed. For example, PDha-*g*-NFPO and PDha-*g*-PEG-LGE, with highly hydrophobic side-chains even became water insoluble. On the other hand, the hydrophilic and ionic side-chains enhanced the water solubility being well-soluble over the entire pH range. As expected, a high DoF (> 50 % in the case of NIPAAm) or long side chains

2. Synthetic routes towards PDha-based copolymers

(PEG) even enable even dissolution in MeOH. Experiments regarding PDha-*g*-PEG showed that low a low DoF resembles the solubility of pristine PDha, while higher grafting densities are soluble in DMF and over the entire pH range. By attaching PEG with a molecular weight of 1,000 instead of 400 g/mol, it became soluble in MeOH and even partly in CHCl₃ (slightly turbid solutions).

Solution properties of selected graft copolymers

Solubility tests already indicate substantial differences in the graft copolymer characteristics. Therefore, after the introduction of a broad range of side-chains featuring a different polarity and charge, the solution properties of some selected graft copolymers were investigated. Exhibiting a polyampholytic backbone their protonation/deprotonation state (potentiometric titration) and overall charge (ζ -potential) is of special interest, determining their interaction with oppositely charged compounds. Besides, for both amphiphilic and DHGCs the aggregation behavior was examined (DLS, UV-Vis spectroscopy and transmission electron microscopy (TEM)).

Amphiphilic PDha-based graft copolymers

Non-polar side-chains were attached to PDha in order to obtain amphiphilic copolymers. As a clear sign of their hydrophobic nature, PDha-*g*-PEG-LGE₃₅ and PDha-*g*-NFPO₆₅ became completely insoluble in water after the reaction. The solution properties PDha-*g*-EOct, bearing a short alkyl chain, were exemplarily studied. While PDha-*g*-EOct₈ with a DoF < 10 reveals clear solutions, when a DoF of 70 % is reached slightly turbid solutions are obtained in aqueous solution (pH 12). As the self-assembly in aqueous solution of amphiphilic block copolymers is well-known, *e.g.*, for the previously described PS-*b*-PDha,¹¹⁴ it is also observed for amphiphilic graft copolymers, where hydrophobic side-chains aggregate to form the core, are stabilized by the hydrophilic backbone in the medium.^{283, 284} Therefore, after the attachment of the hydrophobic side-chains to PDha, self-assembly can also be expected for this amphiphilic graft copolymer. In the case of PDha-*g*-EOct₇₀, the alkyl side-chains can induce aggregation to form hydrophobic domains, stabilized by the ampholytic PDha backbone. These assumptions and the formation of nano-objects were confirmed *via* DLS and TEM (**Figure 25 A and B**). According to DLS, the nano-objects were characterized by a hydrodynamic radius of 16 nm. This is noticeably larger than an individual graft copolymer unimer with only several nm. This observation was further supported by TEM, where loosely defined aggregates with a diameter of 30 nm were visible in the micrographs recorded. The self-assembly of the amphiphilic graft copolymers seems to be rather complex, related to the micellization of polysoaps. Here, three

2. Synthetic routes towards PDha-based copolymers

models exist, and the formation of local, regional and molecular micelles is possible including both intra- and intermolecular interactions of the hydrophobic moieties leading to the aggregation.³⁶ In order to determine the overall charge of the nano-assemblies, the pH dependent ζ -potential was measured (**Figure 25 C**). Therefore, PDha-*g*-EOct₇₀ was first dissolved at pH 13 before being acidified using aqueous HCl. The aggregates present were negatively charged (-15 mV), which was almost constant up until pH 5 as a result of deprotonated carboxylate moieties. Upon further increasing the pH, the dependent ζ -potential approaches zero, before positive values were observed at pH 2, where all amino and carboxylate groups were fully protonated. Hence, the surface charge of the aggregates can be inverted, making these materials interesting candidates for catch and release systems or the encapsulation of hydrophobic guest molecules. Further studies should focus on PDha-*g*-NFPO, exhibiting even more lipophilic fluoro-alkyl entities. Therefore, it is necessary to develop suitable DoF values, or utilize alternative fluoro-alkyl modifiers, since the PDha-*g*-NFPO₆₅ described in this work was completely water-insoluble. However, fluorine-containing amphiphilic copolymers reveal an interesting self-assembly behavior and a high surface activity, and corresponding materials may for example be applied as stabilizers in dispersion polymerization.²⁸⁵

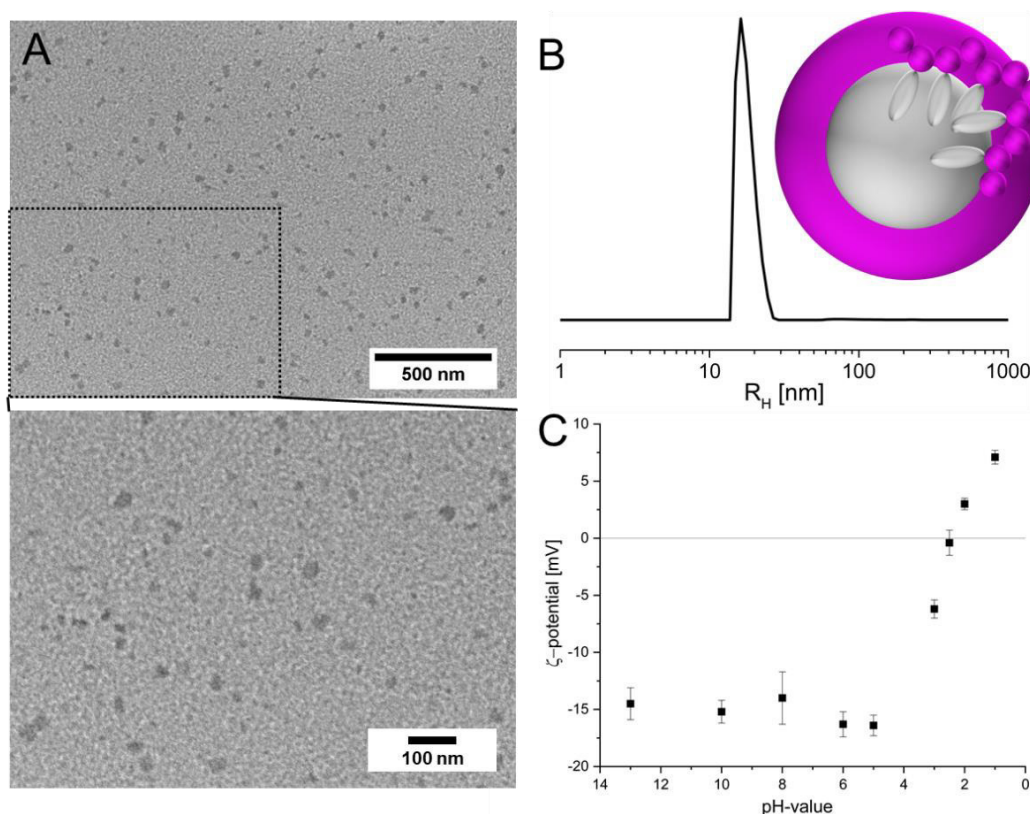


Figure 25. TEM micrographs (A) and DLS CONTIN plot (B) of amphiphilic PDha-*g*-EOct₇₀ in water (pH = 12, *c* = 0.5 g/L). The formed nano-objects that are schematically depicted (B), reveal a hydrophobic core and a PDha corona. The pH-dependent ζ -potential reveals charge neutrality above a pH-value of 2. Adapted from *Polym. Chem.*, **2019**, 10, 3006, with permission of The Royal Society of Chemistry.

2. Synthetic routes towards PDha-based copolymers

Double hydrophilic graft copolymers

By the attachment of polar modifiers onto the PDha backbone, DHGCs were obtained with an enhanced solubility compared to pristine PDha, preventing pH- or metal ion-induced precipitation. As an architectural subclass of linear DHBCs, the graft copolymers usually contain a solubility-promoting and a functional, stimuli-responsive building block. Such macromolecules are gaining research interest due to their versatile solution properties and applications.^{170, 176, 286, 287, 288} However, their self-assembly appears more complex and less studied compared to linear block copolymers, showing tunable collapsing of either the backbone or the side-chains or low aggregation numbers of ~ 2 .²⁸⁹ In this work ionic/ionizable, PEG and low molecular weight, polar moieties were attached to a polyampholytic backbone leading to distinct solution properties and potential application fields. This research on the PDha-based DHGCs will not only be a guideline to develop corresponding materials for specific applications, it will also grant a better fundamental understanding of this polymer class.

Double acidic graft copolymers

Three graft copolymers were prepared featuring additional acidic moieties. This resulted in an excess negative charge compared to unmodified PDha. Being polyanions overall, the anionic charge improves the water solubility while keeping the ampholytic backbone. While PDha-g-PAA and PDha-g-AMPS are functionalized with strongly acidic side-chains (phosphonic and sulfonic acid), PDha-g-COOH contains rather weak carboxylic acid groups, as schematically depicted in **Figure 26 A**. This leads to differences in their solubility, whereby the strong acidic grafts permit solubility at $\text{pH} \leq 1$ due to the deprotonated strong acidic groups that facilitate dissolution, *e.g.*, by electrostatic repulsion. On the other hand, the weak carboxylic groups are protonated under acidic conditions, leading to the slow precipitation of PDha-g-COOH, as previously reported for another graft copolymer with carboxylic groups along the side-chain.²⁸⁰ These observations were supported by ζ -potential measurements. While the ζ -potential of PDha-g-AMPS₂₅ remains negative independent of the pH-value (-50 mV to -13 mV), it is positive for PDha-g-COOH₁₃₀ at pH 2 due to complete protonation of both the carboxylate moieties. Besides, the titration curve of PDha-g-AMPS reveals only two steps at pH 8.1 and 4.3 corresponding to the amino and carboxylic moieties within the backbone, which means that the sulfonic acid is fully deprotonated under the investigated conditions. The potentiometric titration of an alkaline solution (pH 12) of PDha-g-COOH₁₃₀ with 0.1 M HCl was further examined and compared to PDha, derived *via* the same preparation and at similar concentrations (1.5 g/L) (**Figure 26 B**). While the titration curve of unmodified PDha only reveals three steps (corresponding to the protonation of an excess NaOH, the amino moieties and the carboxylic

2. Synthetic routes towards PDha-based copolymers

groups),³² PDha-g-COOH₁₃₀ undergoes four steps. Here, the inflection points can be ascribed to an excess of NaOH, amino moieties and indeed two kinds of carboxylic acids present in the graft copolymer. At first, the titrant is consumed by the excess base, before the amino moieties are protonated. This corresponds to a pK_a of 9.8 ($\alpha_{\text{NH}_2} = 0.5$), which is in line with the value for the PDha homopolymer reported in literature.³² Starting from a pH of 8.3, the first population of carboxylate moieties with a rather low acidity is protonated to form -COOH ($pK_{a,\text{COOH}1} = 6.7$, $\alpha_{\text{COOH}1} = 0.5$) differing remarkably from the second population of highly acidic groups ($pK_{a,\text{COOH}2} = 4.5$, $\alpha_{\text{COOH}2} = 0.5$). Interestingly, the highly acidic groups were not shown for the unmodified PDha revealing only one population with a $pK_{a,\text{COOH}1} = 6.2$, ($\alpha_{\text{COOH}1} = 0.5$).³² However, it is not possible to ascribe the two pK_a values of PDha-g-COOH₁₃₀ directly to the backbone or the side-chain carboxylate moieties, since both of their titration volumes do not fit exactly to the amount of amino moieties. Presumably, the different types of carboxylic groups influence their individual protonation behavior, that could be explained the presence of inductive effects and/or the formation of intramolecular hydrogen bonds.

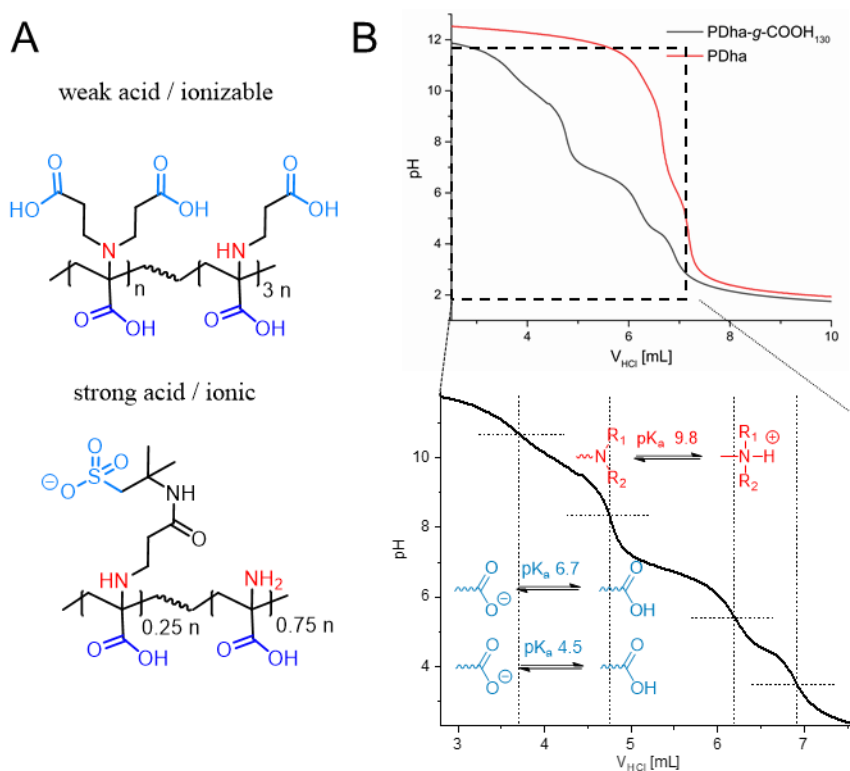


Figure 26. Structure of the PDha-g-COOH and PDha-g-AMPS graft copolymers rendering weak or strong acidic side-chains, respectively (A). The potentiometric titration curve of PDha-g-COOH₁₃₀ presents three steps corresponding to the amino and carboxylic moieties of the PDha backbone and the carboxylic acid grafts (B). Adapted from Polym. Chem., **2019**, 10, 3006, with permission of The Royal Society of Chemistry.

The potentiometric titration was further used to determine the amount of pendant carboxylic acids by comparing the volume of titrant consumed for the amino groups and the carboxylic

2. Synthetic routes towards PDha-based copolymers

acid groups (1.0151 mL vs 2.163 mL). From this, 1.05 carboxylic groups per repeat unit was found (DoF = 105 %), showing that there exists a small amount of di-substituted monomer units within the graft copolymer. Comparing this value to the original DoF of its precursor PDha-g-ACN₁₃₀ calculated from ¹H-NMR spectroscopy, it may be assumed that around 80 % of the formerly nitrile groups were hydrolyzed.

Introducing acidic side-chains offers the possibility to tune the overall charge of PDha while maintaining the functionality of the backbone. This changes the overall solubility of the material and could additionally influence its interaction with oppositely charged compounds or surfaces. PDha-g-COOH₁₃₀ bears a high density of ligands and is therefore interesting as a nanoreactor for the synthesis of inorganic nanoparticles or in biomineralization.^{143, 177, 188} Apart from that, the phosphonic acid groups of PDha-g-PhA are strong anchoring sites, which could enable a strong interaction with inorganic compounds, being an interesting material for the construction of hybrid materials.^{278, 279} Further, PDha-g-PhA and PDha-g-AMPS may be applied as soft matrixes in the photocatalysis due to their solution stability, functional groups and their potential to facilitate proton transfer.^{276, 277} Further research should focus on fine-tuning of the DoF, or on the post-polymerization modification with cationic side-chains, *e.g.*, *N*-[2-(dimethylamino)ethyl]acrylamide, presenting a complementary overall charge (polycationic).

Non-ionic, double hydrophilic graft copolymers

By the attachment of PEG to the polyampholytic backbone, non-ionic, DHGCs, PDha-g-PEG, were obtained. Hereby, two different molecular weights of PEG (400 and 1,000 g/mol, which is denoted as PEG₄₀₀ and PEG_{1,000}, respectively) were introduced, and a DoF between 10 and 50 % tested, influencing the solubility as a function of the PEG content. PEG is known for its biocompatibility and high hydrophilicity,²⁵⁵ and hence, long PEG grafts lead to a better solution stability of the synthesized graft copolymers. The solution behavior was exemplarily investigated for PDha-g-PEG_{1,000,28} (PEG_{1,000} side-chain, DoF = 28 %) assuming pH-dependent changes in conformation and size, since the overall charge and charge density along the backbone are altered, as it is schematically shown in **Figure 27 A**. To get a first hint, ¹H-NMR spectra were measured at acidic, neutral and basic pH values (**Figure 27 B**). While the signal originating from the backbone (-CH₂-C-, 2.90 – 2.30 ppm) is almost completely suppressed at a pH of 2, it is rather broad and shifted at pH 7. This may be the result of a collapsed PDha backbone at lower pH-values, which is stabilized by the PEG side-chains leading to a decreasing intensity of the corresponding proton signals.^{174, 290-292} These observations were further supported by DLS experiments (**Figure 27 C**), presenting distinct apparent R_H

2. Synthetic routes towards PDha-based copolymers

depending on the solution pH. At pH 10 and 9, the largest R_H were measured of 4.5 to 5.5 nm, ascribed to a fully stretched backbone due to electrostatic repulsion of the negatively charged carboxylate groups. In contrast, at pH = 2 a significantly lower R_H of 3 nm was observed, where the carboxylic groups are expected to be fully protonated and the polymer is a polycation. A possible reason for this observation is that under these conditions the intramolecular hydrogen bonds, *e.g.*, between ethylene glycol and carboxylic moieties are pronounced and counteract the electrostatic repulsion. This explanation is supported by the work of J. Hao *et al.*, describing the association of PAA-g-PEG graft copolymers by interchain hydrogen bonding. When the carboxylic acid groups are protonated at low pH values, the size of the formed complexes decreases due to formation of hydrogen bonds between the carboxylic groups in the PAA backbone and the PEG chains.¹⁷¹ However, for the polyampholytic PDha-g-PEG_{1,000,28}, the lowest R_H was found at a pH of around 5. Further research could better elucidate these pH-dependent conformational changes, *e.g.*, via small angle X-ray scattering or small angle neutron scattering.

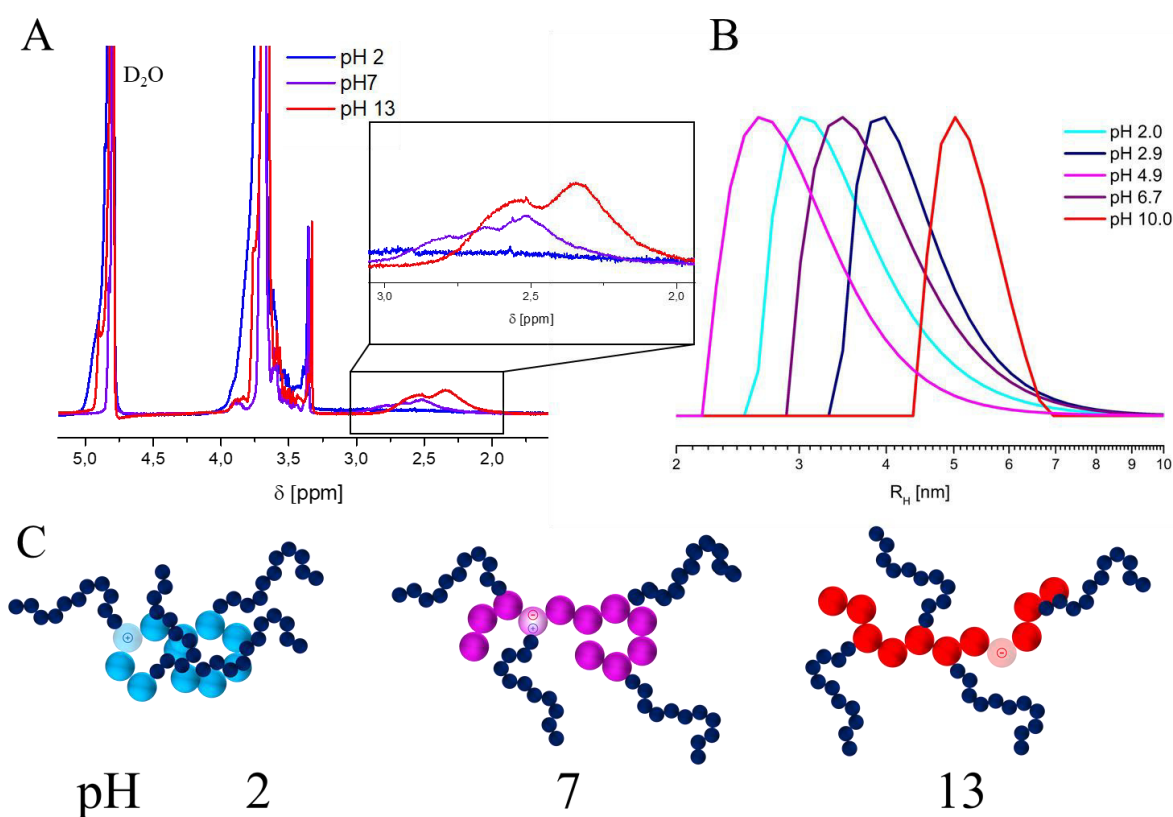


Figure 27. pH-dependent ¹H-NMR spectroscopy (A) and DLS experiments of a PDha-g-PEG_{1,000,28} aqueous solution. The assumed conformational changes are schematically shown (C), with a collapsed backbone at pH 2, partial aggregation at pH 7 and a fully stretched backbone at pH 13. Adapted from *Macromolecules.*, **2020**, 53, 4511-4523. Copyright American Chemical Society.

In summary, the pH-responsive PDha backbone is strongly affected by the environmental pH value and reveals changes in its conformation modulated by charge, as also described for other

2. Synthetic routes towards PDha-based copolymers

DHGCs.¹⁷¹ While the PDha backbone presents functional groups with a tunable charge and the PEG grafts prevent macroscopic aggregation, these materials may be applied in delivery systems,²⁸⁶ or as templates for the preparation of inorganic NPs.²⁸⁰

Triple-responsive, double hydrophilic graft copolymers

Thermoresponsive DHGCs display an interesting aggregation behavior and are mostly based on PNIPAAm, which is found either in the backbone,^{172, 173, 287} or the side-chains.¹⁴⁷ However, thermo-responsive behavior of monomeric NIPAAm is rather unexplored until now. By attaching NIPAAm as a Michael-acceptor onto the PDha backbone, triple-responsive (pH, metal ion and temperature) DHGCs were designed, as shown in **Figure 28 A**. At first, the influence of the DoF on the solution behavior in an aqueous environment was tested, as outlined in **Table 6**. Solubility in water over the entire pH range was achieved starting from DoF = 30 %, and even the dissolution in organic solvents such as methanol and DMF was possible at DoF \geq 50%. This DoF was also found to be the turning point where a thermo-induced cloud point became visible, which was not observed for lower DoF \leq 50 %, presumably due to an insufficient NIPAAm content.

Table 6: Summary of the synthesized PDha-g-NIPAAm graft copolymers, their solubility in aqueous solution and the observation of a thermo-induced cloud point.

Reproduced from Macromol. Rapid Commun., **2021**, 42, 2000671, with permission of WILEY-VCH Verlag GmbH & Co. KGaA, Weinheim.

PDha-g-...	NIPAAm [wt%]	Solubility in water	Thermo-response ?
-		pH > 7	none
NIPAAm ₁₀	9	pH \geq 7	none
NIPAAm ₃₀	24	pH \geq 6 ^b	none
NIPAAm ₅₀	36	pH = 1 - 14	at pH < 7
NIPAAm ₉₅	55	pH = 1 - 14	at pH \leq 7

^a \geq 2 g/L, - \triangleq insoluble, + \triangleq clear solution, +/- slightly turbid;
^b soluble under acidic condition by slow titration starting from pH 7.

Both PDha-g-NIPAAm₅₀ and PDha-g-NIPAAm₉₅ were investigated in respect to their thermo-responsive properties (**Figure 28 B-D**). These graft copolymers differ significantly from PNIPAAm, because the NIPAAm side-chains exhibit different local environments and are in the case of PDha-g-NIPAAm₅₀, are also locally separated. In addition, they are connected to a polyampholytic backbone, with a pH-dependent net charge and distinct water solubility. Hence, the cloud point temperatures (T_{CP}) are also expected to vary from PNIPAAm homopolymers. As a result, PDha-g-NIPAAm₅₀ (36 wt% NIPAAm) does not show any cloud point at a pH \geq 7,

2. Synthetic routes towards PDha-based copolymers

which may be ascribed to the electrostatic repulsion of the negatively charged carboxylate moieties. In contrast, at pH 7, PDha-g-NIPAAm₉₅ (55 wt%) already shows a T_{CP} of 37 °C, which is only slightly affected by changes in the pH and is similar to the cloud point of the PNIPAAm homopolymer with a T_{CP} of 30–35 °C.²⁸¹ However, upon acidification to pH 6, a cloud point also became visible for PDha-g-NIPAAm₅₀, which further decreased from 43 to 28 °C governed by the partial protonation of the carboxylic groups in accordance with potentiometric titration. Hereby, charge neutrality could induce strong electrostatic attraction, which could explain the lowest T_{CP} at pH 5. By further protonation to -COOH the formation of hydrogen bonds and aggregation is facilitated. After complete protonation at pH 1, a polycation may be present and the formation of hydrogen bonds predominate. The corresponding observations were supported by ζ -potential measurements (**Figure 28 B**), revealing an overall negative charge until pH \approx 3, before becoming positive at pH 2.

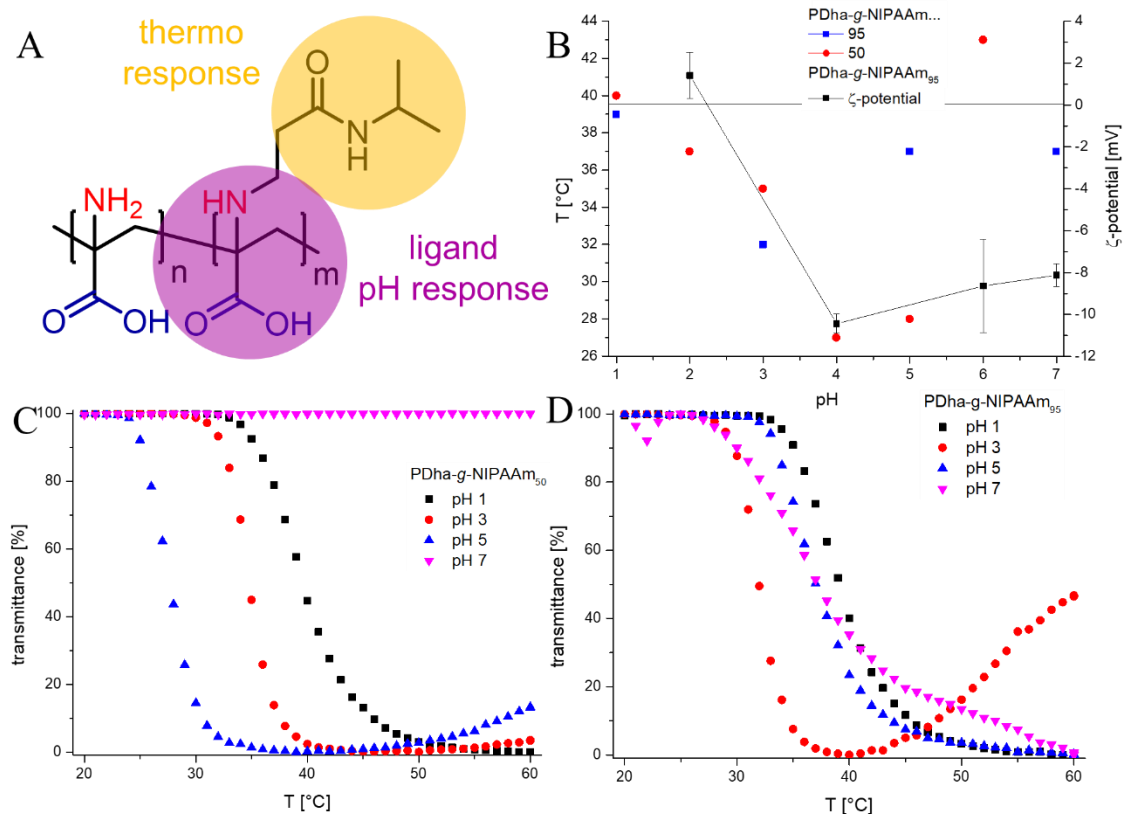


Figure 28. Illustration of the triple-responsive PDha-based graft copolymers featuring pH- and metal ion-responsive carboxylic acid and amino moieties, as well as thermo-responsive NIPAAm side-chains. Cloud points determined from UV-vis measurements of PDha-g-NIPAAm₉₅ and PDha-g-NIPAAm₅₀ (B-D) at different pH values ($c = 1$ mg/mL, rate 0.2 °C/min) and diagram of T_{CP} vs pH value and ζ -potential of PDha-g-NIPAAm₉₅. Reproduced from *Macromol. Rapid Commun.*, **2021**, *42*, 2000671, with permission of WILEY-VCH Verlag GmbH & Co. KGaA, Weinheim.

2. Synthetic routes towards PDha-based copolymers

The reversible aggregation behavior has been exemplarily studied using PDha-g-NIPAAm₉₅ *via* temperature-dependent ¹H-NMR spectroscopy and DLS experiments at pH 1 (**Figure 29 A and B**). Starting from 35 °C, the ¹H-NMR spectra show a decreasing intensity of the -CH₂-backbone at 2.17-2.84 ppm and (-CH₃)₂ NIPAAm protons (0.84-1.14 ppm), due to the collapse of the graft copolymer – both the backbone and side-chains. Cooling the system leads to a stepwise increase in intensity hinting towards swelling, disruption of the aggregates and the unimers are present again. DLS experiments support these observations, since unimeric polymer chains were detected at the beginning and aggregates began forming from 27 °C aggregates with a R_H of 310 nm. Their radius further increased up to 820 nm at 50 °C.

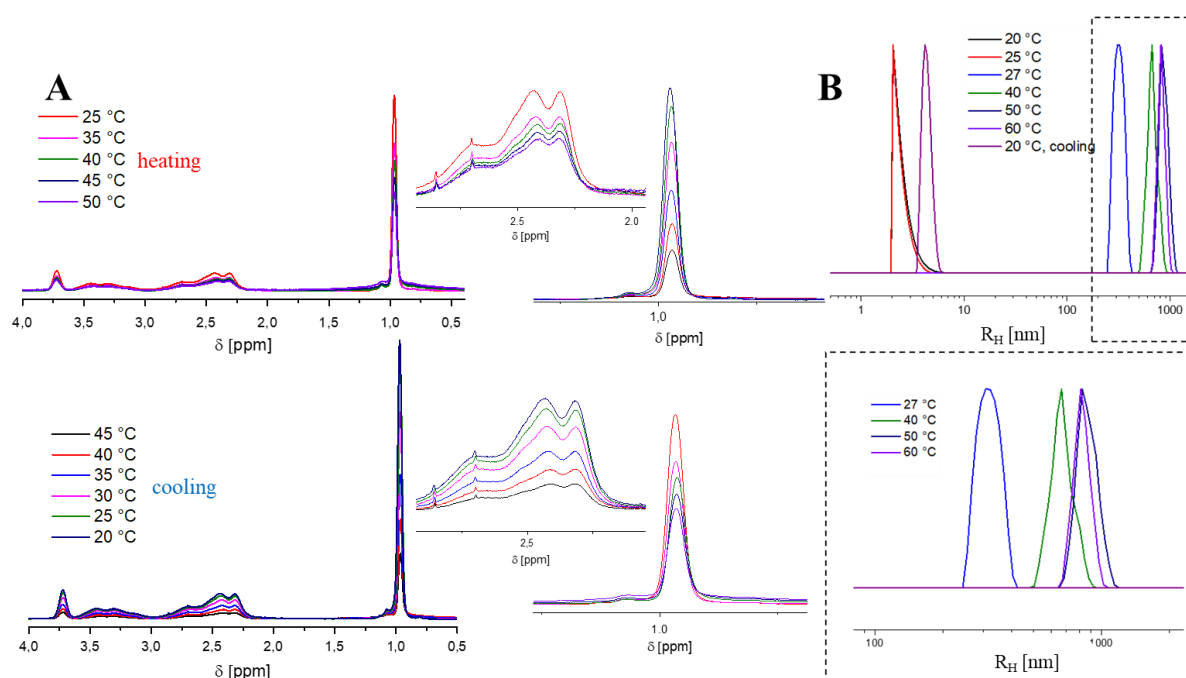


Figure 29: Temperature-induced aggregation behavior of PDha-g-NIPAAm₉₅ elucidated *via* temperature dependent ¹H-NMR spectroscopy (A) and DLS experiments (B) at pH 1. Adapted from Macromol. Rapid Commun., **2021**, *42*, 2000671, with permission of WILEY-VCH Verlag GmbH & Co. KGaA, Weinheim.

The PDha backbone features carboxylic and amino moieties that are strong binding sites for metal ions. While it has not been reported to-date, metal ion-responsive behavior can be expected. Hereby, double hydrophilic copolymers are of special interest, since the NIPAAm side-chains mediate the solubility upon the formation of complexes. Therefore, the chelation ability of PDha-g-NIPAAm₅₀ and PDha-g-NIPAAm₉₅ were investigated in the presence of Cu²⁺ or Pb²⁺ (0.01 mmol/ml). After the addition of a certain volume of the metal ion solution, the graft copolymer solutions (pH 7) became slightly opaque. This is a sign of chelation and aggregation, which was further supported by TEM micrographs and DLS measurements that reveal spherical aggregates with R_H = 11 - 60 nm (**Figure 30**). Differences were observed in the sensitivity as well as the shape and size of the aggregates depending on the type of heavy

2. Synthetic routes towards PDha-based copolymers

metal cation in accordance with literature.^{143, 151} Further, the DoF also appears to have an impact on the aggregation behavior. Upon the addition of Cu^{2+} , aggregation was already apparent at a $\text{Cu}^{2+}/\text{COOH}$ ratio of 1 : 230, while in case of Pb^{2+} a higher amount of metal ions was needed to induce the observable formation of aggregates of 1 : 34. This may be explained by different coordination behaviors of the individual metal ions.¹⁴³ Regarding the morphology, PDha-g-NIPAAm forms rather uniform spherical objects in the presence of Pb^{2+} ions independent on the PDha/NIPAAm and $\text{M}^{2+}/\text{PDha}$ ratios. Therefore, the coordination behavior of Pb^{2+} might be the main driving force. In the presence of Cu^{2+} , the morphology depends on the PDha/NIPAAm ratio. Hereby, the formation of polymer aggregates at already low concentrations and the observed secondary aggregation could be explained by multiple bridging of Cu^{2+} carboxylates.²⁹³

Within this work novel triple-responsive graft copolymers have been described, which demonstrate a high tunability by adjusting the DoF. Also, alternative thermo-responsive acrylamide modifiers could be introduced *via* this straight-forward approach as an additional strategy to fine-tune their thermo-responsive properties.²⁹⁴ The method of attaching molecular NIPAAm side-chains could even be transferred to other amino group containing polymeric backbones. The stimuli-responsive behavior of the PDha-g-NIPAAm graft copolymers has been investigated, rendering them as potential sensing systems, *e.g.*, for the detection of heavy metal ions.¹³⁶

2. Synthetic routes towards PDha-based copolymers

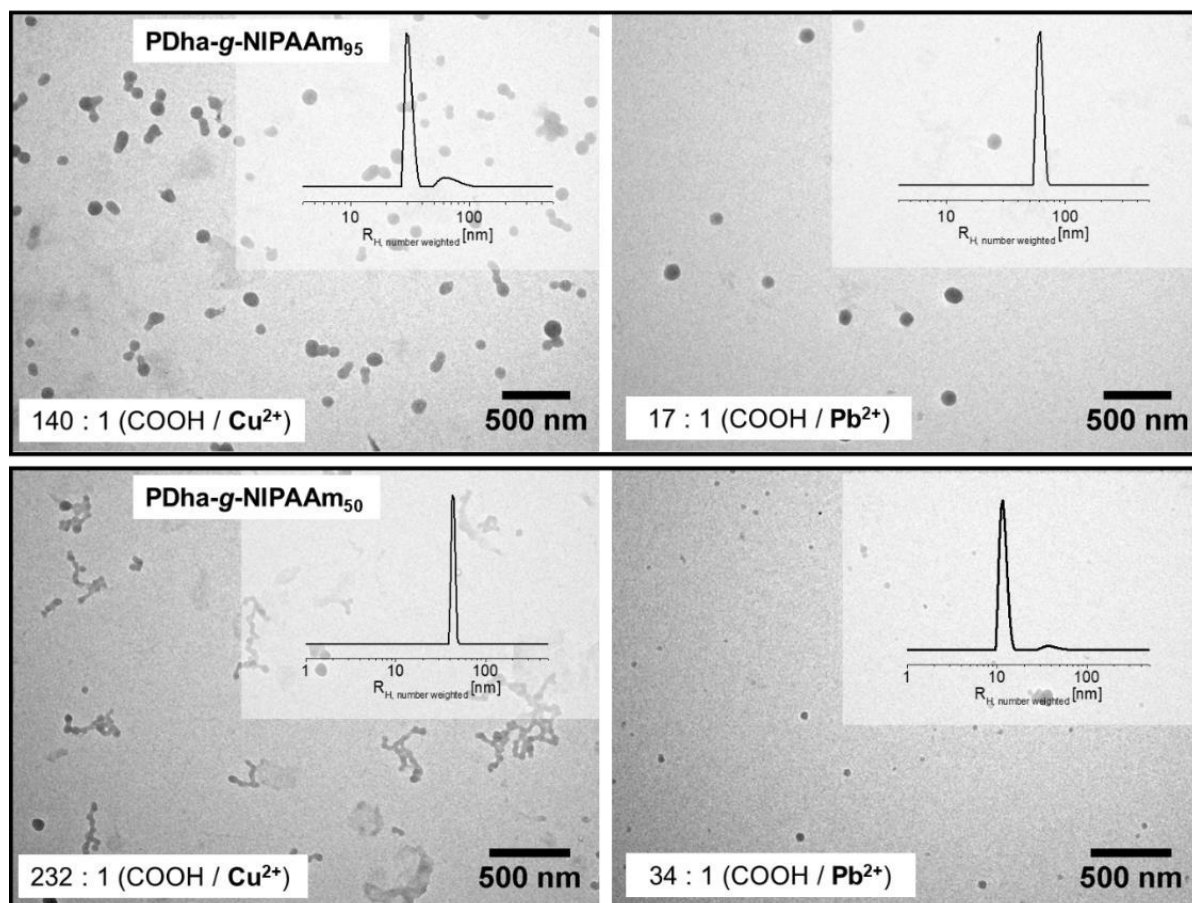


Figure 30: TEM micrographs and DLS CONTIN plots of aggregates formed after addition of Cu^{2+} and Pb^{2+} to the graft copolymer solutions (pH 7). Adapted from *Macromol. Rapid Commun.*, **2021**, *42*, 2000671, with permission of WILEY-VCH Verlag GmbH & Co. KGaA, Weinheim.

Within this chapter, the preparation of a polyampholytic PDha-based graft copolymer library has been described (**Table 7**). A straight-forward post-polymerization modification approach was developed, grafting epoxides and Michael acceptors onto the PDha backbone, to tune its properties. This synthetic route could be further transferred to other modifiers or reactive backbones. The DoF, which can reach up to 135 %, was found to be an additional parameter determining the resulting characteristics and might be easily adjusted by changing the reaction time or concentration of the modifier. A broad variety of side-chains were introduced, both hydrophobic or hydrophilic in nature, and the solution properties tested. The non-polar grafts led to amphiphilic graft copolymers, belonging to the class of polysoaps,³⁶ with a tunable charge and polarity. Their self-assembly in solution was exemplarily tested for PDha-g-EOct, revealing nanosized objects. The application of these materials as surfactants will be examined in the following chapter. On the other DHGCs were obtained presenting an enhanced solution stability over the entire pH range compared to unmodified PDha. PDha-g-PEG containing polymeric side-chains, was investigated with respect to their pH-dependent conformational changes and charge. Further research should be conducted to elucidate the nature of this behavior, *e.g.*, via scattering methods. However, the pH-dependent charge in combination with the solubility

2. Synthetic routes towards PDha-based copolymers

promoting PEG side-chains makes this polymer a promising candidate as a nanoreactor for the preparation of inorganic NPs.^{177, 280} By the attachment of ionic and ionizable side-chains in the form of weak or strong acids, the overall charge was tuned and additional binding sites introduced. The corresponding materials will be implemented as soft matrixes in photocatalytic hydrogen evolution. Finally, polar monomeric NIPAAm moieties were grafted onto PDha and its triple response to pH, T and metal ions was investigated. A specific interaction with individual metal cations was observed and hence, PDha-g-NIPAAm will be applied as a metal sensors, as described for similar ampholytic systems in the literature.¹³⁶ The implementation of the graft copolymers in hybrid materials and their utilization in the mentioned applications will be described in the following chapter.

Table 7: PDha-based graft copolymers prepared in this work, and their corresponding features.

Functional backbone	Modification	Type of modifier	Type of graft copolymer	Feature
PDha-g-..	hydrophobic	alkyl (EOct, PEG-LGE)	amphiphilic	surfactants with tunable charge
		fluoro alkyl (NFPO)		tunable philicity
		aromatic (BGE)		self-assembly in solution
	hydrophilic	polymeric polar (PEG)	double hydrophilic	pH induced conformational changes solution stability
ionic/ionizable (COOH, AMPS, PhA)		double acidic	tunable charge additional binding sites solution stability	
monomeric polar (NIPAAm)		triple-responsive	additional stimuli-response solution stability	

3. PDha-based graft copolymer based hybrid materials and applications

Parts of this chapter have been published in **P1)** J. B. Max, D. V. Pergushov, L. Sigolaeva, and F. H. Schacher, *Polym. Chem.*, **2019**, *10*, 3006, **P3)** J. B. Max, K. Kowalczyk, M. Köhler, C. Neumann, F. Pielenz, L. V. Sigolaeva, D. V. Pergushov, A. Turchanin, F. Langenhorst, and F. H. Schacher, *Macromolecules.*, **2020**, *53*, 4511-4523, **P4)** Johannes B. Max, Afshin Nabiyan, Jonas Eichhorn, and Felix H. Schacher, *Macromol. Rapid Commun.*, **2021**, *42*, 2000671, **P5)** Afshin Nabiyan, Johannes B. Max, Christof Neumann, Magdalena Heiland, Andrey Turchanin, Carsten Streb, and F. H. Schacher, *Chem. Eur. J.*, **2021**, *27*, 1-7, **P6)** A. Nabiyan, J. B. Max, M. Micheel, J. Eichhorn, M. Wächtler, M. Schulz, C. Neumann, B. Dietzek, A. Turchanin and F. H. Schacher, Polyampholytic graft copolymers: A platform to combine sensitizers and catalysts, *in preparation*, **P7)** A. Nabiyan, J. B. Max, F. H. Schacher, Double Hydrophilic Copolymers – Synthetic Approaches, Architectural Variety, and Application Fields, *Chem. Soc. Rev.*, **2022**, DOI: 10.1039/D1CS00086A.

Hybrid materials promise high tunability and performance by combining distinct characteristics with often synergistic effects. By controlling the composition and interactions between components, hybrid materials have already been tailor-made for industrial applications, going beyond fundamental research.^{43-46, 60, 179, 181} While inorganic materials are known to tune the stability, thermal, magnetic or electrical properties, the organic component often tune the hydrophilic/hydrophobic balance or acts as a matrix.^{45, 46} In this respect, polyelectrolytes are often used in water-based hybrid materials acting as dispersants,^{9, 11, 12, 47} stabilizers,^{48, 49} templates and matrices,^{50, 51} and are found in biomedical or catalytic applications.⁵¹⁻⁵³ The above described polyampholytic graft copolymers will be introduced in unprecedented hybrid materials. In a ‘lego-like’ building block approach,¹⁸² the tailor-made macromolecules will be combined with molecular and nanosized inorganic compounds. They will be further exploited for the template assisted synthesis of defined NPs. Both the physical and chemical linkage will be discussed, and their potential applications revealed.

3.1 Smart amphiphilic dispersants

Carbon nanomaterials, *e.g.* CNTs or graphene, exhibit beneficial electrical and electrochemical properties,²⁴⁴ and their combination with amphiphilic polyelectrolytes gives promising hybrid materials for utilization in biosensors.²⁴³ Hydrophobic segments can often attach non-covalently to the aromatic surface of CNTs *via* π - π or π -CH interactions,²⁹⁵ while the electrolytic block ensures solubility and acts as a host matrix for rather polar biomolecules. By employing such polymers, stable dispersions in water can be obtained, *e.g.*, phenoxy-functionalized dextrans are used for the solubilization of single walled CNTs.²⁹⁶ Since

3. PDha-based graft copolymer based hybrid materials and applications

amphiphilic PDha-g-EOct₇₀ already displayed self-assembly due to the presence of non-polar alkyl chains, this polymer appears to be a suitable dispersant for hydrophobic CNTs in water.

For this, dispersions were prepared by mixing an equivalent volume of PDha-g-EOct₇₀ aqueous solution (5 g/L, pH = 12) and MWCNTs (1 g/L, water, pH = 12) *via* sonication, as illustrated in **Figure 31 A**. While MWCNTs quickly settle in water, stable dispersions were obtained by this process as shown in the corresponding photographs (**Figure 31 B**). TEM micrographs (**Figure 31 C**) further visualize the successful dispersion, showing individual MWCNTs with a length of several hundreds of nm, which are presumably coated by PDha-g-EOct₇₀. Since the graft copolymer behaves like a polyanion at pH 12, the negative ζ -potential of the dispersed particles (-22.5 ± 1.8 mV) indicates the coverage of the MWCNTs. The presence of the polymer was further proven *via* thermogravimetric analysis (TGA), allowing the amount of organic matter existing in the hybrid materials to be determined, as shown in **Figure 31 D**.

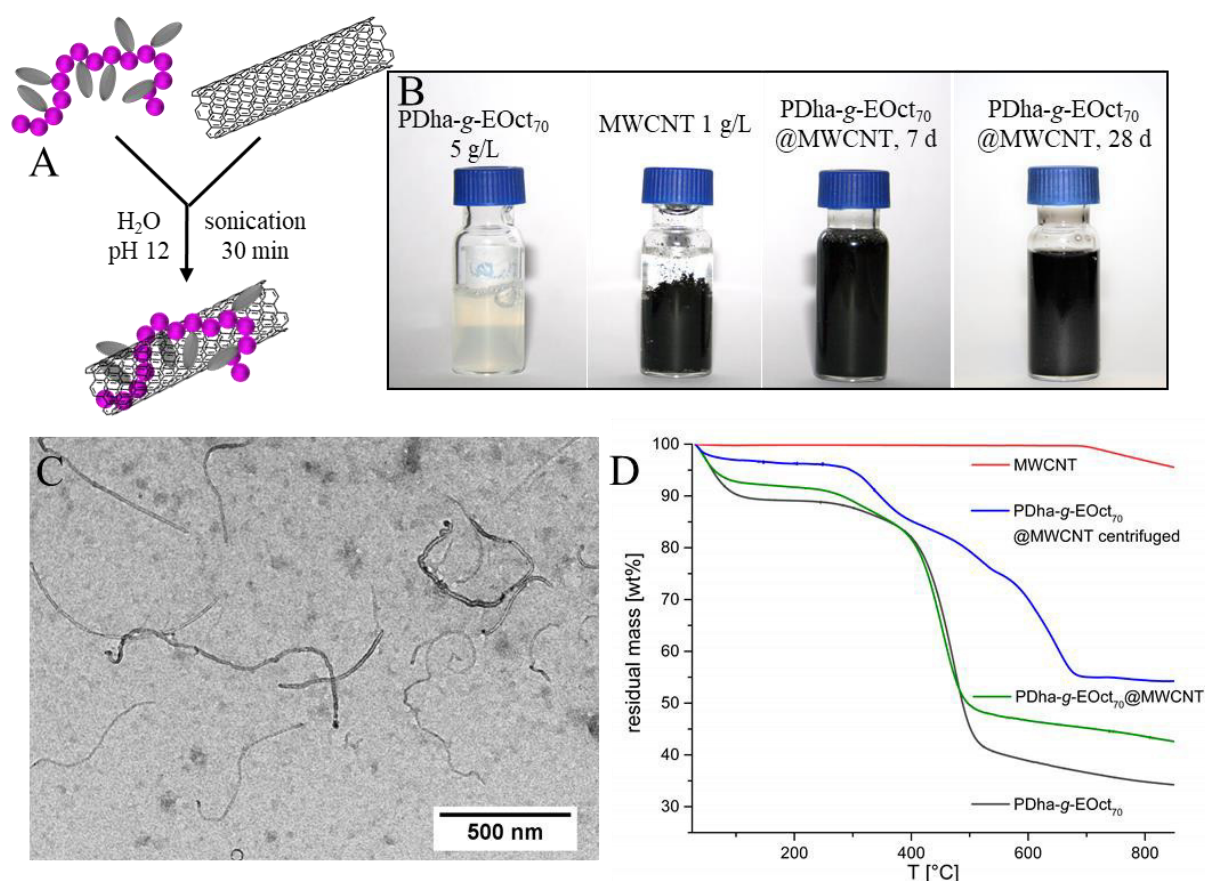


Figure 31: Preparation of PDha-g-EOct₇₀@MWCNT hybrid materials by sonication (A). Photographs (B) show the stable dispersions, even after 28 d of storage compared to pristine MWCNTs in water. TEM micrographs reveal individual MWCNTs (C) and from TGA measurements (D) the presence of the graft copolymer was proven. Adapted from Polym. Chem., **2019**, 10, 3006, with permission of The Royal Society of Chemistry.

The PDha-g-EOct₇₀@MWCNT dispersion was compared with the pristine graft copolymer as well as the pure MWCNTs and all measurements were performed under a nitrogen atmosphere. Before the TGA measurement, the dispersion was treated in two different ways to remove any

3. PDha-based graft copolymer based hybrid materials and applications

salts and to evaluate the amount of unbound polymer. To remove any salt impurities present, the dispersion was precipitated by the addition of 0.5 M HCl and washed several times with Milli-Q water. In another approach, the stable dispersion was centrifuged until precipitation occurred, before also being washed. Afterwards, the resulting materials were freeze-dried. The pristine MWCNTs are thermally stable and the remaining mass stays constant upon heating up to a temperature of 700 °C. For the graft copolymer and the hybrid material, two decomposition steps are observed. The first one, up to 100 °C, can be explained by the evaporation of remaining water, while the second one at around 250 °C corresponds to the decomposition of PDha-g-EOct₇₀ itself. Comparing the weight loss between 250 and 700 °C gives clues about the total mass of the polymer present in the hybrid material, being 52 wt% for PDha-g-EOct₇₀, 46 wt% for precipitated PDha-g-EOct₇₀@MWCNT, and 41 wt% for the one that was centrifuged. The difference in the remaining mass of the two distinctly purified PDha-g-EOct₇₀@MWCNT samples indicates that there is unbound graft copolymer in the solution being removed through centrifugation. Here, a composition of 80 wt% polymer and 20 wt% MWCNTs was calculated for PDha-g-EOct₇₀@MWCNT (centrifuged). Since the initial ratio was 5:1 (m/m), this further suggests the presence of some remaining free polymer in solution. Since, the graft copolymer features pH-dependent aggregation behavior with a high solubility under basic conditions and precipitation in an acidic environment due to strong hydrogen bonding,³² the ability to reversibly disperse CNTs, an example for hydrophobic components, was tested (**Figure 32**). Therefore, a PDha-g-EOct₇₀@MWCNT solution (pH 12) was slowly acidified using aqueous HCl. At a pH of 4 the spontaneous precipitation of the MWCNTs was clearly visible. However, by subsequent addition of NaOH (0.1 M) adjusting again to a pH of 12, it was possible to re-disperse the MWCNTs with brief sonication (5 min). In general, this method could be an interesting way to the purify and/or separate carbon nanomaterials by the utilization of amphiphilic PDha graft copolymers. All in all, PDha-g-EOct₇₀ was found to be a promising dispersant for hydrophobic CNTs in water and the corresponding hybrid materials have been examined. In the future, these hybrids could be implemented in biosensors.

3. PDha-based graft copolymer based hybrid materials and applications

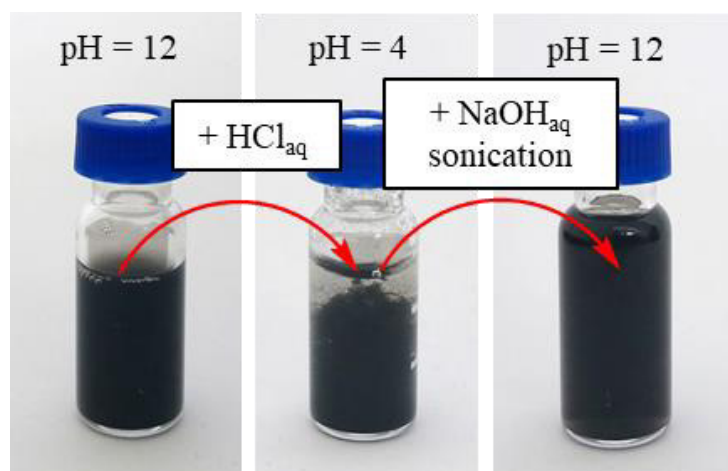


Figure 32: Photographs showing the reversible precipitation / dispersion of PDha-g-EOct70@MWCNT solution by changing the pH-value. Adapted from Polym. Chem., **2019**, 10, 3006, with permission of The Royal Society of Chemistry.

3.2 pH-controlled synthesis of AgAu nanoalloys

The synthesis of well-defined, nanometer sized inorganic composites is often supported by the utilization of structure-directing polymers as templates.^{59, 186, 191, 192} In aqueous environments, this is realized by water-soluble polymers and hydrogels featuring defined and stable micellar or three-dimensional surroundings, *e.g.*, by the formation of poly-ion complexes. This allows controlled growth with simultaneous stabilization, due to the interaction of these materials with the metal ions, before they are, for example, reduced to NPs.^{41, 196, 297, 298} In this respect, metal NPs, such as Ni, Au, Ag or AuAg alloys have been prepared within hydrogel networks or double hydrophilic block or graft copolymers as templates *via* complexation/reduction approaches.^{169, 196, 197, 202, 203, 298} Among these metal NPs, Au is gaining interest, in particular because of its outstanding physiochemical properties, the ease of surface functionalization and high chemical stability.^{251, 299} Besides Au NPs, Ag NPs are found in various applications including biomedicine, nanosensors, catalysis and cosmetics.³⁰⁰ The development of alloys of Au and Ag is promoted by complete miscibility due to almost identical lattice constants and allows the fine-tuning of optical and electronic properties.³⁰¹⁻³⁰³ As a consequence, alloys could outperform pure noble NPs, as it has been exemplarily shown in catalysis.³⁰⁴

The above described PDha-g-PEG graft copolymer presents a tunable charge and high density of functional groups alongside a high solution stability. Therefore, it is seen as a suitable template for the preparation of noble metal NPs in accordance with other graft copolymers.^{169, 203, 280} The formation of Au and Ag NPs in water is significantly influenced by the pH value and temperature,³⁰⁵⁻³¹⁰ while the composition of alloys is, to the best of our knowledge, can only be adjusted by the initial ratio of Au and Ag ions. Ag⁺ are well-known to be complexed by either carboxylates,^{200, 311} or amino moieties. However, the usually utilized [AuCl₄]⁻

3. PDha-based graft copolymer based hybrid materials and applications

preferentially interacts with positively charged ammonium groups.^{305, 306, 310, 312} Since the PDha backbone presents both an amino as well as a carboxylic group in each monomer unit, the simultaneous interaction with oppositely charged Ag^+ and $[\text{AuCl}_4]^-$ is possible. Hence, polyampholytic PDha-g-PEG could be exploited as a smart template for the synthesis of nanoalloys with a pH-controlled composition at a constant Au:Ag ratio. The hypothesized mechanism is illustrated in **Figure 33**. The metal salts will be reduced *via* different approaches and the obtained NPs characterized *via* TEM, UV-vis spectroscopy, X-ray photoelectron spectroscopy (XPS), energy-dispersive X-ray emission spectroscopy (EDX) and TGA to probe their size, shape, composition and optical properties. For the corresponding experiments, PDha-g-PEG_{1,000,28} with a high solubility over the entire pH range has been used; the PEG side-chains are characterized by an $M_n = 1,000$ g/mol.

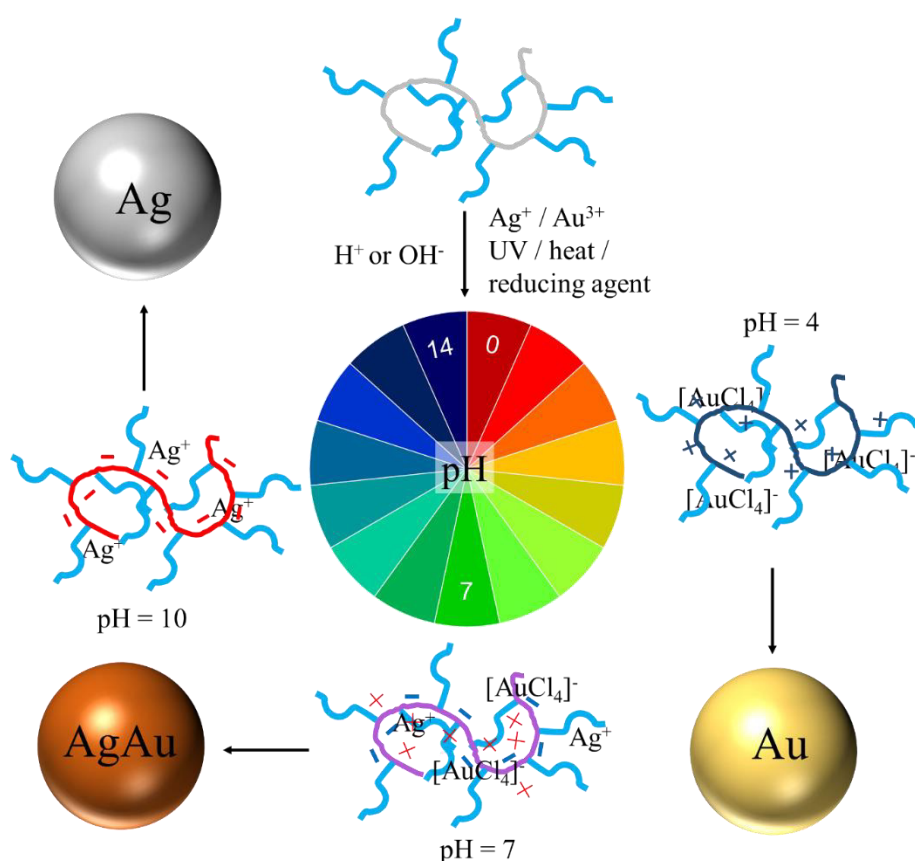


Figure 33: Synthesis of Ag and Au NPs, as well as their bimetallic alloys exploiting polyampholytic PDha-g-PEG as a template. Different reduction methods were applied: irradiation with UV light, heat or the use of a reducing agent. Adapted from *Macromolecules.*, **2020**, 53, 4511-4523. Copyright American Chemical Society.

As a starting point, the preparation of pure Ag and Au NPs was carried out to find suitable reaction conditions, especially considering the environmental pH. The pH value is an important parameter determining both the size and shape of the resulting NPs. It influences not only the association of $[\text{AuCl}_4]^-$ along the polymer chain and the accessibility of functional groups by conformational changes,^{305, 306, 310} but also the initial state of the reagents – reductant and noble-

3. PDha-based graft copolymer based hybrid materials and applications

metal containing ion complex.^{307, 308} A ratio of repeat units to metal ion of 15:1 has been chosen,³¹² and at first NaBH_4 in aqueous solution was used as the reducing agent (one equivalent per metal ion). After addition of the reductant, the clear and colorless graft copolymer/metal ion solutions become yellow or red, respectively, as a sign of NP formation. Different pH values of 10, 7, 4 and 2 were investigated and indeed, a pH-dependence was observed. It turned out that Au NPs are preferably formed under neutral and acidic conditions, exhibiting characteristic absorption maxima of the localized surface plasmon resonance (LSPR) peak between 535 and 515 nm from UV-vis, while Ag NPs are successfully synthesized under neutral and basic conditions with absorption maxima at $\lambda = 400$ and 420 nm. It should be noted that the wave length is affected by the shape and size of the NPs, as well as on their ligand environment and polymer structure.^{199, 310, 313} Next, alternative reduction approaches and the preparation of bimetallic AgAu NPs were tested using UV-vis as a meaningful characterization method (**Figure 34**).

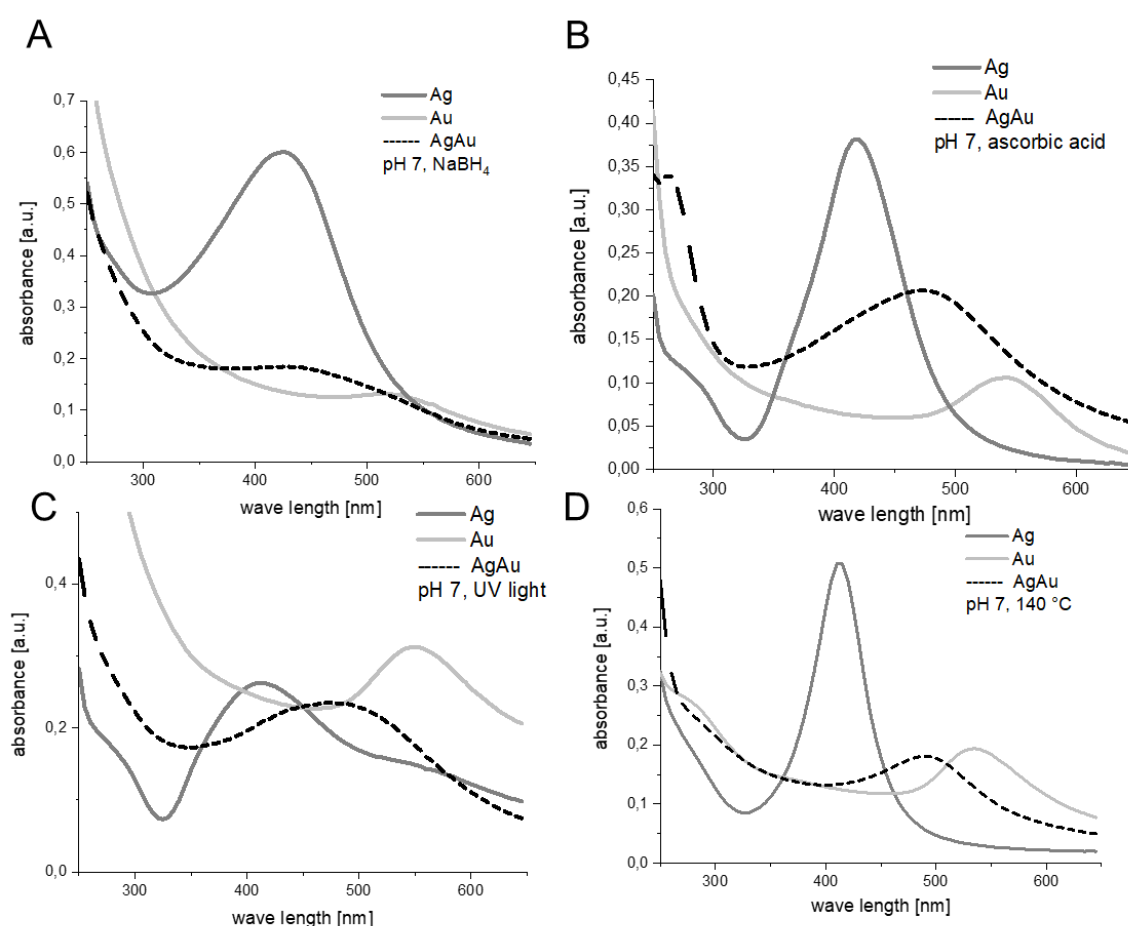


Figure 34: UV-vis measurements of Ag, Au and AgAu NPs prepared *via* different reduction approaches: utilization of chemical reduction agents (NaBH_4 (A)), ascorbic acid (B)), irradiation with UV light for 1 h (C) and heating at 140 °C for 1 h (D). Reprinted from *Macromolecules.*, **2020**, 53, 4511-4523. Copyright American Chemical Society.

3. PDha-based graft copolymer based hybrid materials and applications

Although differences in the absorbance profile were observed, all methods yield the corresponding NPs showing the characteristic absorbance maxima. Revealing a single maximum of the LSPR peak, the successful synthesis of alloys can be assumed, since the physical mixing of individual Ag and Au NP dispersions leads to a bimodal distribution.³¹⁴ Hereby, the absorption maximum of the AgAu NPs is located between the pure NPs, being slightly shifted depending on the preparation approach. This hints to a favored incorporation of Ag using NaBH₄, while thermal reduction leads to a slight excess of Au atoms. However, synthesis using ascorbic acid or light gives nanoalloys with absorption maxima close to the average values of the corresponding Ag and Au NPs.

From these findings, the controlled preparation of AgAu nanoalloys in the presence of a polyampholyte was achieved, and the composition could be controlled by adjusting the pH at a constant 1:1 molar ratio of Ag and Au ions. First, the Ag and Au-containing salts were dissolved in the graft copolymer solution. The pH of the solution was then adjusted by titration with 0.1 M NaOH or HCl to prepare the AgAu nanoalloys. Thermal reduction ($T_{\text{oil bath}} = 140\text{ }^{\circ}\text{C}$, 1 h) was applied in order to avoid any influence of a reducing agent. Differences in the solution color were already visible by eye directly after the synthesis, and are shown in the photographs in **Figure 35 A**. As expected, the colors change from yellow and orange to rather pink with the pH is decreased. These observations were supported by the corresponding UV-vis spectra (**Figure 35 B**), where a clear shift of the LSPR peak to higher wavelengths was detected with decreasing pH and the maximum changes from 460 nm at pH 12 to 540 nm at pH 4. This likely occurs as a result of an increasing incorporation of Au under acidic conditions and Ag under basic conditions. A rather stoichiometric mixture was found at pH 8, showing a maximum closest to the theoretical value of 475 nm.

3. PDha-based graft copolymer based hybrid materials and applications

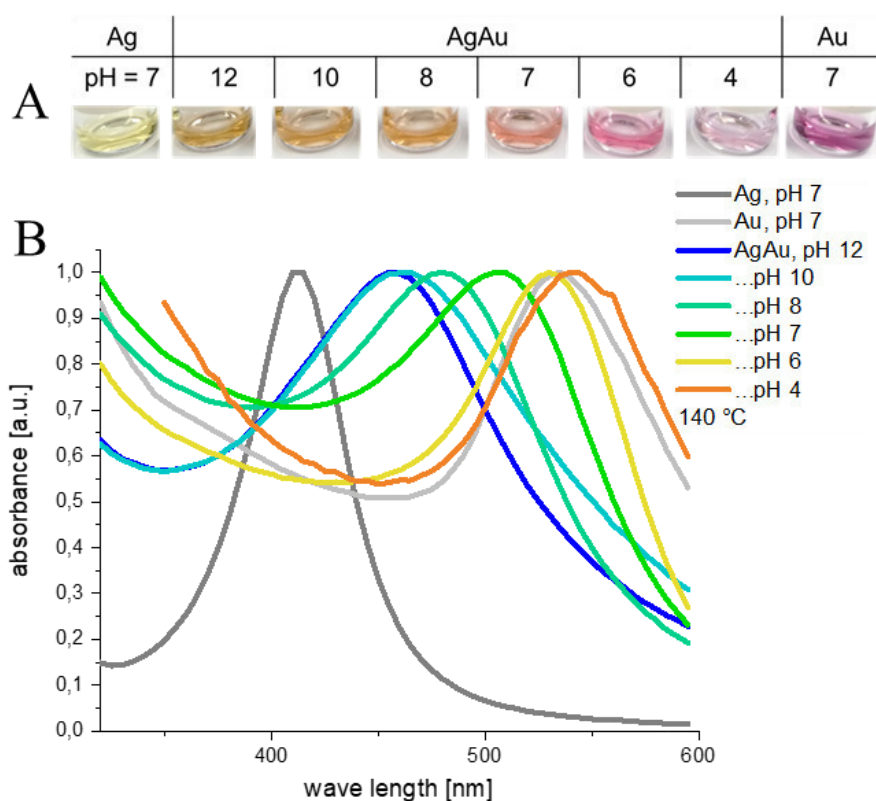


Figure 35: Photographs (A) and UV-vis spectra (B) of the Ag, Au and AgAu NP dispersions obtained at pH values between 4 and 12 at 140 °C. Adapted from *Macromolecules.*, **2020**, 53, 4511-4523. Copyright American Chemical Society.

While the color and absorbance in the UV-vis spectra hints towards the actual nanoalloy composition, the shape, size and ligand environment of the formed NPs can also influence the color and absorbance.^{199, 310, 313} Consequently, XPS was used to quantitatively determine the Ag/Au ratio of purified dispersions, where the expected Ag and Au signals are visible. The high-resolution Au 4f and Ag 3d spectra, which were used to calculate the Ag/Au ratio for all pH values, are exemplarily shown in **Figure 36 A**. The above-mentioned trends are reflected in the XPS data (**Figure 36 B** and **Table 8**), showing the pH dependent nanoalloy composition. The incorporation of Au into the alloys is preferred at pH 4 and 6 (70 at%) and also under neutral condition (pH 7) with 59 at %. Assuming the graft copolymer behaves like a polyampholyte with an excess cationic charge under these pH values (4 and 6), this would explain the favored complexation of negatively charged $[\text{AuCl}_4]^-$.²⁰¹ This corresponds to the potentiometric titration, which reveals an apparent isoelectric point at $\text{pH} \approx 8.05$. At this point an almost equal composition is found with 48 at% Au, before the Ag increases. Consequently, at $\text{pH} > 8$ the graft copolymer resembles a polyanion enhancing the complexation of Ag^+ , and hence, XPS reveals a Ag content of 67 at% at pH 10 and 12. Seemingly, the pH-dependent composition is not a linear function, but rather two plateaus are reached at pH 6 and 10.

3. PDha-based graft copolymer based hybrid materials and applications

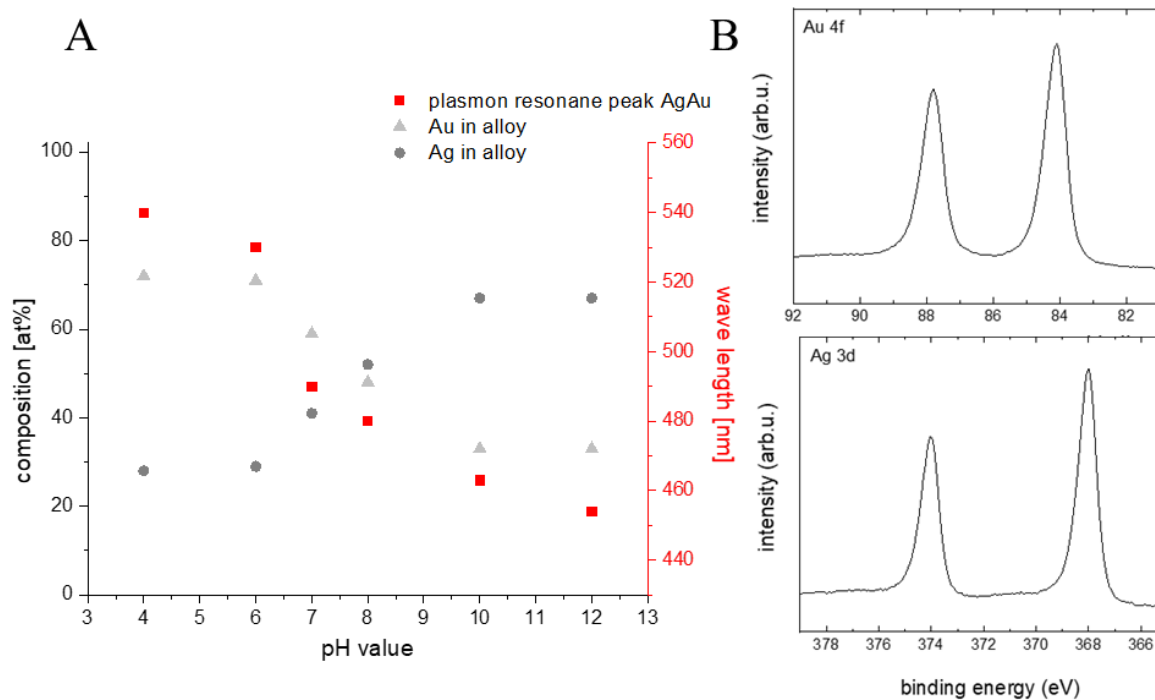


Figure 36: The composition of the NPs as determined from XPS and the absorption maxima of the LSPR as a function of the pH (A). High resolution of the Au 4f and Ag 3d signals from XPS for an AgAu nanoalloy prepared at pH 8 (B). Adapted from *Macromolecules.*, **2020**, 53, 4511-4523. Copyright American Chemical Society.

The formation of bimetallic AgAu nanoalloys was further proven by EDX measurements (**Table 8**), performed on the TEM of individual NPs. The results do, in general, reveal the same trend in the compositions, although slightly different values are found, which can be explained by distinct scales of measurement and sample preparation. In addition, the shape and size of the respective NPs was investigated *via* TEM micrographs (**Table 8**). Here, moderately dispersed NPs with a diameter between 3 and 10 nm were observed. The nanoalloys feature mostly spherical NPs, but prisms and cubes as well as larger aggregates (30 – 50 nm) were also visible. However, no pH-dependent tendency was observed.

3. PDha-based graft copolymer based hybrid materials and applications

Table 8: Summary of the composition and size of the synthesized hybrid materials obtained *via* thermal reduction. Reprinted from *Macromolecules.*, **2020**, 53, 4511-4523. Copyright American Chemical Society.

Sample / pH	Diameter d ^a [nm]	Appearance	Composition Au / Ag [at%] (± 1 at%) ^b	
			XPS	EDX
Au NPs / 7	7 ± 6	mostly spherical, some prisms as well as diffuse aggregates (d = 50 nm)	100 / 0	100
AgAu NPs/ 4	10 ± 3	spherical	72 / 28	80 / 20
AgAu NPs/ 6	10 ± 5	mostly spherical, some prisms/cubes and larger aggregates (d = 30 nm)	71 / 29	75 / 25
AgAu NPs/ 7	5 ± 2	spherical	59 / 41	-
AgAu NPs/ 8	3 ± 1	spherical, few larger aggregates (d = 40 nm)	48 / 52	55 / 45
AgAu NPs/ 10	6 ± 4	mostly spherical, few larger aggregates (d = 50 nm)	33 / 67	37 / 63
AgAu NPs/ 12	7 ± 4	spherical	33 / 67	2 / 98
Ag NPs / 7	9 ± 4	spherical	0 / 100	-

^acalculated from TEM images (at least 50 particles), ^bobtained from XPS measurements.

HR-TEM allowed a detailed look at the isometric NPs (**Figure 37**), presenting almost perfect, sometimes rounded nanocrystals displaying cube and octahedral faces ((100) and (111)). The cubic close packed structures show only minor growth defects, such as stacking faults and microtwins parallel to (111). The amount of graft copolymer shell absorbed onto the NPs was calculated from TGA, as mentioned in the previous chapter for the PDha-g-EOct@MWCNT hybrid materials. A content of 40 wt% polymer material was found for an exemplarily nanoalloy derived at pH 7, hinting towards the presence of unbound polymer in the corresponding dispersions.

3. PDha-based graft copolymer based hybrid materials and applications

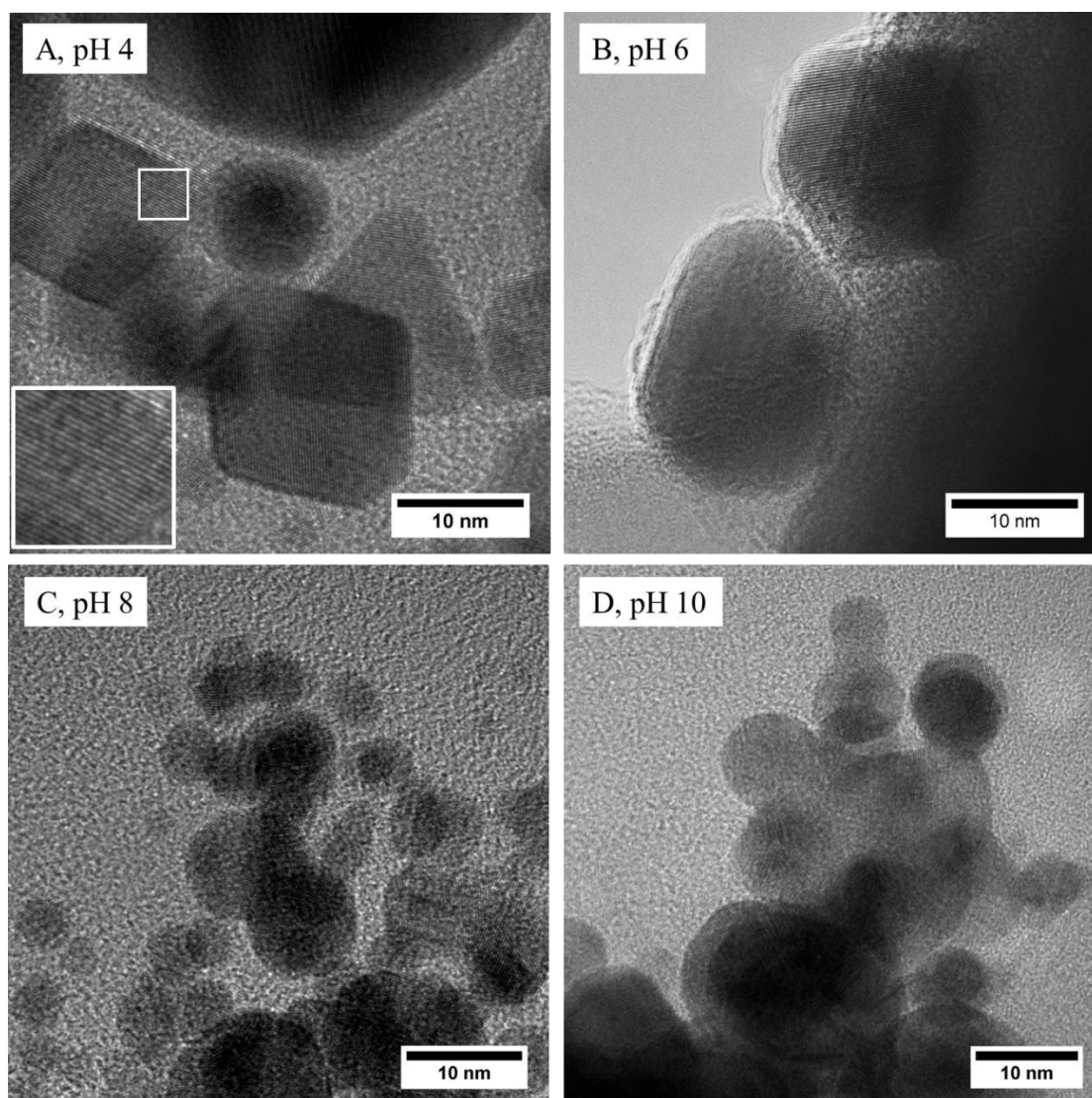


Figure 37: HR-TEM micrographs of AgAu nanoalloys obtained at pH 4, 6, 8 and 10. Reprinted from *Macromolecules.*, **2020**, 53, 4511-4523. Copyright American Chemical Society.

In summary, in **Chapter 2.2** the structure-property relationship of polyampholytic PDha-g-PEG was first described, which was then applied as template for the synthesis of defined Ag, Au and their bimetallic alloy NPs. Therefore, the synthetic route could also be extended to other inorganic (alloy) NPs. Since the functional groups of the PDha backbone feature a tunable net charge and charge density, the DHGC is able to mediate a pH-controlled synthesis of AgAu nanoalloys. Until now, the composition could only be determined by the initial ratio of Au and Ag salts. This behavior corresponds to the overall charge of the polyampholytic backbone at different pH values, which affects the amount and ratio of the Ag^+ and $[\text{AuCl}_4]^-$ complexation. As a result, the incorporation of Ag atoms is favored under basic conditions, while formation of Au is favored under acidic conditions. The composition of the alloys was qualitatively characterized *via* UV-vis measurements, and analysis *via* XPS and EDX was used to obtain quantitative results. From TEM, typical diameters of 3 to 10 nm were observed for the NPs. The herein described NP dispersions are highly stable and their synthesis shows a great

68

3. PDha-based graft copolymer based hybrid materials and applications

tunability with respect to their composition and consequently they could be further introduced in catalysis or biosensors.

3.3 Triple-responsive smart sensors

Sensing systems are often based on smart polymers, translating an external stimulus into detectable (macroscopic) changes in the chemical or physical properties.³¹⁵⁻³¹⁷ In aqueous environment, polyelectrolytes and their hybrid materials are gaining growing research interest in this field due to their high functionality, as outlined in **Table 3**. They were recently used for sensing molecular analytes,^{229, 238} or even environmental parameters, such as pH.²³¹ In this respect, the triple-responsive PDha-g-NIPAAm reported here also belongs in this class of smart, functional polymers. The interplay between its pH and temperature response described above could be exploited to detect minor local changes in the environmental pH by the ON/OFF switching of an apparent T_{CP} . Adjusting the DoF to 50 %, the resulting PDha-g-NIPAAm₅₀ graft copolymer did not show any T_{CP} at pH values above 6, but slightly shifting the pH to below 6, a temperature induced aggregation became visible (**Figure 38 A**). To investigate this behavior, PDha-g-NIPAAm₅₀ was first dissolved at pH 7, and heated to 45 °C, where no T_{CP} was observed. However, after acidification to $pH \leq 6$ by the addition 0.1 M HCl the solution became turbid. This hints towards a lower critical solution temperature (LCST). However, upon cooling the solution to 21 °C, the solution became clear again. This behavior is clearly reversible, as the T_{CP} disappears again after the addition of 0.1 M NaOH. Since its reversible response to pH changes is present within a narrow and biologically relevant range, PDha-g-NIPAAm₅₀ is a promising material for carrier systems in biomedicine.³¹⁸ This phenomenon can be explained by the partial protonation of the carboxylate moieties. While temperature-induced aggregation of NIPAAm was prevented by electrostatic repulsion of the backbone, hydrogen bonding could favor its collapse. Similar behavior was observed for PDha-g-NIPAAm₅₀ upon the addition of metal cations at pH 7 (**Figure 38 B**). Also in the absence of metal cations no T_{CP} was visible. However, after the addition of a certain amount of metal salts a clouding was observed. In this case, the repulsive forces could be overcome by the chelation of the cations through the backbone and a certain blocking of the negatively charged carboxylate groups. As described in **Chapter 2.2**, the sensitivity, as well as the shape and size of the aggregates depends on the type of heavy metal cation, presumably due to different coordination behavior influencing the inter- and intramolecular interactions within the polymer chains.^{143, 151} Exhibiting a high density of functional groups together with a high solubility in water, the PDha-g-NIPAAm₅₀ was investigated as a potential metal ion sensor. Therefore, changes in the hydrodynamic size and/or the T_{CP} should be exploited to signal changes in the presence of metal

3. PDha-based graft copolymer based hybrid materials and applications

ions at low concentrations. The quantitative and qualitative sensing of heavy metal ions is vital from both a health and environmental standpoint.²⁴⁷ This can be realized by the utilization of smart polymers containing specific binding sites for the chelation of metal ions. In response to the addition of metal ions, a change in the optical properties (*e.g.*, absorbance, fluorescence and luminescence),^{132, 319-322} the solution behaviour (*e.g.*, LCST)^{136, 323} or simply the hydrodynamic size³²⁴ will be detected. As an example, J. Cheng *et al.* applied a ampholytic poly(NIPAAm-*co*-maleic acid-*co*-vinylimidazole) terpolymer with a rather high NIPAAm content (> 90 mol %) for the recognition of different metal ions through measuring phase transition temperatures.¹³⁶

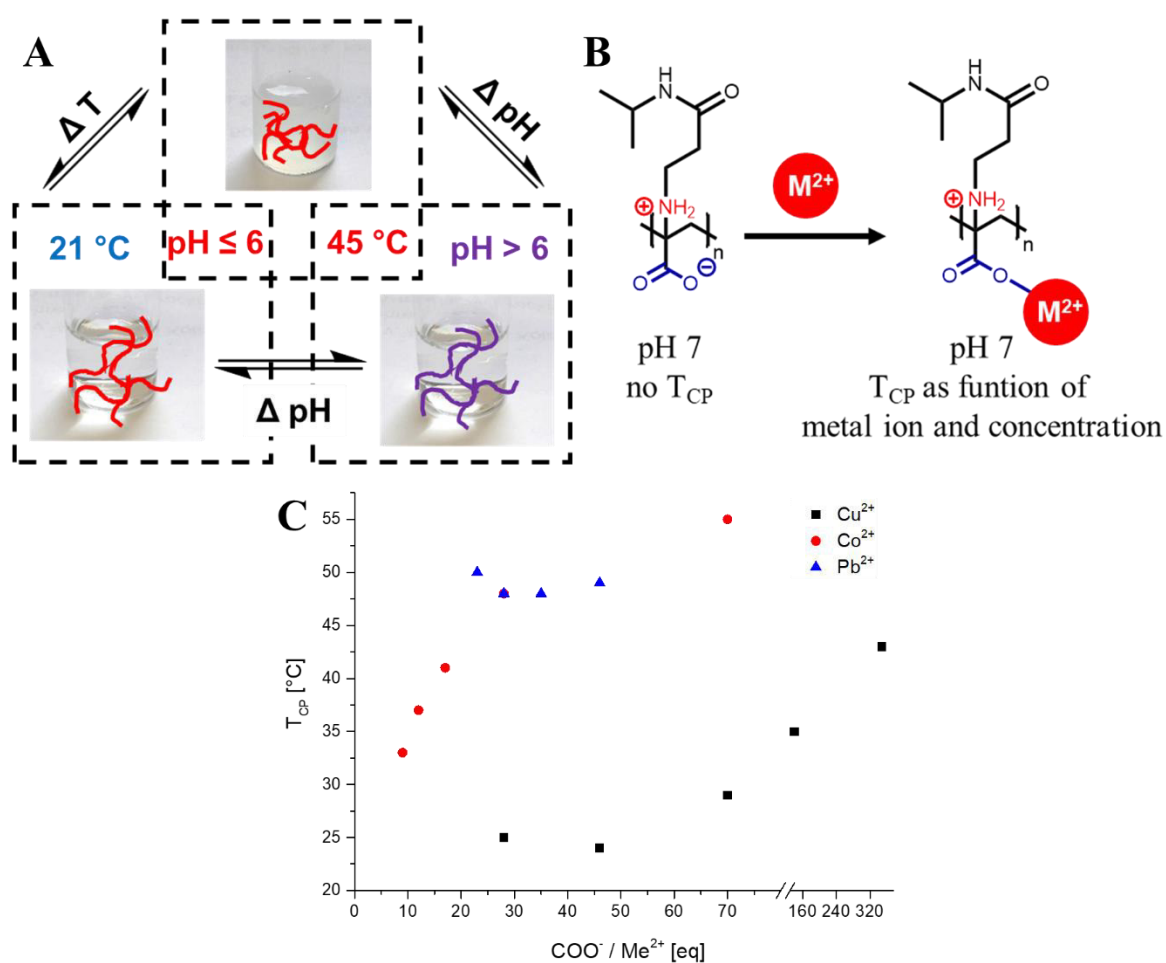


Figure 38: Illustration of the ON/OFF switching of the thermo-responsive behavior of PDha-*g*-NIPAAm₅₀ by narrow changes in the pH value (A) and by the addition of metal cations (B). The T_{CP} as a function of different concentrations of Cu²⁺, Co²⁺ and Pb²⁺ (C) was investigated. Adapted from *Macromol. Rapid Commun.*, **2021**, *42*, 2000671, with permission of WILEY-VCH Verlag GmbH & Co. KGaA, Weinheim.

The cloud point was investigated after the addition of different equivalents of Cu²⁺, Pb²⁺ or Co²⁺ (COO⁻/Me²⁺) to a solution of PDha-*g*-NIPAAm₅₀ at pH 7, as summarized in **Figure 38 C**. Indeed, distinct T_{CP} s were found, that decrease as the metal concentration increases, except for Pb²⁺. This may be explained by an increasing blocking of the negatively charged carboxylates

3. PDha-based graft copolymer based hybrid materials and applications

that prevented the aggregation. For Cu^{2+} , revealing the highest sensitivity, the T_{CP} decreases from 43 °C at a ratio 358: 1 ($\text{COO}^- : \text{Me}^{2+}$, eq : eq) to 25 °C at a ratio of 28 : 1. The detection limits were found to be 0.02 mmol/L, 0.15 mmol/L and 0.1 mmol/L for Cu^{2+} , Pb^{2+} or Co^{2+} , respectively. Further research should focus on lowering these limits, *e.g.* by changing the DoF or the pH of the graft copolymer solutions, and the recognition of further metal ions could be tested. In Chapter 3.2 the utilization of PDha-based graft copolymers as a template for the synthesis of noble metal NPs was discussed. These exhibit strong surface plasmon resonance (SPR) peaks making them applicable as optical sensors, where the corresponding core-shell hybrid materials respond to changes in the temperature, pH and the presence of metal ions (**Figure 39 A**). In this respect, an alternative readout signal to the T_{CP} could be developed. Therefore, Ag NPs ($R_{\text{H}} = 2.5$ nm from DLS) were synthesized in the presence of PDha-g-NIPAAm₅₀ and the response of PDha-g-NIPAAm₅₀@AgNP towards these stimuli investigated. First, Cu^{2+} or Pb^{2+} were exemplarily added and TEM micrographs showed the entrapment of the AgNPs within the above-described polymer/metal ion aggregates (**Figure 39 B**). M. Annadhasan *et al.* describe two processes, which can occur after the addition of metal cations to amino acid-functionalized Au and Ag NPs: one is the aggregation of the NPs by the complexation of the functional groups with the added metal ions and the other is the decoration of the functional groups on the surface with the respective cations. These processes lead either to a blue or a red shift in the SPR.³²⁵ As expected, a clear shift in the SPR peak was observed for PDha-g-NIPAAm₅₀@AgNP upon the complexation of previous described metal ions (**Figure 39 C**), revealing a blue shift in case of Cu^{2+} ($\Delta(\lambda)$ of up to 24 nm) and a red shift for Pb^{2+} and Co^{2+} . The detection limits were independent on the divalent cations, with a concentration of 0.05 mmol/L. Being covered by a triple-responsive shell, the SPR of the AgNPs is further affected by the solution pH and temperature. Upon changing the pH value, the peak shifts in general either to higher (acidic conditions) or lower (basic conditions) wavelengths. By heating, the SPR maximum decreases or even vanishes completely at pH 5 and lower, due to aggregation.

The potential of triple-responsive PDha-g-NIPAAm₅₀ as a sensor of pH and metal cations with a tunable output was investigated. The graft copolymer solution reveals changes of the hydrodynamic size and/or measurable T_{CP} , which were exploited as easily detectable signals. This works for the sensing of narrow changes in the pH as well as the type and concentration of exemplarily metal ions (Cu^{2+} , Pb^{2+} or Co^{2+}) added. Hereby, rather low detection limits of up to 0.02 mmol/L were found. The concept was further extended to PDha-g-NIPAAm₅₀@AgNP core-shell hybrid materials, exhibiting a strong SPR, that was exploited in optical sensing of

3. PDha-based graft copolymer based hybrid materials and applications

pH, the respective metal ions and temperature. The sensing could be extended to other metal cations or real-life samples, *e.g.*, natural water sources. Furthermore, the corresponding graft copolymers have great potential in temperature controlled catalytic applications.³²⁶

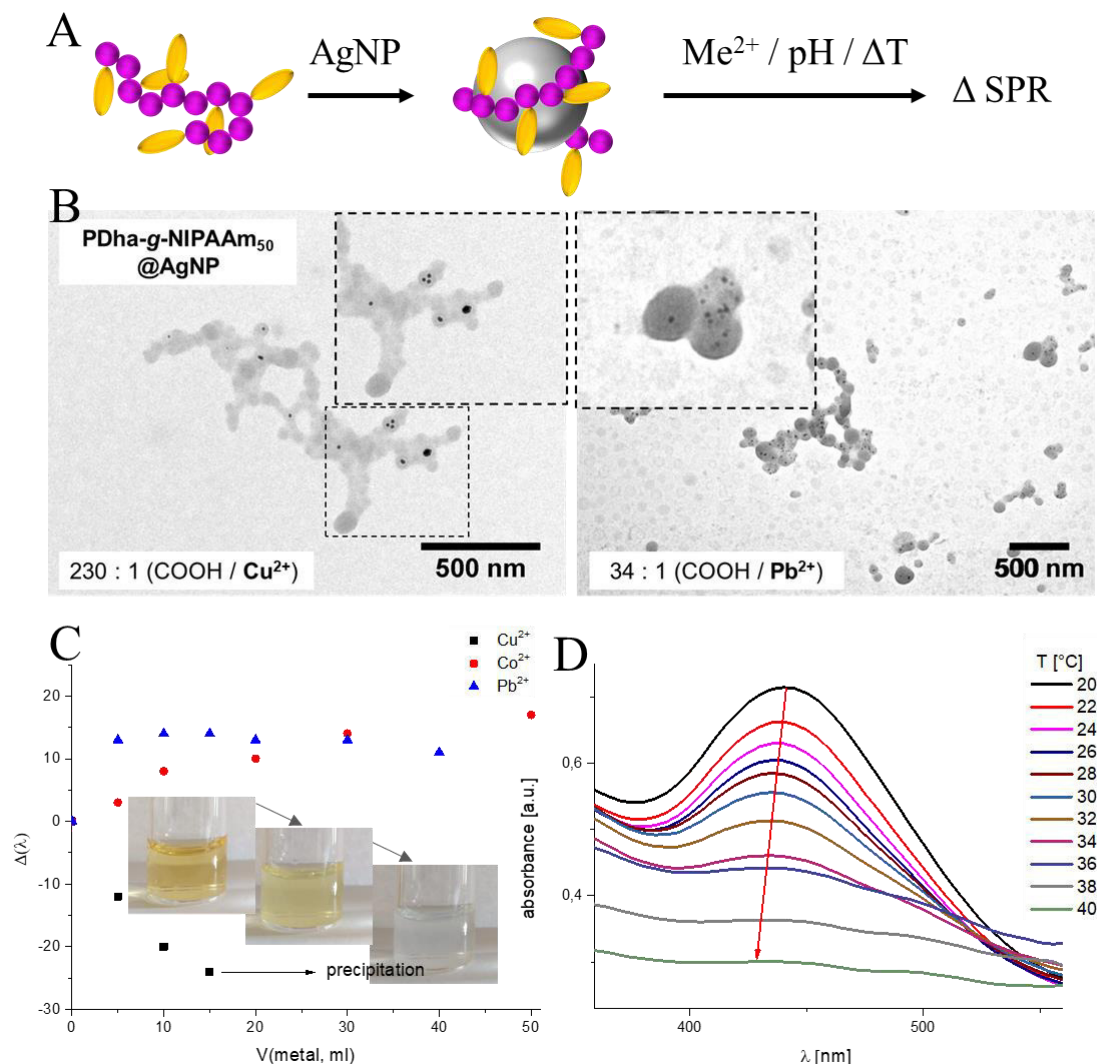


Figure 39: Schematic illustration of the construction of a PDha-g-NIPAAm₅₀@AgNP core-shell hybrids for the sensing of metal ions, pH and changes in temperature by changes of the SPR (A). TEM micrographs show three-component nanomaterials upon the complexation of Cu²⁺ and Pb²⁺ (B). The maximum of the SPR peak shifts depending on the type of metal ion and concentration (C), and is completely quenched when heated at a pH of 5 (D). Adapted from *Macromol. Rapid Commun.*, **2021**, *42*, 2000671, with permission of WILEY-VCH Verlag GmbH & Co. KGaA, Weinheim.

3.4 Soft matrices in light-driven hydrogen evolution

Sustainable clean energy is a crucial aspect to overcome global challenges, such as climate change and overconsumption. Hydrogen is a promising secondary and carbon-free energy carrier and therefore growing research interest is being focused on its production, storage and delivery.^{190, 327, 328} In this context, light-driven catalytic hydrogen evolution is a beneficial carbon-neutral method, based on water and harnessing solar energy.²⁰⁷ The first example of light-induced water splitting was described by A. Fujishima and K. Honda in 1972, using a TiO₂ electrode under UV-light irradiation.³²⁹ From then on, great developments have been made to improve these systems, *e.g.* approaching the harvesting of visible-light, through bandgap engineering,³³⁰ the utilization of photosensitizers,³³¹ the introduction of co-catalysts,²¹¹ electron relays,²¹² or the use of novel semi-conduction materials.³³² The efficiency of multi-component hybrid materials relies on the immobilization of the individual components within a suitable matrix, typically based on solid substrates including carbon nanomaterials,³³³⁻³³⁵ metal oxides,^{336, 337} or semiconductors.³³⁸ Although water-soluble and presenting potential binding sites for diverse components, the utilization of polyelectrolyte-based soft matrices has remained rather unexplored.^{51, 209, 216-218} In this respect, the two novel double acidic graft copolymers, PDha-g-PhA₆₅ and PDha-g-AMPS₂₅, prepared in this work, were tailor-made matrices for light-driven hydrogen evolution, and are as shown in **Figure 40**. The side-chains were chosen in order to promote a high solubility in an aqueous environment and to potentially facilitate a proton transfer.^{276, 277} Furthermore, the phosphonic acid moieties are strong ligand groups,^{278, 279} outperforming carboxylic ones,³³⁹ and can therefore form stable core-shell hybrid materials in combination with photocatalytically active TiO₂ NPs. While the utilization of PDha-g-PhA₆₅ will be discussed in the context of multi-component core-shell materials for the visible-light-driven HER, PDha-g-AMPS₂₅ will be introduced as a universal soft matrix for a multitude of photocatalytically-relevant components resulting in a highly efficient HER.

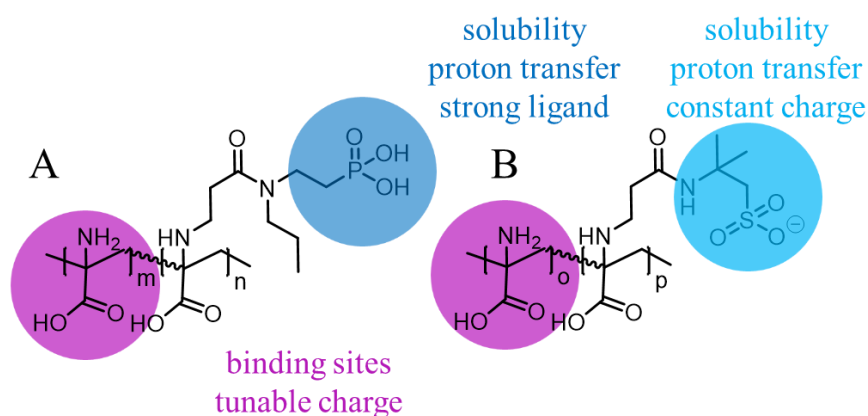


Figure 40. Structures of PDha-g-PhA (A) and PDha-g-AMPS (B) and the proposed features of the corresponding functional groups of the graft copolymers.

3. PDha-based graft copolymer based hybrid materials and applications

Multi-component core-shell hybrid materials for visible light-driven HER

TiO₂ was the first material applied in light-driven water splitting,³²⁹ and is still attracting tremendous interest in this field, being chemically stable, non-toxic and low in cost.³⁴⁰⁻³⁴² However, its utilization was limited earlier due to the use of UV light and the light harvesting of a broader solar energy spectrum is desired. Considering the above-mentioned possibilities to enhance the light-driven hydrogen evolution, TiO₂ can be tuned in order to use visible light by the careful selection of cocatalysts and sensitizers. Recently, the combination of TiO₂ and molybdenum sulfide was found to be a promising composite system.³⁴²⁻³⁴⁵ Thiomolybdates, *e.g.*, [Mo₃S₁₃]²⁻ or [Mo₂S₁₂]²⁻, typically carry a high number of active sites allowing homogenous hydrogen evolution, where already high turnover numbers (>41,000) were found.³⁴⁶⁻³⁴⁸ Polyampholytic PDha-g-PhA₆₅ will be introduced to combine these two low-cost catalysts, as well as Eosin Y (EY) as a dye sensitizer into an unprecedented multicomponent core-shell hybrid materials. The phosphonic acid side-chains will act as a strong anchoring group for TiO₂ to obtain highly stable dispersion,³³⁸ while the amino moieties of the PDha backbone physically interact with the negatively charged EY and [Mo₃S₁₃]²⁻ on the shell. This is a promising and versatile system for visible light-driven catalysis improving the interaction between catalyst, cocatalyst and sensitizer. Although TiO₂ was already combined with EY, the drawbacks of insulation, quenching and stability issues could be solved by a suitable way of interaction.^{327, 349-351} Similarly, EY as a photosensitizer was applied together with MoS₂,³⁵² but experiments with [Mo₃S₁₃]²⁻ failed as a possible result of rather weak interaction.³⁴⁸

At first, the pristine graft copolymer/TiO₂ based core-shell hybrid materials were prepared and characterized. Therefore, commercially available TiO₂ NPs were coated with PDha-g-PhA₆₅ by ultrasonication and two different ratios have been tested: 5:1 and 15:1 (polymer: TiO₂, m/m). The presence and amount of the organic shell material was investigated *via* TGA measurements under air (**Figure 41 A**). After removal of any free polymers in the PDha-g-PhA@TiO₂ dispersion through centrifugation and washing steps, the remaining material was compared with the pristine polymer and NPs. Rather high polymer contents of 29 and 66 wt% were determined for the 5:1 and 15:1 PDha-g-PhA@TiO₂ hybrids, respectively. TEM and DLS (**Figure 41 B and C**) verified the presence of the graft copolymer shell. The TEM micrographs show individual TiO₂ with an average radius approximately 11 nm surrounded by an organic layer with a thickness of several nm. DLS also revealed an increase in the R_H from 11 to 38 nm after the attachment of the polymer. A correspondingly large increase in size could be explained by the formation of multilayers or chain expansion of PDha-g-PhA₆₅.

3. PDha-based graft copolymer based hybrid materials and applications

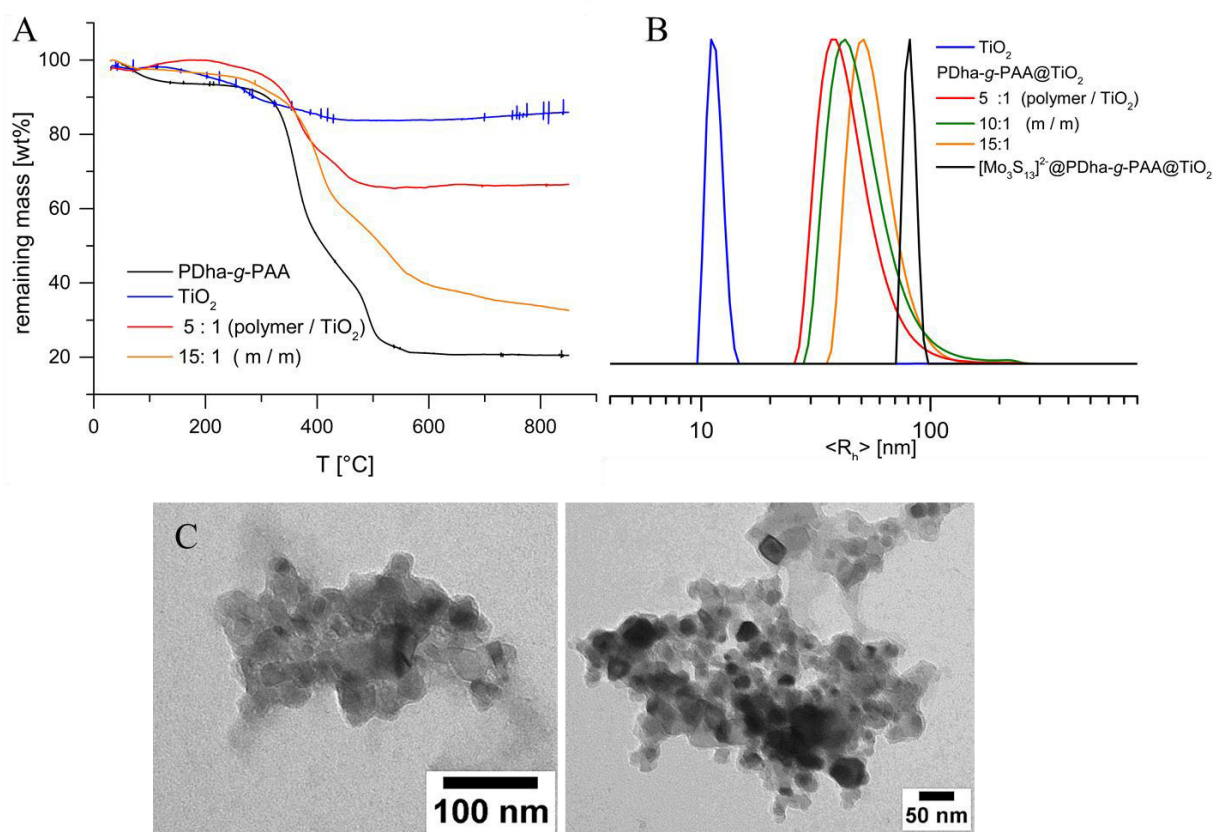


Figure 42. TGA thermograms of PDha-g-PhA, TiO₂ and PDha-g-PhA@TiO₂ with an initial ratio of 5:1 and 15:1 (PDha-g-PhA to TiO₂, m/m) (A) and corresponding R_H from DLS (B). TEM micrographs show PDha-g-PhA@TiO₂ hybrid materials with an initial ratio of 5:1 (PDha-g-PhA to TiO₂, m/m) (C). Adapted from Chem. Eur. J., 2021, 27, 1-7, with permission of WILEY-VCH Verlag GmbH & Co. KGaA, Weinheim.

In order to overcome the recombination of photoexcited carriers, molecular $[\text{Mo}_3\text{S}_{13}]^{2-}$ clusters were introduced as a cocatalyst, in accordance with previous work,²⁰⁹ on the shell of PDha-g-PAA@TiO₂ (**Figure 42 A**). The graft copolymers should act as a linker between both catalysts, both solubilizing the negatively charged thiomolybdate and anchoring on the TiO₂ NP surface, resulting in stable dispersions. This assumption was confirmed by TEM of the solubilized $[\text{Mo}_3\text{S}_{13}]^{2-}$ and $[\text{Mo}_3\text{S}_{13}]^{2-}$ @PDha-g-PAA@TiO₂ three-component hybrid materials (**Figure 42 B-D**). The corresponding micrographs show the presence of dark spots, presumably presenting $[\text{Mo}_3\text{S}_{13}]^{2-}$ clusters, with a distinct contrast within the shell of the above described PDha-g-PAA@TiO₂. The materials were further characterized *via* ζ -potential measurements to further ascertain whether the attachment was successful by regarding the overall charge. TiO₂ NPs reveal a slightly negative charge of -8 ± 2 mV, decreasing to -20 ± 1 after the addition of the graft copolymer, which could be explained by the negatively charged carboxylic acid and phosphonic acid groups. After decoration of the core-shell material with anionic $[\text{Mo}_3\text{S}_{13}]^{2-}$, the ζ -potential further decreases to -32 ± 1 mV and finally to -37 ± 1 mV after the attachment of EY, indicating the successive incorporation of the different components was successful. Although electrostatic repulsion of the negatively charged compounds may be expected, the

3. PDha-based graft copolymer based hybrid materials and applications

polyampholytic PDha backbone still contains positively charged $-\text{NH}_3^+$ at the respective pH of 7-8.³² This would in turn favor the binding of the individual compounds by electrostatic attraction. As described in **Chapter 3.2**, XPS was used as a powerful characterization technique to determine the composition and interaction of the individual materials. **Figure 42 E-G** presents some exemplarily C 1s, P 2p, Mo 3d, N 1s, and O 1s spectra of PDha-g-PAA, PDha-g-PAA@TiO₂, and [Mo₃S₁₃]²⁻@PDha-g-PAA@TiO₂. In the Ti 2p spectra, the doublet was assigned to TiO₂, with Ti 2p_{3/2} at a binding energy of ~459 eV and Ti 2p_{1/2} at a binding energy of ~464.5 eV. The binding energy difference of 5.5 eV between those two peaks of TiO₂ fits well to values found in literature (ΔE from 5.5 to 5.8 eV).^{278, 279} After the grafting of PDha-g-Pha onto the TiO₂ NPs, no significant changes are observed in the Ti 2p spectrum, but a P 2p signal was detected, which was not observed for the TiO₂ reference particles. This confirms the presence of the phosphonic acids on the modified TiO₂ particles and interestingly, the binding energy of phosphonic acid is shifted towards lower binding energies upon coating onto TiO₂ from 133.8 eV for free PDha-g-PAA to 132.9 and 133.4 eV for PDha-g-PAA@TiO₂ and [Mo₃S₁₃]²⁻@PDha-g-PAA@TiO₂, respectively. The observed downshift is another indication for the successful grafting using phosphonic acid as an anchoring group.^{278, 279}

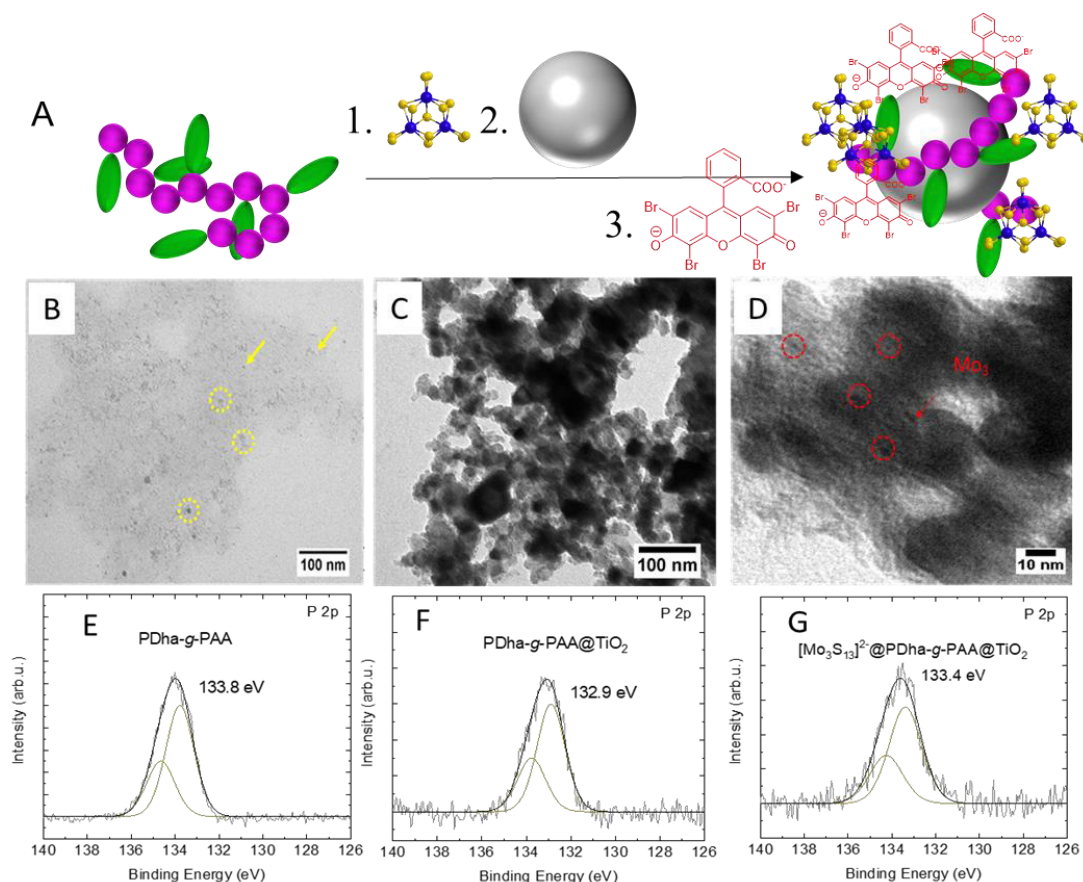


Figure 42. Synthetic route towards [Mo₃S₁₃]²⁻@PDha-g-PhA@TiO₂ (A), TEM micrographs of [Mo₃S₁₃]²⁻@PDha-g-PhA (B), and [Mo₃S₁₃]²⁻@PDha-g-PhA@TiO₂ (C and D) and XPS spectra of P 2p of PhA in PDha-g-PhA (E), PDha-g-PhA@TiO₂ (F), and (G) [Mo₃S₁₃]²⁻@PDha-g-PhA@TiO₂. Adapted from Chem. Eur. J., **2021**, 27, 1-7, with permission of WILEY-VCH Verlag GmbH & Co. KGaA, Weinheim.

3. PDha-based graft copolymer based hybrid materials and applications

After careful construction of the hybrid material, its performance in light-driven hydrogen evolution was investigated using triethanolamine (TEOA) under LED light irradiation (530 ± 50 nm). The outcome using this novel system in terms of the hydrogen product rate and turnover number (TON) as a function of time is depicted in **Figure 43 A and B**, respectively. In general, TiO_2 is inactive under visible light and its combination of EY suffers from a poor interaction and loading capacity.³⁵³ The physically absorbed dye may even desorb into solution during the irradiation resulting in a quick degradation because of the formation of unstable anionic EY^- radicals. As expected, both the bare TiO_2 , as well as the mixture of TiO_2 with EY, shows no to only trace amounts of H_2 evolution activity under visible light, while it was significantly enhanced upon coating with the graft copolymer. Hereby, average rates of 0.301 and 0.276 $\text{mmol g}^{-1} \text{h}^{-1}$ for the ratios of 5:1 and 15:1 PDha-g-PAA to TiO_2 (m/m) were found, respectively, as a possible result of a more effective EY loading through the polyampholytic shell. Even though the material already showed great potential in visible light-driven hydrogen evolution, the efficiency was further improved by the addition of the $[\text{Mo}_3\text{S}_{13}]^{2-}$ clusters. As a control experiment, the physical mixture of $\text{EY}/\text{TiO}_2/[\text{Mo}_3\text{S}_{13}]^{2-}$ was tested, and no hydrogen evolution was observed. However, the TON as the ratio of $[\text{H}_2]/[[\text{Mo}_3\text{S}_{13}]^{2-}]$ reached a value of over 500 for the $(\text{EY}/[\text{Mo}_3\text{S}_{13}]^{2-})@\text{PDha-g-PAA}@\text{TiO}_2$ four-component hybrid material with a continuous hydrogen production over 20 h irradiation. Through the co-catalyst, this is significantly higher than compared to the system without the $[\text{Mo}_3\text{S}_{13}]^{2-}$ (~79 times higher). In accordance with literature,¹⁶⁸ the catalytic activity was even further enhanced by the utilization of MeOH/water solvent mixture under otherwise unchanged conditions, where the active catalytic species may be more stable.

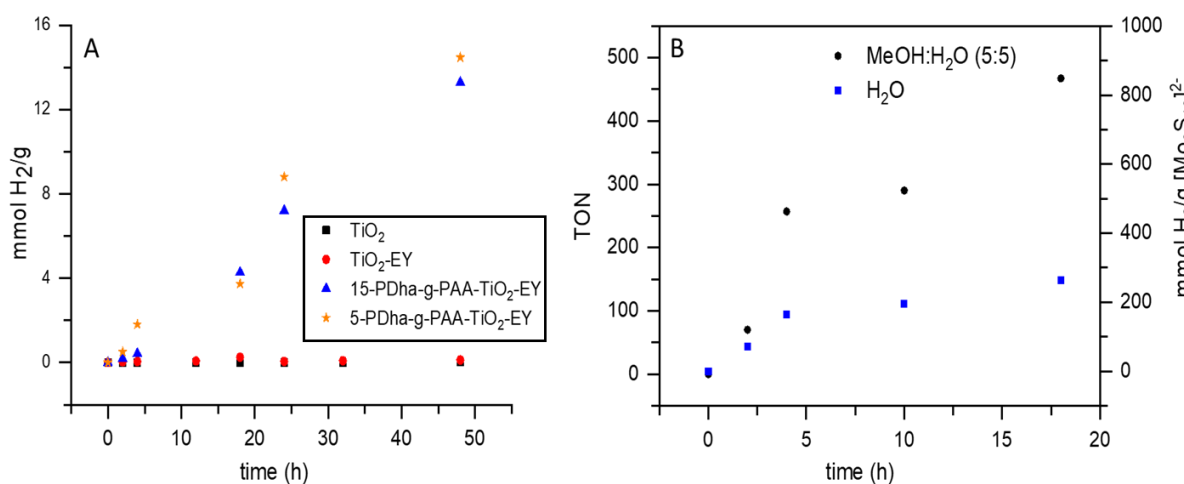


Figure 43. Hydrogen evolution rates for (A): TiO_2 , TiO_2/EY , and $\text{EY}@\text{PDha-g-PAA}@\text{TiO}_2$ with different initial weight ratios (15:1 and 5: 1, m/m) of PDha-g-PAA to TiO_2 in water and (B): Hydrogen evolution rates and the TON, is defined as moles of H_2 produced to moles of $[\text{Mo}_3\text{S}_{13}]^{2-}$ of $(\text{EY}/[\text{Mo}_3\text{S}_{13}]^{2-})@\text{PDha-g-PAA}@\text{TiO}_2$ with an initial ratio of 5:1 (PDha-g-PAA to TiO_2 , m/m) in water and mixture of water/methanol under visible-light irradiation ($\lambda > 520$ nm), with TEOA (0.5 M) as sacrificial donor. Reproduced from Chem. Eur. J., **2021**, 27, 1-7, with permission of WILEY-VCH Verlag GmbH & Co. KGaA, Weinheim.

3. PDha-based graft copolymer based hybrid materials and applications

The polyampholytic graft copolymer, PDha-g-PhA, was applied as a tailor-made coating matrix for the construction of novel multi-component core-shell hybrid material and was used in visible light-driven hydrogen evolution. The main role of the graft copolymer featuring three distinct functional moieties, is to provide close proximity and the potential to interact for all individual elements. In this respect, a catalytically active TiO₂ core was successfully interconnected with a [Mo₃S₁₃]²⁻ co-catalyst and EY as photosensitizer. The underlying approach overcomes the necessity of covalent linking and enables hydrogen evolution under visible light irradiation, reaching TON > 500 under optimized conditions. Further, this versatile soft matrix could also be transferred to other or alternative relevant compounds in the field of water splitting for hydrogen evolution.

An universal polyampholyte-based soft matrix to combine catalysts, sensitizers and electron relays

As already mentioned above, photocatalytic systems for hydrogen production typically consist of multiple components, including photosensitizers, an electron relay mediator, a sacrificial electron donor, and a heterogeneous or homogeneous catalyst.²¹² One of the main challenges that must be addressed is that these systems should exhibit a certain stability in water combined with a high efficiency. Regarding most of the catalysts, the materials suffer from limited aqueous solubility requiring the use of organic solvents and extra organic acids to provide protons. Hence, for the application in water, modifications are necessary, which is challenging from both a design and synthesis point of view. This becomes even more significant for the application of highly hydrophobic carbon nanomaterials, such as graphene, CNT or fullerenes (C60) that are exceptionally stable and efficient, but are insoluble in water.³⁵⁴ While the enhancement of their solubility through covalent functionalization is manipulating the intrinsic properties, non-covalent approaches seem to be beneficial.²⁹⁵ Considering these aspects, polyampholytic PDha-g-AMPS₂₅, with a high functionality and solution stability will be introduced as an universal soft matrix to combine numerous photocatalytically active components exhibiting different properties. This is an unprecedented approach giving access to diverse combinations of catalysts and sensitizers and their stable dispersions. After the characterization of the hybrid materials, their performance in hydrogen evolution will be examined and the role of the polymer discussed.

The utilization of multifunctional PDha-g-AMPS₂₅ as an effective template and stabilizer for several catalytically relevant moieties, which are basically water insoluble and not stable was investigated. Both the template assisted synthesis and a building block approach of readily

3. PDha-based graft copolymer based hybrid materials and applications

prepared precursors is described for the preparation of stable hybrid material dispersions through non-covalent interactions, *e.g.*, electrostatic. The corresponding materials and their synthesis are summarized in **Table 9**.

Table 9. Summary of the PDha-g-AMPS based hybrid material dispersions.

Dispersed components	Synthesis of the hybrid materials	Characterization	Size dimension
Au NP			
Ag NP	template assisted reduction from respective metal ions	XPS, UV-vis, TEM	spherical shape, average diameters 2-4 nm (from TEM)
Pd NP			
Pt NP			
CdS	1. literature synthesis ⁵¹ 2. sonication	XPS, UV-vis, TEM, DLS	R _H = 18-20 nm (DLS) R = 15-25 nm (TEM)
[Mo ₃ S ₁₃] ²⁻	1. literature synthesis ³⁴⁶ 2. sonication	TEM, DLS	R _H 5 nm (DLS)
Pt ₃ Co	1. literature synthesis ³⁵⁵ 2. sonication	XPS, TEM, DLS, TGA	R _H = 15 nm (DLS) R = 15-25 nm (TEM)
MWCNT	commercially available sonication	TEM, TGA	> 100 nm length
C60		TEM	'small dots' several nm

The noble metal NP catalysts were synthesized from the corresponding metal ions at pH 7 using NaBH₄ as a reducing agent as described in **Chapter 3.2**, using PDha-g-AMPS as a template. The successful synthesis was proven *via* XPS and UV-vis measurements revealing the characteristic binding energies and SPR absorbances, respectively. Further, TEM micrographs show relatively narrow dispersed NPs with average diameters of 2 to 4 nm, and this is further supported by photographs that show rather clear dispersions (**Figure 44 A-D**). CdS is one of the most promising semiconductors applied in photocatalytic hydrogen evolution due to its high efficiency and low bandgap energy (2.4 eV).³⁵⁶ Therefore it was synthesized in two steps according to literature, where it was synthesized in the presence of a DHBC as a nanoreactor.⁵¹ First Cd²⁺ was successfully complexed by the graft copolymer, with DLS revealing an increase in size from R_H = 1-2 nm of the pure polymer to an R_H = 8-10 nm after the addition of the metal ion. Afterwards, Na₂S was added and the formation of the nanoaggregates was further indicated by a resulting R_H of 18-20 nm from DLS and the presence of spherical aggregates with radii of 15-25 nm was observed by TEM micrographs (**Figure 44 E**). Moreover, both XPS and UV-vis measurements confirm the successful formation of the CdS nanoparticles, which were stable over weeks.

3. PDha-based graft copolymer based hybrid materials and applications

Thiomolybdates, *e.g.* molecular $[\text{Mo}_3\text{S}_{13}]^{2-}$,³⁴⁶⁻³⁴⁸ and Pt_3Co alloy NPs,³⁵⁵ were found to be promising (co)-catalysts for hydrogen evolution in water, although being insoluble in general. However, after their preparation in accordance with literature,^{346, 355} by mixing with PDha-g-AMPS stable dispersions were formed through sonication for 30 min. Similar to the above-mentioned hybrid materials, DLS and TEM revealed the presence of the resulting aggregates. In case of Pt_3Co the R_H increased from 10 nm for the pristine nanoalloys to 15 nm after mixing with the polymer, hinting towards the formation of an organic shell, which was also visible by TEM (**Figure 43 C**).

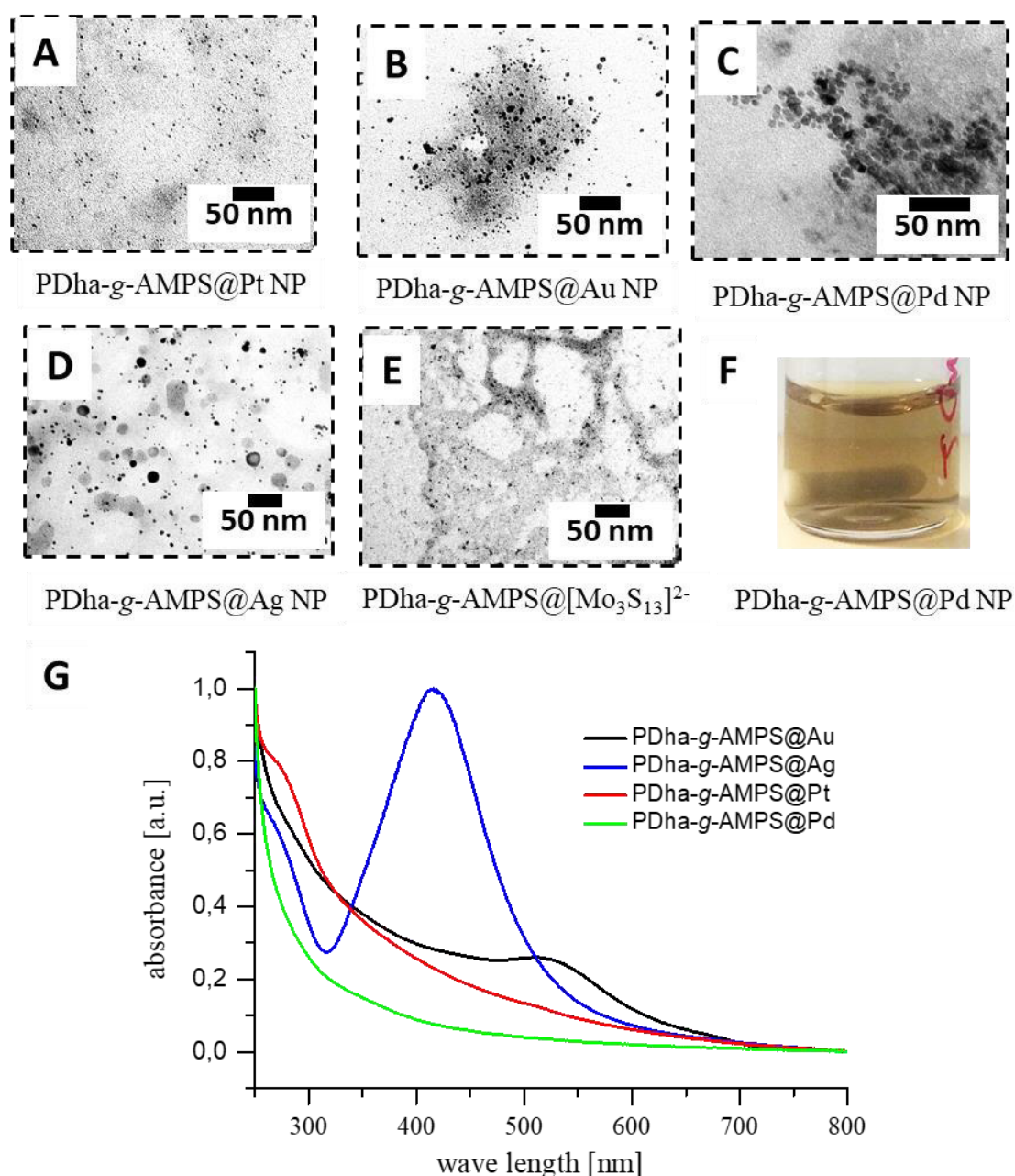


Figure 44. TEM micrographs of PDha-g-AMPS based hybrid materials containing inorganic catalysts: Pt NPs (A), Au NPs (B), Pd NPs (C), Ag NPs (D) and $[\text{Mo}_3\text{S}_{13}]^{2-}$ clusters (E). A representative photograph of a stable noble metal NP dispersion (Pd NPs) is shown in (F). The UV-vis spectra show the characteristic absorbance of the noble metal NPs (G). Adapted from P6 (manuscript *in preparation*).

3. PDha-based graft copolymer based hybrid materials and applications

Due to their outstanding electrical properties CNTs are promising support materials for electrocatalysts.²⁹⁵ Besides CNTs, C60 is also known to enhance the adsorptivity, the absorption capability in the visible light region, and the life span of photoexcited electron–hole pairs in photocatalytic systems.³⁵⁷ Hence, in addition to the described inorganic NPs and molecular cluster, commercially available hydrophobic carbon nanomaterials, *i.e.*, MWCNTs and C60, were dispersed with the assistance of PDha-*g*-AMPS. The successful dispersion was visualized by TEM, as exemplarily shown for CNT/PDha-*g*-AMPS (**Figure 45 A**), where well-separated MWCNTs were visible. Further, no precipitation was observed after several days. The amount of organic content was determined from TGA measurements under air of the pristine MWCNTs, the graft copolymer, the corresponding unmodified PDha, and the hybrid material (**Figure 45 B**) as described in **Chapter 3.1**. After removal of any free polymer through centrifugation and washing steps, a composition of 21 wt% graft copolymer and 79 wt% MWCNTs was found. Seemingly, PDha-*g*-AMPS is not only an effective dispersant for noble metal NPs but also for hydrophobic carbon nanomaterials, which are in general well known to enhance photocatalysis.^{357, 358} Therefore, three-component hybrid materials were constructed by mixing the graft copolymer, PtCo₃ NPs and MWCNTs and subsequent sonication, in order to obtain high performance catalytic systems for hydrogen evolution. The structure of the corresponding hybrids was investigated *via* TEM (**Figure 44 D**), and indicates that the individual components are connected through the polymer. A shell around the MWCNTs is visible that also contains rather dark spots being PtCo₃ NPs. In this respect, the materials are brought in close proximity by the polymer, which could facilitate mass and electron transfer to promote catalysis.

3. PDha-based graft copolymer based hybrid materials and applications

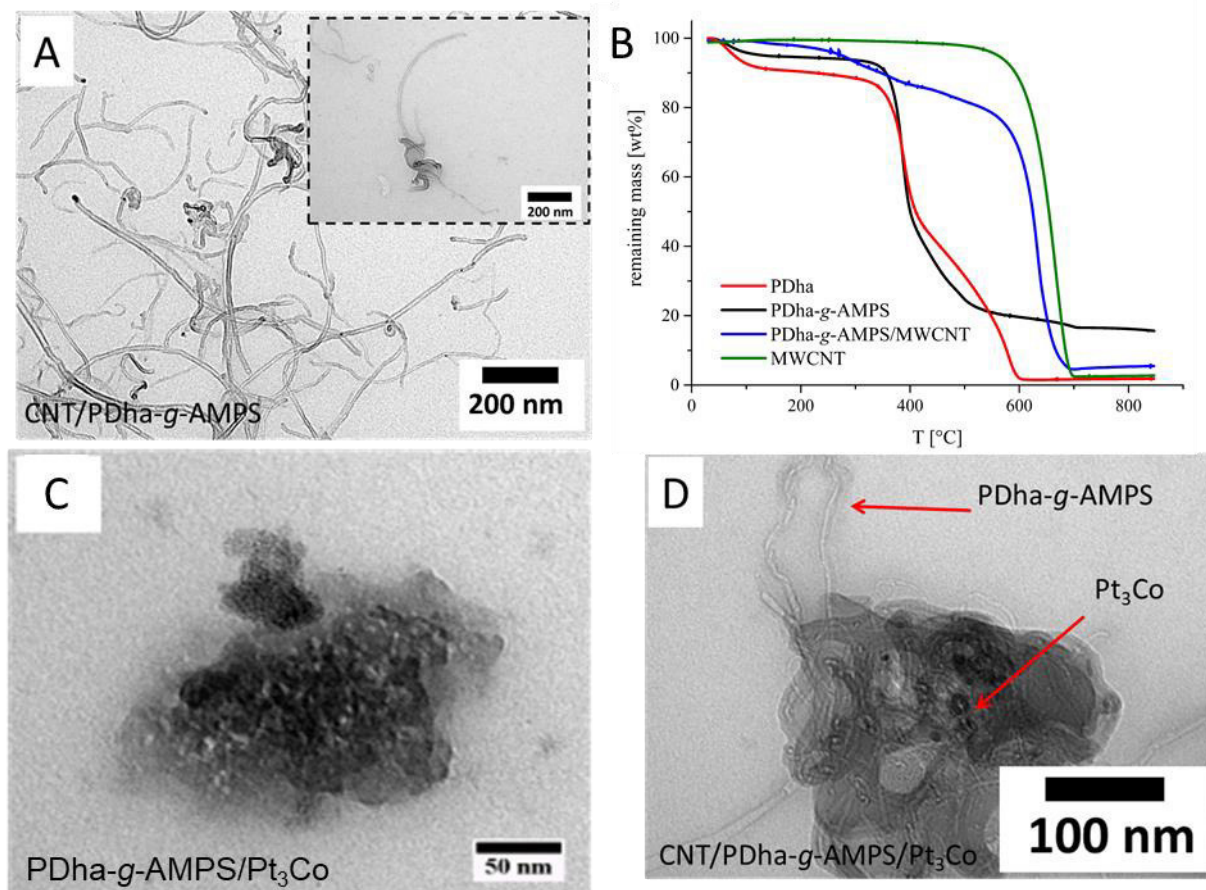


Figure 45. Investigation of three-component hybrid materials, showing the TEM micrographs of MWCNT/PDha-g-AMPS (B), PDha-g-AMPS/Pt₃Co (C) and MWCNT/PDha-g-AMPS/ Pt₃Co-based hybrid materials. TGA measurements reveal the presence of the individual components within the material. Adapted from P6 (manuscript *in preparation*).

The described catalysts and three-component hybrid materials were investigated in the presence and absence of PDha-g-AMPS. Therefore, the hydrogen production activity, as the TON value, was evaluated under LED light ($\lambda = 470$ nm, power output 5 mW/cm^2) irradiation at room temperature for 24 h. TEOA was used as a sacrificial donor and EY as a dye sensitizer (**Figure 46**), similar to the above-described system. First, an exemplarily system based on a Pt₃Co catalyst was examined in detail. As depicted in **Figure 46 A**, the TON was significantly enhanced by a factor of 7.6 after addition of the polymer (EY/Pt₃Co/PDha-g-AMPS), likely due the efficient interaction between Pt₃Co and EY, which are both immobilized on the graft copolymer. By the addition of MWCNTs, the TON was further increased, resulting in a TON of >8,000 for the polymer-containing system. This indicates that PDha-g-AMPS was again able to act as a suitable matrix for hydrophilic EY, Pt₃Co, as well as the hydrophobic MWCNTs. Since the PDha backbone features a pH-responsive polyampholyte, the influence of the pH value was also investigated. Both strongly basic and acidic conditions seem to be disadvantageous, while the highest TON was found at a pH of 8-9, revealing a significant influence of the environmental pH on the photocatalytic activity. This behavior may be

3. PDha-based graft copolymer based hybrid materials and applications

explained by the possible interaction of the graft copolymer and EY influenced by the protonation state of the two components at different pH values. Under harsh acidic conditions, both the carboxyl and amino moieties are protonated ($-\text{COOH}$ and $-\text{NH}_3^+$) and will desorb EY (also $-\text{COO}^-$). On the other hand, under strong basic conditions both the carboxyl and amino moieties will be deprotonated ($-\text{COO}^-$ and $-\text{NH}_2$) and the dye (also $-\text{COO}^-$) will not be absorbed. Hence, an intermediate pH, where the PDha backbone behaves like a zwitterion,³² is favored. However, the excited state of the electron donor agent (TEOA) and the solubility of EY itself strongly depend on the pH value. While the electron donating ability may be reduced after the protonation of TEOA, EY shows a decreased solubility under acidic conditions. Another parameter determining the hydrogen production efficiency is the loading of each individual component, and this will be further investigated.

In the next step, a variety of catalysts, which are summarized in **Table 9**, were evaluated under the optimized conditions (**Figure 46 B**). In all cases, the polymer enhances the TON remarkably, which can be ascribed to the stability of the dispersions and the close connectivity of the components through the support of PDha-*g*-AMPS. The second highest value was hereby achieved using Au NPs as the catalyst, with a 4-fold increase in the TON from 206 to 826 by the utilization of the polymer. Furthermore, C60 was tested as an alternative carbon nanomaterial to MWCNTs. Although with a TON of 3722, which is lower than for the EY/Pt₃Co/PDha-*g*-AMPS/MWCNT system, it is again higher when compared to EY/Pt₃Co/PDha-*g*-AMPS, supporting the assumption that carbon nanomaterials play a significant role in photocatalysis.³⁵⁷

3. PDha-based graft copolymer based hybrid materials and applications

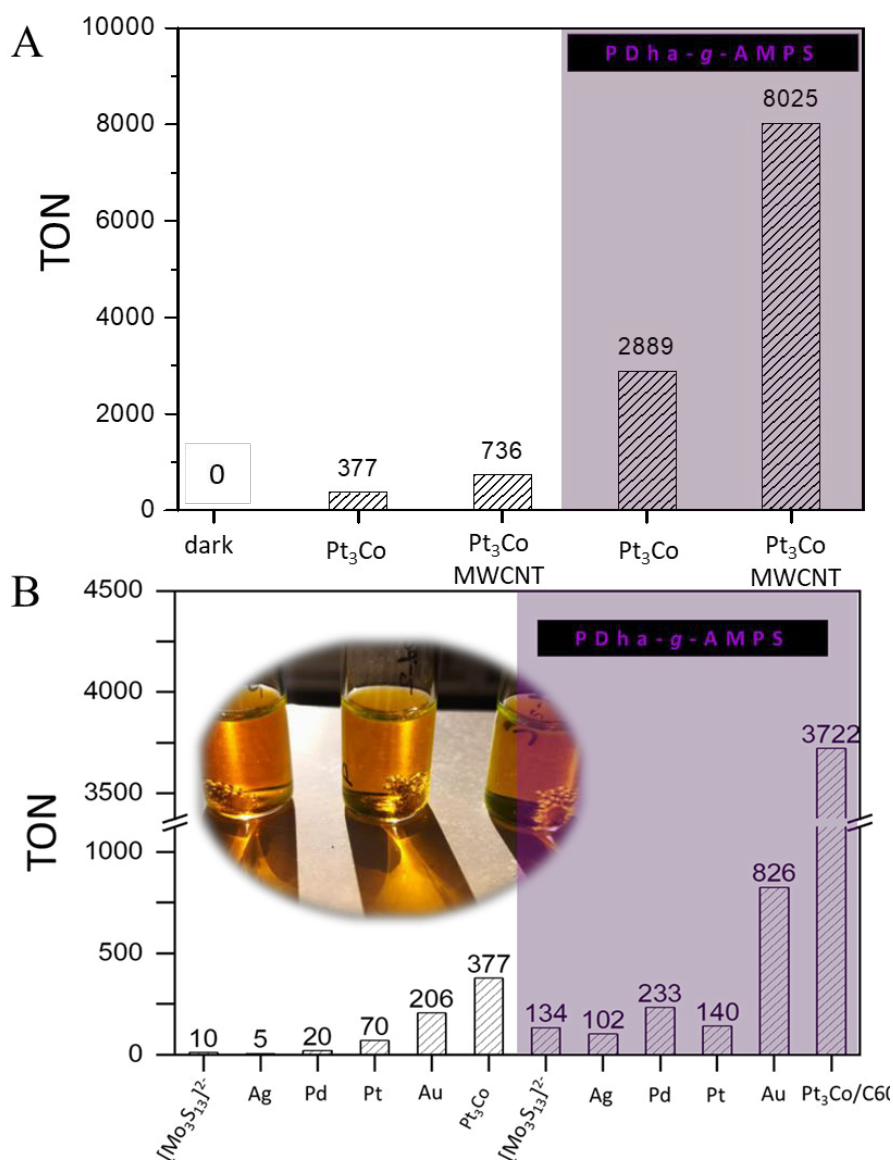


Figure 46. The photocatalytic hydrogen evolution of EY/Pt₃Co, EY/P₃Co/MWCNT, and EY/Pt₃Co/PDha-g-AMPS/MWCNT (A) and alternative catalysts (B). The photographs show bubbles indicating the evolution of hydrogen after irradiation of a photocatalytic system. The TON is defined as (moles of hydrogen produced)/(moles of catalyst) after irradiation for 24 hour. Adapted from P6 (manuscript *in preparation*).

In summary, PDha-g-AMPS₂₅ was introduced as a platform for the construction of stable photocatalytically active hybrid systems. Hereby, the graft copolymer featuring a polyampholytic backbone shows great potential as a soft matrix to connect each individual components for improved catalysis, and further permits the combination of otherwise incompatible and unexplored components. After the preparation of hybrid materials, their ability in light-driven hydrogen evolution was evaluated and the results clearly show a significant enhancement by the utilization of the polymer. Besides, the efficient interaction between a dye sensitizer (EY), Pt₃Co catalyst and carbon nanomaterials have been proven. Compared to other photocatalytic state-of-the-art systems working with EY sensitizers, the

3. PDha-based graft copolymer based hybrid materials and applications

PDha-g-AMPS-based hybrid materials can compete with and even outperform their hydrogen evolution performance (**Table 10**). Further research will elaborate the role of the polymer, *e.g.*, by theoretical calculations, and additional efforts should focus on additional material combinations as well as the optimization of other parameters (*e.g.*, irradiation time, concentration and ratio of the components).

Table 10. Photocatalytic systems based on EY as a photosensitizer described in state-of-the-art literature reports. Adapted from P6 (manuscript *in preparation*).

Photocatalytic system ^{Ref}	Sacrificial donor / Wave length of light irradiation [nm]	TON / Irradiation time [h]
Pt ₃ Co/ PDha-g-AMPS/MWCNT	TEOA / $\lambda \geq 470$	8025 / 24
mpg ¹ -C ₃ N ₄ /Pt ³⁵⁹	TEOA / $\lambda > 420$	275 / 44
[AlSiW ₁₁ (H ₂ O) ₃₉] ⁵⁻ / H ₂ PtCl ₆ ³⁶⁰	TEOA / $\lambda > 420$	473 / 20
[Co(dmbp ²) ₃]Cl ₂ ³⁶¹	TEA ³ / $\lambda > 420$	249.2 / 2
[Co(dmgh ⁴) ₂ py ⁵ Cl] ²⁺ ³⁶²	TEOA / $\lambda > 420$	900 / 14
RGO ⁶ - Co(bpy ⁷) ₃ ²⁺ ³⁶³	TEA / 505	185 / 2.5
[FeFe]-hydrogenase ³⁶⁴	TEOA / 530	60 / 4
Fe ₂ N ³⁶⁵	TEOA / 300 W	57.8 / 1
Pt / TS-1 zeolite ³⁶⁶	TEA / $\lambda \geq 420$	100 / 10

¹mesoporous graphitic (mpg), ²4,4'-dimethyl-2,2'-bipyridyl (dmbp), ³triethyl amine (TEA), ⁴dimethylglyoximate (dmgh), ⁵pyridine (py), ⁶reduced graphene oxide (RGO), ⁷bipyridyl (bpy).

In **Chapter 3**, the tailor-made PDha-based graft copolymers were introduced into various hybrid materials, each profiting from both the backbone and individual side-chain features. Hereby, the organic/inorganic hybrids were derived from either a building block or a template-assisted approach giving access to outstanding materials and advanced applications. The pH-responsive behavior of the polyampholytic backbone, controlling the aggregation behavior and overall charge, was exploited for amphiphilic PDha-g-EOct as a smart dispersant for hydrophobic MWCNTs. In case of double hydrophilic PDha-g-PEG as an intelligent template determining the composition of AgAu nanoalloys. Moreover, triple-responsive PDha-g-NIPAAm was found to be a potential heavy metal ion sensor, as the stimuli gives a measurable output. Last, PDha-g-PAA an PDha-g-AMPS present an exceptionally high solubility and charge density, rendering them suitable soft matrices in photocatalytic hydrogen evolution. The graft copolymers not only grant a high stability to the individual components, but also significantly boosts the hydrogen evolution rate, which can be explained by the successful interconnection of the catalysts and sensitizer.

4. Summary

4. Summary

Water-based polymers and their hybrid materials offer solutions for global challenges in the energy,¹⁹⁰ environmental and medical^{189, 247} sectors from highly efficient photocatalysts,⁵¹ sensors,⁸² to drug delivery systems.¹⁴¹ In the last decades, this field of research has seen dramatic growth, particularly in the implementation of polyampholytes and stimuli-responsive polymers due to their beneficial functions, versatility and performance in aqueous environments.^{41, 57, 70, 127} Within the class of polyampholytes, PDha distinguishes itself by its exceptionally high charge density, tunable charge, a dual pH- and metal ion-response, biocompatibility and reactive handles. Moreover, interacts with other polyelectrolytes, model dyes, proteins or NP surfaces.^{9, 32, 34, 54, 76, 114, 123, 248-250} These characteristics render PDha a highly interesting smart polymer for the construction of unprecedented hybrid materials for applications where a stimuli-response, a multifunctional matrix or (reversible) interactions are demanded.^{51, 165, 225} Still, the utilization of PDha is limited due to its limited solubility under acidic conditions, and its copolymers with more defined tailor-made properties are rather unexplored, due to the synthetic challenge to access such macromolecules and problematic scaling.^{32, 34, 114} From this perspective, the further development of synthetic protocols, modifications, hybridization and application of PDha is the core of this work. The overall approach renders the smart design of water-based multifunctional (hybrid) materials starting from a promising, but rather unexplored, polymer - not only to outcompete existing solutions, but also to add more functionality or different responses.

In **Chapter 2**, PDha-based copolymers were prepared *via* innovative strategies, to obtain both amphiphilic and double hydrophilic materials. The first route involved the preparation of PtBAMA-based block copolymers prior to deprotection, and the second involved the grafting of modifiers onto a readily prepared PDha backbone (**Figure 47**). In this context, double hydrophilic PDha-*b*-PEO block copolymers were prepared containing highly hydrophilic and biocompatible PEO,²⁵⁵ and a multifunctional PDha segment. Its synthesis was not successful before due to the necessary deprotection of its precursor PtBAMA-*b*-PEO resulted in the cleavage of the hydrolytically unstable ester junction. Therefore, a more stable amide junction was introduced despite being synthetically more demanding compared to their ester counterparts.²⁶⁶⁻²⁶⁸ Alternative synthetic approaches were also explored, including click reactions and advanced ATRP techniques (aqueous and SET-LRP), to overcome the limited DPs of PtBAMA and reproducibility. Indeed, the amide junction survives the harsh deprotection conditions and PEO-*b*-PDha was successfully obtained for the first time. As expected, preliminary experiments revealed its pH- and metal ion-responsive behavior through

4. Summary

the formation of nanoaggregates in an aqueous environment. Future research will examine the influence of the PEO / PDha chain lengths on the resulting solution properties and the DHBC will be tested as a highly promising material in biomedical applications,^{259, 39} or as nanoreactor,⁵¹ exhibiting the beneficial features of the polyampholytic PDha segment.

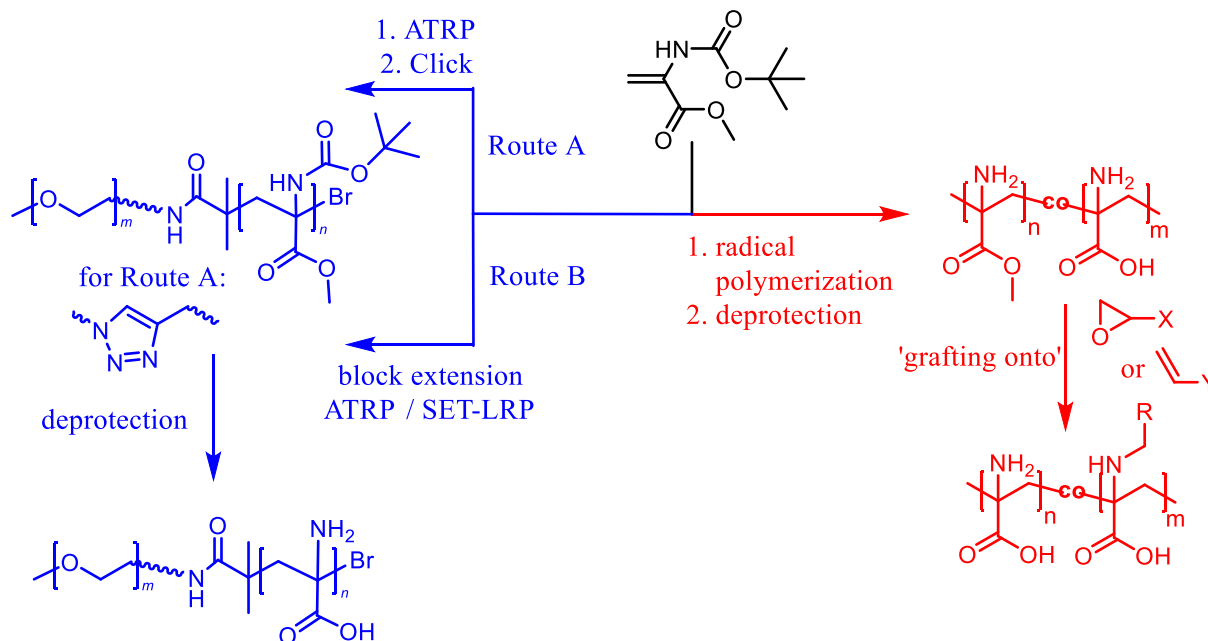
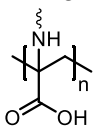
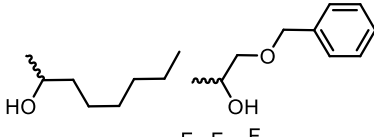
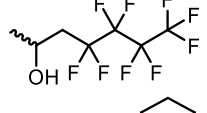
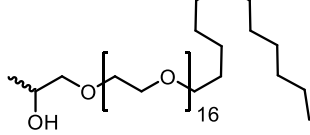
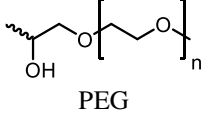
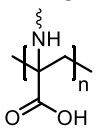
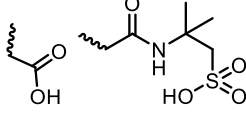
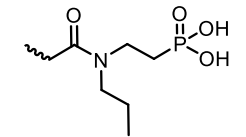
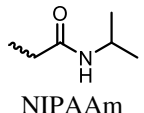


Figure 48. Strategies towards PDha-based copolymers described in this work: (i) synthesis of block copolymers obtained *via* either CuAAC click reaction of functional precursors (Route A) or the chain-extension of a macroinitiator (Route B), depicted in blue; and (ii) post-polymerization modification of a readily prepared PDha precursor in a 'grafting onto' approach.

An alternative approach was further developed based on the post-polymerization modification of the PDha backbone, which is a versatile platform for the functionalization of readily prepared reactive macromolecules.⁵⁸ From this, a broad library of PDha-based graft copolymers was prepared, representing the entire potential of a single polyampholyte by fine-tuning the hydrophobic/hydrophilic balance, the overall charge, potential binding sites and the stimuli-response using the modifiers as distinct molecular building blocks (**Table 11**). Exploiting the amino moieties as reactive handles, the aza Michael addition and the ring-opening of epoxides were found to be suitable,^{58, 118} and the corresponding post-polymerization modifications were thoroughly investigated. The herein described route stands out being a rather simple reaction in water, without the need for inert reaction conditions, and could be transferred to many more modifiers or even their combinations. After characterizing the chemical composition of the graft copolymers, the solution behavior of representative graft copolymers was examined and the expected features were revealed (**Table 11**). The attachment of hydrophobic side-chains gave amphiphilic PDha-g-EOct, which self-assembles in water into nano-sized objects. Still, it presents a pH-dependent overall charge due to the PDha backbone and is foreseen to be a promising surfactant.

4. Summary

Table 11: Graft copolymer library prepared within this work. The structure of the corresponding side-chains is shown, each tuning the properties of PDha with respect to the polarity, charge, binding sites and stimuli-response.

Functional backbone	Modification	Type of modifier / Abbreviation ¹	Resulting characteristic	Revealed features
	hydrophobic	  	amphiphilic 'polysoaps' ³⁶	<ul style="list-style-type: none"> • reduced solubility in water
		EOct, BGE, NFPO, PEG-LGE		<ul style="list-style-type: none"> • self-assembly in aqueous solution
				double hydrophilic
	ionic/ionizable	 	double acidic	<ul style="list-style-type: none"> • enhanced solubility in water • additional pK_a (COOH₂) • overall negative charge independent of pH (strong acid)
		COOH, AMPS, PhA		
	monomeric, polar	NIPAAm		

¹ 1,2-epoxy octane (EOct), benzyl glycidyl ether (BGE), nonafluoropentyloxiran (NFPO), Poly(ethylene glycol) (PEG) glycidyl lauryl ether (PEG-LGE), PEG glycidyl ether (PEG), carboxylic acid (COOH), 2-acrylamido-2-methyl propan sulfonic acid (AMPS), *N*-propyl phosphonic acid acrylamide (PhA), *N*-isopropylacrylamide (NIPAAm).

On the other hand, double hydrophilic graft copolymers were obtained, a rather unexplored but emerging subclass of linear double hydrophilic copolymers, making (fundamental) research in this field even more interesting.^{154, 155, 168, 169, 289} PDha-g-PEG contains highly hydrophilic PEG grafts, resulting in a high solution stability over the entire pH-range, as well as revealing a pH-dependent conformational changes. These characteristics along with potential biocompatibility renders this graft copolymer a promising nanoreactor for the preparation of inorganic NPs^{177, 280} or as a drug-delivery system.¹⁷⁶ The attachment of ionic/ionizable modifiers allowed the overall charge to be tuned. Besides, PDha-g-PhA presents strong anchoring groups, which interact exceptionally strongly with metal oxides, outperforming carboxylic moieties.^{278, 279, 339} These novel double-acidic graft copolymers show great potential in the chelation of metal cations and as soft matrices, due to their high charge density. NIPAAm moieties were also

4. Summary

attached to introduce an additional stimulus response. For the first time, a thermo-responsive behavior of monomeric NIPAAm side-chains was investigated within this work. The prepared PDha-g-NIPAAm graft copolymer showed a triple-responsive behavior towards the presence of metal ions, as well as changes in the pH and temperature.

In **Chapter 3**, the implementation of the graft copolymers in different hybrid materials and their applications were elaborated (**Figure 48**), serving as suitable templates, stabilizers, and matrices. Amphiphilic PDha-g-EOct₇₀ was found to be an efficient dispersant for hydrophobic MWCNTs in water without the need of chemical modifications (**3.1**).²⁹⁵ Exploiting the pH-induced aggregation/disaggregation of the PDha backbone, it was possible to reversibly precipitate and re-disperse the CNTs. This smart mechanism could be used for the purification of CNTs and the obtained dispersions are foreseen to be promising candidates in the sensing of drugs and biomolecules.^{52, 53, 243} Double hydrophilic PDha-g-PEG was applied in the template-assisted synthesis of Ag, Au and bimetallic AgAu NPs *via* the complexation of the corresponding metal ions and subsequent reduction (**3.2**). Due to its tunable charge, the pH governed the final composition of the synthesized AgAu nanoalloys after reduction at a constant initial ratio of Ag⁺ and [AuCl₄]⁻. This is an unprecedented approach to prepare and tune the composition of metallic alloy NPs, which could even be transferred to other metals.

The quantitative and qualitative sensing of heavy metal ions is vital from a health and environmental standpoint and may be realized by exploiting stimuli-responsive polymers.^{127, 128, 136, 247} In this respect, triple-responsive PDha-g-NIPAAm₅₀ allows not only changes in the solution pH to be detected, but also the type and concentration of divalent metal ions (Cu²⁺, Pb²⁺ or Co²⁺) (**3.3**). While the pristine graft copolymer solution undergoes changes in the T_{CP} upon exposure to these triggers, hybrid materials containing Ag NPs (PDha-g-NIPAAm₅₀@AgNP) also provide an optical output. Low detection limits of up to 0.02 mmol/L were found, which may even be tuned by adjusting the polymer concentration or structure. Moreover, future work could test PDha-g-NIPAAm as an interesting candidate for temperature-controlled catalysis.³²⁶

Hydrogen production, especially through photocatalytic water-splitting, became an important issue of the 21st century.^{206, 207} In order to enhance the efficiency and stability of the photocatalytic system, the selection of a suitable matrix is crucial.^{51, 208, 209, 213} Therefore, PDha-based graft copolymers containing acidic side-chains (AMPS and PhA) were designed as multifunctional matrices for photocatalytic hydrogen evolution (**3.4**). In one approach, PDha-g-PhA was grafted onto TiO₂ NPs through the phosphonic acid groups. These core-shell hybrid materials were further decorated with a [Mo₃S₁₃]²⁻ co-catalyst and EY photosensitizer. The

4. Summary

successful interconnection of the individual components by the polyampholytic shell enabled visible light-driven hydrogen evolution. PDha-g-AMPS was introduced as a versatile matrix for various photocatalytically active species and their combinations, including several inorganic catalysts (Au, Ag, Pt, Pd, $[\text{Mo}_3\text{S}_{13}]^{2-}$, Pt_3Co), photosensitizers (EY and CdS), as well as carbon nanomaterials (MWCNTs and C60). For each catalyst, a huge boost in the hydrogen evolution efficiency was observed in the presence of PDha-g-AMPS, and the materials were even outperforming comparable photocatalytic systems found in literature (**Table 10**). Future research should further elucidate the role of the polymer in the hydrogen evolution process and other catalysts should be tested, *e.g.*, superparamagnetic NPs as a recyclable system.^{54, 367, 368}

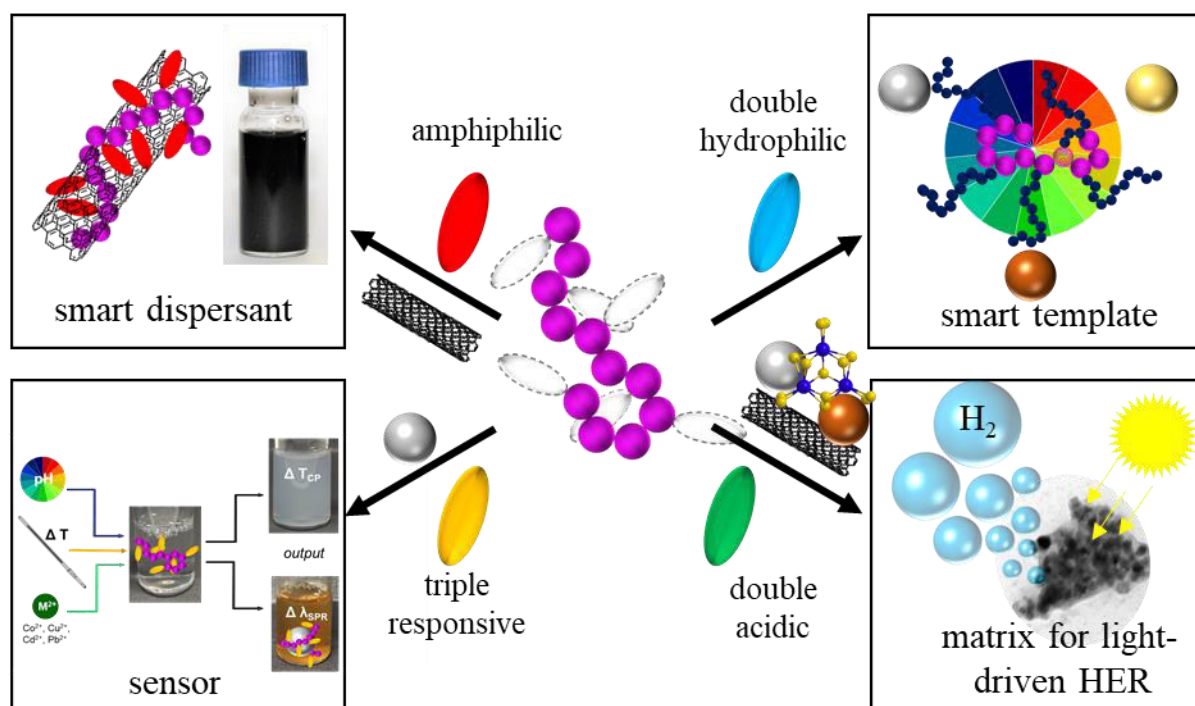


Figure 50. Utilization of the individual graft copolymers as smart dispersants and templates, versatile matrices for photocatalytic HER and pH and metal ion sensors. Parts have been adapted from *Macromol. Rapid Commun.*, **2021**, *42*, 2000671, with permission of WILEY-VCH Verlag GmbH & Co. KGaA, Weinheim.

In summary, the present work describes the development of PDha-based polyampholytic block copolymers or graft copolymers. This allowed the molecular fine-tuning of the properties, before the corresponding tailor-made copolymers were used for the construction of hybrid materials. In particular, the development of the post-polymerization modification gave access to a multitude of graft copolymers, acting as smart dispersants and templates, and were further applicable as sensors or matrixes for light-driven hydrogen evolution revealing a high performance. The herein examined straight-forward pathway could be seen as a general guideline for the construction and application of hybrid materials, where the individual building blocks may be exchanged.

5. Zusammenfassung

Wasserlösliche Polymere und deren Hybridmaterialien bieten durch ihren Einsatz in hochentwickelten Photokatalysatoren,⁵¹ Sensoren⁸² und *drug-delivery* Systemen¹⁴¹ Lösungen für globale Herausforderungen im Bereich von Energie¹⁹⁰ sowie Umwelt und Medizin.^{189, 247} In den letzten Jahrzehnten nahm die Forschung in diesem Gebiet insbesondere durch die Verwendung von Polyampholyten, und *stimuli-responsiven* Polymeren aufgrund ihrer vorteilhaften Funktionen, ihrer Vielseitigkeit und Leistung im wässrigen Milieu drastisch zu.^{41, 57, 70, 127} Poly(dehydroalanin) (PDha) tritt innerhalb der Klasse der Polyampholyte durch eine außerordentliche Ladungsdichte hervor. Es weist nicht nur eine regelbare Ladung, ein pH und Metallion *responsives* Verhalten, Biokompatibilität und reaktive Gruppen auf, sondern interagiert außerdem mit Polyelektrolyten, Modellfarbstoffen, Proteinen, Nanopartikeln (NP) und Oberflächen.^{9, 32, 34, 54, 76, 114, 123, 248-250} Durch diese Eigenschaften ist PDha ein aussichtsreiches, intelligentes Polymer, das für den Aufbau von einzigartigen Hybridmaterialien und deren Anwendungen genutzt werden kann, wo ein *stimuli-response*, eine multifunktionale Matrix oder eine (reversible) Interaktion benötigt wird.^{51, 165, 225} Durch die limitierte Löslichkeit unter sauren Bedingungen ist die Anwendung von PDha begrenzt und zusätzlich sind PDha basierte Copolymere mit maßgeschneiderten Eigenschaften aufgrund der anspruchsvollen Synthese und mäßigen Skalierbarkeit relativ unbekannt.^{32, 34, 114} Daher ist die Entwicklung von Synthesen, Modifikationen, Hybridisierung sowie die Anwendung von PDha der Kern der vorliegenden Arbeit. Ein besonderes Augenmerk wurde auf das intelligente Design von multifunktionalen (Hybrid)materialien ausgehend von einem eher unerforschten Polymer gelegt – nicht nur um existierende Lösungen zu übertreffen, sondern auch um zusätzliche Funktionalität oder unterschiedliche *responses* hinzuzufügen.

In **Kapitel 2** wurde die Herstellung PDha basierter Copolymere durch innovative Methoden beschrieben, um sowohl amphiphile als auch doppelt hydrophile Materialien zu erhalten. Die erste Strategie umfasst die Synthese von Poly(tert-butoxycarbonylaminomethylacrylat) (PtBAMA) basierten Blockcopolymeren und deren Entschützung und die andere Strategie beschreibt das propfen von Modifikatoren auf ein zuvor hergestelltes PDha Rückgrat (**Abbildung 1**). In diesem Zusammenhang wurde PDha-*block*-Polyethylenoxid (PDha-*b*-PEO) hergestellt, bestehend aus einem hydrophilen und biokompatiblen PEO²⁵⁵ und einem multifunktionalen PDha Block. Bis dato war die Synthese nicht erfolgreich, aufgrund der notwendigen Entschützung des Vorgängerpolymers PtBAMA-*b*-PEO, wobei die hydrolyseempfindliche Estergruppe gespalten wurde. Daher wurde eine stabilere Amid-basierte Verknüpfung eingeführt, auch wenn dies im Vergleich zum entsprechenden Ester synthetisch

5. Zusammenfassung

anspruchsvoller ist.²⁶⁶⁻²⁶⁸ Außerdem wurden alternative Vorgehensweisen erforscht um die bisher begrenzten Polymerisationsgrade von PtBAMA zu erhöhen und die Reproduzierbarkeit zu verbessern: die 'Click' Reaktion und fortschrittliche *atom transfer radical polymerization* (ATRP) Techniken (ATRP in wässrigem Medium und *single electron transfer radical polymerization* (SET-LRP)). Durch das Vorhandensein der Amid-basierten Verknüpfung konnte PEO-*b*-PDha nach der Entschützung unter den harschen Bedingungen erhalten werden. Wie erwartet wurde ein pH und Metallionen *responsives* Verhalten aufgedeckt, welches zur Bildung von Nanoaggregaten im Wässrigen führte. Zukünftige Forschung könnte den Einfluss der PEO bzw. PDha Kettenlänge auf die erhaltenen Lösungseigenschaften untersuchen, und das doppelt hydrophile Blockcopolymer (DHBC) mit den Eigenschaften des polyampholytischen PDha Segments in biomedizinischen Anwendungen,^{39, 259} oder als Nanoreaktor⁵¹ testen.

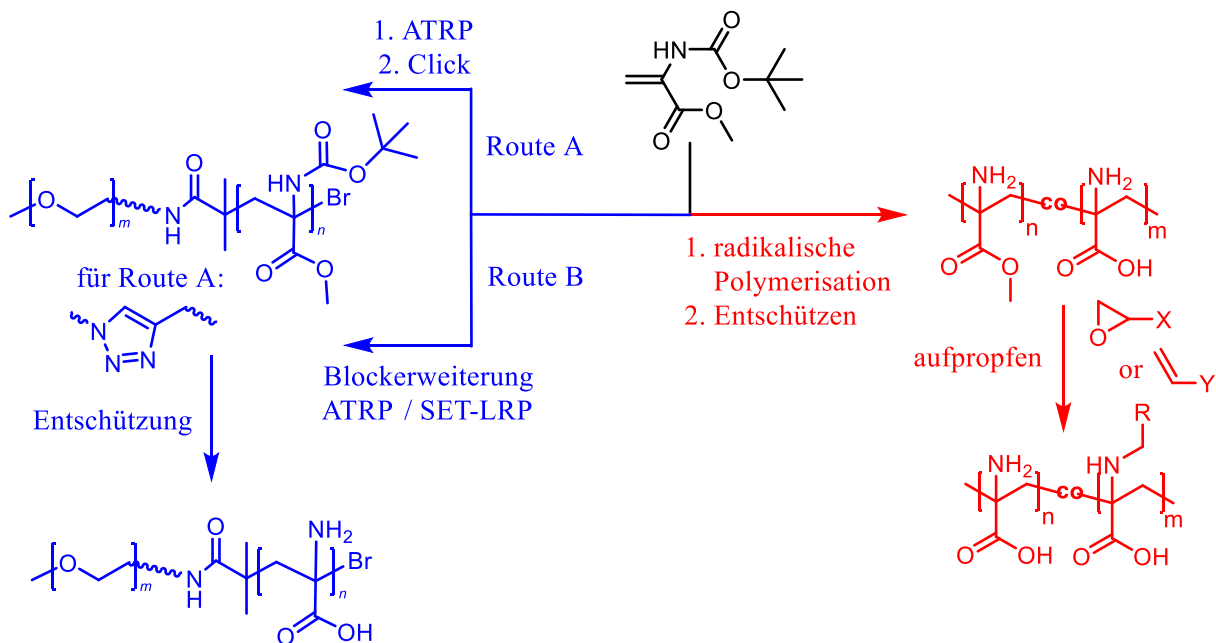


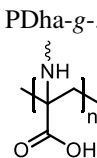
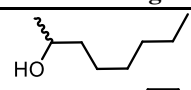
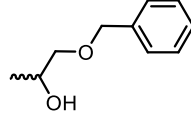
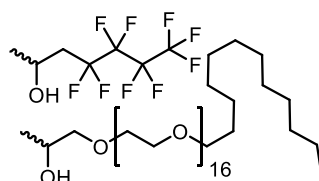
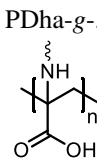
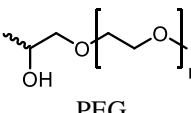
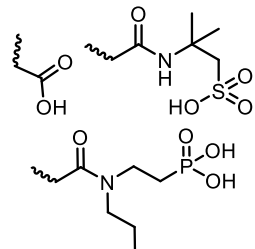
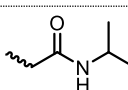
Abbildung 1. Strategien zur Synthese von PDha basierten Copolymeren, die in dieser Arbeit beschrieben wurden: (i) die Synthese von Blockcopolymeren durch eine CuAAC 'Click'-Reaktion von funktionellen Makromolekülen (Route A) und die Kettenverlängerung eines Makroinitiators (Route B), oder die Synthese von Propfcopolymeren über die polymeranaloge Modifikation von hergestelltem PDha durch propfen (ii).

Außerdem wurde ein alternativer Ansatz, die polymeranaloge Umsetzung des PDha Rückgrats, entwickelt, welcher eine vielseitige Plattform für die Funktionalisierung von reaktiven Makromolekülen darstellt.⁵⁸ Auf diese Weise konnte eine weitreichende Bibliothek an PDha-basierten Propfcopolymeren hergestellt werden, die das ganze Potential eines einzigen Polyampholyts abdeckt. Hierbei wurde die die hydrophile/hydrophobe Balance, die Ladung, etwaige Bindungsstellen und der *stimuli-response* durch eine einfache Route und dabei Verwendung von Modifikatoren als unterschiedliche molekulare Bausteine abgestimmt. Die Aminogruppen wurden als reaktive Gruppen für die passende aza-Michael Addition bzw. die Ringöffnung von Epoxiden genutzt,^{58, 118} und die polymeranalogen Modifikationen genau

5. Zusammenfassung

untersucht. Die hier beschriebene Syntheseroute zeichnet sich durch eine recht einfache Durchführbarkeit in Wasser aus, wodurch keine inerten Reaktionsbedingungen nötig sind und kann auf etliche weitere Modifikatoren oder deren Kombinationen übertragen werden. Nach der Strukturaufklärung der Propfcopolymere wurden deren Lösungseigenschaften untersucht und die Besonderheiten aufgedeckt (**Tabelle 1**). Durch das Anbringen von hydrophoben Seitenketten wurde amphiphles PDha-g-EOct erhalten, welches sich in Wasser in Nanoobjekte selbst organisiert. Das PDha Rückgrat zeigte nach wie vor eine pH-abhängige Ladung, daher könnte das Propfcopolymer ein interessantes Tensid darstellen.

Tabelle 1: In dieser Arbeit hergestellte Bibliothek an Propfcopolymeren. Die jeweiligen Strukturen der Seitenketten sind dargestellt, welche die Eigenschaften des PDha Rückgrats, im Hinblick auf die lipophile/hydrophile Balance, die Ladung, Bindungsstellen und *stimuli-response* beeinflussen.

Funktionales Rückgrat	Modifikation	Art des Modifikators / Abkürzung ¹	Resultierende Eigenschaften	Festgestellte Besonderheit
 PDha-g-..	hydrophob	 HO	amphiphil 'Polyseifen' ³⁶	<ul style="list-style-type: none"> • reduzierte Löslichkeit in Wasser • Selbstorganisation in Lösung
		 OH		
		 OH		
		EOct, BGE, NFPO, PEG-LGE		
 PDha-g-..	hydrophili	 OH PEG	doppelt hydrophil	<ul style="list-style-type: none"> • verbesserte Löslichkeit in Wasser (und MeOH) • pH abhängige Konformationsänderungen
	ionisch/ ionisierbar	 COOH, AMPS, PhA	doppelt sauer	<ul style="list-style-type: none"> • verbesserte Löslichkeit in Wasser • zusätzlicher pK_a (COOH₂) • negative Gesamtladung unabhängig vom pH (starke Säure)
	molekular, polar	 NIPAAm	dreifach-responsiv	<ul style="list-style-type: none"> • verbesserte Löslichkeit in Wasser (und MeOH) • Temperatur-responsiv

¹ 1,2-Epoxyoktan (**EOct**), Benzylglycidylether (**BGE**), Nonafluoropentylloxiran (**NFPO**), Poly(ethylen glycol) (PEG) glycidyl lauryl ether (**PEG-LGE**), PEG glycidyl ether (**PEG**), Carbonsäure (**COOH**), 2-Acrylamido-2-methylpropan sulfonsäure (**AMPS**), *N*-Propylphosphonsäureacrylamid (**PhA**), *N*-isopropylacrylamid (**NIPAAm**).

Im Gegensatz dazu wurden doppelt hydrophile Propfcopolymere synthetisiert, als eine relativ unerforschte Unterklasse von linearen DHBC.^{154, 155, 168, 169, 289} PDha-g-PEG trägt hydrophile PEG Seitenketten, was zu einer erhöhten Stabilität in Lösung und pH-abhängiger

5. Zusammenfassung

Gesamtladung und Konformationsänderungen führt. Durch diese Charakteristika zusammen mit einer potentiellen Biokompatibilität ist das Propfcopolymer vielversprechend als Nanoreaktoren zur Herstellung von anorganischen NP,^{177,280} oder als *drug-delivery* Systeme.¹⁷⁶ Durch das Propfen von ionischen/ionisierbaren Modifikatoren wurde die Gesamtladung abgestimmt. Darüber hinaus besitzt PDha-g-PhA starke Ankergruppen, welche noch stärker als Carbonsäuren mit Metalloxiden interagieren können.^{278, 279, 339} Durch die hohe Ladungsdichte zeigen diese neuartigen, doppelt sauren Propfcopolymere großes Potential für die Chelatisierung von Metallkationen und als weiche Matrizen. NIPAAm Gruppen wurden als Seitenketten eingeführt, um einen zusätzlichen *stimuli-response* im resultierenden Polymer zu erhalten. In dieser Arbeit zum ersten Mal das temperatur-*responsive* Verhalten von monomeren NIPAAm Einheiten beschrieben. Das dreifach-*responsive* PDha-g-NIPAAm reagiert auf das Vorhandensein von Metallionen sowie Veränderungen der Temperatur und des pH-Wertes.

In **Kapitel 3** wurde die Verwendung der Propfcopolymere in Hybridmaterialien und deren Anwendungen erforscht, wobei die Polymere als passende *Template*, Stabilisatoren und Matrizen dienen (**Abbildung 2**). Amphiphiles PDha-g-EOct₇₀ stellt ein hervorragendes Dispergiermittel für hydrophobe mehrwändige (multi-walled) carbon nanotubes (CNT) in Wasser dar, ohne deren chemische Modifikation (**3.1**).²⁹⁵ Die pH-induzierte Aggregation/Disaggregation des PDha Rückgrats konnte zudem genutzt werden um die CNTs reversibel auszufällen und zu re-dispergieren. Dieser intelligente Mechanismus könnte für die Aufreinigung von CNTs genutzt werden und die erhaltenen Dispersionen sind aussichtsreiche Materialien für Anwendungen in der Detektion von Medikamenten oder Biomolekülen.^{52, 53, 243} Doppelt hydrophiles PDha-g-PEG wurde für die *Templat*-unterstützte Synthese von Ag, Au und bimetallic AgAu NP durch die Komplexierung der entsprechenden Metallionen und deren nachfolgender Reduktion verwendet (**3.2**). Aufgrund der abstimmbaren Ladung bestimmt der pH-Wert die finale Zusammensetzung von synthetisierten AgAu Nanolegierungen bei einem gleichbleibenden Verhältnis der ursprünglich eingesetzten Ag⁺ und [AuCl₄]⁻ Ionen. Dies ist ein neuartiger Ansatz zur Synthese und Einstellung der Zusammensetzung metallischer NP Legierungen, der auf weitere Metalle übertragen werden könnte. Die quantitative und qualitative Detektion von Schwermetall Ionen verwendet ist aus gesundheitlichen und umwelttechnischen Aspekten essentiell und kann durch die Verwendung von *stimuli-reponsiven* Polymeren realisiert werden.^{127, 128, 136, 247} Das hergestellte PDha-g-NIPAAm₅₀ (Funktionalisierungsgrad = 50 %) erlaubte es nicht nur Änderungen des pH einer Lösung zu detektieren, sondern auch die Art und Konzentration von zweiwertigen Metallionen (Cu²⁺, Pb²⁺ or Co²⁺) (**3.3**). Während in der Propfcopolymer Lösung Änderungen der hydrodynamischen

5. Zusammenfassung

Größe oder des T_{CP} durch diese *Trigger* hervorgerufen wurden, zeigten Hybridmaterialien, die Ag NP beinhalteten (PDha-g-NIPAAm₅₀@AgNP) zusätzlich ein optisches Signal. Insgesamt konnte ein Detektionslimit von 0.02 mmol/L erreicht werden, welches weiterhin durch die Einstellung der Polymerkonzentration oder -struktur (Funktionalisierungsgrad und Seitenkette) angepasst werden könnte. Nicht zuletzt könnte PDha-g-NIPAAm als Material für die temperatur-kontrollierte Katalyse untersucht werden.³²⁶ Die Wasserstoffentwicklung, insbesondere die photokatalytische Wasserspaltung, stellt eine der wichtigsten Aufgaben des 21. Jahrhunderts dar.^{206, 207} Hierbei ist die Verwendung einer geeigneten Matrix entscheidend um die Effizienz und Stabilität des photokatalytischen Systems zu steigern.^{51, 208, 209, 213} Dazu wurden die PDha-basierten Propfcopolymere mit Säuren in der Seitenkette (AMPS und PhA) wurden als multifunktionale Matrizen für die photokatalytische Wasserstoffproduktion hergestellt (3.4). Im ersten Ansatz wurde PDha-g-PhA mit Hilfe der Phosphonsäuregruppen auf TiO₂ NP gepfropft und die Kern-Schale Hybridmaterialien mit [Mo₃S₁₃]²⁻ als Co-Katalysator und Eosin Y (EY) als Photosensibilisator bedeckt. Durch die Verknüpfung der einzelnen Komponenten durch die polyampholytische Schale wurde die durch sichtbares Licht getriebene Wasserstoffentwicklung ermöglicht. In einer anderen Strategie wurde PDha-g-AMPS als eine universelle Plattform für eine Vielzahl an photokatalytisch relevanten Substanzen und deren Kombinationen genutzt: anorganischer Katalysatoren (Au, Ag, Pt, Pd, [Mo₃S₁₃]²⁻, Pt₃Co), Photosensibilisatoren (EY and CdS) und Kohlenstoffnanomaterialien (MWCNTS und C60). Für jeden einzelnen Katalysator wurde durch die Verwendung des PDha-g-AMPS eine signifikante Erhöhung der katalytischen Leistung beobachtet und die Materialien können mitunter literaturbekannte, vergleichbare photokatalytische Systeme übertreffen (Table 10). Zukünftige Forschung könnte die Rolle des Polymers im katalytischen Prozess weiter durchleuchten und andere Katalysatoren könnten getestet werden, etwa superparamagnetische NP, für recyclebare katalytische Systeme.^{54, 367, 368}

Zusammenfassend beschreibt diese Arbeit die Synthese von PDha-basierten polyampholytischen Block- und Propfcopolymeren. Dies ermöglichte die molekulare Abstimmung der Eigenschaften, bevor die entsprechenden maßgeschneiderten Copolymere für den Aufbau von Hybridmaterialien genutzt wurden. Insbesondere die Erforschung von polymeranalogen Modifikationen öffnete den Zugang zu einzigartigen Propfcopolymeren, welche als intelligente Dispergiermittel und Template dienten und als hochleistende Sensoren und Matrizen für die lichtgetriebene Wasserstoffentwicklung verwendet wurden. Die in dieser Arbeit beschriebene Strategie kann außerdem als ein Leitfaden für den Aufbau und die

5. Zusammenfassung

Anwendung von Hybridmaterialien verstanden werden, der weiterhin auf andere Polymere und Materialkombinationen übertragen werden kann.

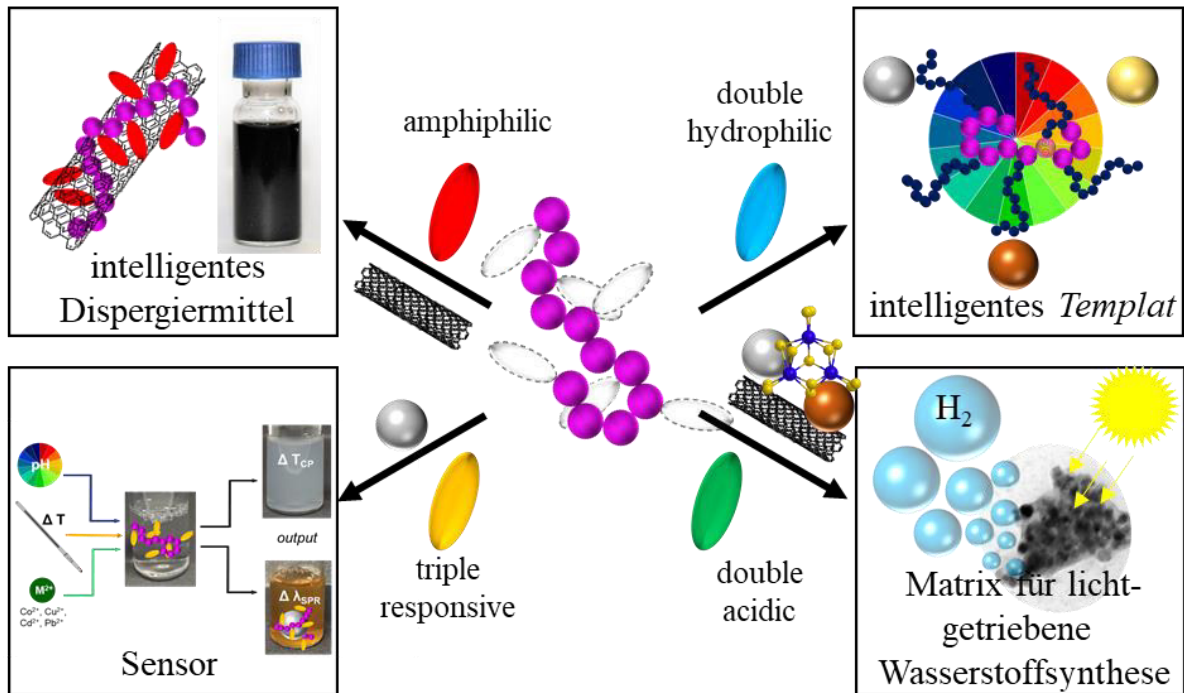


Abbildung 2. Verwendung der Propfcopolymeren als intelligente Dispergiermittel und *Template*, als vielseitige Matrizen für photokatalytische Wasserstoffsynthese und pH- und Metallionen-Sensoren. Ein Teil aus Macromol. Rapid Commun., 2021, 42, 2000671, mit Erlaubnis von WILEY-VCH Verlag GmbH & Co. KGaA, Weinheim.

References

1. H. Namazi, *Bioimpacts*, 2017, **7**, 73-74.
2. P. Musto, *Frontiers in Chemistry*, 2013, **1**.
3. S. Koltzenburg, M. Maskos and O. Nuyken, *Polymere: Synthese, Eigenschaften und Anwendungen*, Springer-Verlag Berlin Heidelberg, 1 edn., 2014.
4. M. Hess, R. G. Jones, J. Kahovec, T. Kitayama, P. Kratochvíl, P. Kubisa, W. Mormann, R. F. T. Stepto, D. Tabak, J. Vohlídal and E. S. Wilks, *Pure and Applied Chemistry*, 2006, **78**, 2067.
5. D. A. Mortimer, *Polymer International*, 1991, **25**, 29-41.
6. P. G. Higgs and J. F. Joanny, *The Journal of Chemical Physics*, 1991, **94**, 1543-1554.
7. A. Ciferri and S. Kudaibergenov, *Macromolecular Rapid Communications*, 2007, **28**, 1953-1968.
8. T. Zhu, Y. Sha, J. Yan, P. Pageni, M. A. Rahman, Y. Yan and C. Tang, *Nature Communications*, 2018, **9**, 4329.
9. P. Biehl, M. von der Lühe and F. H. Schacher, *Macromolecular Rapid Communications*, 2018, **39**, e1800017.
10. P. M. Claesson, E. Poptoshev, E. Blomberg and A. Dedinaite, *Advances in Colloid and Interface Science*, 2005, **114-115**, 173-187.
11. P. Biehl, M. von der Lühe, S. Dutz and F. Schacher, *Polymers*, 2018, **10**, 91.
12. M. von der Lühe, A. Weidner, S. Dutz and F. H. Schacher, *ACS Applied Nano Materials*, 2017, **1**, 232-244.
13. V. S. Meka, M. K. G. Sing, M. R. Pichika, S. R. Nali, V. R. M. Kolapalli and P. Kesharwani, *Drug Discovery Today*, 2017, **22**, 1697-1706.
14. L. Van Haver and S. Nayar, *Algal Research*, 2017, **24**, 167-180.
15. E. M. Wilts, J. Herzberger and T. E. Long, *Polymer International*, 2018, **67**, 799-814.
16. A. Mignon, N. De Belie, P. Dubruel and S. Van Vlierberghe, *European Polymer Journal*, 2019, **117**, 165-178.
17. I. Szilagyí, G. Trefalt, A. Tiraferri, P. Maroni and M. Borkovec, *Soft Matter*, 2014, **10**, 2479-2502.
18. L. Séon, P. Lavalley, P. Schaaf and F. Boulmedais, *Langmuir*, 2015, **31**, 12856-12872.
19. T. Chakrabarty and V. K. Shahi, *Journal of Membrane Science*, 2013, **444**, 77-86.
20. F. Zhicheng, S. Zhengzhong, Y. Jinrong and C. Xin, *Journal of Biomedical Materials Research Part A*, 2008, **86A**, 694-700.
21. E. A. Hassan, M. L. Hassan, C. N. Moorefield and G. R. Newkome, *Carbohydrate Polymers*, 2015, **116**, 2-8.
22. Y. Liu, K. Ogawa and K. S. Schanze, *Journal of Photochemistry and Photobiology C: Photochemistry Reviews*, 2009, **10**, 173-190.
23. S. Y. Bratskaya, A. V. Pestov, Y. G. Yatluk and V. A. Avramenko, *Colloids and Surfaces A: Physicochemical and Engineering Aspects*, 2009, **339**, 140-144.
24. G. J. Copello, L. E. Diaz and V. Campo Dall'Orto, *Journal of Hazardous Materials*, 2012, **217-218**, 374-381.
25. C. S. Patrickios, W. R. Hertler and T. A. Hatton, *Fluid Phase Equilib.*, 1995, **108**, 243-254.
26. C. S. Patrickios, L. R. Sharma, S. P. Armes and N. C. Billingham, *Langmuir*, 1999, **15**, 1613-1620.
27. K. M. Zurick and M. Bernards, *J. Appl. Polym. Sci.*, 2014, **131**.
28. T. Zheng, M. Zhu, M. Waqas, A. Umair, M. Zaheer, J. Yang, X. Duan and L. Li, *RSC Advances*, 2018, **8**, 38818-38830.

References

29. D. V. Pergushov, A. H. Müller and F. H. Schacher, *Chemical Society Reviews*, 2012, **41**, 6888-6901.
30. K. Singh Paresh, K. Singh Vinay and M. Singh, *e-Polymers*, 2007, **7**.
31. J. Sun, C. Wang, Z.-W. Tan and C.-M. Liu, *Polymer Chemistry*, 2020, **11**, 4029-4039.
32. U. Günther, L. V. Sigolaeva, D. V. Pergushov and F. H. Schacher, *Macromolecular Chemistry & Physics*, 2013, **214**, 2202-2212.
33. T. Zayas, M. J. Percino, J. Cardoso and V. M. Chapela, *Polymer*, 2000, **41**, 5505-5512.
34. M. Billing and F. H. Schacher, *Macromolecules*, 2016, **49**, 3696-3705.
35. F. Chen, D. Dai, J. Yang, Z. Fei and M. Zhong, *Journal of Macromolecular Science, Part A*, 2013, **50**, 1002-1006.
36. A. Laschewsky, in *Polysoaps/Stabilizers/Nitrogen-15 NMR*, Springer Berlin Heidelberg, Berlin, Heidelberg, 1995, DOI: 10.1007/BFb0025228, pp. 1-86.
37. I. Iliopoulos, *Current Opinion in Colloid & Interface Science*, 1998, **3**, 493-498.
38. D. Heinz, E. Amado and J. Kressler, *Polymers*, 2018, **10**, 960.
39. A. Harada and K. Kataoka, *Polymer Journal*, 2018, **50**, 95-100.
40. A. El Jundi, S. J. Buwalda, Y. Bakkour, X. Garric and B. Nottelet, *Advances in Colloid and Interface Science*, 2020, **283**, 102213.
41. H. Cölfen, *Macromolecular Rapid Communications*, 2001, **22**, 219-252.
42. Y. Morishima, T. Kobayashi and S.-i. Nozakura, *Polymer Journal*, 1989, **21**, 267-274.
43. R. Mobin, T. A. Rangreez, H. T. N. Chisti, Inamuddin and M. Rezakazemi, in *Functional Polymers*, eds. M. A. Jafar Mazumder, H. Sheardown and A. Al-Ahmed, Springer International Publishing, Cham, 2019, DOI: 10.1007/978-3-319-95987-0_33, pp. 1135-1156.
44. Y. Chujo, *Current Opinion in Solid State and Materials Science*, 1996, **1**, 806-811.
45. S. H. Mir, L. A. Nagahara, T. Thundat, P. Mokarian-Tabari, H. Furukawa and A. Khosla, *Journal of The Electrochemical Society*, 2018, **165**, B3137-B3156.
46. M. S. Saveleva, K. Eftekhari, A. Abalymov, T. E. L. Douglas, D. Volodkin, B. V. Parakhonskiy and A. G. Skirtach, *Frontiers in Chemistry*, 2019, **7**.
47. M. von der Luhe, U. Gunther, A. Weidner, C. Grafe, J. H. Clement, S. Dutz and F. H. Schacher, *RSC Advances*, 2015, **5**, 31920-31929.
48. Z. Q. Tian, S. P. Jiang, Z. Liu and L. Li, *Electrochemistry Communications*, 2007, **9**, 1613-1618.
49. P. Pincus, *Macromolecules*, 1991, **24**, 2912-2919.
50. A. A. Zezin, *Polymer Science Series C*, 2016, **58**, 118-130.
51. A. Nabiyan, M. Schulz, C. Neumann, B. Dietzek, A. Turchanin and F. H. Schacher, *European Polymer Journal*, 2020, **140**, 110037.
52. V. V. Shumyantseva, T. V. Bulko, A. V. Kuzikov, R. A. Masamrekh, A. Y. Konyakhina, I. Romanenko, J. B. Max, M. Köhler, A. A. Gilep, S. A. Usanov, D. V. Pergushov, F. H. Schacher and L. V. Sigolaeva, *Electrochimica Acta*, 2020, **336**, 135579.
53. L. V. Sigolaeva, T. V. Bulko, A. Y. Konyakhina, A. V. Kuzikov, R. A. Masamrekh, J. B. Max, M. Köhler, F. H. Schacher, D. V. Pergushov and V. V. Shumyantseva, *Polymers*, 2020, **12**, 1514.
54. M. von der Lühe, U. Günther, A. Weidner, C. Gräfe, J. H. Clement, S. Dutz and F. H. Schacher, *RSC Advances*, 2015, **5**, 31920-31929.
55. K. Matyjaszewski, in *Controlled Radical Polymerization*, American Chemical Society, 1998, vol. 685, ch. 1, pp. 2-30.
56. A. Laschewsky, *Polymers*, 2014, **6**, 1544.
57. L. D. Blackman, P. A. Gunatillake, P. Cass and K. E. S. Locock, *Chemical Society Reviews*, 2019, **48**, 757-770.
58. G. K. Arda, T. Patrick and K. Harm-Anton, *Journal of Polymer Science Part A: Polymer Chemistry*, 2013, **51**, 1-28.

References

59. M. J. MacLachlan, I. Manners and G. A. Ozin, *Advanced Materials*, 2000, **12**, 675-681.
60. C. Sanchez, P. Belleville, M. Popall and L. Nicole, *Chemical Society Reviews*, 2011, **40**, 696-753.
61. C. L. McCormick, C. E. Hoyle and M. D. Clark, *Polymer*, 1992, **33**, 243-247.
62. S. E. Kudaibergenov and N. Nuraje, *Polymers*, 2018, **10**, 1146.
63. S. E. Kudaibergenov, *Review Journal of Chemistry*, 2020, **10**, 12-39.
64. Y. Cai and S. P. Armes, *Macromolecules*, 2005, **38**, 271-279.
65. A. B. Lowe, N. C. Billingham and S. P. Armes, *Macromolecules*, 1998, **31**, 5991-5998.
66. A. B. Lowe, N. C. Billingham and S. P. Armes, *Chemical Communications*, 1997, DOI: 10.1039/A702116J, 1035-1036.
67. C. Rössel, M. Billing, H. Görls, G. Festag, M. Grube, P. Bellstedt, I. Nischang and F. H. Schacher, *Polymer*, 2017, **127**, 182-191.
68. E. A. Bekturov, S. E. Kudaibergenov and S. R. Rafikov, *Journal of Macromolecular Science, Part C*, 1990, **30**, 233-303.
69. E. A. Bekturov, S. E. Kudaibergenov, R. E. Khamzamalina, V. A. Frolova, D. E. Nurgalieva, R. C. Schulz and J. Zöllner, *Die Makromolekulare Chemie, Rapid Communications*, 1992, **13**, 225-229.
70. S. E. Kudaibergenov and A. Ciferri, *Macromolecular Rapid Communications*, 2007, **28**, 1969-1986.
71. D. A. V., C. R. H. and R. Michael, *Journal of Polymer Science Part B: Polymer Physics*, 2004, **42**, 3513-3538.
72. A. V. Dobrynin and M. Rubinstein, *Progress in Polymer Science*, 2005, **30**, 1049-1118.
73. A. V. Dobrynin, M. Rubinstein and J.-F. Joanny, *Macromolecules*, 1997, **30**, 4332-4341.
74. M. O. Khan, T. Åkesson and B. Jönsson, *Macromolecules*, 2001, **34**, 4216-4221.
75. S. Kudaibergenov, W. Jaeger and A. Laschewsky, in *Supramolecular Polymers Polymeric Betains Oligomers*, Springer Berlin Heidelberg, Berlin, Heidelberg, 2006, DOI: 10.1007/12_078, pp. 157-224.
76. M. von der Lühe, A. Weidner, S. Dutz and F. H. Schacher, *ACS Applied Nano Materials*, 2018, **1**, 232-244.
77. K. L. Morrissey, M. I. Keirn, Y. Inaba, A. J. Denham, G. J. Henry, B. W. Vogler, M. C. Posewitz and M. P. Stoykovich, *Algal Research*, 2015, **11**, 304-312.
78. M. Nazarzadeh, N. Nikfarjam and N. T. Qazvini, *Environmental Engineering Research*, 2017, **22**, 255-265.
79. W. Zhang, Z. Yang, Y. Kaufman and R. Bernstein, *Journal of Colloid and Interface Science*, 2018, **517**, 155-165.
80. B. Saha, N. Choudhury, A. Bhadrans, K. Bauri and P. De, *Polymer Chemistry*, 2019, **10**, 3306-3317.
81. X. Li, L. Kong and G. Gao, *Journal of Materials Chemistry B*, 2021, DOI: 10.1039/D0TB02895A.
82. J. You, H. Hu, J. Zhou, L. Zhang, Y. Zhang and T. Kondo, *Langmuir*, 2013, **29**, 5085-5092.
83. S. E. Kudaibergenov, *Gels*, 2019, **5**.
84. S. Li, Y. Wu, J. Wang, Q. Zhang, Y. Kou and S. Zhang, *Journal of Materials Chemistry*, 2010, **20**, 4379-4384.
85. K. M. Zurick and M. Bernards, *Journal of Applied Polymer Science*, 2014, **131**, n/a-n/a.
86. S. L. Haag and M. T. Bernards, *Gels*, 2017, **3**, 41.
87. Z. Xiong, B. Peng, X. Han, C. Peng, H. Liu and Y. Hu, *Journal of Colloid and Interface Science*, 2011, **356**, 557-565.
88. Z. A. Jamiu, H. A. Al-Muallem and S. A. Ali, *Designed Monomers and Polymers*, 2016, **19**, 128-137.

References

89. C. Lica, M. Segărceanu, M. Pleșca, A. Rikabi and G. Nechifor, *U.P.B. Scientific Bulletin, Series B*, 2014, **76**, 151-158.
90. M. Ferreira, B. Jing, A. Lorenzana and Y. Zhu, *Soft Matter*, 2020, **16**, 10280-10289.
91. J. Eichhorn, Y. D. Gordievskaya, E. Y. Kramarenko, A. R. Khokhlov and F. H. Schacher, *Macromolecules*, 2021, DOI: 10.1021/acs.macromol.0c02344.
92. S. Creutz, J. van Stam, S. Antoun, F. C. De Schryver and R. Jérôme, *Macromolecules*, 1997, **30**, 4078-4083.
93. G. Hadjikallis, S. C. Hadjiyannakou, M. Vamvakaki and C. S. Patrickios, *Polymer*, 2002, **43**, 7269-7273.
94. R. Wang and A. B. Lowe, *Journal of Polymer Science Part A: Polymer Chemistry*, 2007, **45**, 2468-2483.
95. T. Nakaya, M. Yasuzawa and M. Imoto, *Macromolecules*, 1989, **22**, 3180-3181.
96. S. Colak and G. N. Tew, *Langmuir*, 2012, **28**, 666-675.
97. W. Xue, M. B. Huglin and A. T. Russell, *Macromolecular Rapid Communications*, 1999, **20**, 239-243.
98. P.-S. Liu, Q. Chen, S.-S. Wu, J. Shen and S.-C. Lin, *Journal of Membrane Science*, 2010, **350**, 387-394.
99. M. S. Donovan, B. S. Sumerlin, A. B. Lowe and C. L. McCormick, *Macromolecules*, 2002, **35**, 8663-8666.
100. H. Tan, J. Liu, J. Li, X. Jiang, X. Xie, Y. Zhong and Q. Fu, *Biomacromolecules*, 2006, **7**, 2591-2599.
101. S. E. Hankari, B. Motos-Perez, P. Hesemann, A. Bouhaouss and J. J. E. Moreau, *Chemical Communications*, 2011, **47**, 6704-6706.
102. Z. A. Page, V. V. Duzhko and T. Emrick, *Macromolecules*, 2013, **46**, 344-351.
103. J.-S. Wang and K. Matyjaszewski, *Macromolecules*, 1995, **28**, 7901-7910.
104. M. Kato, M. Kamigaito, M. Sawamoto and T. Higashimura, *Macromolecules*, 1995, **28**, 1721-1723.
105. G. Moad and E. Rizzardo, in *Nitroxide Mediated Polymerization: From Fundamentals to Applications in Materials Science*, The Royal Society of Chemistry, 2016, DOI: 10.1039/9781782622635-00001, pp. 1-44.
106. J. Chiefari, Y. K. Chong, F. Ercole, J. Krstina, J. Jeffery, T. P. T. Le, R. T. A. Mayadunne, G. F. Meijs, C. L. Moad, G. Moad, E. Rizzardo and S. H. Thang, *Macromolecules*, 1998, **31**, 5559-5562.
107. K. Matyjaszewski and J. Spanswick, *Materials Today*, 2005, **8**, 26-33.
108. K. Matyjaszewski, *Advanced Materials*, 2018, **30**, 1706441.
109. K. Matyjaszewski, *Macromolecules*, 2012, **45**, 4015-4039.
110. R. Ramirez, J. Woodcock and S. M. Kilbey, *Soft Matter*, 2018, **14**, 6290-6302.
111. E. Čadová, J. Konečný, J. Kříž, R. Svitáková, P. Holler, J. Genzer and P. Vlček, *Journal of Polymer Science Part A: Polymer Chemistry*, 2010, **48**, 735-741.
112. D. Gromadzki, P. Štěpánek and R. Makuška, *Materials Chemistry and Physics*, 2013, **137**, 709-715.
113. B. Liang, G. Zhang, Z. Zhong, T. Sato, A. Hozumi and Z. Su, *Chemical Engineering Journal*, 2019, **362**, 126-135.
114. M. Billing, G. Festag, P. Bellstedt and F. H. Schacher, *Polymer Chemistry*, 2017, **8**, 936-945.
115. J. Nicolas, Y. Guillaneuf, C. Lefay, D. Bertin, D. Gigmes and B. Charleux, *Progress in Polymer Science*, 2013, **38**, 63-235.
116. R. B. Grubbs, *Polymer Reviews*, 2011, **51**, 104-137.
117. E. Rizzardo and D. H. Solomon, *Australian Journal of Chemistry*, 2012, **65**, 945-969.
118. M. A. Gauthier, M. I. Gibson and H.-A. Klok, *Angewandte Chemie International Edition*, 2009, **48**, 48-58.

References

119. A. Narayanan, B. Maiti and P. De, *Reactive and Functional Polymers*, 2015, **91-92**, 35-42.
120. H. Hidaka, T. Onai, M. Murata, K. Fujiwara, M. Takai and M. Moriya, *Journal of Colloid and Interface Science*, 1987, **119**, 565-575.
121. M. Moriya, A. Nishimura, K. Hosoda, M. Takai and H. Hidaka, *Journal of the American Oil Chemists' Society*, 1986, **63**, 263-267.
122. A. Reisch, J.-C. Voegel, G. Decher, P. Schaaf and P. J. Mésini, *Macromolecular Rapid Communications*, 2007, **28**, 2217-2223.
123. J.-H. Kruse, P. Biehl and F. H. Schacher, *Macromolecular Rapid Communications*, 2019, **40**, 1800857.
124. P. L. Golas and K. Matyjaszewski, *Chemical Society Reviews*, 2010, **39**, 1338-1354.
125. M. Jain, R. Rajan, S.-H. Hyon and K. Matsumura, *Biomaterials Science*, 2014, **2**, 308-317.
126. S. Zheng, Q. Yang and B. Mi, *Applied Surface Science*, 2016, **363**, 619-626.
127. M. A. C. Stuart, W. T. S. Huck, J. Genzer, M. Müller, C. Ober, M. Stamm, G. B. Sukhorukov, I. Szleifer, V. V. Tsukruk, M. Urban, F. Winnik, S. Zauscher, I. Luzinov and S. Minko, *Nature Materials*, 2010, **9**, 101-113.
128. R. Brighenti, Y. Li and F. J. Vernerey, *Frontiers in Materials*, 2020, **7**.
129. F. Wendler, M. Sittig, J. C. Tom, B. Dietzek and F. H. Schacher, *Chemistry – A European Journal*, 2020, **26**, 2365-2379.
130. G. Kocak, C. Tuncer and V. Bütün, *Polymer Chemistry*, 2017, **8**, 144-176.
131. A. Halperin, M. Kröger and F. M. Winnik, *Angewandte Chemie International Edition*, 2015, **54**, 15342-15367.
132. T. Hosomi, H. Masai, T. Fujihara, Y. Tsuji and J. Terao, *Angewandte Chemie International Edition*, 2016, **55**, 13427-13431.
133. M. C. García, in *Stimuli Responsive Polymeric Nanocarriers for Drug Delivery Applications*, eds. A. S. H. Makhlof and N. Y. Abu-Thabit, Woodhead Publishing, 2019, DOI: 10.1016/b978-0-08-101995-5.00014-3, pp. 393-409.
134. B. Jiang, W. L. Hom, X. Chen, P. Yu, L. C. Pavelka, K. Kisslinger, J. B. Parise, S. R. Bhatia and R. B. Grubbs, *Journal of the American Chemical Society*, 2016, **138**, 4616-4625.
135. A. L. Black, J. M. Lenhardt and S. L. Craig, *Journal of Materials Chemistry*, 2011, **21**, 1655-1663.
136. J. Cheng, G. Shan and P. Pan, *Industrial & Engineering Chemistry Research*, 2017, **56**, 1223-1232.
137. B. V. K. J. Schmidt, *Macromol Chem Phys*, 2018, **219**, 1700494.
138. C. M. Schilli, M. Zhang, E. Rizzardo, S. H. Thang, Y. K. Chong, K. Edwards, G. Karlsson and A. H. E. Müller, *Macromolecules*, 2004, **37**, 7861-7866.
139. W. Agut, A. Brûlet, D. Taton and S. Lecommandoux, *Langmuir*, 2007, **23**, 11526-11533.
140. M. Arotçaréna, B. Heise, S. Ishaya and A. Laschewsky, *Journal of the American Chemical Society*, 2002, **124**, 3787-3793.
141. E. Molina, J. Warnant, M. Mathonnat, M. Bathfield, M. In, D. Laurencin, C. Jérôme, P. Lacroix-Desmazes, N. Marcotte and C. Gérardin, *Langmuir*, 2015, **31**, 12839-12844.
142. S. Kumar, R. Acharya, U. Chatterji and P. De, *Langmuir*, 2013, **29**, 15375-15385.
143. L. Volkmann, M. Köhler, F. H. Sobotta, M. T. Enke, J. C. Brendel and F. H. Schacher, *Macromolecules*, 2018, **51**, 7284-7294.
144. K. Vijayakrishna, S. K. Jewrajka, A. Ruiz, R. Marcilla, J. A. Pomposo, D. Mecerreyes, D. Taton and Y. Gnanou, *Macromolecules*, 2008, **41**, 6299-6308.
145. Y. Wu, H. Hu, J. Hu, T. Liu, G. Zhang and S. Liu, *Langmuir*, 2013, **29**, 3711-3720.

References

146. N. Chan, S. Y. An, N. Yee and J. K. Oh, *Macromolecular Rapid Communications*, 2014, **35**, 752-757.
147. Y. Cui, X. Jiang, C. Feng, G. Gu, J. Xu and X. Huang, *Polymer Chemistry*, 2016, **7**, 3156-3164.
148. O. Casse, A. Shkilnyy, J. Linders, C. Mayer, D. Häussinger, A. Völkel, A. F. Thünemann, R. Dimova, H. Cölfen, W. Meier, H. Schlaad and A. Taubert, *Macromolecules*, 2012, **45**, 4772-4777.
149. F. Ke, X. Mo, R. Yang, Y. Wang and D. Liang, *Macromolecules*, 2009, **42**, 5339-5344.
150. G. Gotzamanis and C. Tsitsilianis, *Polymer*, 2007, **48**, 6226-6233.
151. A. Nabiyan, P. Biehl and F. H. Schacher, *Macromolecules*, 2020, **53**, 5056-5067.
152. A. Zintchenko, H. Dautzenberg, K. Tauer and V. Khrenov, *Langmuir*, 2002, **18**, 1386-1393.
153. R. Mincheva, F. Bougard, D. Paneva, M. Vachaudéz, N. Manolova, I. Rashkov and P. Dubois, *Biomacromolecules*, 2009, **10**, 838-844.
154. C. Feng, Z. Shen, L. Gu, S. Zhang, L. Li, G. Lu and X. Huang, *Journal of Polymer Science Part A: Polymer Chemistry*, 2008, **46**, 5638-5651.
155. C. Feng, Y. Li, D. Yang, J. Hu, X. Zhang and X. Huang, *Chemical Society Reviews*, 2011, **40**, 1282-1295.
156. P. Cotanda, N. Petzetakis and R. K. O'Reilly, *MRS Communications*, 2012, **2**, 119-126.
157. L. Zhu, Y. Shi, C. Tu, R. Wang, Y. Pang, F. Qiu, X. Zhu, D. Yan, L. He, C. Jin and B. Zhu, *Langmuir*, 2010, **26**, 8875-8881.
158. D.-D. Yao, H. Kubosawa, D. Souma and R.-H. Jin, *Polymer*, 2016, **86**, 120-128.
159. A. Skandalis and S. Pispas, *Journal of Polymer Science Part A: Polymer Chemistry*, 2019, **57**, 1771-1783.
160. L. Wang, Z. Li, P. Huang, Z. He and W. Ding, *Colloid and Polymer Science*, 2018, **296**, 1787-1794.
161. R. Aksakal, M. Resmini and C. R. Becer, *Polymer Chemistry*, 2016, **7**, 171-175.
162. Y.-W. Harn, Y. He, Z. Wang, Y. Chen, S. Liang, Z. Li, Q. Li, L. Zhu and Z. Lin, *Macromolecules*, 2020, **53**, 8286-8295.
163. T. Rudolph, S. Crotty, M. Von der Lühe, D. Pretzel, U. S. Schubert and F. H. Schacher, *Polymers*, 2013, **5**, 1081-1101.
164. Y. Chen, Z. Wang, Y. W. Harn, S. Pan, Z. Li, S. Lin, J. Peng, G. Zhang and Z. Lin, *Angewandte Chemie International Edition*, 2019, **58**, 11910-11917.
165. S. Lee, K. Saito, H.-R. Lee, M. J. Lee, Y. Shibasaki, Y. Oishi and B.-S. Kim, *Biomacromolecules*, 2012, **13**, 1190-1196.
166. F. Wurm, J. Nieberle and H. Frey, *Macromolecules*, 2008, **41**, 1184-1188.
167. L. Sun, Y. Zhou, X. Zhou, Q. Fu, S. Zhao, X. Tu, X. Zhang, L. Ma, M. Liu and H. Wei, *Polymer Chemistry*, 2017, **8**, 500-504.
168. F. Sun, C. Feng, H. Liu and X. Huang, *Polymer Chemistry*, 2016, **7**, 6973-6979.
169. C. Feng, L. Gu, D. Yang, J. Hu, G. Lu and X. Huang, *Polymer*, 2009, **50**, 3990-3996.
170. M. Baško and P. Kubisa, *Macromolecules*, 2002, **35**, 8948-8953.
171. J. Hao, G. Yuan, W. He, H. Cheng, C. C. Han and C. Wu, *Macromolecules*, 2010, **43**, 2002-2008.
172. J. Virtanen, C. Baron and H. Tenhu, *Macromolecules*, 2000, **33**, 336-341.
173. H. Chen, J. Li, Y. Ding, G. Zhang, Q. Zhang and C. Wu, *Macromolecules*, 2005, **38**, 4403-4408.
174. C. Feng, Y. Li, D. Yang, Y. Li, J. Hu, S. Zhai, G. Lu and X. Huang, *Journal of Polymer Science Part A: Polymer Chemistry*, 2010, **48**, 15-23.
175. L. Gu, C. Feng, D. Yang, Y. Li, J. Hu, G. Lu and X. Huang, *Journal of Polymer Science Part A: Polymer Chemistry*, 2009, **47**, 3142-3153.

References

176. D. Zhao, R. Rajan and K. Matsumura, *ACS Applied Materials & Interfaces*, 2019, **11**, 39459-39469.
177. L. Qi, H. Cölfen and M. Antonietti, *Nano Letters*, 2001, **1**, 61-65.
178. M. Nanko, *Advances in Technology of Materials and Materials Processing*, 2009, **11**, 1-8.
179. G. L. Drisko and C. Sanchez, *European Journal of Inorganic Chemistry*, 2012, **2012**, 5097-5105.
180. M. Faustini, L. Nicole, E. Ruiz-Hitzky and C. Sanchez, *Advanced Functional Materials*, 2018, **28**, 1704158.
181. C. Sanchez, B. Julián, P. Belleville and M. Popall, *Journal of Materials Chemistry*, 2005, **15**, 3559-3592.
182. G. Kickelbick, in *Hybrid Materials*, 2006, DOI: 10.1002/9783527610495.ch1, pp. 1-48.
183. H. Gu, C. Liu, J. Zhu, J. Gu, E. K. Wujcik, L. Shao, N. Wang, H. Wei, R. Scaffaro, J. Zhang and Z. Guo, *Advanced Composites and Hybrid Materials*, 2018, **1**, 1-5.
184. A. G. Navrotskaya, D. D. Aleksandrova, E. F. Krivoschapkina, M. Sillanpää and P. V. Krivoschapkin, *Frontiers in Chemistry*, 2020, **8**.
185. M. Decostanzi, Y. Ecochard and S. Caillol, *European Polymer Journal*, 2018, **109**, 1-7.
186. K. J. C. van Bommel, A. Friggeri and S. Shinkai, *Angewandte Chemie International Edition*, 2003, **42**, 980-999.
187. C. G. Schäfer, S. Vowinkel, G. P. Hellmann, T. Herdt, C. Contiu, J. J. Schneider and M. Gallei, *Journal of Materials Chemistry C*, 2014, **2**, 7960-7975.
188. L. Qi, H. Cölfen and M. Antonietti, *Angewandte Chemie International Edition*, 2000, **39**, 604-607.
189. S. Shrivastava, N. Jadon and R. Jain, *TrAC Trends in Analytical Chemistry*, 2016, **82**, 55-67.
190. M. Balat, *International Journal of Hydrogen Energy*, 2008, **33**, 4013-4029.
191. B. Smarsly and M. Antonietti, *European Journal of Inorganic Chemistry*, 2006, **2006**, 1111-1119.
192. B. Weber, *Chemistry – A European Journal*, 2017, **23**, 18093-18100.
193. M. Templin, A. Franck, A. Du Chesne, H. Leist, Y. Zhang, R. Ulrich, V. Schädler and U. Wiesner, *Science*, 1997, **278**, 1795-1798.
194. J. Lee, M. Christopher Orilall, S. C. Warren, M. Kamperman, F. J. DiSalvo and U. Wiesner, *Nature Materials*, 2008, **7**, 222-228.
195. T. von Werne and T. E. Patten, *Journal of the American Chemical Society*, 1999, **121**, 7409-7410.
196. N. Sahiner, H. Ozay, O. Ozay and N. Aktas, *Applied Catalysis A: General*, 2010, **385**, 201-207.
197. J. Song, Y. Zhu, J. Zhang, J. Yang, Y. Du, W. Zheng, C. Wen, Y. Zhang and L. Zhang, *Langmuir*, 2019, **35**, 1563-1570.
198. I. Romanenko, M. Lechner, F. Wendler, C. Hörenz, C. Streb and F. H. Schacher, *Journal of Materials Chemistry A*, 2017, **5**, 15789-15796.
199. A. Pal, S. Shah and S. Devi, *Colloids and Surfaces A: Physicochemical and Engineering Aspects*, 2007, **302**, 51-57.
200. T. C. Wang, M. F. Rubner and R. E. Cohen, *Langmuir*, 2002, **18**, 3370-3375.
201. K.-K. Chia, R. E. Cohen and M. F. Rubner, *Chemistry of Materials*, 2008, **20**, 6756-6763.
202. B. P. Bastakoti, S. Guragain, S.-i. Yusa and K. Nakashima, *RSC Advances*, 2012, **2**, 5938-5940.

References

203. C. Feng, Z. Shen, Y. Li, L. Gu, Y. Zhang, G. Lu and X. Huang, *Journal of Polymer Science Part A: Polymer Chemistry*, 2009, **47**, 1811-1824.
204. E. Seo, T. Lee, K. T. Lee, H.-K. Song and B.-S. Kim, *Journal of Materials Chemistry*, 2012, **22**, 11598-11604.
205. E. Seo, S.-H. Lee, S. Lee, S.-H. Choi, C. J. Hawker and B.-S. Kim, *Polymer Chemistry*, 2017, **8**, 4528-4537.
206. B. Johnston, M. C. Mayo and A. Khare, *Technovation*, 2005, **25**, 569-585.
207. Y. Zhang, Y.-J. Heo, J.-W. Lee, J.-H. Lee, J. Bajgai, K.-J. Lee and S.-J. Park, *Catalysts*, 2018, **8**, 655.
208. V. S. Vyas, V. W.-h. Lau and B. V. Lotsch, *Chemistry of Materials*, 2016, **28**, 5191-5204.
209. I. Romanenko, A. Rajagopal, C. Neumann, A. Turchanin, C. Streb and F. H. Schacher, *Journal of Materials Chemistry A*, 2020, **8**, 6238-6244.
210. J. Zhu, L. Hu, P. Zhao, L. Y. S. Lee and K.-Y. Wong, *Chemical Reviews*, 2020, **120**, 851-918.
211. H. Xing, S. Teng, Z. Xing, L. Bi, Q. Bu, T. Xie and W. Yang, *Applied Surface Science*, 2020, **532**, 147000.
212. X. Liu, Y. Li, S. Peng, H. Lai and Z. Yi, *Journal of Photonics for Energy*, 2016, **6**, 046501.
213. B. L. Wadsworth, D. Khusnutdinova and G. F. Moore, *Journal of Materials Chemistry A*, 2018, **6**, 21654-21665.
214. T.-L. Nghiem, D. Coban, S. Tjaberings and A. H. Gröschel, *Polymers*, 2020, **12**, 2190.
215. A. M. Beiler, D. Khusnutdinova, B. L. Wadsworth and G. F. Moore, *Inorganic Chemistry*, 2017, **56**, 12178-12185.
216. A. S. Weingarten, R. V. Kazantsev, L. C. Palmer, M. McClendon, A. R. Koltonow, A. P. S. Samuel, D. J. Kiebal, M. R. Wasielewski and S. I. Stupp, *Nature Chemistry*, 2014, **6**, 964-970.
217. H. Sai, A. Erbas, A. Dannenhoffer, D. Huang, A. Weingarten, E. Siismets, K. Jang, K. Qu, L. C. Palmer, M. Olvera de la Cruz and S. I. Stupp, *Journal of Materials Chemistry A*, 2020, **8**, 158-168.
218. Z. Hu, X. Zhang, Q. Yin, X. Liu, X.-f. Jiang, Z. Chen, X. Yang, F. Huang and Y. Cao, *Nano Energy*, 2019, **60**, 775-783.
219. M. Rafiq, J. Jing, Y. Liang, Z. Hu, X. Zhang, H. Tang, L. Tian, Y. Li and F. Huang, *Polymer Chemistry*, 2021, **12**, 1498-1506.
220. G. E. Fenoy, E. Maza, E. Zelaya, W. A. Marmisollé and O. Azzaroni, *Applied Surface Science*, 2017, **416**, 24-32.
221. T. Shu, Q. Shen, X. Zhang and M. J. Serpe, *Analyst*, 2020, **145**, 5713-5724.
222. W. Lee, D. Kim, S. Lee, J. Park, S. Oh, G. Kim, J. Lim and J. Kim, *Nano Today*, 2018, **23**, 97-123.
223. B. Sierra-Martin and A. Fernandez-Barbero, *Advances in Colloid and Interface Science*, 2016, **233**, 25-37.
224. L. Shang, J. Xu and G. U. Nienhaus, *Nano Today*, 2019, **28**, 100767.
225. G. Weng, S. Thanneeru and J. He, *Advanced Materials*, 2018, **30**, 1706526.
226. J. Cai, T. Chen, Y. Xu, S. Wei, W. Huang, R. Liu and J. Liu, *Biosensors and Bioelectronics*, 2019, **124-125**, 15-24.
227. T. Shu, Q. Shen, Y. Wan, W. Zhang, L. Su, X. Zhang and M. J. Serpe, *RSC Advances*, 2018, **8**, 15567-15574.
228. X. Shen, X. Yang, C. Su, J. Yang, L. Zhang, B. Liu, S. Gao, F. Gai, Z. Shao and G. Gao, *Journal of Materials Chemistry C*, 2018, **6**, 2088-2094.
229. S. Gou, Y.-e. Shi, P. Li, H. Wang, T. Li, X. Zhuang, W. Li and Z. Wang, *ACS Applied Materials & Interfaces*, 2019, **11**, 6561-6567.

References

230. W. Lu, H. Li, B. Huo, Z. Meng, M. Xue, L. Qiu, S. Ma, Z. Yan, C. Piao and X. Ma, *Sensors and Actuators B: Chemical*, 2016, **234**, 527-533.
231. W. Wu, N. Mitra, E. C. Y. Yan and S. Zhou, *ACS Nano*, 2010, **4**, 4831-4839.
232. Y. Ma, K. Promthaveepong and N. Li, *Analytical Chemistry*, 2016, **88**, 8289-8293.
233. J.-W. Jeon, J. Zhou, J. A. Geldmeier, J. F. Ponder, M. A. Mahmoud, M. El-Sayed, J. R. Reynolds and V. V. Tsukruk, *Chemistry of Materials*, 2016, **28**, 7551-7563.
234. M.-R. Chao, C.-W. Hu and J.-L. Chen, *Microchimica Acta*, 2014, **181**, 1085-1091.
235. C.-W. Lee, H.-S. Park, J.-G. Kim, B.-K. Choi, S.-W. Joo and M.-S. Gong, *Sensors and Actuators B: Chemical*, 2005, **109**, 315-322.
236. C.-W. Lee, H.-S. Park, J.-G. Kim and M.-S. Gong, *Macromolecular Research*, 2005, **13**, 96-101.
237. F. Chen, X. Jiang, T. Kuang, L. Chang, D. Fu, J. Yang, P. Fan and M. Zhong, *Polymer Chemistry*, 2015, **6**, 3529-3536.
238. A. Motorina, O. Tananaiko, I. Kozytska, V. Raks, R. Badía, M. E. Díaz-García and V. N. Zaitsev, *Sensors and Actuators B: Chemical*, 2014, **200**, 198-205.
239. K. Paek, H. Yang, J. Lee, J. Park and B. J. Kim, *ACS Nano*, 2014, **8**, 2848-2856.
240. Y. Fang, S. Guo, C. Zhu, Y. Zhai and E. Wang, *Langmuir*, 2010, **26**, 11277-11282.
241. X. Pang, P. Imin, I. Zhitomirsky and A. Adronov, *Macromolecules*, 2010, **43**, 10376-10381.
242. X. Pang, P. Imin, I. Zhitomirsky and A. Adronov, *Journal of Materials Chemistry*, 2012, **22**, 9147-9154.
243. V. V. Shumyantseva, L. V. Sigolaeva, L. E. Agafonova, T. V. Bulko, D. V. Pergushov, F. H. Schacher and A. I. Archakov, *Journal of Materials Chemistry B*, 2015, **3**, 5467-5477.
244. D. Priftis, *Current Organic Chemistry*, 2015, **19**, 1819-1827.
245. F. Westall and A. Brack, *Space Science Reviews*, 2018, **214**, 50.
246. L. Nicole, L. Rozes and C. Sanchez, *Advanced Materials*, 2010, **22**, 3208-3214.
247. L. A. Malik, A. Bashir, A. Qureashi and A. H. Pandith, *Environmental Chemistry Letters*, 2019, **17**, 1495-1521.
248. P. Biehl, P. Wiemuth, J. G. Lopez, M. C. Barth, A. Weidner, S. Dutz, K. Peneva and F. H. Schacher, *Langmuir*, 2020, **36**, 6095-6105.
249. L. J. Mathias and R. E. Hermes, *Macromolecules*, 1986, **19**, 1536-1542.
250. L. J. Mathias, D. W. Kurz and T. Viswanathan, *Journal of Polymer Science: Polymer Letters Edition*, 1988, **26**, 233-239.
251. Y.-C. Yeh, B. Creran and V. M. Rotello, *Nanoscale*, 2012, **4**, 1871-1880.
252. Y. Lan, Y. Lu and Z. Ren, *Nano Energy*, 2013, **2**, 1031-1045.
253. A. A. Yaqoob, K. Umar and M. N. M. Ibrahim, *Applied Nanoscience*, 2020, **10**, 1369-1378.
254. N. Anzar, R. Hasan, M. Tyagi, N. Yadav and J. Narang, *Sensors International*, 2020, **1**, 100003.
255. S. Khan, J. McCabe, K. Hill and P. A. Beales, *Journal of Colloid and Interface Science*, 2020, **562**, 418-428.
256. Y. Tezuka and H. Oike, *Journal of the American Chemical Society*, 2001, **123**, 11570-11576.
257. Z. Ge, D. Xie, D. Chen, X. Jiang, Y. Zhang, H. Liu and S. Liu, *Macromolecules*, 2007, **40**, 3538-3546.
258. E. Seo, J. Kim, Y. Hong, Y. S. Kim, D. Lee and B.-S. Kim, *The Journal of Physical Chemistry C*, 2013, **117**, 11686-11693.
259. C. Frangville, Y. Li, C. Billotey, D. R. Talham, J. Taleb, P. Roux, J.-D. Marty and C. Mingotaud, *Nano Letters*, 2016, **16**, 4069-4073.

References

260. K. Lipponen, S. Tahka, M. Kostiainen and M. L. Riekkola, *Electrophoresis*, 2014, **35**, 1106-1113.
261. T. Liu and S. Liu, *Analytical Chemistry*, 2011, **83**, 2775-2785.
262. C. Giacomelli, V. Schmidt and R. Borsali, *Macromolecules*, 2007, **40**, 2148-2157.
263. Y. Kakizawa, A. Harada and K. Kataoka, *Biomacromolecules*, 2001, **2**, 491-497.
264. Y.-X. Gao, S.-H. Yu and X.-H. Guo, *Langmuir*, 2006, **22**, 6125-6129.
265. Y. Xu, L. Shi, R. Ma, W. Zhang, Y. An and X. X. Zhu, *Polymer*, 2007, **48**, 1711-1717.
266. D. J. Adams and I. Young, *Journal of Polymer Science Part A: Polymer Chemistry*, 2008, **46**, 6082-6090.
267. A. Limer and D. M. Haddleton, *Macromolecules*, 2006, **39**, 1353-1358.
268. Y. Li, Y. Tang, R. Narain, A. L. Lewis and S. P. Armes, *Langmuir*, 2005, **21**, 9946-9954.
269. J. Edward Semple, B. Sullivan, T. Vojtkovsky and K. N. Sill, *Journal of Polymer Science Part A: Polymer Chemistry*, 2016, **54**, 2888-2895.
270. T. Rudolph, N. Kumar Allampally, G. Fernández and F. H. Schacher, *Chemistry – A European Journal*, 2014, **20**, 13871-13875.
271. G. Lligadas, S. Grama and V. Percec, *Biomacromolecules*, 2017, **18**, 2981-3008.
272. R. A. Cordeiro, N. Rocha, J. P. Mendes, K. Matyjaszewski, T. Guliashvili, A. C. Serra and J. F. J. Coelho, *Polymer Chemistry*, 2013, **4**, 3088-3097.
273. S. H. R. Shin, P. T. McAninch, I. M. Henderson, A. Gomez, A. C. Greene, E. C. Carnes and W. F. Paxton, *Chemical Communications*, 2018, **54**, 9043-9046.
274. W. Choi, K. Min, C. Kim, Y. S. Ko, J. W. Jeon, H. Seo, Y.-K. Park and M. Choi, *Nature Communications*, 2016, **7**, 12640.
275. K. A. McEwan, S. Slavin, E. Tunnah and D. M. Haddleton, *Polymer Chemistry*, 2013, **4**, 2608-2614.
276. K. Wang, L. Yang, W. Wei, L. Zhang and G. Chang, *Journal of Membrane Science*, 2018, **549**, 23-27.
277. M. Phonyiem, S. Chaiwongwattana, C. Lao-ngam and K. Sagarik, *Physical Chemistry Chemical Physics*, 2011, **13**, 10923-10939.
278. C. Viorner, Y. Chevolot, D. Léonard, B.-O. Aronsson, P. Péchy, H. J. Mathieu, P. Descouts and M. Grätzel, *Langmuir*, 2002, **18**, 2582-2589.
279. E. S. Gawalt, G. Lu, S. L. Bernasek and J. Schwartz, *Langmuir*, 1999, **15**, 8929-8933.
280. L. Gu, Z. Shen, C. Feng, Y. Li, G. Lu, X. Huang, G. Wang and J. Huang, *Journal of Materials Chemistry*, 2008, **18**, 4332-4340.
281. H. G. Schild, *Progress in Polymer Science*, 1992, **17**, 163-249.
282. N. Hu, A. Peralta, S. Roy Choudhury, R. Zhang, R. M. Davis and J. S. Riffle, *Polymer*, 2015, **65**, 124-133.
283. A. Ding, J. Xu, G. Gu, G. Lu and X. Huang, *Scientific Reports*, 2017, **7**, 12601.
284. X. Jiang, X. Jiang, G. Lu, C. Feng and X. Huang, *Polymer Chemistry*, 2014, **5**, 4915-4925.
285. D. Alaimo, A. Beigbeder, P. Dubois, G. Broze, C. Jérôme and B. Grignard, *Polymer Chemistry*, 2014, **5**, 5273-5282.
286. D.-H. N. Tran, T. H. Nguyen, T. N. N. Vo, L. P. T. Pham, D. M. H. Vo, C. K. Nguyen, L. G. Bach and D. H. Nguyen, *Journal of Applied Polymer Science*, 2019, **136**, 47544.
287. J. Virtanen and H. Tenhu, *Macromolecules*, 2000, **33**, 5970-5975.
288. K. Sui, X. Zhao, Z. Wu, Y. Xia, H. Liang and Y. Li, *Langmuir*, 2012, **28**, 153-160.
289. T. Jiang, V. Aseyev, J. Niskanen, S. Hietala, Q. Zhang and H. Tenhu, *Macromolecules*, 2020, **53**, 8267-8275.
290. M. M. Akbarzadeh, *RSC Advances*, 2016, **6**, 12081-12083.
291. G. Cerichelli and G. Mancini, *Current Opinion in Colloid & Interface Science*, 1997, **2**, 641-648.

References

292. X. Sun, Y. Zhou and D. Yan, *Science in China Series B: Chemistry*, 2009, **52**, 1703-1710.
293. J. Boonmak, S. Youngme, T. Chotkhun, C. Engkagul, N. Chaichit, G. A. van Albada and J. Reedijk, *Inorganic Chemistry Communications*, 2008, **11**, 1231-1235.
294. S. Chen, K. Wang and W. Zhang, *Polymer Chemistry*, 2017, **8**, 3090-3101.
295. T. Fujigaya and N. Nakashima, *Science and Technology of Advanced Materials*, 2015, **16**, 024802.
296. P. W. Barone and M. S. Strano, *Angewandte Chemie International Edition*, 2006, **45**, 8138-8141.
297. D. Ulker, G. Kocak, C. Tuncer and V. Butun, *Colloid and Polymer Science*, 2019, **297**, 1067-1078.
298. G. Kocak, *Journal of Applied Polymer Science*, 2020, **137**, 48360.
299. V. Amendola, R. Pilot, M. Frascioni, O. M. Maragò and M. A. Iatì, *Journal of Physics: Condensed Matter*, 2017, **29**, 203002.
300. N. Tarannum, Divya and Y. K. Gautam, *RSC Advances*, 2019, **9**, 34926-34948.
301. G. Guisbiers, R. Mendoza-Cruz, L. Bazán-Díaz, J. J. Velázquez-Salazar, R. Mendoza-Perez, J. A. Robledo-Torres, J.-L. Rodriguez-Lopez, J. M. Montejano-Carrizales, R. L. Whetten and M. José-Yacamán, *ACS Nano*, 2016, **10**, 188-198.
302. J. Wilcoxon, *The Journal of Physical Chemistry B*, 2009, **113**, 2647-2656.
303. J. Ando, A. Nakamura, M. Yamamoto, C. Song, K. Murata and R. Iino, *ACS Photonics*, 2019, **6**, 2870-2883.
304. C. Dwivedi, A. Chaudhary, S. Srinivasan and C. K. Nandi, *Colloid and Interface Science Communications*, 2018, **24**, 62-67.
305. L.-Y. Li, W.-D. He, W.-T. Li, K.-R. Zhang, T.-T. Pan, Z.-L. Ding and B.-Y. Zhang, *Journal of Polymer Science Part A: Polymer Chemistry*, 2010, **48**, 5018-5029.
306. R. C. B. Scaravelli, R. L. Dazzi, F. C. Giacomelli, G. Machado, C. Giacomelli and V. Schmidt, *Journal of Colloid and Interface Science*, 2013, **397**, 114-121.
307. É. G. A. Miranda, A. Tofanello, A. M. M. Brito, D. M. Lopes, L. J. C. Albuquerque, C. E. de Castro, F. N. Costa, F. C. Giacomelli, F. F. Ferreira, J. C. Araújo-Chaves and I. L. Nantes, *Frontiers in Chemistry*, 2016, **4**.
308. I. Mukha, N. Vityuk, O. Severynovska, A. Eremenko and N. Smirnova, *Nanoscale Research Letters*, 2016, **11**, 101.
309. K. S. Tan and K. Y. Cheong, *Journal of Nanoparticle Research*, 2013, **15**, 1537.
310. C. Zhai, X. Liu, X. Chen, L. Li, F. Sun and H. Ma, *Journal of Inorganic and Organometallic Polymers and Materials*, 2015, **25**, 687-693.
311. Y. Zhang, P. Filipczak, G. He, G. Nowaczyk, L. Witczak, W. Raj, M. Kozanecki, K. Matyjaszewski and J. Pietrasik, *Polymer*, 2017, **129**, 144-150.
312. M. Zhang, L. Liu, C. Wu, G. Fu, H. Zhao and B. He, *Polymer*, 2007, **48**, 1989-1997.
313. W. Haiss, N. T. K. Thanh, J. Aveyard and D. G. Fernig, *Analytical Chemistry*, 2007, **79**, 4215-4221.
314. A. Pal, S. Shah and S. Devi, *Australian Journal of Chemistry*, 2008, **61**, 66-71.
315. C. Pietsch, R. Hoogenboom and U. S. Schubert, *Angewandte Chemie International Edition*, 2009, **48**, 5653-5656.
316. M. Wei, Y. Gao, X. Li and M. J. Serpe, *Polymer Chemistry*, 2017, **8**, 127-143.
317. J. Hu and S. Liu, *Macromolecules*, 2010, **43**, 8315-8330.
318. Z. Ge and S. Liu, *Chemical Society Reviews*, 2013, **42**, 7289-7325.
319. Y. Chen, K.-Y. Pu, Q.-L. Fan, X.-Y. Qi, Y.-Q. Huang, X.-M. Lu and W. Huang, *Journal of Polymer Science Part A: Polymer Chemistry*, 2009, **47**, 5057-5067.
320. Z. Guo, W. Zhu and H. Tian, *Macromolecules*, 2010, **43**, 739-744.
321. X. Liu, X. Zhou, X. Shu and J. Zhu, *Macromolecules*, 2009, **42**, 7634-7637.

References

322. M. Zhang, P. Lu, Y. Ma and J. Shen, *The Journal of Physical Chemistry B*, 2003, **107**, 6535-6538.
323. P. Mi, L.-Y. Chu, X.-J. Ju and C. H. Niu, *Macromolecular Rapid Communications*, 2008, **29**, 27-32.
324. Q. Luo, Y. Guan, Y. Zhang and M. Siddiq, *Journal of Polymer Science Part A: Polymer Chemistry*, 2010, **48**, 4120-4127.
325. M. Annadhasan, T. Muthukumarasamyvel, V. R. Sankar Babu and N. Rajendiran, *ACS Sustainable Chemistry & Engineering*, 2014, **2**, 887-896.
326. S. Carregal-Romero, N. J. Buurma, J. Pérez-Juste, L. M. Liz-Marzán and P. Hervés, *Chemistry of Materials*, 2010, **22**, 3051-3059.
327. J. O. Abe, A. P. I. Popoola, E. Ajenifuja and O. M. Popoola, *International Journal of Hydrogen Energy*, 2019, **44**, 15072-15086.
328. Z. Chen, X. Duan, W. Wei, S. Wang and B.-J. Ni, *Journal of Materials Chemistry A*, 2019, **7**, 14971-15005.
329. A. Fujishima and K. Honda, *Nature*, 1972, **238**, 37-38.
330. L. Li, Y. Zhu, N. Gong, W. Zhang, W. Peng, Y. Li, F. Zhang and X. Fan, *International Journal of Hydrogen Energy*, 2020, **45**, 2689-2698.
331. P. Wang, S. Guo, H.-J. Wang, K.-K. Chen, N. Zhang, Z.-M. Zhang and T.-B. Lu, *Nature Communications*, 2019, **10**, 3155.
332. M. Chauhan, K. Soni, P. E. Karthik, K. P. Reddy, C. S. Gopinath and S. Deka, *Journal of Materials Chemistry A*, 2019, **7**, 6985-6994.
333. Y. Ouyang, Q. Li, L. Shi, C. Ling and J. Wang, *Journal of Materials Chemistry A*, 2018, **6**, 2289-2294.
334. T. Yang, M. Du, H. Zhu, M. Zhang and M. Zou, *Electrochimica Acta*, 2015, **167**, 48-54.
335. N. Coutard, N. Kaeffer and V. Artero, *Chemical Communications*, 2016, **52**, 13728-13748.
336. J. Willkomm, N. M. Muresan and E. Reisner, *Chemical Science*, 2015, **6**, 2727-2736.
337. N. M. Muresan, J. Willkomm, D. Mersch, Y. Vaynzof and E. Reisner, *Angewandte Chemie International Edition*, 2012, **51**, 12749-12753.
338. J. J. Leung, J. Warnan, D. H. Nam, J. Z. Zhang, J. Willkomm and E. Reisner, *Chemical Science*, 2017, **8**, 5172-5180.
339. K. H. Markiewicz, L. Seiler, I. Misztalewska, K. Winkler, S. Harrisson, A. Z. Wilczewska, M. Destarac and J. D. Marty, *Polymer Chemistry*, 2016, **7**, 6391-6399.
340. J. Ran, J. Zhang, J. Yu, M. Jaroniec and S. Z. Qiao, *Chemical Society Reviews*, 2014, **43**, 7787-7812.
341. C. Wu, J. Zhang, X. Tong, P. Yu, J.-Y. Xu, J. Wu, Z. M. Wang, J. Lou and Y.-L. Chueh, *Small*, 2019, **15**, 1900578.
342. Y. Yuan, H. Lu, Z. Ji, J. Zhong, M. Ding, D. Chen, Y. Li, W. Tu, D. Cao, Z. Yu and Z. Zou, *Chemical Engineering Journal*, 2015, **275**, 8-16.
343. N. Romero, R. B. Guerra, L. Gil, S. Drouet, I. Salmeron-Sánchez, O. Illa, K. Philippot, M. Natali, J. García-Antón and X. Sala, *Sustainable Energy & Fuels*, 2020, **4**, 4170-4178.
344. H. Lai, X. Liu, F. Zeng, G. Peng, J. Li and Z. Yi, *ACS Omega*, 2020, **5**, 2027-2033.
345. S. Li, T. Pu, J. Wang, X. Fang, Y. Liu, S. Kang and L. Cui, *International Journal of Hydrogen Energy*, 2018, **43**, 16534-16542.
346. M. Dave, A. Rajagopal, M. Damm-Ruttensperger, B. Schwarz, F. Nägele, L. Daccache, D. Fantauzzi, T. Jacob and C. Streb, *Sustainable Energy & Fuels*, 2018, **2**, 1020-1026.
347. A. Rajagopal, F. Venter, T. Jacob, L. Petermann, S. Rau, S. Tschierlei and C. Streb, *Sustainable Energy & Fuels*, 2019, **3**, 92-95.

References

348. Y. Lei, M. Yang, J. Hou, F. Wang, E. Cui, C. Kong and S. Min, *Chemical Communications*, 2018, **54**, 603-606.
349. Y. Li, M. Guo, S. Peng, G. Lu and S. Li, *International Journal of Hydrogen Energy*, 2009, **34**, 5629-5636.
350. X. Liu, W. Huang, Y. Lei, Y. Li, Y. Xue, F. Wang and S. Min, *New Journal of Chemistry*, 2018, **42**, 6631-6635.
351. Y. Li, C. Xie, S. Peng, G. Lu and S. Li, *Journal of Molecular Catalysis A: Chemical*, 2008, **282**, 117-123.
352. X. Liu, L. Zhao, H. Lai, Y. Wei, G. Yang, S. Yin and Z. Yi, *RSC Advances*, 2017, **7**, 46738-46744.
353. R. Abe, K. Hara, K. Sayama, K. Domen and H. Arakawa, *Journal of Photochemistry and Photobiology A: Chemistry*, 2000, **137**, 63-69.
354. N. Syed, J. Huang, Y. Feng, X. Wang and L. Cao, *Frontiers in Chemistry*, 2019, **7**.
355. Z. Hu and J. C. Yu, *Journal of Materials Chemistry A*, 2013, **1**, 12221-12228.
356. Y.-J. Yuan, D. Chen, Z.-T. Yu and Z.-G. Zou, *Journal of Materials Chemistry A*, 2018, **6**, 11606-11630.
357. M.-Q. Yang, N. Zhang and Y.-J. Xu, *ACS Applied Materials & Interfaces*, 2013, **5**, 1156-1164.
358. B. Gupta and A. A. Melvin, *Renewable and Sustainable Energy Reviews*, 2017, **76**, 1384-1392.
359. S. Min and G. Lu, *The Journal of Physical Chemistry C*, 2012, **116**, 19644-19652.
360. X. Liu, Y. Li, S. Peng, G. Lu and S. Li, *International Journal of Hydrogen Energy*, 2012, **37**, 12150-12157.
361. H. Rao, Z.-Y. Wang, J. Wang, X.-Z. Hu, Y.-T. Fan and H.-W. Hou, *International Journal of Energy Research*, 2014, **38**, 2003-2009.
362. T. Lazarides, T. McCormick, P. Du, G. Luo, B. Lindley and R. Eisenberg, *Journal of the American Chemical Society*, 2009, **131**, 9192-9194.
363. A. Lewandowska-Andralojc, A. Malolepszy, A. Stritt and A. Grohmann, *Catalysis Science & Technology*, 2020, **10**, 4693-4702.
364. Y. Honda, Y. Shinohara and H. Fujii, *Catalysis Science & Technology*, 2020, **10**, 6006-6012.
365. Z. Cheng, A. Saad, S. Adimi, H. Guo, S. Liu, T. Thomas and M. Yang, *Materials Advances*, 2020, **1**, 1161-1167.
366. X. Zhang, Z. Jin, Y. Li, S. Li and G. Lu, *Applied Surface Science*, 2008, **254**, 4452-4456.
367. A. Bhalkikar, Z. C. Gernhart and C. L. Cheung, *Journal of Nanomaterials*, 2015, **2015**, 264037.
368. B. Movassagh and A. Yousefi, *Monatshefte für Chemie - Chemical Monthly*, 2015, **146**, 135-142.

List of abbreviations

List of abbreviations

ACN	acrylonitrile
AMPS	2-acryl amido-2-methylpropane sulfonic acid
AGET	activators generated by electron transfer
ARGET	activator regenerated by electron transfer
at%	atom percentage
ATRP	atom transfer radical polymerization
BGE	benzyl glycidyl ether
BMP	2-bromo-2-methylpropionamide
boc	<i>tert</i> -butyloxy carbonyl
COOH	carboxylic acid
CNT	carbon nanotube
CuAAC	copper-catalyzed azide-alkyne cycloaddition
Đ	dispersity
DHBC	double hydrophilic block copolymer
DHC	double hydrophilic copolymer
DHGC	double hydrophilic graft copolymer
DLS	dynamic light scattering
DMF	<i>N,N</i> -dimethylformamid
DMSO	dimethyl sulfoxide
dNbpy	4,4'-dinonyl-2,2'-dipyridyl
DoF	degree of functionalization
DP	degree of polymerization
EDX	energy dispersive X-ray scattering
EOct	1,2-epoxyoctane
EY	Eosin Y
FRP	free radical polymerization
FT-IR	fourier-transform infrared
<i>hb</i>	<i>hyperbranched</i>
HER	hydrogen evolution reaction

List of abbreviations

HPAMAM	hyperbranched poly(amidoamine)
IEP	isoelectric point
IPEC	interppolyelectrolyte complex
<i>i</i> PrOH	<i>iso</i> -propanol
λ	wave length
LCST	lower critical solution temperature
LSPR	localized surface plasmon resonance
MeBib	methyl α -bromoisobutyrate
MeOH	methanol
M_n	number average molecular weight
MWCNT	multi-walled carbon nanotube
NMP	nitroxide mediated polymerization
NMR	nuclear magnetic resonance
NP	nanoparticle
NPFO	nonafluoropentaoxriane
P4VPCI	poly(1-methyl-4-vinylpyridinium chloride)
PAA	poly(acrylic acid)
PAGA	poly(2-acrylamido glycolic acid)
PAMA	poly(aminomethylacrylate)
P(AMA- <i>co</i> -Dha)	poly(aminomethylacrylate- <i>co</i> -dehydroalanine)
PDha	poly(dehydroalanine)
PEG	poly(ethylene glycol)
PEG-LGE	poly(ethylene glycol) glycidyl lauryl ether
PEI	poly(ethylene imine)
PEO	poly(ethylene oxide)
PEtOx	poly(ethylene oxide) (PEO)
PG	poly(glycerol)
pH	potential hydrogenii
PhA	phosphonic acid acryl amide
PI	poly(isoprene)

List of abbreviations

PiPrOx	poly(2- <i>iso</i> -propyl-2-oxazoline)
p <i>K</i> _a	logarithmic acidity constant
PMAA	poly(methacrylic acid)
PMDETA	<i>N,N,N',N'',N''</i> -Pentamethyldiethylenetriamine
P <i>n</i> BA	poly(<i>n</i> -butyl acrylate)
PNIPAAm	poly(<i>N</i> -isoproylacrylamide)
POEGMA	poly(oligo(ethylene glycol) monomethyl ether methacrylate)
ppm	parts per million
PS	poly(styrene)
PVA	poly(vinyl alcohol)
RAFT	reversible addition-fragmentation chain transfer
R _H	hydrodynamic radius
SET-LRP	single-electron-transfer living polymerization
SG1	4-(diethoxyphosphinyl)-2,2,5,5-tetramethyl-3-azahexane- <i>N</i> -oxyl
SPR	surface plasmon resonance
<i>t</i> BAMA	<i>tert</i> -butoxy carbonylaminomethyl acrylate
T _{CP}	cloud point temperature
TEM	transmission electron microscopy
TEMPO	2,2,6,6-tetramethyl-1-piperidinyloxy
TFA	trifluoroacetic acid
TGA	thermogravimetric analysis
THF	tetrahydrofuran
TIPNO	2,2,5-trimethyl-4-phenyl-3-azahexane- <i>N</i> -oxyl
TON	turnover number
TPO	trimethylbenzoyl diphenylphosphine oxide
UV-vis	ultraviolet-visible
wt%	weight percentage
XPS	X-ray photoelectron spectroscopy

Publication list

P7: A. Nabiyan, J. B. Max, F. H. Schacher, Double hydrophilic copolymers – synthetic approaches, architectural variety, and current application fields, *Chemical Society Reviews*, 2022, <https://doi.org/10.1039/D1CS00086A>.

P5: A. Nabiyan, J. B. Max, C. Neumann, M. Heiland, A. Turchanin, C. Streb, F. H. Schacher, Polyampholytic Graft Copolymers as Matrix for TiO₂/Eosin Y/[Mo₃S₁₃]₂- Hybrid Materials and Light-Driven Catalysis, *Chemistry a European Journal*, 2021, <https://doi.org/10.1002/chem.202100091>

P4: J. B. Max, A. Nabiyan, J. Eichhorn, F. H. Schacher, Triple-Responsive Polyampholytic Graft Copolymers as Smart Sensors with Varying Output, *Macromolecular Rapid Communication*, 42, 2020, 2000671.

P3: J. B. Max, K. Kowalczyk, M. Köhler, C. Neumann, F. Pielenz, L. V. Sigolaeva, D. V. Pergushov, A. Turchanin, F. Langenhorst, F. H. Schacher, Polyampholytic poly(dehydroalanine) graft copolymers as smart templates for pH-controlled formation of alloy nanoparticles, *Macromolecules*, 2020, 53, 11, 4511-4523.

P2: J. B. Max, P. J. Mons, J. C. Tom, F. H. Schacher, Double hydrophilic poly(ethylene oxide)-block-poly(dehydroalanine) block copolymers: Comparison of two different synthetic routes, *Macromolecular Chemistry and Physics*, 2020, 221, 1900383.

P1: J. B. Max, D. V. Pergushov, L. V. Sigolaeva, F. H. Schacher, Polyampholytic graft copolymers based on polydehydroalanine (PDha) - synthesis, solution behavior and application as dispersants for carbon nanotubes, *Polymer Chemistry*, 2019, 10, 3006-3019.

K. Scheuer, D. Bandelli, C. Helbing, C. Weber, J. Alex, J. B. Max, A. Hocken, O. Stranik, L. Seiler, F. Gladigau, U. Neugebauer, F. H. Schacher, U. S. Schubert, K. D. Jandt, Self-assembly of copolyesters into stereocomplex crystallites tunes the properties of polyester nanoparticles, *Macromolecules*, 2020, 53, 19, 8340-8351.

V. V. Shumyantseva, T. V. Bulko, A. V. Kuzikov, R. A. Masamrek, A. Y. Konyakhina, I. Romanenko, J. B. Max, M. Köhler, A. A. Gilep, S. A. Usanov, D. V. Pergushov, F. H. Schacher, L. V. Sigolaeva, All-electrochemical nanocomposite two-electrode setup for quantification of drugs and study of their electrocatalytical conversion by cytochromes P450, *Electrochimica Acta*, 2020, 336, 135579

D. Bandelli, I. Muljajew, K. Scheuer, J. B. Max, C. Weber, F. H. Schacher, K. D. Jandt, U. S. Schubert, Copolymerization of caprolactone isomers to obtain nanoparticles with constant hydrophobicity and tunable charge, *Macromolecules*, 2020, 53, 13, 5208-5217.

V. Schimpf, J. B. Max, B. Stolz, B. Heck, R. Mülhaupt, Semicrystalline non-isocyanate polyhydroxyurethanes as thermoplastics and thermoplastic elastomers and their use in 3D printing by fused filament fabrication, *Macromolecules*, 2019, 52, 1, 320–331.

Publication list

Patent: V. Schimpf, R. Mülhaupt, J. B. Max, Teilkristalline isocyanatfreie Polyhydroxyurethane mit thermomechanisch programmier- und schaltbaren Eigenschaften. Patent registered on 02/13/2017 at Deutschen Patent- und Markenamt. Aktenzeichen DE10 2017001393A1 and at 01/24/2018 at Europäischen Patentamt, Aktenzeichen EP3360913A1.

Conferences

Poster presentation: J. B. Max, K. Kowalczyk, F. H. Schacher, Post-polymerization modification of polydehydroalanine (PDha) towards functional, tailor-made polyampholytes, European Polymer Congress, Heraklion Crete, Greece, June 2019 (DAAD scholarship).

Poster presentation: J. B. Max, F. H. Schacher, Synthesis and modification of polydehydroalanine (PDha) towards amphiphilic graft copolymers, Biennial Meeting of the GDCh-Division of Macromolecular Chemistry in Karlsruhe, September 2018

Acknowledgements / Danksagung

An dieser Stelle möchte ich allen danken, die mich während meiner Dissertation begleitet und zu ihrem Gelingen beigetragen haben. Dazu gehört sicher nicht nur all das Fachliche, sondern auch all die zwischenmenschlichen Erfahrungen, die ich in dieser Zeit machen durfte.

Ich möchte vorweg meinen Doktorvater Prof. Dr. Felix H. Schacher nennen, der mir von Anfang an großes Vertrauen entgegengebracht hat und mir ermöglichte, in diesem vielseitigen Projekt zu arbeiten. Er schaffte eine ideale Balance aus kreativem Freiraum und zielgerichteter Arbeitsweise, durch die ich zahlreiche Nebenprojekte bewältigen konnte. Mit seinem Fachwissen, das weit über die Polymerchemie hinaus geht, stand er mir jederzeit zur Seite. Darüber hinaus lagen ihm meine privaten Belange immer am Herzen und gerade auch deswegen werde ich die Zeit als Doktorand in guter Erinnerung behalten.

Dankbar bin ich außerdem für die Kooperation mit der Moscow State University, insbesondere Dr. Dmitry V. Pergushov und Dr. Larisa V. Sigolaeva. Durch sie bekam ich nicht nur Einblicke in mir vorher unbekannte Themengebiete eine außergewöhnliche Zeit in Moskau, sondern verbrachte auch eine außergewöhnliche Zeit in Moskau. Ich freue mich sehr über die fruchtbare Zusammenarbeit.

Ich möchte mich bei allen Studierenden bedanken, die ich betreuen durfte und die zu meiner Arbeit beigetragen haben. Durch sie konnte ich über mein eigentliches Thema hinaus forschen und experimentieren, sowie das hohe Pensum an Laborarbeit erfüllen. Außerdem haben mir ein Blick von außen und die richtigen Fragen stets für die eigene Forschung geholfen. Zunächst seien die damaligen Masterstudierenden, Kathrin Kowalczuk, Peter Johannes Mons und Frieda Nagler, erwähnt, die alle drei großartige Arbeit geleistet haben und meine Doktorarbeit bereicherten. Des Weiteren seien die Forschungspraktikanten Katja Geitel und Louis Blechschmidt genannt. Außerdem unterstützten mich im Labor Saurabh Kulkarni, Anjali Dua, Christiana Onyebueke, Cindy Leistner und Anna Nottrott.

Ohne die Unterstützung durch die Analytik an der Universität Jena wäre diese Arbeit kaum möglich gewesen. Hervorzuheben ist die NMR Abteilung, insbesondere Friederike Pielenz und Dr. Peter Bellstedt, die unzählige, oft äußerst aufwendige Proben gemessen und mir bei der Auswertung geholfen haben. Dr. Grit Festtag und Peggy Hermann analysierten für mich nahezu unlösliche SEC Proben innerhalb kürzester Zeit. Prof. Dr. Falko Langenhorst gewährte mir spannende Einblicke in HR-TEM Messungen und Dr. Christof Neumann verbrachte sicherlich viel Zeit mit den XPS Untersuchungen und der Auswertung meiner Proben. Vielen Dank auch

Acknowledgements / Danksagung

an Katja König, die nicht nur unsere SEC Geräte pflegte und schützte, sondern immer ein offenes Ohr für jegliche Belange hatte.

Ich bin froh, ein Teil der Arbeitsgruppe Prof. Dr. Schacher geworden zu sein, durch die ich mich nach meinem Umzug aus Freiburg im Breisgau nach Jena schnell heimisch fühlte. Gerade die angenehme Atmosphäre gaben mir die besten Voraussetzungen für meine Dissertation. Dazu hat jedes einzelne Mitglied beigetragen, von denen ich einige besonders hervorheben möchte.

- Manchmal bedarf es vieler Zufälle, um zur richtigen Zeit am richtigen Ort eine bestimmte Person zu treffen und so freue ich mich Dr. Afshin Nabiyan kennen gelernt zu haben. Selten habe ich einen derart passionierten und kreativen Wissenschaftler getroffen und so kam es schnell zu Kooperationen und gemeinsamen Veröffentlichungen. Noch mehr bin ich allerdings glücklich, einen wahren Freund (دوست) wie Dich zu haben. In diesem Sinne hoffe ich auf viele weitere Fesenjoons.
- Peter Johannes von Mons, Meister der ATRPs, lieferte nicht nur eine hervorragende Masterarbeit ab, sondern half mir bei gemeinsamen Besuchen im Fitnessstudio gesund zu bleiben und den ein oder anderen Muskel aufzubauen. Danke für Deine stetige Unterstützung und die lustigen Abende.
- Moritz Köhler war nicht nur mein Bürokollege, sondern ist auch einer meiner besten Freunde in Jena geworden. Mit wenigen Leuten lässt sich besser ein Bier trinken.
- Danke an das Labor 317, Dr. Philip Biehl, Moritz Köhler und Kathrin Kowalczuk für die schöne Zeit, die tiefgründigen Gespräche und eure Sauberkeit.
- Carsten Rössel, Hüter der Laborgeräte und wandelndes OC Buch, durch den die Konferenz auf Kreta wie ein Urlaub war.
- Yves Carstensen, ein Macher ohnegleichen, der von so ziemlich allem Technischen Ahnung hat und scheinbar jedes Problem beheben kann.
- Der AG Doppelkopf, Dr. Oli Grimm, Costa und Jonas, für die spielerische Pausengestaltung.
- I want to thank Dr. Jessica Tom for sharing her huge knowledge with us, as well as doing a lots of proof-reading and improving my English.
- Ich danke außerdem Dr. Felix Wendler, einem überraschend tiefgründigen Jenaer Urgestein, der mir immer mit Rat und Tat zur Seite stand, Jan Kruse für die vielen Fußballabende und -updates, Johanna Elter die sich immer um den mir so wichtigen Kaffee gekümmert hat, Bob für die Einweisung am SWAXS Gerät und legendäre

Acknowledgements / Danksagung

Kochabende sowie Dr. Iulia Romanesko und Dr. Moritz von der Lühe für den tollen Empfang.

Bis hierher begleiteten mich außerdem meine Studienfreunde Felix, Manuel und Hannes nicht nur bei so mancher Quälerei, sondern vor allem während einer wunderbaren Zeit in Freiburg. Auch meine Schulfreunde waren während des Chemiestudiums und meiner Promotion immer präsent, danke an Maximilian, Johannes, Julian und Mathias.

Diesen Punkt hätte ich sicherlich nicht ohne meine Familie erreicht, durch die ich unerschütterlich bin. Ich danke meinen Großeltern und Eltern genauso für ihre Unterstützung wie meinen Geschwistern. Sicherlich wäre der zweite Abschnitt meiner Promotion nicht annähernd so schön und längst nicht so aufregend gewesen ohne den zweiten Teil meiner Familie hier in Thüringen. Danke für diese besondere Zeit!

Declaration of authorship / Selbständigkeitserklärung

Declaration of authorship / Selbständigkeitserklärung

Ich erkläre, dass ich die vorliegende Arbeit selbständig und unter Verwendung der angegebenen Hilfsmittel, persönlichen Mitteilungen und Quellen angefertigt habe.

Johannes B. Max

Datum

Ort

Unterschrift

Documentation of authorship

Erklärung zu den Eigenanteilen der Promovendin/des Promovenden sowie der weiteren Doktorandinnen/Doktoranden als Co-Autorinnen/-Autoren an den Publikationen und Zweitpublikationsrechten bei einer kumulativen Dissertation

Für alle in dieser kumulativen Dissertation verwendeten Manuskripte liegen die notwendigen Genehmigungen der Verlage („Reprint permissions“) für die Zweitpublikation vor.

Die Co-Autorinnen/-Autoren der in dieser kumulativen Dissertation verwendeten Manuskripte sind sowohl über die Nutzung, als auch über die oben angegebenen Eigenanteile der weiteren Doktorandinnen/Doktoranden als Co-Autorinnen/-Autoren an den Publikationen und Zweitpublikationsrechten bei einer kumulativen Dissertation informiert und stimmen dem zu.

Die Anteile der Promovendin/des Promovenden sowie der weiteren Doktorandinnen/Doktoranden als Co-Autorinnen/Co-Autoren an den Publikationen und Zweitpublikationsrechten bei einer kumulativen Dissertation sind in der Anlage aufgeführt.

Johannes B. Max

Datum

Ort

Unterschrift

Ich bin mit der Abfassung der Dissertation als publikationsbasierte Dissertation, d.h. kumulativ, einverstanden und bestätige die vorstehenden Angaben.

Prof. Dr. Felix H. Schacher

Datum

Ort

Unterschrift

Declaration on authorship contributions to the included publications/Erklärung zu den Eigenanteilen an den enthaltenen Publikationen

“Polyampholytic graft copolymers based on polydehydroalanine (PDha) – synthesis, solution behavior and application as dispersants for carbon nanotubes“

P1 J. B. Max,¹ D. V. Pergushov,² L. Sigolaeva,³ and F. H. Schacher,⁴
Polym. Chem., 2019, 10, 3006.

Author	1	2	3	4
Conceptual development/contribution	X			X
Synthesis and structural characterization of the polymers	X			
Investigation of the solution behavior	X	X	X	
Preparation of manuscript	X	X	X	
Correction of the manuscript	X	X	X	X
Proposed publication equivalent	1.0			

“Double Hydrophilic Poly(ethylene oxide)-*block*-Poly(dehydroalanine) Block Copolymers: Comparison of Two Different Synthetic Routes “

P2 Johannes B. Max,¹ Peter J. Mons,² Jessica C. Tom,³ and Felix H. Schacher,⁴
Macromol. Chem. Phys., 2020, 221, 1900383

Author	1	2	3	4
Conceptual development/contribution	X	X	X	X
Synthesis of the block copolymers, kinetic studies and structural characterization	X	X	X	
Deprotection of the block copolymers	X			
Characterization of the solution behavior	X			
Preparation of manuscript	X	X	X	
Correction of the manuscript	X	X	X	X
Proposed publication equivalent	1.0			

Documentation of authorship

“Polyampholytic Poly(dehydroalanine) Graft Copolymers as Smart Templates for
pH-Controlled Formation of Alloy Nanoparticles. “

P3

J. B. Max,¹ K. Kowalczyk,² M. Köhler,³ C. Neumann,⁴ F. Pielenz,⁵ L. V.
Sigolaeva,⁶ D. V. Pergushov,⁷ A. Turchanin,⁸ F. Langenhorst,⁹ and F. H.
Schacher¹⁰

Macromolecules, 2020, 53, 4511-4523

Author	1	2	3	4	5	6	7	8	9	10
Conceptual development/contribution	X									X
Synthesis of the polymers	X	X								
Structural characterization of the polymers (SEC, FT-IR, NMR)	X	X								
UV-vis of the NP dispersions	X									
Preparation of the nanoparticles	X									
Potentiometric Titration	X					X	X			
ζ-potential measurements	X	X								
TEM measurements	X		X						X	
EDX measurements									X	
XPS measurements	X			X						
eNMR measurements		X			X					
Preparation of manuscript	X	X								
Correction of the manuscript	X	X	X	X	X	X	X	X	X	X
Proposed publication equivalent	1.0									

Documentation of authorship

“Triple-responsive polyampholytic graft copolymers as smart sensors with varying output “

P4 Johannes B. Max,^{1‡} Afshin. Nabiyan,^{2‡} Jonas Eichhorn,³ and Felix H. Schacher⁴
Macromol. Rapid Commun., 2021, 42 2000671.

‡Both authors contributed equally to this work

Author	1	2	3	4
Conceptual development/contribution	X	X		X
Preparation of the polymers	X			
Characterization of the polymers and their solution behavior	X	X		
TEM measurements		X	X	
Preparation of manuscript	X	X		
Correction of the manuscript	X	X	X	X
Proposed publication equivalent	1.0			

“Polyampholytic graft copolymers as matrix for TiO₂/Eosin Y/[Mo₃S₁₃]²⁻ hybrid materials and photocatalysis”

P5 Afshin. Nabiyan,^{1‡} Johannes B. Max,^{2‡} Christof Neumann,³ Magdalena Heiland,⁴ Andrey Turchanin,⁵ Carsten Streb,⁶ and F. H. Schacher⁷
Chem. Eur. J., 2021, 27, 1-7

‡Both authors contributed equally to this work

Author	1	2	3	4	5	6	7
Conceptual development/contribution	X	X					X
Synthesis and characterization of the polymer		X					
Preparation and characterization of the hybrid materials	X	X					
H ₂ measurements	X						
XPS measurements			X				
Preparation of manuscript	X	X					
Correction of the manuscript	X	X	X	X	X	X	X
Proposed publication equivalent		1.0					

Documentation of authorship

“Polyampholytic graft copolymers: A platform to combine sensitizers and catalysts“

P6 A. Nabiyan,¹ J. B. Max,² M. Micheel,³ J. Eichhorn,⁴ M. Wächtler,⁵ M. Schulz,⁶ C. Neumann,⁷ B. Dietzek,⁸ A. Turchanin⁹ and Felix H. Schacher¹⁰

in preparation

Author	1	2	3	4	5	6	7	8	9	10
Conceptual development/contribution	X	X		X						X
Synthesis and characterization of the polymer		X								
Preparation and characterization of the hybrid materials	X	X								
XPS characterizations								X		
Optical characterization	X	X	X							
TEM measurements	X			X						
H ₂ measurements	X	X				X				
Preparation of manuscript	X	X								
Correction of the manuscript	X	X	X	X	X	X	X	X	X	X
Proposed publication equivalent		1.0								

“Double Hydrophilic Copolymers – Synthetic Approaches, Architectural Variety, and Application Fields“

P7 Afshin Nabiyan,^{1,‡} Johannes B. Max,^{2,‡} Felix H. Schacher³

Chem. Soc. Rev., **2022**, DOI: 10.1039/D1CS00086A

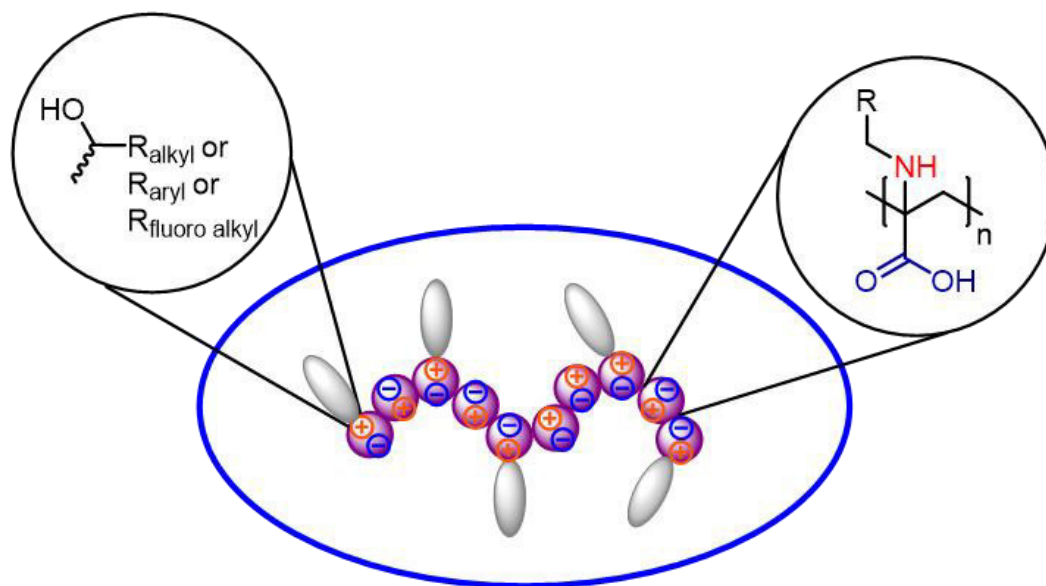
‡Both authors contributed equally to this work

Author	1	2	3
Conceptual development/contribution	X	X	X
Preparation of manuscript	X	X	
Correction of the manuscript	X	X	X
Proposed publication equivalent		0.5	

Publication P1 – P7

Publication P1

“Polyampholytic graft copolymers based on polydehydroalanine (PDha) – synthesis, solution behavior and application as dispersants for carbon nanotubes“

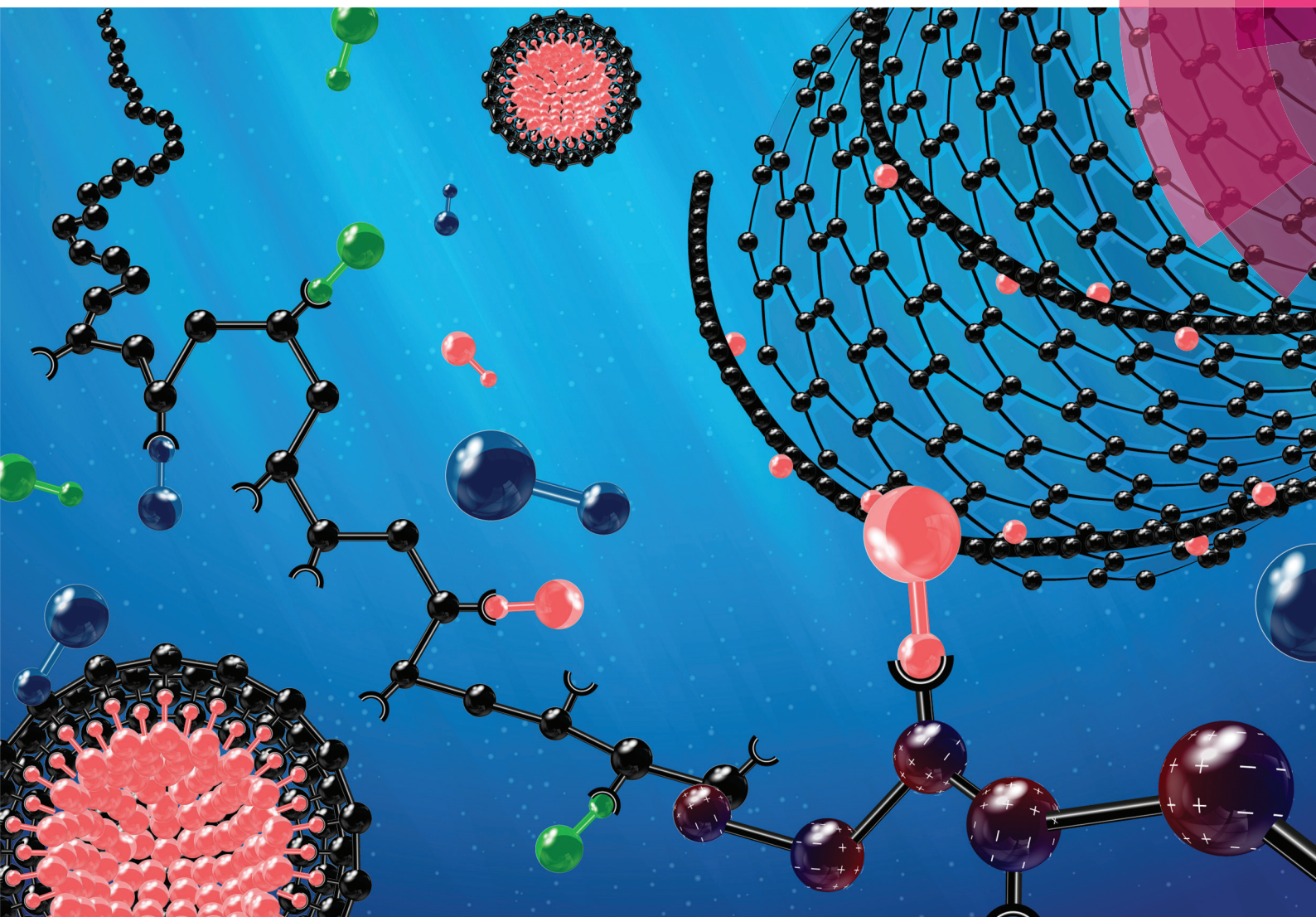


J. B. Max, D. V. Pergushov, L. Sigolaeva, and F. H. Schacher

Polym. Chem., **2019**, 10, 3006

Polymer Chemistry

rsc.li/polymers



Themed issue: Pioneering Investigators 2019

ISSN 1759-9962



ROYAL SOCIETY
OF CHEMISTRY

Celebrating
IYPT 2019

PAPER

F. H. Schacher *et al.*

Polyampholytic graft copolymers based on polydehydroalanine (PDha) – synthesis, solution behavior and application as dispersants for carbon nanotubes



Cite this: *Polym. Chem.*, 2019, **10**, 3006

Polyampholytic graft copolymers based on polydehydroalanine (PDha) – synthesis, solution behavior and application as dispersants for carbon nanotubes†

J. B. Max, ^{a,b,c} D. V. Pergushov,^d L. V. Sigolaeva ^d and F. H. Schacher ^{*a,b,c}

We herein introduce a versatile platform of graft copolymers featuring a polyampholytic backbone and side chains of varying length and polarity using post-polymerization modification of polydehydroalanine (PDha). Nucleophilic substitution of the amino group with various modifiers in water allows the attachment of alkyl, fluoro alkyl, and aryl epoxides as well as a Michael acceptor (acrylonitrile), whereby the overall degree of functionalization (DoF) can be controlled by adjusting both concentration and reaction time. The synthesized graft copolymers were characterized by spectroscopic techniques (¹H-NMR, ¹³C-NMR, solid state ¹³C-NMR, FT-IR), elemental analysis, and size exclusion chromatography (SEC) to prove successful grafting. By introduction of various side-chains, both the overall polarity and charge/charge density of the underlying PDha backbone changes, which is directly reflected in the solution behavior of the graft copolymers. We therefore investigated two examples by potentiometric titrations and ζ -potential measurements. As one example, modification with epoxyoctane led to amphiphilic graft copolymers which formed micelles in aqueous solution as revealed by dynamic light scattering (DLS) and transmission electron microscopy (TEM). Even more, we could show that these materials are promising dispersants for carbon nanomaterials (MWCNTs) and even pH-dependent reversible dispersion formation was possible. In general, the presented synthetic strategy opens up a wide range of novel surfactants with precisely tunable composition, polarity, and functionality.

Received 27th September 2018,
Accepted 26th October 2018

DOI: 10.1039/c8py01390j

rs.c.li/polymers

Introduction

Polyelectrolytes are macromolecules bearing either positive (polycations) or negative charges (polyanions), an equal amount of counterions, and are typically water-soluble. As a subclass, polyampholytes and polyzwitterions feature oppositely charged moieties or ionizable groups either within the polymer backbone or in the side-chain. In case of polyzwitterions, both groups are even located within the same monomer unit.^{1–3} Such materials are not only responsive towards various external triggers such as ionic strength, pH, and temperature

but can also interact with oppositely charged interfaces, surfaces, or polymeric materials.^{4–6} Consequently, this class of polymers is of great interest for a wide range of applications; not only in industrially relevant processes such as flocculants, super absorbers, or dispersing agents,^{2,7} but also in surface coatings,^{8,9} as selective layers in membranes,^{10,11} for the recycling and separation of proteins and/or metal ions from different media,^{12–15} and in biomedical applications including drug delivery and tissue engineering.¹⁶ In particular, polyzwitterions are receiving increasing research interest due to their high hydrophilicity, as well as their tolerance to increasing ionic strength, in contrast to simple polyanions or cations. In addition, many polyzwitterions are structurally analogous to biomacromolecules, and offer the potential to be used as biocompatible materials.¹⁷

The repeat units of such polyzwitterions commonly include cationic ammonium groups, as well as anionic sulfonates, carboxylates, phosphates, phosphonates, or phosphinates.^{5,18–22} The respective polymers can be synthesized either through direct polymerization of zwitterionic monomers, or by the post-polymerization modification of suitable precursor structures; each strategy exhibits inherent advantages and draw-

^aInstitute of Organic Chemistry and Macromolecular Chemistry (IOMC), Friedrich-Schiller-University Jena, Lessingstraße 8, D-07743 Jena, Germany. E-mail: felix.schacher@uni-jena.de

^bJena Center for Soft Matter (JCSM), Friedrich-Schiller-University Jena, Philosophenweg 7, D-07743 Jena, Germany

^cCenter for Energy and Environmental Chemistry (CEEC), Friedrich-Schiller-University Jena, Philosophenweg 7a, D-07743 Jena, Germany

^dDepartment of Chemistry, M.V. Lomonosov Moscow State University, Leninskie Gory 1/3, 119991 Moscow, Russia

† Electronic supplementary information (ESI) available. See DOI: 10.1039/c8py01390j

backs.²³ In general, different synthetic methods can be applied for the synthesis of polyzwitterions including controlled/free radical polymerization or ring-opening metathesis polymerization (ROMP) of various vinyl monomers,^{24–27} step growth polymerizations (*e.g.*, ROP of cyclic esters),²⁸ polyaddition/polycondensation reactions,^{29,30} as well as coupling reactions.³¹ However, many of the available synthetic pathways are challenging and have limitations such as poor solubility of the polyzwitterions in most solvents except water, high melting points, and the presence of ionic groups during the polymerization.¹⁷

An alternative and more promising route is the polymerization of protected monomers, and subsequent deprotection to yield the respective polyzwitterions. Following this route, materials such as polydehydroalanine (PDha) or poly(imidazolyl acrylic acid) (PImAA) with a very high charge density and pH-dependent charge characteristics can be obtained.^{32–34} In case of PDha, the corresponding precursors are typically synthesized *via* radical polymerization of the protected captodative dehydroalanine derivatives – most often, the amino group is protected by an alkyl amide or using a *tert*-butoxy carbonyl (boc) group, while the carboxylic acid is provided by a methyl ester.^{32,33,35–41} PDha was found to exist as polyzwitterion in the pH-range of 6.5 to 10.5, and has already been applied as a coating for magnetic nanoparticles.^{32,42–44} In addition, double hydrophilic or amphiphilic PDha-based block copolymers can be synthesized starting from the corresponding polystyrene- (PS-*b*-PtBAMA) or poly(*n*-butyl methacrylate)-based (PnBA-*b*-PtBAMA) precursors. The subsequent deprotection results in the formation of amphiphilic or double hydrophilic block copolymers with interesting solution properties. In particular PS-*b*-PDha was shown to form core-corona micelles in aqueous solution.^{40,41}

Solution self-assembly is not limited to amphiphilic block copolymers, and has also been observed for other polymeric architectures where the hydrophilic polymer backbones are modified with hydrophobic groups so that hydrophobic interactions compete with ionic interactions in solution.^{23,45} Common architectures apart from block copolymers include star-shaped or graft copolymers, dendrimers, segmented block copolymers or polysoaps, where in the latter case, different structures can also be realized depending on the position of the ionic groups.^{45–47} The multitude of different combinations can also lead to so-called “polyphilicity” as outlined in a recent review.⁴⁸ It is not always possible to access such polymeric architectures *via* a facile or straightforward approach, and this is one reason why more and more interest is being directed towards amphiphilic graft copolymers containing short side-chains. These examples can be easily synthesized *via* various polymerization methods, subsequent post-polymerization modification of the functionalized precursors with hydrophobic entities, or by the copolymerization of hydrophobic and hydrophilic monomers. Nevertheless, the choice of a suitable solvent can be difficult in case of the last route.^{23,46,49} Known examples include the radical copolymerization of acrylic acid with different alkyl amine comonomers, fluorinated acrylates⁵⁰ with added *N*-isopropylacrylamide,⁵¹ or an alternating copolymeriza-

tion of maleic anhydride and octyl vinyl ether, followed by the subsequent hydrolysis of the anhydride groups.⁵² Notably, the polymerization starting from reactive surfactant molecules is basically also possible, but often requires a multi-step synthesis of the respective monomers.^{53–55}

As an alternative, the field of polymer-analogous reactions offers a great variety of possible modifications *via* different mechanisms including addition, substitution, elimination and isomerization reactions.⁵⁶ Hence, the grafting of hydrophobic side-chains onto a hydrophilic backbone or *vice versa*, is a versatile alternative to the direct copolymerization of functional monomers and enables further fine-tuning of the properties by controlling the type and density of grafted moieties.⁴⁶ In this context, amino- and carboxylic acid groups have already been explicitly used, *e.g.* to form hydrophobically modified poly(acids) by amidation or esterification, ring-opening reactions of poly(maleic anhydride),^{57–59} or catalyzed transamidation reactions of poly(acrylic acid).⁶⁰ In addition, polymers containing amino moieties can be modified by reacting with haloalkanes or esters to form various side-chains.^{61–64} Ring-opening reactions are also known; for example, poly(ethylene imine) has been used for subsequent functionalization with epoxyalkanes, as well as acrylic acid *via* a Michael-addition, and the resulting amphoteric polymeric surfactants were pH-responsive and zwitterionic between pH 4 and 10.^{65,66}

We herein present a facile and straightforward route to synthesize graft copolymers of different functionality and polarity using PDha as a polyampholytic backbone. After synthesis and deprotection, the amino groups of PDha were then further functionalized either by ring-opening of various epoxides or by Michael-addition using acrylonitrile. These post-polymerization strategies resulted in the generation of pendants with varying polarity and length with simultaneous control over the grafting density. So far, C₈ and C₁₂, as well as fluorinated alkyl chains, benzyl, nitrile and carboxylic groups have been attached to the PDha backbone. Materials combining the properties of the polyzwitterion PDha with various hydrophobic side-chains are interesting candidates as pH-responsive dispersants or emulsifiers.²³ Therefore, we also highlight the application of such PDha-based graft copolymers for the solubilization of multi-walled carbon nanotubes (MWCNTs), as previous reports indicate that comparable hybrid materials can show excellent properties in the preparation of advanced biosensors.⁶⁷

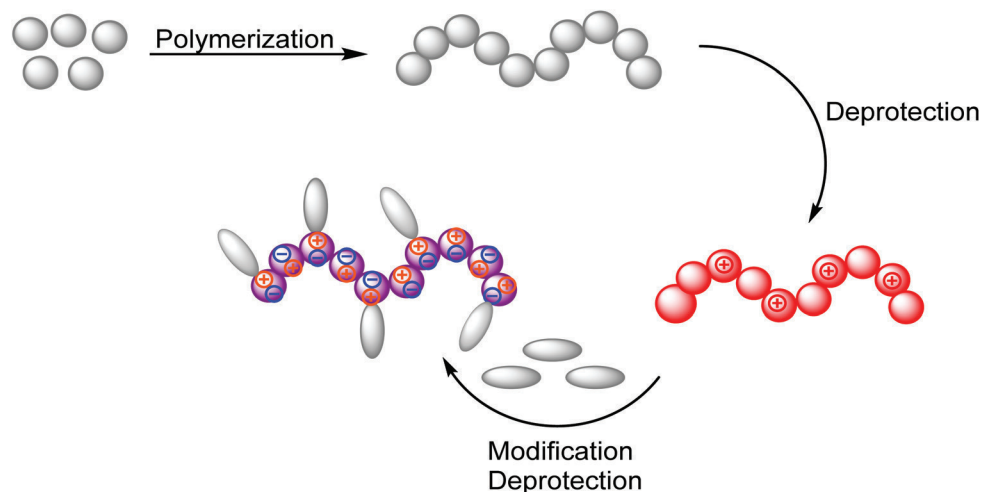
Results and discussion

Synthesis and characterization of PDha-based graft copolymers

Post-polymerization modifications allow the preparation of a variety of functional polymers starting from a single precursor.⁵⁶ We have recently introduced PDha as a versatile polyampholyte, and the synthesis was realized using either free or controlled radical polymerization.^{32,40,41} We also demonstrated that such materials are interesting as coatings for magnetic iron oxide nanoparticles and, depending on the solution pH,

allow reversible electrostatic adsorption of various polyelectrolytes, BSA, and methylene blue.^{44,68} Herein, we introduce a facile strategy where PDha is employed as the backbone for graft copolymers of varying composition, solubility, charge and charge density. The synthesis was carried out in three steps (Scheme 1), starting with the free radical polymerization of *tert*-butoxycarbonylaminoethylacrylate (*t*BAMA), subsequent partial deprotection of poly(*tert*-butoxycarbonylaminoethylacrylate) (PtBAMA) to poly(aminomethylacrylate) (PAMA), before modification and simultaneous deprotection was performed to result in a range of polyzwitterionic graft copolymers.

The synthesis of PtBAMA (Fig. 1A) was carried out *via* free radical polymerization using trimethylbenzoyl diphenylphosphine oxide (TPO) as UV-photoinitiator under dilute conditions as described previously.⁴² The polymer exhibiting a M_n of 14 400 g mol⁻¹ and a D of 5.66 was obtained with a yield of 88% after precipitation in *n*-hexane. The boc protective group was subsequently removed under acidic conditions using 40 eq. of trifluoroacetic acid. After 1 h at 50 °C, the polymer was collected by precipitation in an excess methanol (MeOH) to obtain PAMA (M_n = 7100 g mol⁻¹, D = 2.82, 60% yield). Please note that under these conditions a significant amount of the



Scheme 1 Schematic depiction of the synthesis of amphiphilic PDha-based graft copolymers.

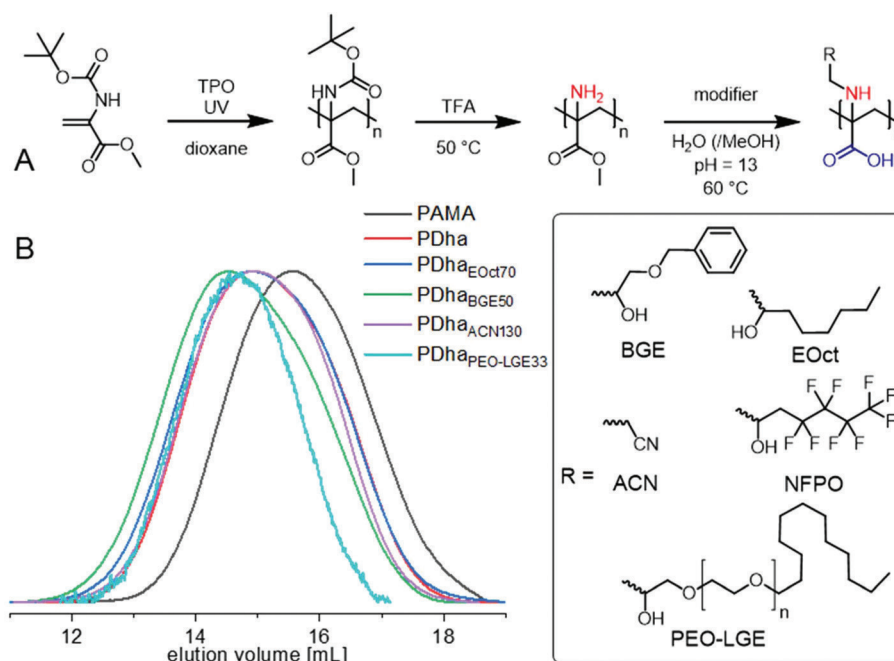


Fig. 1 Synthetic route towards functionalized PDha-based polyampholytic graft copolymers using different modifiers (A) and the corresponding SEC traces of the synthesized polymers and graft copolymers (B).

methyl ester (~80%) is also cleaved simultaneously;³² but the presence of carboxylic acid groups will not affect the following modification reactions, where a complete deprotection towards a polyampholytic PDha backbone will be carried out. The corresponding ¹H-NMR spectra and SEC traces are shown in the ESI (Fig. S1†). Regarding further modification of PAMA, two convenient routes based on the presence of nucleophilic amino groups can be identified. The first possibility is a Michael-addition reaction of electrophilic vinyl compounds as described by Narayanan, Maiti, and De.⁶⁹ The second is the nucleophilic ring-opening of epoxides, which has already been used for the modification of poly(ethylene imine) and poly(glycidyl methacrylate).^{70,71} A great advantage of both strategies is that the respective modifiers are often commercially available; hence, a large variety of different side chains can be introduced directly. Since PAMA is insoluble in common organic solvents except DMSO, the following post-polymerization modifications were carried out in water under basic conditions. Due to the moderate solubility of PAMA, the polymer was dissolved at a relatively low concentration (6.66 g L⁻¹) overnight. A pH of 13 was chosen to increase the nucleophilicity of the amino groups and to better solubilize PAMA. Next, the different modifiers were added at varying ratios with respect to the amino groups and the resulting reaction mixtures were stirred for several days at 60 °C. The non-polar and water-insoluble epoxides were added in methanol (3/1 v/v H₂O/methanol) to adjust the solvent polarity and improve mixing of all reactants. The following electrophiles were used: benzyl glycidyl ether (BGE), 1,2-epoxy octane (EOct), nonafluoropentyl-oxirane (NFPO), poly(ethylene glycol)glycidyl lauryl ether (PEO-LGE), and acrylonitrile (ACN).

After the reaction, the crude products were precipitated in 0.5 M aqueous HCl, and the obtained graft copolymers were washed thoroughly with different solvents to remove unreacted modifier and other impurities. The resulting copolymers are

denoted as PDha_{XY} where X is the added modifier and Y is the determined degree of functionalization (DoF). The successful modifications and presence of introduced side-chains were then confirmed *via* SEC (Fig. 1B and Table 2), FT-IR, and NMR spectroscopy (¹H and ¹³C).

Characterization of PDha_{EOct} and PDha_{BGE}. NMR spectra were measured in basic D₂O (pH = 13); both the polymer backbone and pendant signals are visible, which is exemplarily shown for PDha_{EOct8} and PDha_{BGE50}, as well as for the corresponding epoxides. In the ¹H-NMR spectrum of PDha_{EOct} (Fig. 2A and Fig. S2†), the backbone protons are visible between 2.80 and 1.90 ppm in accordance with the spectrum of non-functionalized PDha (Fig. S3†), which is overlaid by the -N-CH₂- protons of the side-chain. The signals of the alkyl protons are visible between 1.45 and 1.10 (-CH₂-) and 0.85 and 0.65 (-CH₃) ppm. In case of PDha_{BGE} (Fig. S4†), the backbone signals are again visible, and the aromatic protons are observed between 7.50 and 7.00 ppm, which indicates a successful addition of the benzyl glycidyl ether to the amino group. While the ¹³C-NMR spectrum of PDha (Fig. S5†) shows three signals at 180, 65 and 47 ppm corresponding to the carbonyl and backbone carbon atoms, the PDha_{BGE50} spectrum (Fig. 2B) shows additional signals at 138, 128 and 127 ppm, which correspond to the aromatic carbons. For PDha_{EOct} (Fig. S6†), the alkyl chain carbons appear between 35 and 10 ppm. Besides, the signals of the used epoxide disappear.

The DoF was determined from ¹H-NMR spectra whereby the -CH₂- protons of the repeating units were integrated and compared to the integral of the new side-chain protons. For PDha_{EOct}, the -CH₃ group was chosen to compare to the intensity of the backbone signal. For PDha_{BGE}, the signals of the five aromatic protons were integrated and compared to the backbone proton. It was found that the DoF can be varied by changing the concentration of the modifier and reaction time (Table 1). For PDha_{EOct}, the DoF is 8% when 1.5 equivalents of EOct are used, increasing to 70% by increasing the amount of

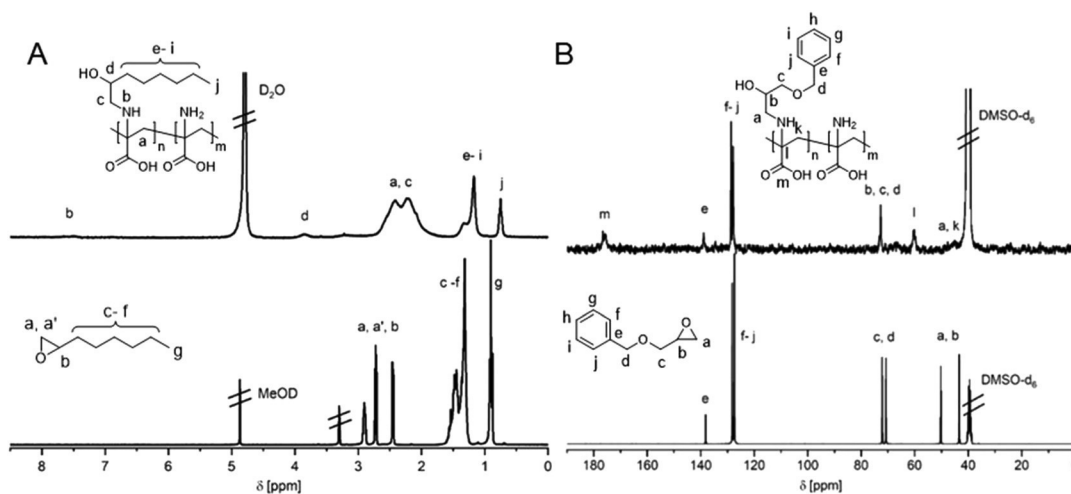


Fig. 2 ¹H-NMR spectrum of EOct (bottom, in MeOD) and PDha_{EOct8} (top, in D₂O + NaOD) (A) and ¹³C-NMR spectrum of BGE (bottom) and PDha_{BGE50} (top) in DMSO-d₆ (B).

Table 1 Summary of analytics, characteristics and solubility of the synthesized PDha-based graft copolymers

Entry	Modifier	Eq. per monomer unit	Degree of functionalization ^a [%]	Solubility ^e			Characterization
				DMF	DMSO	H ₂ O ^c	
0	—	0	0	—	+	+	¹ H-, ¹³ C-NMR, IR
1	EOct	1.5	8	+	+	+	¹ H-, ¹³ C-NMR
2	EOct	10	70	+	+	+/-	¹ H-, ¹³ C-NMR, DLS, TEM
3	BGE	10	20	+	+	+	¹ H-, ¹³ C-NMR
4	LGE	10	—	—	—	—	No reaction
5	ACN	10	130	+	+	+	¹ H-, ¹³ C-NMR, IR
6	EOct	20 ^d	70	+	+	+/-	¹ H-NMR
7	BGE	20 ^d	50	+	+	+	¹ H-NMR
8	LGE	20 ^d	—	—	—	—	No reaction
9	ACN	20 ^d	135	+	+	+	¹ H-NMR, IR
10	PEO-LGE	2	33 ^b	+	+/-	—	¹ H-NMR, solid state ¹³ C-NMR, IR
11	NFPO	10	65 ^b	+	+/-	—	¹ H-, ¹⁹ F-NMR, solid state ¹³ C-NMR, IR

^a Calculated from ¹H-NMR spectroscopy. ^b Calculated from elemental analysis. ^c pH = 12. ^d *t*_{react} = 10 d. ^e As a function of the DoF and the employed modifier: + ≙ well soluble, clear solution; +/- ≙ poorly soluble (by heating), turbid solution, partly precipitation after time, — ≙ insoluble (also after heating).

epoxide to 10 equivalents. This means that excess modifier is necessary to achieve high degrees of functionalization, which can be attributed to non-ideal mixing and possible epoxide ring-opening under basic conditions. For PDha_{BGE}, the DoF increases from 20 to 50% by doubling the reaction time and the amount of epoxide from 10 to 20 equivalents relative to PDha_{BGE}. However, for all graft copolymers irrespective of the excess modifier used, the possible DoF that can be achieved is limited, which we ascribe to steric hindrance.

Characterization of PDha_{NFPO} and PDha_{PEO-LGE}. In addition to the above mentioned modifiers, lauryl glycidyl ether (LGE) was also investigated. However, no significant grafting was observed by NMR, which can be ascribed to phase separation occurring during the reaction due to the poor solubility of LGE in water. Hence, PEO-LGE was used, where the glycidyl ether is linked to a hydrophilic PEO segment (DP = 16), which should facilitate the reaction between the amino groups of PDha and the epoxide. As both PDha_{PEO-LGE} and PDha_{NFPO} exhibit low solubility in water after post-polymerization modification due to their hydrophobic pendants, it was necessary to measure the NMR spectra in DMSO-*d*₆. For this reason, the protons of the PDha backbone are no longer visible as they overlap with the solvent signal (Fig. S7 and S8†). However, the side-chain signals remain visible for PDha_{PEO-LGE} at 3.5 ppm for the PEO segment and between 1.64 and 0.71 for the alkyl chain. It should be noted that the graft copolymers also present limited solubility in DMSO, resulting in rather low quality ¹³C-NMR spectra. Hence, solid-state ¹³C-NMR was performed, where the carbon atoms of the side-chains and the polymer backbone could be detected (Fig. 3 and 4A). The ¹³C-NMR spectrum of PDha_{PEO-LGE} presents signals between 35 and 10 ppm as well as at 70 ppm that originate from the PEO segment in agreement with the NMR spectrum of the corresponding epoxide. The epoxide signals at 52 and 45 ppm disappear, whilst the C=O peak of the PDha backbone at 172 ppm appears.

In the ¹³C-NMR spectrum of PDha_{NFPO65} (Fig. 4A), the signals of the C–F carbon atoms are visible between 120 and

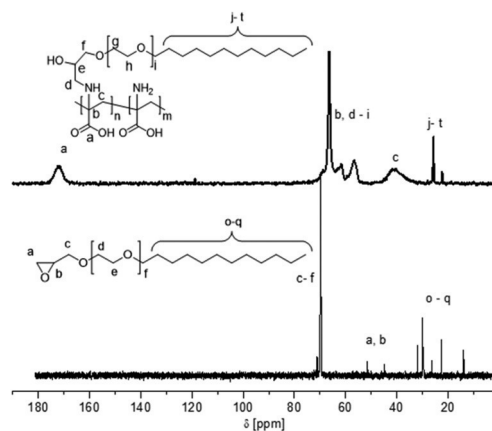


Fig. 3 ¹³C-NMR spectrum of PEO-LGE (bottom, D₂O) and PDha_{PEO-LGE33} (top, solid state).

105 ppm in accordance with the spectrum of NFPO. The ¹⁹F-NMR spectrum for this graft copolymer (Fig. 4B) demonstrates the successful side-chain addition by the presence of fluorine atoms. Here, four signals are observed for fluorine attached to different carbons at –80, –113, –124, and –125 ppm, which are in agreement with the spectrum of the pristine fluorinated epoxide.

For PDha_{NFPO} and PDha_{PEO-LGE}, it was not possible to determine the DoF using ¹H-NMR spectroscopy due to the overlapping solvent signal. Therefore, elemental analysis was performed, where a change in the ratio of nitrogen to carbon in comparison with PDha is observed due to the addition of alkyl chains (ESI eqn (1) and Table 1†). By elemental analysis, a DoF of 65% was determined for the functionalization of PAMA with NFPO using 10 equivalents of the epoxide. This corresponds to the value obtained for PDha_{EOct70}, where the functionalization was performed under similar reaction conditions, and in our opinion corresponds to the maximum DoF achievable. When PEO-LGE was used, the DoF achieved reached only 33%, which

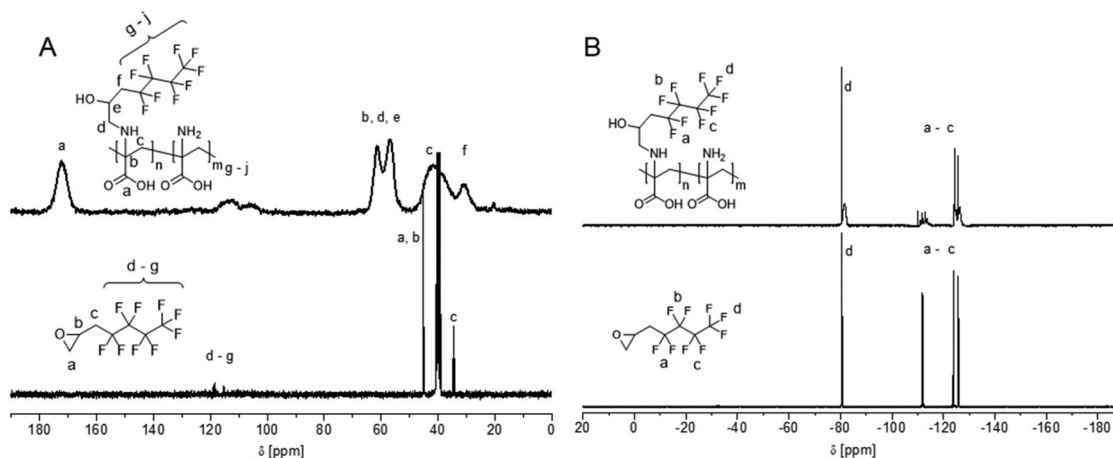


Fig. 4 ^{13}C -NMR spectrum of NFPO (bottom, in DMSO-d_6) and $\text{PDha}_{\text{NFPO}}$ (top, solid state) (A), and the corresponding ^{19}F -NMR spectra in DMSO-d_6 (B).

we attribute to the rather large side chain being introduced, which is accompanied by increased steric hindrance.

Characterization of PDha_{ACN} . In the ^{13}C -NMR spectrum of $\text{PDha}_{\text{ACN}130}$ (Fig. S9[†]), the $\text{C}=\text{O}$ signals at 175 ppm and nitrile at 119 ppm are seen, whilst the vinyl signals associated with the modifier are not visible. In addition, the ^1H -NMR spectrum clearly shows the presence of the $-\text{N}-\text{CH}_2-$ group with signals between 4.08 and 3.12 ppm (Fig. S10[†]) next to the backbone signals. The successful addition of acetonitrile was further confirmed *via* FT-IR spectroscopy, where the CN vibration is visible at 2250 cm^{-1} (Fig. 5B). The DoF was determined as described above for $\text{PDha}_{\text{EOct}}$ and PDha_{BGE} from the ratio of

the $-\text{CH}_2-$ backbone protons to the $-\text{N}-\text{CH}_2-$ protons of the side-chain. From the library of the copolymers described here, $\text{PDha}_{\text{ACN}130}$ exhibits the highest DoF of 130%, which implies that the amino groups are in principle capable of reacting twofold with acetonitrile.

The solubility of the modified PDhas in different solvents is expected to depend on the nature (polarity) of the pendants attached to the backbone. Hence, a coarse solubility profile of the as-synthesized graft copolymers in different solvents was examined and the results are presented in Table 1.

Similar to the PDha backbone, the synthesized graft copolymers are insoluble in common organic solvents including

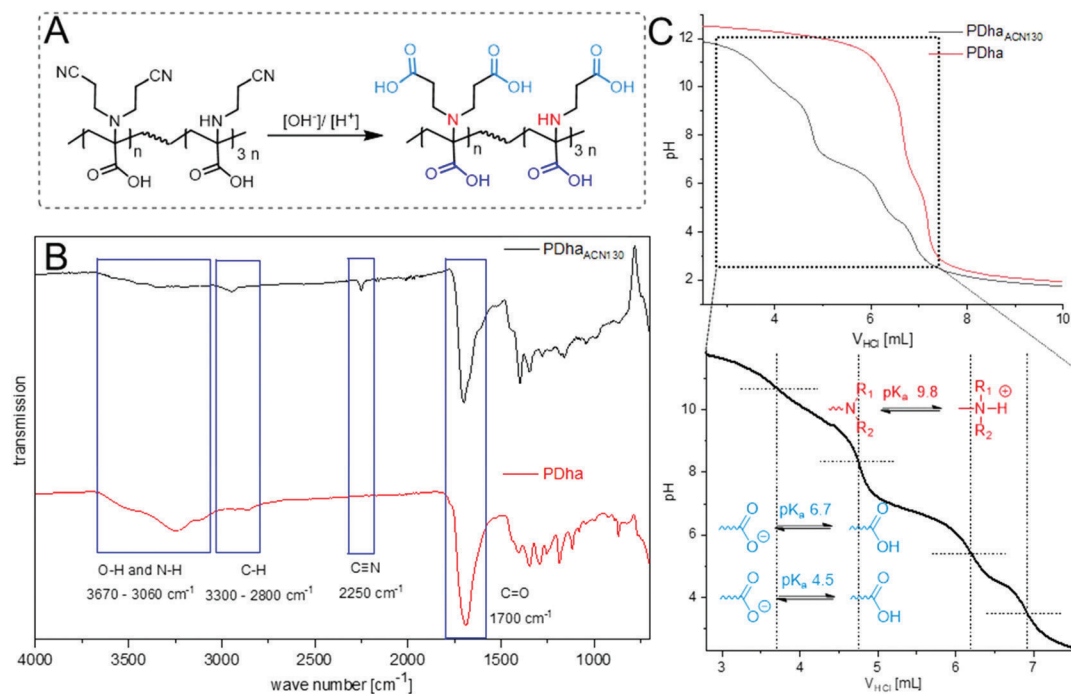


Fig. 5 Schematic structure of $\text{PDha}_{\text{ACN}130}$ before and after hydrolysis (A), comparison of the FT-IR spectra before and after modification of PDha (B), and the corresponding potentiometric titration curve of $\text{PDha}_{\text{ACN}130}$ (C).

methanol, ethyl acetate, dioxane, chloroform, and anisole. However, PDha is well-soluble in DMSO or water at elevated pH, and the synthesized graft copolymers are additionally soluble in DMF. Exceptions are PDha_{NFPO65} and PDha_{PEO-LGE33}, which are insoluble in water because of the highly hydrophobic side-chains. As apparent from PDha_{EOct}, the DoF can also affect the solubility of the prepared graft copolymers. While PDha_{EOct8} is well-soluble in water, at a DoF of 70% the solution is slightly turbid, presumably due to aggregation and the formation of micellar structures.

The graft copolymers were further investigated with respect to their molecular weight and dispersity using size exclusion chromatography (SEC) in DMSO. Upon comparing the SEC traces of the various graft copolymers with their precursor PAMA and the corresponding PDha backbone, a clear shift in the elution volume is observed (Fig. 1B and Table 2). In addition, all samples display monomodal molecular weight distributions, which indicates that there are no significant side reactions occurring, and a uniform functionalization of the PDha chains is achieved. An exception is PDha_{NFPO65} (Fig. S11[†]), which is characterized by a very broad molecular weight distribution, likely due to its poor solubility in DMSO and/or potential interactions with the SEC column material.

Solution behavior of selected graft copolymers

As we can introduce a range of side-chains featuring different polarity and charge, we also investigated the solution properties of some selected graft copolymers in dependence of the attached side chain (hydrophilic vs. hydrophobic).

We first carried out potentiometric titrations for PDha_{ACN130}, where most of the nitrile groups were hydrolyzed to the respective carboxylic acid groups during the reaction under basic conditions and the subsequent acidic work-up (Fig. 5A). The occurring hydrolysis is proven by FT-IR spectroscopy (Fig. 5B), where a shoulder at approximately 1620 cm⁻¹ appears (C=O vibration), which is not visible for the unmodified PDha. The results of a potentiometric titration of an alkaline solution (pH 12) also supports the transformation of nitrile groups into carboxylic acid moieties. Therefore, PDha_{ACN130} and PDha featuring a comparable degree of polymerization derived *via* the same synthetic route and at

comparable concentrations (15 g L⁻¹) were titrated with 0.1 M HCl (Fig. 5C). The titration curve of PDha_{ACN130} (black curve) shows clearly four steps, whereas the titration curve of PDha (red curve) only reveals three.³² The inflection points can be ascribed to the excess of NaOH, amino groups and apparently two kinds of carboxylic groups present in the graft copolymer. First the titrant is consumed for removal of the excess base, followed by the protonation of all amino groups exhibiting a pK_a of 9.8 ($\alpha_{\text{NH}_2} = 0.5$). This is in line with the value for unmodified PDha reported in our earlier work.³² Starting from a pH of 8.3, the first kind of carboxylate groups with a low acidity begin to be protonated to form -COOH. Their pK_a-value ($\alpha_{\text{COOH},1} = 0.5$) differs for about two units from the highly acidic carboxylic groups ($\alpha_{\text{COOH},2} = 0.5$): pK_{a, COOH,1} = 6.7 and pK_{a, COOH,2} = 4.5. Remarkably, the unmodified PDha does not show the presence of highly acidic carboxylic acid groups while only ones with a pK_a of about 6.2 ($\alpha_{\text{COOH}} = 0.5$) are found. For PDha_{ACN130}, it is not possible to ascribe these values directly to the backbone or pendant carboxylate groups, since both their respective titration volumes do not exactly fit to the amount of the amino groups. It is more likely, that the different kinds of carboxylic groups influence each other to change their protonation behavior, *e.g.*, by forming intramolecular hydrogen bonds. If this occurs between protonated and deprotonated groups, this could lead to a distinctly higher acidity. Comparing the amount of titrant consumed for the protonation of all amino groups (1.051 mL) and carboxylate groups (2.163 mL) the number of side-chain carboxylic groups per repeat unit was determined to be 1.05. Thus, the potentiometric titration confirms that a small amount of di-substituted monomer units are present in the polymer. However, this varies from the DoF of 130% calculated from ¹H-NMR, indicating that not all of the nitrile groups were hydrolyzed so far, which is also seen in the corresponding FT-IR spectrum. The ζ -potential of the graft copolymers in aqueous solution (Fig. S12[†]) is negative and stays between -20 and -10 mV within a pH range of 10-4 due to the presence of deprotonated carboxylic groups, the latter exist in PDha_{ACN130} in considerable excess compared to the amino moieties. Starting from a pH of 3, the values of the ζ -potential increase, becoming positive when a pH of 2 is reached due to full protonation of both the carboxylate and the amino groups. In our opinion, such ampholytic graft copolymers with tunable net charge and charge density are very interesting candidates for the reversible complexation of metal ions.

In contrast to the rather hydrophilic graft copolymer PDha_{ACN130}, PDha_{EOct70} formed turbid solutions upon dissolution in water at a pH of 12. Indeed, after attachment of hydrophobic side-chains, self-assembly of the resulting amphiphilic materials can be expected, in slight analogy to our previous work that describes the self-assembly of the amphiphilic block copolymer PS-*b*-PDha.⁴⁰ In case of PDha_{EOct70}, the hydrophobic side-chains induce self-assembly, forming hydrophobic domains, while the ampholytic PDha backbone stabilizes the formed aggregates in aqueous media (Fig. 6). These observations were confirmed using dynamic light scattering (DLS, Fig. 6C), where a hydrodynamic radius (R_h) of 16 nm was

Table 2 Molecular weight and dispersity of PDha-based graft copolymers and corresponding precursors

Polymer	M_n [g mol ⁻¹]	M_w [g mol ⁻¹]	D
PtBAMA ^a	14 400	82 700	5.77
PAMA ^b	7100	20 000	2.82
PDha ^b	12 300	34 700	2.82
PDha _{EOct70} ^b	12 300	40 100	3.25
PDha _{BGE50} ^b	16 900	51 500	3.05
PDha _{ACN130} ^b	14 000	37 600	2.68
PDha _{NFPO65} ^b	3200	64 500	20.03
PDha _{PEO-LGE33} ^b	23 800	45 300	1.95

^a SEC in CHCl₃/iso-propanol/NET₃, PMMA calibration. ^b SEC in DMSO + 0.5% LiBr, PUN calibration.

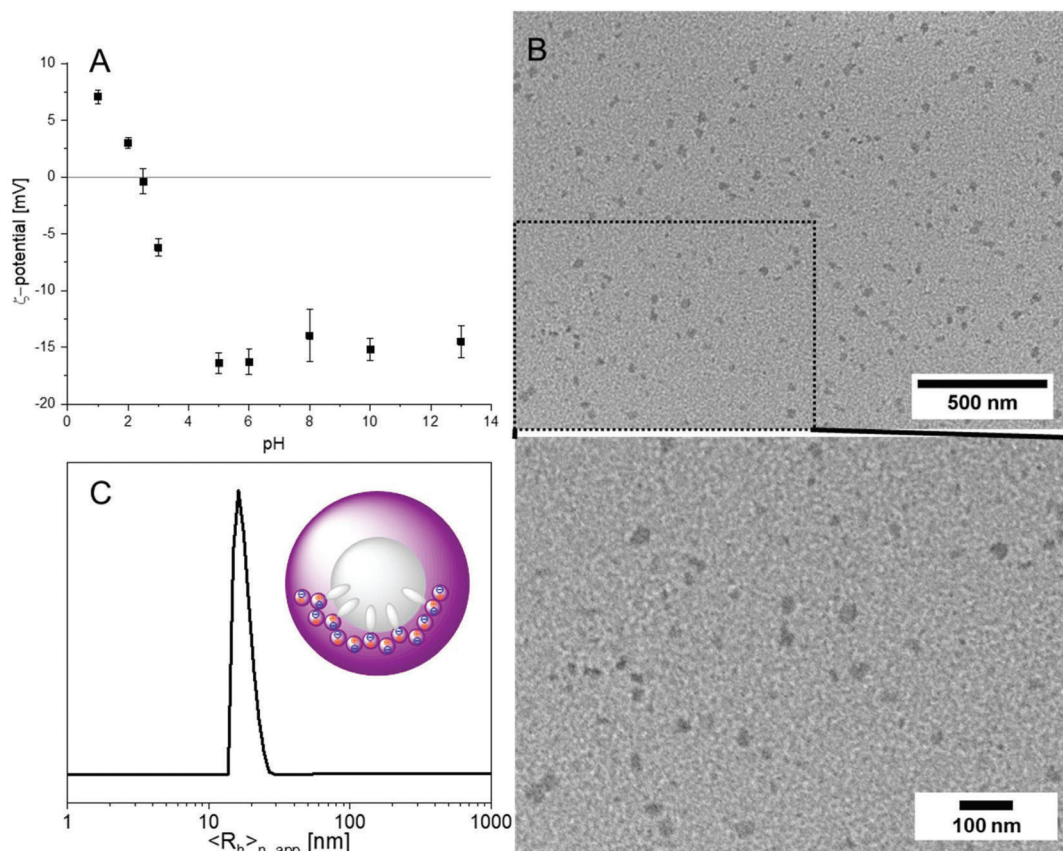


Fig. 6 pH-Dependent ζ -potential of PDha_{EOct70} reveals charge neutrality above a pH-value of 2 (A); TEM micrographs (B) and number-averaged DLS CONTIN plot (C) of PDha_{EOct70} in water (pH = 12) at a concentration of 0.5 g L⁻¹.

found, and this is markedly larger than expected for a single graft copolymer chain. Additional transmission electron microscopy (TEM) experiments also supported these observations as aggregates with an approximate diameter of 30 nm (Fig. 6B) were observed. At the same time, self-assembly of amphiphilic graft copolymers is rather complex, resembling the micellization of polysoaps. Here, three models exist, including the formation of local, regional, and molecular micelles that include both intra- and intermolecular aggregation of the hydrophobic groups.⁴⁶ The ζ -potential of the aggregates present (Fig. 6A) is negative and nearly constant (−15 mV) within a pH-range of 5–13 due to the presence of carboxylate groups. Upon further acidification, the values of the ζ -potential approach zero before becoming positive below a pH of 2, presumably due to the almost complete protonation of the carboxylate and amino moieties. The corresponding titration curve (Fig. S13†) displays two steps at pH-values of approximately 9 and 6.3 as a result of the protonation of the amino and carboxylate groups.

Ampholytic graft copolymers as dispersants for multi-walled carbon nanotubes

Nanocomposites based on amphiphilic polyelectrolytes and carbon nanomaterials, *e.g.*, carbon nanotubes (CNTs), possess

promising properties for use in biosensors.⁶⁷ Basically, the amphiphilic polyelectrolyte can act as both a dispersant for the hydrophobic CNTs and a host matrix for rather polar biomolecules. Quite often non-covalent interactions with the aromatic surface of CNTs using π – π or π –CH interactions of a hydrophobic segment, the polymeric backbone or the side-chain, are exploited to prepare stable dispersions.⁷² One example are phenoxy-functionalized dextrans employed for the solubilization of single walled CNTs (SWCNTs) in water.⁷³

Our previous investigation regarding the solution behavior of amphiphilic PDha_{EOct70} strongly suggests that this polymer should be capable of dispersing CNTs in water due to its hydrophobic C₈ alkyl-chains attached to the polyampholytic backbone (Fig. 7). Hence, we prepared dispersions by mixing a solution of PDha_{EOct70} (5 g L⁻¹, H₂O, pH = 12) and multi walled CNTs (MWCNTs) (1 g L⁻¹, H₂O, pH = 12) with a ratio of 1/1 (v/v), followed by sonication. The corresponding photographs (Fig. 7A and B) show the formation of a stable dispersion and the ζ -potential of the dispersed particles was -22.5 ± 1.8 mV. While the MWCNTs quickly settle in water, no precipitation within more than four months is observed when the dispersion is assisted by PDha_{EOct70}. Since PDha itself forms secondary aggregates under acidic conditions due to strong hydrogen bonding,³² we slowly added aqueous HCl to

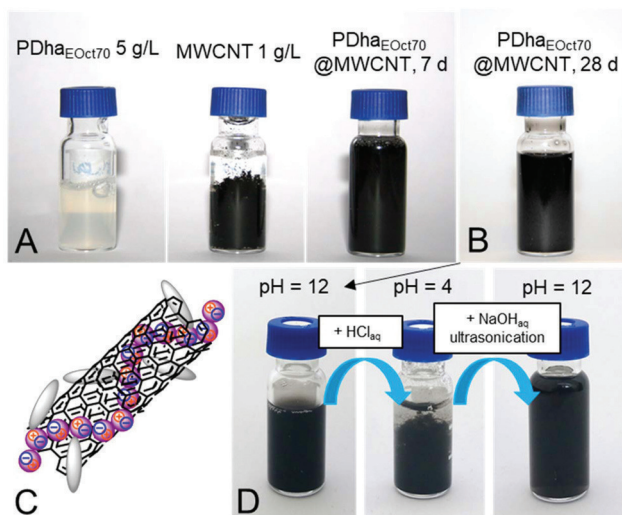


Fig. 7 Photographs of PDha_{EOct70} (5 g L⁻¹, H₂O, pH = 12), pristine MWCNTs (1 g L⁻¹, H₂O, pH = 12) and a mixture of both after sonication and storage for one week (A); the same dispersion after storage for four weeks (B); schematic depiction of a MWCNT after coating with PDha_{EOct70} (C); and the pH-dependent precipitation and re-dispersion of PDha_{EOct70}@MWCNTs (D).

adjust the pH to 4 and immediately observed pronounced precipitation of the MWCNTs (Fig. 7D). Furthermore, the MWCNTs can be re-dispersed by adding 0.1 M NaOH to (again) adjust the pH to 12. After a short sonication for 5 min a stable dispersion is obtained again; and, in our opinion, this renders PDha-based graft copolymers interesting materials for the purification and/or separation of CNTs – in addition to their general capability to disperse such materials in aqueous environment and further transfer them into potential biosensor coatings.

The fact that MWCNTs can be well dispersed in aqueous media by using PDha_{EOct70} suggests that carbon nanomaterials are shielded from water by the adsorbed polymer, which prevents their aggregation and ultimate precipitation. Hence, we examined the surface coverage of the MWCNTs by PDha_{EOct70}, or in other words, the actual amount of the copolymer necessary for the formation of stable dispersions. Therefore, the MWCNTs were dispersed as described above in aqueous solutions of the graft copolymer with different starting concentrations ranging from 0.5 to 6.0 g L⁻¹, while the amount of added carbon nanomaterial was kept constant. A starting polymer concentration of 5 g L⁻¹ led to the most efficient solubilization of the MWCNTs. In all other cases, the formation of aggregates and partial precipitation occurred with material clearly being visible at the bottom of the vials after several days. These observations were further supported by UV-Vis spectroscopy comparing the absorbance at a wavelength of 500 nm in accordance with literature. Since CNTs only absorb light when they are well dispersed, high absorbance values correlate with an efficient dispersion in PDha_{EOct70} solutions.^{74,75}

For this reason, the prepared dispersions were diluted by a factor of 40 and analyzed by UV-Vis spectroscopy, where the

spectrum of the respective graft copolymer solution was used as a baseline (Fig. S14[†]). Again, the highest absorbance was found PDha_{EOct70} initial concentration of 5 g L⁻¹.

Thermogravimetry (TGA) is a straightforward and facile method to determine the amount of organic matter present in hybrid materials. Therefore, TGA measurements of the most stable dispersion that contained 5 g L⁻¹ initial concentration of the graft copolymer were performed under a nitrogen atmosphere and the results were compared to those for the pristine graft copolymer and the pure MWCNTs (Fig. 8). The dispersion was precipitated using 0.5 M HCl, the resultant precipitate was washed several times with Milli-Q water to remove any salts, and then freeze-dried. In another approach, the stable dispersion was centrifuged until precipitation before being washed with Milli-Q water to remove any unbound polymer. While pure MWCNTs are relatively stable and no significant weight loss is observed up to a temperature of 700 °C, there are two decomposition steps visible for the graft copolymer and the hybrid material upon heating. The first can be ascribed to the loss of water when heating up to a temperature of 100 °C, and the second at approximately 250 °C corresponds to the decomposition of the graft copolymer itself. Hence, the weight loss of the samples was compared between 250 and 700 °C. The pure graft copolymer exhibits a weight loss of 52 wt% in this region in the absence of MWCNTs, whilst the hybrid materials show weight losses of 46 wt% and 41 wt% for the PDha_{EOct70}@MWCNTs purified *via* precipitation and centrifugation, respectively. This indicates that there is free graft copolymer in the dispersion that is removed through centrifugation or precipitation. By comparing the remaining mass of PDha_{EOct70}@MWCNT_{centrifuged} with that of the polymer sample without MWCNTs and the mass of MWCNTs itself, a composition of the hybrid material of 80 wt% polymer and 20 wt% MWCNTs can be determined. Since the overall composition of the dispersion after preparation was 5 g L⁻¹ (polymer) to 1 g L⁻¹

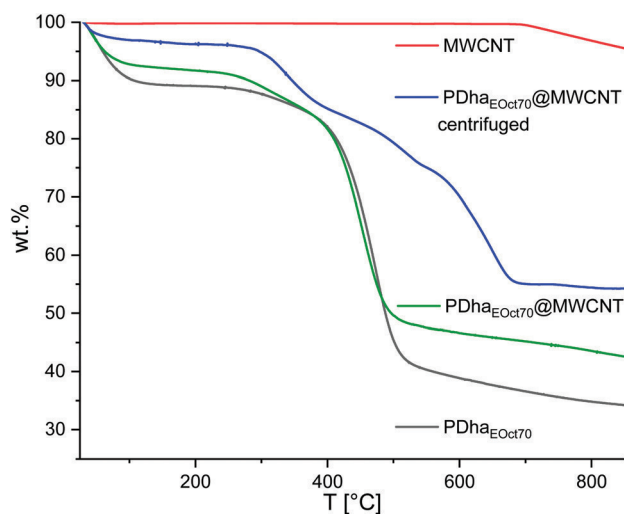


Fig. 8 Thermograms of MWCNTs (red trace), PDha_{EOct70} (black trace), PDha_{EOct70}@MWCNTs (green trace) and PDha_{EOct70}@MWCNTs after centrifugation (blue trace).

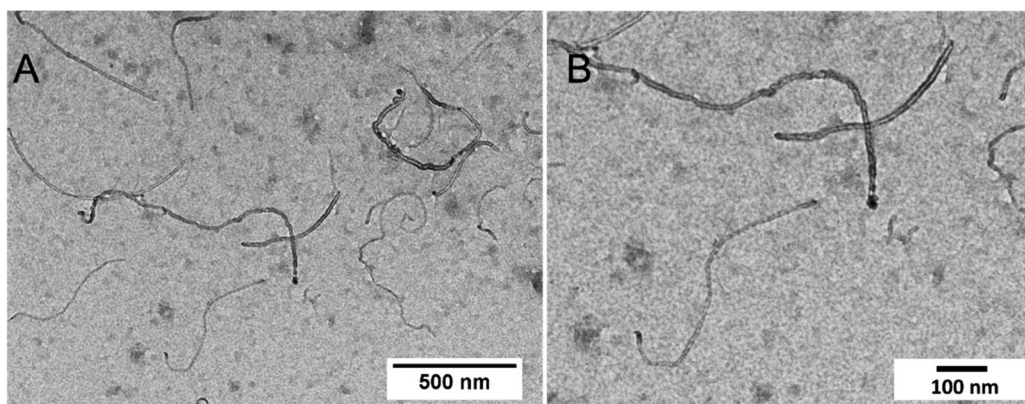


Fig. 9 TEM micrographs of MWCNTs after the non-covalent attachment of PDha_{EOct70}. Samples were taken from stable dispersions at a concentration of the polymer of 5 g L⁻¹.

(MWCNTs), that is 5 : 1 (wt/wt), the presence of some unbound PDha_{EOct70} could be assumed. FT-IR analysis of the freeze-dried supernatant liquid further confirmed these findings.

To further visualize the successful dispersion of the carbon nanomaterial toward individual MWCNTs, TEM micrographs were taken for the formed PDha_{EOct70}@MWCNT dispersion after seven days (Fig. 9A and B). Here, the presence of individual well-separated MWCNTs with lengths of several hundreds of nm could be observed, which are presumably covered by PDha_{EOct70} graft copolymers.

According to the results presented above, our strategy towards PDha-based graft copolymers not only provides access to a library of polymers with tailored charge and hydrophilic–hydrophobic balance, but also allows for rather facile preparation of well-defined and long-term stable aqueous dispersions of carbon nanomaterials such as CNTs. We expect, that such hybrid materials could be used for the fabrication of electrochemical biosensors, in particular those where direct electron transfer is exploited.

Conclusion

We have described a synthetic route to prepare zwitterionic PDha-based graft copolymers *via* post-polymerization modification and their characterization. The amine groups along the polymer backbone are convenient reactive handles that allow the addition of various side-chains. In this way, the addition of a second hydrophilic carboxylic group or various hydrophobic groups can be realized, allowing the polarity and charge of PDha to be adjusted by combining the properties of the poly-ampholyte and the modifier. This resulted in tunable properties of the so-formed graft copolymers, in particular the self-assembly of amphiphilic graft copolymers bearing C₈ side-chains, as evidenced by TEM and DLS measurements. Finally, PDha_{EOct70} was shown to efficiently solubilize MWCNTs as a promising pH-responsive dispersant, where the corresponding pH-change allows for reversible precipitation of the dispersed

carbon nanomaterial. Further research will focus on the introduction of additional modifiers and the application of such new polymeric materials for modification of various surfaces.

Experimental

Chemicals

Benzyl glycidyl ether (>97%), lauryl glycidyl ether (>97%), 2,2,3,3,4,4,5,5,5-nonafluoropentyl oxirane (>98%) and polyethylene glycol glycidyl lauryl ether were purchased from TCI. 1,2-Epoxy octane (96%), acrylonitrile (≥99%) and methanesulfonyl chloride (≥99.7%) were purchased from Sigma-Aldrich. TFA (≥99.9%) was purchased from Roth, triethyl amine (≥99.0%) from CHEMSOLUTE® and *N*-(*tert*-butoxycarbonyl)-L-serinmethylester (98%) from Carbolution Chemicals. Lucirin TPO was kindly supplied by BASF. MWCNTs with an outer diameter of 10–15 nm, an inner diameter of 2–6 nm, and length of 0.1–10 μm were obtained from Sigma-Aldrich. All Chemicals were used as received.

Analytical methods

Nuclear magnetic resonance (NMR) spectroscopy

¹H- and ¹³C-NMR spectroscopy were performed on a Bruker AC 300 MHz spectrometer using CDCl₃, DMSO-d₆ and D₂O/NaOD as solvents at a temperature of 298 K. The spectra were referenced to the residual deuterated solvent signal.

¹⁹F-NMR spectra were measured on a Bruker Avance III 400 MHz spectrometer using DMSO-d₆ as solvent at a temperature of 298 K. CCl₃F was used as an external standard.

¹³C solid-state magic angle spinning (ssMAS) NMR spectra were measured using cross polarization with a contact time of 2 ms and a spinning frequency of 14 kHz on a Bruker Avance III HD 400 MHz spectrometer. The sample temperature was set to 298 K, and the carbon chemical shifts were referenced externally, setting the high-frequency (methylene) signal of adamantane to 38.5 ppm.⁷⁶

Size exclusion chromatography (SEC)

SEC traces in CHCl₃ were measured using a Shimadzu system equipped with a CBM-20 A system controller, an LC-10 VP pump, an RID-10A refractive index detector, and a PSS SDV guard/linear S column. A mixture of chloroform/triethylamine/iso-propanol [94/2/4] (v/v/v) was used as eluent, and measurements were recorded at a flow rate of 1 mL min⁻¹ and 40 °C.

SEC measurements in DMSO were performed on a Jasco instrument using DMSO + 0.5% LiBr as eluent at a flow rate of 0.5 mL min⁻¹ at 65 °C and a Pullulan calibration (Polymer Standards Service GmbH, Germany). The instrument was equipped with PSS NOVEMA 3000 Angström/300 Angström columns, an RI-930 detector, as well as a PU-980 pump.

Dynamic light scattering (DLS)

DLS measurements were performed using an ALV laser CGS3 goniometer equipped with a 633 nm HeNe laser (ALV GmbH, Langen, Germany) at 25 °C at a detection angle of 90°. The CONTIN analysis of the obtained correlation functions was performed using the ALV 7002 FAST Correlator Software.

Transmission electron microscopy (TEM)

TEM images were acquired with a 200 kV FEI Tecnai G2 20 instrument equipped with a 4k × 4k Eagle HS CCD, and a 1k × 1k Olympus MegaView camera for overview images.

Fourier transform infrared spectroscopy (FT-IR)

Infrared spectra were measured on a Perkin Elmer Frontier FT-IR/NIR spectrometer equipped with a Golden Gate ATR unit from Specac. Spectra were recorded between 4000 and 400 cm⁻¹.

Potentiometric titration

Potentiometric titrations were performed with a TitroLine® 7000 titrator equipped with a WA 20 exchangeable unit, magnetic stirrer TM 235, and a ScienceLine pH combination electrodes with temperature sensor A162 from SI Analytics GmbH. The polymers were dissolved in 0.1 M NaOH and titrated against 0.1 M HCl *via* an automatic dynamic pH-titration method.

ζ-Potential measurements

ζ-Potentials were measured on a ZetaSizer Nano ZS from Malvern *via* M3-PALS technique with a 633 nm laser. The detection angle was 13°. The samples were prepared by titration of the polymer in 0.1 M NaOH (0.2 g L⁻¹) with 0.1 M HCl, and 1 mL of the solution was taken at the desired pH-values. The titration and pH-detection was performed on a Metrohm 765 Dosimat titrator with a Greisinger electronic GMH3539 digital pH-/mV-electrode equipped with a thermometer.

Thermogravimetric analysis (TGA)

TGA measurements were carried out under nitrogen flow in a Perkin Elmer TGA800 device by heating from 30 °C to 850 °C with a heating rate of 10 K min⁻¹.

Elemental analysis (EA)

Elemental analysis was performed on a Vario El III (Elementar) elemental analyzer.

Ultrasonication (ultrasonication finger)

Ultrasonication was carried out using a Sonic VibraCellVC505 500 Watt Ultrasonic Processor. To reduce high sound, a Sound Abating Enclosure was used.

Synthesis

Synthesis of *t*BAMA. *N*-(*tert*-Butoxycarbonyl)-L-serine methyl ester (10.0 g, 45.6 mmol, 1.0 eq.) was dissolved in dichloromethane (DCM) (200 mL) before MsCl (6 mL, 77.5 mmol, 1.7 eq.) was added. After cooling in an ice bath, NEt₃ (23 mL, 165.9 mmol, 3.6 eq.) was slowly added dropwise, and the reaction mixture stirred for 1 h at 0 °C. The reaction mixture was then stirred for additional 2 h at room temperature before being washed with potassium bisulfate (1%) to neutrality. The organic phase was dried over Na₂SO₄ before the solvent was removed under reduced pressure. The crude product was further purified *via* column chromatography with silica gel using an ethyl acetate/*n*-hexane mixture of 1/4 (v/v) as eluent. The solvent was removed under reduced pressure to yield the pure product as a colorless oil (8.6 g, 94% yield).

¹H-NMR (300 MHz, CDCl₃, δ): 7.01 (s, 1 H, -NH), 6.16 (s, 1 H, -C=CH-), 5.73 (s, 1 H, -C=CH-), 3.83 (s, 3 H, -O-CH₃), 1.48 (s, 9 H, -COO-C(CH₃)₃) ppm.

Synthesis of *Pt*BAMA. The monomer *t*BAMA and TPO were dissolved in dioxane (50 wt%) before purging the mixture with Ar for 10 min. The reaction vessel was then placed in a UV-cube (100 W) for 10 min before the polymerization was terminated by the addition of methanol. The viscous liquid was diluted with acetone and precipitated into excess *n*-hexane (-25 °C). The product was collected by filtration, and the residue washed three times with *n*-hexane. After drying under vacuum for several hours, the product was obtained as a white powder with a yield of 88%.

¹H-NMR (300 MHz, CDCl₃, δ): 6.00–5.00 (m, -NH), 4.08–3.37 (m, -O-CH₃), 3.32–2.02 (m, -C-CH₂-), 1.75–1.16 (m, -COO-C(CH₃)₃) ppm.

SEC (CHCl₃/*i*-PrOH/NEt₃): *M*_n = 14 000 g mol⁻¹, *M*_w = 79 200 g mol⁻¹, *D* = 5.66.

Deprotection of *Pt*BAMA to yield PAMA. *Pt*BAMA was dissolved in TFA (~20 eq.) and heated to 50 °C. The reaction was stopped after 1 h and the product precipitated into an excess of cold methanol. After filtering and washing with methanol, deionized water and diethyl ether several times, the product was dried under vacuum to give a yellow powder with a yield of 60%.

¹H-NMR (300 MHz, D₂O + NaOD, δ): 3.32 (s, -COO-CH₃), 2.78–1.90 (m, -C-CH₂-) ppm.

Post-polymerization modification of PAMA with epoxides

A concentrated KOH solution was added dropwise to water (15 mL) to adjust the solution pH to 13. After dissolving PAMA (100 mg) overnight, the epoxide (10 eq. per monomer unit) in

MeOH (5 mL) was added. The reaction mixture was then stirred for 5 d at 60 °C before being neutralized using aqueous HCl (0.5 M). The precipitated polymer was filtered off and washed several times with aqueous HCl (0.5 M), deionized water, diethyl ether, methanol or acetone. The isolated white powder was then dried *in vacuo* to give the target polymer.

In the case of NFPO, less MeOH was used (1 mL); and for PEO-LGE, no methanol was added.

EOct. ¹H-NMR (300 MHz, D₂O + NaOD, δ): 7.66–7.36 (m, –N–H), 3.99–3.74 (m, –CH–OH), 2.83–1.77 (m, –C–CH₂–, –N–CH₂–), 1.77–1.51 (m, –C–CH₂–), 0.75 (m, –C–CH₃) ppm. ¹³C-NMR (75 MHz, DMSO-d₆, δ): 176.09 (–COO–), 71.07 (–C–OH), 65.99 (–C–NH–), 59.68 (–C–CH₂–), 34.59 (–CH₂–CH₂–), 33.41 (–CH₂–CH₂–), 31.31 (–CH₂–CH₂–), 28.74 (–CH₂–CH₂–), 25.10 (–CH₂–CH₂–), 22.05 (–CH₂–CH₂–), 13.93 (–CH₂–CH₃) ppm.

Degree of functionalization: 70%.

BGE. ¹H-NMR (300 MHz, D₂O + NaOD, δ): 7.51–7.06 (m, Ar–H), 4.60–4.39 (Ar–CH₂–O–), 3.99–3.74 (m, –O–CH₂–C–OH, –CH–OH), 2.92–1.93 (m, –C–CH₂–, –N–CH₂) ppm.

¹³C-NMR (75 MHz, DMSO-d₆, δ): 175.21 (–COO–), 138.42 (–Ar–C–), 128.20 (–Ar–C–), 127.48 (–Ar–C–), 72.26 (–CH–OH, –CH₂–O–, –NH–CH₂–), 59.71 (–NH–C–CH₂) ppm.

Degree of functionalization: 20%.

NFPO. ¹⁹F-NMR (400 MHz, DMSO-d₆, δ): –79.47 to –82.99 (–CF₃), –109.55 to –115.52 (–C–CF₂–), –123.13 to –125.26 (–C–CF₂–), –125.27 to –127.75 (–C–CF₂–) ppm.

Solid state ¹³C-NMR (75 δ): 172.07 (–COOH), 119.96–101.68 (–CF_x–), 65.30–47.86 (–C–OH, –NH–CH₂–, –CH₂–C–), 40.58 (–C–CH₂–C), 30.48 (–CH₂–CF₂–) ppm.

Degree of functionalization: 65%.

PEO-LGE. ¹H-NMR (300 MHz, DMSO-d₆, δ): 5.16–4.66 (m, N–H), 3.80–3.21 (m, –O–CH₂–C–OH, –CH–OH, –O–CH₂–CH₂, –N–CH₂), 2.78–2.04 (m, –C–CH₂–), 1.46 (m, –CH₂–CH₂–), 1.23 (m, –CH₂–CH₂–), 0.85 (m, –CH₂–CH₃) ppm.

Solid state ¹³C-NMR (75 MHz, δ): 172.10 (–COOH), 71.88–0.51 (–CH–OH, –CH₂–O–, –NH–CH₂) 54.54 (–C–CH₂), 54.54 (–CH₂–C–), 25.75 (–CH₂–CH₂–), 22.26 (–CH₃–CH₂–) ppm.

Degree of functionalization: 35%.

Post-polymerization modification of PAMA with acrylonitrile

A concentrated KOH solution was added dropwise to water (15 mL) to adjust the pH to 13. After dissolving the PAMA (100 mg) overnight, acrylonitrile (400 mg, 7.63 mmol, 10 eq. per monomer unit) was added. The reaction mixture was then stirred for 3 d at 60 °C before being neutralized using aqueous HCl (0.5 M). The precipitated polymer was filtered off and washed with aqueous HCl (0.5 M), deionized water and diethyl ether. The isolated white powder was then dried *in vacuo*.

¹H-NMR (300 MHz, D₂O + NaOD, δ): 3.92–3.10 (m, –CH₂–NH–), 3.06–1.93 (m, –C–CH₂–, –CH₂–CN) ppm.

¹³C-NMR (75 MHz, D₂O + NaOD, δ): 175.75 (–COO–), 119.22 (–CN), 65.51 (–C–NH–), 36.86 (–CH₂–NH–), 32.91 (–CH₂–C–), 15.79 (–CH₂–CN) ppm.

FT-IR: 3670–3060 (O–H, N–H), 3300–2800 (C–H), 2250 (C≡N), 1700 (C=O) cm^{–1}.

Degree of functionalization: 130%.

Preparation of CNT dispersions

MWCNTs were placed in a vial at a concentration of 1 g L^{–1} (0.1 M NaOH). Afterwards the polymer solution (0.1 M NaOH) with different concentrations was added and the mixture placed in an ice bath. Dispersions were then formed by using an ultrasonic finger (20% power, 30 min, pulsed: 59 s on and 30 s off).

Conflicts of interest

There are no conflicts to declare.

Acknowledgements

This research was supported by the Deutsche Forschungsgemeinschaft (DFG, project no. SCHA1640/18-1 and the project C03 within the Collaborative Research Center SFB 1278 “PolyTarget”) and the Russian Science Foundation (RSF, project no. 18-44-04011). We acknowledge Peggy Laudeley for SEC analysis, Moritz Köhler for TEM measurements, and Carsten Rössel and Philip Biehl for helpful discussions. We are further thankful to the NMR department at the Friedrich-Schiller-University Jena for their continuous support.

References

- M. Hess, R. G. Jones, J. Kahovec, T. Kitayama, P. Kratochvíl, P. Kubisa, W. Mormann, R. F. T. Stepto, D. Tabak, J. Vohlidal and E. S. Wilks, *Pure Appl. Chem.*, 2006, **78**, 2067.
- D. A. Mortimer, *Polym. Int.*, 1991, **25**, 29–41.
- P. G. Higgs and J. F. Joanny, *J. Chem. Phys.*, 1991, **94**, 1543–1554.
- K. Singh Paresh, K. Singh Vinay and M. Singh, *e-Polym.*, 2007, **7**, 335–363.
- A. B. Lowe and C. L. McCormick, *Chem. Rev.*, 2002, **102**, 4177–4190.
- A. V. Dobrynin and M. Rubinstein, *Prog. Polym. Sci.*, 2005, **30**, 1049–1118.
- S. Koltzenburg, M. Maskos and O. Nuyken, *Polymere: Synthese, Eigenschaften und Anwendungen*, Springer-Verlag, Berlin Heidelberg, 1 edn, 2014.
- I. Szilagyi, G. Trefalt, A. Tiraferri, P. Maroni and M. Borkovec, *Soft Matter*, 2014, **10**, 2479–2502.
- L. Séon, P. Lavalle, P. Schaaf and F. Boulmedais, *Langmuir*, 2015, **31**, 12856–12872.
- T. Chakrabarty and V. K. Shahi, *J. Membr. Sci.*, 2013, **444**, 77–86.
- F. Zhicheng, S. Zhengzhong, Y. Jinrong and C. Xin, *J. Biomed. Mater. Res., Part A*, 2008, **86A**, 694–700.
- S. Y. Bratskaya, A. V. Pestov, Y. G. Yatluk and V. A. Avramenko, *Colloids Surf., A*, 2009, **339**, 140–144.
- G. J. Copello, L. E. Diaz and V. Campo Dall’Orto, *J. Hazard. Mater.*, 2012, **217–218**, 374–381.

- 14 C. S. Patrickios, W. R. Hertler and T. A. Hatton, *Fluid Phase Equilib.*, 1995, **108**, 243–254.
- 15 C. S. Patrickios, L. R. Sharma, S. P. Armes and N. C. Billingham, *Langmuir*, 1999, **15**, 1613–1620.
- 16 K. M. Zurick and M. Bernards, *J. Appl. Polym. Sci.*, 2014, **131**, 40069.
- 17 A. Laschewsky, *Polymers*, 2014, **6**, 1544.
- 18 L. Der-Jang, L. Wen-Fu, W. Yann-Ching and L. Mei-Chih, *J. Appl. Polym. Sci.*, 1987, **34**, 999–1011.
- 19 K. Rosenheck and A. Katchalsky, *J. Polym. Sci.*, 1958, **32**, 511–514.
- 20 J. Nagaya, H. Uzawa and N. Minoura, *Macromol. Rapid Commun.*, 1999, **20**, 573–576.
- 21 T. Nakaya and Y.-J. Li, *Prog. Polym. Sci.*, 1999, **24**, 143–181.
- 22 A. Laschewsky and A. Rosenhahn, *Langmuir*, 2018, DOI: 10.1021/acs.langmuir.8b01789.
- 23 S. Kudaibergenov, W. Jäger and A. Laschewsky, in *Supramolecular Polymers Polymeric Betains Oligomers*, Springer Berlin Heidelberg, Berlin, Heidelberg, 2006, pp. 157–224, DOI: 10.1007/12_078.
- 24 S. Colak and G. N. Tew, *Langmuir*, 2012, **28**, 666–675.
- 25 W. Xue, M. B. Huglin and A. T. Russell, *Macromol. Rapid Commun.*, 1999, **20**, 239–243.
- 26 P.-S. Liu, Q. Chen, S.-S. Wu, J. Shen and S.-C. Lin, *J. Membr. Sci.*, 2010, **350**, 387–394.
- 27 M. S. Donovan, B. S. Sumerlin, A. B. Lowe and C. L. McCormick, *Macromolecules*, 2002, **35**, 8663–8666.
- 28 T. Nakaya, M. Yasuzawa and M. Imoto, *Macromolecules*, 1989, **22**, 3180–3181.
- 29 H. Tan, J. Liu, J. Li, X. Jiang, X. Xie, Y. Zhong and Q. Fu, *Biomacromolecules*, 2006, **7**, 2591–2599.
- 30 S. E. Hankari, B. Motos-Perez, P. Hesemann, A. Bouhaouss and J. J. E. Moreau, *Chem. Commun.*, 2011, **47**, 6704–6706.
- 31 Z. A. Page, V. V. Duzhko and T. Emrick, *Macromolecules*, 2013, **46**, 344–351.
- 32 U. Günther, L. V. Sigolaeva, D. V. Pergushov and F. H. Schacher, *Macromol. Chem. Phys.*, 2013, **214**, 2202–2212.
- 33 L. J. Mathias and R. E. Hermes, *Macromolecules*, 1986, **19**, 1536–1542.
- 34 C. Rössel, M. Billing, H. Görls, G. Festag, M. Grube, P. Bellstedt, I. Nischang and F. H. Schacher, *Polymer*, 2017, **127**, 182–191.
- 35 R. E. Hermes and L. J. Mathias, *Polym. Bull.*, 1987, **17**, 189–195.
- 36 R. E. Hermes, L. J. Mathias and J. W. Virden, *Macromolecules*, 1987, **20**, 901–903.
- 37 I. Hussain, M. Brust, A. J. Papworth and A. I. Cooper, *Langmuir*, 2003, **19**, 4831–4835.
- 38 L. J. Mathias, D. W. Kurz and T. Viswanathan, *J. Polym. Sci., Polym. Lett. Ed.*, 1988, **26**, 233–239.
- 39 L. J. Mathias and R. E. Hermes, *Macromolecules*, 1988, **21**, 11–13.
- 40 M. Billing, G. Festag, P. Bellstedt and F. H. Schacher, *Polym. Chem.*, 2017, **8**, 936–945.
- 41 M. Billing and F. H. Schacher, *Macromolecules*, 2016, **49**, 3696–3705.
- 42 M. von der Lüche, U. Günther, A. Weidner, C. Grafe, J. H. Clement, S. Dutz and F. H. Schacher, *RSC Adv.*, 2015, **5**, 31920–31929.
- 43 M. von der Lüche, A. Weidner, S. Dutz and F. H. Schacher, *ACS Appl. Nano Mater.*, 2017, **1**, 232–244.
- 44 P. Biehl, M. von der Lüche and F. H. Schacher, *Macromol. Rapid Commun.*, 2018, **39**, e1800017.
- 45 O. V. Borisov and A. Halperin, *Curr. Opin. Colloid Interface Sci.*, 1998, **3**, 415–421.
- 46 A. Laschewsky, in *Polysoaps/Stabilizers/Nitrogen-15 NMR*, Springer Berlin Heidelberg, Berlin, Heidelberg, 1995, pp. 1–86, DOI: 10.1007/BFb0025228.
- 47 P. Anton and A. Laschewsky, *Colloid Polym. Sci.*, 1994, **272**, 1118–1128.
- 48 D. Heinz, E. Amado and J. Kressler, *Polymers*, 2018, **10**, 960.
- 49 P. Anton, P. Köberle and A. Laschewsky, *Makromol. Chem.*, 1993, **194**, 1–27.
- 50 D.-Q. Zhuang, J. C. Ai-hua Da, Y.-X. Zhang, R. Dieing, L. Ma and L. Haeussling, *Polym. Adv. Technol.*, 2001, **12**, 616–625.
- 51 T. L. Lowe, J. Virtanen and H. Tenhu, *Langmuir*, 1999, **15**, 4259–4265.
- 52 P. Deo and P. Somasundaran, *Langmuir*, 2005, **21**, 3950–3956.
- 53 G. Didukh Alexander, R. B. Koizhaiganova, L. A. Bimendina and S. E. Kudaibergenov, *J. Appl. Polym. Sci.*, 2004, **92**, 1042–1048.
- 54 P. Köberle, A. Laschewsky and D. van den Boogaard, *Polymer*, 1992, **33**, 4029–4039.
- 55 A. Laschewsky and I. Zerbe, *Polymer*, 1991, **32**, 2070–2080.
- 56 G. K. Arda, T. Patrick and K. Harm-Anton, *J. Polym. Sci., Part A: Polym. Chem.*, 2013, **51**, 1–28.
- 57 C. L. McCormick, C. E. Hoyle and M. D. Clark, *Polymer*, 1992, **33**, 243–247.
- 58 D. Tsiourvas, C. M. Paleos and P. Dais, *J. Appl. Polym. Sci.*, 1989, **38**, 257–264.
- 59 K. Ping-Lin, N. Sheng-Chung and L. Chien-Chi, *J. Appl. Polym. Sci.*, 1992, **45**, 611–617.
- 60 K. T. Wang, I. Iliopoulos and R. Audebert, *Polym. Bull.*, 1988, **20**, 577–582.
- 61 U. P. Strauss and N. L. Gershfeld, *J. Phys. Chem.*, 1954, **58**, 747–753.
- 62 E. G. Jackson and U. P. Strauss, *J. Polym. Sci.*, 1951, **7**, 473–484.
- 63 I. M. Klotz, G. P. Royer and A. R. Sloniewsky, *Biochemistry*, 1969, **8**, 4752–4756.
- 64 T. Seo, S. Take, K. Miwa, K. Hamada and T. Iijima, *Macromolecules*, 1991, **24**, 4255–4263.
- 65 H. Hidaka, T. Onai, M. Murata, K. Fujiwara, M. Takai and M. Moriya, *J. Colloid Interface Sci.*, 1987, **119**, 565–575.
- 66 M. Moriya, A. Nishimura, K. Hosoda, M. Takai and H. Hidaka, *J. Am. Oil Chem. Soc.*, 1986, **63**, 263–267.
- 67 V. V. Shumyantseva, L. V. Sigolaeva, L. E. Agafonova, T. V. Bulko, D. V. Pergushov, F. H. Schacher and A. I. Archakov, *J. Mater. Chem. B*, 2015, **3**, 5467–5477.
- 68 M. von der Lüche, A. Weidner, S. Dutz and F. H. Schacher, *ACS Appl. Nano Mater.*, 2018, **1**, 232–244.

- 69 A. Narayanan, B. Maiti and P. De, *React. Funct. Polym.*, 2015, **91–92**, 35–42.
- 70 W. Choi, K. Min, C. Kim, Y. S. Ko, J. W. Jeon, H. Seo, Y.-K. Park and M. Choi, *Nat. Commun.*, 2016, **7**, 12640.
- 71 K. A. McEwan, S. Slavin, E. Tunnah and D. M. Haddleton, *Polym. Chem.*, 2013, **4**, 2608–2614.
- 72 T. Fujigaya and N. Nakashima, *Sci. Technol. Adv. Mater.*, 2015, **16**, 024802.
- 73 P. W. Barone and M. S. Strano, *Angew. Chem., Int. Ed.*, 2006, **45**, 8138–8141.
- 74 S. Javadian, A. Motae, M. Sharifi, H. Aghdastinat and F. Taghavi, *Colloids Surf., A*, 2017, **531**, 141–149.
- 75 J. Yu, N. Grossiord, C. E. Koning and J. Loos, *Carbon*, 2007, **45**, 618–623.
- 76 C. R. Morcombe and K. W. Zilm, *J. Magn. Reson.*, 2003, **162**, 479–486.

**Polyampholytic Graft Copolymers based on Polydehydroalanine (PDha) –
Synthesis, Solution Behavior and Application as Dispersants for Carbon
Nanotubes**

J. B. Max,^{1,2,3} D. V. Pergushov,⁴ L. V. Sigolaeva,⁴ F. H. Schacher,^{1,2,3} *

¹ Institute of Organic Chemistry and Macromolecular Chemistry (IOMC), Friedrich-Schiller-
University Jena, Lessingstraße 8, D-07743 Jena, Germany

² Jena Center for Soft Matter (JCSM), Friedrich-Schiller-University Jena, Philosophenweg 7,
D-07743 Jena, Germany

³ Center for Energy and Environmental Chemistry (CEEC), Friedrich-Schiller-University Jena,
Philosophenweg 7, D-07743 Jena, Germany

⁴ Department of Chemistry, M.V. Lomonosov Moscow State University, Leninskie Gory 1/3,
119991 Moscow, Russia

Email: felix.schacher@uni-jena.de

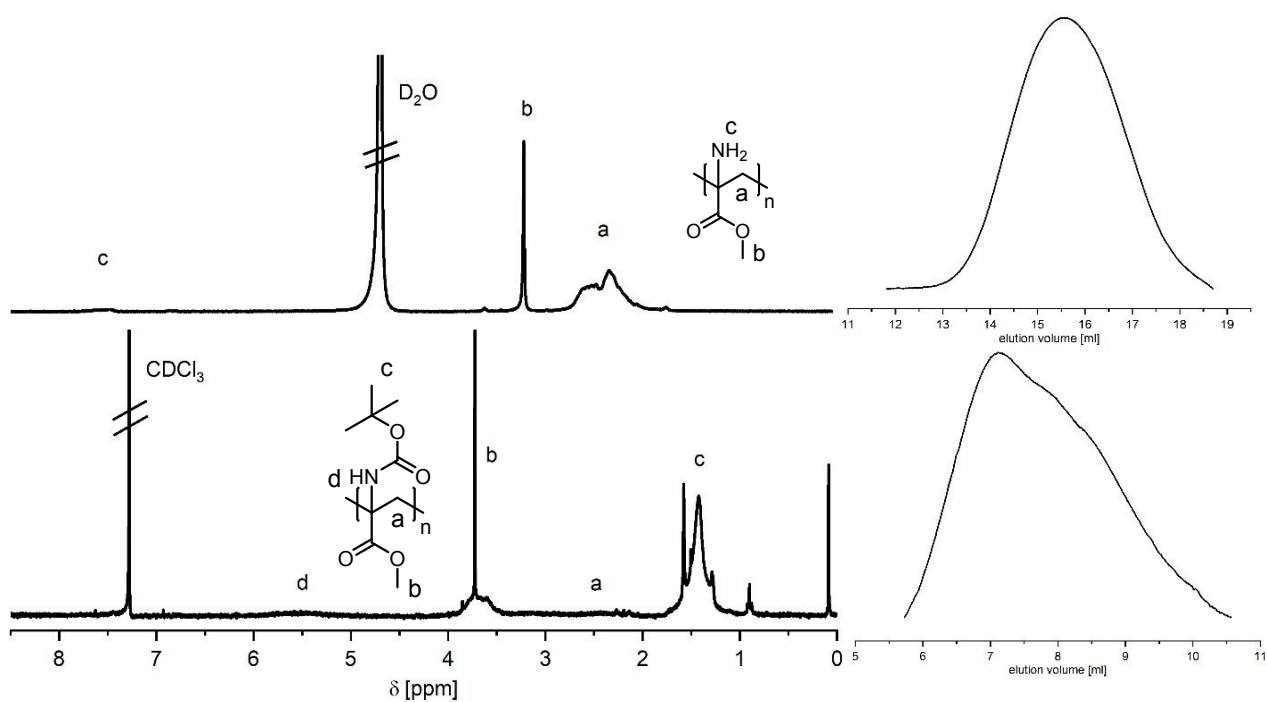


Figure S1: $^1\text{H-NMR}$ spectra of PtBAMA (bottom, in CDCl_3) and PAMA (top, in $\text{D}_2\text{O}+\text{NaOD}$) with the corresponding SEC traces of PAMA (DMSO with 0.5 % LiBr) and PtBAMA ($\text{CHCl}_3/\text{iPrOH}/\text{NEt}_3$).

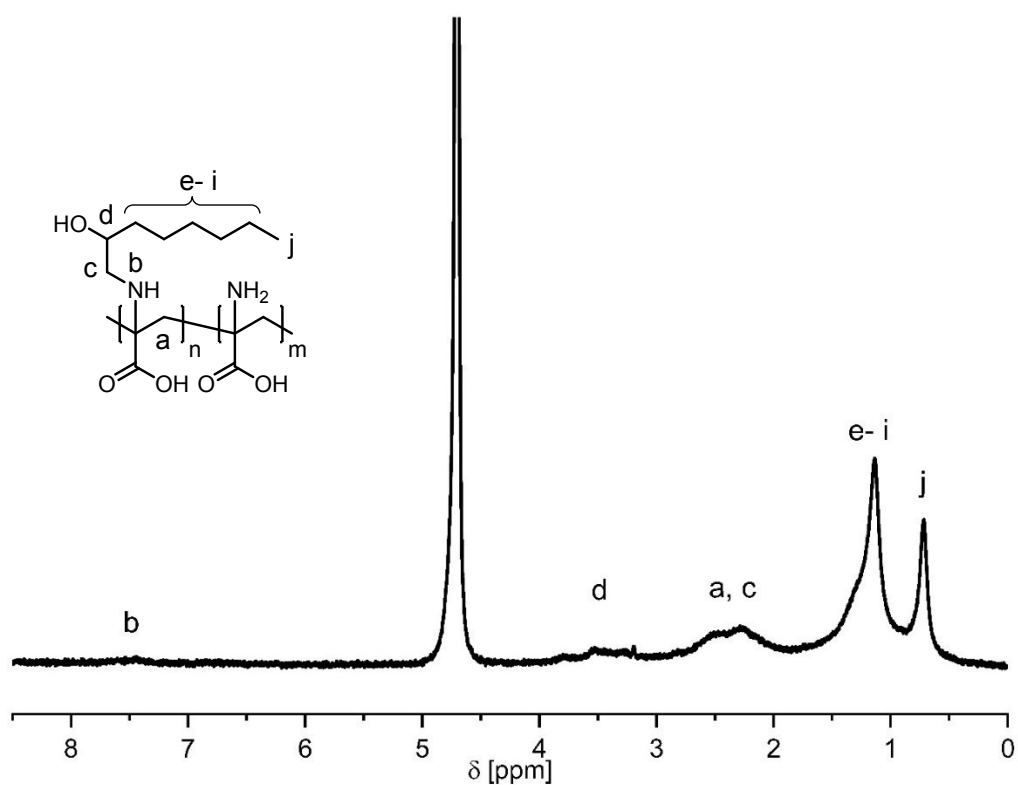


Figure S2: $^1\text{H-NMR}$ spectrum of PDha_{EOct70} in $\text{D}_2\text{O}+\text{NaOD}$.

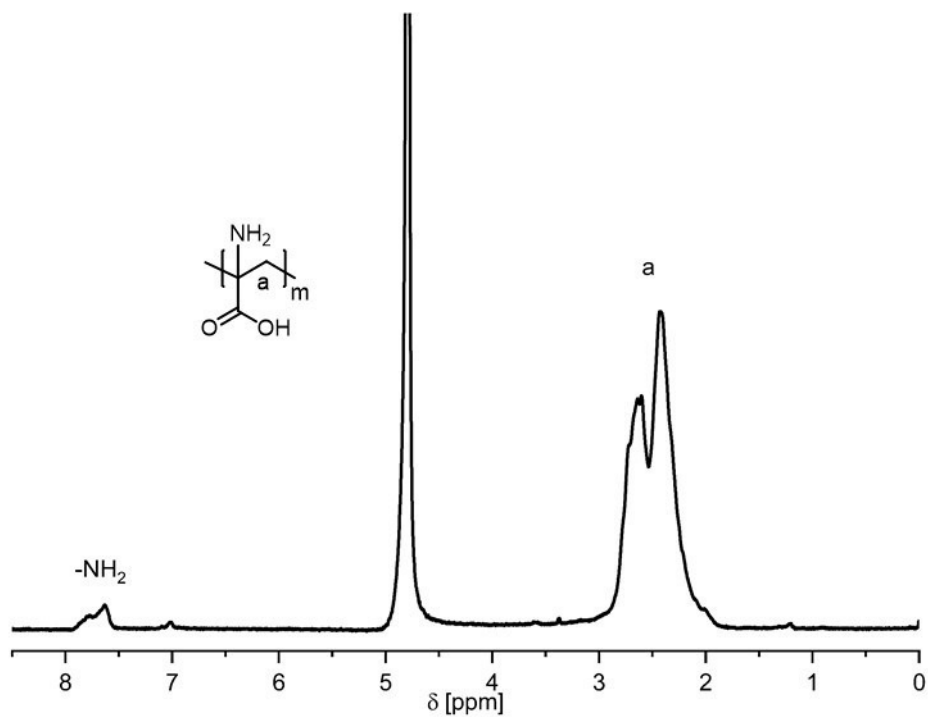


Figure S3: ¹H-NMR spectrum of PDha in D₂O+NaOD.

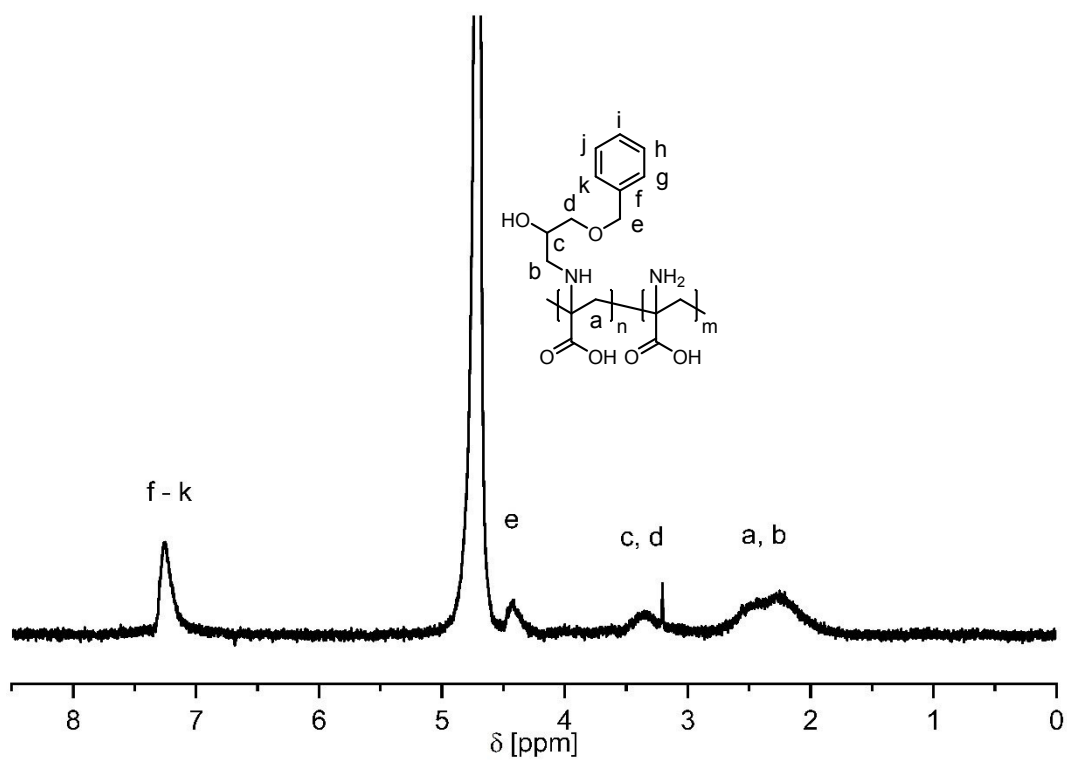


Figure S4: ¹H-NMR spectrum of PDha_{BGE20} in D₂O+NaOD.

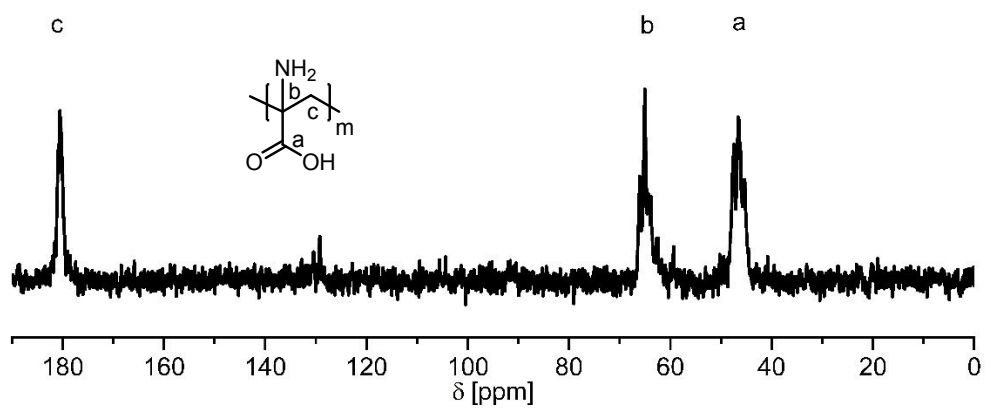


Figure S5: ^{13}C -NMR spectrum of PDha in $\text{D}_2\text{O} + \text{NaOD}$.

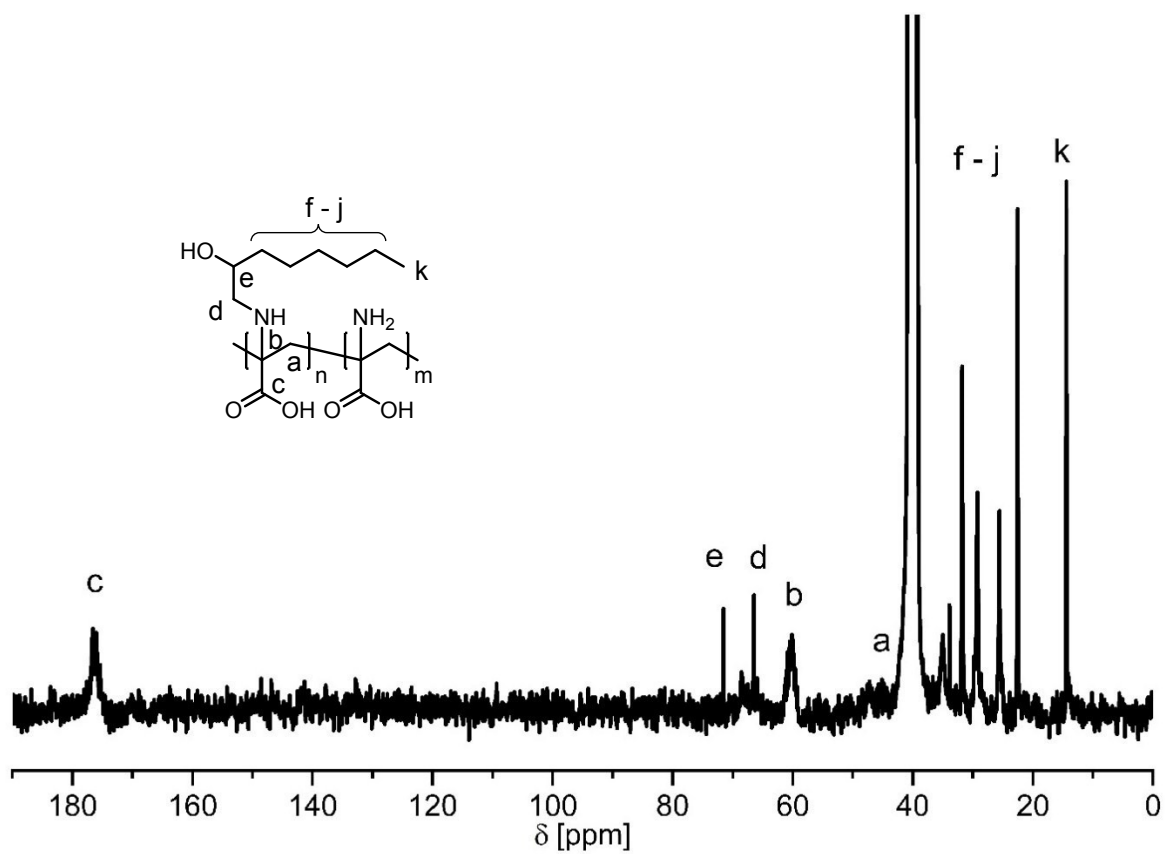


Figure S6: ^{13}C -NMR spectrum of PDha_{EOct70} in DMSO-d_6 .

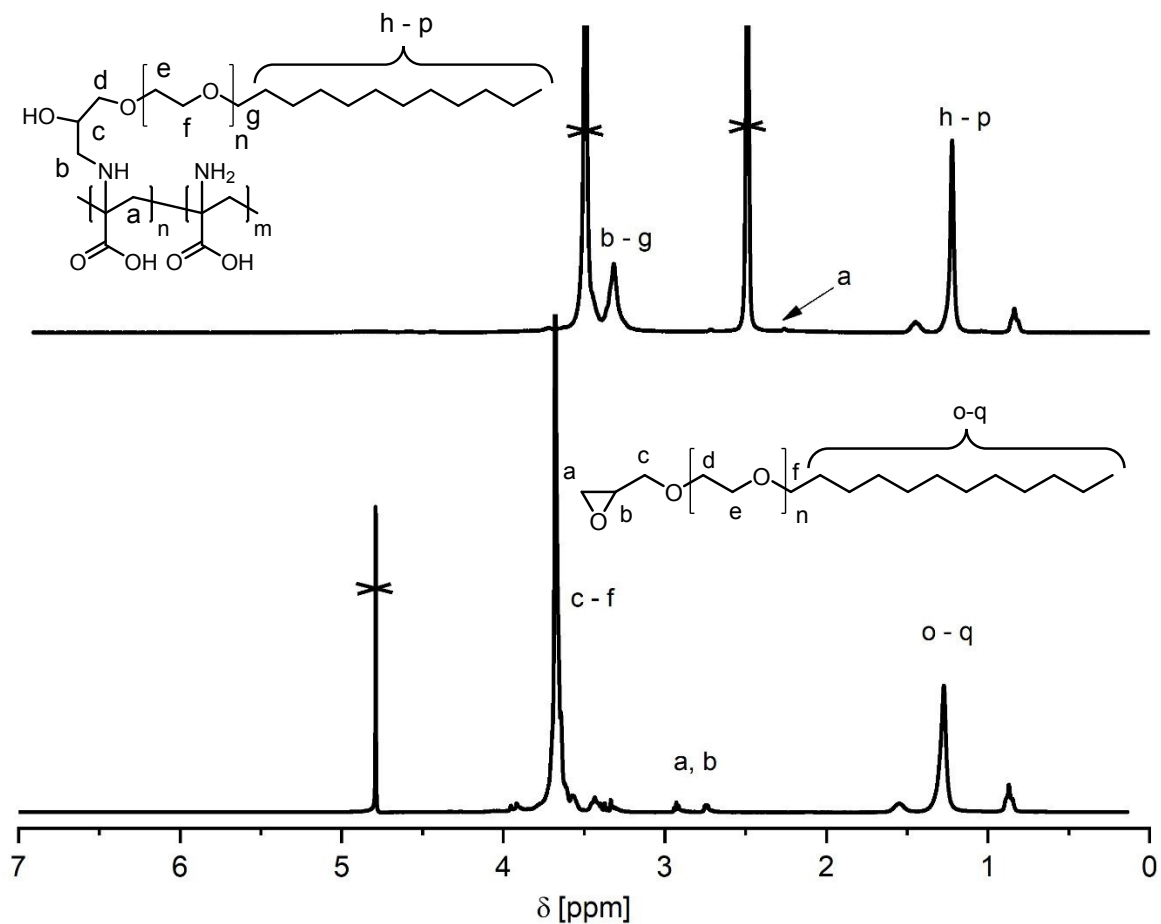


Figure S7: $^1\text{H-NMR}$ spectrum of PEO-LGE (bottom, in D_2O) and $\text{PDha}_{\text{PEO-LGE33}}$ (top, in DMSO-d_6).

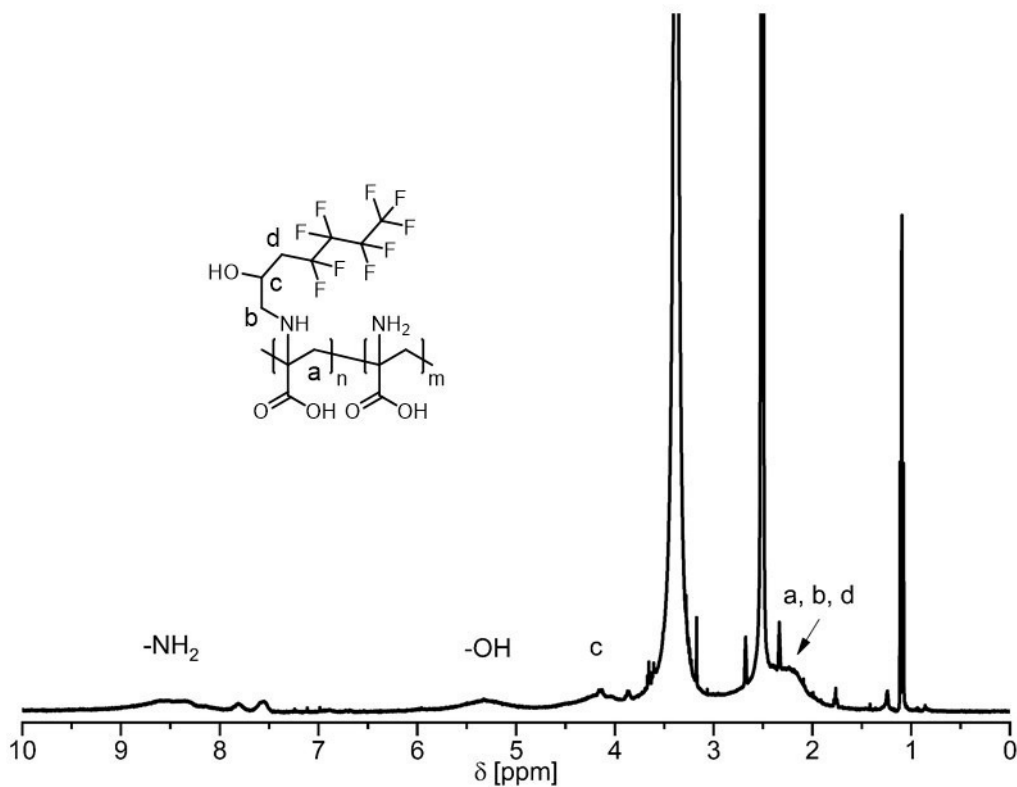


Figure S8: $^1\text{H-NMR}$ spectrum of $\text{PDha}_{\text{NFPO65}}$ in DMSO-d_6 .

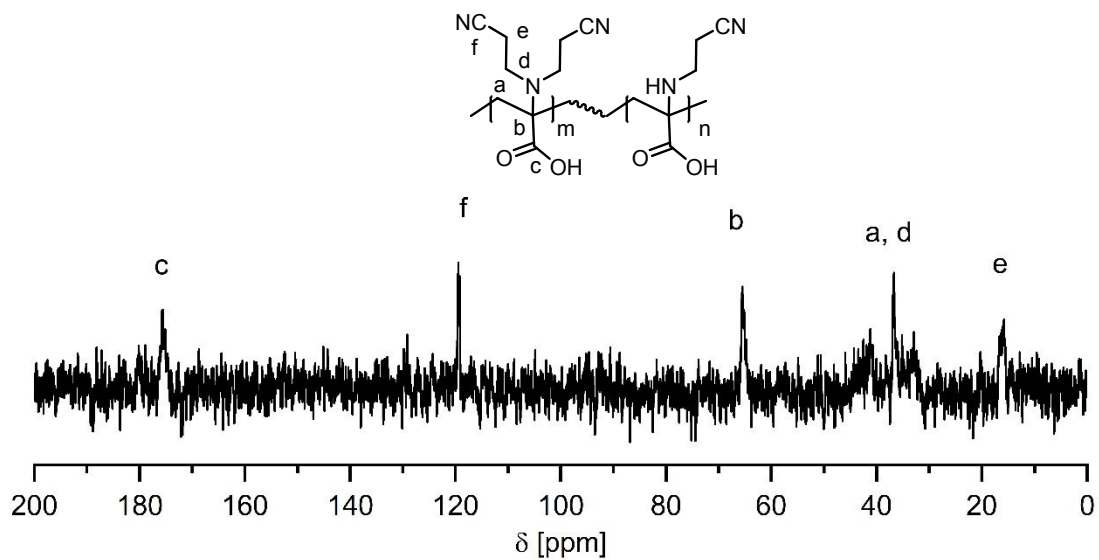


Figure S9: ¹³C-NMR spectrum of PDha_{ACN130} in D₂O+NaOD.

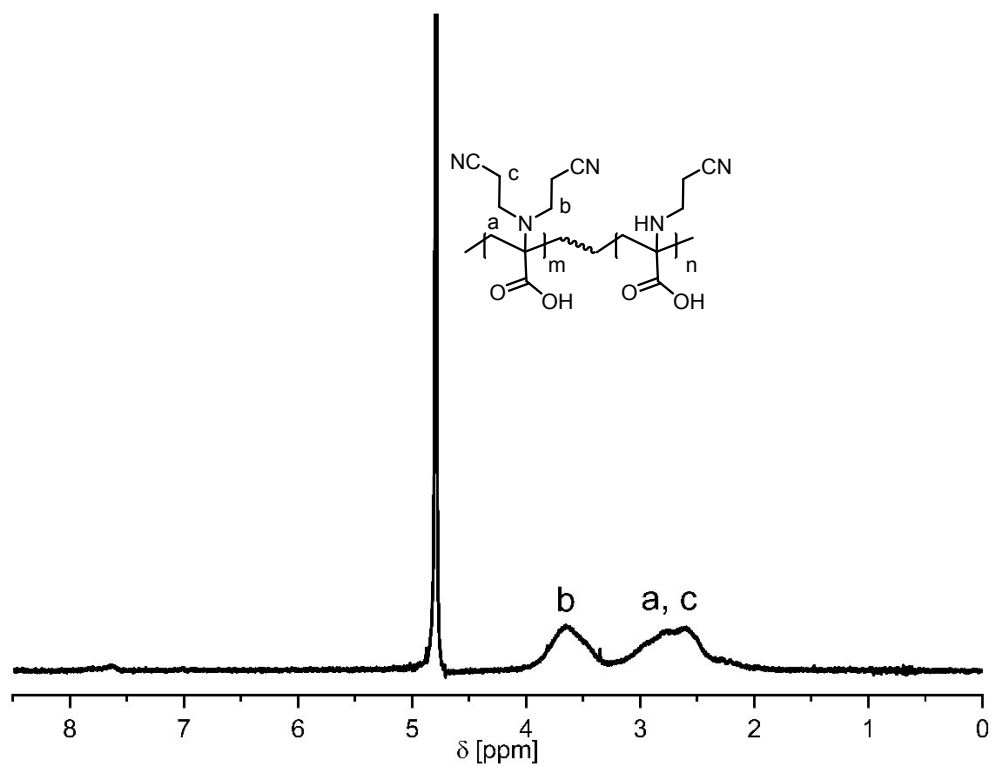


Figure S10: ¹H-NMR spectrum of PDha_{ACN130} in D₂O+NaOD.

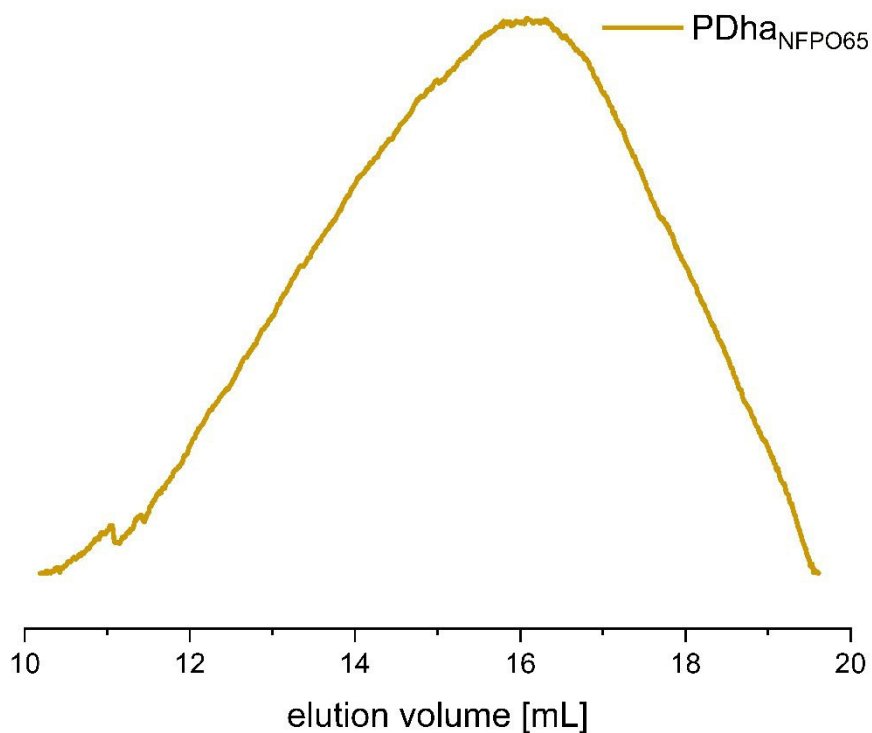


Figure S11: SEC traces of PDha_{NFPO65} measured in DMSO+0.5 % LiBr (Pullulan calibration).

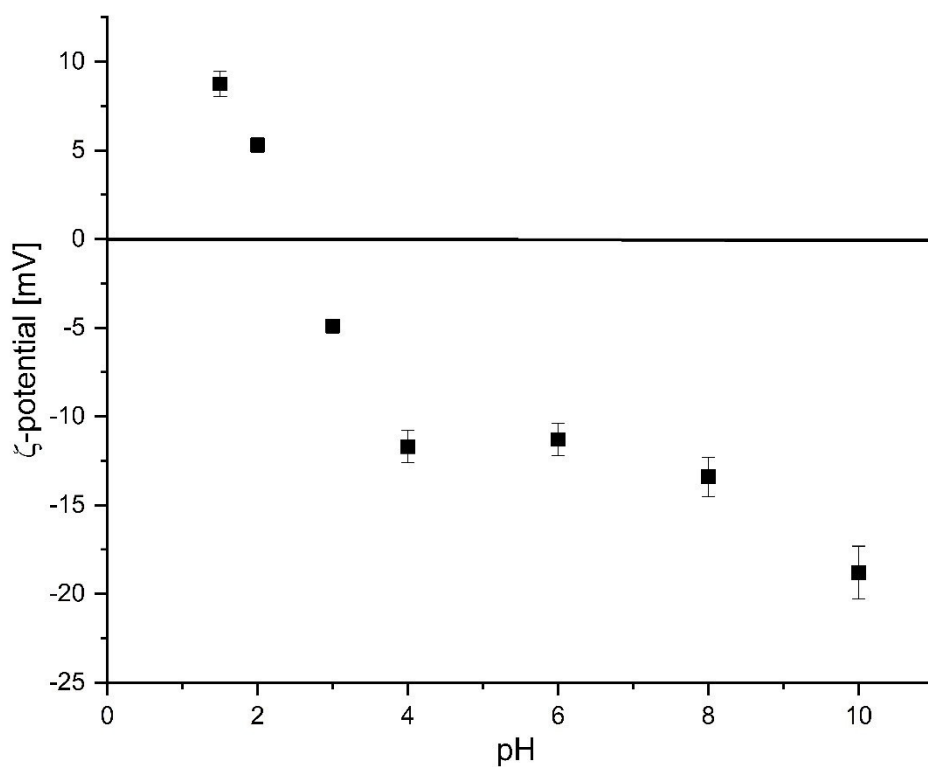


Figure S12: ζ-potential of PDha_{ACN130} at different pH-values revealing charge neutrality above a pH of 2.

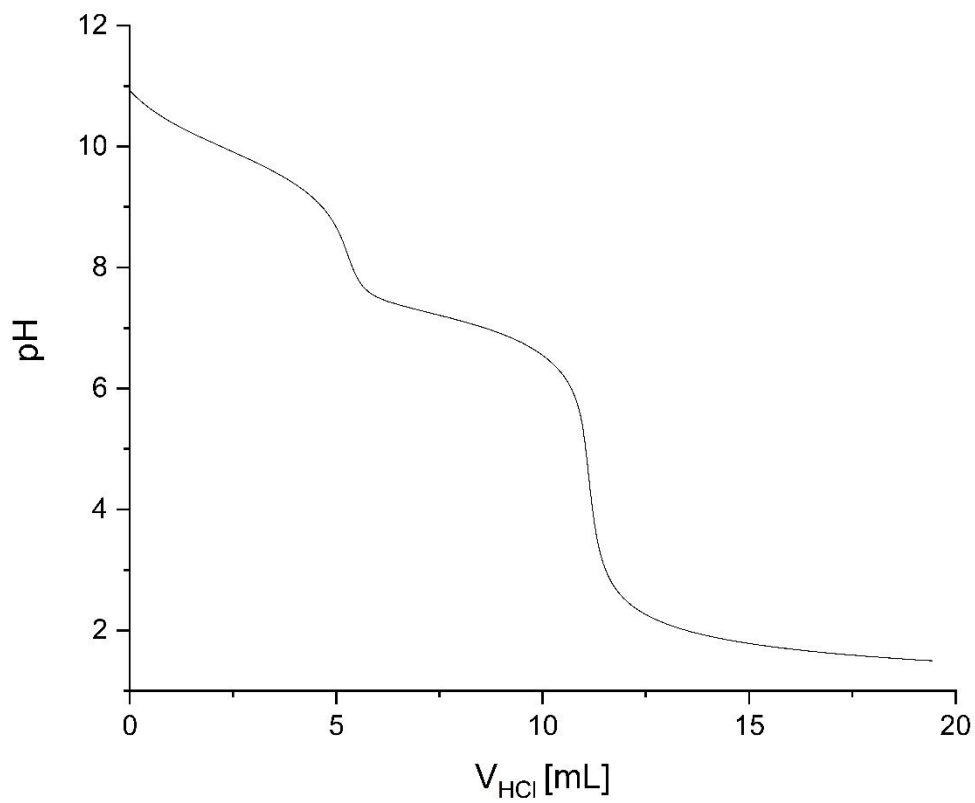


Figure S13: Titration curve of PDha_{EOct70}.

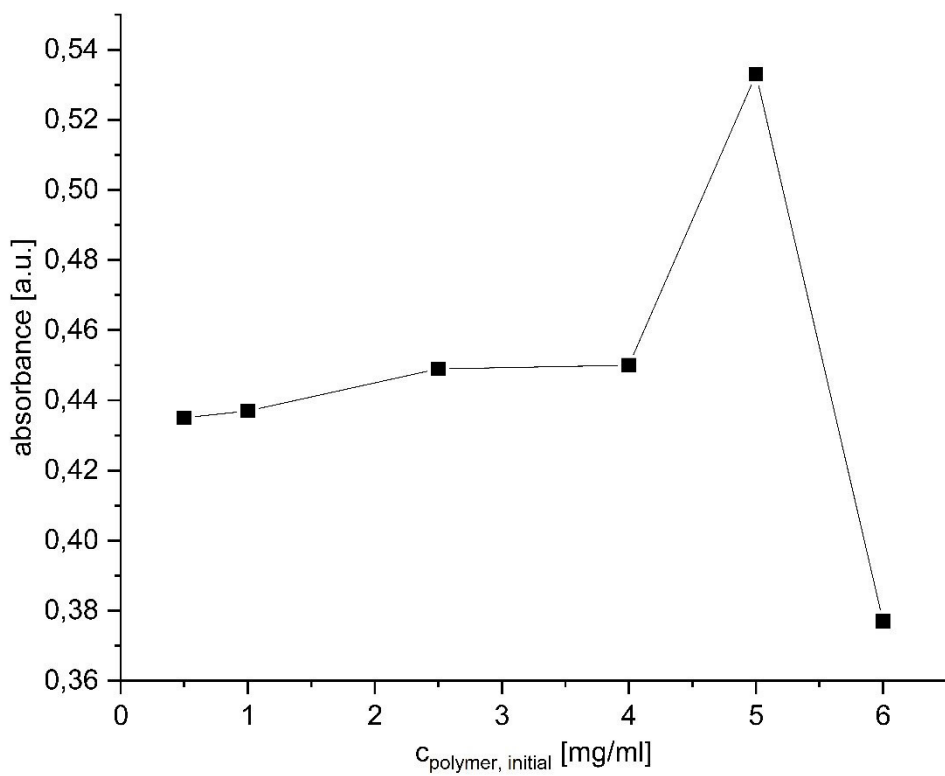


Figure S14: UV-Vis absorbance at a wavelength of 500 nm of the MWCNT (1 mg/mL) dispersions with increasing surfactant (PDha_{EOct70}) starting concentrations.

Equation S1: Calculation of the DF of PDha_{NFPO} and PDha_{PEO-LGE}

$$DoF [\%] = \frac{n(C_{per\ N\ found\ by\ elemental\ analysis}) - n(C_{PDha})}{n(C_{modifier})}$$

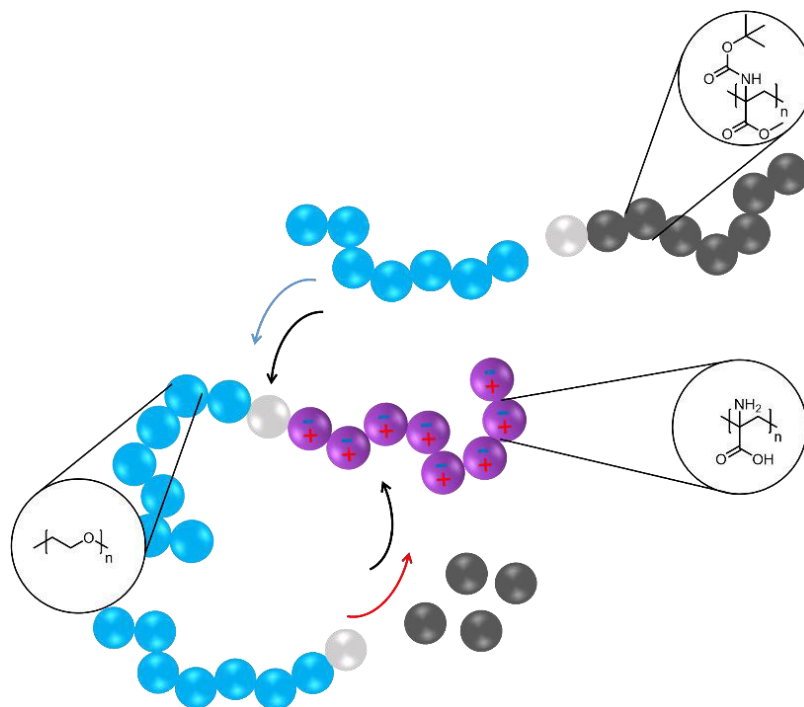
$$n(C_{per\ N\ found\ by\ elemental\ analysis}) = \frac{\frac{wt\% (C)}{M (C)}}{\frac{wt\% (N)}{M (N)}}$$

Table S1: Results of elemental analysis.

composition [%]	PAMA	PDha	PDha _{NFPO}	PDha _{PEO-LGE}
C	41.79	42.76	34.47	55.53
H	5.54	5.23	2.2	8.84
N	15.03	15.9	4.97	3.49
remaining	37.64	36.11	58.36	32.14

Publication P2

“Double Hydrophilic Poly(ethylene oxide)-block-Poly(dehydroalanine) Block Copolymers:
Comparison of Two Different Synthetic Routes”



Johannes B. Max, Peter J. Mons, Jessica C. Tom, and Felix H. Schacher

Macromol. Chem. Phys., **2020**, 221, 1900383



Double Hydrophilic Poly(ethylene oxide)-*block*-Poly(dehydroalanine) Block Copolymers: Comparison of Two Different Synthetic Routes

Johannes B. Max, Peter J. Mons, Jessica C. Tom, and Felix H. Schacher*

Two different synthetic pathways give access to the amphiphilic block copolymer poly(ethylene oxide)-*block*-poly(*tert*-butoxycarbonylaminoethylacrylate). In the first approach, two end-functionalized segments are linked via click chemistry; and in the second approach, a poly(ethylene oxide) (PEO) based macroinitiator is chain extended via atom transfer radical polymerization (ATRP). In both cases the linking unit consists of an amide group, which is necessary to effectively deprotect the corresponding polymer precursor without cleavage of both segments. For this, amide-containing ATRP initiators are employed and successful synthesis by nuclear magnetic resonance (NMR) and size exclusion chromatography (SEC) analyses before comparing both pathways is demonstrated. After deprotection, a novel double hydrophilic block copolymer, poly(ethylene oxide)-*block*-poly(dehydroalanine), is obtained, which is investigated using SEC (aqueous and DMSO) and ¹H-NMR spectroscopy. Containing a potentially zwitterionic PDha segment and a high density of both amino and carboxylic groups, pH-dependent aggregation of the block copolymer is expected and is studied using dynamic light scattering, revealing interesting solution properties. The corresponding polymers are applied in various areas including drug delivery systems or in biomineralization.

due to their diverse applications and unique solution properties in aqueous media.^[1] They typically feature one (functional) block that responds to an external stimulus such as pH, temperature, or ion complexation, to undergo self-assembly into discrete nanostructures.^[1–4] Such materials have thus far been used for the complexation of metal ions or nanoparticles for biomineralization or catalysis,^[5–7] as drug delivery systems in biomedicine,^[8–10] and as surface coatings.^[11–14] DHBCs may consist of an uncharged (e.g., poly(ethylene oxide) or poly(2-methyl-2-oxazoline))^[3] or (pH-dependent) charged segment (e.g., poly(L-lysine), poly(2-vinylpyridine), and poly(ethylene imine) or poly(2-(dimethylamino)ethyl methacrylate)).^[6,9,10,14] In that regard, charged segments, that is, polyelectrolytes and polyampholytes or polyzwitterions as subclasses, are of particular interest as their corresponding homopolymers already exhibit interesting properties and

1. Introduction


Double hydrophilic block copolymers (DHBCs) are a class of water-soluble macromolecules that have gained growing interest

hence, widespread industrial application.^[15,16] Here, one recent example containing two polyelectrolyte blocks is poly(acrylic acid)-*block*-poly(dehydroalanine) (PAA-*b*-PDha), where pH-dependent solubility and aggregation into loosely defined micelles was shown.^[17] PDha, as a polyampholyte segment, exhibits a high charge density and furthermore offers the possibility to perform post-polymerization modifications. To date, PDha has been used as a coating material for magnetic nanoparticles, and pH-dependent charge inversion could be used to reversibly adsorb polyelectrolytes, proteins, and dyes onto such hybrid materials.^[17–23] PDha is typically synthesized from poly(*tert*-butoxycarbonylaminoethylacrylate) (PtBAMA), which is accessed via free or controlled radical polymerization techniques such as atom transfer radical polymerization (ATRP). Hence, block copolymers have also been realized. Afterward, PDha is obtained by the removal of the methyl ester and *tert*-butoxycarbonyl protecting groups using excess LiOH and TFA. These rather harsh deprotection conditions have prevented the preparation of poly(ethylene oxide)-*block*-poly(dehydroalanine) (PEO-*b*-PDha) block copolymers via ATRP, where both segments are typically linked by a vulnerable ester moiety that would also be hydrolyzed under these deprotection conditions. We therefore introduce two strategies here to access such materials. First, an amide linker that is hydrolytically more stable is used in sequential ATRP experiments. However, it is well-known that

J. B. Max, P. J. Mons, Dr. J. C. Tom, Prof. F. H. Schacher
 Institute of Organic Chemistry and Macromolecular Chemistry (IOMC)
 Friedrich-Schiller-University Jena
 Lessingstraße 8, D-07743 Jena, Germany
 E-mail: felix.schacher@uni-jena.de

J. B. Max, P. J. Mons, Dr. J. C. Tom, Prof. F. H. Schacher
 Jena Center for Soft Matter (JCSM)
 Friedrich-Schiller-University Jena
 Philosophenweg 7, D-07743 Jena, Germany

J. B. Max, P. J. Mons, Dr. J. C. Tom, Prof. F. H. Schacher
 Center for Energy and Environmental Chemistry (CEEC)
 Friedrich-Schiller-University Jena
 Philosophenweg 7, D-07743 Jena, Germany

 The ORCID identification number(s) for the author(s) of this article can be found under <https://doi.org/10.1002/macp.201900383>.

© 2019 The Authors. Published by WILEY-VCH Verlag GmbH & Co. KGaA, Weinheim. This is an open access article under the terms of the Creative Commons Attribution License, which permits use, distribution and reproduction in any medium, provided the original work is properly cited.

Kindly note that open access information regarding “Project DEAL” have been added on 15 October 2020 after initial publication.

DOI: 10.1002/macp.201900383

amide-based macroinitiators are prone to excessive termination reactions and poor initiation efficiency compared to their ester-based counterparts.^[24–26] As an alternative approach, we also prepared PEO-*b*-PDha via copper-catalyzed azide-alkyne cycloaddition (CuAAC) to link suitably functionalized segments.^[27] The corresponding poly(ethylene oxide)-*block*-poly(*tert*-butoxycarbonylaminoethylacrylate) (PEO-*b*-PtBAMA) block copolymers were then deprotected in two steps to obtain the desired PEO-*b*-PDha materials. First experiments showed pH-dependent self-assembly in aqueous media, with the potential to complex metal ions for application in water purification, biomineralization, or as templates for the formation of metal nanoparticles. Moreover, utilization in drug delivery systems may also be possible due to the pH-dependent self-assembly behavior of our system.

due to the ester linkage, deprotection to the desired PDha also resulted in the cleavage of both segments at the block junction.^[19] Nevertheless, it was not possible to directly transfer the conditions used in our earlier work to the corresponding amide-based ATRP initiators, which we expected to be a chemically more stable linkage between both blocks. Applying “conventional” ATRP for block extension reactions under similar conditions was not successful and, therefore, we explored alternative approaches with ATRP in aqueous solvent mixtures or single-electron transfer living radical polymerization (SET-LRP), as well as a CuAAC click reaction. In this contribution, both pathways are compared with regard to the access to double hydrophilic PEO-*b*-PDha block copolymers (**Scheme 1**).

In general, both approaches permitted the synthesis of novel well-defined block copolymers, which are summarized in **Table 1**.

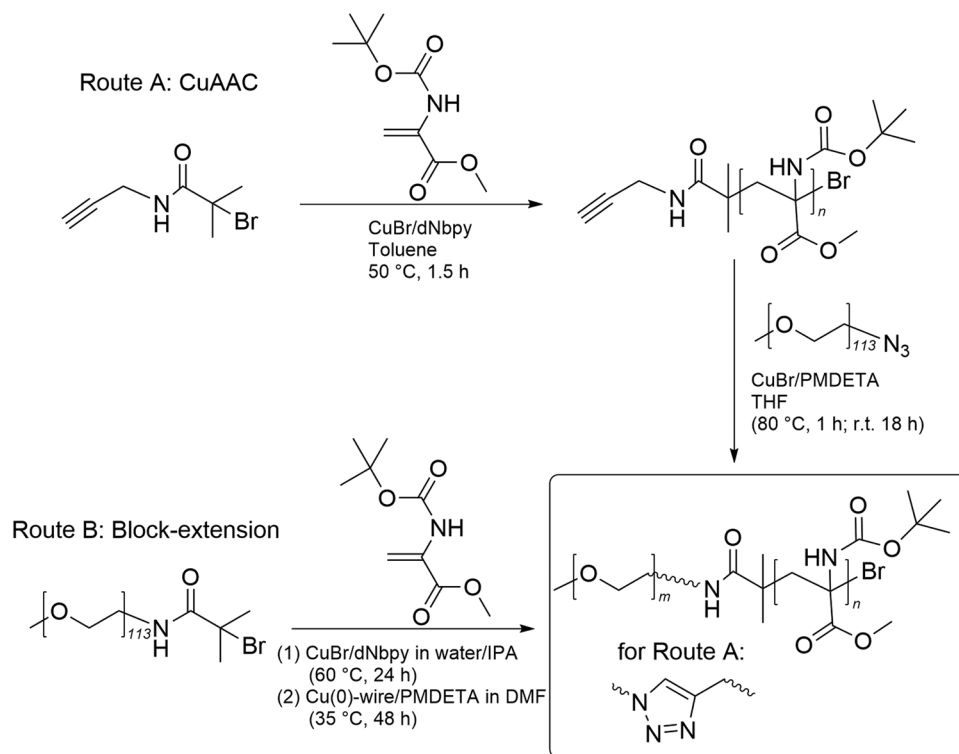
2. Results and Discussion

2.1. Synthesis and Characterization of PEO-*b*-PtBAMA Block Copolymers

PDha is a polyampholyte that exhibits a net positive charge at low pH, a broad zwitterionic regime around its isoelectric point, and is negatively charged at high pH values.^[21] Therefore, a double hydrophilic PEO-*b*-PDha block copolymer is an interesting candidate for reversible self-assembly into discrete nanostructures upon changes in pH or for metal ion complexation. Here, both the amino and carboxyl groups along the PDha backbone are an ideal platform for coordinating metal ions whilst PEO ensures solubility. Although the general synthesis of PEO-*b*-PtBAMA has been reported previously via ATRP,

2.2. Synthesis of PEO-*b*-PtBAMA via Click Chemistry

CuAAC is a powerful tool to covalently link two polymer segments.^[27] In this way, we synthesized the corresponding PEO-*b*-PtBAMA block copolymer by linking alkyne-functionalized PtBAMA with azide-functionalized PEO. Not only does click chemistry allow the conjugation of two readily synthesized and (moderately) well-defined polymers, it also permits the incorporation of higher molecular weight PtBAMA, as the molar mass was found to be limited under ATRP conditions reported earlier.^[19] In general, the controlled radical polymerization of tBAMA by ATRP-based techniques remains quite challenging due to the presence of a nitrogen in each monomer unit that can complex the copper species, its high reactivity, and steric effects.



Scheme 1. Synthetic routes toward PEO-*b*-PtBAMA block copolymers.

Table 1. Summary of the reaction conditions used to synthesize PtBAMA-alkyne and PEO-*b*-PtBAMA, and the corresponding SEC characterization data.

	Cu(I)X [eq.]	Solvent [wt.%]	T [°C]	t [h]	M_n [g mol ⁻¹]	\bar{D}
Route A						
PtBAMA-alkyne ₅₀ ^{a)}	CuBr (1)	Toluene (10)	50	1.5	10 000 ^{d)}	1.45
PtBAMA-alkyne ₄₄ ^{a)}	CuCl (2)	Toluene (10)			8 800 ^{d)}	1.38
PEO ₁₁₃ - <i>b</i> -PtBAMA ₈₅	–	THF (90)	80	1	32 000 ^{f)}	1.42
PEO ₄₄ - <i>b</i> -PtBAMA ₈₅	–	THF (90)	21	18	22 200 ^{f)}	1.55
Route B						
PEO ₁₁₃ - <i>b</i> -PtBAMA ₄₆ ^{b)}	Cu(0) (5 cm)	DMF (33)	60	24	13 900 ^{e)}	1.42
PEO ₁₁₃ - <i>b</i> -PtBAMA ₂₃ ^{b)}	Cu(0) (2.5 cm)	DMF (33)			8 200 ^{e)}	1.06
PEO ₁₁₃ - <i>b</i> -PtBAMA ₁₀ ^{c)}	CuBr (1.5)	H ₂ O/DMF (1/1) (80)	24	24	5 200 ^{e)}	1.03
PEO ₁₁₃ - <i>b</i> -PtBAMA ₃₉ ^{c)}	CuBr (1.5)	H ₂ O/ <i>i</i> PrOH (1/1) (80)			5 800 ^{e)}	1.10

[M]:[I]:[ligand] = ^{a)}100:1:1, L = dNbpy; ^{b)}100:1:1.5, L = PMDETA; ^{c)}100:1.5:1.5, L = dNbpy; THF SEC (^{d)}PS/^{e)}PMMA calibration), ^{f)}CHCl₃/triethylamine/*iso*-propanol [94/2/4], PS calibration.

Synthesis of PEO-N₃ was achieved in accordance with the literature protocols in two steps starting from PEO-OH with either 44 or 113 repeat units.^[28] To obtain PtBAMA-alkyne, an alkyne-containing ATRP initiator, 2-bromo-2-methylpropanamide (BMP), was first synthesized according to literature protocols.^[29] Up until now, only methyl α -bromoisobutyrate (MeBib) has been shown to effectively polymerize *t*BAMA via ATRP. Here, the most promising catalytic system (CuBr/dNbpy) resulted in an M_n below 6500 g mol⁻¹ with a moderately narrow dispersity (\bar{D}) of 1.35 after 24 h. However, attempts to achieve higher molecular weights resulted in poorer control over the reaction.^[19] Further efforts to improve the polymerization control of this reactive monomer were attempted using a different initiator (BMP), and are summarized in Table S1, Supporting Information.

The first experiment (Table 1) using BMP as initiator was performed under similar conditions as for the polymerization initiated using MeBib. However, it should be noted that the use of amide-based initiators is generally more demanding as a result of increased termination reactions and lower initiation efficiency.^[24–26] The reaction using the amide initiator BMP proceeds significantly faster; and after only 1.5 h, an already higher M_n of 10 000 g mol⁻¹ with a corresponding dispersity of 1.45 was found. Lower reaction temperatures of 20/30 °C resulted in higher M_n and broader dispersities, presumably due to slower and incomplete initiation of BMP. Higher concentrations employing only 10 wt. % toluene resulted in highly viscous reaction mixtures after 1 h of polymerization, whilst more dilute systems (33 wt. % toluene) led to a lower M_n of 5600 g mol⁻¹, with only a slightly lower \bar{D} of 1.41. Upon further dilution, no polymerization was observed. Furthermore, the addition of a reversible deactivator, CuBr₂ (0.1 eq. with respect to the initiator), to improve polymerization control proved unsuccessful. Presumably the presence of the deactivating species shifted the equilibrium to the dormant species, which severely lowered the polymerization speed and resulted in no observable polymer formation after a reaction time of 1.5 h. While CuCl has proven unsuccessful in the polymerization of *t*BAMA from MeBib in preliminary experiments, the use of CuCl-based systems using BMP as initiator were promising. Here, an M_n of 8800 g mol⁻¹ and a corresponding \bar{D} of 1.38 could be achieved when 2 eq.

of CuCl relative to BMP was used. As expected, lowering the amount of CuCl further resulted in lower molecular weight polymers with an M_n of 3800 g mol⁻¹ after 4.5 h due to slower initiation, which could be of interest to access lower molecular weight polymers. However, for further experiments, PtBAMA was synthesized using a CuBr/dNbpy catalytic system with a polymerization time of 2.0 h, resulting in \approx 85 repeat units (12 700 g mol⁻¹, \bar{D} of 1.45, THF SEC).

Afterward, PtBAMA₈₅-alkyne was combined with PEO₄₄-N₃ and PEO₁₁₃-N₃ via a CuAAC reaction in accordance with earlier studies.^[30] The azide (1.5 eq.) was used in excess to ensure maximum functionalization of the alkyne moiety. Size exclusion chromatography (SEC) traces reveal a clear shift toward lower elution volumes (**Figure 1A**), and the unreacted PEG-N₃ was successfully removed by washing the crude product thoroughly with water. Hence, the block copolymers PEO₄₄-*b*-PtBAMA₈₅ and PEO₁₁₃-*b*-PtBAMA₈₅ could be successfully prepared with an M_n of 22 200 and 32 000 g mol⁻¹ and a \bar{D} of 1.42 and 1.55 (CHCl₃ SEC), respectively. By further optimizing the homopolymerization of *t*BAMA, which is so far limited in its control via ATRP, it should be possible to obtain more narrowly distributed block copolymers. The M_n values are higher than expected, which may be explained by two possible reasons: 1) the low molecular weight fraction containing a short PtBAMA-alkyne segment may be removed during the washing steps; and 2) the hydrodynamic volume of the block copolymer may vary compared to the single individual blocks. However, since the SEC traces are overlapping, the presence of residual unreacted PtBAMA-alkyne cannot be excluded, although the integral ratio of both blocks by ¹H-NMR fits quite well. The ¹H-NMR spectroscopy results are provided in Figure S1, Supporting Information.

2.3. Synthesis of PEO-*b*-PtBAMA via Block Extension

Block extension of a suitable macroinitiator typically is synthetically less demanding and more straightforward if compared to polymer–polymer ligation approaches. As an alternative to the established ester-based ATRP macroinitiators,^[19] PEO₁₁₃-amide-Br was used under similar conditions for the ATRP

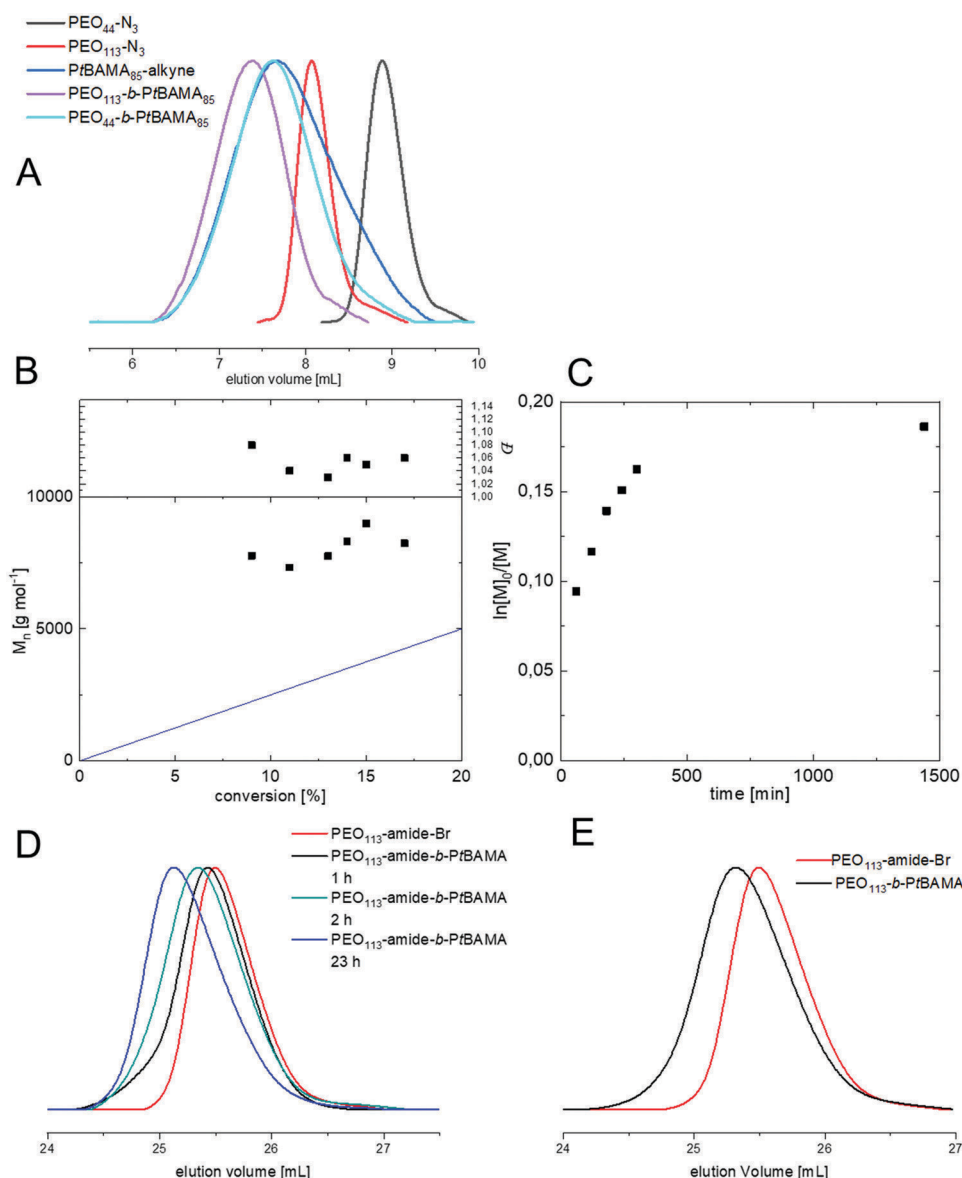


Figure 1. A) SEC traces of PEO-N₃ and PtBAMA₈₅-alkyne before and after CuAAC reaction in CHCl₃; B,C) kinetics of the single-electron transfer living radical polymerization (SET-LRP) block extension (*t*BAMA:ligand:macroinitiator = 100:0.1:1, copper(0) wire length = 2.5 cm, [M]₀ = 0.0248 mmol per 1.25 mL, T = 35 °C) and SEC traces of aqueous ATRPs in a D) DMF and E) iso-propanol solvent mixture. The M_n was obtained by SEC (eluent: THF, PMMA calibration) and conversion determined via ¹H-NMR spectroscopy.

of *t*BAMA. However, the amide initiator suffered from poor reproducibility, and only a maximum of 15 *t*BAMA repeat units could be achieved. Hence, alternative approaches to conventional ATRP were tested, namely SET-LRP and aqueous ATRP. SET-LRP is less sensitive toward oxygen, proceeds faster, and at lower reaction temperatures than conventional ATRP techniques; while aqueous ATRP is more amenable with the water-soluble PEG macroinitiator.

2.4. SET-LRP

DMF was chosen as solvent as it is well suited for controlled SET-LRP.^[31] The polymerizations were carried out at 35 °C,

and the reaction kinetics investigated using varying lengths of copper wire (2.5 and 5 cm). Starting with a copper(0) wire length of 5 cm, an M_n of 13 900 g mol⁻¹ was achieved with a corresponding *D* of 1.42 (Table 1). This corresponds to the addition of 46 monomer units, which is higher than previously achieved using ATRP. The reaction proceeded more slowly in the presence of less Cu(0) wire, and this behavior was further investigated (Figure 1B,C). While previous conversions of up to 60% were possible after 24 h, the chain growth plateaus after less than 20% monomer conversion is reached when lower amounts of copper wire are used. However, while the conversion reached is significantly lower under these conditions, the reaction proceeds in a more controlled manner with a *D* of 1.06 achieved after 24 h at a monomer conversion of

18%. Further decreasing the Cu(0) wire length did not result in any further improvements. While the reaction proceeds in a controlled manner within the first 300 min using a reduced amount of copper wire, the decreasing semilogarithmic plot, which eventually plateaus after 24 h, indicates that the number of active radicals decreases over the course of the polymerization, which may be due to termination reactions occurring. This ultimately limits the conversion, and hence the reachable molecular weight. The relatively low dispersity of 1.06 indicates, however, that this arises predominantly due to the equilibrium rather than the formation of dead chains, and hence we can expect the chains to have living character. Since this is the first report of SET-LRP as suitable candidate to polymerize *t*BAMA in a controlled fashion, future work will focus on further optimizing SET-LRP to synthesize well-defined *Pt*BAMA homopolymers with a targeted molecular weight and low dispersity.

2.5. Aqueous ATRP

Block extension via ATRP can be performed under aqueous conditions, which is favorable for the solubility of the PEO-based macroinitiator. Cordeiro et al. block extended PEO with DMAEMA using ATRP in water/*iso*-propanol mixtures, yielding dispersities below 1.4. We further tested water/DMF (1:1 v/v) mixtures for comparison. A monomer/CuBr/dNbpy/initiator ratio of 100:1.5:1.5:1 was used, and the polymerization performed at a temperature of 60 °C. The chain extension in the DMF/water mixture was monitored via SEC, and samples taken after 1, 2, and 24 h (Figure 1D). With increasing polymerization time, the SEC traces shift toward lower elution volumes. After 24 h, an M_n of 5 200 g mol⁻¹ and \bar{D} of 1.03 is achieved. ¹H-NMR spectroscopy also clearly shows the signals of both blocks, and a degree of polymerization (*DP*) of 10 monomer units was determined. Water/*iso*-propanol mixtures were also explored, and this system permitted the addition of 39 *t*BAMA units with a clear shift in the elution volume observed after 24 h by SEC (Figure 1E). However, a small tailing toward higher elution volume was observed as a possible result of incomplete reinitiation of the macroinitiator chains.

Route B, that is, block extension, was initially considered a more desirable synthetic approach to prepare such block copolymers. Block extension of a PEO macroinitiator requires only one synthetic step and typically results in narrower dispersities of 1.03 compared to 1.42 for conjugation, which is the result of the combination of two already moderately dispersed building blocks. However, Route A (CuAAC) appears more promising for the synthesis of PEO-*b-Pt*BAMA. Block extension suffers from limited conversion, with a maximum of 46 repeat units added under the applied conditions, and hence results in the synthesis of shorter *Pt*BAMA segments. In comparison, the pre-synthesis of the *Pt*BAMA-alkyne homopolymers results in higher *DP*s with more predictable molar masses between 3 200 and 35 000 g mol⁻¹ depending on the reaction time and the copper salt used as shown in Table S1, Supporting Information. However, it should be noted that the main drawback compared to Route B is a broader \bar{D} as a result of the combination of two polymers where the *Pt*BAMA-

alkyne homopolymer is already characterized by a relatively high dispersity ($\bar{D} = 1.45$).

2.6. Deprotection of PEO-*b-Pt*BAMA to PEO-*b-PD*ha

After the successful preparation of PEO-*b-Pt*BAMA block copolymers, we tested the deprotection of the *Pt*BAMA segment, analogous to earlier reports for PS-*b-Pt*BAMA and *Pn*BMA-*b-Pt*BAMA.^[17] We tested both acidic and basic protocols to determine the best conditions to successfully deprotect the *Pt*BAMA segment, and they are depicted in Figure 2A as Routes A and B. Unfortunately, these protocols did not permit the orthogonal deprotection of the *Pt*BAMA segment. However, the corresponding PDha-based block copolymers were obtained after subsequent deprotection steps. The same was observed for PEO-*b-Pt*BAMA, with the exception that long reaction times via Path A exceeding 5 h resulted in complete deprotection in one step. Interestingly, in the case of PEO₄₄-*b-Pt*BAMA₈₅, no cleavage of the block junction was observed according to aqueous SEC (Figure 2C), whereas partial cleavage was found for PEO₁₁₃-*b-Pt*BAMA₈₅ (Figure S3, Supporting Information). We tentatively explain this by slight differences in block copolymer solubility due to the dissimilar PEO chain lengths. Hence, the accessibility of the amide linking group might differ and as a result, PEO₄₄-*b-PD*ha₈₅ may be more stable under the respective conditions. However, since the amide is apparently not stable under such harsh conditions, the deprotection protocol was significantly reduced to 15 min for each step, and a two-step protocol applied (first Route A and then Route B), which allowed quantitative deprotection of *Pt*BAMA to PDha. SEC traces of PEO₁₁₃-*b-PD*ha₈₅ in water did not indicate the presence of cleaved PEO chains, with only a small shoulder visible at higher elution volumes close to the solvent signal (Figure 2B). The distribution at higher elution volumes may result from the formation of aggregates in water, possibly due to attractive interactions between the zwitterionic segments. Dynamic light scattering (DLS) of such samples also showed the presence of some ill-defined larger aggregates. However, SEC traces in DMSO (Figure 2D) show a monomodal distribution, hinting to the presence of intact PEO-*b-PD*ha block copolymer.

Since PEO₁₁₃-*b-PD*ha₈₅ dissolves over a broad pH range (4–14) in water, its solution properties were further investigated via DLS and ζ -potential measurements for comparison.^[21] Therefore, the block copolymer was dissolved at pH 7 and measurements performed after titration to pH = 4 and 9 (Figure 2E). A hydrodynamic radius (R_H) of 4, 16, and 23 nm was found under basic, neutral, and acidic conditions, respectively. These results indicate that aggregation is particularly favored under acidic conditions, where hydrogen bonds lead to strong interactions between different block copolymer unimers. In addition, the chelating ability of these systems for metal ions was investigated by the addition of Cu²⁺ ions.^[5] At pH 7, no significant aggregation was observed in the presence of Cu²⁺, and the R_H also decreased. This observation suggests the successful complexation of Cu²⁺ by PDha, and a certain collapse of the block. At pH 9, an increased R_H of 40 nm is observed in the presence of Cu²⁺, presumably due to higher amounts of

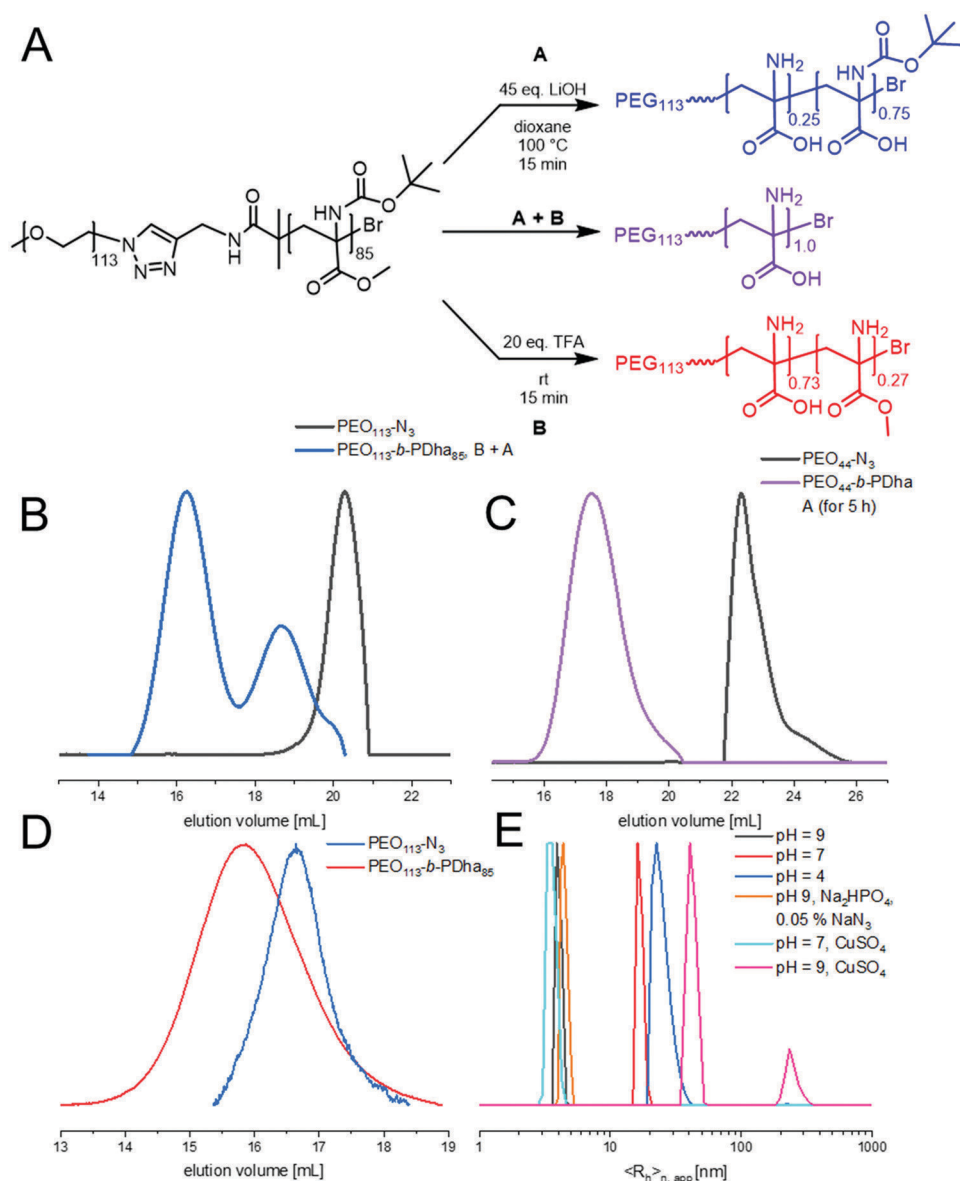


Figure 2. A) Synthetic route toward PEO-*b*-PDha block copolymers via basic and/or acidic deprotection, as well as the corresponding SEC traces of the completely deprotected block copolymers: B) PEO₁₁₃-*b*-PDha₈₅ and C) PEO₄₄-*b*-PDha₈₅ in H₂O; D) PEO₁₁₃-*b*-PDha₈₅ in DMSO. E) DLS measurements of PEO₁₁₃-*b*-PDha₈₅ at different pH values and upon the addition of Cu²⁺ salt.

metal being complexed and the formation of micelles featuring a PDha/Cu²⁺ core and a PEO corona.

The ζ -potential of the PEO₁₁₃-*b*-PDha₈₅ block copolymer was investigated (Figure S4, Supporting Information) in order to determine the overall charge of the polyampholytic segment. Therefore, it was dissolved at pH 12 ($c = 0.2 \text{ mg mL}^{-1}$) and titrated with 0.5 M HCl to carry out measurements in pH steps of 2. PDha behaves like a polyzwitterion in the pH range from 10.5 and 6.5^[21] and, as expected at pH 12 and 10 it reveals negative values around -40 mV due to deprotonated carboxylate moieties. Afterward, the values are slightly increasing until pH 6 (-20 mV) due to partial protonation of the amino groups as well as partial formation of $-\text{COOH}$ groups. At a pH of around

5 the isoelectric point is reached and at pH 4 a value close to neutral of $+1 \text{ mV}$ was found.

3. Conclusion

The successful synthesis of an amphiphilic block copolymer, PEO-*b*-PtBAMA, linked by an amide junction was described via two synthetic strategies: CuAAC and controlled radical polymerization. Both pathways led to well-defined block copolymers with moderately narrow molecular weight distributions according to nuclear magnetic resonance (NMR) and SEC analysis, but differing in the level of control obtained in terms

of dispersity and molecular weight. While block extension of a PEO-amide-Br initiator via SET-LRP and ATRP is synthetically straightforward and results in narrowly distributed block copolymers ($\bar{D} \geq 1.03$), click chemistry affords higher and more controllable molecular weight for the PtBAMA segment. Using experimentally demanding amide-containing initiators, it was possible to link the corresponding polymer segments by a rather stable junction, which permitted the subsequent deprotection under basic and acidic conditions. SEC confirms no cleavage of both segments occurs in contrast to the previously synthesized ester-based ATRP macroinitiators.^[19] This enabled the preparation of double hydrophilic PEO-*b*-PDha block copolymers. First experiments on the solubility and self-assembly in aqueous solution revealed pH-dependent overall charge (negative until pH ≈ 5), as well as aggregation and possible complexation of Cu²⁺ ions. In this regard, the prepared polymers are interesting candidates as templates for metal nanoparticles, cargo carrying systems, or for use in biomineralization. Their potential for use in such applications will be investigated in future studies.

4. Experimental Section

Chemicals: Methanesulfonyl chloride ($\geq 99.7\%$) NaN₃ ($>99.5\%$), propargylamine (98%), 4,4'-di-5-nonyl-2,2'-bipyridine (97%), alpha-bromoisobutyl bromide (98%), copper(I) chloride ($\geq 99.995\%$), Cu(I) bromide (99.999%) and Cu(II) bromide (99%) were purchased from Sigma-Aldrich. TFA ($\geq 99.9\%$) was purchased from Roth, triethylamine ($\geq 99.0\%$) from CHEMSOLUTE, and *N*-(*tert*-butoxycarbonyl)-L-serinmethylester (98%) from Carbolution Chemicals, LiOH monohydrate (56% LiOH) from Acros Organics, pentamethyldiethylenetriamine (98%) from abcr, mPEG₁₁₃-NH₂ from Rapp Polymere, mPEG₁₁₃-OH from JenKem Technology, mPEG₄₄-OH from Fluka. Cu(0) wire ($\geq 99.9\%$, 1 mm diameter) was purchased from Sigma-Aldrich and purified as follows: Copper(0)-wire was wrapped around a magnetic stirrer bar and placed into a flask containing 6 mL HCl (37%) for 6 min under ambient conditions. After which, the acid was removed from the reaction vessel by syringe, and the wire was washed with acetone (10 mL) before being dried under an argon stream for a further 10 min.

Analytical Methods: Nuclear Magnetic Resonance Spectroscopy: ¹H- and ¹³C-NMR spectra were performed on a Bruker AC 300 MHz using CDCl₃ and D₂O/NaOD as solvents at a temperature of 298 K. The spectra were referenced by using the residual signal of the deuterated solvent.

Size Exclusion Chromatography: SEC traces were measured using a Shimadzu system equipped with a CBM-20 A system controller, a LC-10 VP Pump, a RID-10A refraction index detector, and a PSS SDV guard/linear S column. As eluent a mixture of chloroform/triethylamine/isopropanol [94/2/4] v/v/v was used and measurements were recorded with a flow rate of 1 mL min⁻¹ and 40 °C.

SEC measurements in DMSO were measured on a Jasco instrument using DMSO + 0.5% LiBr as solvent at a flow rate of 0.5 mL min⁻¹ at 65 °C and Pullulan calibration. It contains PSS NOVEMA 3000 Angström/300 Angström columns, a RI-930 detector as well as a PU-980 pump.

Aqueous SEC was measured on a Jasco system equipped with a DG-2080-53 degasser, PU-980 pump, and a RI-2031 Plus refractive index detector (Jasco Deutschland Labor- und Datentechnik GmbH, Groß-Umstadt, Germany) with 0.1 M Na₂HPO₄/0.05% NaN₃ pH 9 as eluent and at a flow rate of 1 mL min⁻¹ on a column set of PSS SUPREMA 1000 Å and 30 Å (10 μm) at 30 °C (PSS, Mainz, Germany). PEO was used as calibration.

Dynamic Light Scattering: DLS measurements were performed using an ALV laser CGS3 Goniometer equipped with a 633 nm HeNe laser

(ALV GmbH, Langen, Germany) at 25 °C and at a detection angle of 90°. The CONTIN analysis of the obtained correlation functions was performed using the ALV 7002 FAST Correlator Software.

ξ-Potential: Zeta-potentials were measured on a ZetaSizer Nano ZS from Malvern via M3-PALS technique with a laser beam at 633 nm. The detection angle was 13°. The samples were prepared by titration of the polymer in 0.1 M NaOH (0.2 g/L) with 0.1 M HCl and 1 mL of the solution was taken at the desired pH values. The titration and pH detection was performed on a Metrohm 765 Dosimat titrator with a Greisinger electronic GMH3539 digital pH-/mV-electrode with a thermometer.

Synthesis of tBAMA Boc-Ser-OMe (10.0 g; 45.6 mmol; 1.0 eq.) was dissolved in DCM (200 mL) and MsCl (6 mL; 77.5 mmol; 1.7 eq.) was added. After cooling in an ice bath NEt₃ (23 mL; 165.9 mmol; 3.6 eq.) was slowly added dropwise and the reaction mixture stirred for 1 h at 0 °C. Then it was stirred for additional 2 h at room temperature and afterward washed with potassium bisulfate (1%) to neutrality. The organic phase was dried with Na₂SO₄ and the solvent removed under reduced pressure. The crude product was further purified via column chromatography with silica gel (ethyl acetate/*n*-hexane v/v 1/4). After removal of the solvent under reduced pressure, the product was yielded as a colorless oil (8.6 g, 94%).

¹H-NMR (300 MHz, CDCl₃, δ): 7.01 (s, 1 H, -NH), 6.16 (s, 1 H, -C=CH-), 5.73 (s, 1 H, -C=CH-), 3.83 (s, 3 H, -O-CH₃), 1.48 (s, 9 H, -COO-C(CH₃)₃) ppm.

Synthesis of BMP: Propargylamine (1.00 g, 1 eq.) and NEt₃ (4.6 g, 2.5 eq.) were dissolved in diethylether (20 mL) at 0 °C. Afterward α-bromoisobutylbromide (8.3 g, 2 eq.) was added dropwise and the reaction mixture stirred for 12 h at room temperature. The solution was washed with HCl (0.5 M), NaHCO₃ (3%) and distilled water (1×) until a pH of 1 was reached. The solution was dried over MgSO₄ and the solvent removed under reduced pressure. The crude product was recrystallized in *n*-hexane/toluene at 0 °C and obtained as white crystals.

¹H-NMR (300 MHz, CDCl₃, δ): 7.00–6.75 (-NHCO), 4.08 (-C-CH₂-NHCO), 2.30 (m, H-C-CH₂-), 1.99 (s, -C(CH₃)₂) ppm.

Synthesis of PtBAMA-alkyne: The monomer tBAMA was degassed via four freeze-pump-thaw cycles and afterward added to BMP, Cu(I)Br, and dNbpy under Ar ([100]/[1]/[1]/[1]). Then the reaction mixture was placed in an oil bath at 50 °C and stirred under Ar for 1.5 h. The reaction was terminated by cooling to room temperature and after removal of the Cu-catalyst through an AlOx column, the crude product was precipitated in excess *n*-hexane. The product was filtered off, dried under vacuo, and obtained as a white powder.

¹H-NMR (300 MHz, CDCl₃, δ): 6.00–5.00 (m, -NH), 4.08–3.37 (m, -O-CH₃), 3.32–2.02 (m, -C-CH₂-), 1.75–1.16 (m, -COO-C(CH₃)₃) ppm.

SEC (PS calibration, CHCl₃/*i*-PrOH/NEt₃): M_n = 17000 g mol⁻¹, M_w = 30100 g mol⁻¹, $\bar{D} = 1.77$.

Synthesis of PEO-azide: PEO-OH (M_n \approx 5000 g mol⁻¹, 10.00 g, 1.0 eq.) and NEt₃ (0.51 g, 2.5 eq.) were dissolved in DCM (50 mL) 0 °C. Afterward MsCl (0.046, 2 eq.) was added dropwise and the reaction mixture stirred additional 18 h at room temperature. The reaction mixture was filtered off and precipitated in excess diethyl ether two times before drying under vacuum.

PEO-OMs was dissolved in DMF (50 mL) and NaN₃ (1.3 g, 5 eq.) was added. The turbid reaction mixture was stirred for 24 h at room temperature and then filtered off. DMF was removed in an azeotropic distillation with toluene. The residue was redissolved in DCM before washing with dest. Water (2×) and NaCl (saturated, 1×). The solution was dried over MgSO₄ and precipitated in excess diethyl ether. The product was filtered off, dried under vacuo, and obtained as a white powder (yield: 70%).

¹H-NMR (300 MHz, CDCl₃, δ): 3.68–3.59 (m, -C-CH₂N₃, m, -O-C-CH₂-), 3.38 (s, -O-CH₃) ppm.

SEC (PEO calibration, CHCl₃/*i*-PrOH/NEt₃): M_n = 5700 g mol⁻¹, M_w = 6300 g mol⁻¹, $\bar{D} = 1.10$.

SEC (PEO calibration, CHCl₃/*i*-PrOH/NEt₃): M_n = 2100 g mol⁻¹, M_w = 2300 g mol⁻¹, $\bar{D} = 1.08$.

Synthesis of PEO-*b*-PtBAMA via CuCAAC Click Reaction: PEO-azide (10 mg, 1.0 eq.), PtBAMA-alkyne (20 mg, 1.0 eq.), and PMDETA (0.4 mg, 1.2 eq.) were dissolved in THF (0.2 mL) and the solution degassed via freeze–pump–thaw. Then the mixture was added to CuBr (0.3 g, 1.2 eq.) under Ar. The reaction mixture was stirred at 80 °C for 1 h and after switching off heating for additional 24 h at room temperature. Copper was removed via an AlOx column before the solvent was removed. The crude product was dispersed in water under vigorous stirring for 2 h and the polymer obtained via centrifugation. The polymer was obtained as a white powder after freeze drying.

Synthesis of PEO-*amide*-Br: PEO-NH₂ ($M_n \approx 5000$ g mol⁻¹, 1.00 g, 0.2 mmol) and NEt₃ (0.08 g, 0.8 mmol, 4 eq.) were dissolved in THF (20 mL) at 60 °C. Afterward α -bromoisobutyrylbromide (0.27 g, 1.2 mmol, 6 eq.) was added dropwise and the reaction mixture stirred for 9 h. The solvent of the turbid reaction mixture was removed and the residue redissolved in DCM before washing with Na₂CO₃ (saturated solution, 2 \times), HCl (0.5 M, 2 \times) and dest. Water (2 \times). The solution was dried over MgSO₄ and precipitated in excess diethyl ether. The product was filtered off, dried under vacuo, and obtained as a white powder (yield: 63%).

¹H-NMR (300 MHz, CDCl₃, δ): 3.68–3.59 (m, –C–CH₂NHCO, m, –O–C–CH₂–), 3.38 (s, –O–CH₃), 1.95 (s, –C(CH₃)₂) ppm.

SEC (PEO calibration, CHCl₃/*i*-PrOH/NEt₃): $M_n = 4800$ g mol⁻¹, $M_w = 5400$ g mol⁻¹, $D = 1.12$

Synthesis of PEO-*b*-PtBAMA via ATRP: For the synthesis of PEO₁₁₃-*b*-PtBAMA_{*x*}, tBAMA, CuBr, ligand, and PEO₁₁₃-amide Br were dissolved in the corresponding solvent and deoxygenated using four consecutive freeze–pump–thaw cycles. The polymerization was carried out at 50 °C for 24 h. The reaction was then terminated by cooling in liquid nitrogen followed by the addition of methanol. After removal of the residual copper using an AlOx column, the block copolymer was precipitated into cold *n*-hexane. The desired block copolymer was isolated by removal of the solvent under reduced pressure.

¹H-NMR (300 MHz, CDCl₃, δ): 6.31–4.84 (m, –NH), 4.06–3.47 (m, –O–C–CH₂– and s, –O–CH₃), 3.37 (s, –O–CH₃), 3.30–2.00 (m, –C–CH₂–), 1.78–1.04 (m, –COO–C(CH₃)₃) ppm.

Synthesis of PEO-*b*-PtBAMA via SET-LRP: For the synthesis of PEO₁₁₃-*b*-PtBAMA_{*x*}, tBAMA, Cu(0)-wire, PMDETA, and PEO₁₁₃-amide-Br were dissolved in DMF (1.25 mL), and the mixture deoxygenated by four consecutive freeze–pump–thaw cycles. The polymerization was carried out at 35 °C for 24 h. The reaction was then terminated by cooling in liquid nitrogen followed by the addition of methanol. After removal of copper by an AlOx column, the block copolymer was precipitated into cold *n*-hexane. The desired block copolymer was isolated by removal of the solvent under reduced pressure.

Synthesis of PEO-*b*-PDha: PEO-*b*-PtBAMA (50 mg) was dissolved in 1,4-dioxane (3 mL) and a saturated aqueous LiOH solution (3 mL, ≈ 45 eq. LiOH per monomer unit) was added. The reaction mixture was stirred for 15 min at 100 °C and afterward conc. HCl was added until neutrality of the solution was reached. Afterwards, the polymer was dialyzed against water (6–8 kDa) for 24 h and then the solvent was removed via freeze drying. The polymer was obtained as a white powder (yield: 40%).

¹H-NMR (300 MHz, D₂O, δ): 3.67 (m, –O–C–CH₂–), 3.34 (s, –O–CH₃), 2.95–2.00 (m, –C–CH₂–), 1.28 (m, –C–(CH₃)₃) ppm.

PEO-*b*-PtBAA-*co*-PDha (50 mg) was dissolved in TFA (20 eq.) and stirred for 15 min at room temperature. Then the reaction mixture was precipitated in diethylether, filtered off, and washed with diethylether. The polymer was obtained as a yellowish powder (yield: 50%).

¹H-NMR (300 MHz, D₂O, δ): 3.67 (m, –O–C–CH₂–), 3.34 (s, –O–CH₃), 2.95–2.00 (m, –C–CH₂–) ppm.

Supporting Information

Supporting Information is available from the Wiley Online Library or from the author.

Acknowledgements

This research was supported by the Deutsche Forschungsgemeinschaft (DFG, grant no. TRR 234, project no. SCHA1640/18-1, project A03 within the SFB 1278 “PolyTarget” and TP02 within FOR2811 – project no. 423435478). The authors acknowledge Peggy Laudeley and Dr. Grit Festag for SEC analysis, and they are further thankful to the NMR department at Friedrich-Schiller-University Jena for their continuous support.

Open access funding enabled and organized by Projekt DEAL.

Conflict of Interest

The authors declare no conflict of interest.

Keywords

atom transfer radical polymerization, copper-catalyzed alkyne-azide cycloaddition, double hydrophilic block copolymers, poly(dehydroalanine)

Received: September 10, 2019

Published online: November 26, 2019

- [1] G. Mountrichas, S. Pispas, *J. Polym. Sci., Part A: Polym. Chem.* **2007**, *45*, 5790.
- [2] H. Cölfen, *Macromol. Rapid Commun.* **2001**, *22*, 219.
- [3] O. Casse, A. Shkilnyy, J. Linders, C. Mayer, D. Häussinger, A. Völkel, A. F. Thünemann, R. Dimova, H. Cölfen, W. Meier, H. Schlaad, A. Taubert, *Macromolecules* **2012**, *45*, 4772.
- [4] B. V. K. J. Schmidt, *Macromol. Chem. Phys.* **2018**, *219*, 1700494.
- [5] L. Volkmann, M. Köhler, F. H. Sobotta, M. T. Enke, J. C. Brendel, F. H. Schacher, *Macromolecules* **2018**, *51*, 7284.
- [6] L. M. Bronstein, S. N. Sidorov, A. Y. Gourkova, P. M. Valetsky, J. Hartmann, M. Breulmann, H. Cölfen, M. Antonietti, *Inorg. Chim. Acta* **1998**, *280*, 348.
- [7] N. V. Semagina, A. V. Bykov, E. M. Sulman, V. G. Matveeva, S. N. Sidorov, L. V. Dubrovina, P. M. Valetsky, O. I. Kiselyova, A. R. Khokhlov, B. Stein, L. M. Bronstein, *J. Mol. Catal. A: Chem.* **2004**, *208*, 273.
- [8] J. Du, Y. Tang, A. L. Lewis, S. P. Armes, *J. Am. Chem. Soc.* **2005**, *127*, 17982.
- [9] C. Giacomelli, V. Schmidt, R. Borsali, *Macromolecules* **2007**, *40*, 2148.
- [10] Y. Kakizawa, A. Harada, K. Kataoka, *Biomacromolecules* **2001**, *2*, 491.
- [11] G. B. Webber, E. J. Wanless, S. P. Armes, Y. Tang, Y. Li, S. Biggs, *Adv. Mater.* **2004**, *16*, 1794.
- [12] B. Mahltig, J.-F. Gohy, S. Antoun, R. Jérôme, M. Stamm, *Colloid Polym. Sci.* **2002**, *280*, 495.
- [13] K. Lipponen, S. Tähkä, M. Kostianen, M.-L. Riekkola, *Electrophoresis* **2014**, *35*, 1106.
- [14] S. Luo, J. Xu, Y. Zhang, S. Liu, C. Wu, *J. Phys. Chem. B* **2005**, *109*, 22159.
- [15] D. A. Mortimer, *Polym. Int.* **1991**, *25*, 29.
- [16] A. B. Lowe, C. L. McCormick, *Chem. Rev.* **2002**, *102*, 4177.
- [17] M. Billing, G. Festag, P. Bellstedt, F. H. Schacher, *Polym. Chem.* **2017**, *8*, 936.
- [18] J. B. Max, D. V. Pergushov, L. V. Sigolaeva, F. H. Schacher, *Polym. Chem.* **2019**, *10*, 3220.
- [19] M. Billing, F. H. Schacher, *Macromolecules* **2016**, *49*, 3696.
- [20] P. Biehl, M. von der Luhe, F. H. Schacher, *Macromol. Rapid Commun.* **2018**, *39*, e1800017.
- [21] U. Günther, L. V. Sigolaeva, D. V. Pergushov, F. H. Schacher, *Macromol. Chem. Phys.* **2013**, *214*, 2202.



- [22] M. von der Luehe, U. Günther, A. Weidner, C. Grafe, J. H. Clement, S. Dutz, F. H. Schacher, *RSC Adv.* **2015**, 5, 31920.
- [23] M. von der Luehe, A. Weidner, S. Dutz, F. H. Schacher, *ACS Appl. Nano Mater.* **2018**, 1, 232.
- [24] D. J. Adams, I. Young, *J. Polym. Sci., Part A: Polym. Chem.* **2008**, 46, 6082.
- [25] A. Limer, D. M. Haddleton, *Macromolecules* **2006**, 39, 1353.
- [26] Y. Li, Y. Tang, R. Narain, A. L. Lewis, S. P. Armes, *Langmuir* **2005**, 21, 9946.
- [27] P. L. Golas, K. Matyjaszewski, *Chem. Soc. Rev.* **2010**, 39, 1338.
- [28] J. Edward Semple, B. Sullivan, T. Vojtkovsky, K. N. Sill, *J. Polym. Sci., Part A: Polym. Chem.* **2016**, 54, 2888.
- [29] Z. Xu, K. M. A. Uddin, L. Ye, *Macromolecules* **2012**, 45, 6464.
- [30] T. Rudolph, N. Kumar Allampally, G. Fernández, F. H. Schacher, *Chem.: Eur. J.* **2014**, 20, 13871.
- [31] X. Jiang, S. Fleischmann, N. H. Nguyen, B. M. Rosen, V. Percec, *J. Polym. Sci., Part A: Polym. Chem.* **2009**, 47, 5591.



Supporting Information

for *Macromol. Chem. Phys.*, DOI: 10.1002/macp.201900383

Double Hydrophilic Poly(ethylene oxide)-*block*-Poly
(dehydroalanine) Block Copolymers: Comparison
of Two Different Synthetic Routes

Johannes B. Max, Peter J. Mons, Jessica C. Tom, and Felix H.
Schacher*

Supporting Information

Double hydrophilic poly(ethylene oxide)-*block*-poly(dehydroalanine) (PEO-*b*-PDha) block copolymers – comparison of two different synthetic routes

Johannes B. Max,^{1,2,3} Peter J. Mons,^{1,2,3} Jessica C. Tom,^{1,2,3} Felix H. Schacher,^{1,2,3} *

¹ Institute of Organic Chemistry and Macromolecular Chemistry (IOMC), Friedrich-Schiller-University Jena, Lessingstraße 8, D-07743 Jena, Germany

² Jena Center for Soft Matter (JCSM), Friedrich-Schiller-University Jena, Philosophenweg 7, D-07743 Jena, Germany

³ Center for Energy and Environmental Chemistry (CEEC), Friedrich-Schiller-University Jena, Philosophenweg 7, D-07743 Jena, Germany

Email: felix.schacher@uni-jena.de

Table S1: Synthesis of PtBAMA-alkyne under varying reaction conditions.

polymer	Cu(I)X [y]	toluene [wt.%]	T [°C]	t [h]	M _n [g/mol]	PDI
1	CuBr 1	10	50	1.5	10 000	1.45
2	CuBr 1	10	50	2	12 700	1.45
3	CuBr 1	10	30	1	17 000	1.50
4	CuBr 1	10	20	1.5 18	- 35 000	- 2.07
5	CuBr 1	33	50	1.5	5 600	1.41
6	CuBr 1	66	50	1.5	-	-
7	CuBr 0.5 + CuBr ₂ 0.1	10	50	1.5	-	-
8	CuCl 1	10	50	2	8 800	1.50
9	CuCl 0.5	33	50	1.5 4.5	3 200 3 800	1.82 1.64
10	CuCl 2	10	50	1.5	8 800	1.38
11	CuCl 2	25	50	1.5	7 800	1.46

[M]: [I]: [dNbpy] = 100 :1: 1, THF SEC (PS calibration)

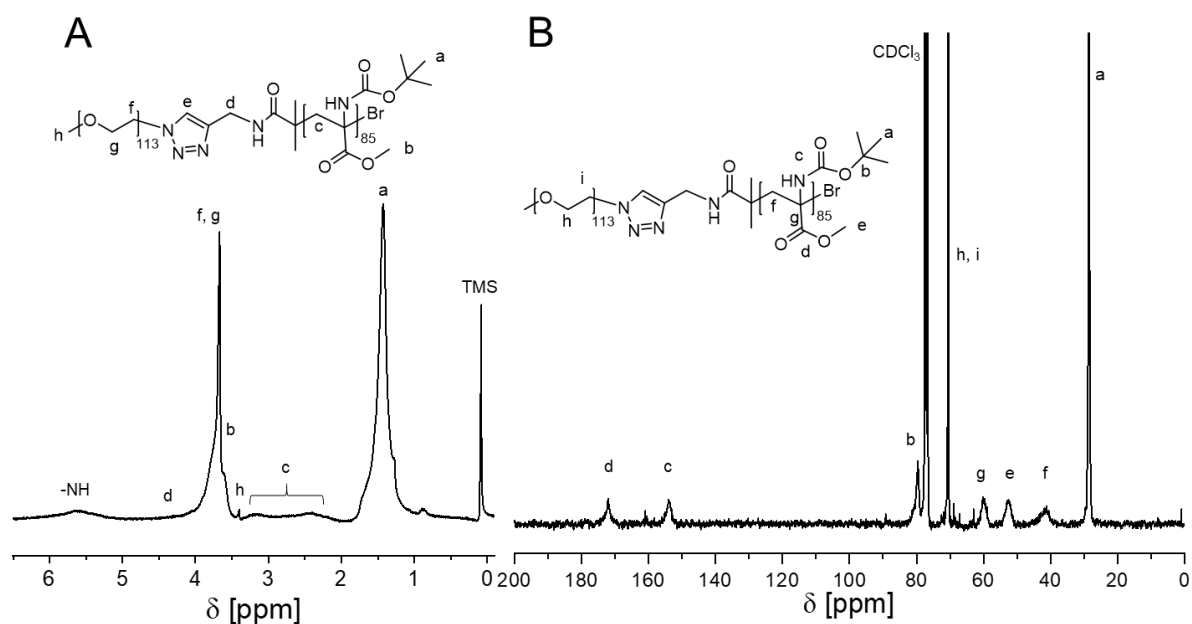


Figure S1: ^1H -NMR (A) and ^{13}C -NMR (B) spectrum of $\text{PEG}_{113}\text{-}b\text{-PtBAMA}_{85}$ block copolymer derived from the CuAAC click-reaction.

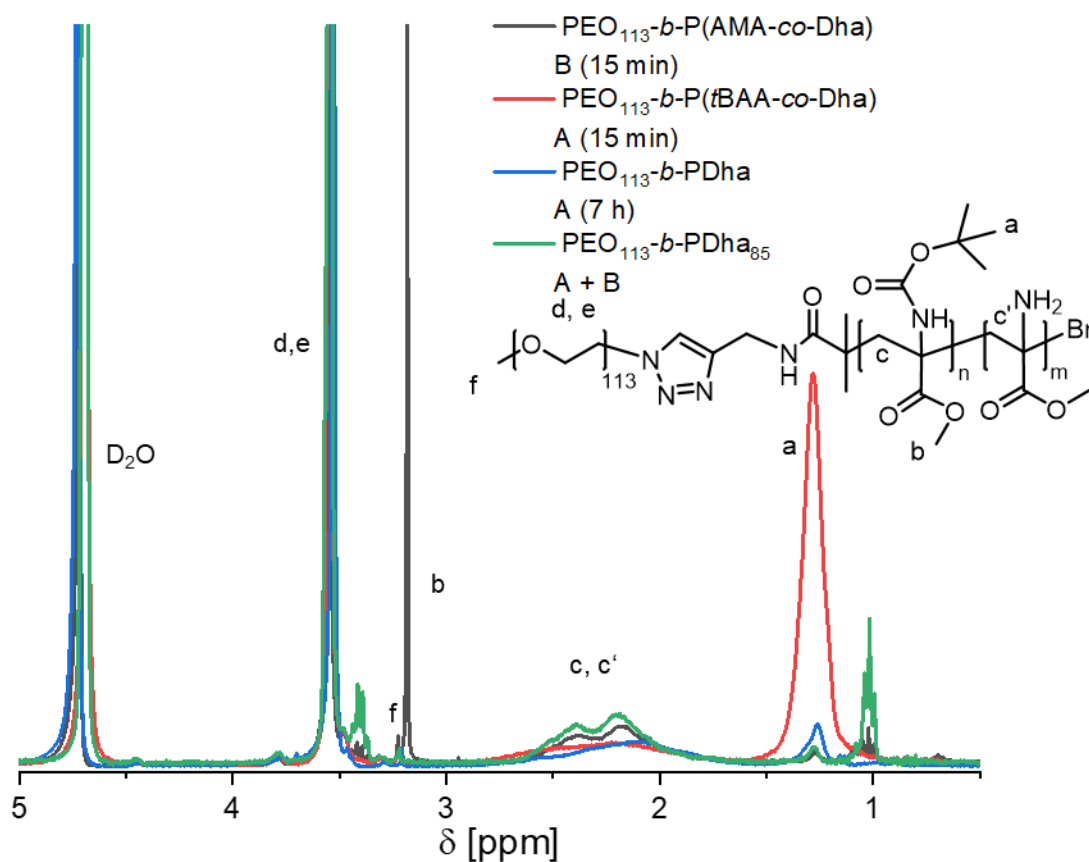


Figure S2: ^1H -NMR spectra of deprotected $\text{PEG-}b\text{-PtBAMA}$ block copolymers: $\text{PEG-}b\text{-PAMA}$ after stirring at rt for 15 min in TFA (black), $\text{PEG-}b\text{-PtBAA}$ after stirring at 100°C in water/dioxane with addition of LiOH for 15 min (red), $\text{PEG-}b\text{-PDha}$ after stirring at 100°C in water/dioxane with addition of LiOH for 7 h (blue) and $\text{PEG-}b\text{-PDha}$ after stirring for 15 min in water/dioxane (45 eq. LiOH) at 100°C and 10 min in TFA at rt (green).

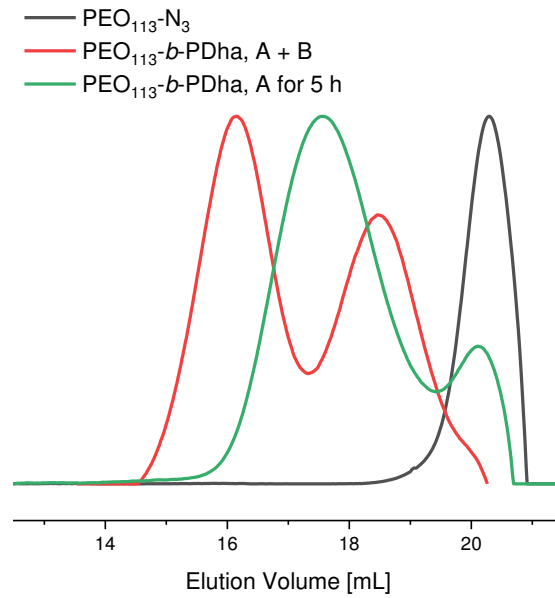


Figure S3: SEC-traces (eluent: water, 0.1 M Na₂HPO₄/0.05% NaN₃ pH 9) of the PEG₁₁₃-N₃ precursor and PEG₁₁₃-*b*-PDha after the deprotection under various conditions.

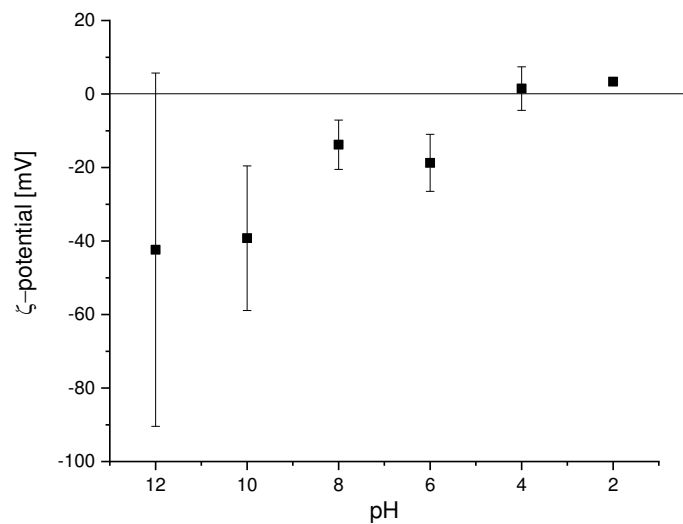
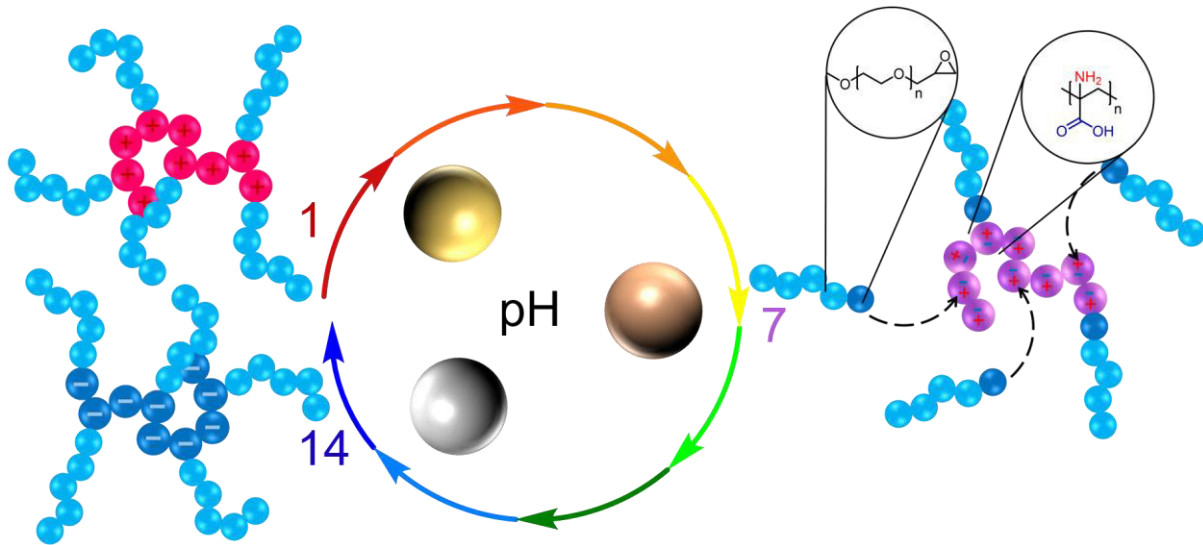


Figure S4: ζ-Potential measurement of PEO₁₁₃-*b*-PDha₈₅ at different pH values between 12 and 2.

Publication P3

“Polyampholytic Poly(dehydroalanine) Graft Copolymers as Smart Templates for pH-Controlled Formation of Alloy Nanoparticles”



J. B. Max, K. Kowalczyk, M. Köhler, C. Neumann, F. Pielenz, L. V. Sigolaeva, D. V. Pergushov, A. Turchanin, F. Langenhorst, and F. H. Schacher

Macromolecules, **2020**, 53, 4511-4523

Polyampholytic Poly(dehydroalanine) Graft Copolymers as Smart Templates for pH-Controlled Formation of Alloy Nanoparticles

J. B. Max, K. Kowalczyk, M. Köhler, C. Neumann, F. Pielenz, L. V. Sigolaeva, D. V. Pergushov, A. Turchanin, F. Langenhorst, and F. H. Schacher*



Cite This: *Macromolecules* 2020, 53, 4511–4523



Read Online

ACCESS |



Metrics & More

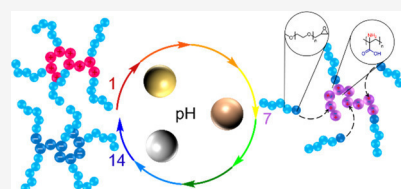


Article Recommendations



Supporting Information

ABSTRACT: Polymer templates are a facile way to control the formation, size, and shape of different inorganic nanomaterials by tuning solution behavior, morphology, or density and the type of functional groups. As a novel class of such templates, we herein introduce polyampholytic graft copolymers, more specifically, poly(dehydroalanine)-graft-poly(ethylene glycol) (PDha-*g*-PEG), which feature a polyampholytic backbone with varying net charge and charge densities at different pH values and PEG *grafts*, providing molecular solubility over the entire pH range. As the PDha backbone features both amino and carboxylic acid groups in each repeat unit, selective interaction with $[\text{AuCl}_4]^-$ and Ag^+ salts is possible, and this permits a straightforward synthesis of Ag, Au, and AgAu alloy nanoparticles. In this regard, we used different approaches: light-induced, thermal, and chemical reduction. As a unique feature, PDha-*g*-PEG enables control over AgAu nanoalloy composition via the pH value, as this directly affects the charge ratio ($-\text{NH}_3^+/-\text{COO}^-$) along the polymeric backbone. The obtained hybrid materials were investigated with respect to structure, shape, composition, and optical properties of nanoparticles via transmission electron microscopy, X-ray photoelectron spectroscopy, energy-dispersive X-ray spectroscopy, thermogravimetric analysis, and UV–vis spectroscopy. In our opinion, this is a facile way to control nanoalloy composition and this can be extended to other mono- or bimetallic nanoparticle examples.



INTRODUCTION

The synthesis of tailor-made, nanostructured inorganic composites such as nanoparticles (NPs) or mesoporous materials can be readily realized by the utilization of structure-directing polymers as templates. Hereby, the organic compounds can be retained as the matrix or stabilizing agent in solution or films or also be removed by thermal decomposition or extraction, giving access to pure inorganic materials afterward.^{1–4} In this regard, inorganic materials with complex and defined structures were synthesized in the presence of block copolymer nanostructures, polymer NPs, or other polymeric matrices and have potential application in catalysis, energy storage, as sensors, in optics, and biomedicines.^{5–9} In case of mesoporous structures, for instance, a poly(isoprene)-*block*-poly(ethylene oxide) block copolymer was used as the template for aluminosilicates¹⁰ or titanium and niobium oxides, where a highly crystalline material was obtained after heating.⁷ Alternatively, covalently linked inorganic/organic hybrid materials can be obtained by controlled radical polymerization, for example, by the utilization of surface-immobilized initiators.¹¹ In an aqueous environment, water-soluble polymers or hydrogels are ideal templates to obtain NPs within a defined surrounding or to support biomineralization.^{12,13} Typically, the interaction of such materials with metal salts leads to the formation of polymer–ion complexes, for example, within a three-dimensional network or micelles. In this way, controlled growth alongside with stabilization of the

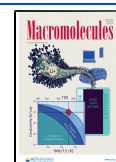
resulting inorganic materials upon reduction is enabled.^{12–15} As one example, Ni, Au, Ag, or AuAg alloy NPs could be prepared within a hydrogel network and applied for catalysis.^{13,14,16} Similarly, Ag nanocapsules were prepared using a thermo-responsive hydrogel core¹⁷ or a complexation/reduction approach, employing double hydrophilic copolymers as templates.^{18,19}

Among all types of metal NPs, Au received tremendous interest over the last decades because of unique physicochemical properties (conductivity and optical properties), excellent chemical stability, and a broad variety of surface functionalizations being possible, for example, using thiolated compounds.^{20,21} In a similar manner, Ag NPs are of interest in biomedical applications such as cancer therapy or photoimaging, as nanosensors, in cosmetics, catalysis, or, as antimicrobial additives.²² Alloys consisting of both Au and Ag, which are completely miscible because of almost identical lattice constants, reveal synergism and allow for fine-tuning both optical and electronic properties.^{23–25} Exemplarily, Ag NPs exhibit a higher refractive index sensitivity but are

Received: February 28, 2020

Revised: April 18, 2020

Published: May 20, 2020



typically more prone to oxidation and less biocompatible, if compared to Au.²⁶ Also, in catalysis, alloy NPs can outperform pure noble-metal NPs.²⁷ As the composition affects spectroscopic properties, shifts in the optical absorbance of the surface plasmon resonance peak can often be directly correlated with the composition of bimetallic particles,^{24,28,29} and this phenomenon was recently exploited in the multicolor tracking of single biomolecules.²⁵ Other examples of bimetallic NPs include Ni, Pt, Pd, Fe, and Cu, as outlined by Sharma et al.³⁰ The synthesis of AgAu NPs can be performed by coreduction of the corresponding metal salts, most often AgNO₃ and H[AuCl₄] in different ratios.^{29,31–39} Stabilization of these nanoalloys is usually achieved by the addition of surfactants, either monomeric, such as sodium dodecyl sulfate,³⁴ or dodecanethiol,⁴⁰ as well as water-soluble polymers, for example, poly(acryl amide),³¹ poly(*N*-vinyl pyrrolidone),³⁷ starch,⁴¹ poly(vinyl alcohol),³⁶ poly(diallyldimethylammonium chloride),²⁷ dendrimers,⁴² or double hydrophilic block copolymers.¹⁵ Besides these examples, polyelectrolyte multilayers, interpolyelectrolyte complexes, or hydrogels also can serve as host matrices,^{14,43} and during the reduction step, both temperature and pH value play an important role.^{44–49} Although energy-dispersive X-ray (EDX),³⁹ atomic absorption spectroscopy,⁵⁰ and X-ray photoelectron spectroscopy (XPS)³⁸ permit absolute determination of the alloy composition, cyclic voltammetry³⁷ and UV–vis spectroscopy⁵¹ give qualitative evidence and are typically used to analyze the electrochemical and optical properties.

Double hydrophilic block copolymers are interesting templates as—besides good solubility in aqueous media—they can feature additional stimuli-responsive properties, rendering both the aggregation state and solution properties dependent on temperature,^{52–54} pH value,^{55–57} ionic strength,^{58,59} irradiation with light,⁶⁰ or the presence of redox-active compounds.⁶¹ In many cases, reversible self-assembly into defined nanostructures upon triggering a suitable stimulus has been reported.^{62,63} This, in turn, with often reported biocompatibility, has led to an increasing interest in such materials,^{12,64} and besides generation of multiresponsive examples,⁶⁵ also aggregation in pure water as a result of different hydrophilicities has been reported.^{66,67} Instead of linear examples, double hydrophilic graft copolymers are another interesting class of materials with regard to templates.⁶⁸ Here, only few reports are available,⁶³ and also, solution behavior is sometimes more complicated, if compared to linear block copolymers.^{69,70} In general, the synthesis can be achieved via three strategies: grafting-through, grafting-onto, and grafting-from.⁷¹ Controlled radical polymerization techniques and their (sequential) combinations provide access to advanced polymer architectures and are hence mainly used.^{19,70,72–75} Besides direct and sequential access, post-polymerization modifications allow the attachment of various side chains to a polymer backbone, as, for instance, realized via amidation reactions toward double hydrophilic polyacetal-graft-PEO copolymers⁷⁶ or Michael addition with subsequent hydrolysis to obtain poly(dehydroalanine)-based (PDha) graft copolymers. Similar to linear block copolymers, double hydrophilic graft copolymers were already applied as templates for nanomaterials,^{19,77} for example, in the preparation of well-defined superparamagnetic Fe₃O₄ NPs, where the side chains form the outer shell while the functional groups along the backbone attach to the iron oxide core.⁶⁸ Moreover, Au NPs were prepared using a PNIPAM-*b*-PEA-*g*-PDEAEMA graft

copolymer, where the amino groups of PDEAEMA allowed the reduction of Au³⁺, and PNIPAM formed the corona.¹⁹

Although both temperature and pH value impact the Au and Ag NP formation in water,^{44–49} to the best of our knowledge, the composition of such alloys is so far only adjusted by the initial ratio of Au and Ag salts. Therefore, we, herein, present a polyampholytic graft copolymer as smart template, allowing control over the nanoalloy composition by varying the pH value at constant Ag/Au ratios. Double hydrophilic graft copolymers based on PDha were synthesized using a combination of radical polymerization and subsequent side-chain modification, and we investigated their solution properties with respect to overall charge, protonation/deprotonation, and self-assembly in aqueous solution. As each repeat unit of the polyampholytic backbone features both an amino as well as a carboxylic acid group, simultaneous interaction with Ag⁺ and [AuCl₄][–] is possible, followed by reduction via chemical, photo-induced, or thermal treatment. The as-prepared alloys were characterized via transmission electron microscopy (TEM), UV–vis spectroscopy, XPS, and thermogravimetric analysis (TGA). We believe that the herein presented approach will allow for a straightforward access to bimetallic NPs and will enable unprecedented control over composition and, with this, alloy properties.

RESULTS AND DISCUSSION

Synthesis of PDha-*g*-PEG Graft-Copolymers. We recently described the synthesis of polyampholytic PDha-based graft copolymers using PDha as polyfunctional reactive backbone.⁷⁸ PDha is accessible using either free or controlled radical polymerization and—depending on the pH value—presents a polycation, polyzwitterion, or polyanion.^{79–84} By subsequent postpolymerization modification, both epoxides and Michael acceptors could be attached to the polymer backbone, exploiting the amino moieties as reactive handles and resulting in amphiphilic and double hydrophilic graft copolymers. Although the solution behavior in water changed after addition of the side chains, solubility at lower pH values was still challenging. Hence, we decided to change to PEG mono glycidyl ethers with 10 and 22 repeat units as modifiers, hoping that this would improve aqueous solubility while maintaining backbone properties and functionality.^{78,79,82,85} The resulting polyampholytic and double hydrophilic graft copolymers will then be utilized as templates for Ag and Au NPs and for the corresponding nanoalloys.

The synthesis of the corresponding graft copolymers is carried out in three steps: first, radical polymerization of *t*BAMA to *Pt*BAMA, followed by acidic deprotection to remove the boc group, and in the last step, a polymer-analogous reaction with the modifier (Figure 1A). Until now, *Pt*BAMA was mainly obtained via free radical polymerization or atom-transfer radical polymerization, but regarding scale-up and reproducibility, we decided to also explore the possibility of using nitroxide-mediated polymerization.^{80,81} Therefore, temperature, solvent, monomer concentration, and addition of the nitroxide radical SG1 were varied, and the most promising conditions, targeting an apparent *M*_n of 10,000 g/mol and a monomodal, relatively narrow dispersity, were [monomer]/[BlocBuilder]/[SG1] ratios of [40]:[1]:[0.65], *T* = 80 °C and a reaction time of 15 min (*M*_n = 11,100 g/mol, *D* = 1.89). This corresponds to around 50 repeat units. The boc group was removed afterward using trifluoroacetic acid (TFA), following a protocol published earlier,⁷⁸ additionally leading to the

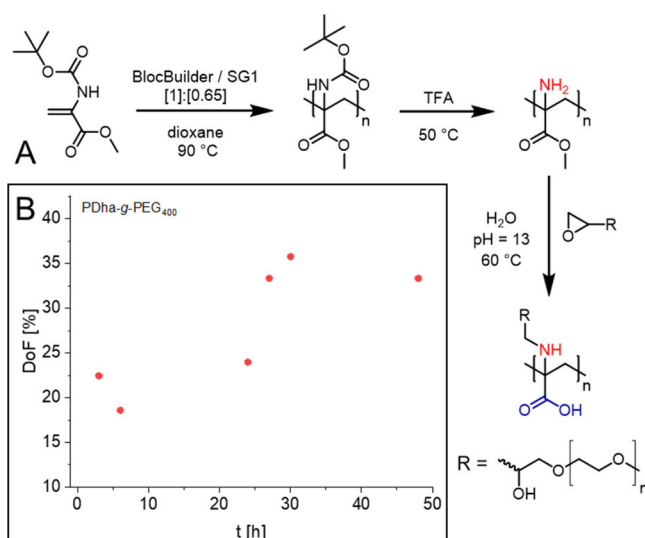


Figure 1. Synthetic route toward PDha-g-PEG double hydrophilic graft copolymers (A) and kinetic investigation of the grafting process for PDha-g-PEG₄₀₀ (B).

cleavage of 91% of the methyl ester. The remaining ester groups were removed during the subsequent postpolymerization modification. PEG glycidyl ethers were synthesized, according to literature reports,⁸⁶ and were well-soluble in water. Hence, all grafting reactions were performed without addition of methanol, as reported earlier for less-polar epoxides at a pH of 13.

Kinetic studies revealed that a maximum degree of functionalization (DoF, defined as the amount of functionalized repeat units in %) of ~45% can be reached after about 48 h, when 0.5 equiv of PEG₁₀₀₀ was used, which corresponds to nearly quantitative conversion. Increasing the amount of glycidyl ether to 1 eq did however not lead to higher DoF values, which we explain by steric hindrance. Regarding the kinetic study for PEG₄₀₀ (Figure 1B), after only 3 h, a DoF of ~23% was reached, but the maximum DoF was only 36%. The polymers were characterized via ¹H- and solid-state ¹³C NMR spectroscopy (Figure S1B), which revealed both the signals of the PDha backbone as well as the PEG side chains. Besides, size exclusion chromatography (SEC) traces of the graft copolymers poly(dehydroalanine)-graft-PEG (PDha-g-PEG_{400,25}) (with 400 g/mol being the molecular weight of the PEG graft and 25% being the degree of grafting) and PDha-g-PEG_{1000,28} revealed a shift to lower elution volumes compared to the precursor poly(aminomethylacrylate)

(PAMA) because of the successful addition of PEG graft (Figure S1A).

Solution Properties of PDha-g-PEG Graft Copolymers. The solution properties of the herein synthesized graft copolymers were investigated with respect to solubility in different solvents, pH-dependent charge, and conformation (Table 1). Five graft copolymers were synthesized having different DoFs, and solubility in water (pH 1 to 14), dimethyl sulfoxide (DMSO), dimethylformamide (DMF), methanol, and chloroform was investigated. Although lower DoF, in case of PDha-g-PEG_{400,10}, rather resembles the solubility of pristine PDha, higher grafting densities like for PDha-g-PEG_{400,25} are also soluble in DMF and over the entire pH range. Further increasing the PEG content allows dissolution in methanol and partly in CHCl₃ (slightly turbid solution).

We were further interested in the pH-dependent solution behavior and, therefore, investigated PDha-g-PEG_{1000,28} via dynamic light scattering (DLS), laser microelectrophoresis, electrophoretic nuclear magnetic resonance (eNMR), and potentiometric titration. For the latter, PDha-g-PEG_{1000,28} was dissolved in aqueous NaOH (pH 12, *c*_{copolymer} = 2.5 g/L) and titrated with 0.1 M HCl. The titration curve (Figure 2C) shows two stages, which we attribute to titration of amino (stage 1) and carboxylate (stage 2) moieties. After the excess base is consumed, the titration of amino groups takes place (stage 1). It is worth noting that there is only one point of inflection in this region, therefore we cannot distinguish the difference between the titration of primary and secondary amino groups, which are formed during the grafting step. The apparent p*K*_a of 9.24 ($\alpha_{(\text{NH}_2+\text{NH})} = 0.5$) is in good agreement with the value for pristine PDha reported earlier.⁸¹ The next step seems to be the titration of carboxylate groups (stage 2), and here, an apparent p*K*_a value of 6.43 ($\alpha_{\text{COOH}} = 0.5$) is found. Please note that the volumes of titrant spent for the titration of both groups are similar (181 μL for amino groups and 140 μL for the carboxylate groups), and the difference might be explained by the accuracy of the assignment of the first inflection point (i.e., the value of *V*₁). This allows us to assume that under these conditions, pH = 8.05 corresponds to an apparent isoelectric point of the PDha-g-PEG_{1000,28} graft copolymer.

We further assumed that the graft copolymer undergoes changes in conformation and size upon pH variation, as net charge and charge density along the backbone are altered. A first hint was observed by ¹H NMR spectroscopy, where the signal of the backbone (2.90–2.30 ppm) is suppressed at pH 2. At pH 7, the signal is rather broad and shifted, as a possible result of a collapsed PDha backbone, which is shielded by the PEG graft. However, after addition of NaOD and reaching a

Table 1. Summary of the Synthesized PDha-g-PEG Copolymers and Their Solubility in Different Environments

PDha-g-...	PEG content [wt %] ^a	solubility ^b				
		water	DMSO	DMF	methanol	CHCl ₃
–	–	pH > 7	+	–	–	–
PEG _{400,10}	28	pH > 7	+	–	–	–
PEG _{400,25} ^c	54	pH = 1–14	+	+	–	–
PEG _{1000,11}	52	pH = 1–14	+	+	+	–
PEG _{1000,28} ^d	74	pH = 1–14	+	+	+	–
PEG _{1000,50}	85	pH = 1–14	+	+	+	±

^aCalculated from DoF. ^b≥ 2 g/L, –Δ insoluble, +Δ clear solution, ±Δ slightly turbid; SEC in DMSO. ^c*M*_n = 10,400 g/mol, *M*_w = 36 100 g/mol, *D* = 3.48. ^d*M*_n = 10,700 g/mol, *M*_w = 39,800 g/mol, *D* = 3.71; PAMA: *M*_n = 7,700 g/mol, *M*_w = 26,100 g/mol, *D* = 3.38.

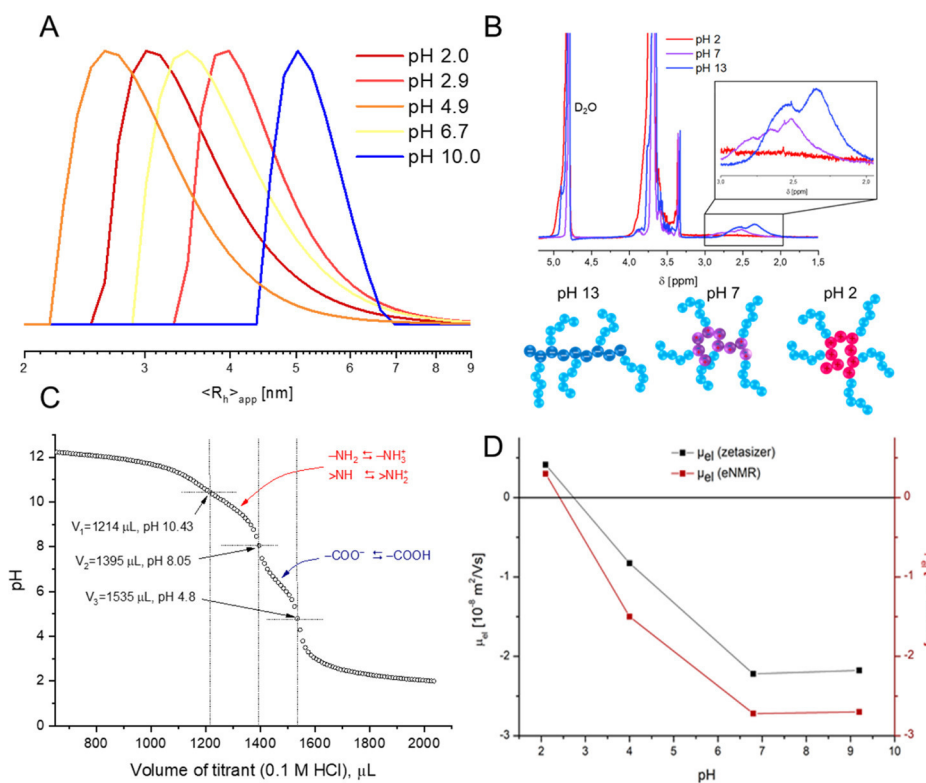


Figure 2. Characterization of PDha-g-PEG_{1000,28} in aqueous solution: DLS measurements at different pH values (A), ¹H NMR spectra at pH 2, 7, and 13 in D₂O/NaOD (B), potentiometric titration using 0.1 M aqueous HCl (C). Comparison of the electrophoretic mobility derived from the zetasizer, and eNMR measurements at pH values between 10 and 2 for PDha-g-PEG_{1000,11} (D).

pH value of 13, the signal can be clearly seen, which can be explained by stretching of the polyampholyte because of electrostatic repulsion. Changes in the nuclear magnetic resonance (NMR) spectra in our opinion can be correlated to at least partial compactization of the PDha backbone at lower pH values and, with this, to a decreasing intensity of the corresponding proton signals.^{72,87–89} This was further supported by DLS experiments (Figures 2A and S2), where different apparent hydrodynamic radii (R_H) dependent on the solution pH were found. At pH 10 and 9, the largest R_H with around 4.5–5.5 nm was observed, which we attribute to fully stretched backbone chains because of electrostatic repulsion of the negatively charged carboxylate groups. In contrast to this, at pH = 2, where the polymer is assumed to be a polycation, the R_H is significantly lower (3 nm). One possible explanation is that under these conditions, intramolecular hydrogen bonds, for example, between PEG and carboxylic moieties, are pronounced and counteract electrostatic repulsion. The lowest R_H was found at pH of about 5. In summary, the PDha backbone is strongly affected by the surrounding pH value and experiences changes in conformation modulated by charge density.

In addition, the electrophoretic mobility (μ_{el}) was measured at different pH values using both zetasizer and eNMR measurements. To enable a direct comparison, both measurements were performed in D₂O ($c_{\text{copolymer}} = 0.2 \text{ g/L}$) for only one set of samples. Here, PDha-g-PEG_{1000,11} as the model polyampholyte was used, as it is already soluble in water over the entire pH range but contains a moderately low amount of PEG, which might influence the measurements. Therefore, a solution of PDha-g-PEG_{1000,11} was adjusted to pH 9.2 with NaOD and subsequently titrated to pH 2.1 using DCl. The

electrophoretic mobility μ_{el} describes the motion of charged molecules in an electric field and is used to determine the ζ -potential, applying the Helmholtz–Smoluchowski equation for electrophoresis. However, some assumptions involved hold only true for ideal, nonporous, and rigid (spherical) particles and, hence, this is just a very rough approximation for coil-shaped polymers in solution.^{90–93} On the other hand, eNMR, as a complementary method, is part of the pulsed-field gradient NMR (PFG NMR) that enables to measure the motion of nuclei (mostly protons) because of the setup of a magnetic field gradient, which cause a reduced signal intensity, depending on the self-diffusion coefficient of the protons.⁹⁴ In case of eNMR measurements, the application of an electric field leads to an additional directed motion of polyelectrolytes, resulting in a phase shift of the signal in dependence of its effective charge.⁹⁵ Both laser microelectrophoresis and eNMR were used for the calculation of μ_{el} (Figure 2D), revealing the same trend within the samples. μ_{el} is negative at pH 9 and stays nearly constant until pH 7 because of deprotonated carboxylic acid groups. Decreasing the pH below 7 leads to an increase of μ_{el} by successive protonation of the carboxylate moieties, and the graft copolymer behavior in this context resembles that of a polyzwitterion. Further addition of DCl yields a point of apparent charge neutrality at around 2.5–2.75 and positive values for μ_{el} at pH 2. The apparent discrepancy to the isoelectric point determined via potentiometric titration might originate from (1) the fact that the graft copolymers do not behave as hard spherical particles, (2) associated counterions influence electrophoretic mobility of the graft copolymers, and (3) a certain effect of the PEG graft, as it has been reported by different groups that PEG exhibits a negative zeta potential in aqueous media.⁹⁶ The obtained values for μ_{el} show a similar

trend but differ in one order of magnitude, although comparable concentrations have been used. μ_{el} calculated from laser microelectrophoresis measurements is in the range of 10^{-8} m²/Vs, the results from eNMR show values in the order of 10^{-9} m²/Vs. In our opinion, the results from zetasizer measurements should be treated with caution.

Application of the Graft Copolymers as Templates for Noble-Metal NPs. We hypothesized that the described polyampholytic graft copolymers resemble versatile templates for the synthesis of metal NPs as well as the corresponding alloys (Figure 3). It is well known that Ag⁺ ions can be

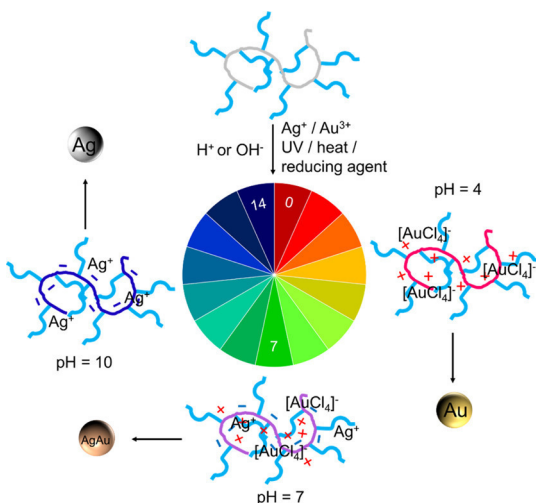


Figure 3. Preparation of NPs and bimetallic alloys in the presence of PDha-g-PEG graft copolymers by reduction of metal-containing salts using a reducing agent, heat, or UV-light.

complexed both by carboxylates^{97,98} as well as amino groups while [AuCl₄]⁻ ions typically interact with positively charged ammonium groups.^{44–46,99} In our case, the polyampholytic nature of PDha-g-PEG features both functionalities in each repeat unit and, in addition, offers the possibility to tune charge density and net charge via pH. Besides this, we also wanted to explore whether temperature and irradiation with light are feasible alternatives to NP synthesis using reducing agents.

Synthesis of Ag and Au NPs under Various Conditions. For the NP preparation, PDha-g-PEG_{1000,28} was chosen, which revealed good solubility and stability over the entire pH range. Typically, a ratio of functional groups to metal-containing ions of 15:1 was chosen, as also often described elsewhere,⁹⁹ and at first, NaBH₄ (one equivalent in respect to metal-containing ions) was used as the reducing agent. Although the solutions appeared clear and colorless after the addition of the noble metal-containing salts, they turned red and yellow after the respective reduction process. It is known that in case of weak polyelectrolytes such as PDMAEMA, the pH value plays an important role and affects both size and shape of the resulting NPs. This stems from a combination of association of [AuCl₄]⁻ alongside the polymeric chain and conformational changes, affecting the accessibility of any functional group.^{44–46} Even more, the initial state of the reagents (reductant and noble metal-containing ion complex) is also influenced by pH.^{47,48} Hence, we decided to first perform the synthesis at different pH values, and UV–vis measurements revealed typical surface plasmon resonance peaks for Au NPs at pH values before reduction of

10, 7, 4, and 2 (Figure 4A). However, under neutral and basic conditions, this absorbance is less distinct, hinting toward a preferred synthesis of Au NPs under acidic conditions. Absorption maxima were observed between 535 and 515 nm

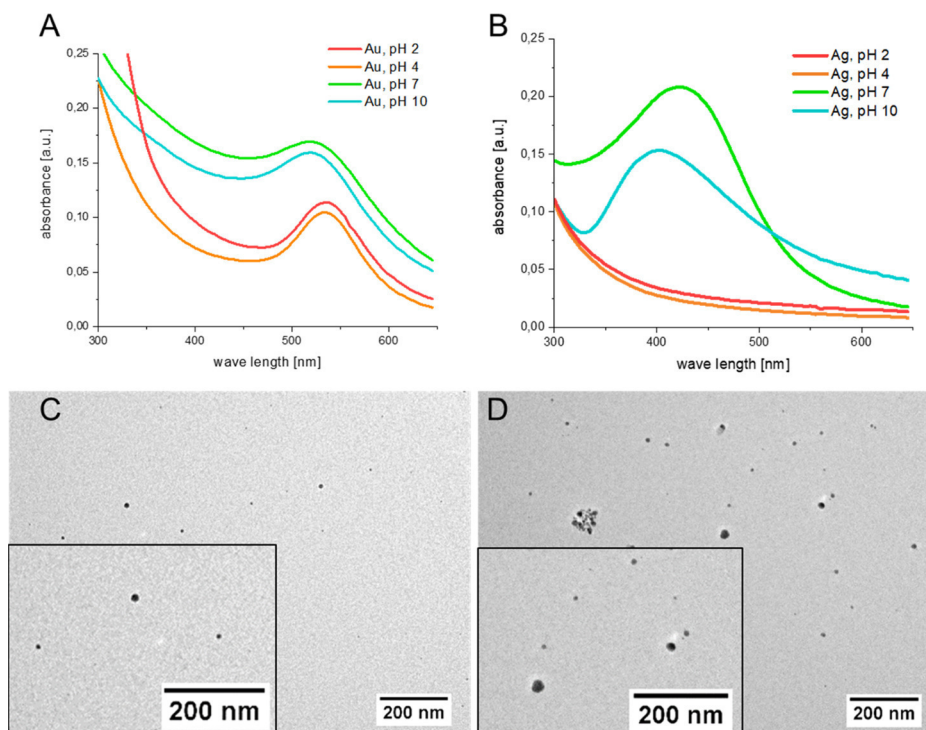


Figure 4. UV–vis spectra of Au NPs (A) and Ag NPs (B) synthesized at pH 2, 4, 7, and 10 using NaBH₄ as the reducing agent. (C,D) show the corresponding TEM micrographs of the Au NPs (C) and Ag NPs (D) prepared at pH 7.

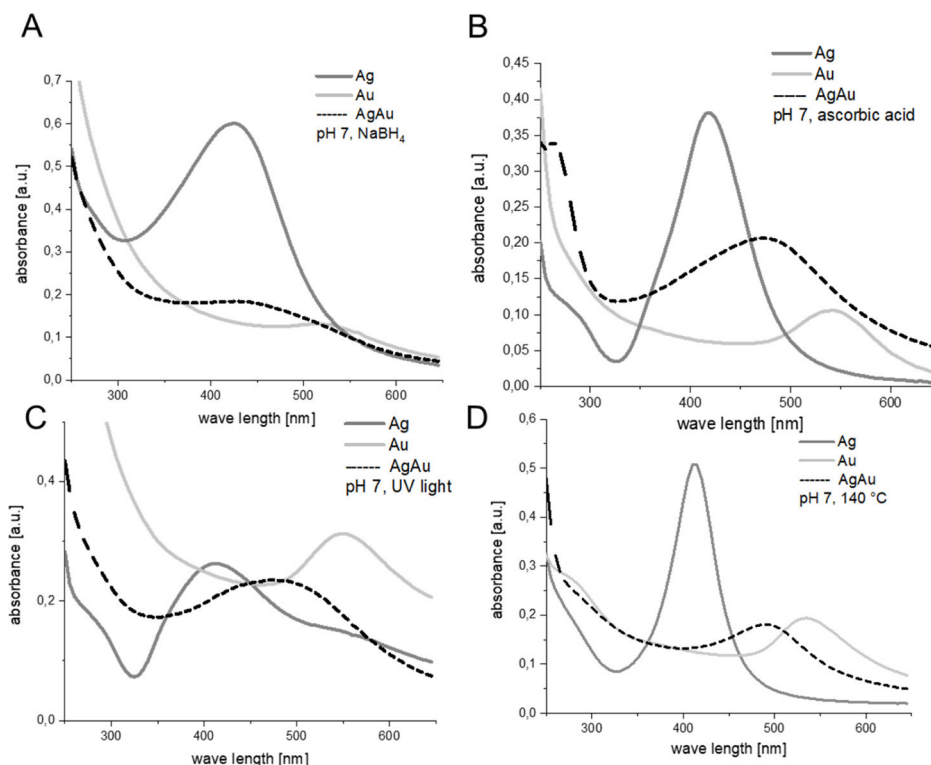


Figure 5. UV-vis spectra of Au NPs, Ag NPs, and AgAu NP alloys prepared at pH 7 via four synthetic routes: using NaBH₄ (A) and ascorbic acid (B) as reducing agents, applying UV-light for 1 h (C), and heating to 140 °C for 1 h (D).

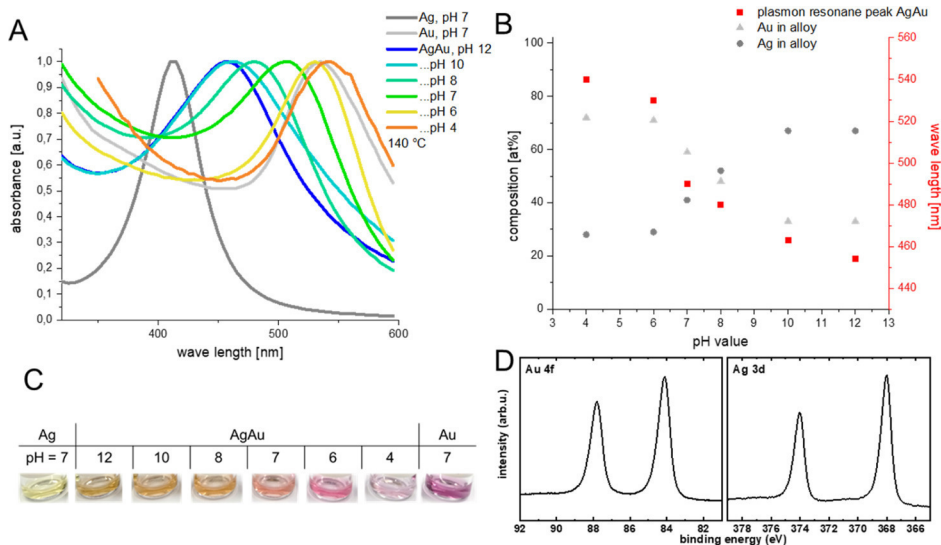


Figure 6. UV-vis spectra of Au NPs, Ag NPs, and AgAu nanoalloys prepared at different pHs from 12 to 4 at 140 °C (A) and images of the NP dispersions (C). The composition of the NPs as determined from XPS as a function of the pH (B) and the Au 4f and Ag 3d signals from XPS for an AgAu nanoalloy prepared at pH 8 (D).

because the wavelength is strongly depending on the size and the shape of the NPs as well as on their ligand environment (chemical nature of the stabilizing polymer) and the polymer structure.^{31,44,100} At pH 7, an average diameter of 6 ± 4 nm (Au) was found from TEM micrographs (Figure 4C), and mostly the spherical shape was observed. The synthesized particles are, hence, in a size range, where quantum size effects can be expected. Next, Ag NPs were prepared under comparable conditions, and also here, a dependence on the pH value was observable. According to subsequent UV-vis

spectra of the dispersions, synthesis was successful under neutral or basic conditions with absorption maxima at $\lambda = 400$ and 420 nm and an average NP diameter of 11 ± 4 nm (Figure 4D). As an alternative to NaBH₄, we also explored reduction using ascorbic acid, heating, or irradiation with light at neutral pH and, besides Ag or Au NPs, we also prepared AgAu alloy NPs at a molar ratio of 1:1.¹⁰¹

In all cases, NP synthesis in the presence of the polyampholytic graft copolymer was successful, resulting in stable dispersions of Ag, Au, and AgAu NPs (Figure 5).

Although Ag NPs and Au NPs in all cases revealed their characteristic absorbance maxima at 415–420 and 525–550 nm, respectively, in case of the resulting alloys, this was found at 440–490 nm, indicating the formation of an alloy instead of both noble-metal NPs individually, because a physical mixture of both individual NPs would result in a bimodal distribution, as shown in Figure S6.³⁴ The peak is shifted to lower or higher wavelengths, leading to the assumption that the amount of Ag or Au atoms incorporated depends strongly on the method used for reduction. Along these lines, NaBH₄ as the reducing agent results in an excess of Ag (440 nm), whereas ascorbic acid and light induced preparation yield nanoalloys with absorption maxima close to the theoretical value (470 and 475 nm). Thermal reduction, however, gave a maximum at 490 nm, hinting to a slightly preferred incorporation of Au.

pH-dependent Preparation of AgAu Nanoalloys. As shown for both Ag and Au NPs using NaBH₄ as the reducing agent, the pH value has a significant influence on NP synthesis in the presence of polyampholytic graft copolymers. Hence, we investigated whether the composition of AgAu nanoalloys at a constant molar ratio (1:1) changes by varying the pH value. To avoid any influence of the reducing agent, thermal reduction was chosen. Both the Ag and the Au precursor salt were dissolved in the graft copolymer solution, and afterward, the pH value was adjusted by titration with aqueous 0.1 M NaOH or HCl, before placing the mixture in an oil bath (140 °C) for 1 h. Afterward, the resulting nanoalloys were investigated via UV–vis spectroscopy, conventional and high-resolution transmission electron microscopy (HR-TEM), and XPS to determine their size, structure, and composition. In the UV–vis spectra (Figure 6A), a clear shift of the plasmon resonance peak to higher wavelengths with decreasing pH is visible as the maximum changes from 460 nm at pH 12 to 540 at pH 4, likely as a result of increasing incorporation of Au. At pH 8, the maximum is closest to the theoretical value of 475 nm for a stoichiometric mixture while more basic conditions favor the incorporation of Ag. This can also be seen visually as the respective solutions change in color from yellow and orange (high pH value) to rather pink at a lower pH value (Figure 6C). Note that, although the color and absorbance in the UV–vis spectra give hints about the actual nanoalloy composition, this is also influenced by both size, shape, and ligand environment of the NPs. Hence, XPS was used for further quantitative analysis of the Ag/Au ratio. Therefore, the dispersions were thoroughly purified by centrifugation and washed with MilliQ water several times. Afterward, the solution was drop-casted onto SiO₂ substrates and dried under ambient conditions. Figure S7 shows the overview spectrum of a sample prepared at pH 8, where the expected Ag and Au signals are visible. In addition, the measured C, N, O, and Si signals can be ascribed to the graft copolymer template and the substrate. The result confirms, furthermore, the successful purification, as no Na and Cl signals could be detected. Figure 6D displays high-resolution (HR) XPS data with Au 4f and Ag 3d signals, which were used to calculate the Ag/Au ratio for all pH values.

According to XPS data (Table 2 and Figure 6B), a clear trend in nanoalloy composition with the pH value can be observed: under acidic conditions, the incorporation of Au is favored, as at pH 4 and 6, about 70 at % Au is found, and also at neutral pH (7), Au is dominant with 59 at %. In our opinion, under acidic conditions, the graft copolymer backbone resembles a polyampholyte with an excess cationic charge

Table 2. Summary of the Composition and Size of the Synthesized Hybrid Materials Obtained via Thermal Reduction

sample/ pH	d^a [nm]	appearance	composition Au/ Ag [at %] (± 1 at %) ^b	
			XPS	EDX
Au NPs/7	7 \pm 6	mostly spherical, some prisms, and diffuse aggregates ($d = 50$ nm)	100/0	100
AgAu NPs/4	10 \pm 3	spherical	72/28	80/20
AgAu NPs/6	10 \pm 5	mostly spherical, some prisms/ cubes, and larger aggregates ($d = 30$ nm)	71/29	75/25
AgAu NPs/7	5 \pm 2	Spherical	59/41	–
AgAu NPs/8	3 \pm 1	spherical, few larger aggregates ($d = 40$ nm)	48/52	55/45
AgAu NPs/10	6 \pm 4	mostly spherical, few larger aggregates ($d = 50$ nm)	33/67	37/63
AgAu NPs/12	7 \pm 4	Spherical	33/67	2/98
Ag NPs/7	9 \pm 4	Spherical	0/100	–

^aCalculated from TEM micrographs (at least 50 particles). ^bObtained from XPS measurements.

(according to potentiometric titration of PDha-g-PEG, the apparent isoelectric point is at a pH of about 8.05) and, with this, favors complexation of [AuCl₄][–].¹⁰² Upon reaching pH 8, an almost stoichiometric composition is found with 48 at % of Au. Upon further increasing the pH to 10 and above, the graft copolymer behaves as a polyanion, and mainly Ag⁺ is complexed, resulting in 67 at % at pH 10 and 12. These values are in good agreement with the data obtained from UV–vis spectra, confirming that the herein described polyampholytic templates are a facile way to control nanoalloy composition via the pH value. However, note that, although we report data from pH 4 to 12, the composition is not a linear function of the pH, but rather two compositional plateaus are reached at pH 6 and 10. Furthermore, from XPS, an increased stability of Ag, typically being rather sensitive toward oxidation, in the alloys is observed. Although the Ag 3d_{5/2} peak of pure Ag NPs is broadened because of oxidized Ag^{x+} species (full width at half-maximum 1.1 eV), it is narrower when Ag is incorporated into the alloys (full width at half-maximum 0.8–0.9 eV). Hence, the presence within an alloy containing Au leads to improved stability. In addition to XPS, EDX measurements were performed on the TEM on individual NPs, confirming the formation of mixed AgAu nanoalloys. In the pH range from 4 to 10, the EDX quantification yields Au-to-Ag ratios that are slightly higher than those obtained by XPS, which can be explained by the different scales of measurements. TEM observations reveal that besides the above-described alloy NPs, few larger structures (30–50 nm) are also found, partially being pure Ag NPs. A considerably larger difference in the Au-to-Ag ratio is observed for the sample synthesized at pH 12, which we ascribe to a heterogeneous distribution of the NPs that could not be statistically conceived by the EDX measurements. Here, we speculate that formation of Ag NPs without the presence of the graft copolymer template might occur as side reaction. As a result, pure Ag NPs were found via EDX, but note that, these

might not be present in case of XPS measurements because of slightly different sample preparation. As UV–vis spectroscopy did not show a bimodal distribution, we expect no slow subsequent formation of Ag NPs taking place.

From TEM micrographs (Figures S3–S5), we extracted also information on both shape and size of the NPs. The NP size is moderately disperse, and particles of around 10 nm in diameter are found for either pure Au or Ag while alloy NPs feature diameters between 3 and 10 nm. Although the smallest nanoalloys were obtained at pH 8 with almost stoichiometric composition, no significant trend over the assessed pH range can be deduced. A detailed look at the isometric NPs using HR-TEM (Figures 7 and S8) shows that they are almost

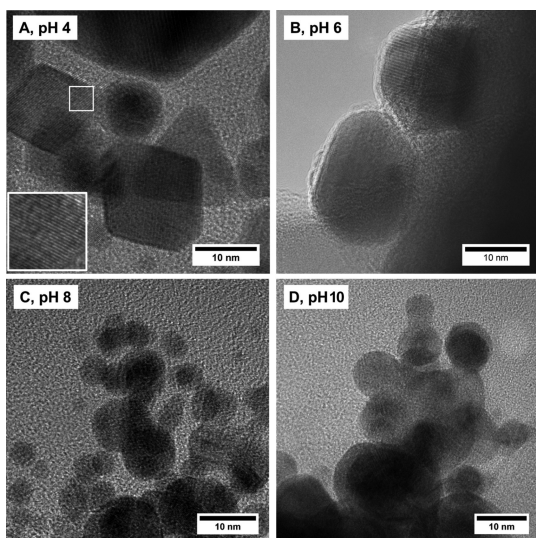


Figure 7. Exemplarily HR-TEM micrographs of AgAu nanoalloys synthesized at pH 4, 6, 8, and 10.

perfect, sometimes rounded nanocrystals, displaying cube and octahedra faces [(100) and (111)]. Only rarely, we observe typical growth defects for closely packed cubic structures, that is, stacking faults and microtwins parallel to (111).

TGA was used to quantify the amount of graft copolymer, which forms the organic shell on the nanoalloy surface for the sample prepared at pH 7. After centrifugation and washing with MilliQ water to remove ions and free graft copolymer, the sample was freeze-dried and measured under air in the range of 0 to 850 °C (10 °C/min heating rate, Figure S9). Although the pristine graft copolymer for comparison is burned in two steps at 200 and 470 °C, for the hybrid material, ~60 wt % remaining mass was observed at ~600 °C. This plateau is ascribed to the inorganic metal NPs, having a stable weight upon heating, and from this value, it can be assumed that the graft copolymer shell represents about 40 wt %. Because the initial ratio of PDha-g-PEG_{1000,28} to inorganic material was 95:5 (wt %/wt %), the dispersions supposedly contain free polymer. The remaining graft copolymer content could be reduced, when an initial polymer concentration of 1 g/L was used. Here, the sample contained only around 15 wt % graft copolymer. However, reducing the amount of stabilizing organic material might influence the dispersion stability in general.

CONCLUSIONS

We herein described the synthesis of a novel polyampholytic double hydrophilic graft copolymer based on PDha, which

besides featuring interesting solution properties could be used as a template for the preparation of Au, Ag, and AgAu alloy NPs. Although several reduction pathways (UV-light, chemical reduction, and heating) yielded comparable results, the graft copolymer itself was able to determine AgAu nanoalloy composition by the solution pH. We ascribe this to the pH-dependent variation in net charge and charge density, and this directly affects the amount and ratio of Ag⁺ and [AuCl₄]⁻ complexation upon mixing. As a result, the incorporation of Ag into the nanoalloy is favored under basic conditions, whereas Au is overrepresented in acidic media. Although this is, in our opinion, the first example of nanoalloy composition control using a smart template, we think that these results can also be transferred to other metals/alloys including Cu, Pd, or Pt. In this way, template-mediated access to different mono- or bimetallic NPs with application in catalysis or biosensing would be possible.

EXPERIMENTAL PART

Chemicals. Methanesulfonyl chloride (≥ 99.7%), epichlorhydrin (≥ 99%), L-ascorbic acid (99%), NaH (60% dispersion in mineral oil), and AgNO₃ (≥ 99.0%) were purchased from Sigma-Aldrich (St. Louis, USA). TFA (≥ 99.9%) and NaOH (0.1 N) were purchased from Roth (Karlsruhe, Germany), triethyl amine (≥ 99.0%) was purchased from CHEMSOLUTE (Renningen, Germany), and *N*-(*tert*-butoxycarbonyl)-*L*-serin methylester (98%) was purchased from Carbolution Chemicals (St. Ingbert, Germany). NaBH₄ (> 98%) was obtained from Acros Organics (Schwerte, Germany), and PEG mono methyl ether (1000 and 400 g/mol) was purchased from TCI chemicals (Tokyo, Japan). HAuCl₄ × 3 H₂O (99.99%) was purchased from Alfa Aesar (Haverhill, USA), and HCl (37% solution) was purchased from Fischer Scientific (Hampton, USA). Blocbuilder and SG1 were synthesized according to literature.^{103,104}

Analytical Methods. NMR Spectroscopy. ¹H- and ¹³C NMR spectroscopies were performed on Bruker AC 300 MHz, using CDCl₃, DMSO-*d*₆, and D₂O/NaOD as solvents at a temperature of 298 K. The spectra were referenced by using the residual signal of the deuterated solvent.

¹³C solid-state magic-angle spinning NMR spectra were measured by using cross-polarization with a contact time of 2 ms and a spinning frequency of 14 kHz on a Bruker AVANCE III HD 400 MHz spectrometer. Sample temperature was set to 298 K, and the carbon chemical shifts were referenced externally, setting the high-frequency (methylene) signal of adamantane to 38.5 ppm.¹⁰⁵

For the eNMR measurements, a Bruker 400 MHz spectrometer with an Avance III panel and a 5 mm BBFO probe head with *z*-gradient ($G_{\max} = 0.5$ T/m) was used. The determination of the electrophoretic mobility was carried out with a setup of P&L Scientific (Sweden), working with the Pd electrode ($U_{\max} = 1$ kV).

Size Exclusion Chromatography. SEC traces were measured using a Shimadzu system equipped with a CBM-20 A system controller, a LC-10 VP Pump, a RID-10A refraction index detector, and a PSS SDV guard/linear S column. As an eluent, a mixture of chloroform/triethylamine/*iso*-propanol [94/2/4] (v/v/v) was used, and measurements were recorded with a flow rate of 1 ml/min and 40 °C.

SEC measurements in DMSO were performed on a Jasco instrument, using DMSO +0.5% LiBr as the solvent at a flow rate of 0.5 mL/min at 65 °C and Pullulan calibration. It was equipped with PSS NOVEMA 3000 Angström/300 Angström columns, a RI-930 detector, and a PU-980 pump.

Dynamic Light Scattering. DLS measurements were performed using an ALV laser CGS3 Goniometer equipped with a 633 nm HeNe laser (ALV GmbH, Langen, Germany) at 25 °C and at a detection angle of 90°. The CONTIN analysis of the obtained correlation functions was performed using the ALV 7002 FAST Correlator Software.

Transmission Electron Microscopy. TEM images were acquired with 200 kV FEI Tecnai G2 20 equipped with $4k \times 4k$ Eagle HS CCD and a $1k \times 1k$ Olympus MegaView camera for overview images.

Laser Microelectrophoresis. Electrophoretic mobilities were measured on ZetaSizer Nano ZS from Malvern via M3-PALS technique with a laser beam at 633 nm. The detection angle was 13° . The samples were prepared by titration of the polymer in 0.1 M NaOH (0.2 g/L) with 0.1 M HCl, and 1 mL of the solution was taken at the desired pH values. The titration and pH detection were performed on a Metrohm 765 Dosimat titrator with a Greisinger electronic GMH3539 digital pH-/mV-electrode with a thermometer.

Potentiometric Titration. Potentiometric titration was performed using a digital pH meter (Orion), equipped with a combined glass/reference electrode, and calibrated with standard buffer solutions of pH 4.0, 7.0, and 10.0 (Oacon, Orion). The polymer was dissolved in 0.1 M NaOH at a concentration of 2.5 g/L. HCl (0.1 M) was used as the titrant, which was added by 10 μ L portions to a 3 mL of polymer solution at a constant temperature (25°C) and under intensive stirring. pH readings were registered after establishing the equilibrium state, when the pH reached a constant value after each step of titrant addition. For the calculation of the pK_a values, the Henderson–Hasselbalch equation was used.

X-ray Photoelectron Spectroscopy. The AgAu NP solutions were drop-casted on silicon substrates with native oxide and dried under ambient conditions. The silicon substrates were pre-cleaned by O_2 plasma and dipping in ethanol.

XPS was performed using a UHV multiprobe system (Scienta Omicron) with a monochromatic X-ray source (Al K_{α}) and an electron analyzer (Argus CU) with a 0.6 eV spectral energy resolution. The spectra were fitted using Voigt functions after background subtraction. The spectra were calibrated using the Si 2p peak (Si, 99.4 eV). For quantitative analysis, the relative sensitivity factors of the Au 4f (17.1) and Ag 3d (18) peaks were used.

HR-TEM and Energy-Dispersive X-ray Emission Spectroscopy. For TEM observations, we used FEI Technai G²FEG TEM, equipped with a 2K CCD camera (Gatan Ultrascan), a HAADF STEM detector (Fischione), and an X-Maxn80 T SDD EDX system (Oxford Instruments) for chemical measurements. The TEM was operated at 200 kV, and images were obtained in conventional bright-field and HR modes. Diffraction data were obtained by the selected area electron diffraction technique.

UV–Vis. UV–vis measurements were performed on an Agilent Cary 60 spectrometer in a Hellma quartz glass cuvette with a path length of 10 mm at room temperature in the solvent. The absorbance was measured in a range from 200 to 800 nm in 5 nm steps.

UV Cube. UV irradiations were carried out using Hoehnle UVACUBE 100 equipped with a 100 W lamp.

Thermogravimetric Analysis. TGA measurements were carried out under air flow in a PerkinElmer TGA800 device by heating from 30 to 850°C with a heating rate of 10 K/min.

Synthesis. **Synthesis of tBAMA.** Boc-Ser-OMe (10.0 g, 45.6 mmol; 1.0 equiv) was dissolved in dichloromethane (200 mL), and MsCl (6 mL; 77.5 mmol; 1.7 equiv) was added. After cooling in an ice bath, triethylamine (23 mL; 165.9 mmol; 3.6 equiv) was slowly added dropwise, and the reaction mixture was stirred for 1 h at 0°C . After additional 2 h at room temperature, the mixture was afterward washed with potassium bisulfate (1%) to neutrality. The organic phase was dried with Na_2SO_4 , and the solvent was removed under reduced pressure. The crude product was further purified via column chromatography with silica gel (ethyl acetate/*n*-hexane v/v 1/4). After removal of the solvent under reduced pressure, the product was yielded as a colorless oil (8.6 g, 94%).

$^1\text{H NMR}$ (300 MHz, CDCl_3 , δ): 7.01 (s, 1 H, –NH), 6.16 (s, 1 H, –C=CH–), 5.73 (s, 1 H, –C=CH–), 3.83 (s, 3 H, –O–CH₃), 1.48 (s, 9 H, –COO–C(CH₃)₃) ppm.

Synthesis of PtBAMA. tBAMA, BlocBuilder and SG1 ([40]/[1]/[0.65]) were dissolved in 1,4-dioxane (66 wt %). The reaction mixture was degassed via four freeze–pump–thaw circles and stirred for 15 min at 80°C under Ar. Afterward, the crude product was

precipitated in cold *n*-hexane, washed three times with hexane, and dried under vacuum. The product was obtained as a white powder.

$^1\text{H NMR}$ (300 MHz, CDCl_3 , δ): 6.00–5.00 (m, –NH), 4.08–3.37 (m, –O–CH₃), 3.32–2.02 (m, –C–CH₂–), 1.75–1.16 (m, –COO–C(CH₃)₃) ppm.

SEC (CHCl_3 /*i*-PrOH/ NET_3 , PS calibration): $M_n = 11,000$ g/mol, $M_w = 20,790$ g/mol, $D = 1.89$.

Deprotection of PtBAMA to PAMA. PtBAMA was dissolved in TFA (~ 4 equiv per monomer unit) and heated to 50°C . The reaction was stopped after 1 h, and the product was precipitated in cold methanol. After filtering and washing with methanol and diethyl ether several times, the product was dried under vacuum and obtained as a yellow powder. Yield: 60%

$^1\text{H NMR}$ (300 MHz, $\text{D}_2\text{O} + \text{NaOD}$, δ): 3.32 (s, –COO–CH₃), 2.78–1.90 (m, –C–CH₂–) ppm.

Synthesis of PEG-GE (400 and 1000 g/mol). Epichlorohydrin (1.6 mL; 0.02 mol) and NaH (60% in mineral oil; 0.8 g; 0.02 mmol) were dissolved in THF (200 mL) under argon and heated to 40°C . Then, mPEG-OH (1000 g/mol, 10 g; 0.01 mmol) was added, and the reaction mixture was stirred for 2 h at 40°C . After cooling to room temperature, the crude reaction mixture was filtered, and the solvent was evaporated. The remaining product was redissolved in dichloromethane and, afterward, precipitated in cold diethylether. After filtration, the product was dried *in vacuo* and obtained as a white powder (3.8 g; 38%).

$^1\text{H NMR}$ (300 MHz, CDCl_3 , δ) 3.70–3.60 (m, –O–CH₂–CH₂–), 3.37 (s, –O–CH₃), 3.16 (m, –O–CH–CH₂–), 2.79 (m, –O–CH–CH₂–), 2.61 (m, –O–CH₂–CH) ppm.

In case of PEG-GE with $M_n = 400$ g/mol, the work-up was slightly different. After the reaction, the solution was filtered off, the solvent was removed, and the remaining viscous oil was redissolved in water. The product was obtained after extraction with dichloromethane (3 \times) as a slightly yellowish oil (8.9 g, 89%).

Postpolymerization Modification of PAMA with PEG-GE. A concentrated KOH solution was dropwise added to water (15 mL) to adjust a pH value of 13. Afterward, PAMA (100 mg) was dissolved overnight, and the epoxide (0.5 equiv per monomer unit) was added. The reaction mixture was stirred for a certain time at 60°C and then it was neutralized using aqueous HCl (0.5 M). The crude product was dialyzed against deionized water (MWCO = 3.5 kDa) for 1–3 days and, afterward, freeze-dried to obtain a colorless polymer powder.

$^1\text{H NMR}$ (300 MHz, D_2O , δ) 3.87–3.30 (m, –O–CH₂–CH₂–), 3.26 (m, –O–CH₃–), 3.01–2.07 (m, –C–CH₂) ppm.

Solid-state $^{13}\text{C NMR}$ (75 MHz, δ): 177.30 (–COO–), 70.72 (–O–CH₂–CH₂–, –C–OH, –CH₂–NH, –CH₂–O–), 61.36 (–C–NH–), 53.92–37.11 (–CH₂–C–) ppm.

Preparation of Noble-Metal NPs. Pdha-g-PEG_{28,1000} was dissolved in MilliQ water (5 g/L, 15 equiv), and a solution of AgNO_3 and/or $\text{H[AuCl}_4]$ (10 mM, 1 equiv) was added. Afterward, the pH was adjusted by addition of 0.1 M NaOH or 0.1 M HCl, and the solution was stirred for 30 min for appropriate mixing. Then, the reduction agent, NaBH_4 or ascorbic acid (10 mM, 1 equiv), was added at once under constant stirring, and the reaction mixture turned colored immediately. In case of thermal reduction, the reaction mixture was diluted (50 v %), placed in a microwave vial, and stirred at 140°C for 1 h. Light-induced reduction was performed in an UV cube under stirring for 1.5 h.

■ ASSOCIATED CONTENT

Supporting Information

The Supporting Information is available free of charge at <https://pubs.acs.org/doi/10.1021/acs.macromol.0c00474>.

NMR, SEC traces, DLS curves, TEM micrographs, UV–vis spectrum, XPS overview, HR-TEM micrographs, and TGA curves (PDF)

■ AUTHOR INFORMATION

Corresponding Author

F. H. Schacher – Institute of Organic Chemistry and Macromolecular Chemistry (IOMC), Jena Center for Soft Matter (JCSM), and Center for Energy and Environmental Chemistry (CEEC), Friedrich-Schiller-University Jena, D-07743 Jena, Germany; orcid.org/0000-0003-4685-6608; Email: felix.schacher@uni-jena.de

Authors

J. B. Max – Institute of Organic Chemistry and Macromolecular Chemistry (IOMC), Jena Center for Soft Matter (JCSM), and Center for Energy and Environmental Chemistry (CEEC), Friedrich-Schiller-University Jena, D-07743 Jena, Germany

K. Kowalczyk – Institute of Organic Chemistry and Macromolecular Chemistry (IOMC), Jena Center for Soft Matter (JCSM), and Center for Energy and Environmental Chemistry (CEEC), Friedrich-Schiller-University Jena, D-07743 Jena, Germany

M. Köhler – Institute of Organic Chemistry and Macromolecular Chemistry (IOMC), Friedrich-Schiller-University Jena, D-07743 Jena, Germany

C. Neumann – Jena Center for Soft Matter (JCSM), Center for Energy and Environmental Chemistry (CEEC), and Institute of Physical Chemistry (IPC), Friedrich-Schiller-University Jena, D-07743 Jena, Germany

F. Pielenz – Institute of Organic Chemistry and Macromolecular Chemistry (IOMC), Friedrich-Schiller-University Jena, D-07743 Jena, Germany

L. V. Sigolaeva – Department of Chemistry, M.V. Lomonosov Moscow State University, 119991 Moscow, Russia

D. V. Pergushov – Department of Chemistry, M.V. Lomonosov Moscow State University, 119991 Moscow, Russia

A. Turchanin – Jena Center for Soft Matter (JCSM), Center for Energy and Environmental Chemistry (CEEC), and Institute of Physical Chemistry (IPC), Friedrich-Schiller-University Jena, D-07743 Jena, Germany; orcid.org/0000-0003-2388-1042

F. Langenhorst – Institute of Geoscience, Friedrich-Schiller-University Jena, D-07743 Jena, Germany

Complete contact information is available at:

<https://pubs.acs.org/10.1021/acs.macromol.0c00474>

Notes

The authors declare no competing financial interest.

■ ACKNOWLEDGMENTS

This research was supported by the Deutsche Forschungsgemeinschaft (DFG, project SCHA1640/18-1; project 316213987/SFB 1278 PolyTarget/project C03; project 364549901/TRR 234 CataLight, project Z02; EXC2051 Microverse), as well as the Russian Science Foundation (RSF, project no. 18-44-04011). We acknowledge Peggy Laudeley for SEC analysis and the NMR department at Friedrich-Schiller-University Jena for their continuous support. Further, we are thankful for the cryo-TEM/TEM facilities of the Jena Center for Soft Matter (JCSM) that were established with a grant from the German Research Council (DFG) and the European Funds for Regional Development (EFRE). We acknowledge also the access to the TEM facilities at the Institute of Geoscience which were funded by the Gottfried-Wilhelm-Leibniz prize (LA830/14-1).

■ REFERENCES

- (1) Weber, B. Synthesis of Coordination Polymer Nanoparticles using Self-Assembled Block Copolymers as Template. *Chem. Eur. J.* **2017**, *23*, 18093–18100.
- (2) Smarsly, B.; Antonietti, M. Block Copolymer Assemblies as Templates for the Generation of Mesoporous Inorganic Materials and Crystalline Films. *Eur. J. Inorg. Chem.* **2006**, *2006*, 1111–1119.
- (3) van Bommel, K. J. C.; Friggeri, A.; Shinkai, S. Organic Templates for the Generation of Inorganic Materials. *Angew. Chem., Int. Ed.* **2003**, *42*, 980–999.
- (4) MacLachlan, M. J.; Manners, I.; Ozin, G. A. New (Inter)Faces: Polymers and Inorganic Materials. *Adv. Mater.* **2000**, *12*, 675–681.
- (5) Schäfer, C. G.; Vowinkel, S.; Hellmann, G. P.; Herdt, T.; Contiu, C.; Schneider, J. J.; Gallei, M. A polymer based and template-directed approach towards functional multidimensional micro-structured organic/inorganic hybrid materials. *J. Mater. Chem. C* **2014**, *2*, 7960–7975.
- (6) Ying, J. Y.; Mehnert, C. P.; Wong, M. S. Synthesis and Applications of Supramolecular-Templated Mesoporous Materials. *Angew. Chem., Int. Ed.* **1999**, *38*, 56–77.
- (7) Lee, J.; Christopher Orilall, M.; Warren, S. C.; Kamperman, M.; DiSalvo, F. J.; Wiesner, U. Direct access to thermally stable and highly crystalline mesoporous transition-metal oxides with uniform pores. *Nat. Mater.* **2008**, *7*, 222–228.
- (8) Toombes, G. E. S.; Mahajan, S.; Thomas, M.; Du, P.; Tate, M. W.; Gruner, S. M.; Wiesner, U. Hexagonally Patterned Lamellar Morphology in ABC Triblock Copolymer/Aluminosilicate Nanocomposites. *Chem. Mater.* **2008**, *20*, 3278–3287.
- (9) Toombes, G. E. S.; Mahajan, S.; Weyland, M.; Jain, A.; Du, P.; Kamperman, M.; Gruner, S. M.; Muller, D. A.; Wiesner, U. Self-Assembly of Four-Layer Woodpile Structure from Zigzag ABC Copolymer/Aluminosilicate Concertinas. *Macromolecules* **2008**, *41*, 852–859.
- (10) Templin, M.; Franck, A.; Du Chesne, A.; Leist, H.; Zhang, Y.; Ulrich, R.; Schädl, V.; Wiesner, U. Organically Modified Aluminosilicate Mesostructures from Block Copolymer Phases. *Science* **1997**, *278*, 1795–1798.
- (11) Pyun, J.; Matyjaszewski, K. Synthesis of Nanocomposite Organic/Inorganic Hybrid Materials Using Controlled/"Living" Radical Polymerization. *Chem. Mater.* **2001**, *13*, 3436–3448.
- (12) Cölfen, H. Double-Hydrophilic Block Copolymers: Synthesis and Application as Novel Surfactants and Crystal Growth Modifiers. *Macromol. Rapid Commun.* **2001**, *22*, 219–252.
- (13) Sahiner, N.; Ozay, H.; Ozay, O.; Aktas, N. New catalytic route: Hydrogels as templates and reactors for in situ Ni nanoparticle synthesis and usage in the reduction of 2- and 4-nitrophenols. *Appl. Catal., A* **2010**, *385*, 201–207.
- (14) Kocak, G. Preparation and catalytic properties of modified PGMA-based pH-responsive hydrogel films as a novel template for in situ synthesis of Au, Ag, and Au:Ag nanoparticles. *J. Appl. Polym. Sci.* **2020**, *137*, 48360.
- (15) Ulker, D.; Kocak, G.; Tuncer, C.; Butun, V. Preparation of monometallic and bimetallic alloy nanoparticles stabilized with sulfobetaine-based block copolymer and their catalytic activities. *Colloid Polym. Sci.* **2019**, *297*, 1067–1078.
- (16) Song, J.; Zhu, Y.; Zhang, J.; Yang, J.; Du, Y.; Zheng, W.; Wen, C.; Zhang, Y.; Zhang, L. Encapsulation of AgNPs within Zwitterionic Hydrogels for Highly Efficient and Antifouling Catalysis in Biological Environments. *Langmuir* **2019**, *35*, 1563–1570.
- (17) Bryan, W. W.; Medhi, R.; Marquez, M. D.; Rittikulsittichai, S.; Tran, M.; Lee, T. R. Porous silver-coated pNIPAM-co-AAc hydrogel nanocapsules. *Beilstein J. Nanotechnol.* **2019**, *10*, 1973–1982.
- (18) Bastakoti, B. P.; Guragain, S.; Yusa, S.-i.; Nakashima, K. Novel synthesis route for Ag@SiO₂ core-shell nanoparticles via micelle template of double hydrophilic block copolymer. *RSC Adv.* **2012**, *2*, 5938–5940.
- (19) Feng, C.; Gu, L.; Yang, D.; Hu, J.; Lu, G.; Huang, X. Size-controllable gold nanoparticles stabilized by PDEAEMA-based double hydrophilic graft copolymer. *Polymer* **2009**, *50*, 3990–3996.

- (20) Amendola, V.; Pilot, R.; Frascioni, M.; Maragò, O. M.; Iati, M. A. Surface plasmon resonance in gold nanoparticles: a review. *J. Phys.: Condens. Matter* **2017**, *29*, 203002.
- (21) Yeh, Y.-C.; Czeran, B.; Rotello, V. M. Gold nanoparticles: preparation, properties, and applications in bionanotechnology. *Nanoscale* **2012**, *4*, 1871–1880.
- (22) Tarannum, N.; Divya, D.; Gautam, Y. K. Facile green synthesis and applications of silver nanoparticles: a state-of-the-art review. *RSC Adv.* **2019**, *9*, 34926–34948.
- (23) Guisbiers, G.; Mendoza-Cruz, R.; Bazán-Díaz, L.; Velázquez-Salazar, J. J.; Mendoza-Perez, R.; Robledo-Torres, J. A.; Rodríguez-Lopez, J.-L.; Montejano-Carrizales, J. M.; Whetten, R. L.; José-Yacamán, M. Electrum, the Gold–Silver Alloy, from the Bulk Scale to the Nanoscale: Synthesis, Properties, and Segregation Rules. *ACS Nano* **2016**, *10*, 188–198.
- (24) Wilcoxon, J. Optical Absorption Properties of Dispersed Gold and Silver Alloy Nanoparticles. *J. Mater. Chem. B* **2009**, *113*, 2647–2656.
- (25) Ando, J.; Nakamura, A.; Yamamoto, M.; Song, C.; Murata, K.; Iino, R. Multicolor High-Speed Tracking of Single Biomolecules with Silver, Gold, and Silver–Gold Alloy Nanoparticles. *ACS Photonics* **2019**, *6*, 2870–2883.
- (26) Loiseau, A.; Asila, V.; Boitel-Aullen, G.; Lam, M.; Salmain, M.; Boujday, S. Silver-Based Plasmonic Nanoparticles for and Their Use in Biosensing. *Biosensors* **2019**, *9*, 78.
- (27) Dwivedi, C.; Chaudhary, A.; Srinivasan, S.; Nandi, C. K. Polymer Stabilized Bimetallic Alloy Nanoparticles: Synthesis and Catalytic Application. *Colloid Interface Sci. Commun.* **2018**, *24*, 62–67.
- (28) Devarajan, S.; Vimalan, B.; Sampath, S. Phase transfer of Au–Ag alloy nanoparticles from aqueous medium to an organic solvent: effect of aging of surfactant on the formation of Ag-rich alloy compositions. *J. Colloid Interface Sci.* **2004**, *278*, 126–132.
- (29) Link, S.; Wang, Z. L.; El-Sayed, M. A. Alloy Formation of Gold–Silver Nanoparticles and the Dependence of the Plasmon Absorption on Their Composition. *J. Mater. Chem. B* **1999**, *103*, 3529–3533.
- (30) Sharma, G.; Kumar, A.; Sharma, S.; Naushad, M.; Prakash Dwivedi, R.; Allothman, Z. A.; Mola, G. T. Novel development of nanoparticles to bimetallic nanoparticles and their composites: A review. *J. King Saud Univ. Sci.* **2019**, *31*, 257–269.
- (31) Pal, A.; Shah, S.; Devi, S. Synthesis of Au, Ag and Au–Ag alloy nanoparticles in aqueous polymer solution. *Colloids Surf., A* **2007**, *302*, 51–57.
- (32) Abhijith, K. S.; Sharma, R.; Ranjan, R.; Thakur, M. S. Facile synthesis of gold–silver alloy nanoparticles for application in metal enhanced bioluminescence. *Photochem. Photobiol. Sci.* **2014**, *13*, 986–991.
- (33) Rioux, D.; Meunier, M. Seeded Growth Synthesis of Composition and Size-Controlled Gold–Silver Alloy Nanoparticles. *J. Phys. Chem. C* **2015**, *119*, 13160–13168.
- (34) Pal, A.; Shah, S.; Devi, S. Preparation of Silver–Gold Alloy Nanoparticles at Higher Concentration Using Sodium Dodecyl Sulfate. *Aust. J. Chem.* **2008**, *61*, 66–71.
- (35) Pal, A.; Shah, S.; Devi, S. Preparation of silver, gold and silver–gold bimetallic nanoparticles in w/o microemulsion containing TritonX-100. *Colloids Surf., A* **2007**, *302*, 483–487.
- (36) Pyne, S.; Sarkar, P.; Basu, S.; Sahoo, G. P.; Bhui, D. K.; Bar, H.; Misra, A. Synthesis and photo physical properties of Au @ Ag (core @ shell) nanoparticles disperse in poly vinyl alcohol matrix. *J. Nanoparticle Res.* **2011**, *13*, 1759–1767.
- (37) Saw, E. N.; Grasmik, V.; Rurainsky, C.; Epple, M.; Tschulik, K. Electrochemistry at single bimetallic nanoparticles – using nano impacts for sizing and compositional analysis of individual AgAu alloy nanoparticles. *Faraday Discuss.* **2016**, *193*, 327–338.
- (38) Mott, D.; Thuy, N. T. B.; Aoki, Y.; Maenosono, S. Aqueous synthesis and characterization of Ag and Ag–Au nanoparticles: addressing challenges in size, monodispersity and structure. *Philos. Trans. R. Soc., A* **2010**, *368*, 4275–4292.
- (39) Ristig, S.; Prymak, O.; Loza, K.; Gocyla, M.; Meyer-Zaika, W.; Heggen, M.; Raabe, D.; Epple, M. Nanostructure of wet-chemically prepared, polymer-stabilized silver–gold nanoalloys (6 nm) over the entire composition range. *J. Mater. Chem. B* **2015**, *3*, 4654–4662.
- (40) Han, S. W.; Kim, Y.; Kim, K. Dodecanethiol-Derivatized Au/Ag Bimetallic Nanoparticles: TEM, UV/VIS, XPS, and FTIR Analysis. *J. Colloid Interface Sci.* **1998**, *208*, 272–278.
- (41) Malathi, S.; Ezhilarasu, T.; Abiraman, T.; Balasubramanian, S. One pot green synthesis of Ag, Au and Au–Ag alloy nanoparticles using isonicotinic acid hydrazide and starch. *Carbohydr. Polym.* **2014**, *111*, 734–743.
- (42) Liu, H.; Shen, M.; Zhao, J.; Guo, R.; Cao, X.; Zhang, G.; Shi, X. Tunable synthesis and acetylation of dendrimer-entrapped or dendrimer-stabilized gold–silver alloy nanoparticles. *Colloids Surf., B* **2012**, *94*, 58–67.
- (43) Shang, L.; Jin, L.; Guo, S.; Zhai, J.; Dong, S. A Facile and Controllable Strategy to Synthesize Au–Ag Alloy Nanoparticles within Polyelectrolyte Multilayer Nanoreactors upon Thermal Reduction. *Langmuir* **2010**, *26*, 6713–6719.
- (44) Zhai, C.; Liu, X.; Chen, X.; Li, L.; Sun, F.; Ma, H. Facile Synthesis of Intelligent Polymers Modified Gold Nanoparticles in Aqueous Solution. *J. Inorg. Organomet. Polym. Mater.* **2015**, *25*, 687–693.
- (45) Li, L.-Y.; He, W.-D.; Li, W.-T.; Zhang, K.-R.; Pan, T.-T.; Ding, Z.-L.; Zhang, B.-Y. Thermal and pH-sensitive gold nanoparticles from H-shaped block copolymers of (PNIPAM/PDMAEMA)-b-PEG-b-(PNIPAM/PDMAEMA). *J. Polym. Sci., Part A: Polym. Chem.* **2010**, *48*, 5018–5029.
- (46) Scaravelli, R. C. B.; Dazzi, R. L.; Giacomelli, F. C.; Machado, G.; Giacomelli, C.; Schmidt, V. Direct synthesis of coated gold nanoparticles mediated by polymers with amino groups. *J. Colloid Interface Sci.* **2013**, *397*, 114–121.
- (47) Miranda, É. G. A.; Tofanello, A.; Brito, A. M. M.; Lopes, D. M.; Albuquerque, L. J. C.; de Castro, C. E.; Costa, F. N.; Giacomelli, F. C.; Ferreira, F. F.; Araújo-Chaves, J. C.; Nantes, I. L. Effects of Gold Salt Speciation and Structure of Human and Bovine Serum Albumins on the Synthesis and Stability of Gold Nanostructures. *Front. Chem.* **2016**, *4*, 13.
- (48) Mukha, I.; Vityuk, N.; Severynovska, O.; Eremenko, A.; Smirnova, N. The pH-Dependent Structure and Properties of Au and Ag Nanoparticles Produced by Tryptophan Reduction. *Nanoscale Res. Lett.* **2016**, *11*, 101.
- (49) Tan, K. S.; Cheong, K. Y. Advances of Ag, Cu, and Ag–Cu alloy nanoparticles synthesized via chemical reduction route. *J. Nanoparticle Res.* **2013**, *15*, 1537.
- (50) Ristig, S.; Chernousova, S.; Meyer-Zaika, W.; Epple, M. Synthesis, characterization and in vitro effects of 7 nm alloyed silver–gold nanoparticles. *Beilstein J. Nanotechnol.* **2015**, *6*, 1212–1220.
- (51) Verbruggen, S. W.; Keulemans, M.; Martens, J. A.; Lenaerts, S. Predicting the Surface Plasmon Resonance Wavelength of Gold–Silver Alloy Nanoparticles. *J. Phys. Chem. C* **2013**, *117*, 19142–19145.
- (52) Schilli, C. M.; Zhang, M.; Rizzardo, E.; Thang, S. H.; Chong, Y. K.; Edwards, K.; Karlsson, G.; Müller, A. H. E. A New Double-Responsive Block Copolymer Synthesized via RAFT Polymerization: Poly(N-isopropylacrylamide)-block-poly(acrylic acid). *Macromolecules* **2004**, *37*, 7861–7866.
- (53) Agut, W.; Brûlet, A.; Taton, D.; Lecommandoux, S. Thermoresponsive Micelles from Jeffamine-b-poly(l-glutamic acid) Double Hydrophilic Block Copolymers. *Langmuir* **2007**, *23*, 11526–11533.
- (54) Arotçaréna, M.; Heise, B.; Ishaya, S.; Laschewsky, A. Switching the Inside and the Outside of Aggregates of Water-Soluble Block Copolymers with Double Thermoresponsivity. *J. Am. Chem. Soc.* **2002**, *124*, 3787–3793.
- (55) Lee, S.; Saito, K.; Lee, H.-R.; Lee, M. J.; Shibasaki, Y.; Oishi, Y.; Kim, B.-S. Hyperbranched Double Hydrophilic Block Copolymer Micelles of Poly(ethylene oxide) and Polyglycerol for pH-Responsive Drug Delivery. *Biomacromolecules* **2012**, *13*, 1190–1196.

- (56) Molina, E.; Warnant, J.; Mathonnat, M.; Bathfield, M.; In, D.; Jérôme, C.; Lacroix-Desmazes, P.; Marcotte, N.; Gérardin, C. Drug–Polymer Electrostatic Complexes as New Structuring Agents for the Formation of Drug-Loaded Ordered Mesoporous Silica. *Langmuir* **2015**, *31*, 12839–12844.
- (57) Kumar, S.; Acharya, R.; Chatterji, U.; De, P. Side-Chain Amino-Acid-Based pH-Responsive Self-Assembled Block Copolymers for Drug Delivery and Gene Transfer. *Langmuir* **2013**, *29*, 15375–15385.
- (58) Volkmann, L.; Köhler, M.; Sobotta, F. H.; Enke, M. T.; Brendel, J. C.; Schacher, F. H. Poly(2-acrylamidoglycolic acid) (PAGA): Controlled Polymerization Using RAFT and Chelation of Metal Cations. *Macromolecules* **2018**, *51*, 7284–7294.
- (59) Vijayakrishna, K.; Jewrajka, S. K.; Ruiz, A.; Marcilla, R.; Pomposo, J. A.; Mecerreyes, D.; Taton, D.; Gnanou, Y. Synthesis by RAFT and Ionic Responsiveness of Double Hydrophilic Block Copolymers Based on Ionic Liquid Monomer Units. *Macromolecules* **2008**, *41*, 6299–6308.
- (60) Wu, Y.; Hu, H.; Hu, J.; Liu, T.; Zhang, G.; Liu, S. Thermo- and Light-Regulated Formation and Disintegration of Double Hydrophilic Block Copolymer Assemblies with Tunable Fluorescence Emissions. *Langmuir* **2013**, *29*, 3711–3720.
- (61) Chan, N.; An, S. Y.; Yee, N.; Oh, J. K. Dual Redox and Thermoresponsive Double Hydrophilic Block Copolymers with Tunable Thermoresponsive Properties and Self-Assembly Behavior. *Macromol. Rapid Commun.* **2014**, *35*, 752–757.
- (62) Schmidt, B. V. K. J. Double Hydrophilic Block Copolymer Self-Assembly in Aqueous Solution. *Macromol. Chem. Phys.* **2018**, *219*, 1700494.
- (63) Cui, Y.; Jiang, X.; Feng, C.; Gu, G.; Xu, J.; Huang, X. First double hydrophilic graft copolymer bearing a poly(2-hydroxyethyl acrylate) backbone synthesized by sequential RAFT polymerization and SET-LRP. *Polym. Chem.* **2016**, *7*, 3156–3164.
- (64) Mountrichas, G.; Pispas, S. Novel double hydrophilic block copolymers based on poly(p-hydroxystyrene) derivatives and poly(ethylene oxide). *J. Polym. Sci., Part A: Polym. Chem.* **2007**, *45*, 5790–5799.
- (65) Khimani, M.; Yusa, S.-i.; Aswal, V. K.; Bahadur, P. Aggregation behavior of double hydrophilic block copolymers in aqueous media. *J. Mol. Liq.* **2019**, *276*, 47–56.
- (66) Casse, O.; Shkilnyy, A.; Linders, J.; Mayer, C.; Häussinger, D.; Völkel, A.; Thünemann, A. F.; Dimova, R.; Cölfen, H.; Meier, W.; Schlaad, H.; Taubert, A. Solution Behavior of Double-Hydrophilic Block Copolymers in Dilute Aqueous Solution. *Macromolecules* **2012**, *45*, 4772–4777.
- (67) Ke, F.; Mo, X.; Yang, R.; Wang, Y.; Liang, D. Association of Block Copolymer in Nonselective Solvent. *Macromolecules* **2009**, *42*, 5339–5344.
- (68) Gu, L.; Shen, Z.; Feng, C.; Li, Y.; Lu, G.; Huang, X.; Wang, G.; Huang, J. Synthesis of PPEGMEA-g-PMAA densely grafted double hydrophilic copolymer and its use as a template for the preparation of size-controlled superparamagnetic Fe₃O₄/polymer nano-composites. *J. Mater. Chem.* **2008**, *18*, 4332–4340.
- (69) Laschewsky, A. Molecular concepts, self-organisation and properties of polysoaps. *Polysoaps/Stabilizers/Nitrogen-15 NMR*; Springer Berlin Heidelberg: Berlin, Heidelberg, 1995; pp 1–86.
- (70) Feng, C.; Shen, Z.; Gu, L.; Zhang, S.; Li, L.; Lu, G.; Huang, X. Synthesis and characterization of PNIPAM-*b*-(PEA-g-PDEA) double hydrophilic graft copolymer. *J. Polym. Sci., Part A: Polym. Chem.* **2008**, *46*, 5638–5651.
- (71) Feng, C.; Li, Y.; Yang, D.; Hu, J.; Zhang, X.; Huang, X. Well-defined graft copolymers: from controlled synthesis to multipurpose applications. *Chem. Soc. Rev.* **2011**, *40*, 1282–1295.
- (72) Feng, C.; Li, Y.; Yang, D.; Li, Y.; Hu, J.; Zhai, S.; Lu, G.; Huang, X. Synthesis of well-defined PNIPAM-*b*-(PEA-g-P2VP) double hydrophilic graft copolymer via sequential SET-LRP and ATRP and its “schizophrenic” Micellization behavior in aqueous media. *J. Polym. Sci., Part A: Polym. Chem.* **2010**, *48*, 15–23.
- (73) Gu, L.; Feng, C.; Yang, D.; Li, Y.; Hu, J.; Lu, G.; Huang, X. PPEGMEA-g-PDEAEMA: Double hydrophilic double-grafted copolymer stimuli-responsive to both pH and salinity. *J. Polym. Sci., Part A: Polym. Chem.* **2009**, *47*, 3142–3153.
- (74) Sun, F.; Feng, C.; Liu, H.; Huang, X. PHEA-g-PDMAEA well-defined graft copolymers: SET-LRP synthesis, self-catalyzed hydrolysis, and quaternization. *Polym. Chem.* **2016**, *7*, 6973–6979.
- (75) Zhao, D.; Rajan, R.; Matsumura, K. Dual Thermo- and pH-Responsive Behavior of Double Zwitterionic Graft Copolymers for Suppression of Protein Aggregation and Protein Release. *ACS Appl. Mater. Interfaces* **2019**, *11*, 39459–39469.
- (76) Baško, M.; Kubisa, P. Synthesis of Double Hydrophilic Graft Copolymers with a Polyacetal Backbone. *Macromolecules* **2002**, *35*, 8948–8953.
- (77) Qi, L.; Cölfen, H.; Antonietti, M. Synthesis and Characterization of CdS Nanoparticles Stabilized by Double-Hydrophilic Block Copolymers. *Nano Lett.* **2001**, *1*, 61–65.
- (78) Max, J. B.; Pergushov, D. V.; Sigolaeva, L. V.; Schacher, F. H. Polyampholytic graft copolymers based on polydehydroalanine (PDha) – synthesis, solution behavior and application as dispersants for carbon nanotubes. *Polym. Chem.* **2019**, *10*, 3006–3019.
- (79) Biehl, P.; von der Lühne, M.; Schacher, F. H. Reversible Adsorption of Methylene Blue as Cationic Model Cargo onto Polyzwitterionic Magnetic Nanoparticles. *Macromol. Rapid Commun.* **2018**, *39*, No. e1800017.
- (80) Billing, M.; Schacher, F. H. ATRP of tert-Butoxycarbonylaminoethyl acrylate (tBAMA): Well-Defined Precursors for Polyelectrolytes of Tunable Charge. *Macromolecules* **2016**, *49*, 3696–3705.
- (81) Günther, U.; Sigolaeva, L. V.; Pergushov, D. V.; Schacher, F. H. Polyelectrolytes with Tunable Charge Based on Polydehydroalanine: Synthesis and Solution Properties. *Macromol. Chem. Phys.* **2013**, *214*, 2202–2212.
- (82) von der Lühne, M.; Weidner, A.; Dutz, S.; Schacher, F. H. Reversible Electrostatic Adsorption of Polyelectrolytes and Bovine Serum Albumin onto Polyzwitterion-Coated Magnetic Multicore Nanoparticles: Implications for Sensing and Drug Delivery. *ACS Appl. Nano Mater.* **2018**, *1*, 232–244.
- (83) Billing, M.; Festag, G.; Bellstedt, P.; Schacher, F. H. Amphiphilic and double hydrophilic block copolymers containing a polydehydroalanine block. *Polym. Chem.* **2017**, *8*, 936–945.
- (84) Kruse, J. H.; Biehl, P.; Schacher, F. H. Different Routes to Ampholytic Polydehydroalanine: Orthogonal versus Simultaneous Deprotection. *Macromol. Rapid Commun.* **2019**, *40*, 1800857.
- (85) von der Lühne, M.; Günther, U.; Weidner, A.; Grafe, C.; Clement, J. H.; Dutz, S.; Schacher, F. H. SPION@polydehydroalanine hybrid particles. *RSC Adv.* **2015**, *5*, 31920–31929.
- (86) Sung, S.-J.; Min, S. H.; Cho, K. Y.; Lee, S.; Min, Y.-J.; Yeom, Y. I.; Park, J.-K. Effect of Polyethylene Glycol on Gene Delivery of Polyethylenimine. *Biol. Pharm. Bull.* **2003**, *26*, 492–500.
- (87) Akbarzadeh, M. M. Nano-micellar Zn(Cys)₂ complex mimics the chloroperoxidase active site. *RSC Adv.* **2016**, *6*, 12081–12083.
- (88) Cerichelli, G.; Mancini, G. NMR techniques applied to micellar systems. *Curr. Opin. Colloid Interface Sci.* **1997**, *2*, 641–648.
- (89) Sun, X.; Zhou, Y.; Yan, D. Drug release property of a pH-responsive double-hydrophilic hyperbranched graft copolymer. *Sci. China, Ser. B: Chem.* **2009**, *52*, 1703–1710.
- (90) Lowry, G. V.; Hill, R. J.; Harper, S.; Rawle, A. F.; Hendren, C. O.; Klaessig, F.; Nobbmann, U.; Sayre, P.; Rumble, J. Guidance to improve the scientific value of zeta-potential measurements in nanoEHS. *Environ. Sci.: Nano* **2016**, *3*, 953–965.
- (91) Delgado, A. V.; González-Caballero, F.; Hunter, R. J.; Koopal, L. K.; Lyklema, J. Measurement and interpretation of electrokinetic phenomena. *J. Colloid Interface Sci.* **2007**, *309*, 194–224.
- (92) Aljamali, N. M. Zetasizer Technique in Biochemistry. *Biochem. Anal. Biochem.* **2015**, *04*, 1000168.
- (93) Lobaskin, V.; Dünweg, B.; Holm, C. Electrophoretic mobility of a charged colloidal particle: a computer simulation study. *J. Phys.: Condens. Matter* **2004**, *16*, S4063–S4073.
- (94) Packer, K. J. The study of slow coherent molecular motion by pulsed nuclear magnetic resonance. *Mol. Phys.* **1969**, *17*, 355–368.

(95) Pagès, G.; Gilard, V.; Martino, R.; Malet-Martino, M. Pulsed-field gradient nuclear magnetic resonance measurements (PFG NMR) for diffusion ordered spectroscopy (DOSY) mapping. *Analyst* **2017**, *142*, 3771–3796.

(96) Barthel, M. J.; Rinkenauer, A. C.; Wagner, M.; Mansfeld, U.; Hoepfner, S.; Czaplowska, J. A.; Gottschaldt, M.; Träger, A.; Schacher, F. H.; Schubert, U. S. Small but Powerful: Co-Assembly of Polyether-Based Triblock Terpolymers into Sub-30 nm Micelles and Synergistic Effects on Cellular Interactions. *Biomacromolecules* **2014**, *15*, 2426–2439.

(97) Wang, T. C.; Rubner, M. F.; Cohen, R. E. Polyelectrolyte Multilayer Nanoreactors for Preparing Silver Nanoparticle Composites: Controlling Metal Concentration and Nanoparticle Size. *Langmuir* **2002**, *18*, 3370–3375.

(98) Zhang, Y.; Filipczak, P.; He, G.; Nowaczyk, G.; Witczak, L.; Raj, W.; Kozanecki, M.; Matyjaszewski, K.; Pietrasik, J. Synthesis and characterization of Ag NPs templated via polymerization induced self-assembly. *Polymer* **2017**, *129*, 144–150.

(99) Zhang, M.; Liu, L.; Wu, C.; Fu, G.; Zhao, H.; He, B. Synthesis, characterization and application of well-defined environmentally responsive polymer brushes on the surface of colloid particles. *Polymer* **2007**, *48*, 1989–1997.

(100) Haiss, W.; Thanh, N. T. K.; Aveyard, J.; Fernig, D. G. Determination of Size and Concentration of Gold Nanoparticles from UV–Vis Spectra. *Anal. Chem.* **2007**, *79*, 4215–4221.

(101) Daruich De Souza, C.; Ribeiro Nogueira, B.; Rostelato, M. E. C. M. Review of the methodologies used in the synthesis gold nanoparticles by chemical reduction. *J. Alloys Compd.* **2019**, *798*, 714–740.

(102) Chia, K.-K.; Cohen, R. E.; Rubner, M. F. Amine-Rich Polyelectrolyte Multilayer Nanoreactors for in Situ Gold Nanoparticle Synthesis. *Chem. Mater.* **2008**, *20*, 6756–6763.

(103) Grimaldi, S.; Finet, J.-P.; Le Moigne, F.; Zeghdaoui, A.; Tordo, P.; Benoit, D.; Fontanille, M.; Gnanou, Y. Acyclic β -Phosphonylated Nitroxides: A New Series of Counter-Radicals for “Living”/Controlled Free Radical Polymerization. *Macromolecules* **2000**, *33* (4), 1141–1147.

(104) Harrisson, S.; Couvreur, P.; Nicolas, J. Simple and efficient copper metal-mediated synthesis of alkoxyamine initiators. *Polymer Chemistry* **2011**, *2* (8), 1859–1865.

(105) Morcombe, C. R.; Zilm, K. W. Chemical shift referencing in MAS solid state NMR. *J. Magn. Reson.* **2003**, *162*, 479–486.

Supplementary Information

Polyampholytic Poly(dehydroalanine) graft copolymers as smart templates for pH-controlled formation of alloy nanoparticles

J. B. Max,^{1,2,3} K. Kowalczyk,^{1,2,3} M. Köhler, C. Neumann,^{2,3,4} F. Pielenz,¹ L. V. Sigolaeva,⁵ D. V. Pergushov,⁵ A. Turchanin,^{2,3,4} F. Langenhorst,⁶ F. H. Schacher,^{1,2,3} *

¹ Institute of Organic Chemistry and Macromolecular Chemistry (IOMC), Friedrich-Schiller-University Jena, Lessingstraße 8, D-07743 Jena, Germany

² Jena Center for Soft Matter (JCSM), Friedrich-Schiller-University Jena, Philosophenweg 7, D-07743 Jena, Germany

³ Center for Energy and Environmental Chemistry (CEEC), Friedrich-Schiller-University Jena, Philosophenweg 7, D-07743 Jena, Germany

⁴ Institute of Physical Chemistry (IPC), Friedrich-Schiller-University Jena, Lessingstraße 10, D-07743 Jena, Germany

⁵ Department of Chemistry, M.V. Lomonosov Moscow State University, Leninskie Gory 1/3, Moscow 119991, Russia

⁶ Institute of Geoscience, Friedrich-Schiller-University Jena, Carl-Zeiss-Promenade 10, D-07743 Jena, Germany

Email: felix.schacher@uni-jena.de

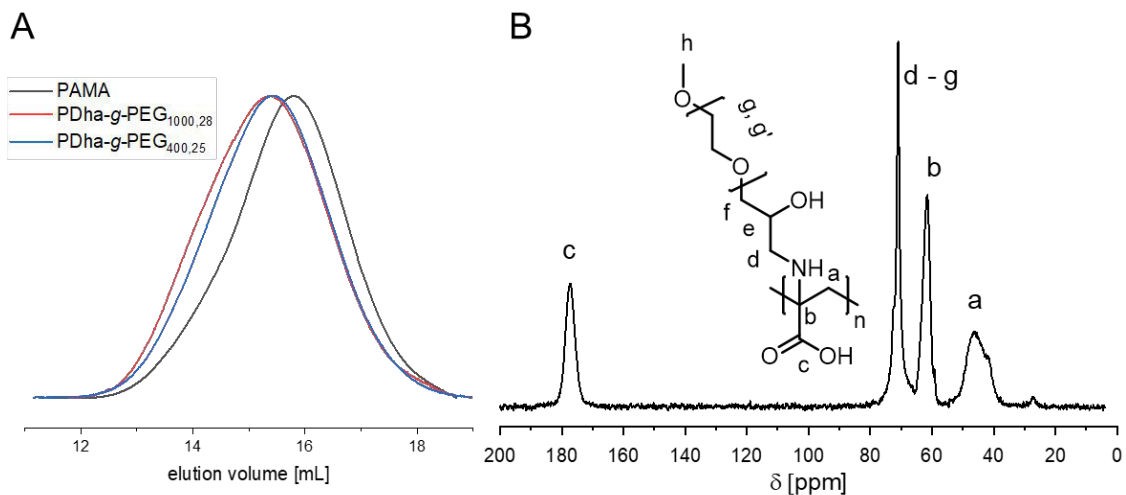


Figure S1: Exemplarily SEC traces before and after the post-polymerization modification of PDha-*g*-PEG_{400,25} and PDha-*g*-PEG_{1000,28} (A, measured in DMSO) and solid-state ¹³C-NMR spectrum of PDha-*g*-PEG_{1000,28} (B).

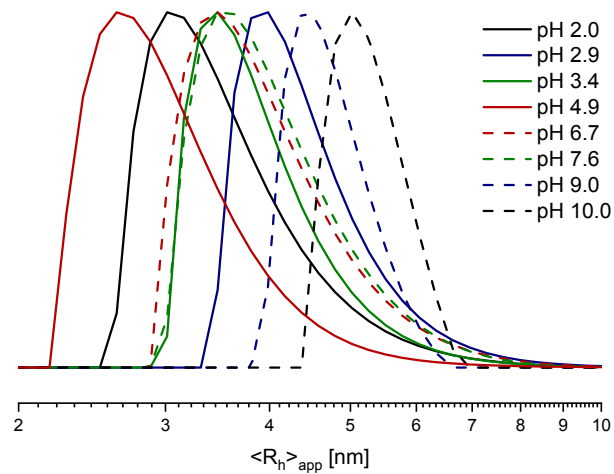


Figure S2: DLS measurements PDha-*g*-PEG_{1000,28} in aqueous solution at different pH values.

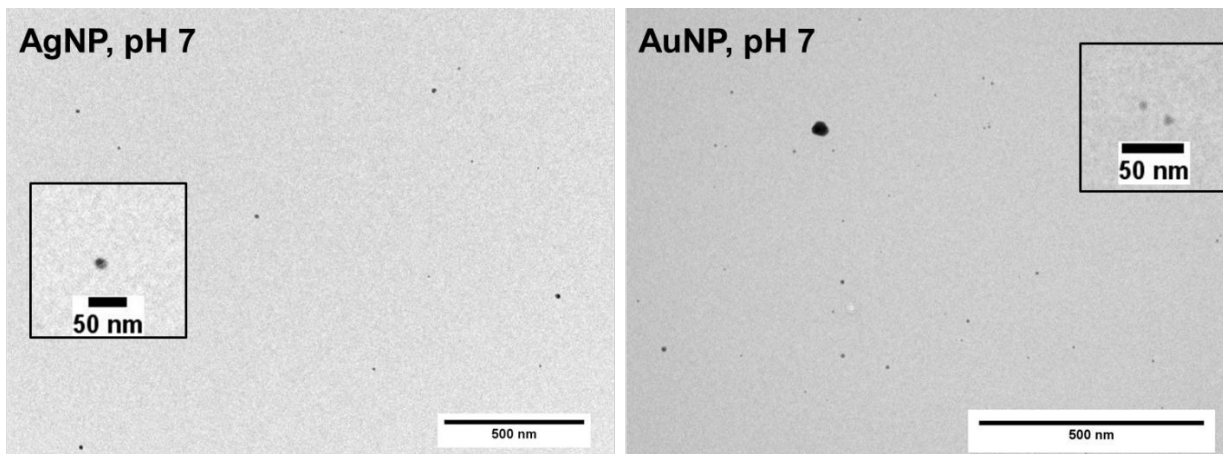


Figure S3: TEM micrographs of PDha-*g*-PEG_{1000,28}@Ag and Au NPs in aqueous solution derived at 140 °C at pH 7, including an enlarged inset.

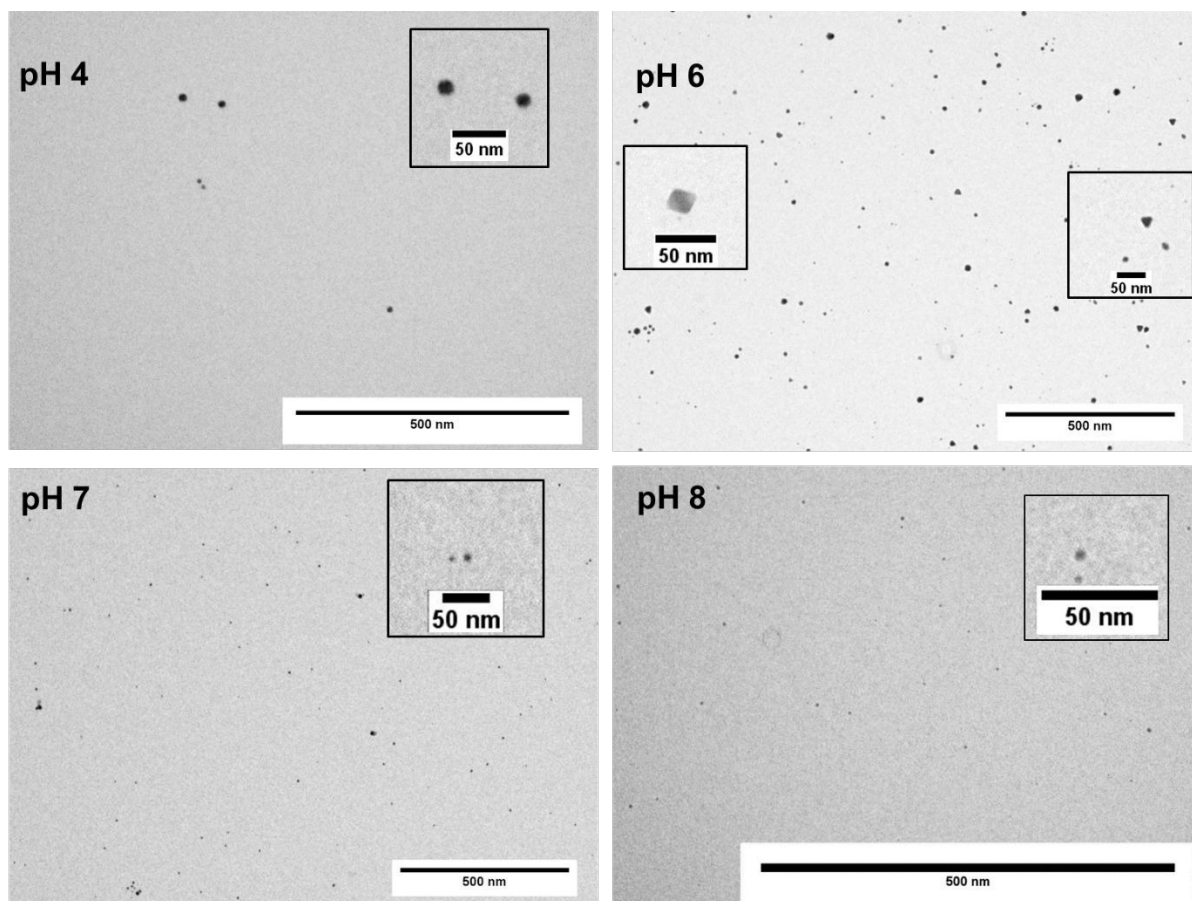


Figure S4: TEM micrographs of PDha-*g*-PEG_{1000,28}@AgAu NPs in aqueous solution derived at 140 °C at different pH values, including an enlarged inset.

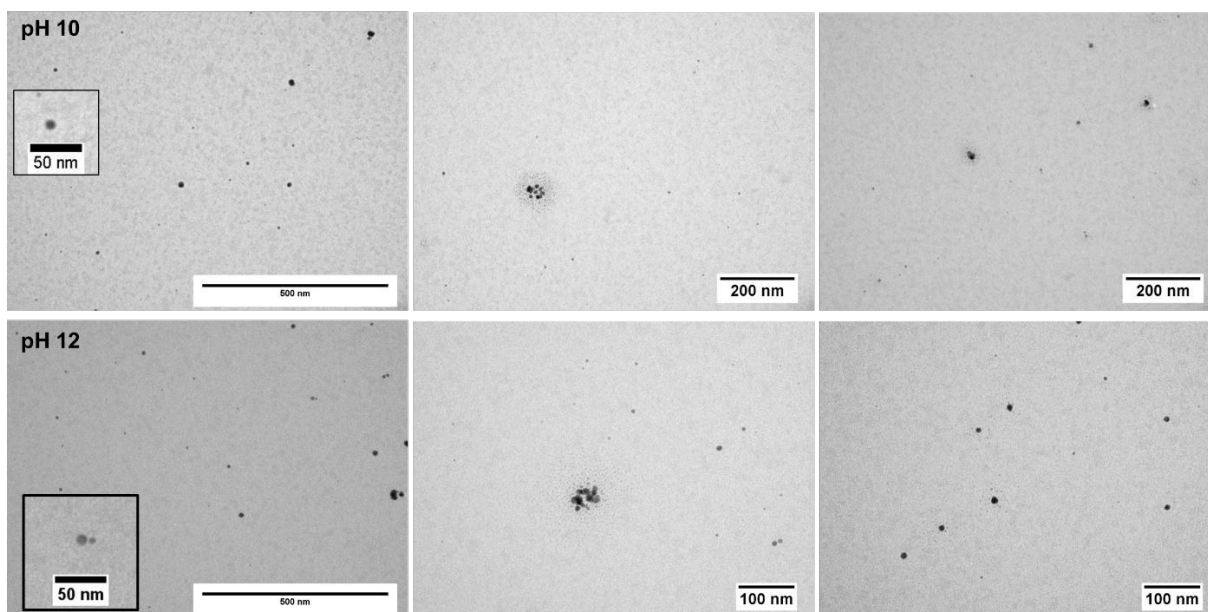


Figure S5: TEM micrographs of PDha-g-PEG_{1000,28} @AgAu NPs in aqueous solution derived at 140 °C at different pH values, including an enlarged inset.

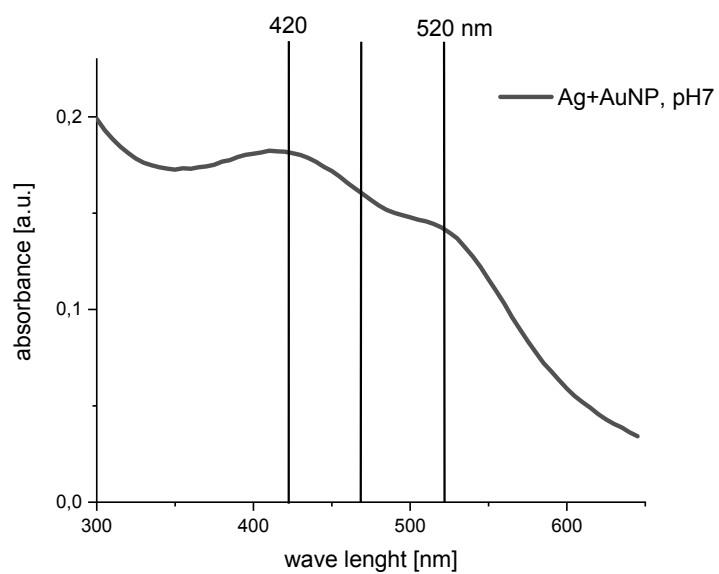


Figure S6: UV-Vis spectrum of a physical mixture of Ag and Au NPs derived thermally at pH 7.

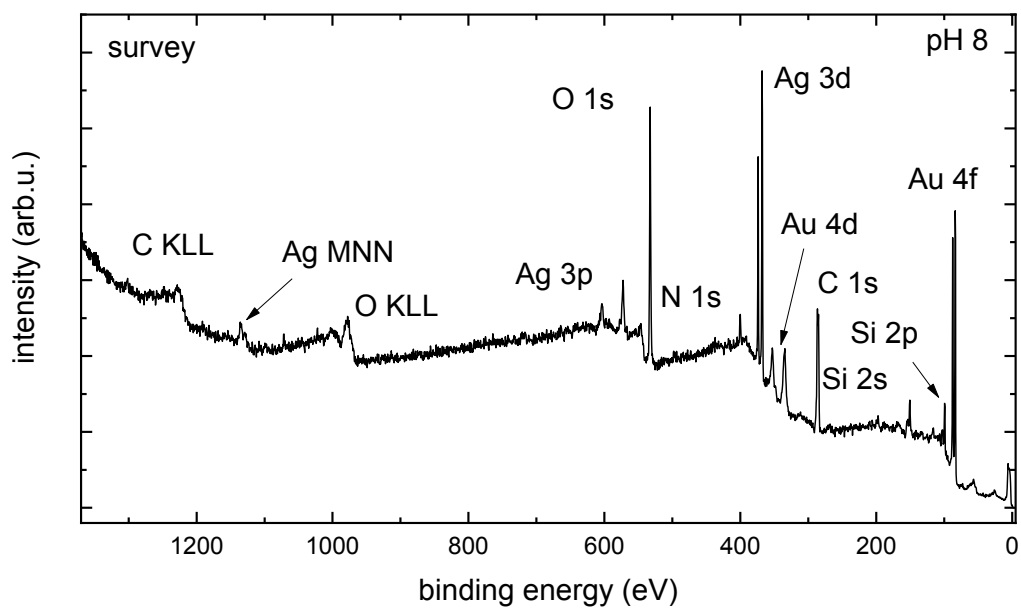


Figure S7: XP overview spectrum of the AgAu NPs prepared at pH 8 after drop-casting the solution onto Si substrates with native oxide.

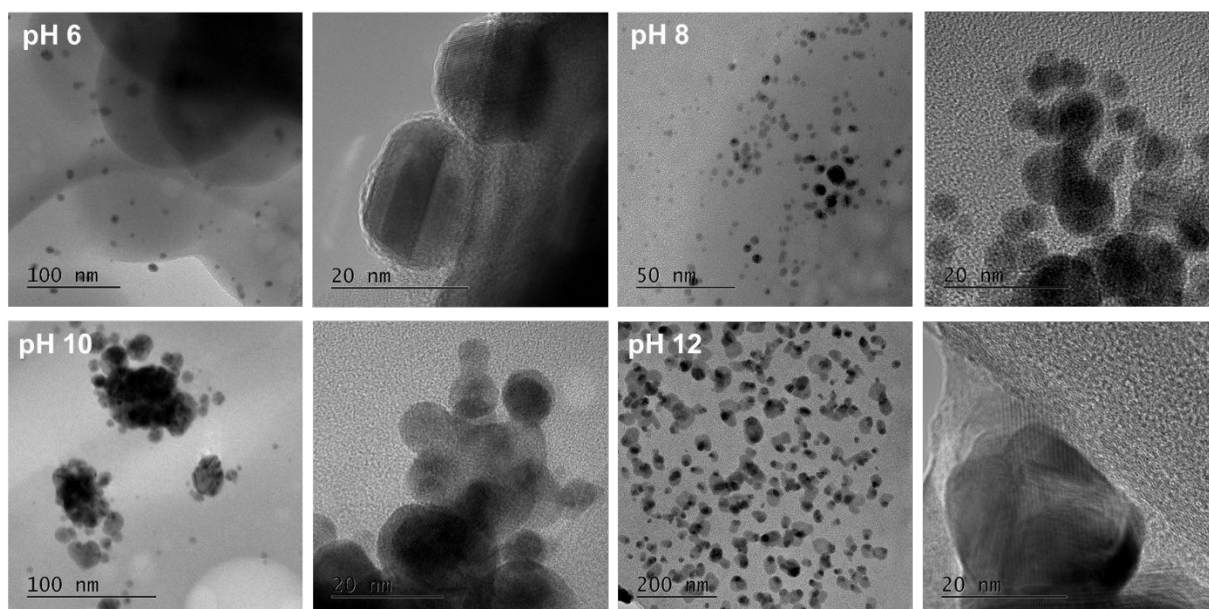


Figure S8: HR-TEM micrographs of PDha₅₀-g-PEG_{1000,28}@AgAu NPs from aqueous solutions derived at 140 °C at different pH values.

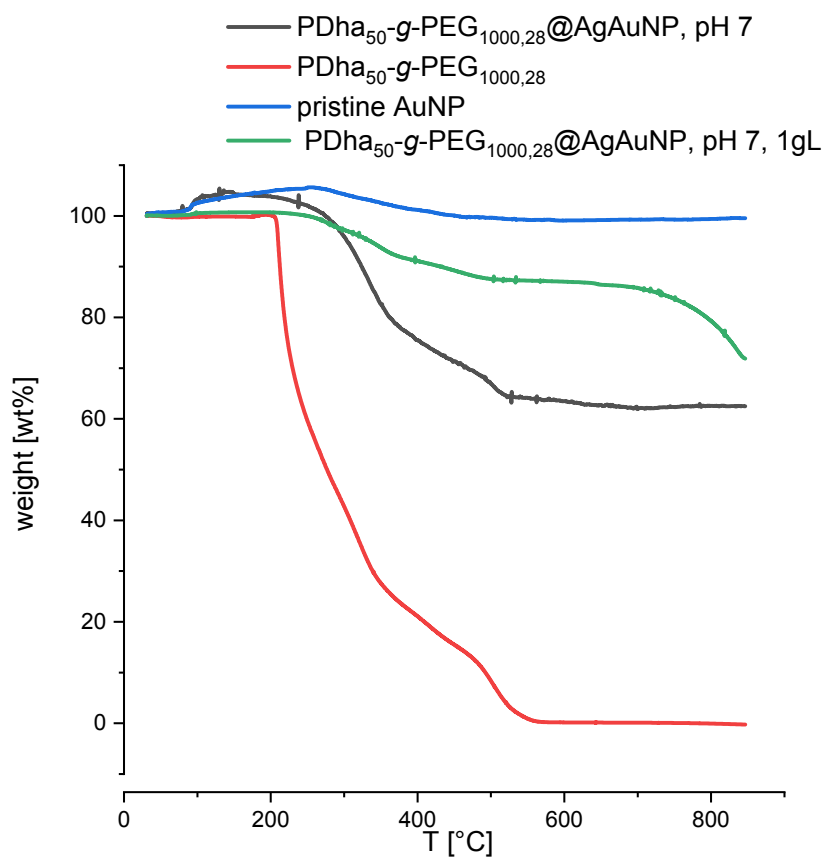
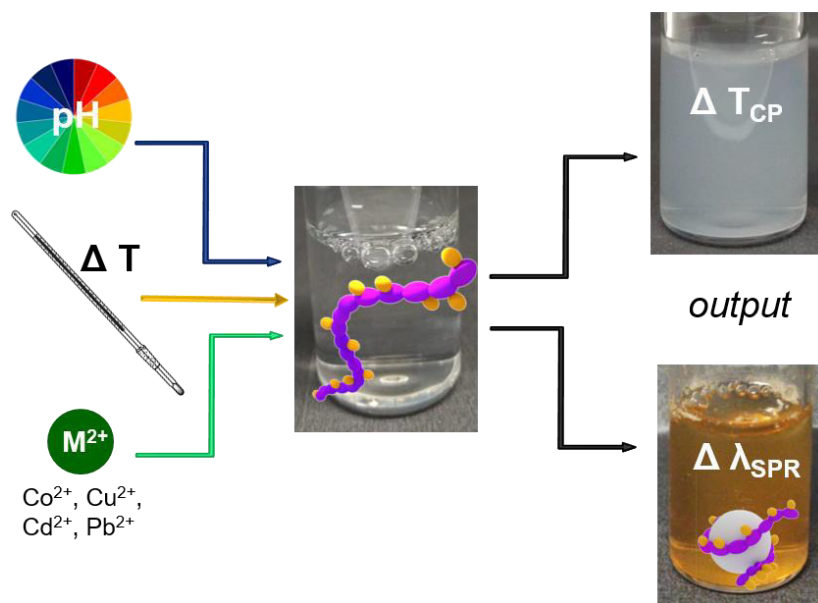


Figure S9: Thermograms of pristine Au NPs, PDha₅₀-g-PEG_{1000,28}@AgAu NPs and PDha₅₀-g-PEG_{1000,28} measured under air with a heating rate of 10 K/min.

Publication P4

“Triple-responsive polyampholytic graft copolymers as smart sensors with varying output “



Johannes B. Max,[‡] Afshin. Nabiyan,[‡] Jonas Eichhorn, and Felix H. Schacher

Macromol. Rapid Commun., **2021**, 42 2000671.

[‡]Both authors contributed equally to this work



Triple-Responsive Polyampholytic Graft Copolymers as Smart Sensors with Varying Output

Johannes B. Max, Afshin Nabiyan, Jonas Eichhorn, and Felix H. Schacher*

Three triggers result in two measurable outputs from polymeric sensors: multiresponsive polyampholytic graft copolymers respond to pH-value and temperature, as well as the type and concentration of metal cations and therefore, allow the transformation of external triggers into simply measurable outputs (cloud point temperature (T_{CP}) and surface plasmon resonance (SPR) of encapsulated silver nanoparticles). The synthesis relies on poly(dehydroalanine) (PDha) as the reactive backbone and gives straightforward access to materials with tunable composition and output. In particular, a rather high sensitivity toward the presence of Cu^{2+} , Co^{2+} , and Pb^{2+} metal cations is found.

From health and environmental perspectives, heavy metal sensing is of special interest for quantitative and qualitative analyses of aqueous systems.^[1] Among others, promising materials for corresponding sensors are smart polymers, which can translate external stimuli such as light, temperature, pH, or the presence of metal ions into a physical or chemical readout.^[2–4] If such materials contain specific binding sites for different metal ions, the optical properties such as absorbance, fluorescence, and luminescence^[5–9] or the solution behavior, e.g., the lower critical solution temperature (LCST)^[10,11] or simply the hydrodynamic size,^[12] of a responsive polymer will significantly change upon metal chelation. Hereby, recent progress in the polymerization of functional monomers allows us to incorporate strong ligands such as bipyridine units,^[9] crown ethers,^[10] carboxylates, or imidazoles.^[11] However, as recently shown for materials featuring both carboxylate and hydroxyl moieties, complexation also

strongly depends on coordination behavior and concentration of the respective metal ion, affecting inter- and intramolecular interactions within polymer chains.^[13,14]

Polyelectrolytes exhibit ionizable groups in each repeat unit^[15] and, therefore, are an interesting polymer class for metal ion sensing,^[16,17] but also for separation and flocculation processes,^[18,19] catalysis,^[20] or as antimicrobially active materials.^[21] Further tuning of material properties can be achieved by combining ionic and hydrophobic monomers,^[22] different polymerization techniques,^[23,24] or postpo-

lymerization modification reactions. Of particular interest are examples, which maintain solubility in water even after metal complexation, as shown for double hydrophilic co-polyelectrolytes^[13,14,25] or multistimuli-responsive copolymers.^[26,27] Going even further, the combination of different stimuli within one material opens up a wide space of sensing applications, as shown for chitosan-g-poly(*N*-isopropylacrylamide) (PNIPAAm) graft copolymers featuring a pH-responsive polyelectrolyte backbone and thermoresponsive side chains.^[27]

Poly(dehydroalanine) (PDha), a polyampholyte featuring high charge density and both amine and carboxylate moieties in every repeat unit,^[28] was introduced recently as a versatile platform to obtain tailor-made copolymers with defined hydrophilicity,^[29,30] as a building block in double hydrophilic block copolymers,^[31] or as a template for the pH-controlled formation of Au/Ag alloy nanoparticles.^[32] Hereby, the polyampholytic PDha backbone offers pH-dependent net charge and a high density of functional groups as anchoring points for grafts or as binding sites for metal ions.^[31,32] We now introduce thermoresponsive PDha-based graft copolymers by grafting one single NIPAAm unit. While PNIPAAm is probably the most studied LCST polymer overall,^[33] this effect has so far not been shown for short side chains. However, high NIPAAm contents (>90 mol%) in poly(*N*-isopropylacrylamide-*co*-maleic acid-*co*-1-vinylimidazole) terpolymers were shown to be of interest for metal ion recognition.^[11] In our case, we combine thermoresponsive of NIPAAm grafts with pH-dependent charge and metal ion complexation of the PDha backbone, resulting in triple-responsive graft copolymers. These materials are highly sensitive sensors, where even the output can be tuned.

We have shown recently that grafting different side chains to PDha backbones allows us to tune solubility and surface affinity.^[30,32] We now performed aza-Michael additions under basic aqueous conditions to attach NIPAAm side chains and, with that, create triple-responsive graft copolymers (**Scheme 1**). PDha with an apparent molecular weight of $M_n = 10\,000\text{ g mol}^{-1}$ was used,^[32] and successful synthesis was proven *via* ^1H - and

J. B. Max, A. Nabiyan, J. Eichhorn, Prof. F. H. Schacher
Institute of Organic Chemistry and Macromolecular Chemistry
Friedrich-Schiller-Universität Jena
Lessingstraße 8, Jena 07743, Germany
E-mail: felix.schacher@uni-jena.de

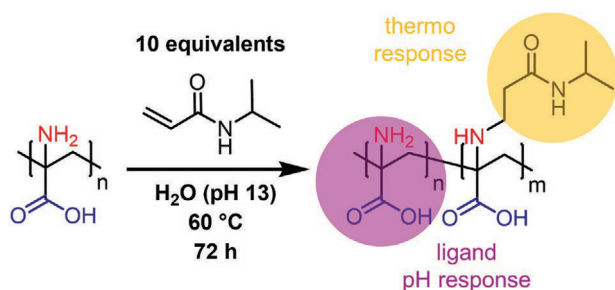
J. B. Max, A. Nabiyan, J. Eichhorn, Prof. F. H. Schacher
Jena Center for Soft Matter (JCSM)
Friedrich-Schiller-Universität Jena
Philosophenweg 7, Jena 07743, Germany

J. B. Max, A. Nabiyan, J. Eichhorn, Prof. F. H. Schacher
Center for Energy and Environmental Chemistry (CEEC)
Friedrich-Schiller-Universität Jena
Philosophenweg 7, Jena 07743, Germany

The ORCID identification number(s) for the author(s) of this article can be found under <https://doi.org/10.1002/marc.202000671>.

© 2020 The Authors. Macromolecular Rapid Communications published by Wiley-VCH GmbH. This is an open access article under the terms of the Creative Commons Attribution-NonCommercial-NoDerivs License, which permits use and distribution in any medium, provided the original work is properly cited, the use is non-commercial and no modifications or adaptations are made.

DOI: 10.1002/marc.202000671



Scheme 1. Synthetic route toward the synthesis of a triple-responsive graft copolymer based on PDha.

^{13}C -NMR spectroscopy, as well as fourier transformation infrared spectroscopy (FT-IR spectroscopy) and size exclusion chromatography (SEC) measurements (Figure S1, Supporting Information).

Kinetic investigations (Figure S2, Supporting Information) of the grafting process revealed a linear increase of the degree of functionalization (DoF) with time and a maximum of 95% grafting density upon use of 20 equivalents of the Michael acceptor. Thus, the amount of NIPAAm side chains can be precisely adjusted, and it strongly influenced the solubility of the resulting PDha-g-NIPAAm graft copolymers. Solubility in water even under acidic conditions, where PDha is typically insoluble, could be achieved starting from DoF = 30% and the dissolution in organic solvents such as methanol and *N,N*-dimethyl formamide DMF at DoF \geq 50% (Table S1, Supporting Information) was possible. The ζ -potential and titration curve (Figure S3, Supporting Information) of PDha-g-NIPAAm₉₅ (where the subscript represents the DoF) still resemble the parent ampholytic PDha homopolymer, showing pH-dependent charge through protonation/deprotonation of

carboxylic and amino groups.^[32,34] By exploiting the PDha backbone as a reactive handle, also other acrylamides can be used, broadening the range of accessible graft copolymers.^[35]

Since both PDha-g-NIPAAm₅₀ and PDha-g-NIPAAm₉₅ were soluble over the entire pH range, these graft copolymers were chosen for the investigation of their thermoresponsive properties (Figure 1). In comparison to PNIPAAm, monomeric NIPAAm side chains exhibit a different local environment and are, especially in case of PDha-g-NIPAAm₅₀, also locally separated. Besides, the polyampholytic backbone exhibits pH-dependent net charge and solubility. As a result, no cloud points could be detected at pH 7 and above for PDha-g-NIPAAm₅₀, which we ascribe to electrostatic repulsion of the negatively charged carboxylates along the PDha backbone. However, in case of PDha-g-NIPAAm₉₅ at pH 7, a cloud point temperature (T_{CP}) of 37 °C can be observed. Upon decreasing the pH to 6, a cloud point became apparent for PDha-g-NIPAAm₅₀, which decreases from 43 to 28 °C at pH 5 as a result of partial protonation of the carboxylic groups in accordance with potentiometric titrations (Figure S3, Supporting Information). Charge neutrality could lead to strong electrostatic attraction as a possible explanation for the lowest T_{CP} at pH 5. Further protonation of carboxylic groups enables the formation of hydrogen bonds and aggregation is facilitated. At pH 1 all carboxylic groups would be protonated and the hydrogen bonds predominate the behavior of the polycation. These observations were further proven by ζ -potential measurements (Figure 1D), revealing an overall negative charge until a pH of around 3, before positive values are obtained at pH 2.

While a clear increase of the T_{CP} from 28 to 40 °C from pH 5 to 1 is observed for PDha-g-NIPAAm₅₀ (36 wt% NIPAAm, Figure 1D), in case of PDha-g-NIPAAm₉₅ (55 wt% NIPAAm),

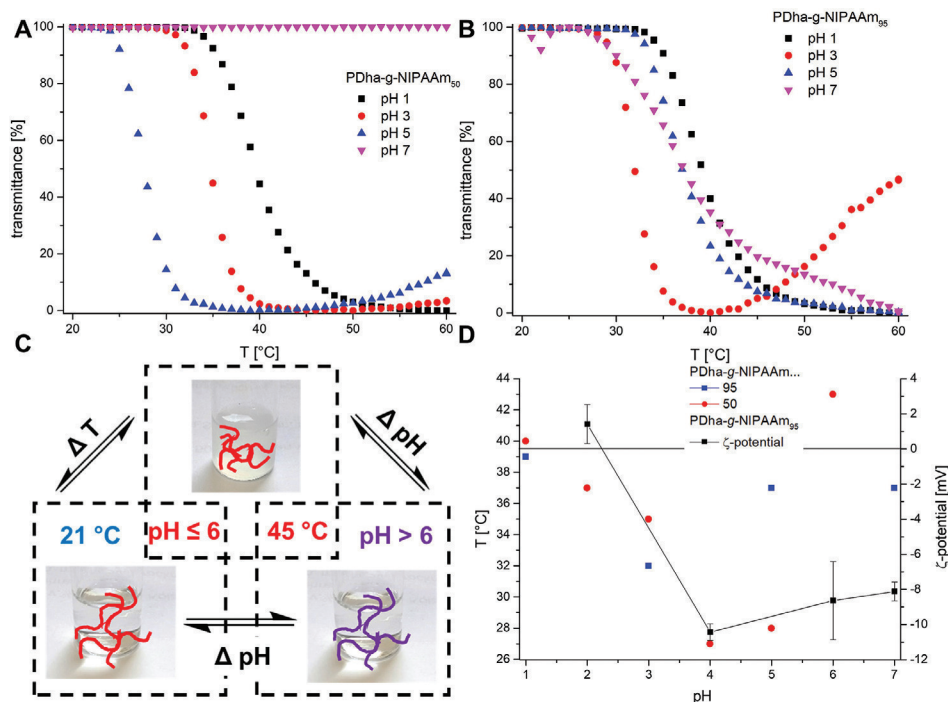


Figure 1. A,B) Cloud points determined from UV-vis measurements of PDha-g-NIPAAm₉₅ and PDha-g-NIPAAm₅₀ at different pH values ($c = 1 \text{ mg mL}^{-1}$, rate $0.2 \text{ }^\circ\text{C min}^{-1}$). C) Schematic illustration of the on/off switching of the thermoresponsive behavior of PDha-g-NIPAAm₅₀ by changes in pH value. D) Diagram of T_{CP} versus pH value and ζ -potential of PDha-g-NIPAAm₉₅.

less variation is observed and the observed T_{CP} values are closer to those reported for the PNIPAAm homopolymer with a T_{CP} of 30–35 °C.^[33] Exemplarily, at pH 1 we investigated the reversible aggregation of PDha-g-NIPAAm₉₅ by temperature-dependent ¹H-NMR spectroscopy and dynamic light scattering (DLS) measurements (Figure S4, Supporting Information). Regarding ¹H-NMR, the integrals of the –CH₂– backbone at 2.17–2.84 ppm and (–CH₃)₂ NIPAAm protons (0.84–1.14 ppm) decrease in intensity starting from 35 °C, as a result of the collapse of the graft copolymer. Upon cooling, a stepwise increase in intensity hints toward swelling and dissolving of the aggregates being formed. These observations were supported by DLS measurements (Figure S4B, Supporting Information), where first individual polymer chains were detected, and starting from 27 °C, aggregates with a hydrodynamic radius (R_H) of 310 nm were found, further increasing in size up to 820 nm at 50 °C.

As a first and simple example of sensing, the T_{CP} can be used to monitor changes in local pH, as it is schematically shown in Figure 1C. At first, a solution of PDha-g-NIPAAm₅₀ (pH ≈ 7) was heated to 45 °C, where no T_{CP} was observed. After

addition of 0.1 M HCl so that a pH of ≤6 was reached, the solution became turbid, indicating LCST behavior. Upon returning to 21 °C the solution became clear again, and increasing the pH by addition of 0.1 M NaOH led to similar behavior as observed initially. This reversible response to changes in pH within a moderately narrow and biologically relevant window renders such graft copolymers interesting materials for biomedical applications, e.g., in carrier systems.^[36]

The PDha backbone offers strong binding sites for metal ions and can act as a template for the formation of noble metal nanoparticles.^[32] Simultaneously, solubility is mediated by remaining backbone and NIPAAm side-chain functionalities, and we therefore used both PDha-g-NIPAAm₅₀ and PDha-g-NIPAAm₉₅ for the chelation of metal ions. Cu²⁺ or Pb²⁺ (0.01 mmol mL⁻¹) was added until the graft copolymer solutions (pH 7) became slightly opaque, indicating chelation and aggregation. Independent of the DoF, spherical aggregates were formed (Figure 2) with a size of R_H = 11–60 nm according to DLS (Figure S5, Supporting Information) and this was confirmed by transmission electron microscopy (TEM).

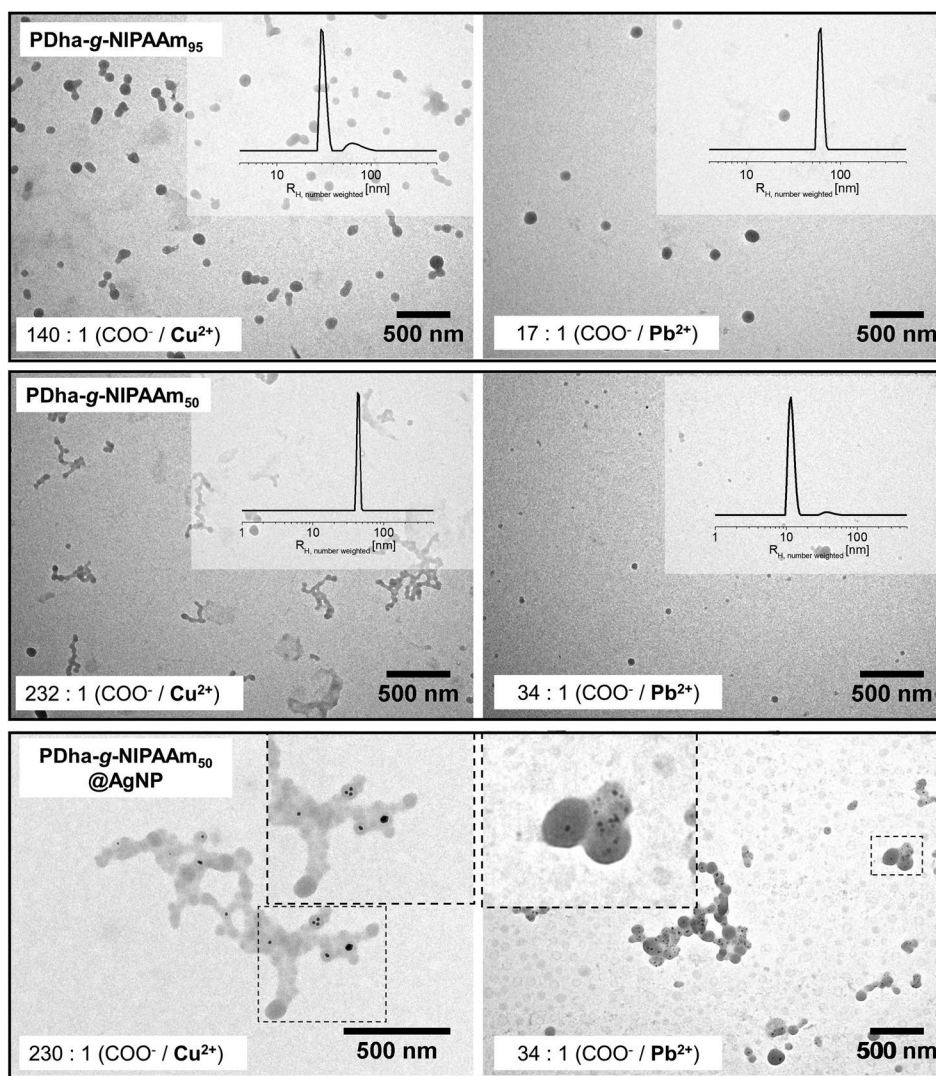


Figure 2. TEM micrographs of aggregates formed after addition of Cu²⁺ and Pb²⁺ to the graft copolymer solutions and AgNP dispersions.

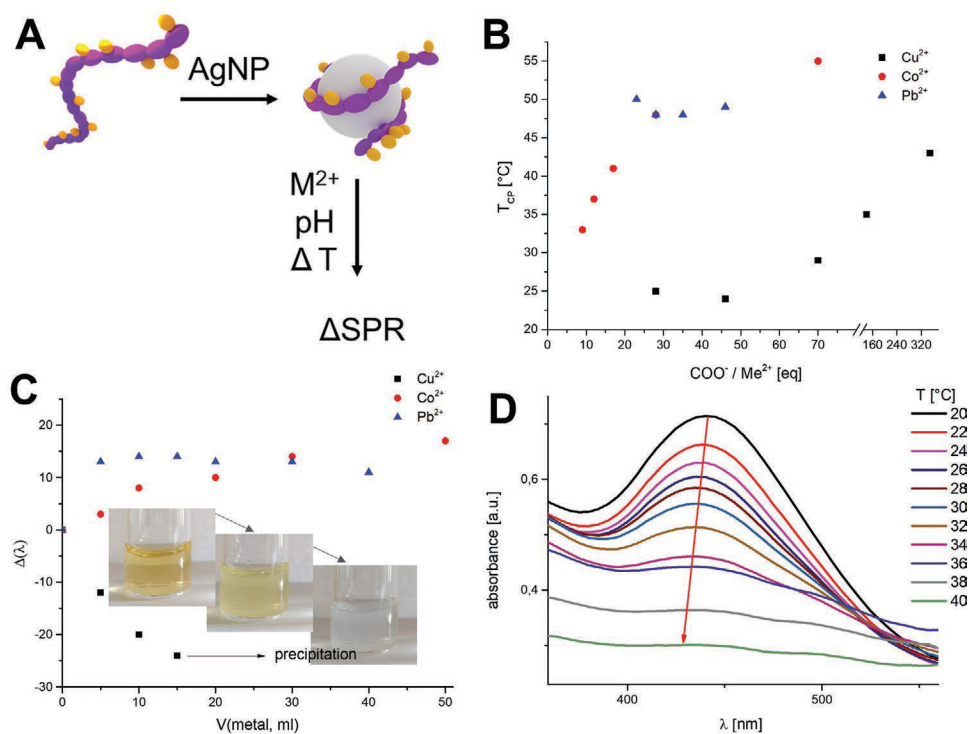


Figure 3. A) Formation of PDha-g-NIPAAm₅₀ and AgNP hybrid materials being responsive to metal cations, pH, and temperature changes. B) T_{CP} as a function of metals and their concentration after addition to PDha-g-NIPAAm₅₀. C) Shift of the SPR wavelength maximum in presence of PDha-g-NIPAAm₅₀ as a function of metals and their concentration. D) The SPR is quenched when heated at pH 5 or lower.

We observed a high sensitivity toward the addition of Cu²⁺, as already at a ratio of 1:230 (Cu²⁺/COO⁻) visible aggregation occurred, while in case of Pb²⁺ ions, a higher amount of metal ions was necessary to induce the formation of aggregates (1:34). We tentatively ascribe this to different coordination behavior, in line with earlier studies on the complexation of different metal ions with poly(acrylamidoglycolic acid) (PAGA).^[14] In addition, our results indicate that size and shape of the aggregates seem to depend on the type of metal ion and concentration, in accordance with literature examples,^[13,14] as well as the DoF of NIPAAm side chains. We found that the morphology of PDha-g-NIPAAm in the presence of Pb²⁺ ions remains regularly spherical even though we vary both the PDha/NIPAAm and M²⁺/PDha ratios. As these parameters show no significant influence on aggregate morphology, we hypothesize that the main driving force is the coordination behavior of Pb²⁺. In the presence of Cu²⁺, we have observed a morphological dependence mainly on the PDha/NIPAAm ratio. Multiple bridging of Cu²⁺ carboxylates is well known,^[37] and this could lead to the formation of polymer aggregates and secondary aggregation at already low metal concentrations.

However, this, in our opinion, renders these graft copolymers even more applicable in sensing, using the hydrodynamic size and/or measurable T_{CP} as signals for changes in pH or the presence of (traces of) metal ions. Complexation of the metal ions correlates also with inter- and intramolecular interactions and blocking of functional groups. As a result, thermoresponsiveness was found for PDha-g-NIPAAm₅₀ even at pH 7, where previously aggregation was prevented by repulsive forces of the ionized moieties. We investigated the cloud points after Cu²⁺, Pb²⁺, or Co²⁺ addition for different concentrations (Figure 3B)

and found distinct T_{CP} s. Except for Pb²⁺, T_{CP} is decreasing with higher metal concentrations that we attribute to an increased blocking of functional groups. Hereby, we found detection limits of 0.02, 0.15, and 0.1 mmol L⁻¹ for Cu²⁺, Pb²⁺, and Co²⁺, respectively. It is worth noting that these limits could be further adjusted by varying polymer concentration, DoF, or the pH value of the solution. Besides, other transition and main group metals could be recognized using the graft copolymer.

As an alternative readout signal, we exploited the ability of PDha-based materials to act as a template for the formation of noble metal nanoparticles and introduced silver nanoparticles (AgNPs) (Figure 3A), thereby imparting a strong surface plasmon resonance (SPR) signal within these hybrid materials. The SPR can then be used as an optical sensor responding to temperature, pH, and the presence of metal ions.^[32,38,39] We were able to obtain AgNPs ($R_H = 2.5$ nm from DLS) in the presence of PDha-g-NIPAAm₅₀ using NaBH₄ as the reducing agent (Figure S6, Supporting Information). After addition of either Cu²⁺ or Pb²⁺, the AgNPs were entrapped in the above-described aggregates, forming three-component nanomaterials as can be seen in TEM micrographs (Figure 2) and DLS (Figure S5, Supporting Information). As anticipated, a clear shift of the SPR peak was observed for PDha-g-NIPAAm₅₀@AgNP core-shell nanomaterials upon complexation of metal ions (Figure 3C), resulting in a blueshift in case of Cu²⁺ ($\Delta\lambda$) of up to 24 nm and a redshift for Pb²⁺ and Co²⁺. This process could be explained by either aggregation of AgNPs or decoration of the functional groups on the surface with the corresponding cations,^[40] and this is also dependent on the metal concentration. Here, the detection limit was found to be 0.05 mmol L⁻¹ for each metal

tested. Being covered by a thermo- and pH-responsive shell, SPR of the AgNPs is further affected by the solution pH and temperature (Figures S7 and S8, Supporting Information). While the maximum SPR peak shifts by changing the pH value, it vanishes completely by heating due to aggregation at pH 5 and lower (Figure 3D; Figure S8 and Table S2, Supporting Information), further proving the concept of a multiresponsive graft copolymer and a sensitive detector for changes in pH, temperature, or the presence of metal ions.

In summary, we describe a facile strategy to obtain polyampholytic PDha-based triple-responsive graft copolymers. The materials feature tuneable output in terms of solubility or the SPR of immobilized AgNPs. Thereby, the measured output again depends on the amount of metal ion being present, the overall concentration, and the pH value of the medium. Although shown for AgNPs as a well-studied model system, the concept of using this graft copolymer as a template could be transferred to other metal NPs. In this regard, PDha-g-NIPAAm in our opinion is also an interesting starting point for soft-matter-based temperature-controlled catalysis.^[41]

Supporting Information

Supporting Information is available from the Wiley Online Library or from the author.

Acknowledgements

This research was supported by the Deutsche Forschungsgemeinschaft (DFG, Project No. SCHA1640/18-1 and TRR234 “CataLight,” Project No. 364549901, project B5). The authors are grateful to Peggy Laudeley for SEC analysis and the NMR department at Friedrich-Schiller-University Jena for their continuous support. Further, the authors acknowledge the cryo-TEM/TEM facilities of the Jena Center for Soft Matter (JCSM), which were established with a grant from the German Research Council (DFG) and the European Funds for Regional Development (EFRE).

Open access funding enabled and organized by Projekt DEAL.

Conflict of Interest

The authors declare no conflict of interest.

Keywords

graft copolymers, metal sensors, polyampholyte, smart polymers, stimuli responsive materials

Received: November 9, 2020

Revised: November 27, 2020

Published online:

[1] L. A. Malik, A. Bashir, A. Qureshi, A. H. Pandith, *Environ. Chem. Lett.* **2019**, *17*, 1495.

[2] J. Hu, S. Liu, *Macromolecules* **2010**, *43*, 8315.

[3] M. Wei, Y. Gao, X. Li, M. J. Serpe, *Polym. Chem.* **2017**, *8*, 127.

[4] C. Pietsch, R. Hoogenboom, U. S. Schubert, *Angew. Chem., Int. Ed.* **2009**, *48*, 5653.

[5] Y. Chen, K.-Y. Pu, Q.-L. Fan, X.-Y. Qi, Y.-Q. Huang, X.-M. Lu, W. Huang, *J. Polym. Sci., Part A: Polym. Chem.* **2009**, *47*, 5057.

[6] Z. Guo, W. Zhu, H. Tian, *Macromolecules* **2010**, *43*, 739.

[7] T. Hosomi, H. Masai, T. Fujihara, Y. Tsuji, J. Terao, *Angew. Chem., Int. Ed.* **2016**, *55*, 13427.

[8] X. Liu, X. Zhou, X. Shu, J. Zhu, *Macromolecules* **2009**, *42*, 7634.

[9] M. Zhang, P. Lu, Y. Ma, J. Shen, *J. Phys. Chem. B* **2003**, *107*, 6535.

[10] P. Mi, L.-Y. Chu, X.-J. Ju, C. H. Niu, *Macromol. Rapid Commun.* **2008**, *29*, 27.

[11] J. Cheng, G. Shan, P. Pan, *Ind. Eng. Chem. Res.* **2017**, *56*, 1223.

[12] Q. Luo, Y. Guan, Y. Zhang, M. Siddiq, *J. Polym. Sci., Part A: Polym. Chem.* **2010**, *48*, 4120.

[13] A. Nabiyani, P. Biehl, F. H. Schacher, *Macromolecules* **2020**, *53*, 5056.

[14] L. Volkmann, M. Köhler, F. H. Sobotta, M. T. Enke, J. C. Brendel, F. H. Schacher, *Macromolecules* **2018**, *51*, 7284.

[15] M. Hess, R. G. Jones, J. Kahovec, T. Kitayama, P. Kratochvíl, P. Kubisa, W. Mormann, R. F. T. Stepto, D. Tabak, J. Vohlídal, E. S. Wilks, *Pure Appl. Chem.* **2006**, *78*, 2067.

[16] T. Zhu, Y. Sha, J. Yan, P. Pageni, M. A. Rahman, Y. Yan, C. Tang, *Nat. Commun.* **2018**, *9*, 4329.

[17] Y. Liu, K. Ogawa, K. S. Schanze, *J. Photochem. Photobiol., C* **2009**, *10*, 173.

[18] B. L. Rivas, E. Pereira, R. Cid, K. E. Geckeler, *J. Appl. Polym. Sci.* **2005**, *95*, 1091.

[19] G. Craciun, E. Manaila, D. Ighigeanu, *Polymers* **2019**, *11*, 234.

[20] T. Zheng, M. Zhu, M. Waqas, A. Umair, M. Zaheer, J. Yang, X. Duan, L. Li, *RSC Adv.* **2018**, *8*, 38818.

[21] E. A. Hassan, M. L. Hassan, C. N. Moorefield, G. R. Newkome, *Carbohydr. Polym.* **2015**, *116*, 2.

[22] Y. Morishima, T. Kobayashi, S.-i. Nozakura, *Polym. J.* **1989**, *21*, 267.

[23] F. Schacher, T. Rudolph, F. Wieberger, M. Ulbricht, A. H. E. Müller, *ACS Appl. Mater. Interfaces* **2009**, *1*, 1492.

[24] X. Zhang, K. Matyjaszewski, *Macromolecules* **1999**, *32*, 1763.

[25] C. Frangville, Y. Li, C. Billotey, D. R. Talham, J. Taleb, P. Roux, J.-D. Marty, C. Mingotaud, *Nano Lett.* **2016**, *16*, 4069.

[26] C. M. Schilli, M. Zhang, E. Rizzardo, S. H. Thang, Y. K. Chong, K. Edwards, G. Karlsson, A. H. E. Müller, *Macromolecules* **2004**, *37*, 7861.

[27] N. do Nascimento Marques, A. M. da Silva Maia, R. de Carvalho Balaban, *Polímeros* **2015**, *25*, 237.

[28] E. A. Bekturov, S. E. Kudaibergenov, S. R. Rafikov, *J. Macromol. Sci., Part C: Polym. Rev.* **1990**, *30*, 233.

[29] M. Billing, G. Festag, P. Bellstedt, F. H. Schacher, *Polym. Chem.* **2017**, *8*, 936.

[30] J. B. Max, D. V. Pergushov, L. V. Sigolaeva, F. H. Schacher, *Polym. Chem.* **2019**, *10*, 3006.

[31] J. B. Max, P. J. Mons, J. C. Tom, F. H. Schacher, *Macromol. Chem. Phys.* **2020**, *221*, 1900383.

[32] J. B. Max, K. Kowalczyk, M. Köhler, C. Neumann, F. Pielenz, L. V. Sigolaeva, D. V. Pergushov, A. Turchanin, F. Langenhorst, F. H. Schacher, *Macromolecules* **2020**, *53*, 4511.

[33] H. G. Schild, *Prog. Polym. Sci.* **1992**, *17*, 163.

[34] U. Günther, L. V. Sigolaeva, D. V. Pergushov, F. H. Schacher, *Macromol. Chem. Phys.* **2013**, *214*, 2202.

[35] S. Chen, K. Wang, W. Zhang, *Polym. Chem.* **2017**, *8*, 3090.

[36] Z. Ge, S. Liu, *Chem. Soc. Rev.* **2013**, *42*, 7289.

[37] J. Boonmak, S. Youngme, T. Chotkhun, C. Engkagul, N. Chaichit, G. A. van Albada, J. Reedijk, *Inorg. Chem. Commun.* **2008**, *11*, 1231.

[38] M. von der Lüche, U. Günther, A. Weidner, C. Gräfe, J. H. Clement, S. Dutz, F. H. Schacher, *RSC Adv.* **2015**, *5*, 31920.

[39] M. von der Lüche, A. Weidner, S. Dutz, F. H. Schacher, *ACS Appl. Nano Mater.* **2017**, *1*, 232.

[40] M. Annadhasan, T. Muthukumarasamyvel, V. R. Sankar Babu, N. Rajendiran, *ACS Sustainable Chem. Eng.* **2014**, *2*, 887.

[41] S. Carregal-Romero, N. J. Buurma, J. Pérez-Juste, L. M. Liz-Marzán, P. Hervés, *Chem. Mater.* **2010**, *22*, 3051.



Supporting Information

for *Macromol. Rapid Commun.*, DOI: 10.1002/marc.202000671

Triple-Responsive Polyampholytic Graft Copolymers as
Smart Sensors with Varying Output

Johannes B. Max, Afshin Nabiyan, Jonas Eichhorn, and
Felix H. Schacher*

Supporting Information

Triple-responsive polyampholytic graft copolymers as smart sensors with varying output

Johannes B. Max,^{abc} Afshin Nabiyan,^{abc} Jonas Eichhorn,^{abc} and Felix H. Schacher^{abc}*

^aInstitute of Organic Chemistry and Macromolecular Chemistry

Friedrich-Schiller-Universität Jena, Lessingstraße 8, 07743 Jena, Germany

^bJena Center for Soft Matter (JCSM)

Friedrich-Schiller-Universität Jena, Philosophenweg 7, 07743 Jena, Germany

^cCenter for Energy and Environmental Chemistry (CEEC)

Friedrich-Schiller-Universität Jena, Philosophenweg 7, 07743 Jena, Germany

E-mail: felix.schacher@uni-jena.de

Experimental Part

Chemicals

N-Isopropylacrylamide was purchased from TCI chemicals (>98 %). CoCl₂ (≥98.0 %), CuCl₂ (99 %) and PbCl₂ (98%) were purchased from Sigma-Aldrich. All chemicals were used as received. PDha_{0.80}-*stat*-PAMA_{0.20} was synthesized as described in our earlier work starting from *Pt*BAMA ($M_n = 10\,000$ g/mol, $\bar{D} = 2.46$).^[1]

Analytical methods

Nuclear magnetic resonance (NMR) spectroscopy

¹H- and ¹³C-NMR spectra were performed on a Bruker AC 300 MHz using CDCl₃, DMSO-d₆ and D₂O/NaOD as solvents at a temperature of 298 K. The spectra were referenced by using the residual signal of the deuterated solvent.

Size exclusion chromatography (SEC)

An Agilent 1260 Infinity System, equipped with a 1260 IsoPump (G1310B), an 1260 ALS (G1310B) autosampler and three consecutive PSS SDV, 5 μm, 8x300mm columns was used for SEC measurements in THF. The flow rate was 1 ml/min and the columns were heated to

at 30 °C. The signals were collected using a 1260 DAD VL (GG1329B) and a 1260 RID (G1315D) detector.

SEC measurements in DMSO were performed on a Jasco instrument using DMSO + 0.5 % LiBr as solvent at a flow rate of 0.5 ml/min at 65 °C and Pullulan calibration. It was equipped with PSS NOVEMA 3000 Angström / 300 Angström columns, a RI-930 detector as well as a PU-980 pump.

Dynamic Light Scattering (DLS)

DLS measurements were performed using an ALV laser CGS3 Goniometer equipped with a 633 nm HeNe laser (ALV GmbH, Langen, Germany) at 25 °C and at a detection angle of 90°. The CONTIN analysis of the obtained correlation functions was performed using the ALV 7002 FAST Correlator Software.

Transmission Electron Microscopy (TEM)

TEM images were acquired with a 200 kV FEI Tecnai G2 20 equipped with a 4k x 4k Eagle HS CCD and a 1k x 1k Olympus MegaView camera for overview images.

ξ-Potential

Zeta-potentials were measured on a ZetaSizer Nano ZS from Malvern via M3-PALS technique with a laser beam at 633 nm. The detection angle was 13°. The samples were prepared by titration of the polymer in 0.1 M NaOH (0.2 g/L) with 0.1 M HCl and 1 mL of the solution was taken at the desired pH values. The titration and pH detection was performed on a Metrohm 765 Dosimat titrator with a Greisinger electronic GMH3539 digital pH-/mV-electrode with a thermometer.

Potentiometric titration

Potentiometric titrations were performed with a TitroLine® 7000 titrator equipped with a WA 20 exchangeable unit, magnetic stirrer TM 235, and a ScienceLine pH combination electrodes with temperature sensor A162 from SI Analytics GmbH. The polymers were dissolved in 0.1 M NaOH at a concentration of 1.5 g/L and titrated against 0.1 M HCl *via* an automatic dynamic pH-titration method.

UV-Vis

UV/Vis measurements were performed on a Agilent Cary 60 in a Hellma quartz glass cuvette with a pathlength of 10 mm at room temperature in solvent. The absorbance was measured in a range from 200 nm to 800 nm in 5 nm steps.

Synthesis

Post-polymerization modification of PDha-*stat*-PAMA with NIPAM

PDha_{0.80}-*stat*-PAMA_{0.20} (100 mg) and NIPAAm (10 eq per monomer unit) were dissolved in water (5 ml each, pH 13, KOH). Afterwards the clear solutions were mixed and placed in an oil bath at 60 °C for constant stirring. The reaction was terminated after 48 h, by adding aqueous HCl (0.5 M) until a pH of 7 was reached. Then, the crude product was dialyzed against deionized water (MWCO = 3.5 kDa) for 2 days and afterwards freeze-dried to obtain a colorless polymer powder.

¹H-NMR (300 MHz, D₂O, δ) = 3.93 – 3.70 (m, -CH), 3.70 – 3.07 (m, -C(=O)-CH₂-), 2.99 – 1.92 (m, -C-CH₂-, and -NH-CH₂-), 1.22 – 0.95 (m, -CH-(CH₃)₂) ppm.

¹³C-NMR (75 MHz, D₂O δ): 175.29 (-COOH), 171.50 (-CONH-), 65.78 (-HN-C-COOH), 41.81 (-C-CH₂-, and -CH), 34.19 and 38.72 (-CH₂-CH₂-), 21.51 (-(CH₃)₂) ppm.

Complexation of metal ions

PDha-*g*-NIPAAm was dissolved in deionized water (1 mg/ml) and a solution of the corresponding metal (0.01 mmol/ml) was added dropwise under continuous stirring. Increasing the amount of metal led to slightly turbid solutions.

Complexation of metal ions

To a solution of PDha-*g*-NIPAAm₅₀ (1 mg/ml), aqueous AgNO₃ (0.01 mmol/ml, 17 eq per monomer unit) was added. After stirring for 15 min NaBH₄ (0.01 mmol/mol, 1 eq per silver ion) was added dropwise and the color turned orange.

Figures and Tables

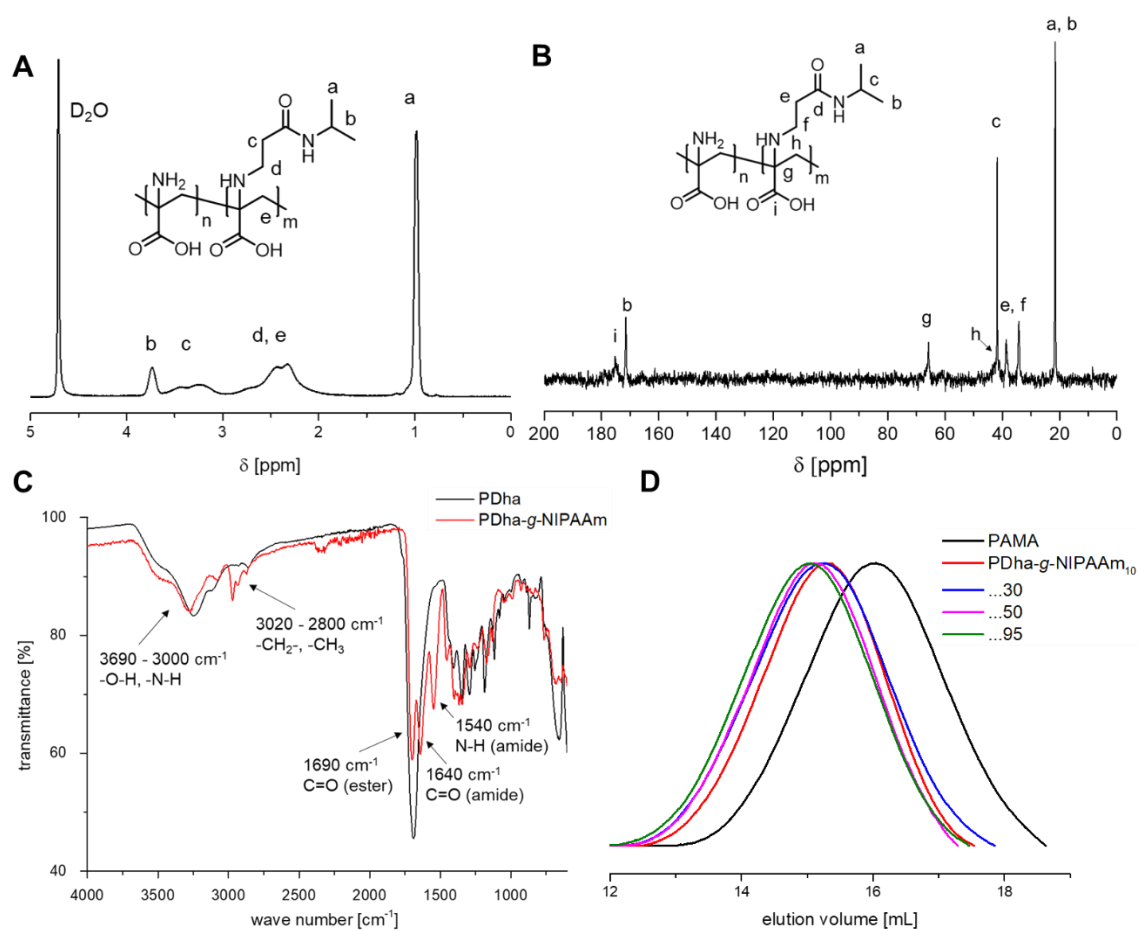


Figure S1: Characterization of PDha-g-NIPAAm₉₅ double hydrophilic graft copolymer *via* $^1\text{H-NMR}$ (A) and $^{13}\text{C-NMR}$ spectroscopy (B) and FT-IR spectroscopy (C). SEC traces (in DMSO) of the synthesized graft copolymers with different DoF.

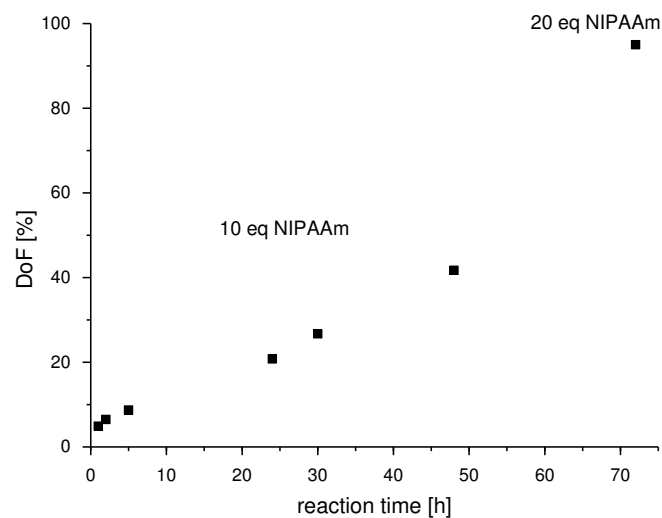


Figure S2: Kinetic study of the post-polymerization modification of PDha with NIPAAm derived from $^1\text{H-NMR}$ spectroscopy.

Table S1: Summary of the synthesized PDha-g-NIPAAm graft copolymers and their solubility in different environments.

PDha-g-...	NIPAAm [wt%]	solubility ^a			
		water	DMSO	DMF	methanol
-		pH > 7	+	-	-
NIPAAm ₁₀	9	pH ≥ 7	+	-	-
NIPAAm ₃₀	24	pH ≥ 6 ^b	+	-	-
NIPAAm ₅₀	36	pH = 1 - 14	+	+	+
NIPAAm ₉₅	55	pH = 1 - 14	+	+	+

^a ≥ 2 g/L, - ≙ insoluble, + ≙ clear solution, +/- slightly turbid; ^b soluble under acidic condition by slow titration starting from pH 7.

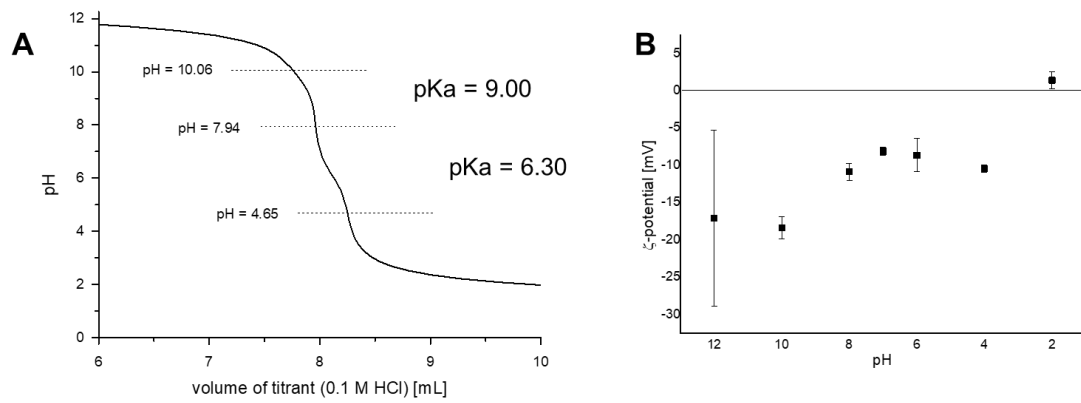


Figure S3: Potentiometric titration (A) and ζ -potential measured with a zetasizer (B) of PDha-g-NIPAAm₉₅.

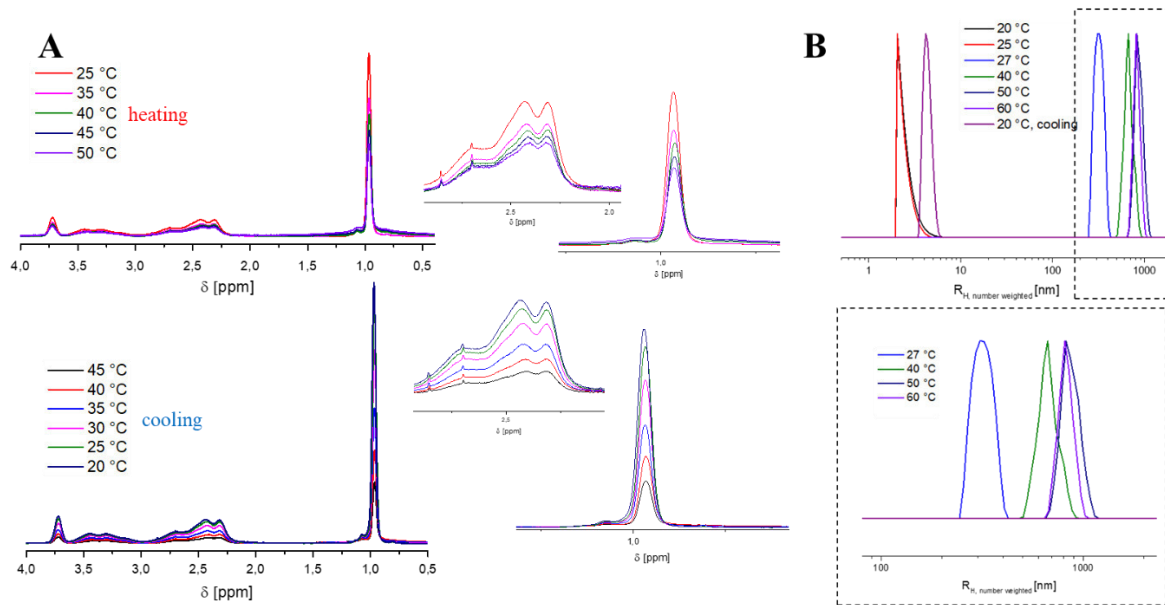


Figure S4: Investigation of the thermoresponsive behaviour of PDha-g-NIPAAm₉₅ via temperature dependent ¹H-NMR spectroscopy (A) and DLS measurements (B) at pH 1.

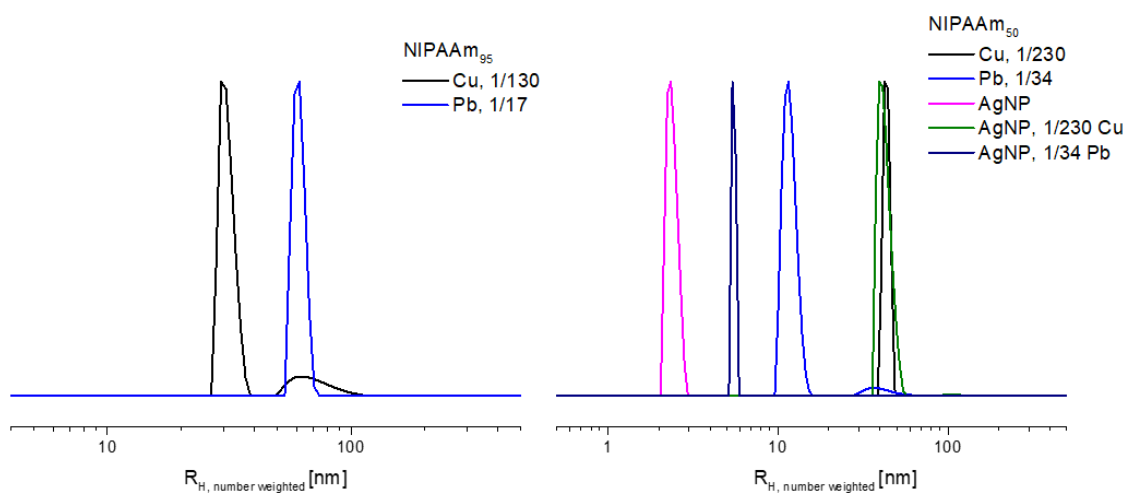


Figure S5: DLS measurements of PDha-g-NIPAAm solutions after metal addition.

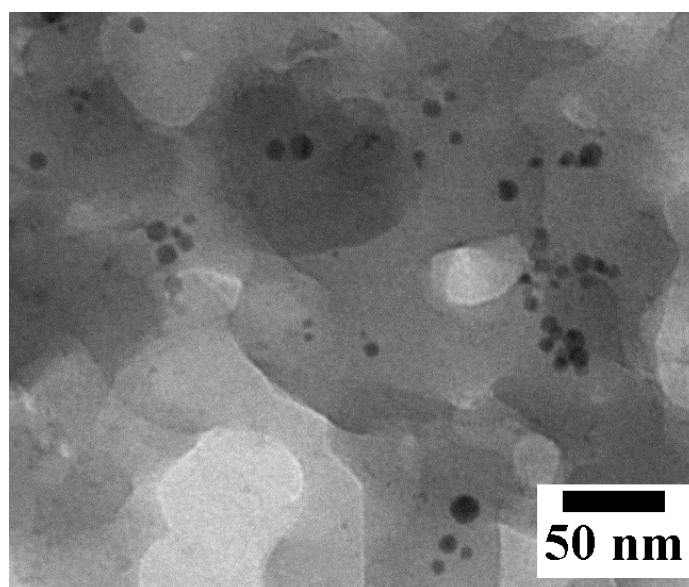


Figure S6: TEM micrographs of PDha-g-NIPAAm₅₀@Ag NPs.

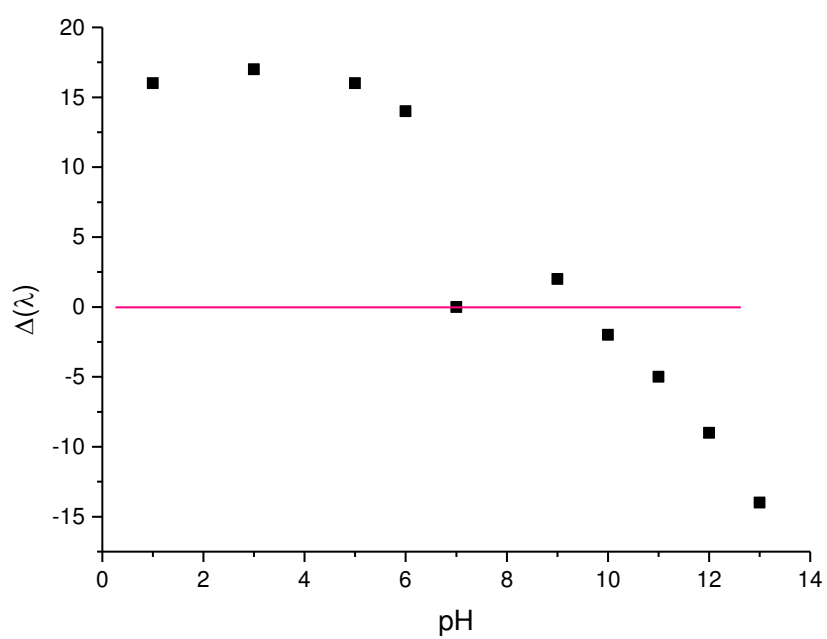


Figure S7: pH dependent absorption maximum of the surface plasmon resonance peak of PDha-g-NIPAAm₅₀@Ag NPs.

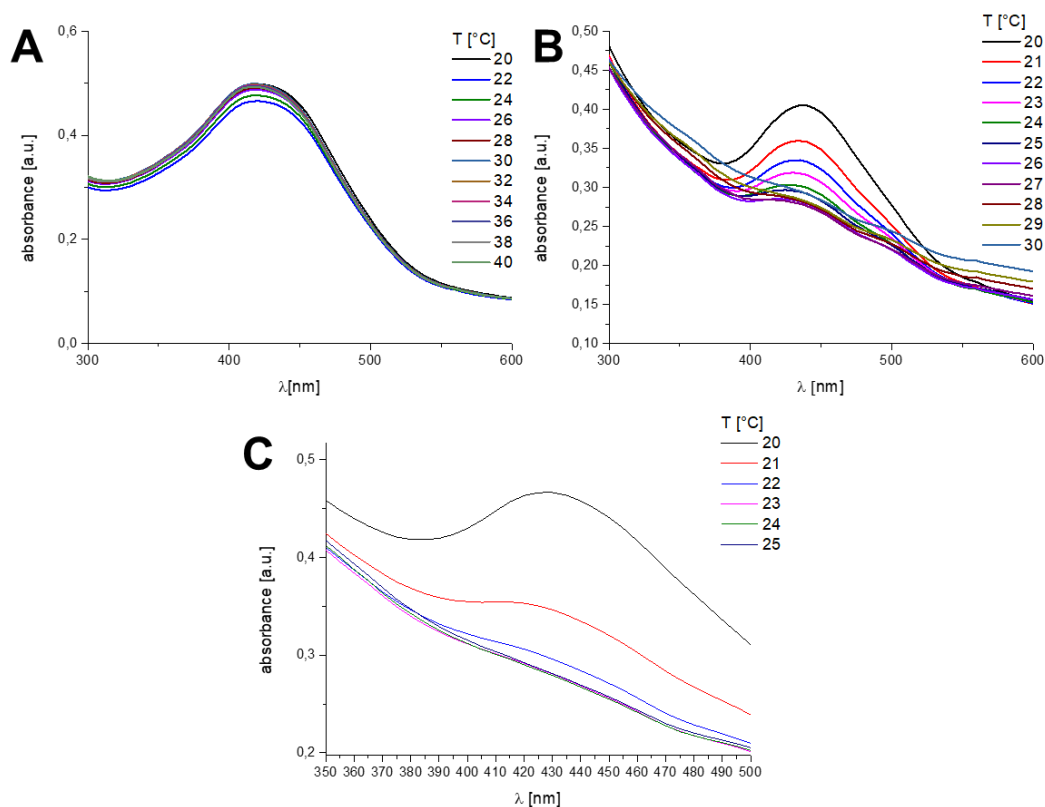


Figure S8: Temperature dependent absorption maxima of the surface plasmon resonance peak of PDha-g-NIPAAm₅₀@Ag NPs at pH 7 (A), 3 (B), and 1 (C).

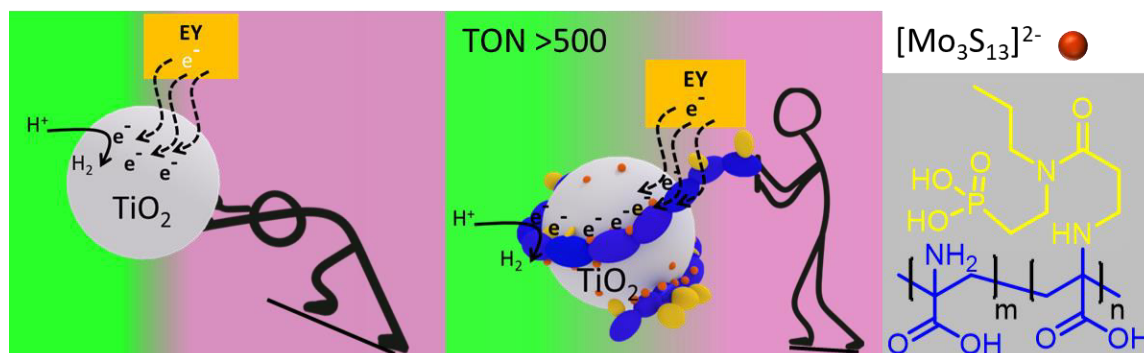
Table S2: Summary of cloud points temperatures of PDha-g-NIPAAm₅₀@Ag NP and temperature, where the surface plasmon resonance peak is fully quenched.

pH	T _{CP} [°C]	T _{quenching} [°C]
7	none	none
5	34	40
3	32	29
1	36	22

[1] J. B. Max, K. Kowalczyk, M. Köhler, C. Neumann, F. Pielenz, L. V. Sigolaeva, D. V. Pergushov, A. Turchanin, F. Langenhorst, F. H. Schacher, *Macromolecules* **2020**, *53*, 4511.

Publication P5

“Polyampholytic graft copolymers as matrix for $\text{TiO}_2/\text{Eosin Y}/[\text{Mo}_3\text{S}_{13}]^{2-}$ hybrid materials and photocatalysis”



Afshin. Nabiyan,[‡] Johannes B. Max,[‡] Christof Neumann, Magdalena Heiland, Andrey Turchanin, Carsten Streb, and F. H. Schacher

Chem. Eur. J., **2021**, 27, 1-7

[‡]Both authors contributed equally to this work

Photocatalysis

SPECIAL
ISSUEPolyampholytic Graft Copolymers as Matrix for TiO₂/Eosin Y/[Mo₃S₁₃]²⁻ Hybrid Materials and Light-Driven CatalysisAfshin Nabiyan,^[a, b, c] Johannes Bernhard Max,^[a, b, c] Christof Neumann,^[b, c, d] Magdalena Heiland,^[e] Andrey Turchanin,^[b, c, d] Carsten Streb,^[e] and Felix Helmut Schacher*^[a, b, c]

Abstract: An effective strategy to enhance the performance of inorganic semiconductors is moving towards organic-inorganic hybrid materials. Here, we report the design of core-shell hybrid materials based on a TiO₂ core functionalized with a polyampholytic (poly(dehydroalanine)-graft-(*n*-propyl phosphonic acid acrylamide) shell (PDha-*g*-PAA@TiO₂). The PDha-*g*-PAA shell facilitates the efficient immobilization of the photosensitizer Eosin Y (EY) and enables electronic interactions between EY and the TiO₂ core. This resulted in high visible-light-driven H₂ generation. The enhanced light-driven

catalytic activity is attributed to the unique core-shell design with the graft copolymer acting as bridge and facilitating electron and proton transfer, thereby also preventing the degradation of EY. Further catalytic enhancement of PDha-*g*-PAA@TiO₂ was possible by introducing [Mo₃S₁₃]²⁻ cluster anions as hydrogen-evolution cocatalyst. This novel design approach is an example for a multi-component system in which reactivity can in future be independently tuned by selection of the desired molecular or polymeric species.

Introduction

Global challenges such as climate change and overconsumption urgently require the supply of sustainable clean energy.

[a] A. Nabiyan, J. B. Max, Prof. Dr. F. H. Schacher
Institute of Organic Chemistry and Macromolecular Chemistry (IOMC)
Friedrich Schiller University Jena
Lessingstraße 8, 07743 Jena (Germany)
E-mail: felix.schacher@uni-jena.de

[b] A. Nabiyan, J. B. Max, Dr. C. Neumann, Prof. Dr. A. Turchanin,
Prof. Dr. F. H. Schacher
Jena Center for Soft Matter (JCSM)
Friedrich Schiller University Jena
Philosophenweg 7, 07743 Jena (Germany)

[c] A. Nabiyan, J. B. Max, Dr. C. Neumann, Prof. Dr. A. Turchanin,
Prof. Dr. F. H. Schacher
Center for Energy and Environmental Chemistry Jena (CEEC Jena)
Friedrich Schiller University Jena
Philosophenweg 7a, 07743 Jena (Germany)

[d] Dr. C. Neumann, Prof. Dr. A. Turchanin
Institute of Physical Chemistry and Abbe Center of Photonics
Friedrich Schiller University Jena
Lessingstr. 10, 07743 Jena (Germany)

[e] M. Heiland, Prof. Dr. C. Streb
Institute of Inorganic Chemistry I
Ulm University
Albert-Einstein-Allee 11, 89081 Ulm (Germany)

Supporting information and the ORCID identification number(s) for the author(s) of this article can be found under:
<https://doi.org/10.1002/chem.202100091>.

© 2021 The Authors. Chemistry - A European Journal published by Wiley-VCH GmbH. This is an open access article under the terms of the Creative Commons Attribution License, which permits use, distribution and reproduction in any medium, provided the original work is properly cited.

Part of a Special Issue on Contemporary Challenges in Catalysis.

This could be tackled by the utilization of hydrogen as a secondary, carbon-free energy carrier. Therefore, tremendous efforts have been invested in the direction of production, storage, and delivery of hydrogen.^[1] Light-driven catalytic hydrogen evolution is a favourable carbon-neutral method, exploiting solar energy.^[2] The first example of light-induced water splitting was described in 1972 by utilisation of a TiO₂ electrode, though it was limited to irradiation with UV light.^[3] Although being chemically stable, non-toxic, and a low cost material, light harvesting using a broader solar energy spectrum is desirable.^[4] Recent approaches towards hydrogen evolution are therefore targeting visible-light harvesting through band gap engineering,^[5] utilization of photosensitizers,^[6] introduction of co-catalysts,^[7] electron relays such as polyoxometalates,^[8] or the use of novel semi-conducting materials.^[9] In this context, TiO₂ as potential candidate can be tuned for visible-light-driven hydrogen evolution by the addition of different cocatalysts and sensitizers. Recently, combining TiO₂ and molybdenum sulfide was identified as a promising composite system.^[4c, 10]

Molybdenum sulfides (MoS_x) as (co)catalysts are gaining considerable interest due to low cost, long-term stability, and earth-abundance. In that regard both, 2D structured MoS_{2+x} as well as molecular molybdenum sulfides (thiomolybdates), for example, [Mo₃S₁₃]²⁻ or [Mo₂S₁₂]²⁻ have been investigated in combination with different sensitizers and (co)catalysts.^[4b, 11] Thiomolybdates typically carry a high number of active sites and allow homogenous hydrogen evolution with high turnover numbers (> 41 000).^[11b, c, 12]

With respect to multi-component hybrid materials, immobilization of different compounds within suitable matrices plays a

key role in connecting individual elements of light-driven catalytic systems and has been realized on solid substrates such as carbon nanomaterials,^[13] metal oxides^[14] or semiconductors such as p-Si.^[15] Although being well soluble in aqueous environment and exhibiting potential binding sites for both different catalysts and sensitizers, only few examples focus on soft matrices based on polyelectrolytes. Romanenko et al. described the preparation of block copolymer membranes, where the molecular catalyst $[\text{Mo}_3\text{S}_{13}]^{2-}$ and photosensitizer $[\text{Ru}(\text{bpy})_3]^{2+}$ were immobilized using positively charged groups along the poly(*N,N*-dimethylaminoethyl methacrylate) (PDMAEMA) segment.^[16] Besides, polyelectrolyte-based hydrogels are promising scaffolds and in this regard Weingarten et al.^[17] and H. Sai et al.^[18] attached perylene monoimide as well as suitable catalysts for efficient hydrogen production. Also 'free' polymers could molecularly interact with catalysts as it has been shown by Hu et al., exploiting conjugated polyelectrolytes for the interaction with Pt catalysts in hydrogen evolution reactions,^[19] or double-hydrophilic block copolymers as templates for CdS nanoparticles.^[20]

Polyampholytic polydehydroalanine (PDha) is a suitable template featuring a high density of functional (charged) groups and strongly interacting with metal oxides, metal nanoparticles and dyes in water, which led us to the assumption that this is a promising matrix for light-driven catalysis.^[21] PDha exhibits both positively charged amino groups as well as negatively charged carboxylic acid moieties for the specific interaction with various compounds. Furthermore, it was found to be a platform for modification reactions to obtain materials with tailored solubility, for example, as sensors, smart dispersants, or templates.^[21c,22] Besides this, PDha-*g*-PEG was already successfully used as dispersant for a water-insoluble perylene-based photosensitizer.^[23] In this regard, we prepared tailor-made PDha graft copolymers for the application in visible-light driven hydrogen evolution. We herein introduce a novel catalytic system consisting of promising and low cost catalysts TiO_2 and $[\text{Mo}_3\text{S}_{13}]^{2-}$, as well as Eosin Y (EY) as dye sensitizer in the presence of the sacrificial agent triethanol amine (TEOA), revealing >800 fold increased activity compared to bare EY/ TiO_2 hybrids. This is realized by the attachment of phosphonic acid side-chains for increased solution stability against sedimentation and as strong anchor groups for TiO_2 .^[15] The overall combination not only leads to visible light-driven catalysis, but also enables the physical combination of materials, which has not been possible before. The mere combination of TiO_2 and EY has already been reported, but efficient hydrogen evolution strongly depends on the way of interaction due to insulating, quenching and stability issues.^[1c,24] On the other hand, while EY was successfully used as a photosensitizer together with MoS_2 ,^[25] it failed in case of $[\text{Mo}_3\text{S}_{13}]^{2-}$ presumably due to rather weak interactions with the catalyst.^[11b]

Results and Discussion

Synthesis of phosphonic acid modified graft copolymers

In our earlier work we have shown that post-polymerization modification of PDha by grafting is a powerful synthetic route to fine-tune solution properties and functionality.^[21c,22a] To develop the applicability of PDha as a coating for TiO_2 NPs, both increasing its water solubility at pH values <7 and the attachment of an additional, strong anchor group was desired. Therefore, PDha with an average of 60 repeat units was used as a reactive backbone, obtained from deprotection of PtBAMA ($M_n = 13\,200$, $\bar{D} = 2.55$), and *n*-propyl phosphonic acid acrylamide (PAA) was successfully grafted via an aza-Michael addition (Figure 1 A).

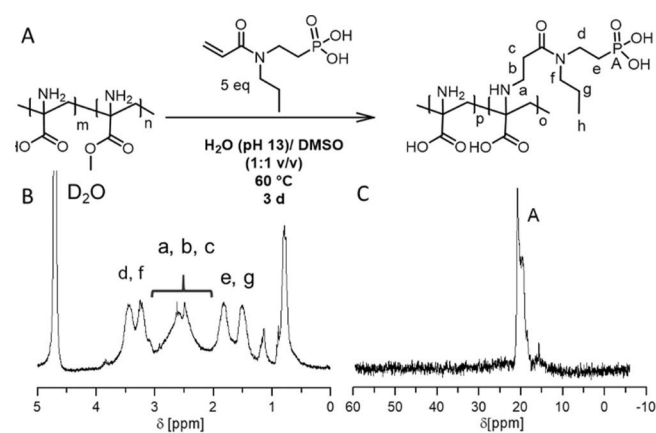


Figure 1. Synthesis of PDha-*g*-PAA graft copolymers (A) and corresponding ^1H -NMR (B) and ^{31}P -NMR (C) spectra.

The modifier was synthesized in accordance with the protocol of Hu et al.^[26] Hereby, 66% of the monomer units were functionalized when 5 equivalents of the acryl amide were used. The degree of functionalization was determined from ^1H NMR spectroscopy in accordance with our previous work.^[22a] As expected, the obtained graft copolymer was soluble over the entire pH-range as well as in methanol. NMR (^{31}P , ^1H and ^{13}C) spectroscopy (Figure 1 A, B; Figure S2) shows the presence of both the PDha backbone as well as phosphonic acid side groups and SEC traces reveal a narrowing of the elution traces in comparison to the pristine polymer, while still maintaining a monomodal distribution. Regarding the multiple peaks in the ^{31}P NMR spectrum being in close proximity, we assume a random distribution of the side-chains along the backbone leading to different chemical environments of the phosphonic acid groups. Besides that, protonation might also play a role.

Formation of TiO_2 based core-shell hybrids

The amino and carboxylic acid moieties of PDha are exceptionally strong ligands for inorganic NPs as already proven for stable dispersions with iron oxide, gold, silver, or Ag/Au nano-

alloy particles.^[21a,c,27] However, the readily grafted phosphonic acid side-chains are additional strong ligands for TiO₂ surfaces and besides that they implement pH solution stability as well as additional negative charges, the latter possibly facilitating proton transfer processes.^[28] Therefore, we utilized PDha-*g*-PAA as coating for TiO₂ NPs using simple ultra-sonication (Figure 2A) and the successful formation of core-shell hybrid materials was proven by thermogravimetric analysis (TGA), transmission electron microscopy (TEM), X-ray photoelectron spectroscopy (XPS) and dynamic light scattering (DLS) (Figures S3–S6).

To determine the amount of organic shell material, TGA was measured under air for the pristine TiO₂, PDha-*g*-PAA and the hybrid materials with different polymer to TiO₂ ratios (5:1 and 15:1 (w/w) polymer/TiO₂, Figure S3). Any free polymer was removed by dialysis and three washing steps after centrifugation of the solid material. For the TiO₂ NPs a weight loss of around 17 wt% was observed between 30 °C and 450 °C, which is mainly assigned to the loss of water. In case of PDha-*g*-PAA three weight-loss steps were observed, the first step between rt and 140 °C as a result of loss of residual water, and two further steps at 290 and 470 °C as a result of polymer decomposition. No further weight loss is observed at $T > 600$ °C (residual mass: 20 wt%). Regarding the hybrid material, similar decomposition steps were observed between 290 and 600 °C, providing evidence for the presence of the polymer shell. High polymer contents of 29 wt% and 66 wt% were calculated, respectively. To confirm these results, TEM images of PDha-*g*-PAA@TiO₂ (Figure 2 and Figures S4 and S5) show individual TiO₂ NPs with an average radius of around 11 nm and an organic layer with a thickness of several nm is clearly visible. Additionally, in DLS an increase of the hydrodynamic radius (R_H) from 11 to 38 nm was observed after shell formation (Figure S3). We attribute this significant increase in size to multilayer formation and chain expansion of the grafted polymers.

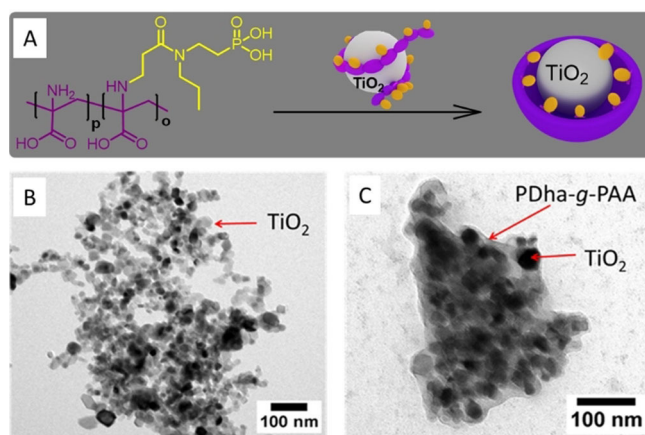


Figure 2. Preparation of PDha-*g*-PAA@TiO₂ core-shell hybrid materials (A), TEM images of TiO₂ (B) and PDha-*g*-PAA@TiO₂ with 15:1 (w/w, polymer/TiO₂) as initial ratio of PDha-*g*-PAA/TiO₂.

[Mo₃S₁₃]²⁻ as cocatalyst modification

To further overcome the recombination of photoexcited carriers, cocatalyst modification was explored for the PDha-*g*-PAA@TiO₂ core-shell hybrid system. Thereby, as a co-catalyst we used [Mo₃S₁₃]²⁻ clusters in accordance with our earlier work.^[16] Hereby, PDha-*g*-PAA on one hand solubilizes negatively charged molybdenum sulfide, and on the other hand is anchored on the surface of the TiO₂ nanoparticles (Figure 3A), therefore bringing both building blocks in close proximity while at the same time mediating solubility.

The resulting [Mo₃S₁₃]²⁻@PDha-*g*-PAA and [Mo₃S₁₃]²⁻@PDha-*g*-PAA@TiO₂ hybrid materials were characterized via DLS and TEM (Figure 3 and Figure S3, S4). TEM data indicates small aggregates with the size of only a few nm for [Mo₃S₁₃]²⁻@PDha-*g*-PAA (Figure 3B). After successful solubilisation of [Mo₃S₁₃]²⁻, TiO₂ NPs were added before further sonication and the resulting three-component hybrid material ([Mo₃S₁₃]²⁻@PDha-*g*-PAA₁₅@TiO₂) was subjected to TEM investigations (Figure 3C, D and Figure S9), where in addition to the above-described core-shell nanoobjects additional dark spots with different contrast could be found. We ascribe these likely to the presence of the co-catalyst as schematically shown in Figure 3A and Figure S8. However, DLS reveals a significant increase of the R_H of the three-component hybrid material compared to PDha-*g*-PAA@TiO₂ (15 w/w) from 38 to 82 nm, which could be the result of multilayer formation, chain expansion, and some secondary aggregation taking place.

In addition, ζ -potential measurements were carried out and while the overall charge of the TiO₂ NP was found to be slightly negative with -8 ± 2 mV, it decreased to -20 ± 1 after addition of the graft copolymer. We ascribe this to the negatively charged carboxylic acid and phosphonic acid groups. After decoration of the core-shell material with anionic [Mo₃S₁₃]²⁻ the ζ -potential became $-32 \pm$ and finally -37 ± 1 after attachment of EY, indicating successive incorporation of the different compounds. This is noteworthy as electrostatic repulsion might also be expected—nevertheless, additional (attractive) interactions, for example, with exposed -NH₃⁺ functional groups from the PDha backbone or of hydrophobic nature seem to favor binding of the individual components. Indeed, the amine groups of the polyampholytic backbone should be protonated at the corresponding pH of 7–8, although an overall negative charge is observed.^[21c,22a,29]

In order to further investigate the interactions between PDha-*g*-PAA with [Mo₃S₁₃]²⁻ and TiO₂, X-ray photoelectron spectroscopy (XPS) was used. The C 1s, P 2p, Mo 3d, Ti 2p, N 1s, and O 1s spectra obtained by XPS for different samples are shown in Figure 3E–G and Figures S5, S6. In the Ti 2p spectra, the doublet was assigned to TiO₂, with Ti 2p_{3/2} at a binding energy of ≈ 459 eV and Ti 2p_{1/2} at a binding energy of ≈ 464.5 eV. The binding energy difference of 5.5 eV between those two peaks of TiO₂ corresponds well to literature values (ΔE from 5.5 to 5.8 eV).^[30] Following grafting of PDha-*g*-PAA, no significant changes are observed in the Ti 2p spectrum. After grafting of the polymer, a P 2p signal was detected, which was not observed for the TiO₂ reference particles. This

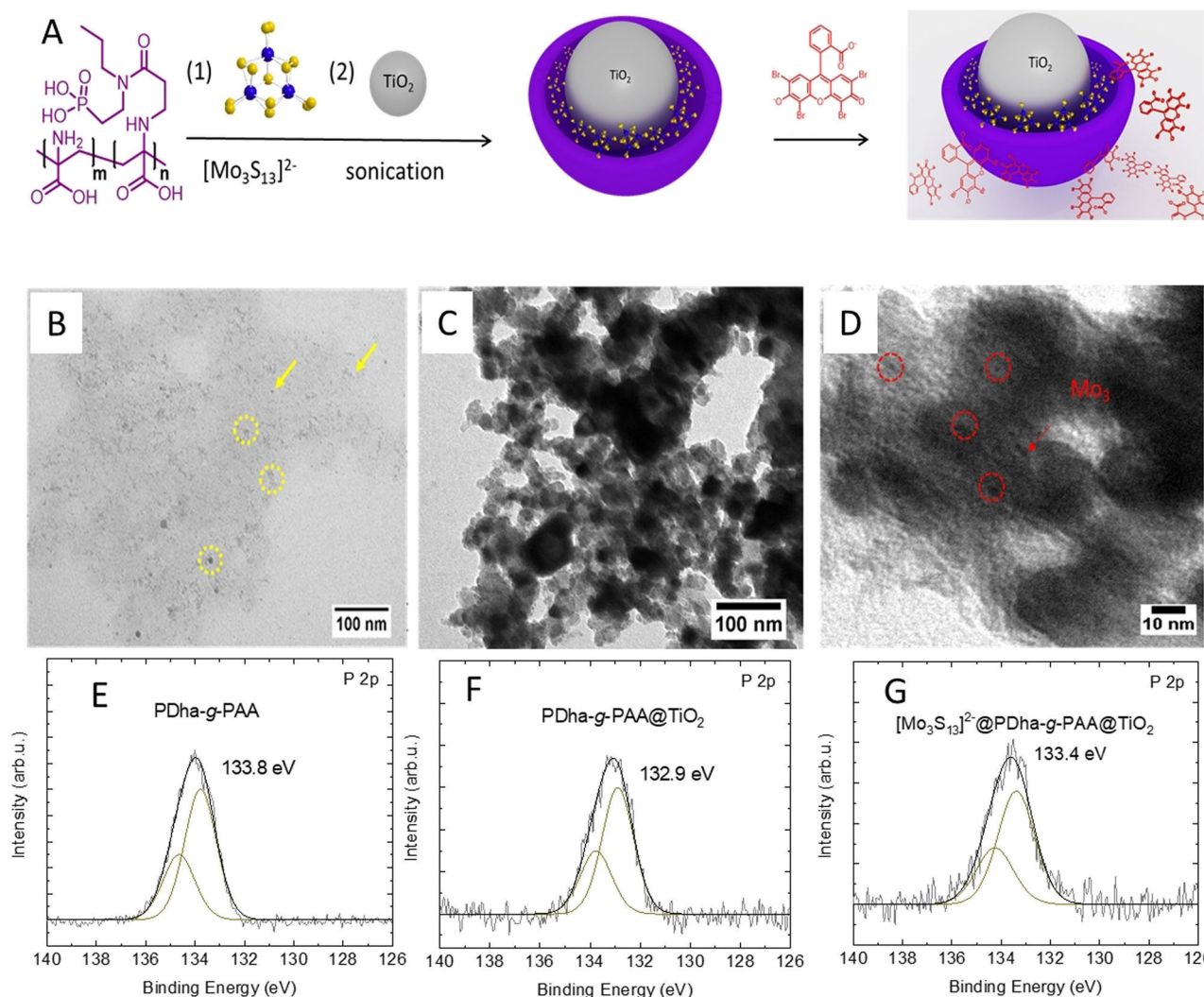


Figure 3. (A): Preparation route of $[\text{Mo}_3\text{S}_{13}]^{2-}@\text{PDha-g-PAA}@\text{TiO}_2$, TEM images of $[\text{Mo}_3\text{S}_{13}]^{2-}@\text{PDha-g-PAA}$ (B), and (C and D): $[\text{Mo}_3\text{S}_{13}]^{2-}@\text{PDha-g-PAA}@\text{TiO}_2$ and (E–G): XPS spectra of P 2p of PAA in PDha-g-PAA (E), PDha-g-PAA@TiO₂ (F), and (G) $[\text{Mo}_3\text{S}_{13}]^{2-}@\text{PDha-g-PAA}@\text{TiO}_2$.

confirms the presence of the phosphonic acids on the modified TiO₂ particles. Interestingly, the binding energy of phosphonic acid is shifted towards lower binding energies upon grafting onto TiO₂ from 133.8 eV for free PDha-g-PAA to 132.9 and 133.4 eV for PDha-g-PAA@TiO₂ and $[\text{Mo}_3\text{S}_{13}]^{2-}@\text{PDha-g-PAA}@\text{TiO}_2$, respectively (Figure 3 E–G). The observed downshift is another indication for successful grafting using phosphonic acid as anchoring group.^[30a,31]

Visible-light driven hydrogen evolution

Light-driven catalytic H₂ evolution performances of the samples were evaluated in the presence of TEOA (0.5 M) as sacrificial reagent under LED light irradiation (530 nm (with ± 50 nm; 281 mW; 330 mA; 3.1 V) in a 3D-printed irradiation reactor with a fan (Figure S1). To investigate the effect of each compound of our system different tests were made. Figure 4 A shows the time courses of H₂ production for TiO₂, TiO₂/EY, and EY/PDha-g-PAA/TiO₂ with different weight percent (wt%) of polymer. TiO₂ without EY and physical mixtures of TiO₂ with EY show no or

trace H₂ evolution activity under these conditions. We could explain this by inactivity of TiO₂ under visible light irradiation and the lack of firmly bound EY to the TiO₂ surface.^[32] Besides low loading of TiO₂ via a weak ester-like linkage, physically adsorbed dyes tend to desorb into the solution during irradiation, leading to quick degradation due to the formation of unstable anion radicals (EY⁻), and decreasing efficiency in H₂ evolution catalysis. In sharp contrast, coating TiO₂ with PDha-g-PAA significantly increased the H₂ production under visible light. Overall, during irradiation, EY/PDha-g-PAA/TiO₂ with 5:1 and 15:1 of PDha-g-PAA to TiO₂ (w/w) exhibits high stability for hydrogen production with average rates of 0.301 and 0.276 mmol g⁻¹ h⁻¹, respectively.

The enhanced activity of EY/PDha-g-PAA/TiO₂ is attributed to an effective EY loading by PDha-g-PAA and stable fixation of EY within the polyampholyte shell. The maximum loading amount of EY by PDha-g-PAA and TiO₂ NPs was evaluated by a UV/Vis study (Figure S7 and Table S1). Our data revealed capacity values of 151 μg mg⁻¹ for TiO₂, and 102 and 76 μg mg⁻¹ for EY/PDha-g-PAA/TiO₂ with 5:1 and 15:1 (w/w) of graft copo-

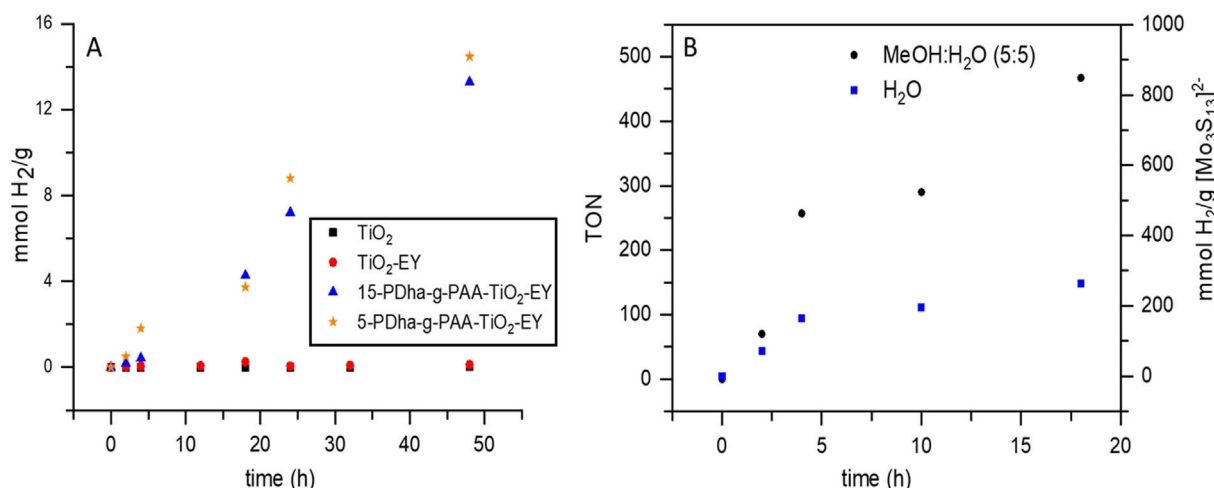


Figure 4. Hydrogen evolution rates for (A): TiO₂ (300.0 μmol L⁻¹), TiO₂/EY (20.0 μmol), and EY/PDha-*g*-PAA/TiO₂ with different initial weight percent (5 and 15 w/w) of PDha-*g*-PAA to TiO₂ in water and (B): Hydrogen evolution rates and the turnover number (TON, is defined as moles of hydrogen produced to moles of [Mo₃S₁₃]²⁻ (3 μmol L⁻¹)) of EY/PDha-*g*-PAA/(TiO₂/[Mo₃S₁₃]²⁻) with 5:1 w/w initial weight (PDha-*g*-PAA to TiO₂) in water and mixture of water/methanol under visible-light irradiation (λ > 520 nm), with TEOA (0.5 M) as sacrificial donor.

lymer, respectively. The maximum loading capacity for the EY/PDha-*g*-PAA/TiO₂ coating material resembled the capacity of PDha-*g*-PAA as well, whereas it was slightly lower compared to pristine TiO₂, probably due to the rather high surface area of TiO₂. Nevertheless, this might also enhance the fast decomposition of dye during irradiation, leading to lower hydrogen evaluation rates. On the other hand, although PDha-*g*-PAA/TiO₂ shows lower capacity for EY adsorption, it is seemingly enough adsorbed and stable to inject the electron through the graft copolymer shell to the TiO₂ core.

For improving the performance of PDha-*g*-PAA/TiO₂ core-shell hybrids, additional loading with thiomolybdate [Mo₃S₁₃]²⁻ nanoclusters as a molecular mimic of MoS₂ edge sites was investigated. Hereby, PDha-*g*-PAA was used first to solubilize [Mo₃S₁₃]²⁻ and afterwards PDha-*g*-PAA/[Mo₃S₁₃]²⁻ was grafted onto TiO₂ NPs as described above (Figure 3A). However, EY/TiO₂/[Mo₃S₁₃]²⁻ were also physically mixed as control experiment and here no hydrogen evolution could be observed under the conditions reported. In contrast, under optimum reaction conditions for the EY/PDha-*g*-PAA/(TiO₂/[Mo₃S₁₃]²⁻) system, the H₂ production under visible light irradiation was continuous during 20 h of reaction time. The H₂ evolution turnover number (TON = [H₂]/[Mo₃S₁₃]²⁻) reaches > 500 within 20 h of irradiation. As we can see from H₂ production data, the activities of H₂ production from EY/PDha-*g*-PAA/(TiO₂/[Mo₃S₁₃]²⁻) system are significantly improved compared to the system without [Mo₃S₁₃]²⁻ (e.g. EY/PDha-*g*-PAA/TiO₂), and average hydrogen production rates increased from 0.301 mmol g⁻¹ h⁻¹ (EY/PDha-*g*-PAA/TiO₂) to 23.9 mmol g⁻¹ h⁻¹ (EY/PDha-*g*-PAA/(TiO₂/[Mo₃S₁₃]²⁻)). The high catalytic activity of EY/PDha-*g*-PAA/(TiO₂/[Mo₃S₁₃]²⁻) system (increase by a factor of ≈ 79) is assigned to the high activity of the molecular co-catalyst [Mo₃S₁₃]²⁻ when compared with the rather low hydrogen evolution performance of pure TiO₂. Catalyst accessibility and surface effects might further contribute to the observed increase and will be studied in more detail.

Finally, previous studies by Streb et al.^[11c] indicated that [Mo₃S₁₃]²⁻ shows higher catalytic activity in methanol/water mixtures compared to pure water. Therefore, we also investigated our EY/PDha-*g*-PAA/(TiO₂/[Mo₃S₁₃]²⁻) system in a methanol/water (1:1) mixture under otherwise unchanged conditions. As shown in Figure 4B, we observe increased H₂ evolution rates in methanol-water as well as higher apparent stability (i.e. prolonged reactivity compared to the system in water as exclusive solvent). This is in line with previous studies, which suggested that ligand exchange on [Mo₃S₁₃]²⁻ in water is a major deactivation pathway.^[11c] Indeed, our data indicates that [Mo₃S₁₃]²⁻ in water shows promising activity but fast catalyst deactivation because of complete exchange of the terminal disulfides resulting in decreased catalytic activity. In contrast, in methanol-water mixtures, significantly higher reactivity is achieved by stabilizing highly active catalytic species. We could attribute this enhancement to partial exchange of one or two terminal disulfides with aqua ligands which leads to the formation of more active species. Compared to earlier studies where EY was covalently or electrostatically grafted to the surface of TiO₂, this work demonstrates that PDha-based polyampholytic graft copolymers are a simple, tunable, and effective method to achieve stable EY sensitization on TiO₂ with enhanced activity and stability for light-driven H₂ evolution.

Conclusion

In summary, we report the successful grafting of a tailor-made polyampholytic graft copolymer to TiO₂ nanoparticles, which enabled the binding of EY photosensitizer and [Mo₃S₁₃]²⁻ hydrogen evolution cocatalysts. Our results reveal that this is a straightforward approach for the preparation of a tunable and versatile soft matter matrix which can effectively co-integrate several molecular components relevant for light-driven catalysis. The main role of the graft copolymer is to provide close proximity and the potential to interact for all individual com-

ponents. Specifically, we find that the obvious improvement of the light-driven catalytic activity for hydrogen production was found by immobilizing $[\text{Mo}_3\text{S}_{13}]^{2-}$ clusters, reaching TONs > 500. Our strategy indicates that we can use polyampholytic graft copolymers to improve and regulate different molecular catalytic systems by immobilization on TiO_2 . This strategy introduces a system, which could be valuable for other molecular catalysts, dyes or semiconducting sensitizers.

Acknowledgements

This research was supported by the Deutsche Forschungsgemeinschaft (DFG, project SCHA1640/18-1 and TRR234 "Catalight", Project No. 364549901, projects A5, B5, and Z2). We acknowledge Peggy Laudeley for SEC analysis, as well as Jonas Eichhorn, Peter Mons and the NMR department at Friedrich-Schiller-University Jena for their support. We thank Martin Schulz for GC hydrogen quantification and further, we are thankful for the cryo-TEM/TEM facilities of the Jena Center for Soft Matter (JCSM), which were established with a grant from the German Research Council (DFG) and the European Fonds for Regional Development (EFRE). Open access funding enabled and organized by Projekt DEAL.

Conflict of interest

The authors declare no conflict of interest.

Keywords: hybrid materials · hydrogen evolution reaction · photocatalysis · polyampholytes · thiomolybdates

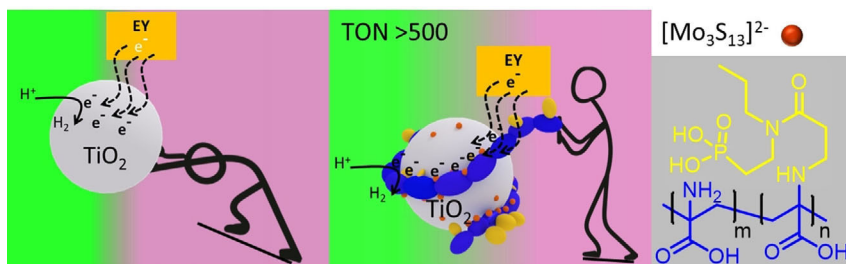
- [1] a) Z. Chen, X. Duan, W. Wei, S. Wang, B.-J. Ni, *J. Mater. Chem. A* **2019**, *7*, 14971–15005; b) M. Balat, *Int. J. Hydrogen Energy* **2008**, *33*, 4013–4029; c) J. O. Abe, A. P. I. Popoola, E. Ajenifuja, O. M. Popoola, *Int. J. Hydrogen Energy* **2019**, *44*, 15072–15086.
- [2] Y. Zhang, Y.-J. Heo, J.-W. Lee, J.-H. Lee, J. Bajgai, K.-J. Lee, S.-J. Park, *Catalysts* **2018**, *8*, 655.
- [3] A. Fujishima, K. Honda, *Nature* **1972**, *238*, 37–38.
- [4] a) J. Ran, J. Zhang, J. Yu, M. Jaroniec, S. Z. Qiao, *Chem. Soc. Rev.* **2014**, *43*, 7787–7812; b) C. Wu, J. Zhang, X. Tong, P. Yu, J.-Y. Xu, J. Wu, Z. M. Wang, J. Lou, Y.-L. Chueh, *Small* **2019**, *15*, 1900578; c) Y. Yuan, H. Lu, Z. Ji, J. Zhong, M. Ding, D. Chen, Y. Li, W. Tu, D. Cao, Z. Yu, Z. Zou, *Chem. Eng. J.* **2015**, *275*, 8–16.
- [5] L. Li, Y. Zhu, N. Gong, W. Zhang, W. Peng, Y. Li, F. Zhang, X. Fan, *Int. J. Hydrogen Energy* **2020**, *45*, 2689–2698.
- [6] P. Wang, S. Guo, H.-J. Wang, K.-K. Chen, N. Zhang, Z.-M. Zhang, T.-B. Lu, *Nat. Commun.* **2019**, *10*, 3155.
- [7] H. Xing, S. Teng, Z. Xing, L. Bi, Q. Bu, T. Xie, W. Yang, *Appl. Surf. Sci.* **2020**, *532*, 147000.
- [8] X. Liu, Y. Li, S. Peng, H. Lai, Z. Yi, *J. Photonics Energy* **2016**, *6*, 046501.
- [9] M. Chauhan, K. Soni, P. E. Karthik, K. P. Reddy, C. S. Gopinath, S. Deka, *J. Mater. Chem. A* **2019**, *7*, 6985–6994.
- [10] a) N. Romero, R. B. Guerra, L. Gil, S. Drouet, I. Salmeron-Sánchez, O. Illa, K. Philippot, M. Natali, J. García-Antón, X. Sala, *Sustainable Energy Fuels* **2020**, *4*, 4170–4178; b) H. Lai, X. Liu, F. Zeng, G. Peng, J. Li, Z. Yi, *ACS Omega* **2020**, *5*, 2027–2033; c) S. Li, T. Pu, J. Wang, X. Fang, Y. Liu, S. Kang, L. Cui, *Int. J. Hydrogen Energy* **2018**, *43*, 16534–16542.
- [11] a) M.-L. Grutza, A. Rajagopal, C. Streb, P. Kurz, *Sustainable Energy Fuels* **2018**, *2*, 1893–1904; b) Y. Lei, M. Yang, J. Hou, F. Wang, E. Cui, C. Kong, S. Min, *Chem. Commun.* **2018**, *54*, 603–606; c) M. Dave, A. Rajagopal, M. Damm-Ruttensperger, B. Schwarz, F. Nägele, L. Daccache, D. Fantauzzi, T. Jacob, C. Streb, *Sustainable Energy Fuels* **2018**, *2*, 1020–1026; d) M. Dinari, A. Nabiyan, A. A. Ensafi, M. Jafari-Asl, *RSC Adv.* **2015**, *5*, 100996–101005; e) A. Baloglou, M. Plattner, M. Ončák, M.-L. Grutza, P. Kurz, M. K. Beyer, *Angew. Chem. Int. Ed.* **2021**, *60*, 5074–5077; *Angew. Chem.* **2021**, *133*, 5133–5137.
- [12] A. Rajagopal, F. Venter, T. Jacob, L. Petermann, S. Rau, S. Tschierlei, C. Streb, *Sustainable Energy Fuels* **2019**, *3*, 92–95.
- [13] a) Y. Ouyang, Q. Li, L. Shi, C. Ling, J. Wang, *J. Mater. Chem. A* **2018**, *6*, 2289–2294; b) T. Yang, M. Du, H. Zhou, M. Zhang, M. Zou, *Electrochim. Acta* **2015**, *167*, 48–54; c) N. Coutard, N. Kaeffer, V. Artero, *Chem. Commun.* **2016**, *52*, 13728–13748.
- [14] a) J. Willkomm, N. M. Muresan, E. Reisner, *Chem. Sci.* **2015**, *6*, 2727–2736; b) N. M. Muresan, J. Willkomm, D. Mersch, Y. Vaynzof, E. Reisner, *Angew. Chem. Int. Ed.* **2012**, *51*, 12749–12753; *Angew. Chem.* **2012**, *124*, 12921–12925.
- [15] J. J. Leung, J. Warnan, D. H. Nam, J. Z. Zhang, J. Willkomm, E. Reisner, *Chem. Sci.* **2017**, *8*, 5172–5180.
- [16] I. Romanenko, A. Rajagopal, C. Neumann, A. Turchanin, C. Streb, F. H. Schacher, *J. Mater. Chem. A* **2020**, *8*, 6238–6244.
- [17] A. S. Weingarten, R. V. Kazantsev, L. C. Palmer, M. McClendon, A. R. Koltonow, A. P. S. Samuel, D. J. Kiebała, M. R. Wasielewski, S. I. Stupp, *Nat. Chem.* **2014**, *6*, 964–970.
- [18] H. Sai, A. Erbas, A. Dannenhoffer, D. Huang, A. Weingarten, E. Siimets, K. Jang, K. Qu, L. C. Palmer, M. Olvera de la Cruz, S. I. Stupp, *J. Mater. Chem. A* **2020**, *8*, 158–168.
- [19] Z. Hu, X. Zhang, Q. Yin, X. Liu, X.-f. Jiang, Z. Chen, X. Yang, F. Huang, Y. Cao, *Nano Energy* **2019**, *60*, 775–783.
- [20] A. Nabiyan, M. Schulz, C. Neumann, B. Dietzek, A. Turchanin, F. H. Schacher, *Eur. Polym. J.* **2020**, *140*, 110037.
- [21] a) P. Biehl, M. von der Luhe, F. H. Schacher, *Macromol. Rapid Commun.* **2018**, *39*, 1800017; b) P. Biehl, P. Wiemuth, J. G. Lopez, M. C. Barth, A. Weidner, S. Dutz, K. Peneva, F. H. Schacher, *Langmuir* **2020**, *36*, 6095–6105; c) J. B. Max, K. Kowalczyk, M. Köhler, C. Neumann, F. Pielenz, L. V. Sigolaeva, D. V. Pergushov, A. Turchanin, F. Langenhorst, F. H. Schacher, *Macromolecules* **2020**, *53*, 4511–4523.
- [22] a) J. B. Max, D. V. Pergushov, L. V. Sigolaeva, F. H. Schacher, *Polym. Chem.* **2019**, *10*, 3006–3019; b) J. B. Max, A. Nabiyan, J. Eichhorn, F. H. Schacher, *Macromol. Rapid. Commun.* DOI: <https://doi.org/10.1002/marc.202000671>.
- [23] D. Costabel, A. Skabeev, A. Nabiyan, Y. Luo, J. Max, A. Rajagopal, D. Kowalczyk, B. Dietzek, M. Wächtler, H. Görls, D. Ziegenbalg, Y. Zagranyski, C. Streb, F. H. Schacher, K. Peneva, *Chem. Eur. J.* **2021**, *27*, 4081–4088.
- [24] a) Y. Li, M. Guo, S. Peng, G. Lu, S. Li, *Int. J. Hydrogen Energy* **2009**, *34*, 5629–5636; b) X. Liu, W. Huang, Y. Lei, Y. Li, Y. Xue, F. Wang, S. Min, *New J. Chem.* **2018**, *42*, 6631–6635; c) Y. Li, C. Xie, S. Peng, G. Lu, S. Li, *J. Mol. Catal. A* **2008**, *282*, 117–123.
- [25] X. Liu, L. Zhao, H. Lai, Y. Wei, G. Yang, S. Yin, Z. Yi, *RSC Adv.* **2017**, *7*, 46738–46744.
- [26] N. Hu, A. Peralta, S. Roy Choudhury, R. Zhang, R. M. Davis, J. S. Riffle, *Polymer* **2015**, *65*, 124–133.
- [27] a) M. von der Lühe, U. Gunther, A. Weidner, C. Grafe, J. H. Clement, S. Dutz, F. H. Schacher, *RSC Adv.* **2015**, *5*, 31920–31929; b) M. von der Lühe, A. Weidner, S. Dutz, F. H. Schacher, *ACS Appl. Nano Mater.* **2018**, *1*, 232–244.
- [28] K. Wang, L. Yang, W. Wei, L. Zhang, G. Chang, *J. Membr. Sci.* **2018**, *549*, 23–27.
- [29] U. Günther, L. V. Sigolaeva, D. V. Pergushov, F. H. Schacher, *Macromol. Chem. Phys.* **2013**, *214*, 2202–2212.
- [30] a) C. Viornery, Y. Chevolut, D. Léonard, B.-O. Aronsson, P. Péchy, H. J. Mathieu, P. Descouts, M. Grätzel, *Langmuir* **2002**, *18*, 2582–2589; b) J. L. Ong, C. W. Prince, L. C. Lucas, *J. Biomed. Mater. Res.* **1995**, *29*, 165–172.
- [31] E. S. Gawalt, G. Lu, S. L. Bernasek, J. Schwartz, *Langmuir* **1999**, *15*, 8929–8933.
- [32] R. Abe, K. Hara, K. Sayama, K. Domen, H. Arakawa, *J. Photochem. Photobiol. A* **2000**, *137*, 63–69.

Manuscript received: January 9, 2021

Accepted manuscript online: February 5, 2021

Version of record online: ■■■■■ 0000

FULL PAPER



A tailor-made polyampholyte matrix enables effective interaction of different components in light-driven hydrogen evolution reaction, in our case TiO₂ nanoparticles, thiomolybdate [Mo₃S₁₃]²⁻

clusters, and Eosin Y as photosensitizer. Altogether, high photocatalytic activity for H₂ generation under visible-light irradiation was observed for well-defined hybrid materials.

 Photocatalysis

A. Nabiyan, J. B. Max, C. Neumann, M. Heiland, A. Turchanin, C. Streb, F. H. Schacher*

■ ■ - ■ ■

Polyampholytic Graft Copolymers as Matrix for TiO₂/Eosin Y/[Mo₃S₁₃]²⁻ Hybrid Materials and Light-Driven Catalysis



Chemistry–A European Journal

Supporting Information

Polyampholytic Graft Copolymers as Matrix for TiO₂/Eosin Y/[Mo₃S₁₃]²⁻ Hybrid Materials and Light-Driven Catalysis

Afshin Nabiyan,^[a, b, c] Johannes Bernhard Max,^[a, b, c] Christof Neumann,^[b, c, d]
Magdalena Heiland,^[e] Andrey Turchanin,^[b, c, d] Carsten Streb,^[e] and
Felix Helmut Schacher*^[a, b, c]

Experimental Part

Chemicals

Diethyl vinylphosphonate (>98 %) was purchased from TCI Chemicals and acryloyl chloride (96 %) from Alfa Aesar, ammonium polysulfide solution from Fisher Chemical™ and triethyl amine (≥ 99.0 %) from CHEMSOLUTE®. Triethanolamine (98 %), titanium (IV) oxide (≥99.5 %, 21 nm primary particle size (TEM)), bromotrimethylsilane (97%) and propylamine (98 %), Eosin Y disodium salt (≥85 %) and $(\text{NH}_4)_6\text{Mo}_7\text{O}_{24} \cdot 4\text{H}_2\text{O}$ (99.98 %) were purchased from Sigma-Aldrich. All chemicals were used as received.

PDha_{0.90}-*stat*-PAMA_{0.10} was synthesized as described earlier starting from PtBAMA with a molecular weight of $M_n = 13\,200$ g/mol and $\bar{D} = 2.55$ (THF SEC, PS calibration).¹

Analytical methods

Nuclear magnetic resonance (NMR) spectroscopy

¹H- and ¹³C-NMR spectra were performed on a Bruker AC 300 MHz using CDCl₃, MeOD-d₄ and D₂O/NaOD as solvents at a temperature of 298 K. The spectra were referenced by using the residual signal of the deuterated solvent.

Size exclusion chromatography (SEC)

Size exclusion chromatography (SEC) measurements were made on a Shimadzu system equipped with a G1330B pump, a G1362A refractive index detector, a DAD G1315D UV-vis detector and a Polymer Standards Service GmbH (Mainz, Germany) SDV guard/100/1000/100 000 °A, 5 mm column (8 x 300 mm). As eluent THF was used with a flow rate of 1 mL/min. The temperature of the column oven was set to 30 °C and a calibration with low dispersity PS standards was used (M_n ranging from 474 to 2 520 000 g/mol).

SEC measurements in DMSO were performed on a Jasco instrument using DMSO + 0.5 % LiBr as solvent at a flow rate of 0.5 ml/min at 65 °C and Pullulan calibration. It was equipped with PSS NOVEMA 3000 Ångström / 300 Ångström columns, a RI-930 detector as well as a PU-980 pump.

Dynamic Light Scattering (DLS)

DLS measurements were performed using an ALV laser CGS3 Goniometer equipped with a 633 nm HeNe laser (ALV GmbH, Langen, Germany) at 25 °C and at a detection angle of 90°. The CONTIN analysis of the obtained correlation functions was performed using the ALV 7002 FAST Correlator Software.

Transmission Electron Microscopy (TEM)

TEM images were acquired with a 200 kV FEI Tecnai G2 20 equipped with a 4k x 4k Eagle HS CCD and a 1k x 1k Olympus MegaView camera for overview images.

Laser Microelectrophoresis (Zeta-potential measurements)

Electrophoretic mobilities were measured on a ZetaSizer Nano ZS from Malvern via M3-PALS technique with a laser beam at 633 nm. The detection angle was 13°. The samples were prepared by titration of the polymer in 0.1 M NaOH (0.2 g/L) with 0.1 M HCl and 1 mL of the solution was taken at the desired pH values. The titration and pH detection was performed on a Metrohm 765

Dosimat titrator with a Greisinger electronic GMH3539 digital pH-/mV-electrode with a thermometer.

Adsorption and Desorption Studies

An aqueous Eosin Y solution (0.01 mmol/mL) was added to 2 mg/mL of TiO₂ or PDha-*g*-PAA@TiO₂. The resulting suspension was shaken intensively and kept overnight. The following day the particles were removed by centrifugation (14000 RPM), and the supernatant was investigated by UV-vis spectroscopy. In case of solutions with too high concentration, a 10-fold dilution was carried out. The particles were then washed at least 3 times with 1 mL of solution per washing step to remove unbound dye.

X-ray Photoelectron Spectroscopy (XPS)

XPS was performed using a UHV multiprobe system (Scienta Omicron) with a monochromatic X-ray source (Al K_α) and an electron analyzer (Argus CU) with a 0.6 eV spectral energy resolution. For individual samples, charge compensation during data acquisition was realized by an electron flood gun (NEK150, Staib, Germany) at 6 eV and 50 μA. The spectra were fitted using Voigt functions after background subtraction. The spectra were calibrated using the Si 2p peak at 103.5 eV (SiO₂) and the C 1s peak (C-C, 285.5 eV), respectively.

UV-vis spectroscopy

UV-vis measurements were performed on an Agilent Cary 60 spectrometer in a Hellma quartz glass cuvette with a pathlength of 10 mm at room temperature in solvent. The absorbance was measured in a range from 200 nm to 800 nm in 5 nm steps.

Thermogravimetric analysis (TGA)

TGA measurements were carried out under air flow in a Perkin Elmer TGA800 device by heating from 30 °C to 850 °C with a heating rate of 10 K/min.

Ultrasonication (Ultrasonication Finger)

Ultrasonication was carried out using a Sonic VibraCellVC505 500 Watt Ultrasonic Processor. To reduce high sound, a Sound Abating Enclosure was used.

Light-driven catalysis

The light-driven catalytic hydrogen evolution experiments were performed in a 5 or 10 mL Pyrex flask, the openings of which were sealed with a silicone rubber septum, at ambient temperature and atmospheric pressure. A LED light (with max λ = 530 nm (with ± 50 nm; 281 mW; 330 mA; 3.1 V) in a 3D-printed irradiation reactor with a fan) was used as a visible light source to trigger the catalytic reaction and was positioned 2 cm away from the reactor. In a typical light-driven catalytic experiment, the desirable amount of catalyst was dissolved in 2 mL of a mixed aqueous solution containing 0.5 TEOA, and the system was then bubbled with nitrogen for 20 min to remove the dissolved oxygen and create anaerobic conditions. A 0.2 mL sample of the generated gas was collected intermittently through the septum, and the hydrogen content was analyzed by gas chromatography with a thermal conductivity detector (TCD). The turnover number (TON) is determined as moles of hydrogen produced to initial moles of [Mo₃S₁₃]²⁻ (C: 3.0 μmol/mL as initial amount that was used in formation of [Mo₃S₁₃]²⁻@PDha-*g*-PAA@TiO₂).

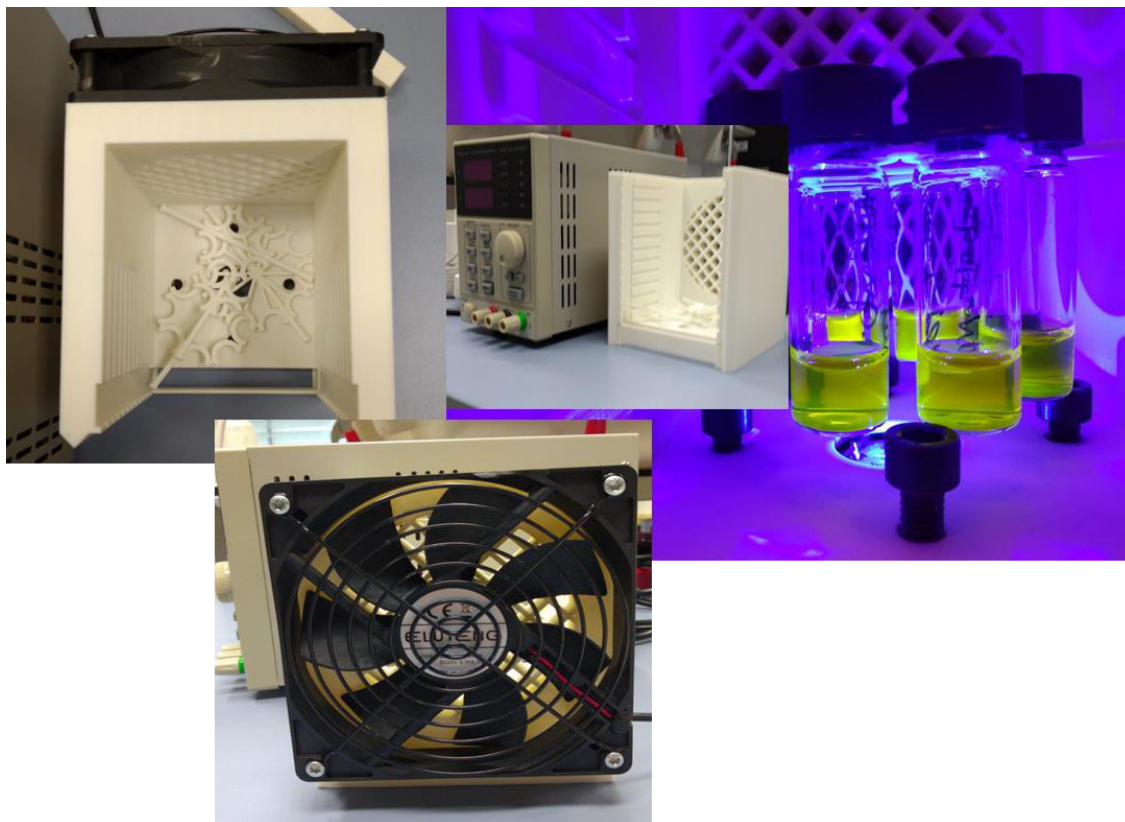


Figure S1: Setup for the light-driven catalytic hydrogen production experiments

Synthesis

Synthesis of PAA in accordance with a literature protocol²

N-propyl amine (1.00 g; 17 mmol, 1 eq) and water (20% v.%) were put in an oil bath at 45 °C and afterwards diethyl vinyl phosphate (2.36 g, 14 mmol, 0.85 eq) was added dropwise. The solution was stirred for 18 h before dichloromethane (DCM, ~ 20 ml) was added. Afterwards the reaction mixture was dried with Na₂SO₄, filtrated and the solvent evaporated under vacuum.

The reaction product (1.5 g, 7 mmol, 1 eq) and NEt₃ (1.0 g, 10 mmol, 1.5 eq) were dissolved in distilled DCM (20 ml) and cooled in an ice bath. Acrolyl chloride (0.8 g, 9 mmol, 1.3 eq) was added dropwise and the ice bath removed afterwards. The reaction mixture was stirred for 18 h before it was diluted with more DCM (30 ml). It was washed with 0.1 M NaOH (3 x 30 ml), 0.2 M HCl (2 x 30 ml) and water (2 x 30 mL), dried over Na₂SO₄ and the solvent evaporated under vacuum. The product (1) was obtained as an orange, viscous oil (85 %).

¹H NMR (300 MHz, CDCl₃, δ) = 6.69 – 6.44 (m, CH₂=CH-), 6.41 – 6.21 (m, -CH=CH₂), 5.70 – 5.58 (m, -CH=CH₂), 4.26 – 3.98 (P-O-CH₂-), 3.76-3.50 (m, -N-CH₂), 3.42 – 3.23 (m, -N-CH₂), 2.25 – 1.89 (m, -CH₂-CH₂-CH₃), 1.76 – 1.52 (m, -CH₂-P=O), 1.45 – 1.19 (m, -CH₂-CH₃), 1.03- 0.80 (m, -CH₂-CH₃) ppm.

Afterwards, the ethyl ester was cleaved. Therefore 1 was dissolved in anhydrous DCM under Ar atmosphere and TMSBr added through a syringe. The reaction mixture was stirred at 21 °C for 24 h. Remaining TMSBr and DCM were removed *via* evaporation and methanol was added. Then

the reaction mixture was stirred at 21°C for another 24 h. After drying under vacuum for several hours the product was obtained as an orange, waxy solid (90%).

^1H NMR (300 MHz, MeOD, δ) = 6.76 – 6.56 (m, $\text{CH}_2=\text{CH}-$), 6.23 – 5.96 (m, $-\text{CH}=\text{CH}_2$), 5.82 – 5.54 (m, $-\text{CH}=\text{CH}_2$), 3.35 - 3.20 (m, $-\text{N}-\text{CH}_2$), 3.39 – 3.19 (m, $-\text{N}-\text{CH}_2$), 1.96 – 1.72 (m, $-\text{CH}_2-\text{CH}_2-\text{CH}_3$), 1.60 – 1.33 (m, $-\text{CH}_2-\text{P}=\text{O}$), 0.94 - 0.70 (m, $-\text{CH}_2-\text{CH}_3$) ppm.

Post-polymerization modification of PDha-co-PAMA with PAA

PDha_{0.85}-*stat*-PAMA_{0.15} (100 mg) and PAA (10 eq per monomer unit) were dissolved in water (5 ml each, pH 13, KOH). Afterwards the clear solutions were mixed and placed in an oil bath at 60 °C for constant stirring. The reaction was terminated after 48 h, by adding aqueous HCl (0.5 M) until a pH of 7 was reached. Then, the crude product was dialyzed against deionized water (MWCO = 3.5 kDa) for 2 days and afterwards freeze-dried to obtain a colorless polymer powder.

PDha-co-PAMA (50 mg) was dissolved in water (10 ml, pH 13 KOH-solution) and PAA (5 eq per monomer units) was in DMSO (10 ml). The reaction mixture was stirred for 72 h at 70 °C and then it was neutralized using aqueous HCl (0.5 M). For purification, the crude product was dialyzed against deionized water (MWCO = 3.5 kDa) for 48 h and afterwards freeze-dried to obtain a slightly orange powder.

^1H -NMR (300 MHz, D₂O, δ) = 3.64 – 3.02 ($-\text{CH}_2-\text{N}-\text{C}=\text{O}-$ and $-\text{CH}_2-\text{N}-\text{C}=\text{O}-$) 2.94 – 2.08 ($-\text{C}-\text{CH}_2-$, $-\text{NH}-\text{CH}_2-$, $-\text{CH}_2-\text{CON}-$) 2.07 – 1.32 ($-\text{CH}_2-\text{CH}_3$ and $-\text{CH}_2-\text{PO}_3\text{H}_2$) 1.29 – 1.07 ($-\text{NH}-$ or $-\text{NH}_2$), 1.00 - 0.49 ($-\text{CH}_3$) ppm.

^{13}C -NMR (75 MHz, D₂O δ): 177.59 ($-\text{COOH}$), 171.94 ($-\text{CONH}-$), 62.53 - 60.25 ($-\text{HN}-\text{C}-\text{COOH}$), 49.81, 30.74, 27.28, 26.23, 21.37, 20.28 (side-chain: $-\text{CH}_2-\text{NH}$, $-\text{CH}_2-\text{PO}_3\text{H}_2$, $-\text{CH}_2-\text{N}-\text{C}=\text{O}$, $-\text{CH}_2-\text{N}-\text{C}=\text{O}$, $-\text{CH}_2-\text{CON}-$, $-\text{CH}_2-\text{CH}_3$), 45.50 – 42.20 ($-\text{C}-\text{CH}_2-$), 10.50 ($-\text{CH}_3$) ppm.

Adsorption study of Eosin Y

An aqueous Eosin Y solution (0.01 mmol/mL) was added to 1 mg/mL of TiO₂ or its compositions that were separated by centrifugation from solution. The resulting supernatant was investigated by UV-vis spectroscopy. In case of solutions that were too concentrated, a 10-fold dilution was carried out. The particles were then washed at least 3 times with 1 mL of solution per washing step to remove unbound dye.

(NH₄)₂[Mo₃S₁₃]*2H₂O was synthesized according to the literature.³ Briefly, to a solution of (NH₄)₆Mo₇O₂₄*4H₂O (4.0 g, 3.2 mmol in 20 mL water) a ammonium polysulfide solution (120 ml, 25 wt%) was added. The reaction mixture was covered and heated to 96°C without stirring for five days. Dark red crystals were isolated by filtration, washed with water, ethanol, carbon disulfide and ether before air drying. Yield: 5.6 g, dark red crystals (97.9% based on Mo).

Preparation of PDha-g-PAA@TiO₂

The desired amount of polymer was added to the target concentration of TiO₂ in water. Afterwards the mixture was placed in an ice bath. Dispersions were then formed by using an ultrasonic finger (20% power, 60 min, pulsed: 60 s on and 30 s off). For purification, the obtained core-shell hybrid solutions were dialyzed against deionized water (MWCO = 14 kDa) for 48 h.

Preparation and loading of $[\text{Mo}_3\text{S}_{13}]^{2-}$ in PDha-*g*-PAA@TiO₂

0.5 mg $[\text{Mo}_3\text{S}_{13}]^{2-}$ were first dispersed with aqueous PDha-*g*-PAA solution (1 mg/mL) with assistance of sonication (1 hour). Afterwards, the stabilized $[\text{Mo}_3\text{S}_{13}]^{2-}$ /PDha-*g*-PAA dispersion was grafted on TiO₂ nanoparticles (2 mg.mL). The grafting process was carried out by 1-hour additional sonication. For purification, the obtained hybrid solutions were dialyzed against deionized water (MWCO = 14 kDa) for 24 h.

XPS analysis

The different preparation steps were characterized using XPS. Besides the Ti 2p spectra discussed in the main paper, the TiO₂ particles show a characteristic feature at a binding energy of ~530.3 eV in the O 1s spectra, which is not present for PDha-*g*-PAA alone (Figure S6). After grafting of PDha-*g*-PAA on TiO₂, the characteristic groups of the polymer are visible in the C 1s spectra as shoulders at binding energies of ~286.6 eV (C-N, C-P) and ~ 288.5 eV (COOH, N-C=O) confirming the presence of PDha-*g*-PAA (Figure S7). Furthermore, P 2p (Figure 3) and N 1s (Figure S7) signals were detected, which were not present on the pure TiO₂ particles before. Finally, the structure of the co-catalyst Mo₃S₁₃ was characterized. The Mo 3d signal shows mainly a doublet assigned to Mo₃S₁₃ together with a small second doublet ascribed to oxidized Mo. The S 2p signal shows the typical structure for Mo₃S₁₃ with two species assigned to bridge/apical and terminal S, respectively. This is in agreement with previously published results.⁴

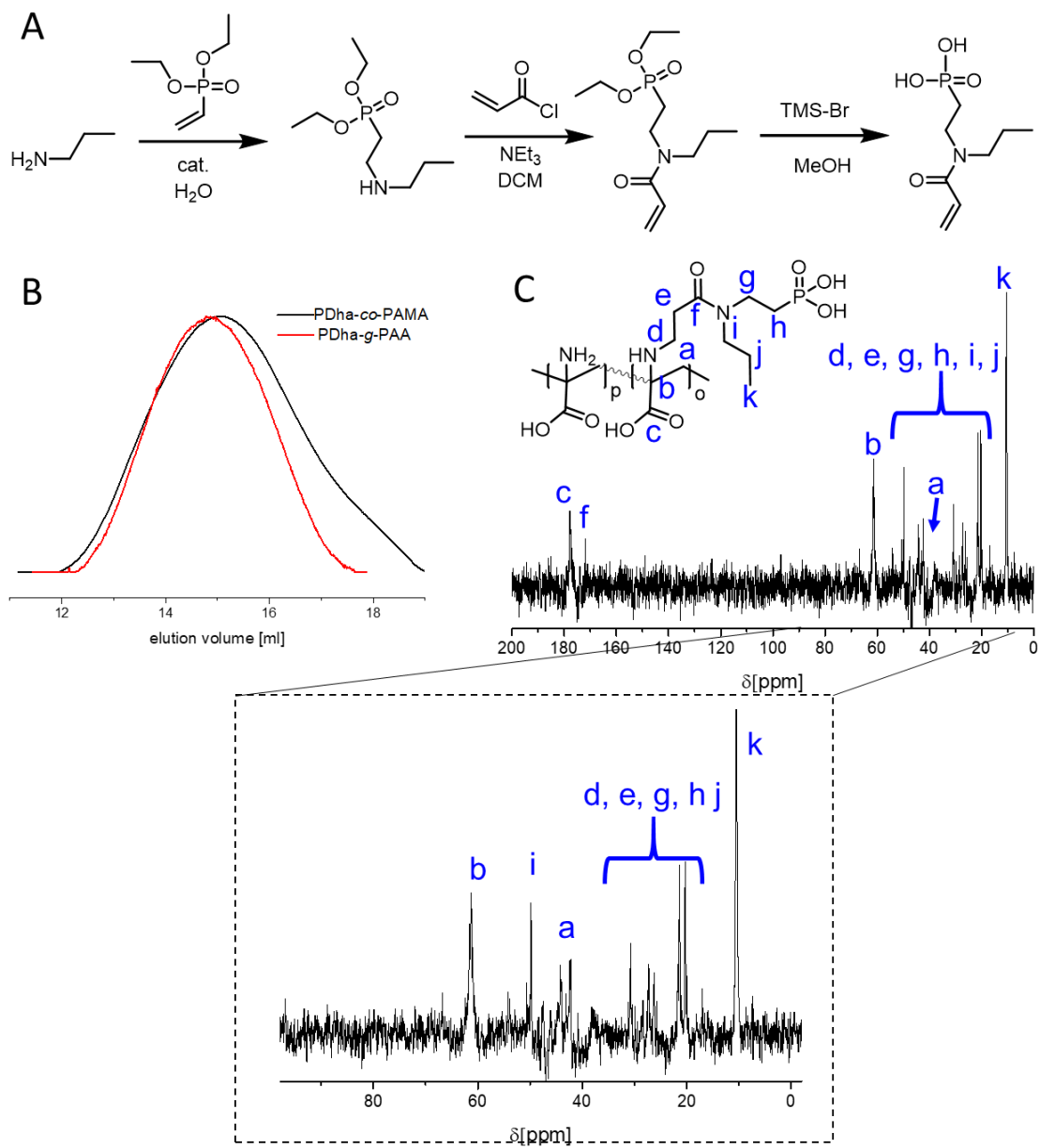


Figure S2: Synthesis of the PAA monomer (A); corresponding SEC trace of PDha-co-PAMA and PDha-g-PAA (B); ^{13}C NMR spectra of PDha-g-PAA (C).

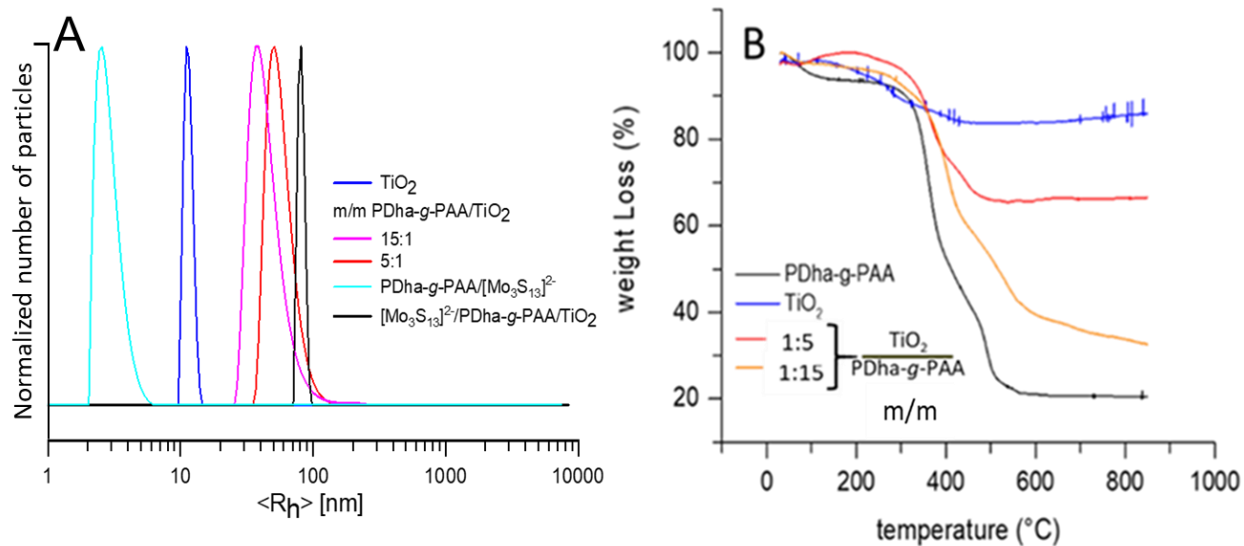


Figure S3: (A): DLS CONTIN plots of TiO_2 , PDha-g-PAA, PDha-g-PAA@ TiO_2 , $[\text{Mo}_3\text{S}_{13}]^{2-}$ @PDha-g-PAA@ TiO_2 , and $[\text{Mo}_3\text{S}_{13}]^{2-}$ @PDha-g-PAA and (A) and (B): Thermograms of TiO_2 , PDha-g-PAA, PDha-g-PAA@ TiO_2 with different ratios of added graft copolymer.

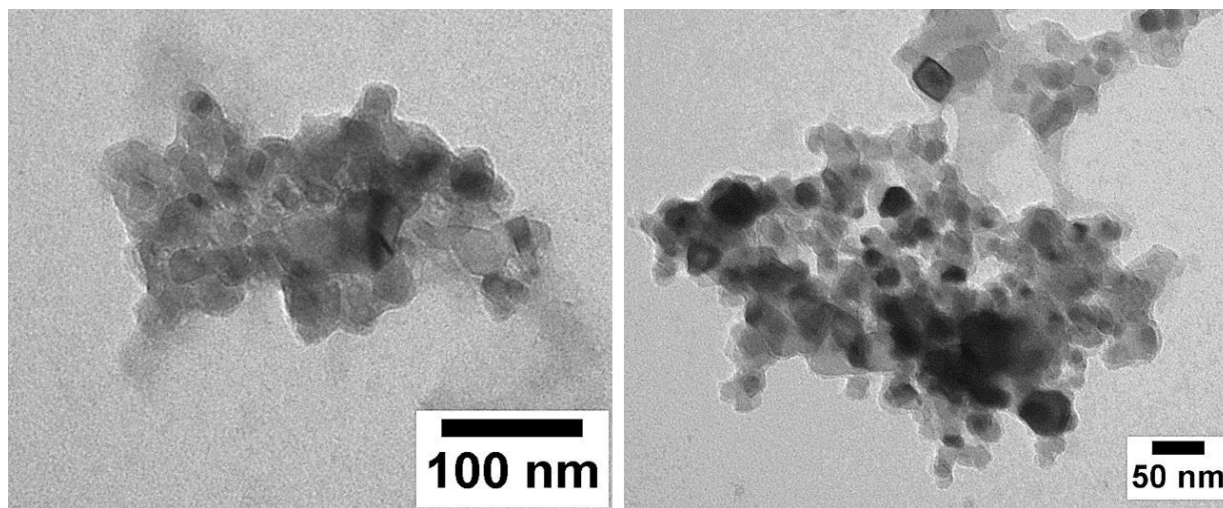


Figure S4: TEM micrographs of PDha-g-PAA@ TiO_2 with ratio of 5:1 m/m (PDha-g-PAA : TiO_2).

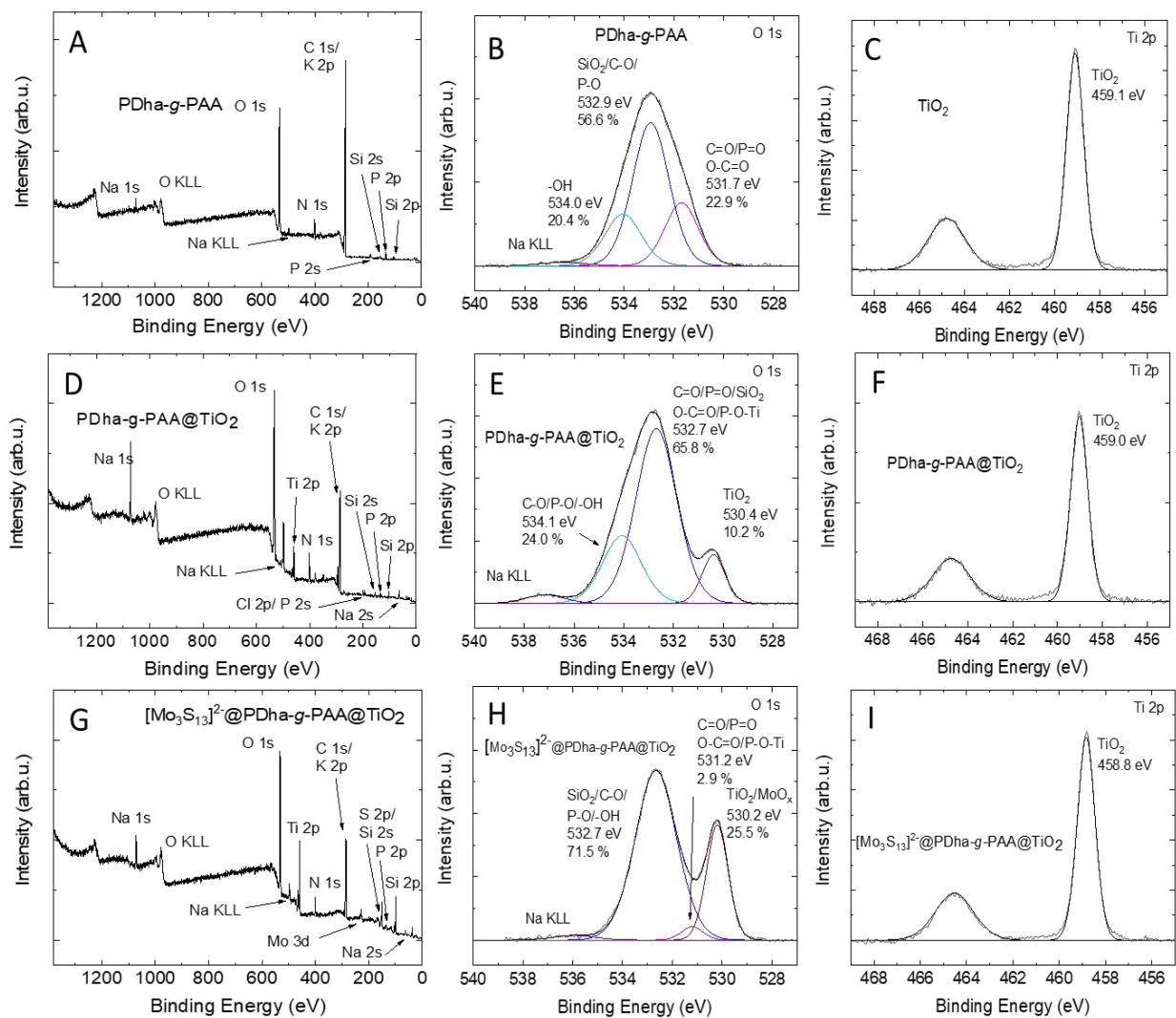


Figure S5: XPS spectra of O 1s and Ti 2p of PDha-g-PAA, PDha-g-PAA@TiO₂ (5:1) and [Mo₃S₁₃]²⁻@PDha-g-PAA@TiO₂.

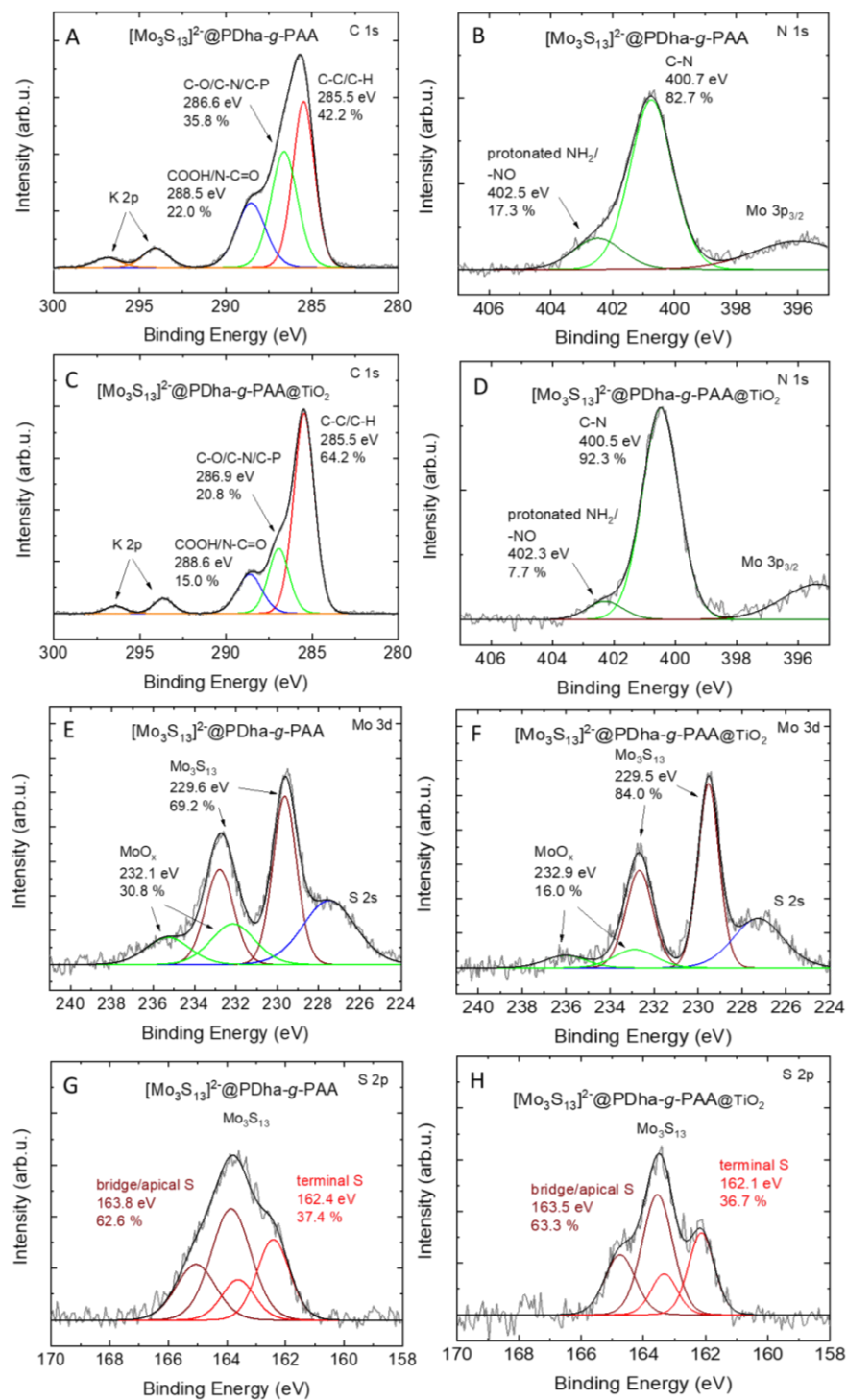


Figure S6: XPS spectra of C 1s, N 1s, Mo 3d, and S 2p of $[\text{Mo}_3\text{S}_{13}]^{2-}@PDha-g-PAA$ and $[\text{Mo}_3\text{S}_{13}]^{2-}@PDha-g-PAA@TiO_2$.

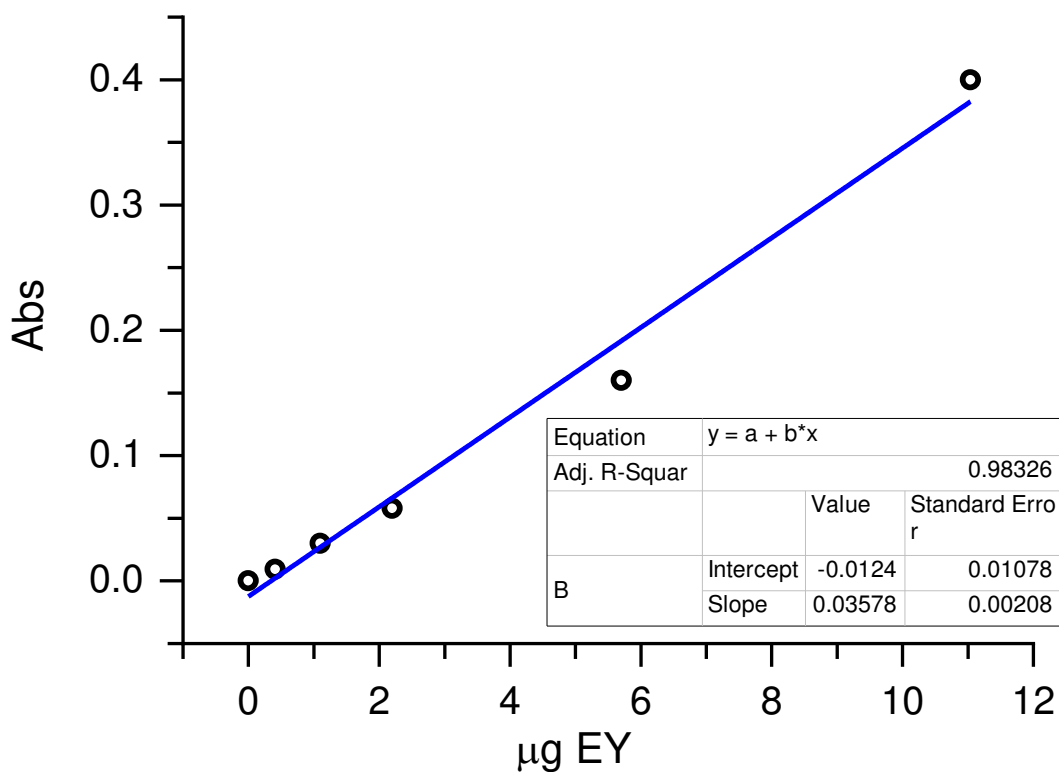
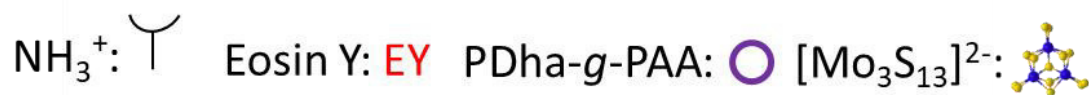
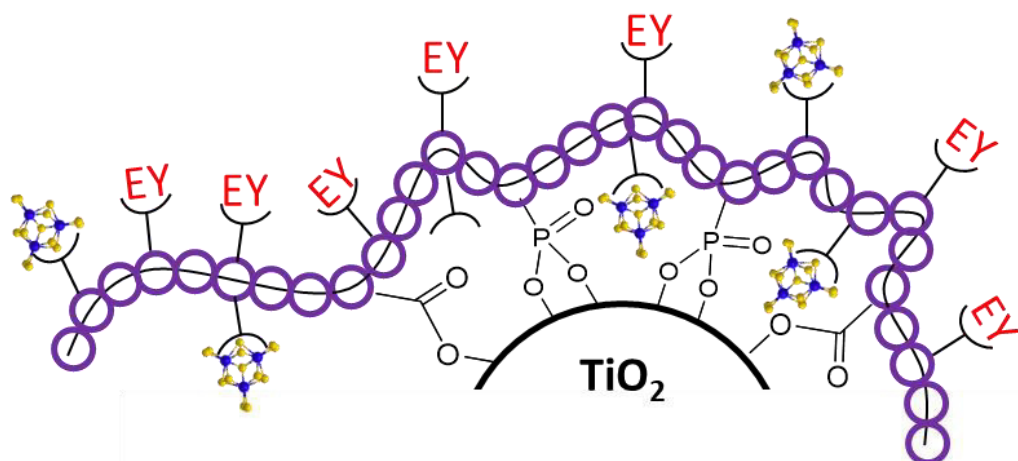


Figure S7: Calibration curves for concentration calculation of EY.

Table S1: Amount of EY absorbed on the different hybrid materials.

sample	Abs 515 nm	^a µg EY ^a	µg EY/mg TiO ₂
TiO ₂	0.2572	7.53	151
PDha-g-PAA@TiO ₂ (1:5)	0.1708	5.12	102
PDha-g-PAA@TiO ₂ (1:15)	0.1237	3.8	76

^a Calculated after washing the samples with water for 3 times and then re-dispersing by 10 minutes ultra-sonication.



$[\text{Mo}_3\text{S}_{13}]^{2-}$ @PDha-g-PAA

$[\text{Mo}_3\text{S}_{13}]^{2-}$ @PDha-g-PAA@TiO₂



Figure S8: Schematic illustration of proposed (attractive) interactions between PDha-g-PAA and TiO₂, Eosin Y, and $[\text{Mo}_3\text{S}_{13}]^{2-}$.

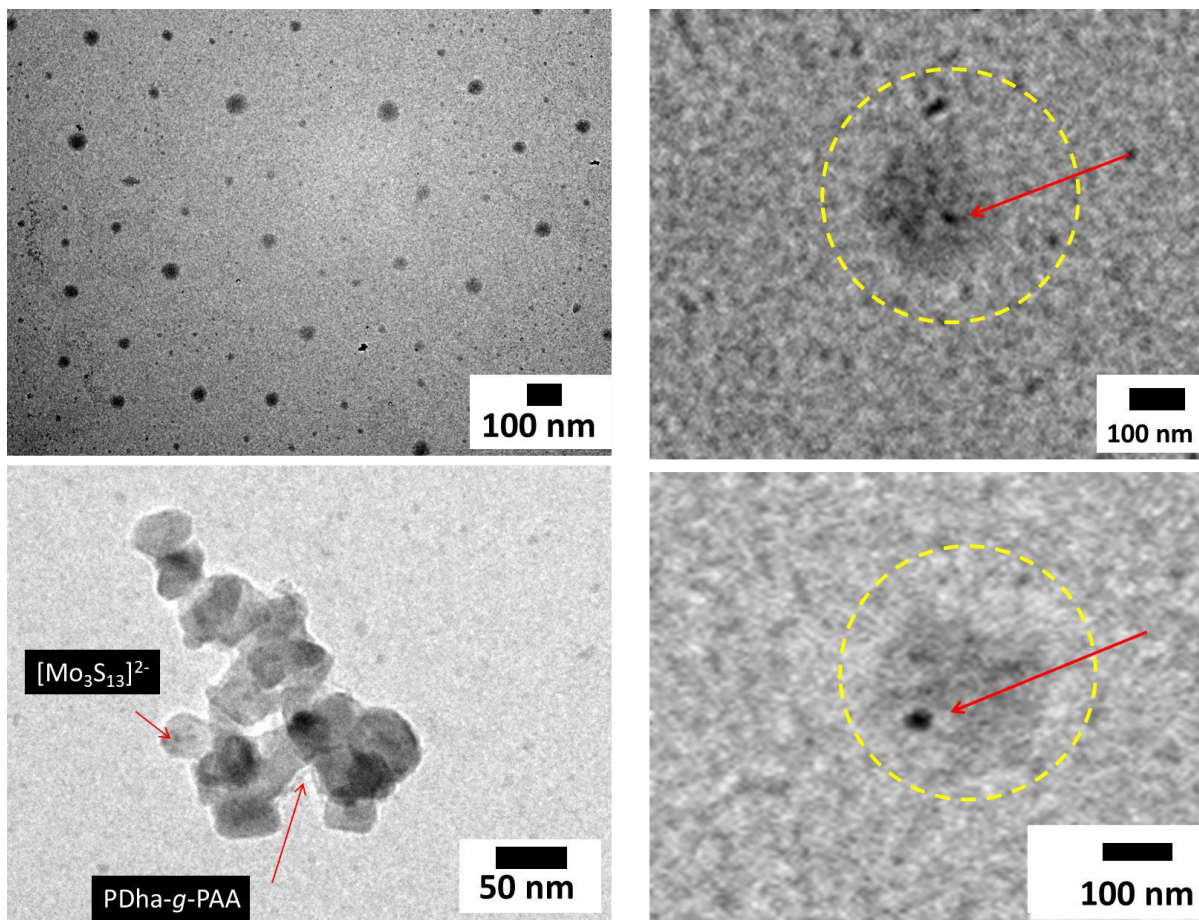


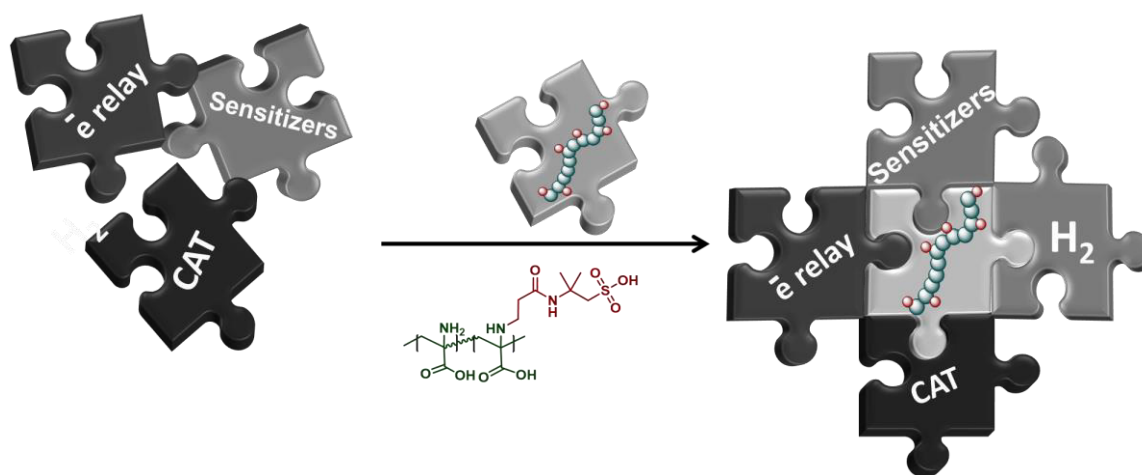
Figure S9: TEM micrographs of $[\text{Mo}_3\text{S}_{13}]^{2-}@\text{PDha-g-PAA}@\text{TiO}_2$.

References:

1. J. B. Max, K. Kowalczyk, M. Köhler, C. Neumann, F. Pielenz, L. V. Sigolaeva, D. V. Pergushov, A. Turchanin, F. Langenhorst and F. H. Schacher, *Macromolecules*, 2020, **53**, 4511-4523.
2. N. Hu, A. Peralta, S. Roy Choudhury, R. Zhang, R. M. Davis and J. S. Riffle, *Polymer*, 2015, **65**, 124-133.
3. A. Rajagopal, F. Venter, T. Jacob, L. Petermann, S. Rau, S. Tschierlei and C. Streb, *Sustainable Energy & Fuels*, 2019, **3**, 92-95.
4. I. Romanenko, A. Rajagopal, C. Neumann, A. Turchanin, C. Streb and F. H. Schacher, *Journal of Materials Chemistry A*, 2020, **8**, 6238-6244.

Publication P6

“Polyampholytic graft copolymers: A platform to combine sensitizers and catalysts“



A. Nabiyan, J. B. Max, M. Micheel, J. Eichhorn, M. Wächtler, M. Schulz, C. Neumann, B. Dietzek, A. Turchanin and Felix H. Schacher

in preparation

ARTICLE

Polyampholytic graft copolymers: A platform to combine sensitizers and catalysts

Afshin Nabiyan^a, Johannes B. Max^a, Mathias Micheel,^{c,e} Jonas Eichhorn,^a Christof Neumann,^{b,c,d} Maria Wächtler^{c,e}, Martin Schulz,^{c,e} Benjamin Dietzek,^{c,d,e} Andrey Turchanin,^{b,c,d} and Felix H. Schacher^{a,b,d}*

Received 00th January 20xx,
Accepted 00th January 20xx

DOI: 10.1039/x0xx00000x

Inorganic–organic hybrid systems offer unique opportunities in functional materials for tailor-made properties and enhanced energy conversion efficiency. We herein introduce a novel polyampholytic graft copolymer, poly(dehydroalanine)-*graft*-(2-acrylamido-2-methyl propane sulfonic acid) (PDha-*g*-AMPS), with tunable charge, that not only serves as a platform for formation and stabilization of nanoparticles and carbon nanomaterials known to be effective in catalysis, but also exhibits a significant role in the enhancement of hydrogen production from water. Hereby, we immobilized a series of photocatalytic systems including various catalyst/sensitizer/electron mediator combinations (such as Eosin Y (EY)/Pt, Au, Pd, and Ag, EY/Pt₃Co, EY/Pt₃Co/carbon nanotubes (CNT), EY/Pt₃Co/fullerene (C60), and CdS) in environments of PDha-*g*-AMPS and we investigate their photocatalytic activity. With assistance of our polymer, high hydrogen production efficiency was achieved in neutral aqueous media with a turnover number >8000. Our observations show that PDha-*g*-AMPS acts as immobilizing platform for multi-component materials and we proof this by catalytic and optical studies. In our opinion, this is a general and novel approach towards the effective combination of different photocatalysis components using polyelectrolytes and this can be also extended to many other catalytic reactions.

Introduction

A great example of the harnessing the solar energy is photocatalytic hydrogen production which is nowadays a considerable target in sustainable and clean energy. Utilizing soft matrix in such photocatalytic reaction draw great attention due to versatility and providing toolbox of organic chemistry for tailoring and tuning the functions.^{1–3} Although soft materials illustrate great developments, integrating the light-harvesting with charge-transport and catalytic functions to produce solar fuels is still a great challenge.³

Polymers provide unique opportunities in the development of hybrid structures by assembling soft materials onto solid supports. Typically, the polymer matrix was introduced as microenvironment, which can facilitate the charge transfer to redox-active sites, manage the delivery of chemical substrates, improve the product specificity during catalytic transformations, and lend the chemical protection to

underpinning solid-state supports as well as embedding the components.⁴ Among various organic polymers, polyelectrolytes have attracted extensive attention by possessing many ionizable groups.^{5,6} The combination of polymeric and electrolyte behaviour gives them a number of unique abilities such as changing drastically the fluid properties of aqueous solutions and suspensions, interacting with neutral particles, small ions and oppositely charged macromolecules.^{5,6} Polyelectrolytes are defined as polymers containing either positive (polycations) or negative charges (polyanions), an equal amount of counterions, and are typically water-soluble. As a subclass for polyelectrolytes, there are polyampholytes and polyzwitterions. These types of polyelectrolytes feature oppositely charged moieties or ionizable groups either within the polymer backbone or in the side-chain.⁷ In case of polyzwitterions, both groups are even located within the same monomer unit. The typical repeat units of polyzwitterions commonly include cationic ammonium groups, as well as anionic sulfonates, carboxylates, phosphates, phosphonates, or phosphinates.^{8,9}

Polyelectrolytes have a wide variety of applications that include ion exchange, chelation to bind trace metals, sewage treatment, soil conditioning, paper reinforcement, pigment retention, and formulation in shampoos and hair conditioners.^{8,10,11} Recently they are emerged as substrate for photocatalysis. This fascinating materials have been highlighted by several research groups as promising scaffolds for facile photocatalytic water reduction. For example, Wasielewski *et al.* report the light-driven production of hydrogen inside a hydrogel

^a Institute of Organic Chemistry and Macromolecular Chemistry (IOMC), Friedrich-Schiller University Jena, Lessingstraße 8, D-07743 Jena, Germany.

^b Jena Center for Soft Matter (JCSM), Friedrich Schiller University Jena, Philosophenweg 7, D-07743 Jena, Germany.

^c Institute of Physical Chemistry and Abbe Center of Photonics, Friedrich Schiller University Jena, Helmholtzweg 4, 07743 Jena, Germany.

^d Center for Energy and Environmental Chemistry Jena (CEEC Jena), Philosophenweg 7a, 07743 Jena, Germany.

^e Department Functional Interfaces, Leibniz Institute of Photonic Technology (IPHT), Albert-Einstein-Strasse 9, 07745 Jena, Germany.

† Footnotes relating to the title and/or authors should appear here.

Electronic Supplementary Information (ESI) available: [details of any supplementary information available should be included here]. See DOI: 10.1039/x0xx00000x

scaffold built by a polyelectrolyte from poly(diallyl dimethyl ammonium) chloride.³ Besides Stupp *et al.* indicate photocatalytic hydrogen production by assistance of chromophore from polyelectrolytic hydrogels.¹² In general, based on our understanding of polyelectrolytic ability and potential of them, although they exhibited a great potential in catalysis, they are not well applied and studied in alien of catalytic reactions. Indeed, the application of them in catalysis is still poor and their improvement and utilization are highly desirable.

Photocatalytic systems for H₂ production typically consist of a photosensitizer, an electron relay, a sacrificial electron donor, and either a heterogeneous or a homogeneous catalyst. Recently, considerable efforts have conducted to the identification and modification of various metal complexes, carbon nanomaterials, dyes and photosensitizers for hydrogen production catalysts. However, most of the catalysts have limited aqueous solubility and require the use of organic solvents and extra organic acids to provide protons. For those water-soluble catalysts, systemic modification of molecular structures is challenging from both design and synthesis points of view, making further activity improvements very difficult. This dilemma is increasing significantly for carbon nanomaterials such as graphene, carbon nanotubes (CNT) and fullerene (C60). For instance, CNTs have a lack of solubility and the difficult manipulation in solvent have imposed great limitations on the usage of CNTs. Indeed, freshly synthesized CNTs are insoluble and poorly usable in all organic solvents and aqueous solutions. Many researcher, to cope of solubility issues of the CNT introduced covalent surface modification of CNT. Although the covalent approach is efficient in functionalizing and stabilizing CNTs, the covalent bonding inevitably disrupts the long range π conjugation of CNTs, leading to decrease electrical properties.¹³ On the other hand, non-covalent approach can avoid the destruction of the chemical structure, and retain the electric properties of CNTs. Recently, our group introduced a novel polyampholyte based on Poly(dehydroalanine) (PDha) as dispersants for CNTs.¹³ Now, our aim is to show that not only our elaborate polyampholytes can solve the problem of CNT dispersing and boosting the hydrogen production, but also it can be used as universal platform to combine many other catalysis and photosensitizer, which were not before well combinable for the photocatalysis. PDha exhibits amino and carboxylic moieties in each repeat unit and therefore, it offers a high density of functional groups and charge. These groups allow pH-dependent changes of the overall charge and provide strong ligands. These properties were already exploited for the controlled nanoparticle formation and stabilization, but so far different nano-materials were not combined and hydrogen production not yet tested.^{13–15}

We herein report the design and characterizations of polyampholytes copolymer as meeting point in platform for localizing and effectively combining the different catalyst, sensitizer, and electron relay mediator. The resulting catalytic hybrid materials were shown to be highly active in photocatalytic H₂ production with assistance of polyampholytes

platform. To understand why a higher efficiency of hydrogen production could be achieved by polyampholytes platform, we performed comprehensive studies on interaction of polymer with catalyst, sensitizer, and electron relay mediator by studying catalytic performance and optical properties. Our results indicate that the electron transfer can be improve significantly by polymer from sensitizer to catalyst and electron acceptor. This work, we illustrate the fact that instead of revising molecular structures that is difficult from design and synthesis points of view, we can use polyampholytes to improve, combine and regulate catalyst features.

Results and discussion

The following sections are divided into three parts: (i) synthesis and characterization of PDha-*g*-AMPS by aza-Michael addition and then formation, stabilization and investigation of different inorganic nanoparticles and carbon nanomaterials, (ii): investigation of hydrogen production of system with Eosin Y (EY) as a photosensitizer, CNT as an electron relay mediator for efficiently accepting and transporting electrons, and Pt₃Co nanoparticles works as catalyst, which were localized in PDha-*g*-AMPS polyampholytic graft copolymer. Furthermore, the function of PDha-*g*-AMPS in enhancement of photosensitized hydrogen production activity and the probable mechanism were also discussed and (iii) extending the hypothesis of polymer role for enhancement of hydrogen production activity were tested for alternative systems including C60, CdS, Au, Ag, Pt, Pd, and [Mo₃S₁₃]²⁻.

Preparation of hybrid materials

Tailor-made PDha based graft copolymer as dispersant for metal catalysts:

Synthesis of PDha-*g*-AMPS: Post-polymerization modification of PDha allows the synthesis of tailor-made polyampholytes with tuneable charge as well as strong binding sites for ions, metal nanoparticles and carbon nanomaterials.¹⁶ Through the grafting reactions, different functional side-chains were attached by the reaction of the amino moieties with epoxides or Michael acceptors.^{14,16} For our purpose, we were interested in a PDha based graft copolymer with a high water-solubility and charge density as well as the possibility to disperse simultaneously carbon nanomaterials, metal nanoparticles and dyes. Therefore, we chose the attachment of 2-Acrylamido-2-methyl propane sulfonic acid (AMPS) fulfilling these demands. Further, sulfonic acid groups were meant to be suitable moieties for an efficient proton transfer, which could facilitate the hydrogen production reaction.¹⁷ PDha-*stat*-PAMA with roughly 65 repeat units was used as a precursor and reacted with AMPS in an aza-Michael addition (Figure 1A). A reaction time of 72 h resulted in 0.25 AMPS side-chains per repeat unit and the successful synthesis was proven by ¹³C-NMR (Figure 1B) and ¹H-NMR spectroscopy (Figure S1B), where signals of the PDha backbone as well as AMPS were found. SEC revealed a clear shift of the elution volume as a result of grafting and an

increase in the molecular weight of the polymer (Figure 1C). Besides, FT-IR spectroscopy analysis proof the presence of the sulfonic acid groups (Figure S1A).

While the other PDha based polymers exhibit an overall positive charge at a pH < 3 as found from ζ -potential measurements, PDha-*g*-AMPS carries a constant negative charge independent

of the pH value due to the deprotonated sulfonic acid groups (Figure S1C). Nevertheless, the ionizable carboxylic and amino moieties of the backbone can be protonated and deprotonated by changing the pH-value as the potentiometric titration shows pKa values of 8.1 and 4.3, respectively (Figure S1D).

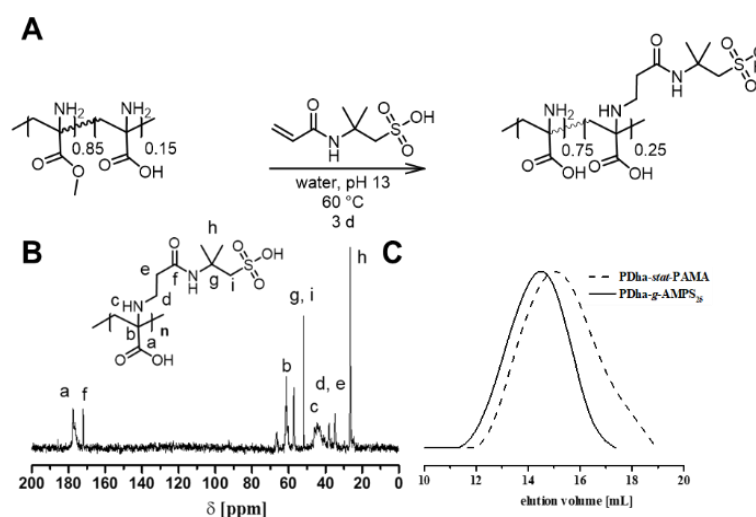


Figure 1: Synthetic route towards the synthesis of a template graft copolymer based on PDha (A), characterization of PDha-*g*-AMPS double hydrophilic graft copolymer via ^{13}C -NMR (B) and ^{13}C -NMR spectroscopy (C) SEC (DMSO) trace of PAMA-*g*-AMPS and PDha-*g*-AMPS.

Dispersion of metal catalyst: Enormous efforts in the immobilization of catalysts onto solid supports is currently being carried out.¹⁸ This general method has shown drawbacks such as additional functionalization of the catalyst ligand and solid surface, and changes in chemical reactivity.¹⁹ As an alternative noncovalent interactions, *e.g.* electrostatic attraction, are emerging as a powerful tool that gives rise to supported catalysts without chemical modification of the catalysts.²⁰ Here, we aimed to effectively disperse and stabilize the metal catalyst such as Pt_3Co or $[\text{Mo}_3\text{S}_{13}]^{2-}$ by the support of the polyampholytic PDha-*g*-AMPS under mild reaction conditions. We are interested to these catalysts since $[\text{Mo}_3\text{S}_{13}]^{2-}$ nanoclusters and Pt_3Co alloys exhibit higher activity in many reaction especially in water splitting with different dyes and semiconductors.^{21,22} Despite these success stories, the use of Pt alloys and molybdenum clusters for photocatalytic hydrogen production with Eosin Y has not been reported. The formed hybrids were studied in respect of stabilization, size and morphology by the dynamic light scattering (DLS) and transmission electron microscopy (TEM) respectively.

Pt_3Co or $[\text{Mo}_3\text{S}_{13}]^{2-}$ as our exemplary catalyst for hydrogen production have poor solubility in water, featuring an overall rather positive and negative charge, respectively. Simultaneously, our polymer backbone behaves like a polyzwitterion at pH 7 leading to electrostatic attraction of either the amino or carboxylic moieties. This combination of functional groups makes the materials amenable for catalyst deposition. To introduce our soft matter matrix for the catalyst

immobilization, we mixed directly Pt_3Co or $[\text{Mo}_3\text{S}_{13}]^{2-}$ with our graft copolymer *via* ultrasonication. After 30 min, both catalyst in PDha-*g*-AMPS solution mixture became a homogeneous dispersion without any sign of precipitation for even weeks. This observation is the results of the anchoring and stabilization of the catalyst by the polymer.

The size of the hybrids materials was controlled by DLS. PDha-*g*-AMPS/ $[\text{Mo}_3\text{S}_{13}]^{2-}$ hybrids have a R_h below 5 nm in radii and TEM micrograph (Figure 4, E) show the nanoaggregates with average size of 2 nm in radii that are randomly distributed in the organic phase (Figure 4, E). We assume an electrostatic attraction of the negatively charged catalyst and positively charged amino moieties. We also investigated the size of Pt_3Co nanoparticles before and after stabilization by PDha-*g*-AMPS. DLS measurement of PDha-*g*-AMPS/ Pt_3Co showed an increased radius of 15 nm compared to 10 nm for the pristine Pt_3Co (Figure S2). Increasing of the average particle size of ~ 5 nm is in reasonable agreement with forming a shell around the nanoparticles. Corresponding TEM micrographs contain information about the aggregation behavior as well as the shell thickness. TEM micrographs do not necessarily represent the state of the particles in dispersion because of drying artifacts and possible melting of the organic matter as a result of the electron beam. In PDha-*g*-AMPS/ Pt_3Co , again both aggregates and single core-shell particles can be seen (see also TEM micrographs at lower magnification in Figures S3). Furthermore, a shell of organic material can be observed around the particles, proofing our concept of the formation of hybrid particles and

the adsorption of organic material, as observed in DLS measurements. The thickness of the organic shell was qualitatively determined via gray-scale analysis of different particles to be approximately 5 nm. This is in good accordance with the calculated values from the DLS results. To sum it up, our polymer is an exceptionally efficient dispersant for inorganic catalysts and also other ones, with different surface charges could be tested. This effective interaction and coating can be explained by the interactions between particles and functional groups of the polymer. Indeed, the polyampholytic backbone of PDha containing amino and carboxylic groups, is suitable for electrostatic binding of either anionic or metal catalyst, that could be extended to a great variety of other nanoparticles

Dispersing of carbon nanomaterials: Lack of solubility as a result of strong aggregation and hydrophobicity has imposed great limitations on the usage of carbon nanomaterials. In order to overcome solubility issues, we utilized a non-covalent approach for stabilization to obtain well dispersed CNT and C60, as exemplarily carbon nanomaterials with different shapes and size. However, in this approach, we would avoid the destruction of the chemical structure, and retain the electric and mechanical properties of carbon nanomaterials which afterwards show significant impact on photocatalytic performance of our hybrids.²³ Here, PDha with polyampholytic nature was used to provide electrostatic interaction with CNT and C60 to stabilize them in aqueous solution. As exemplary stabilization test, a polymer solution (1 mg mL⁻¹, pH 7) was added to CNTs or C60 (1.0 mg), and treated with ultra-

sonication for 60 min. Afterwards, stable dispersions with the appearance of black or brownish inks, respectively, were formed.

Thermogravimetry (TGA) was used to determine the amount of organic matter present in hybrid materials. Therefore, TGA measurements of CNT dispersion as our exemplary case that contained 1 g L⁻¹ initial concentration of the graft copolymer were performed under an air and nitrogen atmosphere and the results were compared to those for the pristine graft copolymer and the pure CNTs (Figure. S4, B). The dispersion was precipitated by high-speed centrifugation and the resultant precipitate was washed several times with Milli-Q water to remove any free polymer, and then freeze-dried. While pure CNTs are relatively stable and no significant weight loss is observed up to a temperature of 500 °C, there are two decomposition steps visible for the graft copolymer and the hybrid material upon heating. The first can be ascribed to the loss of water when heating up to a temperature of 100 °C, and the second at approximately 250 °C corresponds to the decomposition of the graft copolymer itself. Hence, the weight loss of the samples was compared between 250 and 5000 °C. The pure graft copolymer exhibits a weight loss of 74 wt% in this region in the absence of CNTs, whilst the hybrid materials show weight losses of 16 wt% for the PDha-*g*-AMPS/CNTs purified via centrifugation. By comparing the remaining mass of PDha-*g*-AMPS/CNTs with that of the polymer sample without CNTs and the mass of CNTs itself, a composition of the hybrid material of 21 wt% polymer and 79 wt% CNTs can be determined.

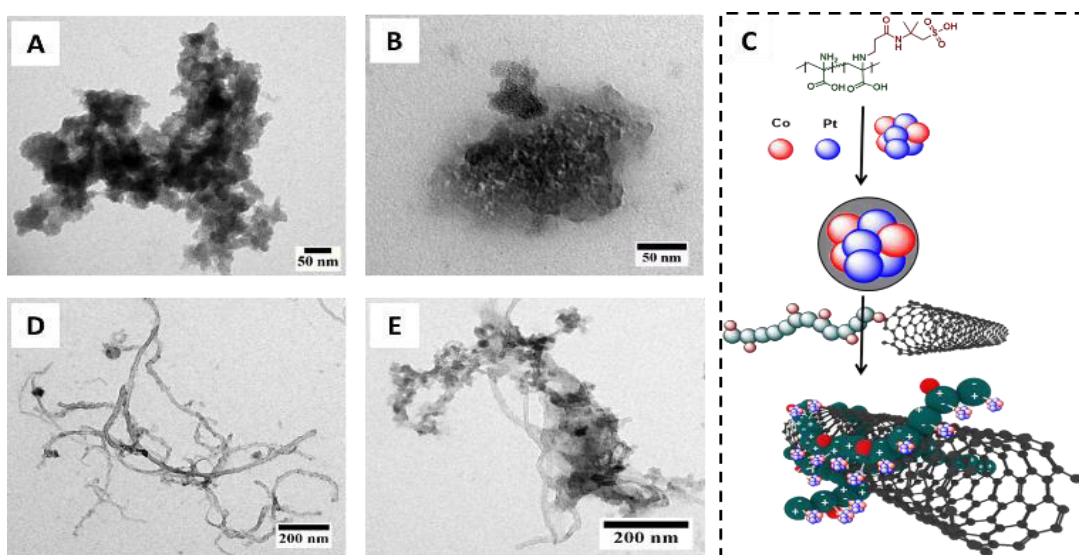


Figure 2: (A): TEM micrographs of Pt₃Co, (B): PDha-*g*-AMPS at Pt₃Co, (C-D): PDha-*g*-AMPS/Pt₃Co/CNT and (D): schematic formation of PDha-*g*-AMPS/Pt₃Co/CNT hybrids.

For further visualizing the successful dispersion of the carbon nanomaterial toward individual CNTs and C60, TEM micrographs were taken for the formed PDha-*g*-AMPS/CNTs

and C60 dispersion after several days (Figure S4, A and Figure S5). Here, the presence of individual well-separated CNTs with lengths of several hundred nm and small polymeric shell as well

as small dots of C60 distributed at organic phase could be observed, which are presumably covered by PDha-*g*-AMPS graft copolymers.

As we have shown, PDha-*g*-AMPS is able to disperse either hydrophobic carbon nanomaterials or metal NPs. We were now interested into stabilizing the both nano-materials simultaneously. Thus, Pt₃Co was coated with PDha-*g*-AMPS and this hybrid directly was used for stabilization of the CNT or C60. The obtained hybrids were investigated for the visualizing the interactions and amount of organic shell by TEM and TGA respectively.

Figure S4 shows the TGA curves of the PDha-*g*-AMPS, PDha-*g*-AMPS/CNT and PDha-*g*-AMPS/CNT/Pt₃Co as our case of study. As weigh loss comparison of all of samples shows, comparing the remaining mass of PDha-*g*-AMPS/CNTs and PDha-*g*-AMPS/CNT/Pt₃Co, a composition of the hybrid material of xx wt% polymer, xx wt% CNTs and Pt₃Co can be determined.

To visualize the interaction behavior of PDha-*g*-AMPS/Pt₃Co with CNT, the hybrid structures from the well dispersion inks were investigated by drop-casting the solution onto TEM grids and corresponding images of PDha-*g*-AMPS/CNT/Pt₃Co hybrids are illustrated in Figure 2 (D-E) and Figure S4, D. TEM results shows well dispersed CNTs with high aspect ratio. At higher magnification, polymeric shell around of the CNT particles is visible, is also shared between several CNTs. Further, the linkage of Pt₃Co nanoparticles to the CNT by the polymer was observed as dark spots with a size of several nanometers. This linking could facilitate mass and electron transfer and promote catalysis.

Template for the synthesis of CdS: In addition to using PDha-*g*-AMPS as an effective dispersant, we were interested in template supported synthesis of inorganic catalysts. Our recent investigations have revealed that the double-hydrophilic block copolymers, which consist of one hydrophilic block interacting strongly with appropriate inorganic materials and another hydrophilic block mainly promoting solubilization in water, can be used as template for CdS crystals formation.²⁴ CdS has high visible light-driven photoactivity for H₂ production and low bandgap energy (2.4 eV), and therefore is acknowledged as one of the most attractive semiconductor photocatalysts.²⁵ Here, we were now interest to show that our double-hydrophilic graft copolymer can also facially form and stabilize CdS nanocrystals in aqueous solution at room temperature. Thereby, CdS nanoparticles were synthesized with a two-step approach. First, PDha-*g*-AMPS was used as template for chelation of Cd²⁺ ions presumably by -COO⁻ functional groups. In the next step, these immobilized ions will serve as nucleation point for the formation of CdS nanoparticles by addition of Na₂S (1 equivalent to Cd²⁺). Immediately, the color of the solution changed from colorless to yellow (Figure 3, A) and the mixture was stirred under argon for 24 hours. During that time, the rather high concentration of Cd²⁺ in the polymer backbones reacts with S²⁻ and forms CdS which afterwards were investigated regarding size, morphology, and optical properties. Size of forming aggregates was studied by DLS. Figure 3, B illustrate the size of the PDha-*g*-AMPS after addition of Cd²⁺ ions and afterwards forming the CdS nanoparticles. While PDha-*g*-

AMPS is unimeric in solution with hydrodynamic radii of 1–2 nm, after adding desirable equivalents of Cd²⁺ ions due to complexation our hybrids exhibit a Rh of 8–10 nm. The dispersions of these aggregates shows clear appearance without no precipitation or sedimentation within 1 week after preparation as a result of effective interaction between the polymer and Cd²⁺ ions in water. After addition of Na₂S DLS indicates the forming of nanoaggregates with average size of 18–20 nm. The stability of formed aggregates was controlled for one weeks and our visual observation indicate a stable colloidal solution.

PDha-*g*-AMPS/CdS sample were further characterized using TEM to obtain further insight into the aggregate morphology. The micrographs in Figure 3, (B-C) reveal spherical structures of 15–25 nm in radii. Both the inorganic (multi)core and the organic shell are visible. However, spherical structures are formed seemingly from several cluster of CdS which are appear as black spot in the center of the spherical aggregates. The sizes of the formed aggregates observed by TEM are significantly smaller than those found in DLS experiments. Some of the micrographs additionally reveal a larger superstructure (several multi core) apparently consisting of several of the smaller aggregates that is formed by secondary aggregation.

UV/Vis spectroscopy was used to analyze the optical properties of PDha-*g*-AMPS, PDha-*g*-AMPS/Cd²⁺ and PDha-*g*-AMPS/CdS solutions (Figure 3, A). PDha-*g*-AMPS and PDha-*g*-AMPS/Cd²⁺ shows only one weak characteristic absorption band centered at ~260 nm and upon formation of CdS a new absorption shoulder appears from 530 nm, which we attribute to quantum confinement effects of CdS.

In principle, the position of the band edge absorption with either a distinct shoulder or a band edge from quantum confinement can be used to calculate particle sizes and size distributions. From the shoulder (λ_{sh}) and the band edge (λ_e) positions of the absorption spectrum of CdS (Figure 3, A), we calculated a CdS crystal diameter (Table 1). Here, the average size of CdS crystals was determined using Henglein's empirical model, which relates the diameter of the CdS crystals to the onset of their light absorption (equation S1 and Table 1).²⁶ CdS crystals show an average of 5.3 to 9.8 nm in diameter and this average size is smaller than what we observed from TEM and DLS, which indicates that the nanoaggregates in TEM results are clearly loaded with more than one CdS crystal.

Table 1: Parameters obtained from the analysis of the absorption spectra of PDha-*g*-AMPS/CdS.

sample	^a λ_{sh}	^a λ_e (nm)	^b D λ_{sh}	^b D (λ_e)
PDha- <i>g</i> -AMPS/CdS	545	490	9.8	5.3

^a Absorption shoulder and edge features (λ_{sh} and λ_e) were obtained from the intersection of the sharply decreasing region of the spectra with the baseline. The calculation of the mean average diameters of D CdS (λ_{sh}) and D CdS (λ_e) can be found in the Supporting Information. ^b diameter of the CdS crystals (nm) which are stabilized by PDha-*g*-AMPS.

To gain further insight into the synthesis of CdS by our double hydrophilic copolymer system (PDha-*g*-AMPS/CdS), we used X-

Ray photoelectron spectroscopy (XPS) for analysis of PDha-*g*-AMPS/CdS (Figure S6). Our investigation reveal signals connected to the copolymer backbone such as C 1s, N 1s and S 2p. The high-resolution C 1s XP spectrum can be assigned to C-C, C-S, and C-N (red ~ 286 eV), C-O (green, 287–288 eV), and C=O and COOH (blue, 289.5 eV) bonds for the PDha-*g*-AMPS backbone. The N 1s component at 400–410 eV is assigned to N-C bonds, whereas protonated N can be found at 402 eV. The XPS peaks for S 2p appear as a broad sulfur signal with low intensity which could be attributed to the AMPS functional groups. After

background subtraction different contributions according to SO_4^- (~167–168 eV) and SO_3^- (168–170 eV) become visible. After the formation of CdS, PDha-*g*-AMPS/CdS exhibited signals for Cd 3d and S 2p. As Figure S6 presents the deconvolution peaks of Cd 3d_{5/2} and Cd 3d_{3/2} located at ~406 and 413 eV with splitting energy of ~8 eV according to the spin-orbit coupling. The presence of sulfur of CdS is confirmed by S 2p, where signals are found at 164.7 and 165.9 eV and can be allocated to S 2p_{3/2} and S 2p_{1/2} in CdS (Figure S6).

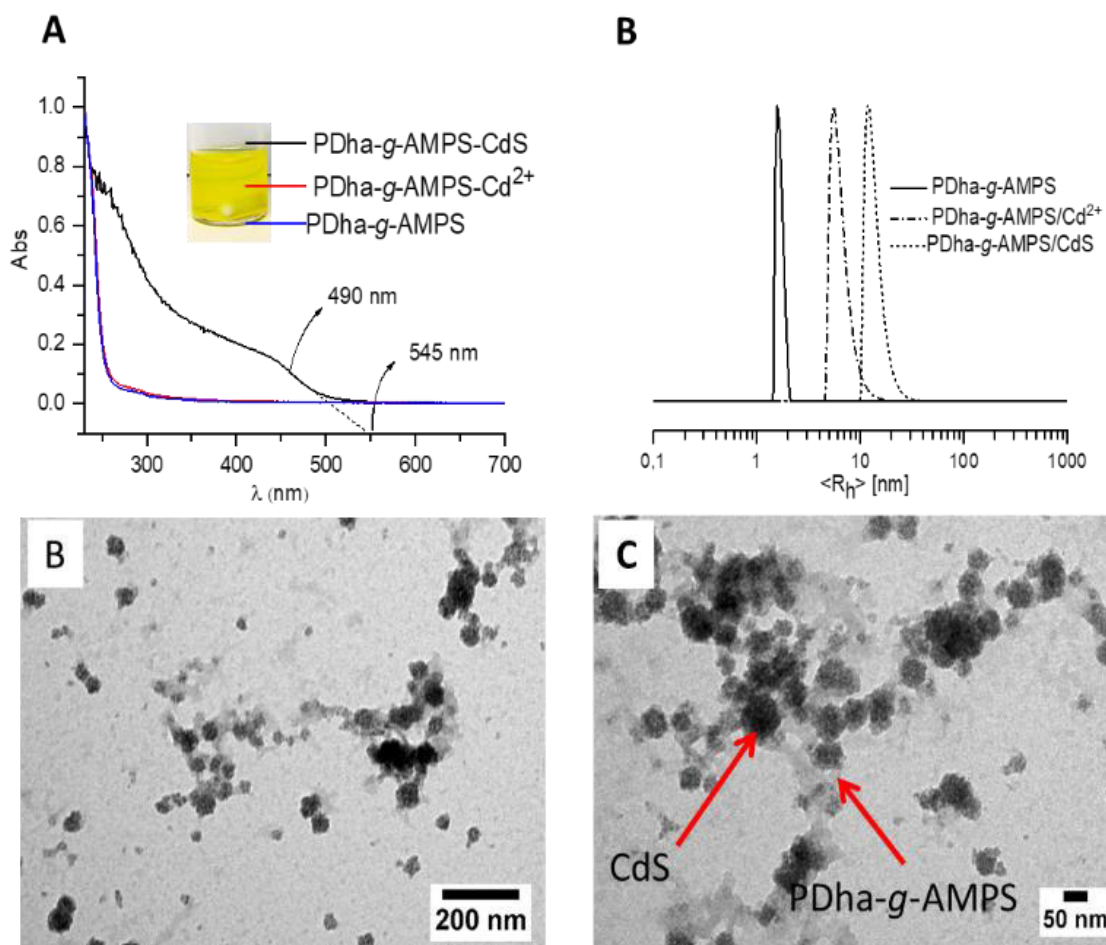


Figure 3 (A): UV/Vis absorption spectra of PDha-*g*-AMPS, PDha-*g*-AMPS/Cd²⁺, and PDha-*g*-AMPS/CdS in water (ratio of CdS to PDha is X equivalents), (B): DLS CONTIN plot for PDha-*g*-AMPS, PDha-*g*-AMPS/Cd²⁺, and PDha-*g*-AMPS/CdS in water, and (C-D): TEM images of PDha-*g*-AMPS/CdS with different magnification scale.

Synthesis of noble-metal nanoparticles: The properties of metal nanoparticles are strongly dependent on their size, shape, solid or hollow interiors, and composition. Moreover, in the case of multicomponent nanostructures, properties also depend on the elemental distribution within the particle. By tuning and controlling these physical and chemical parameters, one can, therefore, alter and optimize the desired property for a target application.^{27,28} For instance, in the case of catalysis, it

is expected that the surface area, size, surface composition, and the nature of exposed facets (shape) should strongly affect catalytic activities and selectivity (geometric and electronic effects).^{29,30} Here, we aimed to show our platform not only can produce the different noble metal catalysts, but it can also control small size and increase the particle distribution, which are lately influenced on the photocatalytic performance. We hypothesized that the described polyampholytic graft

copolymers resembles as template for the synthesis of metal nanoparticles. Thereby, in order to grow noble metal nanocrystal in polymer matrix, firstly, PDha-*g*-AMPS solution was mixed with desirable amount of the Ag^+ , Au^{3+} , Pt^{2+} , and Pd^{2+} ions. It is well known that Ag^+ , Au^{3+} , Pt^{2+} , and Pd^{2+} ions can be complexed by carboxylates as well as amino groups. In our case, the polyampholytic nature of PDha-*g*-AMPS features both functionalities in each repeat unit. Besides AMPS side-chains ensure high solubility over the entire pH range and prevent

precipitation after metal ion addition. After the complexation of the respective ions, the nanoparticles are formed by reduction agent. NaBH_4 was used as reducing agent (one equivalent in respect to metal-containing ions) performing the synthesis at pH 7. We decided to use a selection of different noble metals, that show catalytic activity. The obtained different nanoparticles are investigated by UV-Vis, TEM, and XPS.

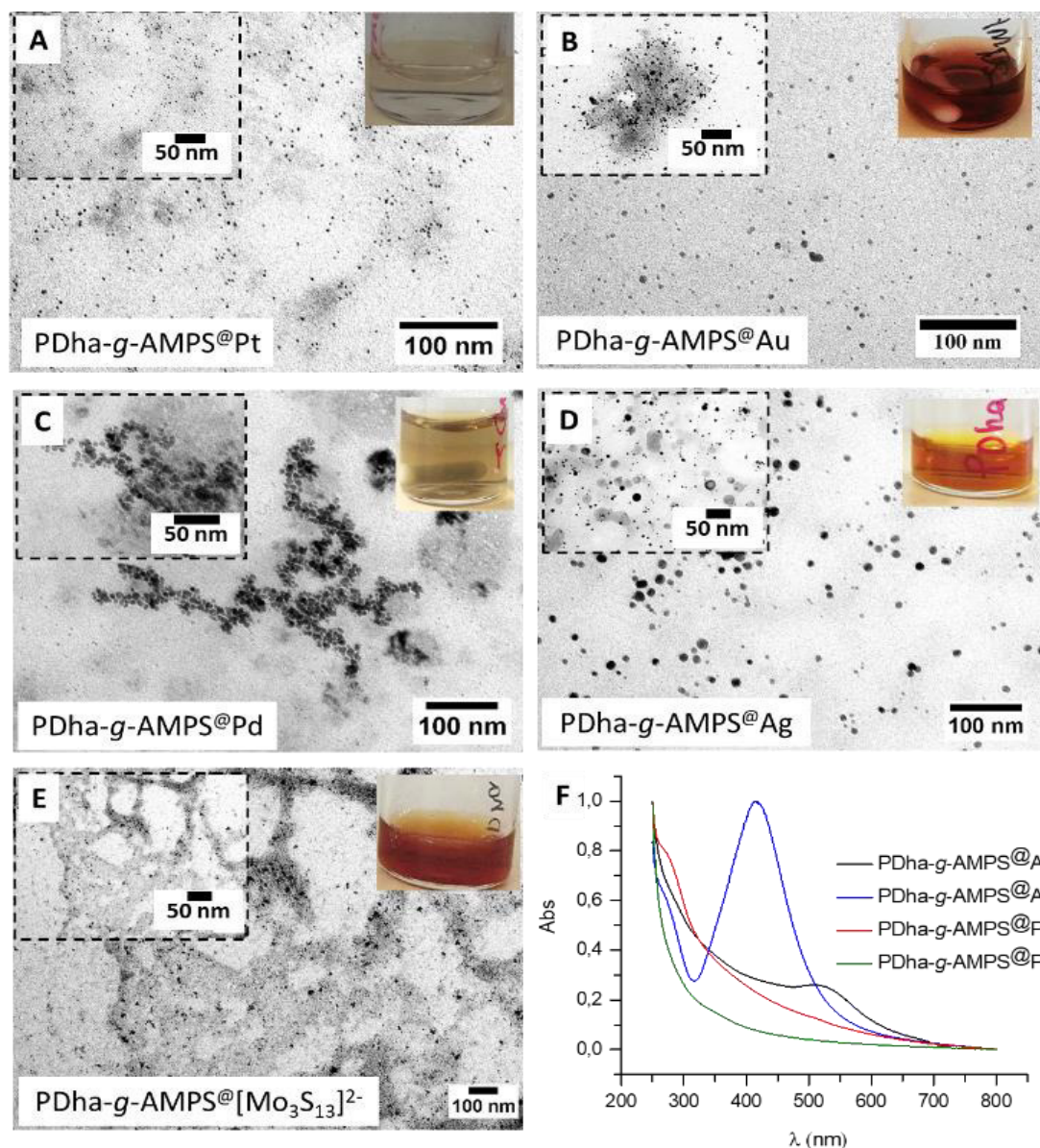


Figure 4: (A-E) TEM images of PDha-*g*-AMPS/Pt, Au, Pd, Ag and $[\text{Mo}_3\text{S}_{13}]^{2-}$ nanoparticles respectively and (F) UV-Vis spectrum of PDha-*g*-AMPS/ Pt, Au, Pd, and Ag nanoparticles.

Figure (4, F) and Figure (S7) show UV/Vis spectra of Ag^+ , Au^{3+} , Pt^{2+} , and Pd^{2+} /PDha-*g*-AMPS before and after reduction. UV-vis measurements revealed typical surface plasmon resonance peaks for Au and Ag nanoparticles (Figure 4, F). The palladium

nanoparticle formation has been revealed by comparison of UV-visible spectra of palladium species before and after reduction by NaBH_4 . Pd ions shows absorption bands, attributed to the absorption of palladium (II) species in the starting

solution. After reduction, the peaks vanished, this absence of the absorption peaks above 355 nm shows the full reduction of the initial Pd (II) ions.³¹ Our data indicate that due to the ligand-to-metal charge transfer transition of the Pt ions before reduction, we can observe peak at 370 nm in its UV/Vis spectrum as shown in Figure S7. During the reduction with NaBH₄ solution, the color of the solution gradually changed to nearly colorless. The peak at 370 nm disappeared after the reaction as shown in Figure 4, a, indicating that the Pt ions were completely reduced. The Pt nanoparticles had absorption in all ranges of the UV/Vis spectrum and the absorption increased with the decrease of wavelength.

To achieve a further insight into the formation of nanoparticles, X-ray photoelectron spectroscopy was applied to obtain hybrids. Figure S8 illustrates the clear signatures of Pt, Au, Ag and Pd nanoparticles. Pt nanoparticles show the Pt 4f_{7/2} and 4f_{5/2} doublet with the binding energies of 71.4 and 74.8 eV (Figure S8, A). These are typical values for Pt⁰, indicating the formation of Pt nanoparticles. The XPS results also identified binding energies of 533.2 and 553 eV, were attributed to 3p_{3/2} and 3p_{1/2} incarcerated Pd⁰ respectively. Figure S8 also depicts 3d spectral region of Ag showing two peaks at 368.04 eV and 373.54 eV respectively corresponding to Ag 3d_{5/2} and Ag 3d_{3/2}. The 4f spectral region of Au is depicted in Figure S8 showing two main peaks at 83.3 eV and 87.0 eV corresponding to Au 4f_{7/2} and Au 4f_{5/2} respectively.

From TEM investigation (Figure 4, A-D), we extracted also information on both shape and size of the nanoparticles. Our TEM observation indicates that nanoparticles are clearly immobilized and distributed at organic surface. All of nanoparticles (*e.g.* Ag, Au, Pd, and Pt) were spherical in shape with a narrow size distribution. The average diameter of the spherical particles is 2–4 nm. Further investigations could focus on alternative reduction routes or the utilization of additional metals or even alloys.

Photocatalytic Proton Reduction

Most of catalysts, carbon nanomaterials, dye-sensitizer, or semiconductor which nowadays are popular for utilization in H₂ production, have limitations such as aqueous solubility, requiring of organic solvents, low solution stability, high tendency for agglomeration, decomposition, low-separation efficiency of electron–hole pairs, secondary aggregation and etc.^{32–34} As a solution for those obstacles, a systemic modification of molecular structures is suggested but it is challenging from both design and synthesis points of view, making further activity improvements very difficult.³⁴ Here, we aimed to show how we can overcome some of these drawbacks such as agglomeration, electron transfer, solution stabilization, and etc., by implementing our polyampholytic platform as a meeting point for effectively combining different catalysis with different dye-sensitizers or semiconductors. Therefore, we designed several different systems based on various catalysts, carbon nanomaterials, dye-sensitizer, and semiconductor and conducted a systematic investigation for them. We started by investigating H₂ production of the simple catalytic combination

of the Eosin Y (EY) as dye-sensitizer with Pt₃Co catalyst in presence and absence of PDha-*g*-AMPS. Our results show significant enhancement can be achieved in presence of our polyampholytic network. Afterwards, we developed our model by introducing the CNT. We evaluate carefully the probable mechanism and role of each element with details for photocatalytic H₂ production. The results are summarized in Figure 5 and 6. However, to further highlight our boosting of H₂ production by immobilizing with polyampholytic approaches, we investigated some other alternative catalytic systems including C60, CdS, instead of CNT, EY respectively and Au, Ag, Pt, Pd, and [Mo₃S₁₃]²⁻ instead of Pt₃Co. However, the photocatalytic activities of all systems for H₂ evolution were evaluated under LED light ($\lambda = 470$ nm, power output 5 mW/cm²) at room temperature using TEOA as sacrificial donor. Control experiments indicated that in the absence of either sacrificial agents and light or both and photosensitizer (EY or CdS) the photocatalyst was practically inactive, indicating that the photocatalytic process, hole scavenger and photosensitizers are necessary for H₂ production.

EY has been shown a successful photocatalytic H₂ production because of high quantum yield of triplet formation, long excited-state lifetime, and proper redox properties of its excited states.^{35,36} The hydrogen production turnover number (TON) of catalyst systems including EY with Pt₃Co, P₃Co/CNT, and Pt₃Co/PDha-*g*-AMPS/CNT are obtained and shown in Figure 5, A. These photocatalytic activities were obtained after considering the optimization effects of CNT, TEOA, and PDha-*g*-AMPS loading amounts, pH values of TEOA aqueous solution, and weight ratios of EY to Pt₃Co (Figure S10–S12). When the photocatalysis conditions were fixed (*i.e.* EY, PDha-*g*-AMPS and CNT with concentrations of 0.5 μ M, 0.5 mg mL⁻¹, and 0.1 mg mL⁻¹ respectively; 0.5 M TEOA solution; pH = 8–9), we indicate H₂ production turnover number (TON) based on amount of evolved H₂ and used Pt₃Co in mole. Our observations indicate that EY/Pt₃Co could produce hydrogen from water reduction, but the hydrogen production TON was only 377 after 24 hours irradiation. After introduction of appropriate amount of polymer and CNT, the highest H₂ production TON based on EY/Pt₃Co/PDha-*g*-AMPS and EY/Pt₃Co/PDha-*g*-AMPS/CNT were 2889 and 8025, respectively. As can be seen, the introduction of CNT and polymer in the presence of EY and Pt₃Co is crucial for improving the photocatalytic activity of this photosensitized system.

The photocatalytic activity of the EY/Pt₃Co/PDha-*g*-AMPS is obviously enhanced as compared to EY/Pt₃Co system. This value exceeds that of the EY/Pt₃Co/PDha-*g*-AMPS system by a factor of 7.6. Most likely, this is due to an efficient interaction between the Pt₃Co and the host photosensitizer (EY) immobilized in the confined backbone of the PDha-*g*-AMPS. To describe this hypothesis, we illustrate Figure S9. As you can see, we can consider PDha backbone as meeting point of the Pt₃Co and EY. Our TEM investigation indicates that Pt₃Co can strongly interact with functional groups of the PDha-*g*-AMPS and this resulted in an organic layer which coats the Pt₃Co nanoparticles (Figure 2, B). However, in our last investigation we indicated the PDha backbone has great interaction for the adsorption of the organic

dyes.¹⁵ Thus here, counting on above described interaction, considering the PDha-*g*-AMPS as meeting point of the sensitizer

and catalyst is key factor to explaining the effects of PDha-*g*-AMPS in enhancement of the H₂ production activity.

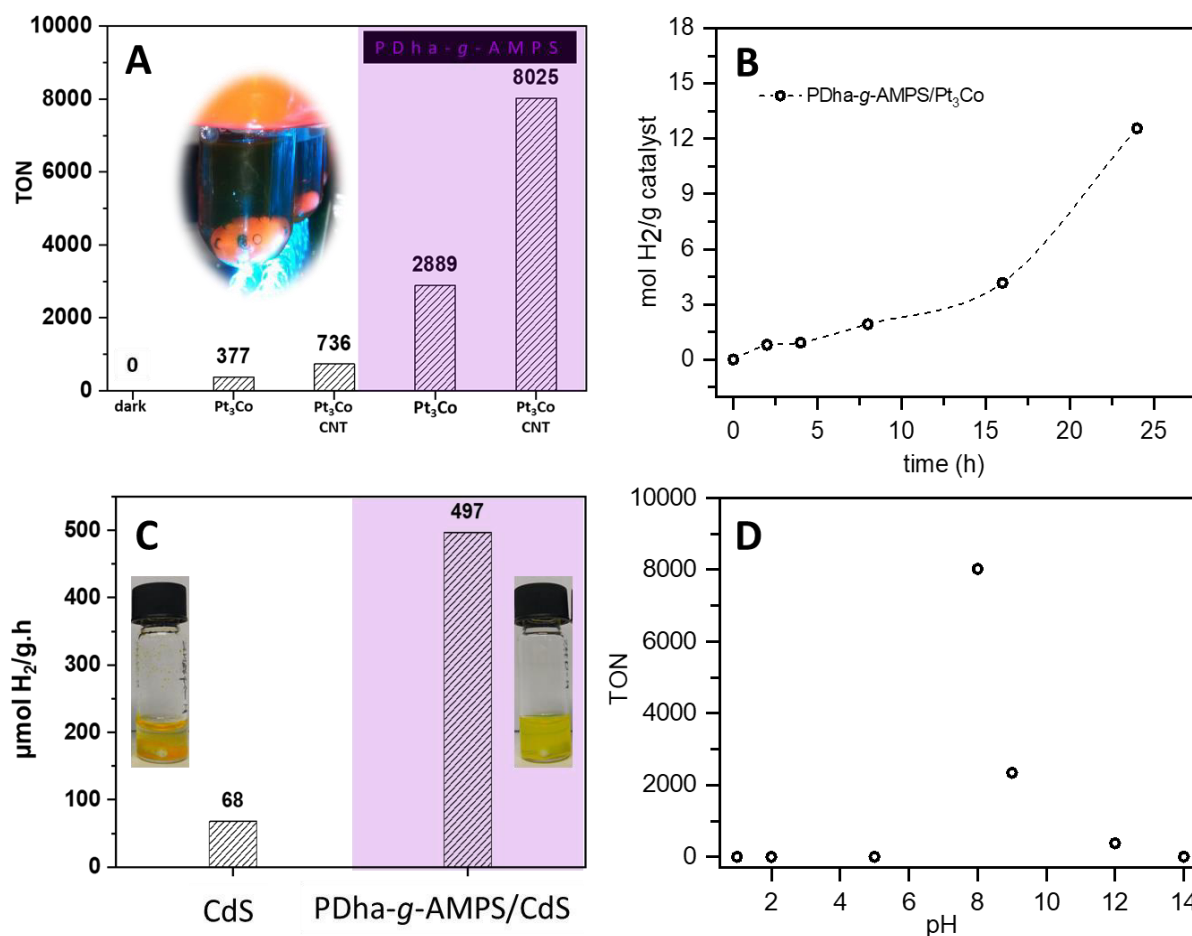


Figure 5: (A): Photocatalytic hydrogen production performance for EY/Pt₃Co, EY/Pt₃Co/CNT, and EY/Pt₃Co/PDha-*g*-AMPS/CNT, where the turnover number (TON) is defined as (moles of hydrogen produced)/(moles of catalyst) after illumination for 24 hour, (B) The time courses of hydrogen evolution over EY/Pt₃Co/PDha-*g*-AMPS/CNT photocatalysts (Reaction conditions: EY, PDha-*g*-AMPS and CNT with concentrations of 100 mmol L⁻¹, 0.5 mg mL⁻¹, and 75 μg mL⁻¹ respectively; 0.5 M TEOA solution; pH = 8-9), (C): hydrogen production rate of CdS and PDha-*g*-AMPS/CdS obtained after 24 h of irradiation (Reaction conditions: TEOA (0.5 M), PDha-*g*-AMPS with concentration of 0.5 mg mL⁻¹ at room temperature and (D): Effect of pH value on photocatalytic activity for hydrogen generation over EY/Pt₃Co/PDha-*g*-AMPS/CNT (Reaction conditions: EY, PDha-*g*-AMPS and CNT with concentrations of 0.5 μM, 0.5 mg mL⁻¹, and 0.1 mg mL⁻¹ respectively; 0.5 M TEOA solution).

Observation of TON 736 for EY/Pt₃Co/CNT reveals that CNT can further improve the TON of H₂ production (1.9 times higher). This enhancement is due to the efficient transfer of the electrons photogenerated from the excited dye to the Pt₃Co catalyst through CNT matrix. This enhancement of the activity becomes remarkably (21.2 times better) when CNTs are coated and dispersed by PDha-*g*-AMPS/Pt₃Co. We could explain this by the interaction of the EY with CNT. Generally, non-functionalized CNTs are highly hydrophobic and the adsorption of EY at the surface of CNT is low. This sheds light on the fact that EY and Pt₃Co have negligible interaction and adsorption on the surface of non-functionalized and highly hydrophobic CNT. On the other hand, according to our TEM and TGA observations, PDha-*g*-AMPS/Pt₃Co can coat and disperse the CNT. As our hydrogen production data indicate that CNT can act effectively as electron traps and charge separation, when polyampholytic

PDha-*g*-AMPS is stabilized and coated the non-functionalized CNT. Consequently, PDha-*g*-AMPS play again the role of the meeting point to connect the electron relay mediator (CNT), catalyst (Pt₃Co) and dye-sensitizer (EY).

The time courses of H₂ evolution of EY/Pt₃Co/PDha-*g*-AMPS/CNT are shown in Figure 5, B. In this system, the initial rate for H₂ evolution is lower. This rate has been maintained for ~10-15 h before significantly increasing with increasing irradiation time. This behavior is due to probably forming stronger interaction between elements of the catalytic system after illumination for a certain time. In this regard, during the light irradiation, the charge can gradually accumulate in the hybrid system. CNT is a popular candidate in this area and it can accept and store electrons.³⁷ On the other side, PDha-*g*-AMPS/Pt₃Co/EY has a great affinity for interaction with charged materials. Thus, this two combinations can make stronger

interaction which be later increase hydrogen production activity after certain time.

PDha-*g*-AMPS copolymer is a pH responsive polyampholyte and the pH value often has a remarkable effect on a photocatalytic reaction. As shown in (Figure 5, D) the best photocatalytic activity was obtained at pH 8-9. The average of hydrogen generation TON was 8025. It is known that a strong basic or acidic environment which our hybrids shows low TON, is disadvantageous to hydrogen production. These results can be speculated as several factors. First, the pH values can influence the adsorption between EY and PDha-*g*-AMPS. In the acidic solution, functional groups of PDha such as -COOH and -NH₂ were protonated by proton ions, so the EY can be release effectively. However, the EY has also low solubility in low pH. In the strong basic solution, the carboxyl groups of EY were deprotonated and the amino groups of PDha deprotonated, so the dye could not adsorb on PDha effectively because of less electrostatic force between PDha and EY functional groups. Moreover, the pH values can also influence the existing state of the electron donor reagent. TEOA was protonated in acidic solution, so its ability of donating electrons would be weakened, which might influence the regeneration of oxidized dye molecules. Thus our hybrids showed low hydrogen production activity.

Optimization of the Photocatalytic Reaction: The photocatalytic activity for hydrogen evolution over the EY/Pt₃Co/PDha-*g*-AMPS/CNT photocatalyst was optimized by considering the effects of PDha-*g*-AMPS, EY, and CNT loading amounts (Figure S10-S12).

Our early investigations show that the PDha-*g*-AMPS content is essential factor for H₂ production activity and the photocatalytic activity of EY/Pt₃Co/PDha-*g*-AMPS/CNT is found to be strongly dependent on the amount of PDha-*g*-AMPS loaded. To evaluate the influence of the PDha-*g*-AMPS on TON of H₂ production, we change the polymer content systematically from 0 to 8.0 mg mL⁻¹ and we collect the hydrogen production activity for system containing CNT with concentrations of 75 μg mL⁻¹, EY with concentration of 0.1 mg mL⁻¹, 0.5 M TEOA solution and pH = 8-9 respectively as reaction condition. As our data shows in Figure S10, the amount of hydrogen production increases with increasing PDha-*g*-AMPS loading amount to a maximum at 0.5 mg mL⁻¹, beyond which it decreases again. The mean reason for this behaviour is probably decreasing the connection between EY and Pt₃Co with accessible surface of the CNT. When the amounts of PDha-*g*-AMPS content is increasing, it can result a thicker coating layer on CNT. Consequently, this thickness of coating can significantly reduce probably the access to surface of the CNT for catalyst and dye as an effect of insulation.

The concentration of EY plays also a key role in the number of excited electrons. Figure S11 is illustrate the effect of the concentration of EY on the photocatalytic activity of EY/Pt₃Co/PDha-*g*-AMPS/CNT system containing: (PDha-*g*-AMPS, CNT and TEOA solution with concentrations of 1 mg mL⁻¹ and 1 μg mL⁻¹ and 0.5 M respectively at pH = 8-9). As can be seen from Figure S11, the activity increases with the increase of EY, arrives at a maximum number when EY = 0.1 mmol L⁻¹, and afterwards gradually show decreases. We can attribute this

variation to the adsorption of EY. The adsorption amount of EY increases as the increase of EY concentration in solution and in surface local of the PDha-*g*-AMPS/CNT, and reaches saturation at approximately EY = 0.1 mmol L⁻¹. The highest photocatalytic activity obtained at this concentration can be interpreted as the following: when EY concentration is low, most of the dyes produce the electrons which is used for hydrogen production increase. When the adsorption of EY to PDha-*g*-AMPS/CNT approaches the saturation level, it is disadvantageous to photocatalytic activity if EY increases further. This is because the free dye molecules in solution cannot participate anymore in electron transfer. In sharp contrast, they absorb a part of illuminated light and lead to loss of the effective portion of the incident light for hydrogen production. Then the photocatalytic activity declines accordingly.

CNT functions as a strong electron acceptor and transporter because of excellent electron conductivity. Our investigation indicate that, by even a small amount of CNT, we can noticeably increase H₂ production activity. Thus, the H₂ production activity is also dependent of amount of the CNT and we evaluate this effect on EY/Pt₃Co/PDha-*g*-AMPS/CNT system containing: (PDha-*g*-AMPS, EY and TEOA solution with concentrations of 0.5 mg mL⁻¹ and 75 mol L⁻¹ and 0.5 M respectively at pH = 8-9). Figure S12 display photocatalytic activity of EY/Pt₃Co/PDha-*g*-AMPS/CNT catalyst in present different amount of CNT. In the presence of a small amount of CNT (2.5 to 25 μg mL⁻¹), the TON of sample EY/Pt₃Co/PDha-*g*-AMPS/CNT was slightly enhanced from 3310 to 3874, perhaps because the amount of CNT was not enough to efficiently to adsorb EY.

When the CNT content was (75 μg mL⁻¹), the H₂-production rate reached the highest TON of 6093 (Figure S12). In this regard, the photocatalytic activity of sample EY/Pt₃Co/PDha-*g*-AMPS/CNT exceeds that of EY/Pt₃Co/PDha-*g*-AMPS by a factor of 2.1. However, a further increase in the CNT content led to a deterioration of the catalytic performance. In particular, at the CNT content of (100 μg mL⁻¹), the photocatalytic activity gradually decreased, with an H₂-production TON 5623. It is reasonable because the introduction of a large percentage of black CNT led to rapidly decreased the intensity of light through the depth of the reaction solution, which could be called a "shielding effect".^{38,39} As a consequence, a suitable content of CNT is crucial for optimizing the photocatalytic activity of EY/Pt₃Co/PDha-*g*-AMPS/CNT hybrid system.

Stability of EY/Pt₃Co/PDha-*g*-AMPS/CNT: The stability of EY/Pt₃Co/PDha-*g*-AMPS/CNT catalyst at the optimum experimental conditions is listed in Figure S13, where the reaction condition was: EY, PDha-*g*-AMPS and CNT with concentrations of 100 mmol L⁻¹, 0.5 mg mL⁻¹, and 75 μg mL⁻¹ respectively; 0.5 M TEOA solution; pH = 8-9. The stability performance of EY/Pt₃Co/PDha-*g*-AMPS/CNT was tested over three cycles.

The TON of hydrogen production was reached to 105 in the first run, without renewing the TEOA and EY, the hydrogen-production performance was measured in the next cycle. After two more cyclic of irradiation and measurement, samples then reached the maximum TON at the third run (684), and then declined slightly in the consecutive runs. The slight decrease in

the consecutive runs was probably caused by the consumption of electron donor (TEOA) and the partial decomposition of EY dye. However, when another fresh portion of EY and TEOA were added to the system after reaction, the photocatalytic activity was recovered.

Mechanism: When the EY molecules are directly adsorbed on CNT by Pt₃Co/PDha-*g*-AMPS and excited with visible light

irradiation, a large energy band offset form between EY* and CNT, and then the excited electrons most likely transfer to the Pt₃Co/PDha-*g*-AMPS/CNT hybrids (Figure 6). To justify this hypothesis, the UV/Vis and photoluminescence spectra of EY in present of PDha-*g*-AMPS/CNT and Pt₃Co/PDha-*g*-AMPS/CNT were investigated and shown in Figure 6.

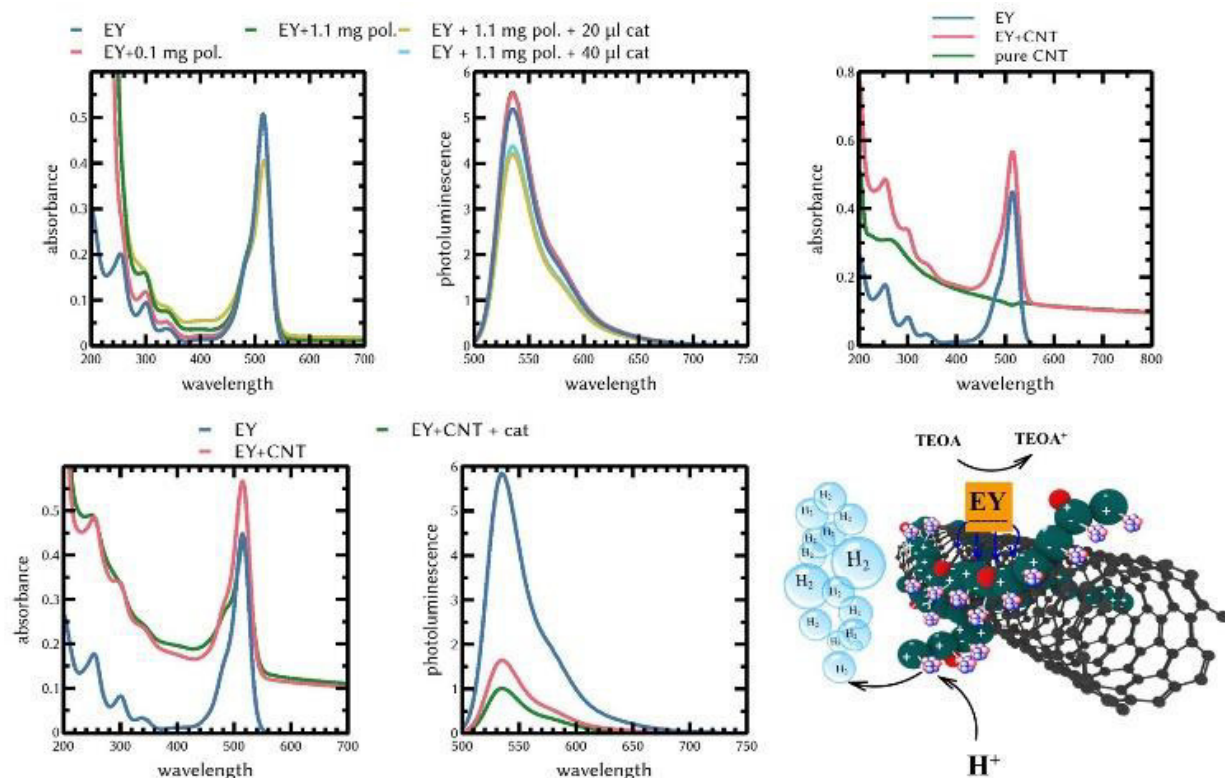


Figure 6: (A-E) Absorption and fluorescence spectra of EY in presents of PDha-*g*-AMPS, PDha-*g*-AMPS/CNT and Pt₃Co/PDha-*g*-AMPS/CNT and (F): Schematic illustration of the charge separation and transfer in the Pt₃Co/PDha-*g*-AMPS/CNT system under visible light.

UV-vis spectroscopy was used to study the ground-state interaction between different components of hybrid system including: EY with PDha-*g*-AMPS, PDha-*g*-AMPS/CNT and Pt₃Co/PDha-*g*-AMPS/CNT. Hereby, the absorption spectra of EY is shown in Figure 6. This spectrum is also recorded with adding different amount of PDha-*g*-AMPS and certain amount of PDha-*g*-AMPS/CNT and Pt₃Co/PDha-*g*-AMPS/CNT. During the measurements, the concentration of EY in water was kept constant, and PDha-*g*-AMPS was varied in the concentration. Our observation indicates, that at first sight, absorption of EY solution slightly decreased in the presence of PDha-*g*-AMPS. These spectral results proof EY interaction with PDha-*g*-AMPS in the ground state. Nevertheless, this interaction is weak and the dye always exists in an equilibrium between the free EY and EY adsorbed on the PDha-*g*-AMPS. However, in the next step, when we add PDha-*g*-AMPS/CNT to same concentration of the EY solution, we observed more pronounced decreasing in the absorption spectrum of EY/PDha-*g*-AMPS/CNT. Surprisingly,

with incorporation of the Pt₃Co, EY solution indicate a remarkable decreasing in absorption in present of Pt₃Co/PDha-*g*-AMPS/CNT. This decrease in the absorbance represents a trapped electrons are transferred to Pt₃Co/PDha-*g*-AMPS/CNT hybrids strongly.

For deeper understanding the electron transferring, photoluminescence and quantum yields (QY) of EY solution was again controlled in presents of PDha-*g*-AMPS, PDha-*g*-AMPS/CNT and Pt₃Co/PDha-*g*-AMPS/CNT and the results are shown in Figure 6. The excitation wavelength of the light source was 460 nm. EY solution shows an intensive emission peak centred at XXX nm with a strong fluorescence intensity of about xxx and QY of xxx because of its conjugated xanthene structure and strong recombination of excited charge pairs upon visible light excitation. As PDha-*g*-AMPS, PDha-*g*-AMPS/CNT and Pt₃Co/PDha-*g*-AMPS/CNT are introduced into the EY solution, a considerable fluorescence quenching is observed and the fluorescence intensity of EY decreases to XXX along with the

slight blue shift of emission peak (XXX nm). This small blue shift in emission band could be the result of the noncovalent π - π stacking interaction between aromatic regions of the PDha-*g*-AMPS/CNT and EY. Surprisingly, this quenching is significantly remark for Pt₃Co/PDha-*g*-AMPS/CNT. Accordingly, we could suggest the electron transfer from the excited state of EY to Pt₃Co/PDha-*g*-AMPS/CNT which is similar to the previous reports on a dye-sensitize functionalized CNT and GO.

PDha-*g*-AMPS as Support for Other Photocatalytic System

Hydrogen production with assistance of PDha-*g*-AMPS is extraordinary high for the described system. Our results indicate that the PDha-*g*-AMPS has significant role for the activity of this reaction. However, our data was competitive with the performance of other catalysts reported in the literature (Table S1). We were interested in highlighting the effective supporting and multifunctionality of our system, that could be transferred to a series of catalyst include: Ag, Au, Pd, Pt, [Mo₃S₁₃]²⁻ and CdS nanoparticles are produced or grafted with/without PDha-*g*-AMPS platform. Afterwards, they are evaluated for hydrogen production in presence and absence of PDha-*g*-AMPS.

CdS nanoparticles which were characterized above, were evaluated for hydrogen production. Figure 5, C shows the comparison of the activities of CdS produced with PDha-*g*-AMPS and CdS formed without assistance of the polymer. The photocatalytic H₂ production rate of CdS without polymer is 68 $\mu\text{mol/h.g}$. This rate is close to what literature reported and also we observed in our previous study.²⁴ This performance of the CdS free nanoparticles is low because of the rapid recombination of photoexcited electrons and holes. However, the Figure 5, C illustrate the hydrogen production rate of the CdS nanoparticles produced and immobilized with assistance of PDha-*g*-AMPS double hydrophilic copolymer. As expected, PDha-*g*-AMPS/CdS activity is greatly enhanced to 497 $\mu\text{mol/h.g}$ in the presence of 1 PDha-*g*-AMPS, probably because of immobilization of crystals by polymer, better solution stability and preventing the CdS for forming the aggregation and secondary aggregation by PDha-*g*-AMPS polyelectrolyte.

Noble metal cocatalysts such as Pt, Pd, Ag, and Au can function as efficient H₂ productin catalyst or cocatalyst. For photocatalysts such as EY, these metals are believed to be the efficient catalyst due to its high work function and low overpotential for H₂ evolution. Hereby, we produced these series of metal catalyst with assistance of the PDha-*g*-AMPS. Afterwards, EY/noble metal catalyst were carried out for the hydrogen production activity in presents (Pt, Pd, Ag, and Au/PDha-*g*-AMPS/EY) and absent (Pt, Pd, Ag, and Au/EY) of PDha-*g*-AMPS graft copolymer. Our results indicate that PDha-*g*-AMPS has again great influence in enhancing the

photocatalytic hydrogen production activity. Figure 7 shows the comparison of the photocatalytic hydrogen production TON of Pt, Pd, Ag, and Au/EY and Pt, Pd, Ag, and Au/PDha-*g*-AMPS/EY. For catalyst without polymeric support (e.g. Pt, Pd, Ag, and Au/EY, a hydrogen production TON 50, 20, 70, 260 can be achieved for Pt, Pd, Ag, and Au respectively. When we loaded the (1.0 mg/mL) PDha-*g*-AMPS with corresponding noble metal catalyst (*i.e.* Pt, Pd, Ag, and Au/PDha-*g*-AMPS/EY), all different Pt, Pd, Ag, and Au/PDha-*g*-AMPS/EY shows a great enhancement of hydrogen production activity. For example, the TON of Au increased from 206 to 826, which was 4-fold enhancement. These results suggested that the PDha-*g*-AMPS could easily and effectively immobilize dye sensitizer with other catalyst. The system based PDha-*g*-AMPS competes favourably with other state of the art photocatalysts in terms of hydrogen production ability (Table S1). As shown in Figure 7 and Figure 5, the system generates bubbles that are clearly observed in a matter of min under LED irradiation or even sun light. It is worth noting, that these systems could be further improved as we did for the above described system in respect of concentration and composition

Pristine fullerene (C60) is a semiconductor and possesses a similar electrical conductivity in accepting and transporting electrons to its analogies such as CNTs and graphene.^{40,41} We showed that C60 can also be stabilized with PDha-*g*-AMPS graft copolymer. We are now interest to activity of C60 in our catalytic system. Hereby, Pt₃Co/PDha-*g*-AMPS with concentration of 0.5 mg mL⁻¹ was used for coating and stabilizing the C60 (0.5 mg mL⁻¹). Afterwards, the obtained hybrid structures (Pt₃Co/PDha-*g*-AMPS/C60) was added to solution of EY with concentration of 0.1 mmol L⁻¹ and the hydrogen production TON was calculated after 24 hours irradiation under blue LED light. Figure 7 illustrate the TON of Pt₃Co/PDha-*g*-AMPS/EY and Pt₃Co/PDha-*g*-AMPS/C60/EY. As we can see, the TON was increased from 377 to 3722 after loading the PDha-*g*-AMPS/C60. Most likely, this enhancement is due to a forming strong interaction by PDha-*g*-AMPS between the C60 and EY. Then C60 can operate effectively as electron mediator for hydrogen evolution.

Thiomolybdate [Mo₃S₁₃]²⁻ nanoclusters, as a molecular mimic of MoS₂ edge sites, showed high efficiency in photochemical H₂ production.⁴² We introduce [Mo₃S₁₃]²⁻ as negative charged and non-noble metal catalyst which can interact with PDha-*g*-AMPS catalytic system. Hereby, the poor water soluble [Mo₃S₁₃]²⁻ salts are evaluated for hydrogen production in presence of 0.5 M TEOA and 100 mmol L⁻¹ EY in water. Figure 7 display the TON of [Mo₃S₁₃]²⁻ which are evaluated in absent and presents of PDha-*g*-AMPS platform. As our data shows, when [Mo₃S₁₃]²⁻ are stabilized with PDha-*g*-AMPS polyampholytic network, the TON of hydrogen production was increase from 10 to 134 after 24 hours irradiation. Most probably, this 13.4 times enhancement is due to a strong interaction between the [Mo₃S₁₃]²⁻ and the EY by polyampholytic scaffold.

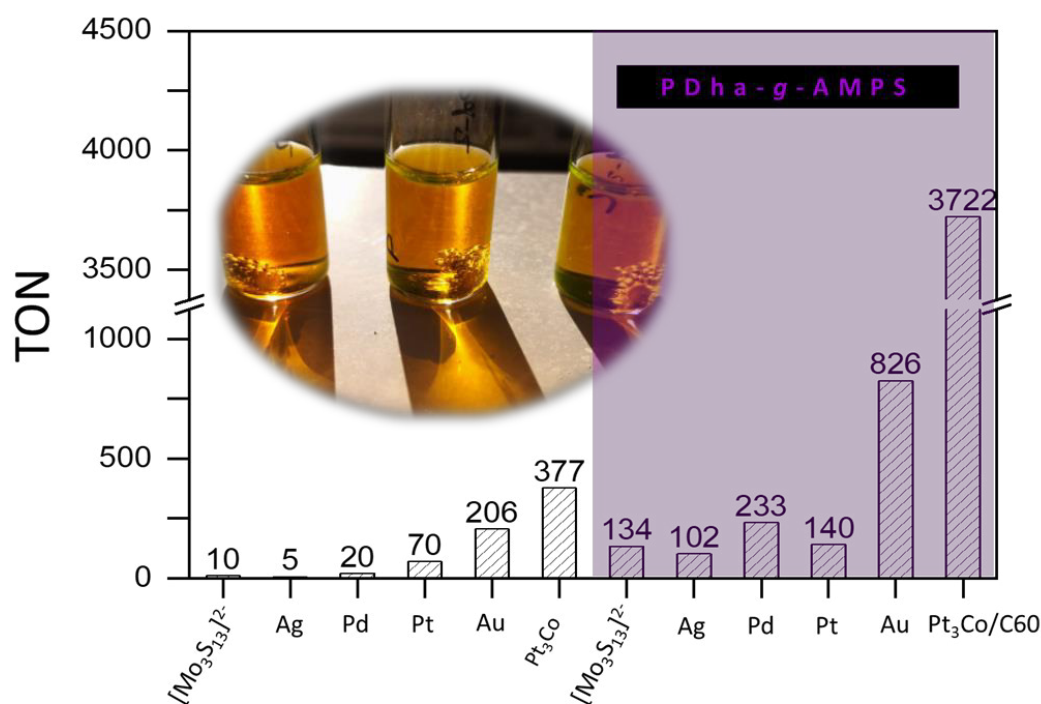


Figure 7: Photocatalytic hydrogen production performance for different photocatalyst system in present and absent of PDha-g-AMPS, where the turnover number (TON) is defined as (moles of hydrogen produced)/(moles of catalyst) after illumination for 24 hour, (Reaction conditions: EY and PDha-g-AMPS with concentrations of 0.1 mmol L^{-1} and 0.5 mg mL^{-1} respectively; 0.5 M TEOA solution; $\text{pH} = 8-9$).

Conclusions

In conclusion, we report a novel polyampholytic copolymer as a multifunctional platform for effectively combining different catalysts, electron mediators and sensitizers for photocatalytic hydrogen production. We have also demonstrated PDha-g-AMPS as a template for the preparation and stabilization of different metal nanoparticles and carbon nanomaterial.

Our results reveal, that we could facially achieve the enhancement of the photocatalytic hydrogen production by adding the polymer as a matrix for variety of system including dye or semiconductor sensitizer, alloy, noble metals and non-noble metal catalyst, and carbon nanomaterials as electron mediator. The role of the graft copolymers in enhancement of the photocatalytic reaction was carefully tested by varying the concentration as well as the types of sensitizer, catalyst and

electron mediator. Specifically, we find that the obvious improvement of the photocatalytic activity for hydrogen production was found by immobilizing non-functionalized CNT with PDha-g-AMPS. $\text{Pt}_3\text{Co}/\text{PDha-g-AMPS}/\text{CNT}$ shows the best activity ($\text{TON} > 8000$). Our strategy indicates, that instead of revising molecular structures, which is challenging from both design and synthesis points of view, we can use the polyampholytic copolymers to improve and regulate different molecular catalytic systems by immobilization. This strategy introduce a systems could be valuable for other molecular catalysts. Optimization of H_2 production and introducing the alternative catalyst, and dye or semiconductor sensitizer such as perylene and BiOVO_4 for these systems will be the subject of further investigations.

Conflicts of interest

In accordance with our policy on [Conflicts of interest](#) please ensure that a conflicts of interest statement is included in your manuscript here. Please note that this statement is required for all submitted manuscripts. If no conflicts exist, please state that “There are no conflicts to declare”.

Acknowledgements

We thank Peggy Laudeley for SEC measurements. The Deutsche Forschungsgemeinschaft is gratefully acknowledged for financial support within the framework of TRR234 “CataLight” (Project ID: 364549901, projects B4, B5 and Z2) as well as a research infrastructure grant (INST 275/257-1 FUGG). The TEM facilities of the Jena Center for Soft Matter (JCSM) were established with a grant from the German Research Council (DFG) and the European Fund for Regional Development (EFRE).

Notes and references

- M. W. Kanan and D. G. Nocera, *Science (80-.)*, 2008, **321**, 1072–1075.
- T. A. Faunce, W. Lubitz, A. W. B. Rutherford, D. MacFarlane, G. F. Moore, P. Yang, D. G. Nocera, T. A. Moore, D. H. Gregory and S. Fukuzumi, *Energy Environ. Sci.*, 2013, **6**, 695–698.
- A. S. Weingarten, R. V. Kazantsev, L. C. Palmer, M. McClendon, A. R. Koltonow, A. P. S. Samuel, D. J. Kiebal, M. R. Wasielewski and S. I. Stupp, *Nat. Chem.*, 2014, **6**, 964–970.
- B. L. Wadsworth, D. Khusnutdinova and G. F. Moore, *J. Mater. Chem. A*, 2018, **6**, 21654–21665.
- D. V. Pergushov, A. H. E. Müller and F. H. Schacher, *Chem. Soc. Rev.*, 2012, **41**, 6888–6901.
- A. F. Thünemann, M. Müller, H. Dautzenberg, J.-F. Joanny and H. Löwen, in *Polyelectrolytes with defined molecular architecture II*, Springer, 2004, pp. 113–171.
- M. Hess, R. G. Jones, J. Kahovec, T. Kitayama, P. Kratochvíl, P. Kubisa, W. Mormann, R. F. T. Stepto, D. Tabak and J. Vohlidal, *Pure Appl. Chem.*, 2006, **78**, 2067–2074.
- A. B. Lowe and C. L. McCormick, *Chem. Rev.*, 2002, **102**, 4177–4190.
- I. Szilagy, G. Trefalt, A. Tiraferri, P. Maroni and M. Borkovec, *Soft Matter*, 2014, **10**, 2479–2502.
- J. C. Salamone and W. C. Rice, *Mark, HF*, 1988, 514–530.
- A. Nabiyan, P. Biehl and F. H. Schacher, *Macromolecules*.
- H. Sai, A. Erbas, A. Dannenhoffer, D. Huang, A. Weingarten, E. Siismets, K. Jang, K. Qu, L. C. Palmer and M. O. De La Cruz, *J. Mater. Chem. A*, 2020, **8**, 158–168.
- J. B. Max, D. V. Pergushov, L. V. Sigolaeva and F. H. Schacher, *Polym. Chem.*, 2019, **10**, 3006–3019.
- J. B. Max, P. J. Mons, J. C. Tom and F. H. Schacher, *Macromol. Chem. Phys.*, 2020, **221**, 1900383.
- P. Biehl, P. Wiemuth, J. G. Lopez, M.-C. Barth, A. Weidner, S. Dutz, K. Peneva and F. H. Schacher, *Langmuir*.
- J. B. Max, K. Kowalczyk, M. Köhler, C. Neumann, F. Pielenz, L. V. Sigolaeva, D. V. Pergushov, A. Turchanin, F. Langenhorst and F. H. Schacher, *Macromolecules*.
- M. Phonyiem, S. Chaiwongwattana, C. Lao-Ngam and K. Sagarik, *Phys. Chem. Chem. Phys.*, 2011, **13**, 10923–10939.
- C. W. Jones, *Top. Catal.*, 2010, **53**, 942–952.
- D. J. Cole-Hamilton, *Science (80-.)*, 2003, **299**, 1702–1706.
- J. M. Fraile, J. I. Garcia and J. A. Mayoral, *Chem. Rev.*, 2009, **109**, 360–417.
- Z. Hu and C. Y. Jimmy, *J. Mater. Chem. A*, 2013, **1**, 12221–12228.
- A. Rajagopal, F. Venter, T. Jacob, L. Petermann, S. Rau, S. Tschierlei and C. Streb, *Sustain. energy fuels*, 2019, **3**, 92–95.
- J. Zou, S. I. Khondaker, Q. Huo and L. Zhai, *Adv. Funct. Mater.*, 2009, **19**, 479–483.
- A. Nabiyan, M. Schulz, C. Neumann, B. Dietzek, A. Turchanin and F. H. Schacher, *Eur. Polym. J.*, 2020, 110037.
- Y.-J. Yuan, D. Chen, Z.-T. Yu and Z.-G. Zou, *J. Mater. Chem. A*, 2018, **6**, 11606–11630.
- H. Weller, H. M. Schmidt, U. Koch, A. Fojtik, S. Baral, A. Henglein, W. Kunath, K. Weiss and E. Dieman, *Chem. Phys. Lett.*, 1986, **124**, 557–560.
- Y. Xia, Y. Xiong, B. Lim and S. E. Skrabalak, *Angew. Chemie Int. Ed.*, 2009, **48**, 60–103.
- Z. Fan and H. Zhang, *Chem. Soc. Rev.*, 2016, **45**, 63–82.
- P. F. M. de Oliveira, R. M. Torresi, F. Emmerling and P. H. C. Camargo, *J. Mater. Chem. A*, 2020, **8**, 16114–16141.
- C. T. Campbell, S. C. Parker and D. E. Starr, *Science (80-.)*, 2002, **298**, 811–814.
- P.-F. Ho and K.-M. Chi, *Nanotechnology*, 2004, **15**, 1059.
- X. Ning and G. Lu, *Nanoscale*, 2020, **12**, 1213–1223.
- X. Zhang, T. Peng and S. Song, *J. Mater. Chem. A*, 2016, **4**, 2365–2402.
- L. Xie, J. Tian, Y. Ouyang, X. Guo, W. Zhang, U.-P. Apfel, W. Zhang and R. Cao, *Angew. Chemie*.
- T. Lazarides, T. McCormick, P. Du, G. Luo, B. Lindley and R. Eisenberg, *J. Am. Chem. Soc.*, 2009, **131**, 9192–9194.
- A. Lewandowska-Andraśojć, D. Larowska, E. Gacka, T. Pedzinski and B. Marciniak, *J. Phys. Chem. C*, 2020, **124**, 2747–2755.
- A. Kongkanand and P. V. Kamat, *ACS Nano*, 2007, **1**, 13–21.
- J. Yu, T. Ma and S. Liu, *Phys. Chem. Chem. Phys.*, 2011, **13**, 3491–3501.
- Q. Li, B. Guo, J. Yu, J. Ran, B. Zhang, H. Yan and J. R. Gong, *J. Am. Chem. Soc.*, 2011, **133**, 10878–10884.
- P. V. Kamat, *J. Phys. Chem. Lett.*, 2010, **1**, 520–527.
- S. Min and G. Lu, *J. Phys. Chem. C*, 2011, **115**, 13938–13945.
- M. Dave, A. Rajagopal, M. Damm-Ruttensperger, B. Schwarz, F. Nägele, L. Daccache, D. Fantauzzi, T. Jacob and C. Streb, *Sustain. Energy Fuels*, 2018, **2**, 1020–1026.

Polyampholytic graft copolymers: A platform to combine sensitizers and catalysts

Afshin Nabiyan ^a, Johannes B. Max ^a, Mathias Micheel,^{c,e} Jonas Eichhorn, ^a Christof Neumann,^{b,c,d} Maria Wächtler,^{c,e} Martin Schulz, ^{c,e} Benjamin Dietzek,^{c,d,e} Andrey Turchanin,^{b,c,d} and Felix H. Schacher ^{a,b,d} *

^a*Institute of Organic Chemistry and Macromolecular Chemistry (IOMC), Friedrich-Schiller University Jena, Lessingstraße 8, D-07743 Jena, Germany.*

^b*Jena Center for Soft Matter (JCSM), Friedrich Schiller University Jena, Philosophenweg 7, D-07743 Jena, Germany..*

^c*Institute of Physical Chemistry and Abbe Center of Photonics, Friedrich Schiller University Jena, Helmholtzweg 4, 07743 Jena, Germany.*

^d*Center for Energy and Environmental Chemistry Jena (CEEC Jena), Philosophenweg 7a, 07743 Jena, Germany.*

^e*Department Functional Interfaces, Leibniz Institute of Photonic Technology (IPHT), Albert-Einstein-Strasse 9, 07745 Jena, Germany.*

Experimental

General

Triethanolamine ($\geq 99.7\%$), Fullerene ($\geq 99\%$), Palladium(II) chloride (99%), 2-Acrylamido-2-methylpropane sulfonic acid, and AgNO_3 ($\geq 99.0\%$), Potassium tetrachloroplatinate ($\geq 99.9\%$) were purchased from Sigma-Aldrich (St. Louis, USA). TFA ($\geq 99.9\%$) and NaOH (0.1 N) were purchased from Roth (Karlsruhe, Germany), triethyl amine ($\geq 99.0\%$) was purchased from CHEMSOLUTE (Renningen, Germany), and N-(tert-butoxycarbonyl)-L-serin methylester (98%) was purchased from Carbolution Chemicals (St. Ingbert, Germany). NaBH_4 ($> 98\%$) was obtained from Acros Organics (Schwerte, Germany) was purchased from TCI chemicals (Tokyo, Japan). $\text{HAuCl}_4 \times 3 \text{H}_2\text{O}$ (99.99%) was purchased from Alfa Aesar (Haverhill, USA), and HCl (37% solution) was purchased from Fischer Scientific (Hampton, USA). We synthesized the blocbuilder and SG1 according to literature.[1,2]

Instrumentation

Nuclear magnetic resonance (NMR) spectroscopy

^1H - and ^{13}C -NMR spectra were performed on a Bruker AC 300 MHz using CDCl_3 , DMSO-d_6 and $\text{D}_2\text{O/NaOD}$ as solvents at a temperature of 298 K. The spectra were referenced by using the residual signal of the deuterated solvent.

Gas chromatography

Hydrogen was quantified by manual injection of a 200 μL sample from the headspace of the sealed cell into an Agilent 7820A gas chromatograph equipped with a Hayesep Q pre-column and a mol. sieve 5A separation column and a thermal conductivity detector (TCD). Nitrogen was used as carrier gas under isothermal conditions (130°C). The concentration of hydrogen was determined by a calibration curve obtained from known concentrations of H_2 .

Size exclusion chromatography (SEC)

An Agilent 1260 Infinity System, equipped with a 1260 IsoPump (G1310B), an 1260 ALS (G1310B) autosampler and three consecutive PSS SDV, 5 μm , 8x300mm columns was used for SEC measurements in THF. The flow rate was 1 ml/min and the columns were heated to at 30 °C. The signals were collected using a 1260 DAD VL (GG1329B) and a 1260 RID (G1315D) detector.

SEC measurements in DMSO were performed on a Jasco instrument using DMSO + 0.5 % LiBr as solvent at a flow rate of 0.5 ml/min at 65 °C and Pullulan calibration. It was equipped with PSS NOVEMA 3000 Angström / 300 Angström columns, a RI-930 detector as well as a PU-980 pump.

Dynamic Light Scattering (DLS)

DLS measurements were performed using an ALV laser CGS3 Goniometer equipped with a 633 nm HeNe laser (ALV GmbH, Langen, Germany) at 25 °C and at a detection angle of 90°. The CONTIN analysis of the obtained correlation functions was performed using the ALV 7002 FAST Correlator Software.

Transmission Electron Microscopy (TEM)

TEM images were acquired with a 200 kV FEI Tecnai G2 20 equipped with a 4k x 4k Eagle HS CCD and a 1k x 1k Olympus MegaView camera for overview images.

ξ-Potential

Zeta-potentials were measured on a ZetaSizer Nano ZS from Malvern via M3-PALS technique with a laser beam at 633 nm. The detection angle was 13°. The samples were prepared by titration of the polymer in 0.1 M NaOH (0.2 g/L) with 0.1 M HCl and 1 mL of the solution was taken at the desired pH values. The titration and pH detection was performed on a Metrohm 765 Dosimat titrator with a Greisinger electronic GMH3539 digital pH-/mV-electrode with a thermometer.

Potentiometric titration

Potentiometric titrations were performed with a TitroLine® 7000 titrator equipped with a WA 20 exchangeable unit, magnetic stirrer TM 235, and a ScienceLine pH combination electrodes with temperature sensor A162 from SI Analytics GmbH. The polymers were dissolved in 0.1 M NaOH at a concentration of 1.5 g/L and titrated against 0.1 M HCl *via* an automatic dynamic pH-titration method.

UV-Vis

UV/Vis measurements were performed on a Agilent Cary 60 in a Hellma quartz glass cuvette with a pathlength of 10 mm at room temperature in solvent. The absorbance was measured in a range from 200 nm to 800 nm in 5 nm steps.

Synthesis

Synthesis of *tBAMA*

Boc-Ser-OMe (10.0 g, 45.6 mmol; 1.0 equiv) was dissolved in dichloromethane (200 mL), and MsCl (6 mL; 77.5 mmol; 1.7 equiv) was added. After cooling in an ice bath, triethylamine (23 mL; 165.9 mmol; 3.6 equiv) was slowly added dropwise, and the reaction mixture was stirred for 1 h at 0 °C. After additional 2 h at room temperature, the mixture was afterward washed with potassium bisulfate (1%) to neutrality. The organic phase was dried with Na₂SO₄, and the solvent was removed under reduced pressure. The crude product was further purified via column chromatography with silica gel (ethyl acetate/*n*-hexane v/v 1/4). After removal of the solvent under reduced pressure, the product was yielded as a colorless oil (8.6 g, 94%).

¹H NMR (300 MHz, CDCl₃, δ): 7.01 (s, 1 H, -NH), 6.16 (s, 1 H, -C=CH-), 5.73 (s, 1 H, -C=CH-), 3.83 (s, 3 H, -O-CH₃), 1.48 (s, 9 H, -COO-C(CH₃)₃) ppm.

Synthesis of *PtBAMA*

tBAMA, BlocBuilder and SG1 ([40]/[1]/[0.65]) were dissolved in 1,4-dioxane (66 wt %). The reaction mixture was degassed via four freeze-pump-thaw circles and stirred for 15 min at 80 °C under Ar. Afterward, the crude product was precipitated in cold *n*-hexane, washed three times with hexane, and dried under vacuum. The product was obtained as a white powder.

¹H NMR (300 MHz, CDCl₃, δ): 6.00–5.00 (m, -NH), 4.08–3.37 (m, -O-CH₃), 3.32–2.02 (m, -C-CH₂-), 1.75–1.16 (m, -COO-C(CH₃)₃) ppm.

SEC (CHCl₃/*i*-PrOH/NEt₃, PS calibration): $M_n = 11,000$ g/mol, $M_w = 20,790$ g/mol, $\bar{D} = 1.89$.

Deprotection of *PtBAMA* to *PAMA*

PtBAMA was dissolved in TFA (~ 40 equiv per monomer unit) and heated to 50 °C. The reaction was stopped after 1 h, and the product was precipitated in cold methanol. After filtering and washing with methanol and diethyl ether several times, the product was dried under vacuum and obtained as a yellow powder. Yield: 60%

^1H NMR (300 MHz, D_2O + NaOD, δ): 3.32 (s, $-\text{COO}-\text{CH}_3$), 2.78–1.90 (m, $-\text{C}-\text{CH}_2-$) ppm.

Post-polymerization modification of PDha-*stat*-PAMA with AMPS

PDha_{0.85}-*stat*-PAMA0.15 (100 mg) and AMPS (10 eq per monomer unit) were dissolved in water (5 ml each, pH 13, KOH). Afterwards the clear solutions were mixed and placed in an oil bath at 60 °C for constant stirring. The reaction was terminated after 48 h, by adding aqueous HCl (0.5 M) until a pH of 7 was reached. Then, the crude product was dialyzed against deionized water (MWCO = 3.5 kDa) for 2 days and afterwards freeze-dried to obtain a colorless polymer powder.

Carbon nanomaterials dispersion

Desirable amount of polymer was added to target concentration of MWCNTs or C60 in water. Afterwards the mixture placed in an ice bath. Dispersions were then formed by using an ultrasonic finger (20% power, 30 min, pulsed: 60 second on and 30 s off).

Catalysis fabrication and immobilization

Nobel metal fabrication: PDha-*g*-AMPS was dissolved in distilled water (1 mg.mL⁻¹), and a solution of AgNO₃, K₂PdCl₄, K₂PtCl₄ and/or H[AuCl₄] (0.01 mmol. mL⁻¹) was added. Afterward, the solution was stirred for 20 min for appropriate mixing. Then, the reduction agent, NaBH₄ (0.01 mmol. mL⁻¹), was added at once under constant stirring, and the reaction mixture turned colored dispersion immediately.

Pt₃Co was prepared by a modification of the synthesis reported Yu et al by reduction of Pt and Co salts together in ethylene glycol.[3] Briefly, 5.72 mg H₂PtCl₆ (corresponding to 2.7 mg Pt) and 0.66 mg CoCl₂ (corresponding to 0.3 mg Co) were dissolved in 20 mL ethylene glycol (pH was adjusted to 11 by NaOH) to form a homogeneous and light green solution. The solution was then transferred to a 100 mL Schlenk flask with Teflon septum and heated at 200 °C for 15 h. The black precipitate was then filtered and washed with deionized water, acetone and absolute alcohol to remove soluble species before being dried in a vacuum oven at 70 °C overnight.

(NH₄)₂[Mo₃S₁₃].2H₂O was synthesized according to the literature. [4] Briefly, to a solution of (NH₄)₆Mo₇O₂₄·4H₂O (4.0 g, 3.2 mmol) was added ammonium polysulfide solution (120 ml, 25 wt%). The reaction mixture was covered and heated to 96°C without stirring for five days. Dark red crystals were isolated by filtration, washed with water, ethanol, carbon disulfide and ether before air drying. Yield: 5.6 g, dark red crystals (97.9% based on Mo).

CdS fabrication: To induce formation of CdS, the desirable amount of CdCl₂ with concentration of 0.01 mol L⁻¹ was added to 1 mg.mL⁻¹ solution of PDha-*g*-AMPS during of string under Argon. After 1 hours, 1 similar equivalences of Na₂S with concentration of 0.01 M was added slowly to polymer solution and the color of the dispersion changed immediately to yellow. The dispersion was then kept at 25 °C overnight with magnetic stirring. The mixture was protected from light by wrapping the reaction vial in aluminum foil to prevent photo bleaching in 5 °C.

Photocatalysis

The photocatalytic hydrogen production experiments were performed in a 5 or 10 mL Pyrex flask, the openings of which were sealed with a silicone rubber septum, at ambient temperature and atmospheric pressure. A LED lamp with max ($\lambda_{\text{max}} = 470 \text{ nm}$) was used as a visible light source to trigger the photocatalytic reaction and was positioned 2 cm away from the reactor. In a typical photocatalytic experiment, 1 mg of the prepared desired hybrids nanomaterials was dissolved in 2 mL of a mixed aqueous solution containing 0.5 TEOA, and the system was then bubbled with nitrogen for 20 min to remove the dissolved oxygen and create an anaerobic condition. A 0.2 mL sample of the generated gas was collected intermittently through the septum, and hydrogen content was analyzed by gas chromatography with a thermal conductivity detector (TCD).

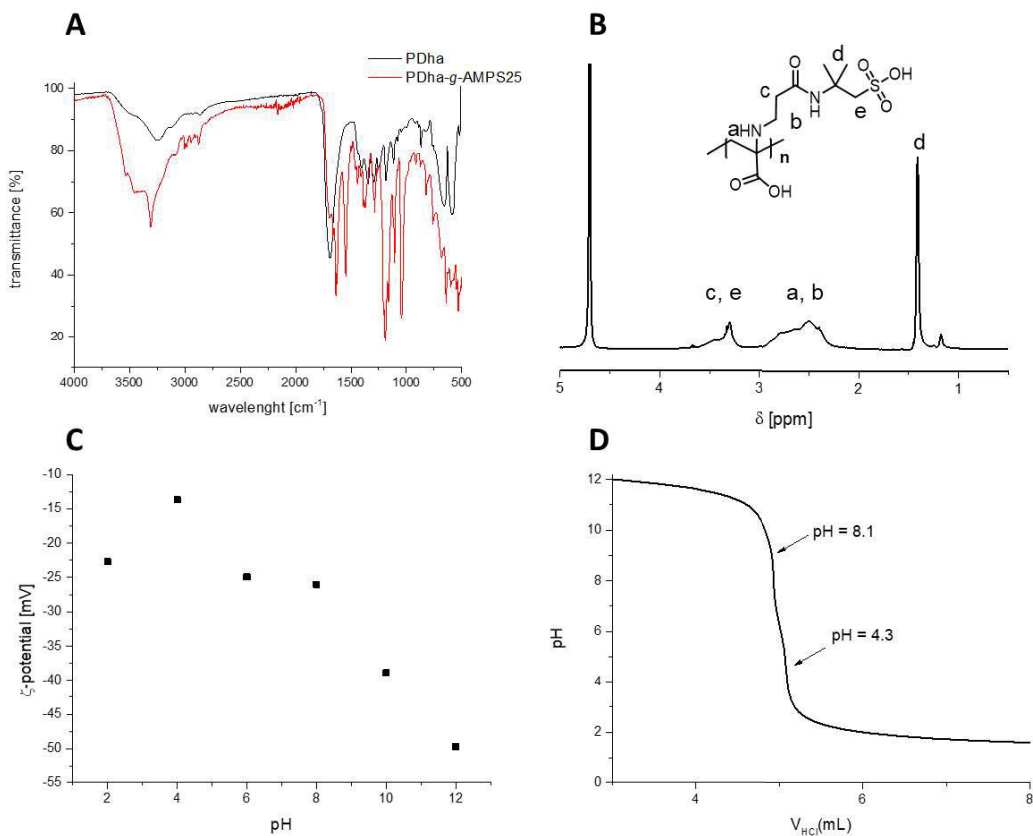


Figure S1: Characterization of PDha-g-AMPS double hydrophilic graft copolymer via (A): FT-IR spectroscopy, (B): $^1\text{H-NMR}$ and (C): ζ -potential measured with a zetasizer and (D): Potentiometric titration.

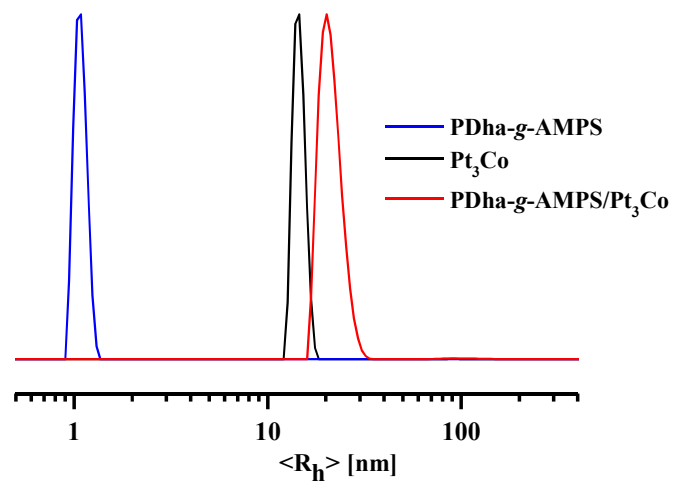


Figure S2: DLS CONTIN plot for PDha-*g*-AMPS, Pt₃Co, and PDha-*g*-AMPS/ Pt₃Co in water.

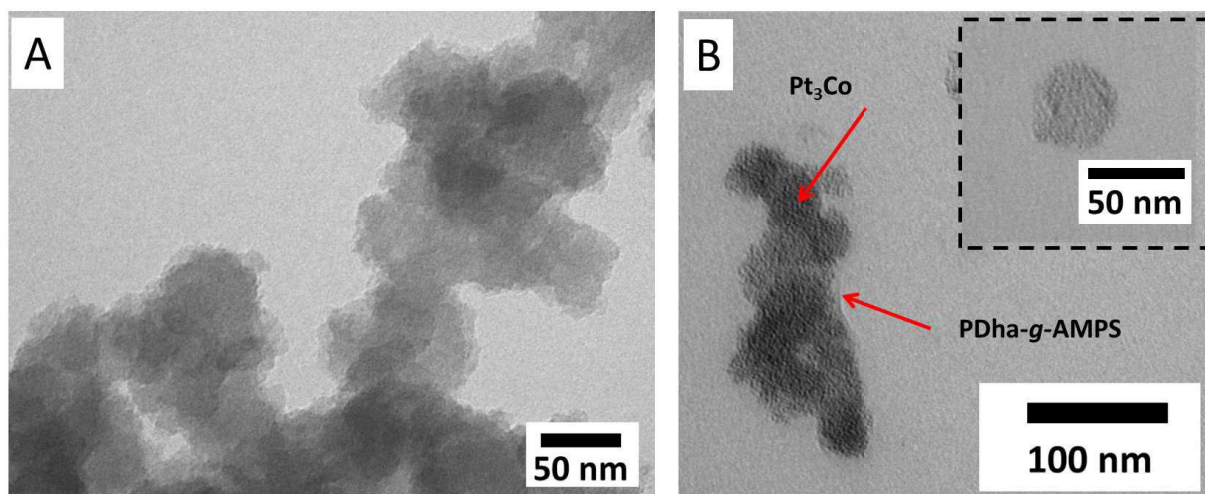


Figure S3: (A-B): TEM micrographs of PDha-*g*-AMPS/Pt₃Co with different magnification.

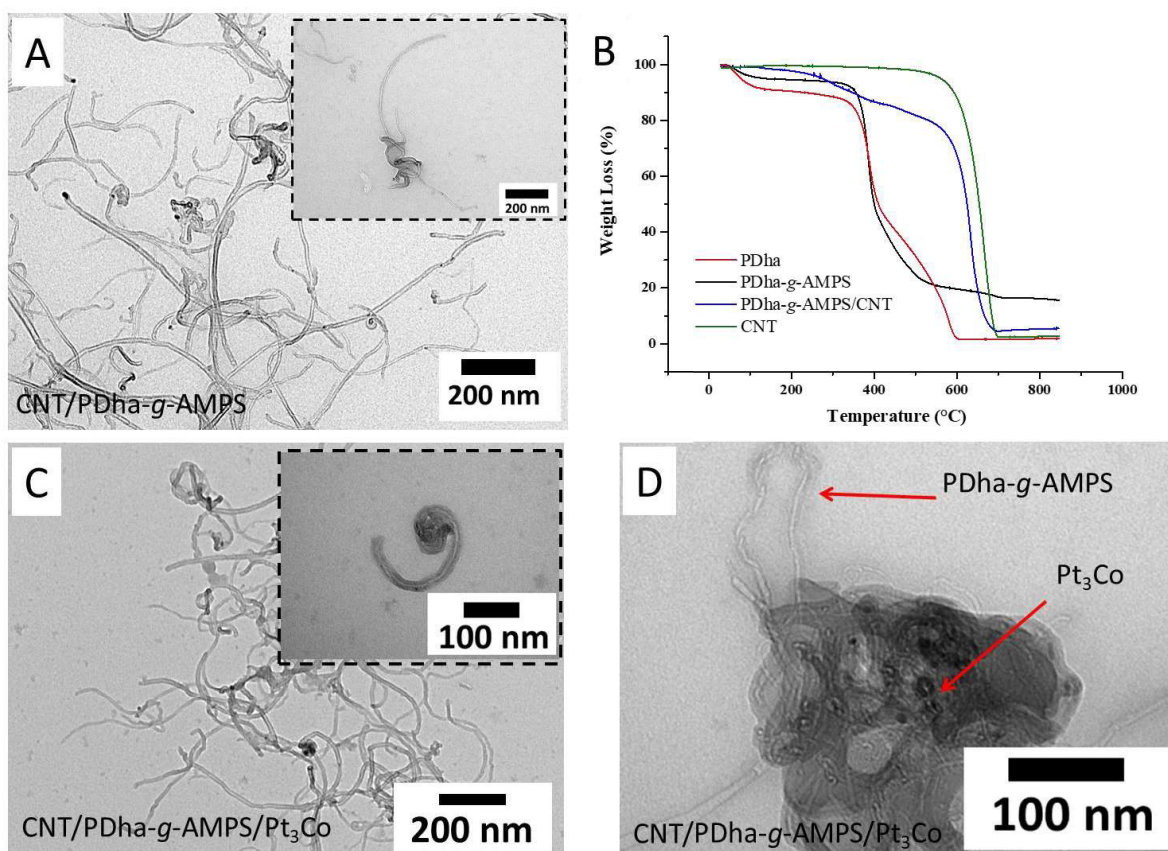


Figure S4: (A): TEM micrographs of PDha-g-AMPS/CNT with different magnification, (B): Thermograms of PDha, PDha-g-AMPS, PDha-g-AMPS/CNT and CNT, (C-D): TEM micrographs of CNT/PDha-g-AMPS/ Pt₃Co .

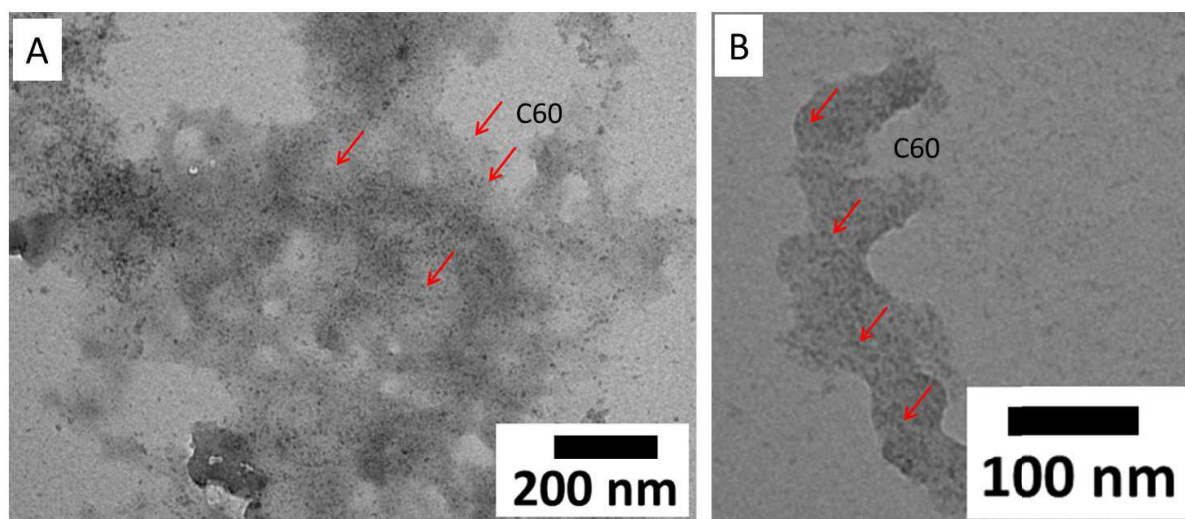


Figure S5: (A): TEM micrographs of PDha-g-AMPS/C60 with different magnification

The average sizes of CdS nanoparticles were determined using Hengleins [5,6] empirical model, which relates the diameter of the CdS nanoparticle ($2R$) to the exciton absorption, shoulder, and edge in the UV-vis spectra according to Equation S1.

$$2R(\text{nm}) = \frac{0.10}{0.1338 - 0.0002345 * \lambda} \quad (1)$$

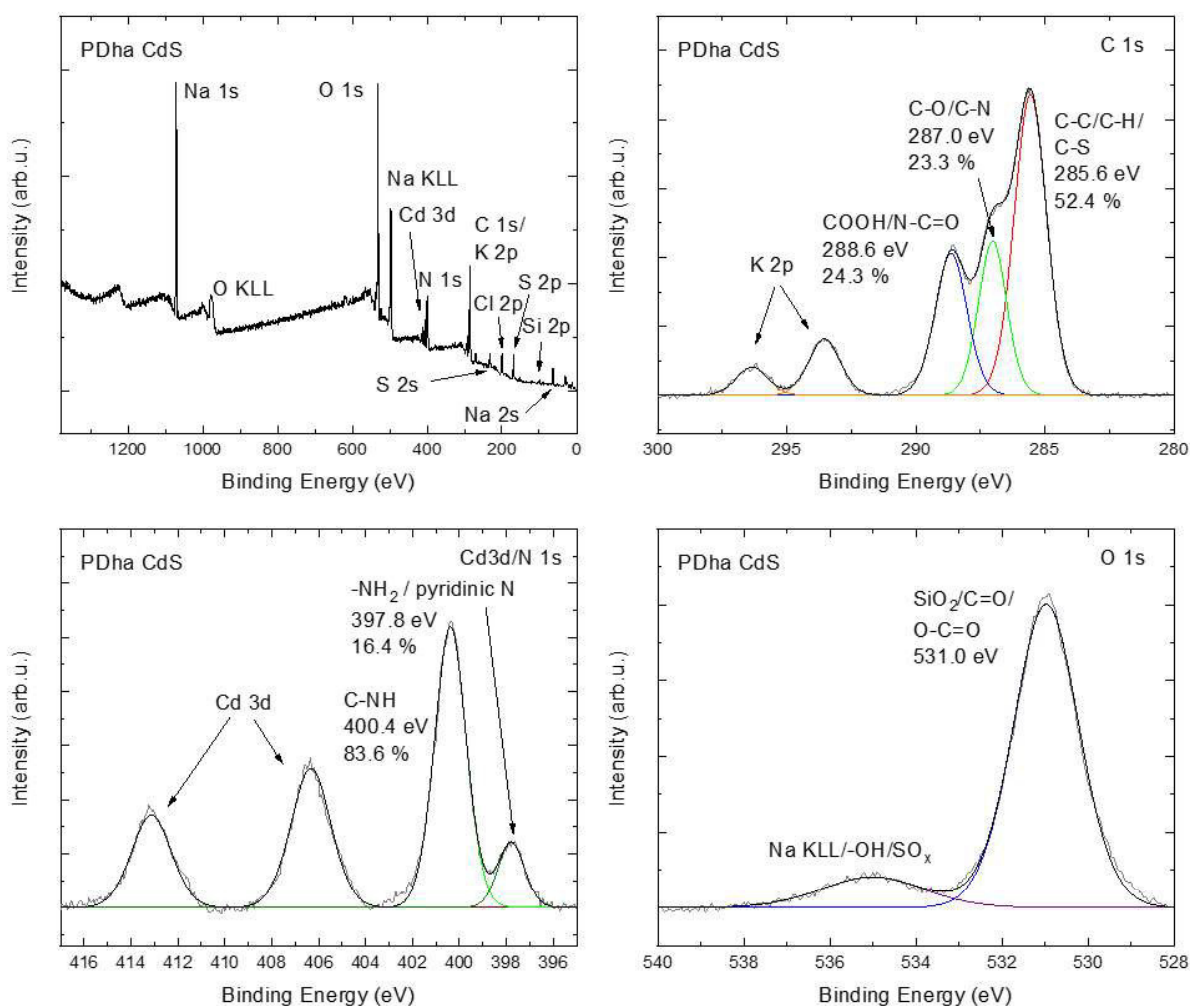


Figure S6: XPS deconvolution of PDha-*g*-AMPS/CdS.

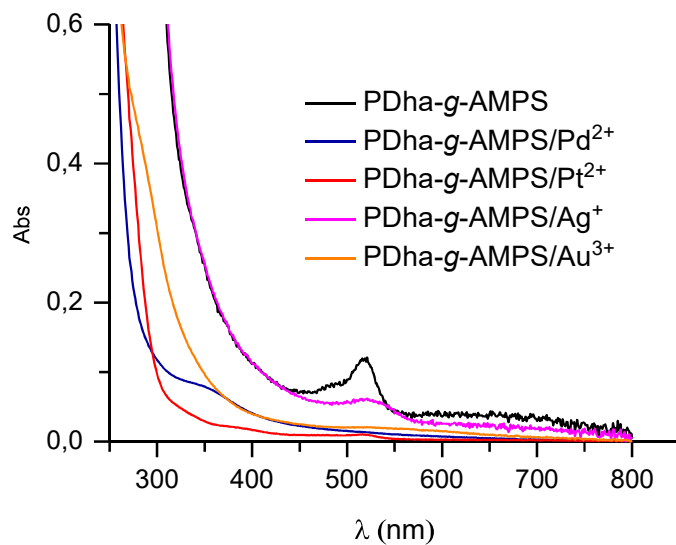


Figure S7: UV/Vis spectrum of PDha-g-AMPS/ Pt²⁺, Au³⁺, Pd²⁺, and Ag⁺ ions before reduction with NaBH₄.

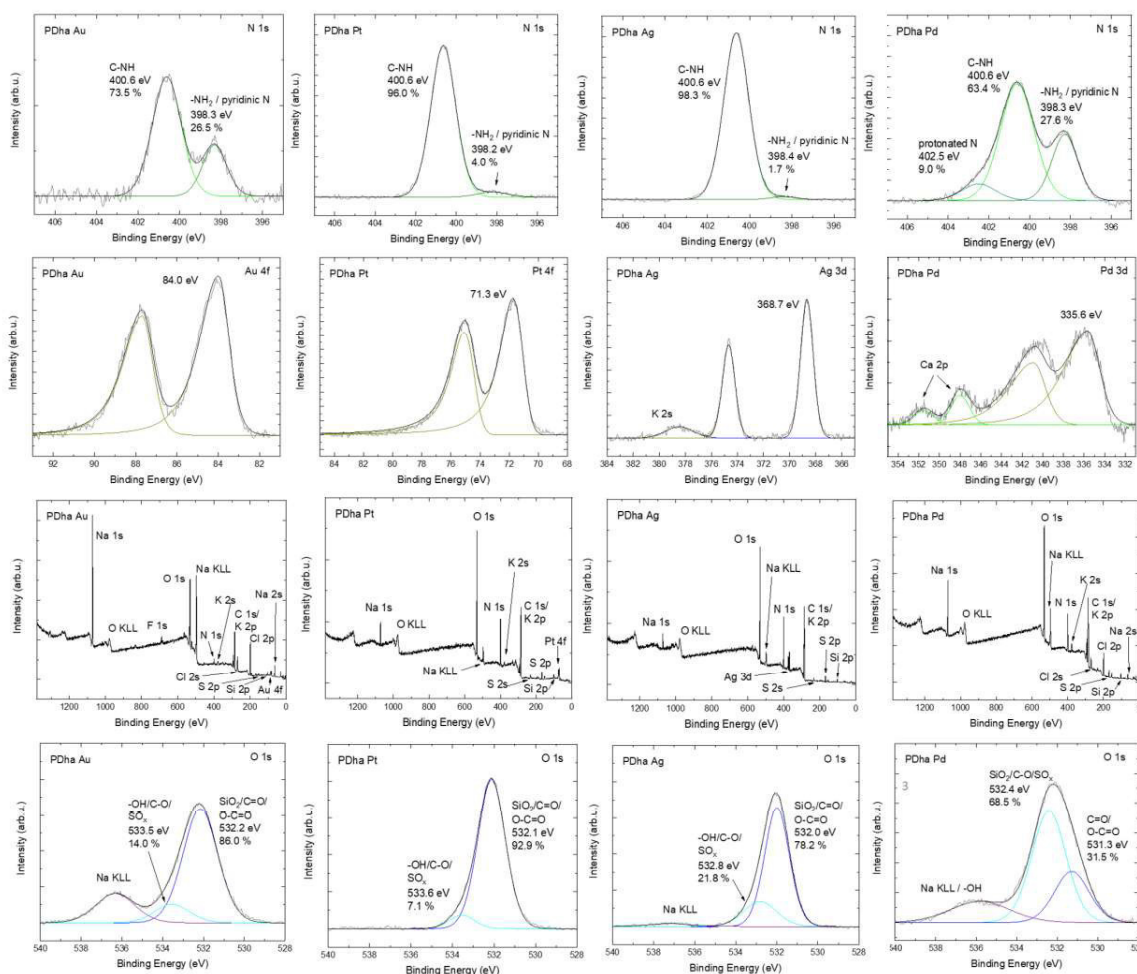


Figure S8: XPS of PDha-g-AMPS/ Pt, Au, Pd, and Ag nanoparticles.

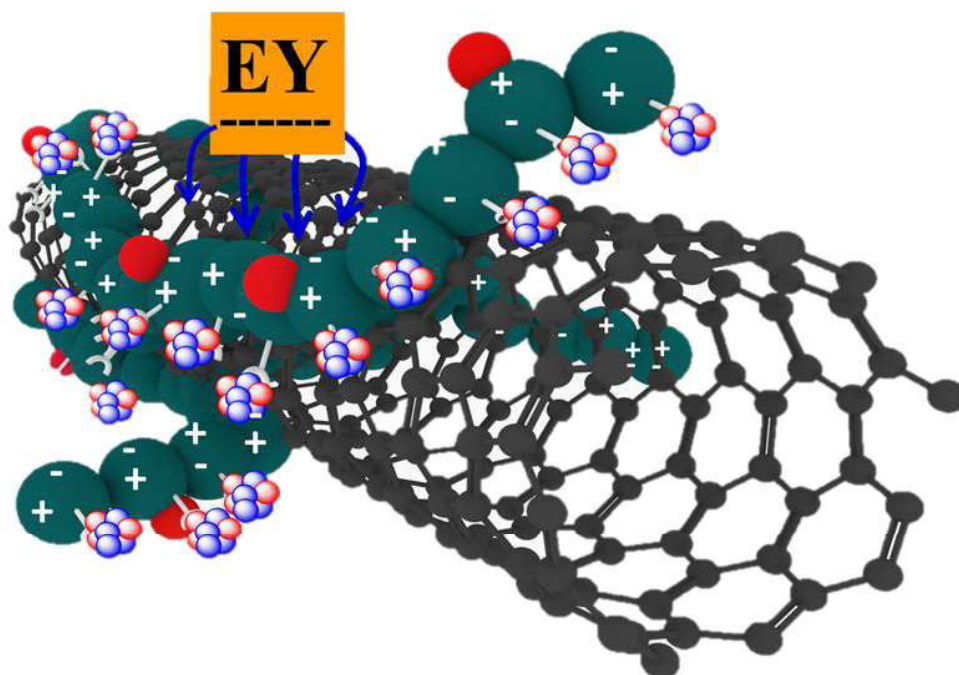


Figure S9: schematic for PDha backbone as meeting point of CNTs, Pt₃Co and EY.

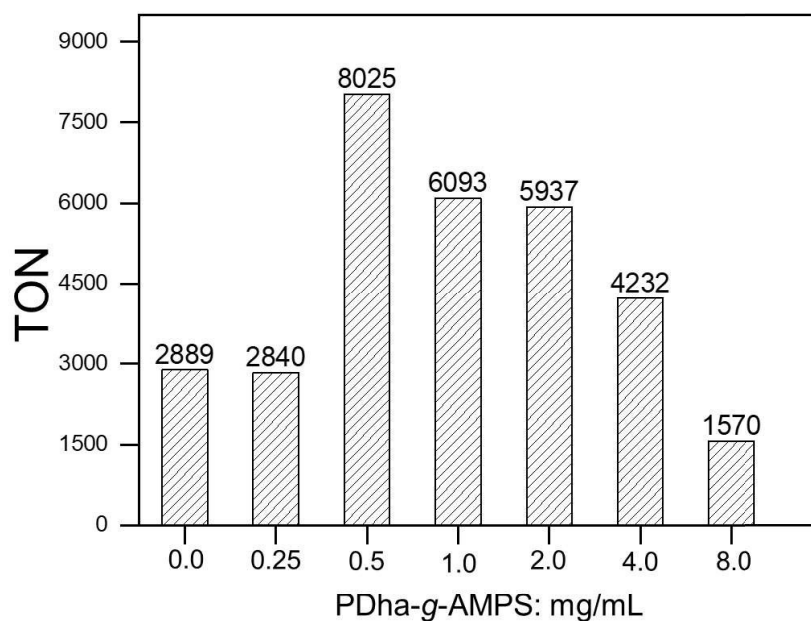


Figure S10: Photocatalytic hydrogen production performance (TON) for EY/Pt₃Co/PDha-g-AMPS/CNT with different amount of PDha-g-AMPS, after illumination for 24 hour (Reaction conditions: EY, and CNT with concentrations of 1mmol L⁻¹, 0.5 mg mL⁻¹, and 75 μg mL⁻¹ respectively; 0.5 M TEOA solution; pH = 8-9).

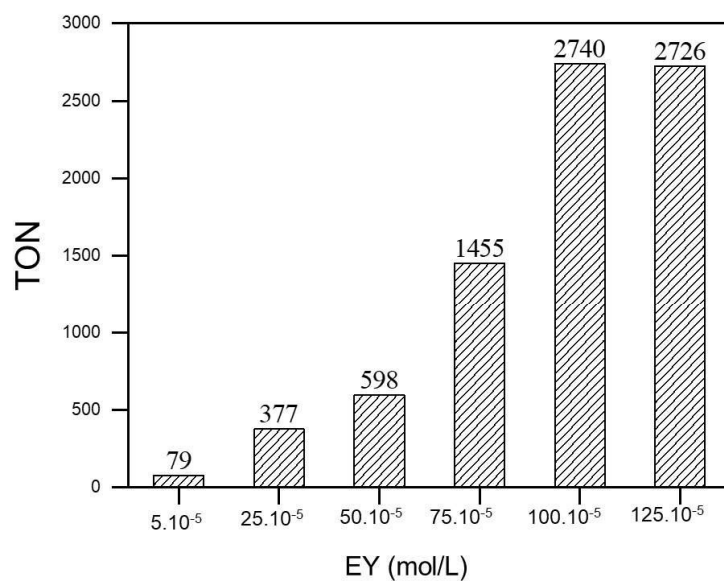


Figure S11: Photocatalytic hydrogen production performance (TON) for EY/Pt₃Co/PDha-*g*-AMPS/CNT with different amount of EY, after illumination for 24 hour (Reaction conditions: PDha-*g*-AMPS, and CNT with concentrations of, 1 mg mL⁻¹, and 1 μg mL⁻¹ respectively; 0.5 M TEOA solution; pH = 8-9).

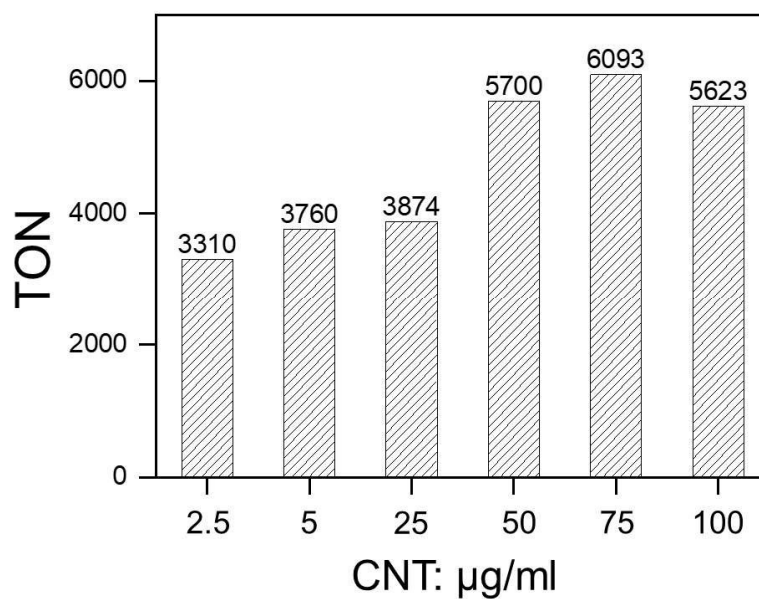


Figure S12: Photocatalytic hydrogen production performance (TON) for EY/Pt₃Co/PDha-*g*-AMPS/CNT with different amount of CNT, after illumination for 24 hour (Reaction conditions: PDha-*g*-AMPS, and EY with concentrations of, 1 mg mL⁻¹, and 0.75 mmol L⁻¹ respectively; 0.5 M TEOA solution; pH = 8-9).

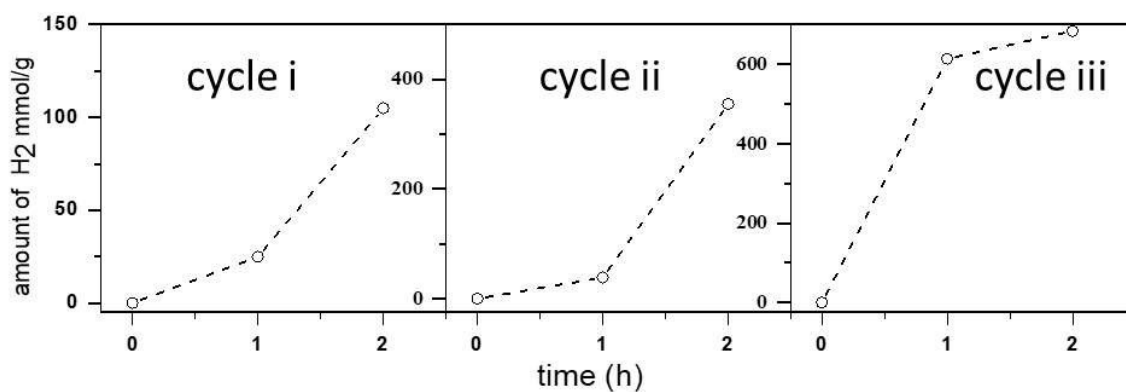


Figure S13: LED light -driven photocatalytic hydrogen production over EY/Pt₃Co/PDha-*g*-AMPS/CNT with during 6 h with measuring the amount of H₂ (TON) every 1h (Reaction conditions: PDha-*g*-AMPS, EY, and EY with concentrations of, 1 mg mL⁻¹, 0.1 mmol/L, and 0.75 mmol L⁻¹ respectively; 0.5 M TEOA solution; pH = 8-9).

Table S1: Brief survey of CdS and EY photocatalysts reported in literature.

photocatalyst	sacrificial reagent/hv	TON	activity (mmol /h.g)	Ref.
CdS				
CdS	TEOA LED, $\lambda \geq 470$ nm		0.068	This work
PDha-g-AMPS/CdS	TEOA LED, $\lambda \geq 470$ nm		0.497	This work
CdS	Na ₂ S–Na ₂ SO ₃ , $\lambda > 420$ nm		0.17	[7]
CdS	Na ₂ S–Na ₂ SO ₃ 320–780 nm,		0.001	[8]
CdS	TEOA, $\lambda > 420$ nm		0.035	[9]
CdS	Na ₂ S–Na ₂ SO ₃ , $\lambda > 420$ nm		0.0073	[10]
CdS	Na ₂ S–Na ₂ SO ₃ , $\lambda > 420$ nm		0.029	[11]
CdS	lactic acid, $\lambda > 420$ nm		0.23	[12]
EY				
Pt ₃ Co/ PDha-g-AMPS/CNT	TEOA, LED, $\lambda \geq 470$ nm	8025, 24h	-	This work
mpg-C3N4/Pt	TEOA $\lambda > 420$ nm	275, in 44h	-	[13]
AlSiW ₁₁ -H ₂ PtCl ₆	TEOA $\lambda > 420$ nm	473, 20h		[14]
[Co(dmbp) ₃]Cl ₂	TEA $\lambda > 420$ nm	249.2, 2h		[15]
[Co(dmgh) ₂ pyCl] ²⁺	TEOA, $\lambda > 420$ nm	900, 14h		[16]
RGO- Co(bpy) ₃ ²⁺	TEA, LED with 505 nm	185, 2.5h		[17]
[FeFe]-hydrogenase	TEOA, 530 nm LED	60, 4h		[18]
Fe ₂ N	TEOA, 300 W xenon lamp	57.8, 1h		[19]
Pt- TS-1 zeolite	TEA, $\lambda \geq 420$ nm	100, 10h		[20]

References:

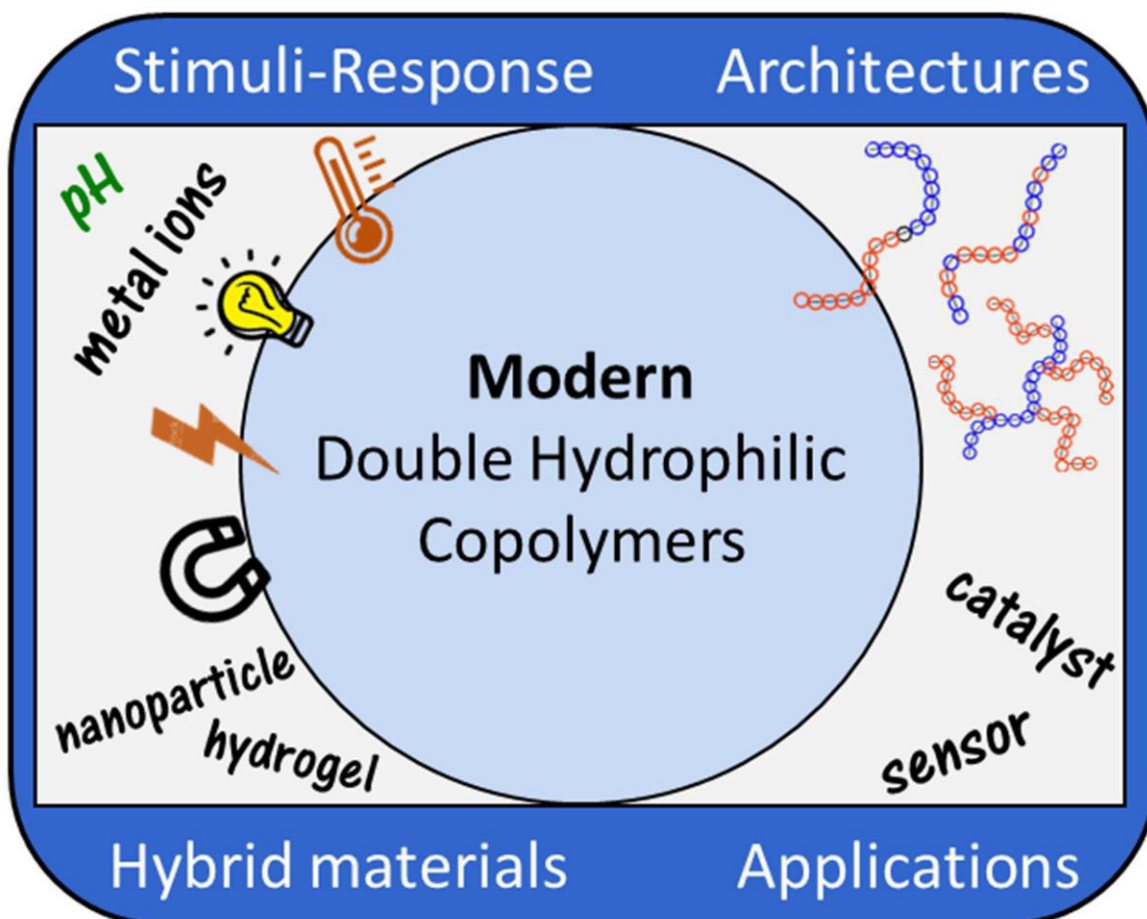
- [1] J.B. Max, K. Kowalczyk, M. Köhler, C. Neumann, F. Pielenz, L. V Sigolaeva, D. V Pergushov, A. Turchanin, F. Langenhorst, F.H. Schacher, Polyampholytic Poly (dehydroalanine) Graft Copolymers as Smart Templates for pH-Controlled Formation of Alloy Nanoparticles, *Macromolecules*. (2020).
- [2] S. Harrison, P. Couvreur, J. Nicolas, Simple and efficient copper metal-mediated synthesis of alkoxyamine initiators, *Polym. Chem.* 2 (2011) 1859–1865.
- [3] Z. Hu, C.Y. Jimmy, Pt 3 Co-loaded CdS and TiO 2 for photocatalytic hydrogen evolution from water, *J. Mater. Chem. A*. 1 (2013) 12221–12228.
- [4] A. Rajagopal, F. Venter, T. Jacob, L. Petermann, S. Rau, S. Tschierlei, C. Streb, Homogeneous visible light-driven hydrogen evolution by the molecular molybdenum sulfide model [Mo 2 S 12] 2-, *Sustain. Energy Fuels*. 3 (2019) 92–95.
- [5] H. Weller, H.M. Schmidt, U. Koch, A. Fojtik, S. Baral, A. Henglein, W. Kunath, K. Weiss, E. Dieman, Photochemistry of colloidal semiconductors. Onset of light absorption as a function of size of extremely small CdS particles, *Chem. Phys. Lett.* 124 (1986) 557–560.
- [6] R. He, X. Qian, J. Yin, H. Xi, L. Bian, Z. Zhu, Formation of monodispersed PVP-capped ZnS and CdS nanocrystals under microwave irradiation, *Colloids Surfaces A Physicochem. Eng. Asp.* 220 (2003) 151–157.
- [7] H. Park, W. Choi, M.R. Hoffmann, Effects of the preparation method of the ternary CdS/TiO 2/Pt hybrid photocatalysts on visible light-induced hydrogen production, *J. Mater. Chem.* 18 (2008) 2379–2385.
- [8] D. Ma, J.-W. Shi, Y. Zou, Z. Fan, X. Ji, C. Niu, Highly efficient photocatalyst based on a CdS quantum dots/ZnO nanosheets 0D/2D heterojunction for hydrogen evolution from water splitting, *ACS Appl. Mater. Interfaces*. 9 (2017) 25377–25386.
- [9] J. Ran, J. Yu, M. Jaroniec, Ni (OH) 2 modified CdS nanorods for highly efficient visible-light-driven photocatalytic H 2 generation, *Green Chem.* 13 (2011) 2708–2713.
- [10] J. Yuan, J. Wen, Q. Gao, S. Chen, J. Li, X. Li, Y. Fang, Amorphous Co 3 O 4 modified CdS nanorods with enhanced visible-light photocatalytic H 2-production activity, *Dalt. Trans.* 44 (2015) 1680–1689.
- [11] J. Liu, K. Chen, G.-M. Pan, Z.-J. Luo, Y. Xie, Y.-Y. Li, Y.-J. Lin, Z.-H. Hao, L. Zhou, S.-J. Ding, Largely enhanced photocatalytic hydrogen production rate of CdS/(Au–ReS 2) nanospheres by the dielectric–plasmon hybrid antenna effect, *Nanoscale*. 10 (2018) 19586–19594.
- [12] Q. Li, B. Guo, J. Yu, J. Ran, B. Zhang, H. Yan, J.R. Gong, Highly efficient visible-light-driven photocatalytic hydrogen production of CdS-cluster-decorated graphene nanosheets, *J. Am. Chem. Soc.* 133 (2011) 10878–10884.
- [13] S. Min, G. Lu, Enhanced electron transfer from the excited eosin Y to mpg-C3N4 for highly efficient hydrogen evolution under 550 nm irradiation, *J. Phys. Chem. C*. 116 (2012) 19644–19652.
- [14] X. Liu, Y. Li, S. Peng, G. Lu, S. Li, Photocatalytic hydrogen evolution under visible light irradiation by the polyoxometalate α -[AlSiW11 (H2O) O39] 5--Eosin Y system, *Int. J. Hydrogen Energy*. 37 (2012) 12150–12157.
- [15] H. Rao, Z. Wang, J. Wang, X. Hu, Y. Fan, H. Hou, H2 Generation from a homogeneous photocatalytic

system containing noble-metal-free Co (II) complex under the irradiation of visible light, *Int. J. Energy Res.* 38 (2014) 2003–2009.

- [16] T. Lazarides, T. McCormick, P. Du, G. Luo, B. Lindley, R. Eisenberg, Making hydrogen from water using a homogeneous system without noble metals, *J. Am. Chem. Soc.* 131 (2009) 9192–9194.
- [17] A. Lewandowska-Andralojc, A. Malolepszy, A. Stritt, A. Grohmann, Modification of eosin Y and cobalt molecular catalyst system with reduced graphene oxide for enhanced photocatalytic hydrogen production, *Catal. Sci. Technol.* 10 (2020) 4693–4702.
- [18] Y. Honda, Y. Shinohara, H. Fujii, Visible light-driven, external mediator-free H₂ production by a combination of a photosensitizer and a whole-cell biocatalyst: *Escherichia coli* expressing [FeFe]-hydrogenase and maturase genes, *Catal. Sci. Technol.* 10 (2020) 6006–6012.
- [19] Z. Cheng, A. Saad, S. Adimi, H. Guo, S. Liu, T. Thomas, M. Yang, Metal organic framework-derived porous Fe₂N nanocubes by rapid-nitridation for efficient photocatalytic hydrogen evolution, *Mater. Adv.* 1 (2020) 1161–1167.
- [20] X. Zhang, Z. Jin, Y. Li, S. Li, G. Lu, Photocatalytic hydrogen generation over Eosin Y-Sensitized TS-1 zeolite, *Appl. Surf. Sci.* 254 (2008) 4452–4456.

Publication P7

“Double Hydrophilic Copolymers – Synthetic Approaches, Architectural Variety, and Application Fields“



Afshin Nabiyan,[‡] [Johannes B. Max](#),[‡] Felix H. Schacher

Chem. Soc. Rev., **2022**, DOI: 10.1039/D1CS00086A

[‡]Both authors contributed equally to this work



Cite this: DOI: 10.1039/d1cs00086a

Double hydrophilic copolymers – synthetic approaches, architectural variety, and current application fields

 Afshin Nabiyan,^{abc} Johannes B. Max^{abc} and Felix H. Schacher *^{abc}

Solubility and functionality of polymeric materials are essential properties determining their role in any application. In that regard, double hydrophilic copolymers (DHC) are typically constructed from two chemically dissimilar but water-soluble building blocks. During the past decades, these materials have been intensely developed and utilised as, e.g., matrices for the design of multifunctional hybrid materials, in drug carriers and gene delivery, as nanoreactors, or as sensors. This is predominantly due to almost unlimited possibilities to precisely tune DHC composition and topology, their solution behavior, e.g., stimuli-response, and potential interactions with small molecules, ions and (nanoparticle) surfaces. In this contribution we want to highlight that this class of polymers has experienced tremendous progress regarding synthesis, architectural variety, and the possibility to combine response to different stimuli within one material. Especially the implementation of DHCs as versatile building blocks in hybrid materials expanded the range of water-based applications during the last two decades, which now includes also photocatalysis, sensing, and 3D inkjet printing of hydrogels, definitely going beyond already well-established utilisation in biomedicine or as templates.

Received 30th August 2021

DOI: 10.1039/d1cs00086a

rsc.li/chem-soc-rev

^aInstitute of Organic Chemistry and Macromolecular Chemistry (IOMC), Friedrich-Schiller University Jena, Lessingstraße 8, D-07743 Jena, Germany. E-mail: felix.schacher@uni-jena.de

^bJena Center for Soft Matter (JCSM), Friedrich Schiller University Jena, Philosophenweg 7, D-07743 Jena, Germany

^cCenter for Energy and Environmental Chemistry Jena (CEEC Jena), Philosophenweg 7a, 07743 Jena, Germany

Introduction

Copolymers are composed of two or more chemically distinct polymer segments or monomer units that are covalently linked.^{1–3} The design and the preparation of copolymers allows us to access polymeric materials with additional degrees of


Afshin Nabiyan

Afshin Nabiyan received his BSc and MSc degrees in pure chemistry and organic chemistry at Isfahan University of Technology (Iran) in 2015. Later, he obtained his PhD degree under the supervision of Felix. H. Schacher at Friedrich-Schiller-Universität Jena (Germany) in 2021. In late 2021, he was awarded the Cata-Light Young Scientist Support, and recently, he became a postdoctoral researcher at the group of Felix. H. Schacher. His research interests mainly include the synthesis and self-assembly of water-soluble (co)polymers and hybrid materials to construct hierarchical structures for sensing and photocatalysis.


Johannes B. Max

Johannes B. Max received his MSc degree at the university of Freiburg im Breisgau (Germany) in 2017, where his bachelor and master theses were supervised by Rolf Mülhaupt. After an internship at Covestro AG in Leverkusen, he started his PhD studies in the work group of Felix H. Schacher in Jena (Germany). Recently, he is working as a postdoctoral researcher at the Otto Schott Institute of Materials Research. Johannes' research interests include the synthesis of smart and stimuli-responsive polymers via different routes, their self-assembly, utilization in hybrid materials and applications, e.g., sensors and photocatalysis.

Johannes B. Max received his MSc degree at the university of Freiburg im Breisgau (Germany) in 2017, where his bachelor and master theses were supervised by Rolf Mülhaupt. After an internship at Covestro AG in Leverkusen, he started his PhD studies in the work group of Felix H. Schacher in Jena (Germany). Recently, he is working as a postdoctoral researcher at the Otto Schott Institute of Materials Research.

freedom and properties compared to homopolymers.^{1–3} Among the copolymer families, water-soluble double hydrophilic copolymers (DHCs), consisting of two distinct hydrophilic blocks or monomers, have recently gained scientific attention due to their interesting solution properties and the growing number of water-based applications.⁴ Moreover, a large number of copolymer architectures derived from different preparation strategies, ranging from linear block and random copolymers to stars, brushes and macrocycles, have been reported.^{5–8} Among them, linear double hydrophilic block copolymers (DHBCs) are the most familiar and oldest subclass of DHCs, consisting of at least two different water-soluble blocks. Since their discovery almost 50 years ago,⁹ the field of DHBC research has continued to develop, not only because of synthetic developments in the field of macromolecular science, but also because of their interesting structure–property relationships, their potential functionality in solution, and their potential application in important sectors of modern life.^{10,11}

Today, DHBCs are important building blocks at the interface of multidisciplinary research including chemistry, biomedicine, material science and nanotechnology. They offer tailor-made solutions, *e.g.*, matrices for photocatalytic hydrogen evolution as a sustainable energy source,¹² the sensing of heavy metal ions or biological analytes,^{13–16} enabling the 3D printing of hydrogels,¹⁴ or the delivery of anti-cancer drugs.^{4,17,18}

Typically, DHBCs consist of one solubility promoting segment, as well as a second hydrophilic and functional segment. Hence, the number of reported individual polymers is vast, as there exists an almost uncountable number of possible combinations of rather common, *e.g.* ethylene oxide,¹⁶ acrylic acid,¹⁹ and vinyl pyridine,²⁰ or less frequently reported hydrophilic monomer units, *e.g.* featuring charges.^{21,22} From this perspective,

there is an almost endless potential to tune both composition and the resulting characteristics of such materials.

The main characteristics of DHBCs arise from the interplay between the constituting segments. Self-assembly in different environments is mostly driven by one segment turning water-insoluble either through an external stimulus such as pH,²³ temperature,²⁴ light,²⁵ or the presence of metal ions,²⁶ or the interaction with molecular,²⁷ or nano-sized compounds²⁸ and surfaces,²⁹ while the second block maintains its solubility in water. This provides access to exceptional assemblies in water, but self-assembly is sometimes even observed in pure water without any additional trigger.³⁰ In that regard, there are also several examples of permanently double hydrophilic copolymers.³¹

The role of each segment is not always strictly defined. For example, if both of the segments are functional, both of them may switch from hydrophilic to non-hydrophilic nature upon exposure to a certain trigger, resulting in a ‘schizophrenic’ (micellisation) behaviour.^{32,33} A single block may even exhibit multiple roles; for example, poly(ethylene glycol) PEG represents both a high hydrophilicity along with biocompatibility.³⁴ Indeed, recently multi hydrophilic block copolymers (MHBCs) were also introduced exhibiting an indefinite number of segment combinations.³⁵ Besides, the diverse topologies found in macromolecular chemistry are more frequently exhibiting double hydrophilic nature. The choice of a suitable topology can be seen as an additional parameter defining the material properties.³⁶ Therefore, the corresponding architectures presenting solely hydrophilic segments, *e.g.*, star,³⁷ graft, hyperbranched³⁸ or macrocyclic,⁸ are closely related to the class of linear DHBCs.

Regarding the synthesis of DHBCs, access is often realised in a similar way compared to common linear block copolymers, making use of controlled polymerisation techniques for the successive addition of different monomers, or by exploiting click chemistry to link readily prepared segments.^{21,39} However, especially the synthesis of nonlinear DHBCs is rather advanced and usually either multi-site initiators^{40–42} or bi-functional monomers⁴³ are required, as well as multiple steps.^{16,44} Further, often different controlled radical polymerisation (CRP) methods are combined, such as atom transfer radical polymerisation (ATRP) and reversible addition–fragmentation chain-transfer polymerisation (RAFT).⁴⁵ ‘Alternative’ approaches have also been reported, which could be seen as an additional advantage having access to an even broader preparative toolbox, such as grafting-onto reactions to obtain double hydrophilic graft copolymers.⁴⁶ Liu *et al.*⁴⁷ concisely describe the self-assembly and stimulus-responsive behavior of some non-linear amphiphilic and double-hydrophilic copolymer architectures. Herein, the tunable self-assembly using non-linear architectures is emphasized. From this perspective, the classical concept of linear DHBCs will be extended in this review, highlighting the different double hydrophilic copolymer (DHC) architectures that are accessible, including crosslinked 3D structures. They will be divided first into their subclasses: (a) graft, (b) star and miktoarm, (c) toothbrush and centipede-like, (d) hyperbranched and dendritic, (e) macrocyclic and (f) crosslinked; and before their synthesis is discussed, individual features and solution behaviour are examined.



Felix H. Schacher

Felix H. Schacher studied chemistry at the Universities of Bayreuth (Germany) and Lund (Sweden) and obtained his diploma in 2006. After his PhD under the supervision of Axel H. E. Müller in 2009, he joined the group of Ian Manners at the University of Bristol as DAAD postdoctoral fellow. In 2010 he was appointed Juniorprofessor at the Friedrich-Schiller-Universität Jena and became Full Professor at this institution in 2015. He has

been awarded the Dr-Hermann-Schnell-Fellowship in 2013 and the Carl-Duisberg Memorial Award of the GDCh in 2020. His scientific interests include controlled/living polymerization techniques, block copolymers, polyelectrolytes, and polyampholytes – all in the context of using (directed) self-assembly processes for material design in the fields of membranes, hybrid materials, and biomedicine.

The properties of DHCs are often superior compared to their linear DHBC counterparts, and are already foreseen to be promising materials in different application fields, *e.g.*, sensing,¹⁵ catalysis^{12,48} or as drug delivery systems.¹⁷ Together with the concept of multi-hydrophilicity, the topology can be seen as an additional parameter to tune the DHC properties to tailor-make water-soluble polymeric materials. In addition to these DHBCs, double hydrophilic random copolymers that reveal interesting solution properties and applications will also be considered, even though their chemical structure is less defined.

Major developments are also observed in the application of DHCs. Earlier work from Helmut Cölfen in 2001 emphasised the application of DHBCs as surfactants, stabilisers and structure directing materials, *e.g.*, to control crystallisation processes and as templates, in addition to their utilisation in drug delivery.¹¹ In another perspective review, Nottelet *et al.*⁴⁹ focus mostly on DHBCs that combine a biocompatible non-ionic block with a degradable functional block such as polysaccharides, polypeptides, polyesters or similar. In this context, the described DHBCs are promising candidates for biomedical applications. However, the application field of DHCs expanded rapidly, and this polymer class is recently used in biomedical applications, as nanocarriers and imaging/contrast agents, in catalysis, sensing, or within hybrid materials and this is also highlighted here.^{12,15,33,44,48–50} Their water-solubility, together with their potential binding sites, renders DHBCs suitable organic components for hybrid materials in aqueous environments, and their combination with various inorganic materials was found to yield high performance materials.^{33,51}

In general, hybrid materials are one of the most emerging material classes due to the possibility to tune the physical and chemical properties, often profiting from synergistic effects. While the polymers are mainly acting as stabilisers or templates, the inorganic materials contribute advantageous stability, as well as optical and electrical properties.^{52–54} For this, the rather novel applications of DHCs will be outlined with a special focus on hybrid materials. Since their utilisation is often based on their response to external stimuli, further progress in this field will be discussed as well. Besides giving a broad overview of recent literature in the field of DHCs, this review also covers general trends used in polymer chemistry towards this class of materials. However, within this review, the functions of the DHCs will be unveiled (Fig. 1) and through understanding their structure–property relationship versatile applications were accessed, that are described in the last section of the review.

Three general functions may be identified: (A) interaction and encapsulation of metal ions or molecules, forming nano-reactors and nanocarriers. Corresponding assemblies are often used as templates. These properties are often required in the construction of defined hybrid nanomaterials, catalysis, or delivery systems. (B) DHCs as stabilizing or dispersing agents, being attached to (nanoparticle) surfaces, granting their stability in aqueous environment and often tuning their properties. This function is found, where inorganic nanoparticles are applied in solution. (C) Responding to the exposure to an

external stimulus (pH, temperature, light, ions, ...) stimuli-responsive DHCs give a response or an output, *e.g.*, through changing the physical properties of the surrounding solution. Especially sensing applications rely on this mechanism.

Synthetic approaches towards a variety of architectures

Today, researchers in polymer science have access to a wide range of controlled/living polymerization techniques, such as anionic/cationic or controlled radical polymerization. One consequence of those techniques being readily available was the preparation of polymers with various architectures. Among them, linear block copolymers (both amphiphilic and double hydrophilic examples) have been the focus of a very large number of studies. Those typically contain a straightforward synthetic approach, defined structures, and self-assembly studies in the bulk and in selective solvents, rendering such materials interesting for a broad range of applications. Their self-assembly has been intensively investigated, and in solution, this is particularly affected by the block copolymer composition, concentration, solvent, or the presence of additives.^{2,47,55–57} Linear double hydrophilic block copolymers as one interesting subgroup drew also considerable attention. Quite often, this category of linear block copolymers can reversibly switch between micellar and unimer states upon the application of external stimuli. For this reason, many excellent reports can be found in the literature that have been focused on the synthesis of new double hydrophilic linear block copolymers.^{2,47,55–57}

Recently, non-linear copolymers have also attracted the attention of many researchers. In this regard, a broad variety of possible topologies (architectures) exists, each influencing the properties and function of a given macromolecule.³⁶ Hence, the general concept of block copolymers is extended to non-linear architectures, such as graft, star, miktoarm, centipede, or cyclic, which is supported by recent synthetic advances (Fig. 1).^{2,57} The supramolecular self-assembly of some representative non-linear copolymers was described by Liu *et al.*⁴⁷ Herein, the high potential to tune self-assembly by adjusting the topology is highlighted.

For double-hydrophilic copolymers, the architecture also significantly affects the solution properties, such as the solubility or viscosity.^{17,31,37,41} This can be considered an additional design element in the preparation of defined materials offering tailor-made solutions for a given dilemma. Moreover, the micellization behaviour of non-linear copolymers differs significantly from that of linear counterparts,^{58,59} as chain-end effects play a more important role,⁴³ and the functionality itself, as well as the local density of functional groups, differs as well.^{37,38} As compared to traditional DHBCs, the utilisation of an alternative architecture may often be advantageous, *e.g.*, branched *versus* block as templates.⁶⁰ Hence, quite complex materials can be obtained considering both the inherent feature of a specific architecture and the molecular composition, *e.g.*, charge, polarity, segment length and density of side-chains in a double hydrophilic material.^{12,15,33,48,61}

However, in many cases, the preparation of non-linear topologies is more demanding. It is often necessary to use

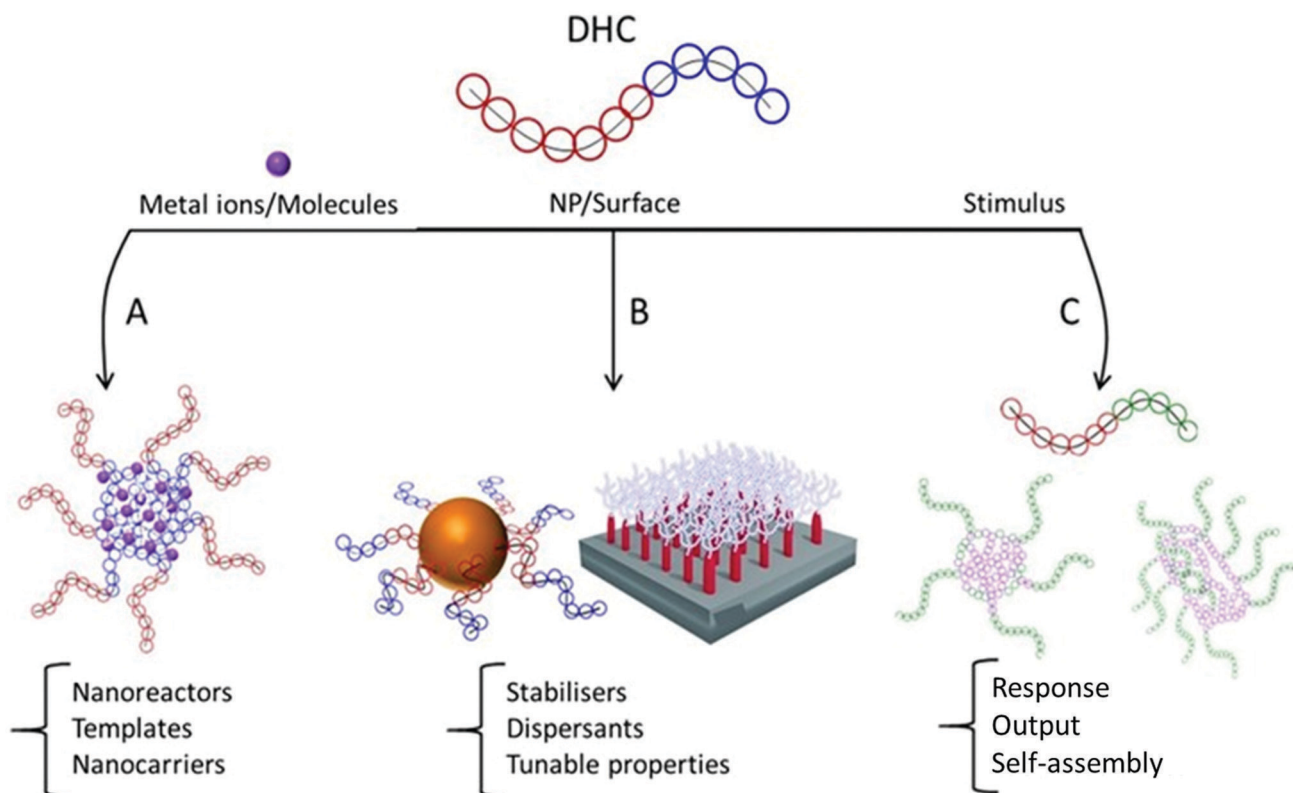


Fig. 1 General functions of DHCs, being divided in their interaction with metal ions or molecules (A), nanoparticles (NPs) and surfaces (B), and the response to an external trigger (C).

multi-functional initiators, or to combine polymerisation techniques and post-polymerisation modifications. In addition, they often reveal more complex and rather unexplored self-assembly.^{7,31,41,62} The resulting morphologies may be less defined due to more complicated structures, and this renders characterisation more challenging.^{21,46,63} From this point of view, the development and utilisation of diverse DHC architectures still bear a lot of potentials. The corresponding copolymers are promising materials for future applications in 3D inkjet printing,¹³ catalysis,⁴⁸ sensing¹⁵ and biomedicine.¹⁷ The distinct topologies that are found in the literature (star and miktoarm, graft, crosslinked and others) will be highlighted in this section (Fig. 2). Crosslinked DHCs, forming chemically linked 3D nano-objects, will also be discussed.^{64–66} Furthermore, multi-hydrophilic block copolymers (MHBCs) will be introduced, combining even more functionalities.⁶⁷

In general, DHCs are prepared in a similar way compared to other segmented polymers usually following two different strategies. Here, especially controlled/living polymerization techniques, either ionic or radical, allow the construction of well-defined polymers by the sequential addition of monomers. As an alternative, two readily synthesized blocks with active end-groups are linked, *e.g.*, *via* click chemistry.⁵⁷ Also, other post-polymerization modification techniques exploiting a reactive polymer backbone give access to defined copolymers, such as graft copolymers.⁶⁸ However, regarding DHCs some

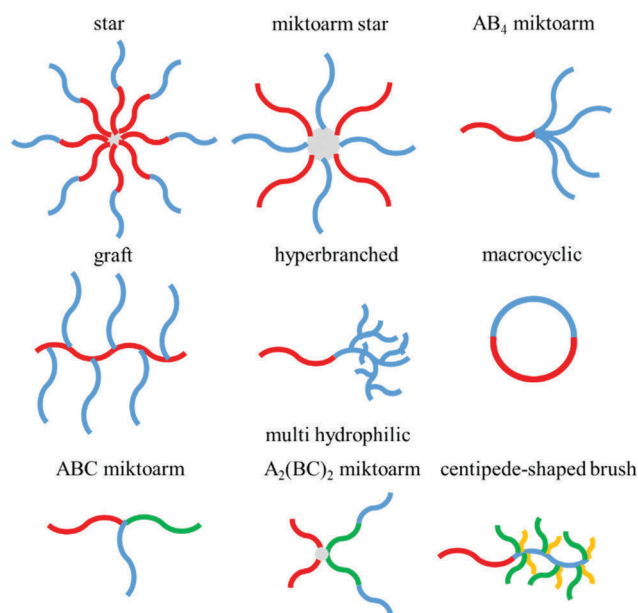


Fig. 2 Schematic depiction of representative DHC architectures, with the individual segments in blue and red: star,³⁹ miktoarm star,³⁷ AB₄ miktoarm,⁵⁹ graft,⁴⁶ hyperbranched,³⁸ and macrocyclic.⁸ Multi-hydrophilic copolymers (MHCs) containing additional hydrophilic segments, depicted in green and yellow, for ABC miktoarm,⁹⁸ A₂(BC)₂ miktoarm,⁶⁷ and centipede-shaped copolymers.⁶²

challenges may be identified. The choice of solvent is often limited, since most of the monomers are polar, ionizable, or even bear permanent charge.^{26,33,61} Thus, some limitations with regard to the choice of polymerization technique can be faced.^{26,33,61} DHCs usually contain functional moieties, *e.g.*, acids and bases, and hence, initiators and ligands have to be compatible with the corresponding monomers.^{26,33} Finally, some of the repeat units could not be introduced *via* a simple polymerization making the use of protective group chemistry necessary.^{21,42,69} Indeed, great attention should be taken to properly select suitable reaction conditions when designing a specific system. In polymer science, the ultimate goal is mostly to introduce inexpensive, biocompatible, multifunctional, and ideally non-toxic polymers.^{4,70} At the same time, the methods that are used to polymerize novel hydrophilic (co)polymers may be harmful because of the toxicity and other incompatibilities associated with either catalyst or certain additives.^{4,70–72} Regarding non-linear architectures, the synthetic approaches become even more complex such as the necessity to use multifunctional initiators. Challenges may also arise from the subsequent characterization both in terms of absolute molar mass as well as the architecture itself, *e.g.*, the number of arms or grafts. For instance, in the case of hydrophilic miktoarm star (co)polymers, it is challenging to construct well-defined structures with multiple precisely designed arms as a consequence of the strict requirements of the complicated preparation and purification procedures.^{72,73}

Graft copolymers (DHGC)

Graft copolymers feature a polymer backbone and chemically different side-chains. They typically present a compact and confined structure, strong chain-end effects and complex self-assembly, *e.g.*, the formation of worm-like micelles, even unimolecular aggregation, as well as lower aggregation numbers compared to linear structures have been reported.^{7,43,68,74,75} In addition to the choice of various potential backbone or side-chain moieties, *e.g.*, ionic or non-ionic,^{15,46,76} DHGCs differ in the density and length of side-chains, strongly influencing the resulting characteristics, and allowing broad tuneability.^{46,77,78} However, while the backbone is generally one of the hydrophilic segments, two distinct hydrophilic blocks can also be linked to the same backbone.^{79,80}

In general, graft copolymers can be synthesised *via* three approaches, which are also found in the field of double-hydrophilic graft copolymers: grafting-through, grafting-onto and grafting-from.⁶⁸ Following this, the existing DHGCs were divided into these synthetic routes, and their unique features and potential applications are summarised in Table 1. The pathway selected strongly depends on the desired monomer, each of those three approaches reveals unique advantages and challenges. The grafting-to strategy is based on connecting specific side chains to a linear hydrophilic backbone using a suitable coupling reaction. As the linear backbone and side chains are constructed separately, they could be prepared using appropriate polymerization methods and their chain lengths can be precisely tuned. In case of grafting-through, graft

copolymers could be prepared *via* the polymerization of hydrophilic macromonomers and here, the grafting density and the length of side chains can be tuned as well during macromonomer synthesis. Finally, the grafting-from requires a macroinitiator which already carries the respective initiation sites. This macromolecule can be prepared directly from the initiation-group-containing monomer or by the introduction of initiating functional groups to a specific precursor.⁶⁸

The grafting-onto and grafting-through methods often benefit from a one-pot synthesis, sometimes even performed in water, starting from readily prepared functional precursors. This enables the characterisation of each individual building block, and a single reactive backbone can be used for functionalisation with various modifiers. However, a rather random distribution of the side-chains can be assumed and often the adjustment to a certain degree of functionalisation (DoF) is crucial to control structure–property relationships.^{15,46,63,81}

In this respect, Max *et al.*^{15,61,63} prepared a library of graft copolymers starting from a pH- and ion-responsive poly-(dehydroalanine) (PDha) backbone bearing amino moieties in each repeat unit as reactive handles (Fig. 3). By slightly changing the reaction conditions, various modifiers such as PEG, phosphonic acid, acrylic acid, or *N*-isopropyl acrylamide (NIPAAm) were grafted *via* either an aza-Michael addition or the ring-opening of epoxides to obtain tailor-made materials. Hereby, it was found that the DoF and the chain-length significantly influence the solubility, as shown for PEG side-chains.^{15,46,48,61,63}

Controlled polymerisation techniques typically provide good control over the side-chain length and \bar{D} .^{43,45,48,79,80,82,83} Sun and Cui⁴³ prepared DHGCs with a hydrophilic poly(2-hydroxy ethyl acrylate) (PHEA) backbone and poly(*N*-isopropyl acrylamide) (PNIPAAm) or poly(2-(dimethyl amino) ethyl methacrylate) (PDMAEMA) side-chains. They started with a single-electron transfer-living radical polymerization (SET-LRP) initiator-containing monomer (2-hydroxyethyl-2-((2-chloropropanoyloxy)methyl)acrylate), which was first polymerised *via* RAFT (Fig. 4). Afterwards, the second monomer was grafted *via* SET-LRP to obtain graft copolymers with a narrow molecular weight distribution and grafts, as well as hydroxyl groups in each repeat unit.^{43,45}

In another pathway, Gu *et al.*^{79,80} synthesised DHGCs based on a poly[poly(ethylene glycol)methyl ether acrylate] (PPEGMA) backbone grafted with both PDMAEMA and PMAA side-chains. In the first step, PEGMA was polymerised *via* ATRP before functionalising the backbone with an ATRP initiator using lithium diisopropylamide and 2-bromopropionylchloride (DoF = 75%). In the third step, the second monomer was grafted by another ATRP reaction. To obtain poly(methacrylic acid) (PMAA), subsequent hydrolysis of the protected precursor was carried out.

As in the case of linear DHBCs, the graft copolymers usually contain a solubility promoting block and a functional, stimuli-responsive building block. However, self-assembly is more complex and has not been exhaustively studied yet. In this respect, the side-chains may stabilise the graft copolymer after the DHGC becomes amphiphilic upon exposure to a stimulus,

Table 1 Synthesis, properties and utilisation of double hydrophilic graft copolymers found in the literature

DHGC	Synthesis	Feature/suggested application	Ref.
Grafting onto			
PDha- <i>g</i> -PEG PDha- <i>g</i> -NIPAAm PDha- <i>g</i> -PAA Gelatine- <i>g</i> -PEG	Grafting of epoxides and Michael-acceptors	Multi-responsive application as a template, dispersant, in photocatalysis and sensing	15, 46, 48, 61 and 63
poly(acetal) _{hydrolysed} - <i>g</i> -PEG PNIPAAm- <i>g</i> -PEG	Grafting of mPEG-NH ₂ on poly(acetal), subsequent hydrolysis Grafting of PEG-NH ₂ onto P(NIPAAm- <i>co</i> -glycidyl methacrylate) or P(NIPAAm- <i>co</i> - <i>N</i> -acrylylsuccinimide)	Formation of nanogels with curcumin drug delivery in cancer treatment Interaction with inorganic crystals Stable spherical aggregates above LCST	18 76 77 and 78
PAA- <i>g</i> -PEO	Grafting of mPEG-NH ₂ (using ETC/HOBt)	Encapsulating and delivering cationic or hydrogen-accepting agrochemicals or drugs	84
P(AMPSNa- <i>co</i> -ANa)- <i>g</i> -PNIPAAm P(AMPSNa- <i>co</i> -ANa)- <i>g</i> -PNIPAAm- <i>g</i> -PDMAM	Grafting of PNIPAAm-NH ₂ /PDMAM-NH ₂	Complexation of surfactants, tunable aggregation behavior	85
Grafting from			
P(L-Lysine)- <i>g</i> -P(sulfobetaine) PSBM- <i>g</i> -P(OEGMA- <i>co</i> -DEGMA)	(1) Grafting a RAFT CTA onto the backbone (2) RAFT polymerisation of the sulfobetaine (1) FRP of SBM and BIHPM (ATRP initiator containing monomer) (2) ATRP copolymerisation of OGMA and DEGMA	Suppression of protein aggregation and protein release Zwitterionic backbone temperature and salt response tunable self-assembly	82 75
PHEA- <i>g</i> -PDMAEA	Initiator functionalised monomer (1) RAFT (2) SET-LRP (3) Quaternisation	Self-catalysed hydrolysis of PDMAEA; micelle formation in the organic phase	43
PHEA- <i>g</i> -PNIPAAm	Sequential RAFT and SET-LRP starting from trifunctional HECPPMA	Thermo-response	45
PEO- <i>g</i> -PDMAEMA	(1) Functionalisation of P(EO- <i>co</i> -glycidol) with the initiator (2) ATRP of DMAEMA	Brush-like structure nanoelectronics, sensing, enhanced oil recovery, and drug and gene delivery systems	83
PPEGMEA- <i>g</i> -PMAA and PPEGMEA- <i>g</i> -PDEAEMA	(1) ATRP (2) Functionalisation with an initiator (3) ATRP (4) Hydrolysis	Biomedicine, <i>e.g.</i> , drug carrier	79 and 80
PMA- <i>g</i> -PEG/PDMA	Initiator-functionalised monomer (1) RAFT (2) ATRP	Coating material protein resistant	86
Grafting through			
PNIPAAm- <i>g</i> -PEO	FRP of PNIPAAm and PEO macromonomers	Aggregation above the LCST	81

Abbreviations: P(AMPSNa-*co*-ANa)-*g*-PNIPAAm-*g*-PDMAM: poly(sodium-2-acrylamido-2-methylpropanesulfonate-*co*-sodium acrylate)-*graft*-poly(*N*-isopropyl acrylamide)-*graft*-poly(*N,N*-dimethylacrylamide) PSBM-*g*-P(OEGMA-*co*-DEGMA): poly(sulfobetaine methacrylate)-*graft*-poly[oligo(ethylene glycol) methyl ether methacrylate]-*co*-di(ethylene glycol) methyl ether methacrylate]; PHEA-*g*-PDMAEA: poly(2-hydroxyethyl acrylate)-*g*-poly(2-dimethylamino ethylacrylate); PPEGMEA-*g*-PMAA: poly[poly(ethylene glycol) methyl ether acrylate]-*graft*-poly(methacrylic acid); PPEGMEA-*g*-PDEAEMA: poly[poly(ethylene glycol) methyl ether acrylate]-*graft*-poly(2-(diethylamino)ethyl methacrylate).

as shown for PEG-*g*-NIPAAm. Here, the PEG side chains can stabilise core-shell nanostructures at temperatures above the lower critical solution temperature (LCST), while some of them still interact with PNIPAAm in the core.^{77,78,81}

Gu *et al.* described the synthesis of PPEGMEA-*g*-PMAA and PPEGMEA-*graft*-poly(2-(diethylamino)ethyl methacrylate) (PDEAEMA) graft copolymers. While the carboxylic acid groups containing graft copolymer was a suitable stabiliser and template for Fe₃O₄ NPs through ionic interactions, the pH- and salt response of PPEGMEA-*g*-PDEAEMA was studied. For this DHGC, the reversible formation of micelles depends on both the pH and the NaCl concentration, where the PDEAEMA chains collapse within the core. T. Jiang *et al.*⁷⁵ also described the tuneable self-assembly of poly(sulfobetaine methacrylate)-*graft*-poly[oligo(ethylene glycol)methyl ether methacrylate]-*co*-di(ethylene glycol)methyl ether

methacrylate] (PSBM-*g*-P(OEGMA-*co*-DEGMA)), containing a zwitterionic backbone.

The aggregation strongly depends on the temperature, salt concentration, and the polymer structure itself (longer or shorter side-chains). This allows the formation of distinct nano-objects, where either the backbone or the grafts collapse within the core. However, in case of longer side-chains, low aggregation numbers of around 2 were found for the micelles.⁷⁵

Due to their versatile solution behaviour and efficient interaction with inorganic nanoparticles,^{15,79} ions,¹⁵ proteins,⁸² or drugs, DHGCs are already found in various applications such as sensing,¹⁵ catalysis,^{12,48} suppression of protein aggregation,⁸² or cancer treatment.¹⁸ Further utilisation in carrier systems, nanoelectronics, oil recovery, and as dispersants is foreseen.^{46,83,84}

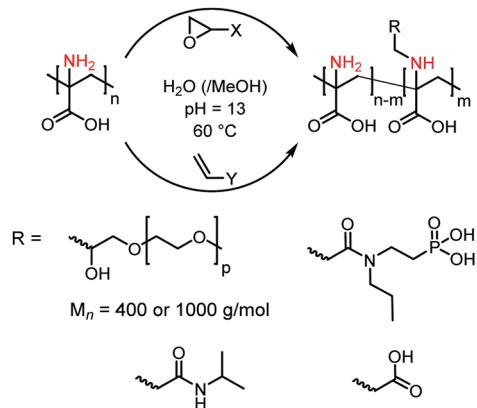


Fig. 3 PDha-based graft copolymers derived *via* an aza-Michael addition and the ring-opening of epoxides in a grafting-onto approach. The amino moieties (red) were exploited as reactive handles.^{15,46,48,61,63}

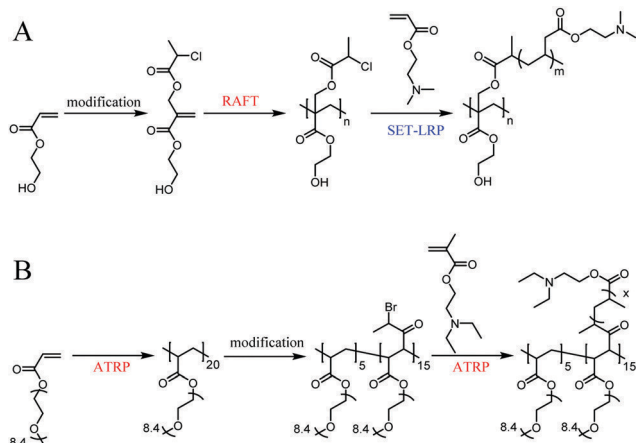


Fig. 4 Synthesis of PHAEA-*g*-PDMAEA and PPEGMA-*g*-PDMAEA *via* the grafting-onto approach and the smart combination of monomer or polymer modification and controlled polymerisation techniques (RAFT, SET-LRP and ATRP), corresponding to literature reports.^{43,80}

Stars and miktoarm star copolymers

Star-shaped double-hydrophilic copolymers benefit from a higher density of functional groups compared to linear block copolymers with both internal and peripheral functional moieties. This is leading to higher loading capacities and lower aggregation numbers as well as often micellar structures with increased stability. Besides, they exhibit a lower solution viscosity due to less entanglements being formed.^{37,87}

The structural diversity in the field of segmented, double-hydrophilic star and miktoarm copolymers is broad. They differ in arm number (3, 4, 8, 21 and more), and their arrangement: block copolymers, or individual blocks (arms) linked through the core. In this respect, different types of miktoarm star exist: star block copolymers, miktoarm stars and A_xB_y -type non-linear block copolymers, and the variety of these topologies and the hydrophilic segments are depicted in Table 2. Regarding the synthetic access, in any case, the utilisation of multi-site initiators or crosslinking points is necessary, besides the smart

combination of controlled polymerisation techniques and end-group modifications.

The arm-first approach is based on the utilisation of reactive arms as macromonomers. Rudolph *et al.*³⁹ synthesised poly(ethylene oxide)-*block*-poly(2-ethyl-2-oxazoline)₈ (PEO-*b*-PEtOx)₈ starting from star-shaped (PEO)₈ with azide end-groups. Afterwards, alkyne-functionalised PEtOx were linked to the PEO precursor *via* a copper-catalysed azide-alkyne cycloaddition click reaction (CuAAC). Alternatively, the star block copolymer was obtained by the CROP of EtOx from a [PEO-Ts]₈ macro-initiator. In a similar approach, Skandalis *et al.*^{37,88} synthesised (PDMAEMA_{*n*}POEGMA_{*m*})_{*p*} miktoarm star polymers with 24 arms each. First, the PDMAEMA homopolymer was synthesised *via* RAFT and then crosslinked with ethylene glycol dimethacrylate (EGDM), a difunctional monomer, to obtain a crosslinked core. Hereby, the chain transfer agent (CTA) was transferred to the core and chain-extended with OEGMA to graft the POEGMA arms. On the other hand, (PDMAEMA-*b*-POEGMA)_{*n*} star block copolymers were synthesised *via* a core first approach. After the EGDM core containing the CTA was synthesised, DMAEMA and OEGMA were polymerised sequentially. In both strategies, the star-star coupling cannot be excluded, but the core-first approach provides improved control and straightforward purification, *i.e.*, the removal of the remaining monomer or homo star polymers.

The PDMAEMA segments or arms were further quaternised to tune the hydrophilicity.³⁷ An alternative architecture was realised by Taghavi-Kahagh *et al.*,⁸⁹ preparing polyampholytic PDMAEMA-*star*-PMAA DHCs, containing hydrophilic PDMAEMA arms and a hydrophilic PMAA core. Therefore, the arms were synthesised first *via* RAFT, such that they possessed functional CTA end-groups. Afterwards, MAA and dual-functional N,N' -methylenebis(acrylamide) were added in a distillation-preparation technique to form the core. Changing the arm length (*i.e.*, their molecular weight) and/or arm number is then straightforward to further tune the solution properties.⁸⁹

The core first approach is more often exploited in the synthesis of star block copolymers, starting from multifunctional initiator cores and followed by CRP. For this, cyclodextrin (21 arms)^{42,69,90} dendritic polyesters (nine arms)^{13,91} and glycerol ethoxylate (3 arms)⁹² were used for the defined synthesis of the block copolymer. For the polymerisation of the corresponding block copolymers, in addition to conventional ATRP, SET-LRP and photo ATRP were applied to precisely control the segment length. It should be noted that for the synthesis of poly(acrylic acid) (PAA)-containing star block copolymers, deprotection of the protected PtBAA segment is necessary.^{42,90} The use of a dual-functional, four-arm ATRP/RAFT initiator, as shown in Fig. 5, was used to synthesise non-linear miktoarm block copolymers (AB₃, A₂B₂) by combining both CRP techniques.⁴⁰ This pathway also gives access to multi-hydrophilic DHCs, A₂(BC)₂ and (AB)₂C₂, by the sequential addition of monomers.^{67,93–95}

However, Cai and Armes^{31,41,99} applied another trifunctional initiator, 2-(diethanolamino)acetyloxyethyl 2-bromoisobutyrate, to construct Y-shaped (AB₂) and zwitterionic DHCs using only ATRP. After the polymerisation of PDEA, the hydroxyl groups of

Table 2 Schematic structure of star and miktoarm-shaped DHCs and the corresponding polymers

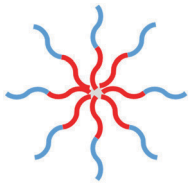
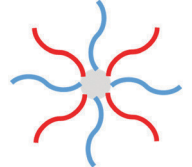
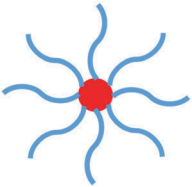
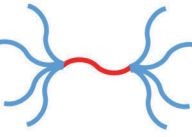
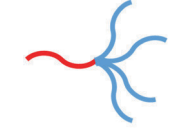
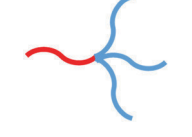



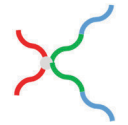

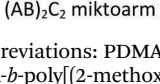
Schematic depiction	Polymers	Ref.
 star block copolymer	PNIPAAm- <i>b</i> -PDMA or PHEAm (3 arms) PEO- <i>b</i> -PEtOx (8 arms) P(OEGA)- <i>b</i> -PAA (9 arms) PAA- <i>b</i> -P(MEA-co-OEGA ₄₈₀) (21 arms) P4VP- <i>b</i> -PAA (21 arms) PNIPAAm- <i>b</i> -PAA (21 arms) (PDMAEMA- <i>b</i> -POEGMA) _{<i>n</i>} (<i>n</i> arms)	13, 37, 39, 42, 69 and 90–92
 miktoarm star	(PDMAEMA) _{<i>n</i>} (POEGMA) _{<i>m</i>} (<i>n</i> and <i>m</i> = 24)	37
 star copolymers	PDMAEMA- <i>star</i> -PMAA (34, 35, 38 arms)	89
 A ₂ BA ₂ and A ₄ BA ₄ miktoarm	PDEA ₄ - <i>b</i> -poly(propylene oxide)- <i>b</i> -PDEA ₄	58
 AB ₄ miktoarm	PNIPAAm- <i>b</i> -PDEA ₄	59
 AB ₃ miktoarm	PNIPAAm- <i>b</i> -PAA ₃ PAA- <i>b</i> -PNIPAAm ₃	93
 AB ₂ miktoarm (Y-shaped)	PDEA- <i>b</i> -PSEMA ₂ PPO/PEO (Jeffamine)- <i>b</i> -...P GMA, HEMA, HEA, MEMA, MPC, DEA, DMA PZLL- <i>b</i> -(PBLG) ₂	31, 41 and 96
 A ₂ B ₂ miktoarm	(PNIPAAm) ₂ -(PAA) ₂	93

Table 2 (continued)

Schematic depiction	Polymers	Ref.
	PEG(- <i>b</i> -PMAA)- <i>b</i> -PDEA PEG(- <i>b</i> -PDEA)- <i>b</i> -PNIPAAm	97 and 98
ABC miktoarm star 	(PNIPAAm) ₂ -(PNVP- <i>b</i> -PAA) ₂ (PNIPAAm- <i>b</i> -PAA) ₂ -(PNVP) ₂	67
A ₂ (BC) ₂ 	(PNIPAM- <i>b</i> -PAA) ₂ -(PVP) ₂ (PNIPAM) ₂ -(PVP- <i>b</i> -PAA) ₂	93–95
(AB) ₂ C ₂ miktoarm 		

Abbreviations: PDMA: poly(*N,N*-dimethylacrylamide); PEO-*b*-PETox: poly(ethylene oxide)-*block*-poly(2-ethyl-2-oxazoline); PAA-*b*-P(MEA-*co*-OEGA₄₈₀): PAA-*b*-poly[(2-methoxyethyl acrylate)-*co*-(oligo(ethylene glycol) acrylate)]; P4VP: poly(4-vinyl pyridine); POEGMAm: poly(oligo(ethylene glycol) methacrylate); PSEMA: poly(succinyloxyethyl methacrylate); PPO/PEO (Jeffamine)-*b*-...GMA, HEMA, HEA, MEMA, MPC, DEA, DMA: poly(alkylene oxides)-*block*-...glycerol monomethacrylate, 2-hydroxyethyl methacrylate, 2-hydroxyethyl acrylate, 2-(*N*-morpholino ethyl methacrylate, 2-methacryloyloxyethyl phosphorylcholine, 2-(diethylamino)ethyl methacrylate; 2-(dimethylamino)ethyl methacrylate; PZLL-*b*-(PBLG)₂: poly(ϵ -benzyloxycarbonyl-L-lysine)-*block*-poly(γ -benzyl-L-glutamate).

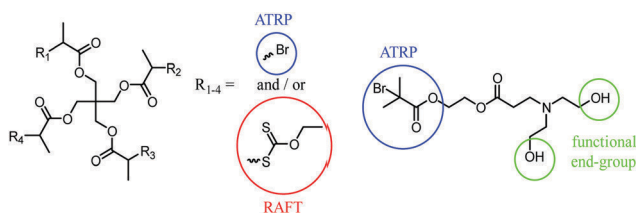


Fig. 5 Four-arm initiator-containing sites for ATRP and RAFT polymerisation (left). It can contain one or three of each moiety, and allows the combination of both methods.⁴⁰ Trifunctional initiators allow for the post-polymerisation modification of the hydroxyl groups for additional ATRPs.⁴¹

the initiator were esterified to obtain a dual-functional ATRP macroinitiator for subsequent polymerisation.⁴¹

Other miktoarm DHCs were synthesised starting from an end-group functionalised segment, where either commercially available^{31,58} or readily synthesised examples³⁸ containing amino moieties were used. These were transformed into multi-functional ATRP initiators by Michael-addition reactions or the ring opening of epoxides and subsequent esterification.^{31,38,58} In this respect, AB₂, AB₄, A₂BA₂ and A₄BA₄ miktoarm DHCs were synthesised after polymerisation of the second monomer. Liu *et al.* describe the preparation of ABC miktoarm star terpolymers in a multi-step approach including the synthesis of a trifunctional initiator, ATRP, CuAAC click reactions, and a deprotection step.^{97,98}

Although the synthetic access to the above-described architectures is not always straightforward, star and miktoarm DHCs exhibit interesting solution self-assembly. One might expect that while more than two sorts of polymer segments

are arranged in a non-linear DHBC, their solution self-assembly could be more complex and attractive. In general, the self-assembly of miktoarm and stars copolymer is less studied since this architecture class is generally less studied and most experimental works involve linear block copolymers.^{97,100,101} So far from literature reports we could realize that they often show more complex self-assembly patterns if compared to linear block copolymers.^{15,31,41,58,59,67,93} The micellisation behaviour could differ, *e.g.*, with respect to the unimer-to-micelle transition kinetics, the stability of the resulting aggregates, or the dimension and one decisive factor clearly is that junction points of more than two chemically distinct segments exist.^{31,41,58,59,67,87,93}

Due to their unique properties, star-shaped DHCs show great potential in biomedical applications and even in 3D inkjet printing for the preparation of hydrogels. For this, hydrogels were constructed using the individual arms of P(OEGA)-*b*-PAA as dynamic physical crosslinking points complexing different metal cations.^{13,91} The exciting micellisation behaviour is shown in the case of PDEA₄-*block*-poly(propylene oxide)-*block*-PDEA₄ (A₄BA₄) copolymers, where both unimolecular or flower-like micelles were found depending on the temperature and pH value.⁵⁸ For star block copolymers, unimolecular micelles were also found for 21 arm, dual pH-responsive P4VP-*b*-PAA (Fig. 6A).

Under basic conditions, the PAA segment is stretched, and the P4VP blocks collapse to form the core. On the other hand, in an acidic environment, inverse unimolecular micelles are formed with P4VP extending into the solution. However, at intermediate pH values, aggregation between the star block copolymers was observed, resulting from apparent zero net charge and polyelectrolyte complex formation (Fig. 6A).⁴²

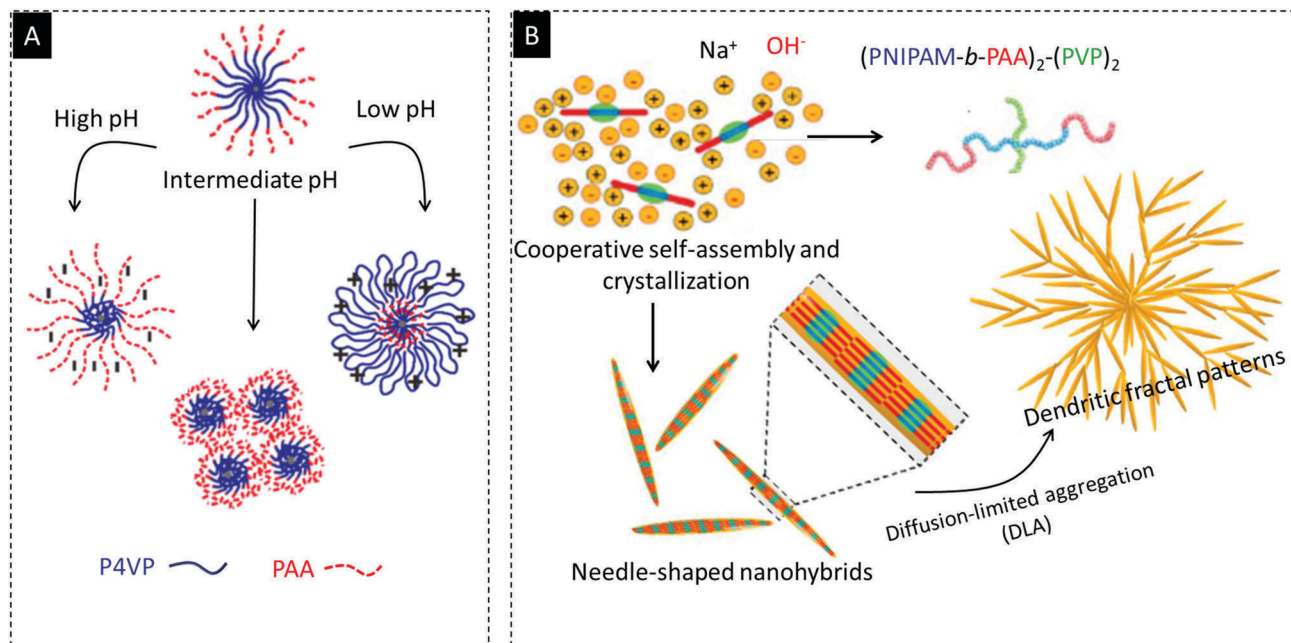


Fig. 6 (A) Schematic depiction of the self-assembly of a dual pH-responsive P4VP-*b*-PAA star block copolymer at different pH-values. Adopted with permission from ref. 42. Copyright © 2020 American Chemical Society. (B) Cooperative self-assembly of (PNIPAAm-*b*-PAA)₂-(PVP)₂ in NaOH solution. Here, dendritic fractal patterns were formed. Adapted from ref. 93. with permission of Royal Society of Chemistry.

However, aggregation in pure water was also observed without any stimulus, and this phenomenon was ascribed to the different hydrophilicity of the constituting segments.^{37,39}

Within this architectural class, MHBCs can introduce additional complexity by including multiple functionalities – thereby further tuning eventual phase transitions, water-solubility, or biocompatibility.^{67,93} The zwitterionic ABC miktoarm star terpolymers (PEG(*b*-PMAA)-*b*-PDEA) from Liu *et al.*, for example, consist of an anionic and a cationic segment, as well as a non-ionic PEG block. This enables multiple phase-transitions by changing the pH-value, giving polyion, hydrogen-bonded, or even hydrophobic cores.⁹⁸ Sun *et al.* describes the cooperative self-assembly and crystallisation of miktoarm (PNIPAAm-*b*-PAA)₂(PVP)₂ in an alkaline solution, as shown in Fig. 6B. The investigated nanohybrids of the DHC and the alkali salts form well-defined micro-sized objects (needles and dendritic patterns). Each segment has its own function: the PAA interacts with the metal cations acting as a scaffold, PVP forms hydrogen bonds with the PNIPAAm segment, and PNIPAAm reveals self-concentration and intermolecular association. The obtained materials are interesting candidates for use, *e.g.*, in sensors or microprinting.⁹³

Toothbrush and centipede-like architectures

Toothbrush and centipede-like architectures have also been reported for DHGCs, which exhibit a linear block and a segment containing grafts with different lengths, revealing exceptional self-assembly.^{6,7,43,45,62,79,80,83,84,102} A centipede-shaped brush even exhibits two chemically distinct chains connected to each grafting point.⁶² In this context, switching between different morphologies, *e.g.*, vesicles to micelles or worm-like assemblies to micelles, as well as the formation of

schizophrenic micelles has been described. An advantage of this architecture is, that the high density of chains in a brush-like segment can increase the colloidal stability of the formed aggregates, if compared to linear segments.⁵¹ The corresponding materials show interesting thermo or pH-induced micellisation in water to form unimolecular or spherical micelles and vesicles.¹⁰² While Sun *et al.* prepared PNIPAAm-*b*-POEGMA *via* sequential RAFT of NIPAAm and OEGMA with three or eight OEGMA units as brushes,¹⁰² C. Feng *et al.* synthesised such DHCs in a grafting-from approach, using either ATRP or SET-LRP. First, the linear segment was synthesised in a controlled manner before it was chain-extended with hydroxyethyl acrylate (HEA). Afterwards, the hydroxyl groups were converted into ATRP initiators and the third monomer was polymerised to obtain PNIPAAm-*b*-(PEA-*g*-P2VP) and PNIPAAm-*b*-(PEA-*g*-PDEAEMA).⁵⁻⁷ PNIPAAm-*b*-(PEA-*g*-PDEAEMA) the latter was found to be a suitable stabiliser and template for the preparation of AuNPs in water,⁷⁴ and other applications are foreseen in biomedicine,¹⁰² as biological vectors or protective shells for sensitive enzymes.^{6,7}

PEO-*b*-[PGMA-*g*-(PDEA)(PMEOMA)] is a special case of MHBC. It is a centipede-like MHBC, which was prepared using two ATRP steps, post-polymerisation modification reactions, as well as CuAAC chemistry. Nevertheless, the dual-responsive polymer exhibits a ‘schizophrenic’ micellisation behaviour, switching between worm-like unimers and two different types of micellar objects.⁶² Jeong *et al.* investigated the influence of the molecular geometry on the colloidal properties and the controlled drug release by comparing a typical PAA-*b*-PEG block copolymer with brush-like PAA-*b*-PEGMA. Hereby, micellar structures containing the bulky brush-like chains in the shell

exhibit fundamentally different self-association kinetics compared to the linear chains in the shell, and significantly influenced the release of cisplatin complexed in the PAA core (Fig. 7A). This is an interesting example of how the core/corona structures can be synthetically tuned and how this affects potential application scenarios.⁵¹ Regarding the above-mentioned examples, toothbrush shaped DHCs reveal great potential to be applied as templates,⁷⁴ protective shells^{6,7} and for the controlled delivery of drugs.⁵¹

Hyperbranched and dendritic architectures

In general, there exist two types of hyperbranched and dendritic DHCs. One consists of a linear PEG linked to a hyperbranched segment, and the other is based on polyamidoamine dendrimers (HPAMAM) containing PEG or poly(lysine) grafts (Fig. 7B). Hyperbranched linear DHCs feature an enhanced water solubility, a high density of the polymer itself, polyfunctionality, and a high local concentration of functional end-groups.^{17,38,60} This results in increased loading capacities, and more effective chelation of metal ions compared to linear DHCs as investigated by Qi *et al.*,⁶⁰ rendering them suitable for drug-delivery and catalytic systems or templates.^{17,38,60} PEG-*b*-poly(glycerol) was synthesised starting from PEG-OH in four steps. First, it was chain-extended with ethoxyethyl glycidol ether, and the hydroxyl group deprotected and deprotonated before branches were introduced using glycidol.⁶⁰ Lee *et al.* exploited the polyfunctional hydroxyl groups for the attachment of the anticancer drug doxorubicin *via* hydrazone-based bonds. The obtained micelles were successfully tested as drug delivery systems.¹⁷ On the other hand, PEG-*b*-PEI were found to be suitable nanoreactors for the synthesis and stabilisation of CdS and Pd, Cu, Rh and Pt NPs. The amino moieties allow a strong interaction with the NP surface, and the corresponding

systems are interesting candidates for catalysis in water or biomineralisation.^{60,108}

Multi-arm dendritic polymers form highly stable (unimolecular) micelles and feature a functional interior, rendering these materials useful nanocapsules and nanoreactors to be applied in the template-assisted synthesis of nanoparticles and drug-delivery systems.^{103–107} The hydrophilic PEG or poly(lysine) side-chains, respectively, hereby promote the formation of core-shell structures,¹⁰³ increase transfection efficiency and reduce cytotoxicity.^{104,107} The HPAMAM core is prepared from an AB monomer (methyl acrylate) and a C₄ monomer (ethylene diamine) by Michael-addition reactions followed by amidation.^{103,105} In a grafting-onto approach, the peripheral amine groups were converted with activated PEGs containing an *N*-hydroxysuccinimide (NHS) ester¹⁰⁵ or succinimide carbonate moiety.¹⁰⁴ Also, the HPAMAM end-groups can be activated before grafting PEG, which was already realised for hydrazones,¹⁰³ oligoamines, and alkynes.¹⁰⁶ The grafting-from approach is also possible for this topology class, as already studied by Pan *et al.* They polymerised modified lysine from the dendrimers before a subsequent deprotection step. The obtained polymers form nanoplexes with DNA and were found to be effective gene vectors.¹⁰⁷

Macrocyclic DHCs

Until now, cyclic- or ring-shaped polymers remained relatively unexplored as a consequence of the complex synthetic procedures required. However, they exhibit unique properties due to their lack of end-groups or reduced hydrodynamic radii, and developments in their synthesis have led to increased interest in these architectures.^{109,110} Z. Ge *et al.* synthesised linear α,ω -heterodifunctional poly(2-(2-methoxy-ethoxy)-ethyl methacrylate)-*block*-poly(oligo(ethylene glycol)methyl ether methacrylate),

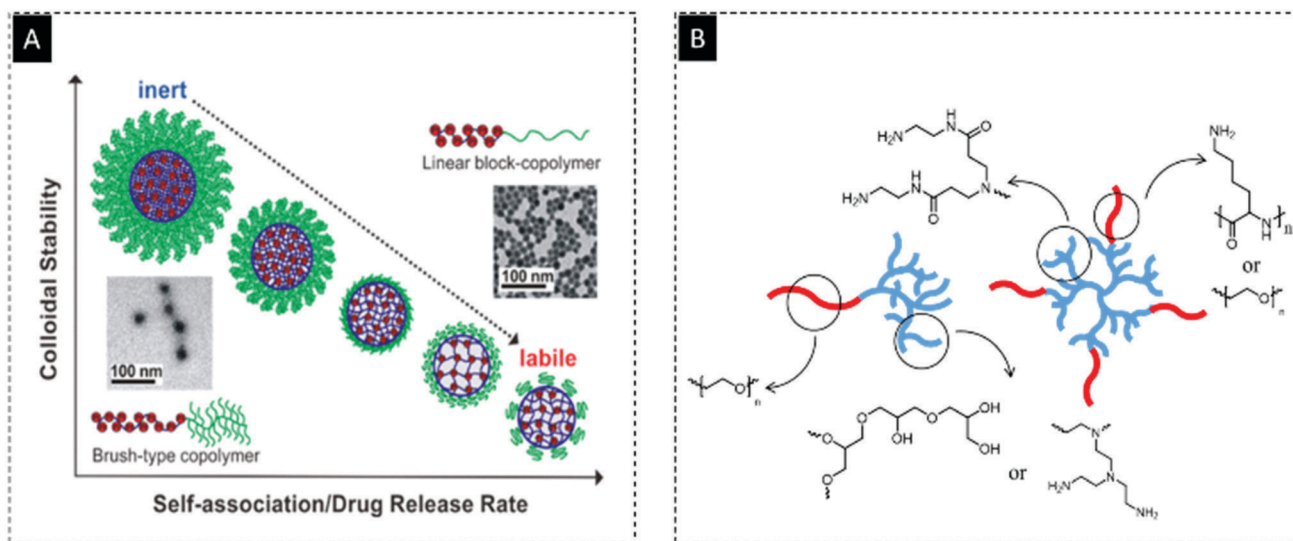


Fig. 7 (A) Schematic depiction of the influence of the micellar geometry on the self-association and drug release of DHCs. Reprinted with permission from ref. 51. Copyright © 2018 American Chemical Society and (B) schematic depiction of linear, branched, and dendritic DHCs, and the structural elements of the corresponding segments. Linear hyperbranched DHCs typically consist of a PEG segment and hyperbranched glycerol^{17,38} or PEI.⁶⁰ Dendritic DHCs usually consist of a HPAMAM core and either PEG^{103–106} or PLL side-chains.¹⁰⁷

alkenyl- PMEO_2MA - b - POEGMA-N_3 block copolymers *via* successive ATRP and end-group functionalisation, which form micelles at 40 °C in water. This leads to the spatial separation of the alkenyl and azide moieties, and under suitable conditions for click chemistry only released unimers will react intramolecularly. This procedure allows the reaction of relatively high concentrations of linear precursors, which is unusual for the synthesis of macrocycles and the corresponding *cyclic*- PMEO_2MA - b - POEGMA were able to form flower-like micelles. Using the same procedure, pH-responsive *cyclic*- PDMA - b - PDEA was synthesised and compared to the linear precursors. Their self-assembly differs resulting in higher critical micelle concentrations (CMC), more compact hydrodynamic radii, and lower aggregation numbers.⁸

There appears to be a lot of potential in the design of ring-shaped DHCs and even novel architectures, *e.g.*, multicycles or tadpoles could be implemented.

Crosslinking of DHCs

Crosslinked nanostructures consisting of DHBCs could be considered a separate architectural subclass, which forms 3D structures where at least one part is crosslinked. While assemblies from linear DHBCs may dissociate under dilute conditions such as within body fluids, crosslinked nano-objects benefit from higher stability and longer lifetime.^{64,65,111} Hence, they are promising candidates as drug delivery systems, *e.g.*, in cancer treatment loading doxorubicin or cisplatin in the core,^{111,112} which justifies additional steps in the synthetic protocol. In the literature, three morphologies exist: core cross-linked micelles,^{111–114} vesicles,^{64–66} and nanogels.¹¹⁵ The cross-linking of preformed 3D objects was, for example, achieved starting from polymerisation-induced self-assembly (PISA),

complexation with metal ions, or even from DHBC aggregates in pure water. The crosslinking can be viewed as an additional design element, by determining the density or the type of linker, *e.g.*, resulting in degradable or non-degradable junction points.

In general, PISA is an emerging technique for the preparation of block copolymer nanostructures *via* various controlled polymerisation methods. Hereby, well-soluble segments are chain-extended with a solvophobic monomer, decreasing solubility and inducing aggregation at a certain degree of polymerisation, resulting in the formation of nano-objects.^{116,117} PISA was exploited for the preparation of crosslinked poly(ethylene glycol) methyl ether methacrylate-*block*-poly(glycerol methacrylate-*co*-bis(2-methacryloyl)oxyethyl disulfide)) PPEGMA-*b*-(PGLMA/PBMOD) vesicles. At first, PPEGMA macroinitiators were synthesised *via* reversible complexation mediated polymerisation before polymerising the second segment consisting of hydrophobic solketal methacrylate and bis(2-methacryloyl)oxyethyl disulfide as crosslinker. The obtained crosslinked amphiphilic ABC vesicles were then hydrolysed to obtain double hydrophilic PPEGMA-*b*-(PGLMA/PBMOD) vesicles with hydrodynamic diameters of 190 nm, as shown in Fig. 8A.⁶⁶

Upon employing a disulfide-based crosslinking strategy, the corresponding nano-objects could be cleaved in the presence of glutathione, which is found in tumour cells, leading to the dissolution of the nanostructures and rendering these materials highly interesting nanocarriers.⁶⁶ Qu *et al.*¹¹⁴ synthesised cross-linked poly[poly(ethylene glycol)methyl ether methacrylate-*block*- N,N' -di(methyl amino)ethyl methacrylate-*block*-methacrylic acid] PPEGMEMA-*b*-PDMAEMA-*b*-PMAA micelles starting from micellar PPEGMEMA-*b*-PDMAEMA-*b*-poly(*tert* butyl methacrylate) (P*t*BMA)

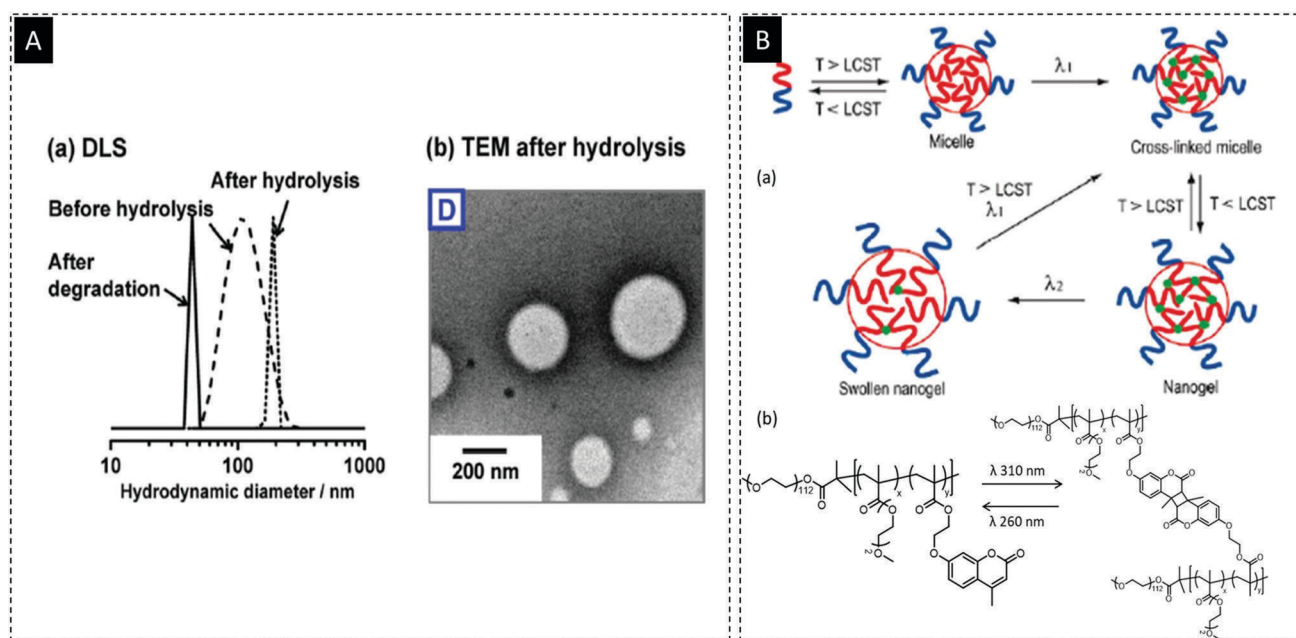


Fig. 8 (A) DLS measurements (a) and TEM micrographs (b) of the crosslinked double hydrophilic vesicles described by Sarkar *et al.*⁶⁶ Adapted from ref. 66. with permission of Royal Society of Chemistry. (B) Preparation of a nanogel by the photo-induced crosslinking of the coumarin containing core.¹¹⁸ Reprinted with permission from ref. 118. Copyright © 2009 American Chemical Society.

triblock terpolymers. In this case, hydrophobic *Pt*BMA segments, bearing reactive end-groups, self-assemble within the core. Then, the addition of a bifunctional crosslinker stabilises the structures before the *tert*-butyl groups are cleaved to obtain hydrophilic PMAA. Each segment exhibits its own function in this system: PPEGMA acts as a stabiliser in the corona and increases biocompatibility, PDMAEMA induces pH-dependent charge, *Pt*BMA promotes the self-assembly and its product PMAA acts as a proton sponge.¹¹⁴

Willersinn *et al.* described the self-assembly of PEO-*b*-poly(*N*-vinyl pyrrolidone)-*co*-(*N*-vinyl imidazole) and pullulan-*block*-poly(*N*-vinyl pyrrolidone) in water, without an external stimulus, forming vesicles. This behaviour is not fully understood yet, but probably results from the different hydrophilicity of each segment, differences in chain rigidity, and the volume fraction may also be a contributing factor.^{64,65}

While the vinyl imidazole-containing polymer was cross-linked with a dihalide,⁶⁴ in case of pullulan segments this was realised by cysteamine dihydrochloride, yielding stable vesicles with a diameter of 700 nm.⁶⁵ Upon using this cross-linking agent, the pH- or redox-induced disassembly is possible, leading to an increased amount of unimer species.

Bronich *et al.*,¹¹³ Kim *et al.*,¹¹¹ and Bontha *et al.*¹¹² exploited the polyion-metal complex formation of PMA and Ca²⁺ (Ba²⁺ and Sr²⁺ are also possible) to induce micellisation. Here, commercially available PEO-*b*-PMA was complexed by adding CaCl₂ and the resulting physically crosslinked micelles were converted with 1-(3-dimethyl amino propyl)-3-ethylcarbodiimide hydrochloride and 1,2-ethylenediamine to obtain further crosslinks. The obtained micelles were purified by dialysis and revealed diameters of around 170 nm, which were constant even upon 100-fold dilution. The core-crosslinked micelles were further tested as nanocarriers by loading doxorubicin and cisplatin.^{111–113} A similar approach was applied for graft-comb Pluronic-PAA copolymers, leading to stable nano-gels with pH-dependent swelling.¹¹²

In addition to the well-defined nano-sized micelles and vesicles described above, covalently crosslinked double hydrophilic nanogels and hydrogels must be mentioned in the context of 3D architectures, although a concise distinction is difficult. The synthesis of nanogels by various approaches has been reviewed by Khoee and Asadi.¹¹⁹ Herein, the preparation from polymer precursors or monomers is described *via* different crosslinking reactions. The corresponding materials exhibit high water uptake, biocompatibility, and promising mechanical properties. Among others, for example, photo-crosslinkable PEG-*b*-P(DMAEMA-*co*-2-cinnamoyloxyethyl acrylate),¹²⁰ or PEO-*b*-P(MEOMA-*co*-4-methyl-[7-(methacryloyl)oxyethoxy]coumarin) nanogels were examined and the thermo and light-responsive behaviour is depicted in Fig. 8B.¹¹⁸ Although not mentioned in this review, another interesting example is a core-shell PSB-*b*-PNIPAAm nanogel, revealing a dual-thermo response with both upper critical solution temperature (UCST) and LCST behaviour.¹²¹ It is also noteworthy that PEG-PEI nanogels, which were first introduced in 1999, are promising drug delivery systems.^{122–124}

Stimuli-responsive polymers

The last decades have witnessed tremendous progress in the field of stimuli-responsive polymers. This is predominantly owed to the new strategies available for the polymerisation of “functional” monomers and the active development of post-polymerisation modifications.^{125–133} During the revolutionary stage of developing stimuli-responsive polymeric systems, DHC have also emerged as a subclass in this family, adding notable contributions to possible compositions and applications. The stimuli-responsive behaviour is indeed an important concept within DHCs, in general, since most of them also exhibit at least one type of response, and this then significantly governs the solution behaviour. As a result, their response to triggers is exploited for self-assembly, to interact with metal ions, catch-and-release mechanisms, or for translation into a measurable readout.^{15,32,33,133–135} This expands the range of applications of DHCs to include *e.g.*, sensors, which will be described later.

In general, most of the above described DHCs with different topologies also exhibit a stimuli-responsive in one way or another. So far, Ge *et al.*¹⁰ discussed several stimuli responsive hydrophilic copolymers for drug delivery and enhanced imaging, summarising some interesting combinations. Herein, we will focus on combinations of different monomers, yielding DHCs which contain at least one stimuli-responsive building block. As many excellent systems have been developed, we will highlight some pioneering work in several categories including double and multi-stimuli responsive hydrophilic copolymers (DHCs and multi hydrophilic copolymers (MHCs)). A general understanding of stimuli-responsive DHCs could help tailor their properties for their implementation to fulfil certain tasks.

In the following section, stimuli-responsive DHCs are presented. The DHCs were categorised as follows: stimuli-responsive DHCs reacting towards the exposure of one or more triggers, and MHCs exhibiting at least one stimuli-response with more than two segments.

Stimuli-responsive DHCs

Thermo-responsive polymers. In addition to amphiphilic thermo-responsive polymers, DHCs have been studied intensively. The majority of these DHCs described involve a combination of thermo-responsive moieties with either non-ionic or ionic (*i.e.*, polyelectrolyte) segments to control the morphology and complexation,^{26,33} self-assembly,^{33,136,137} hydrogel formation,^{138–140} or tuning of the LCST/UCST points.^{24,141–143} Some thermo-responsive DHCs with ionic and non-ionic segments are summarised in Table 3, with some of the interesting and representative works highlighted below. It is worth noting, that most of the thermo-responsive DHCs contain PNIPAAm segments, being also one of the most studied thermo-responsive homopolymers.

One of the first examples of ionic segments was reported by Laschewsky in 2002 (Fig. 9A). They reported a “schizophrenic” thermo-responsive DHC, which was constructed from non-ionic NIPAAm and the zwitterionic monomer 3-[*N*-(3-methacrylamido propyl)-*N,N*-dimethyl] ammonium propane sulfonate (SPP) by

Table 3 Selected examples of thermo-responsive DHCs, showing their structure and potential features. In addition to their thermo-response, the materials are responsive towards pH and metal ions

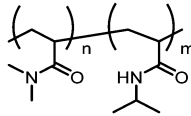
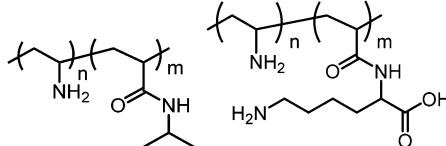
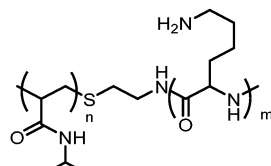
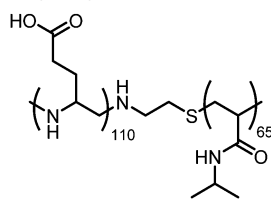
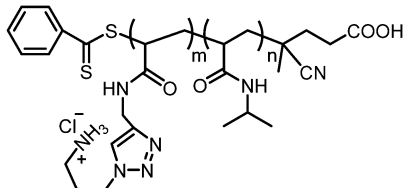
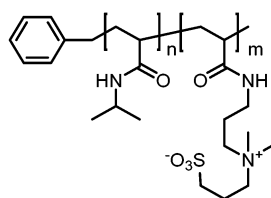
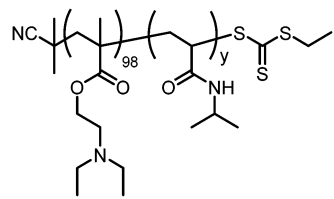
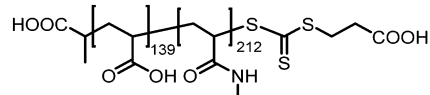
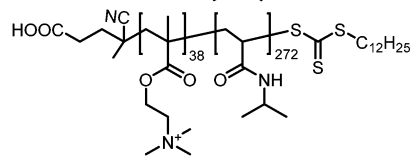
(Co)polymer structures	Special features	Ref.
(Co)polymers containing PNIPAAm units		
	Room temperature synthesis of PNIPAAm Temperature-induced self-assembly Nanostructured hydrogels Dual thermo-responsive	138, 153 and 154
	Formation of polyplex micelles Thermo- and pH-responsive	137 and 155
	Thermo- and pH-responsive	156
	Coil-to-helix transitions based on polypeptide Thermo- and pH-responsive	157
	Gold nanoparticle incorporated core and shell Thermo- and pH-responsive	158
	Schizophrenic micelles Dual thermo-responsive	24
	“Schizophrenic” self-assembly: from micelles to vesicles Thermo- and pH-responsive	159
	Co-assembly of double-hydrophilic block copolymer and interpolyelectrolyte complex Thermo- and pH-responsive	88
		

Table 3 (continued)

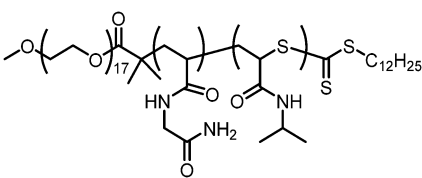
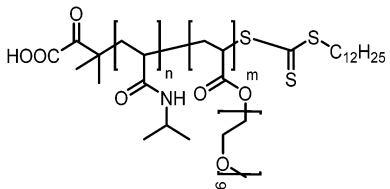
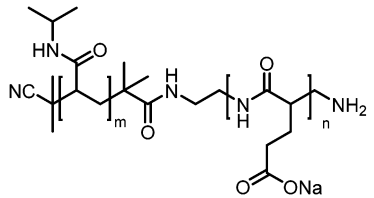
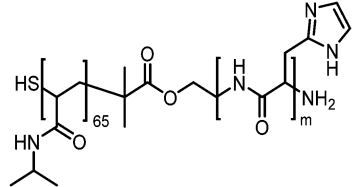
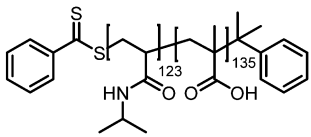
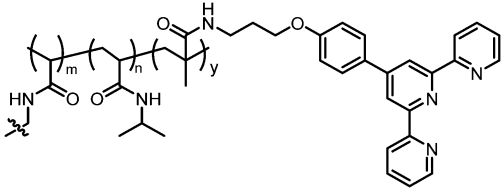
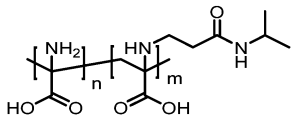
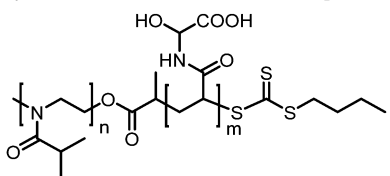
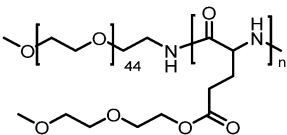
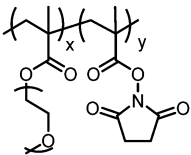
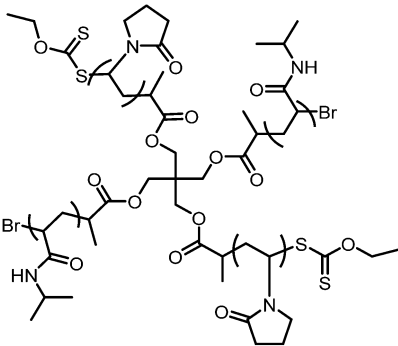
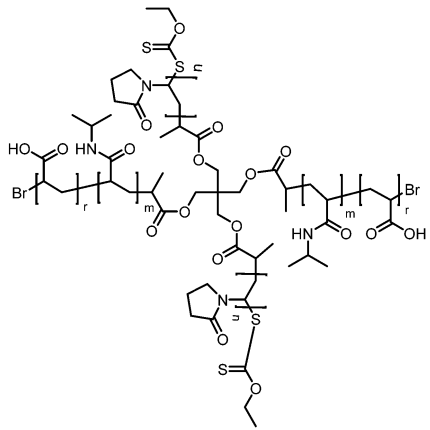
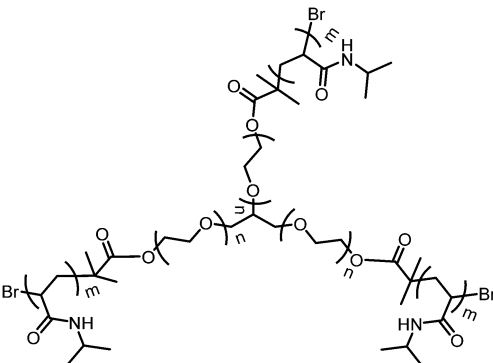
(Co)polymer structures	Special features	Ref.
	Triple hydrophilic UCST-LCST block Copolymers Thermo- and pH-responsive	141
	Formation of circular micelles with a sunflower-like structure Dual thermo-responsive	160
	Tunable morphology Thermo- and pH-responsive	161
	Controlled drug delivery Thermo- and pH-responsive	162
	Preparation and stabilisation of AuNPs Thermo- and pH-responsive	163
	Stimuli-responsive microgels and their assembly through metal-ligand interactions Thermo- and metal ion-responsive	164
	Polyampholytic graft copolymers Self-assembly in solution Triple thermo-, pH- and metal ion-responsive	15
(Co)polymers based on other thermoresponsive units		
	Self-assembly in solution Thermo- and metal ion-responsive	33

Table 3 (continued)

(Co)polymer structures	Special features	Ref.
	Step-wise self-assembly Thermo-responsive	165
	Functionalisation of quantum dots Thermo-responsive	166
Non-linear thermoresponsive (co)polymers		
	Non-linear multi-responsive, multi-hydrophilic block copolymers Thermo- and pH-responsive	67 and 94
	Multi-hydrophilic block copolymers Thermo- and pH-responsive	9 3 and 95
	Pentablock star-shaped polymers Thermo-responsive	92

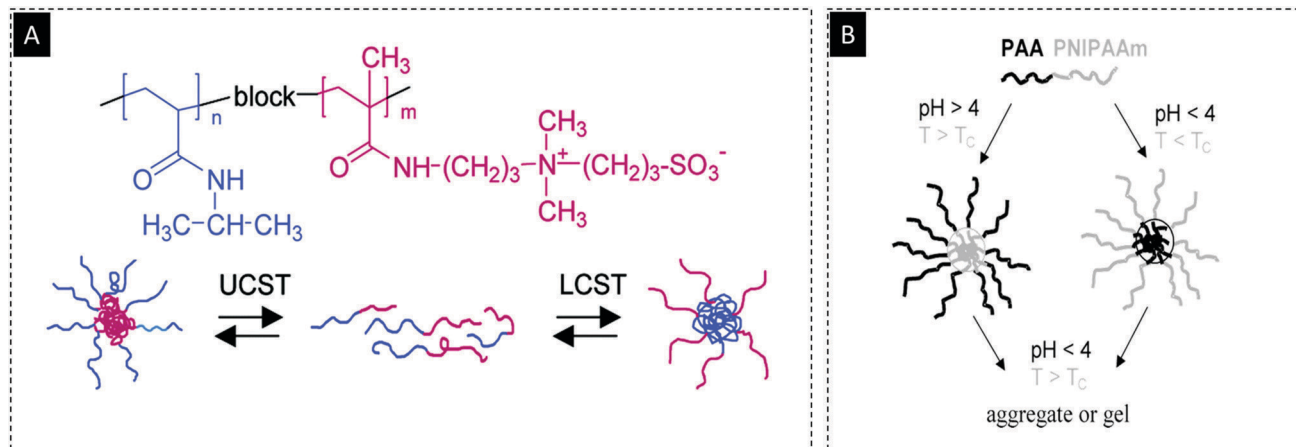


Fig. 9 (A) Simplified model of the self-assembly of PNIPAAm-*b*-PSPP block copolymers with temperature.²⁴ Reprinted with permission from ref. 24. Copyright © 2002 American Chemical Society and (B) illustration of the aggregate formation for PNIPAAm-*b*-PAA in aqueous solution in dependence of pH and temperature. Reprinted with permission from ref. 144. Copyright © 2002 American Chemical Society.

RAFT polymerisation (Fig. 9A). This block copolymer showed double thermo-responsive behaviour in water. Both segments of these DHC dissolve in aqueous solution at intermediate temperatures, while at high temperatures, the NIPAAm segment collapses due to the LCST. At lower temperature the SPP chains collapse due to UCST behaviour.

In another interesting example, Müller *et al.*¹⁴⁴ also reported PNIPAAm-*b*-PAA by RAFT polymerisation (Fig. 9B), where the formation of larger aggregates at pH 4.5 and temperatures above the LCST point was reported. However, their study also confirmed that the solution behaviour is strongly dependent on hydrogen bonding interactions between the acrylic acid and NIPAAm segments.³³ Indeed, they were also able to tune the cloud point of PNIPAAm from $T_c = 32\text{ °C}$ to 35 °C by adjusting the pH value. This is due to the fact that acrylic acid segments are highly charged at pH 5–7 and thereby increase the cloud point temperature. However, below pH 4.5 charge density decreases, which has an adverse effect. In another key example, Max *et al.*,¹⁵ presented a triple-responsive graft copolymer based on PDha featuring monomeric NIPAAm side chains (PDha-*g*-NIPAAm), which after being used as a template for the preparation of AgNPs could be used as a sensor for pH, temperature, as well as the presence of multivalent metal ions.

Thermo-responsive DHC-containing non-ionic segments mostly feature PEG, and as one interesting and early work, Zhang *et al.*¹⁴⁵ reported thermo-responsive micellisation of poly(ethylene glycol)-*block*-poly(*N*-isopropylacrylamide) (PEG-*b*-PNIPAAm) in aqueous solution. Their observation indicated the formation of micellar structures, which could be tuned by the block copolymer concentration and composition.

Poly(2-alkyl-2-oxazoline)s, *e.g.*, featuring methyl, ethyl, propyl, or isopropyl side chains, have also received great attention for constructing DHCs.^{146–148} Two representative recent examples are DHC of poly(2-methyl-2-oxazoline)-*block*-poly(2-ethyl-2-oxazoline) (PMeOx-*b*-PEtOx) and poly(2-isopropyl-2-oxazoline)-*block*-poly(2-methyl-2-oxazoline) (PiPrOx-*b*-PMeOx) reported by Guégan *et al.*¹⁴⁹ They show a pathway to obtain DHBCs in

a two-step procedure, with an inside cationic part and a hydrophilic and neutral outer part that are very promising for polyplex formation towards non-viral gene delivery. In another key work for poly(2-alkyl-2-oxazoline)s, Takahashi *et al.*¹⁴⁸ combined poly(2-isopropyl-2-oxazoline) and poly(*N*-isopropylacrylamide) (PiPrOx-*b*-PNIPAAm), and they reported that the dehydration of each block does not occur independently. However, non-ionic blocks like PEG were also attached to thermo-responsive units such as PNIPAAm and poly(2-oxazoline)s for different applications, one example being hydrogel formation.^{150,151} Sanson *et al.*¹⁵⁰ reported microgels from NIPAAm in the presence of poly(ethylene glycol)methacrylate (PEG) as a macro-comonomer and methylene bisacrylamide (MBA) as crosslinker.

Pullulan, another non-ionic block, was also combined with thermo-responsive PiPrOx. Here, Morimoto *et al.*¹⁵² reported the preparation of polymeric biphasic, gel/crystal nanocomposites using simple heat treatment in water. According to their observations, an appropriate selection of the length of the PiPrOx can lead to reversibly thermo-responsive nano-gels and permanently fixed crystalline/amorphous nano-assemblies.

pH-Responsive DHCs

In the previous section, we showed that the properties of thermo-responsive DHCs can be tuned by adding pH-responsive segments. Now, we will show that pH-responsive materials are influenced by the incorporation of either thermo-responsive or other non-ionic segments.

The concept of “pH-responsive polymers” predominantly describes polymers with ionisable acidic or basic functional groups where the overall charge varies with the solution pH. These groups can either accept or release protons upon changes in local pH, and this topic has seen a tremendous amount of contributions already.^{129,130,167} In this direction, DHCs containing pH-responsive functional groups have also become increasingly popular during the past few years.

In general, DHCs with pH-responsive segments commonly can either exhibit reversible changes in solubility or conformational

properties as a function of pH. Functional groups are mostly ionic moieties that can dissociate into charged groups or form ionic groups upon protonation. In response to changes in solution pH, one of the segments becomes less hydrophilic, which usually leads to aggregation. The respective DHCs contain a range of suitable comonomers, and are summarised in Table 4. Their solution behaviour is mainly based on ionic interactions, which lead to variations in the chain stretching due to electrostatic repulsions, rendering such materials of interest for different applications as stabilisers, templates for NP formation, drug and gene delivery, as surfactants, dispersants, sensors, in catalysis, or as surface modifiers, complexants, or building blocks for the formation of hydrogels.^{15,46,91,168–170}

Structures of pH-responsive DHCs vary in architecture and, similar to stimuli-responsive polymers in general, typical examples of pH-responsive groups are carboxyl, pyridine, sulfonic acids, phosphates, or tertiary amines. However, polyampholytic or polyzwitterionic segments bear both basic and acidic groups, sometimes even within the same monomer unit.^{15,24,63,171,172} In addition, the combination of ionic groups can be chosen depending on any desired application or targeted composition.

A well-known combination is poly(ethylene oxide)-*block*-poly(methacrylic acid) which was reported by Murata *et al.*¹⁷³ in 2002. They reported nanoaggregate formation upon metal ion chelation in water.¹⁷³ Later in 2005, Bronich *et al.*¹¹³ developed PEO-*b*-PAA/Ca²⁺ by crosslinking the core (Fig. 10A). Almost simultaneously, Tjandra *et al.*¹⁷⁴ reported the use of PEO-*b*-PMAA, which was prepared by ATRP, as a template for the formation of hydroxyapatite.

PEO-*b*-PMAA was further investigated for understanding the solution behaviour in the presence of Ca²⁺ ions by Sondjaja *et al.*¹⁷⁶ They observed that the aggregates not only depend on the Ca²⁺/block copolymer ratio, but that structural rearrangements of the resulting Ca²⁺/PEO-*b*-PMAA complex were also triggered by changes of the water activity itself. In 2008, Gérardin *et al.*¹⁷⁵ reported another innovative strategy to construct mesoporous materials at room temperature in aqueous medium using PEO-*b*-PAA (Fig. 10B). Later, Ra Schin *et al.*²³ reported vesicle formation of PEO-*b*-PAA by self-assembly and degradation in response to the pH value (Fig. 10C). In another example, Hao *et al.*⁸⁴ investigated the solution behaviour of PAA-*g*-PEO, and their results indicated the formation of large inter-chain complexes, which also depended on the pH value and salt concentration.

The complexation between DHCs presenting oppositely charged ionic segments has also been of great interest for the construction of well-defined nano-objects.^{44,177,178} This is also known as polyion complexation (PIC) or interpolyelectrolyte complex formation (IPEC), and pioneering work in this field has been described by Kataoka and Harada, focusing on the application of these systems as potential nanocarrier systems.⁴⁴ In this review, they indicate that extensive studies have been carried out on polyion complex micelles from DHC systems. As an interesting example, we should highlight the research by Yusa *et al.*¹⁷⁸ Here, they described the RAFT polymerisation of diblock copolymers consisting of a hydrophilic poly(2-(methacryl

oxy)ethyl phosphoryl choline) (PMPC) block and either a cationic or anionic block was prepared from (3-(methacrylamido)propyl)trimethyl ammonium chloride (MAPTAC) or sodium 2-(acrylamido)-2-methylpropanesulfonate (AMPS) (Fig. 11A). Polyion complex vesicles were afterwards formed upon mixing and stoichiometric charge neutralisation.

Another interesting subclass of pH-responsive DHCs are materials featuring polypeptide/amino acid units (amino acids, Tables 3 and 4). Prominent examples are poly(L-glutamic acid) (PLGA), poly(dehydroalanine) (PDha), poly(histidine) (PHIS), or poly(aspartic acid) (PASA).^{15,126,162,167,179–181} Some of these polymers are inherently biocompatible and even degradable.^{126,167} Aside from being biocompatible, such examples are able to synergistically combine features from synthetic and natural polymers, such as their design, synthetic access and biomimicking properties.¹²⁶ Selected examples include the work of Kataoka *et al.*,^{182–184} or Rodríguez-Hernández *et al.*¹⁷⁷ In the latter case, the reversible self-assembly of schizophrenic vesicles for zwitterionic diblock copolymers from poly(L-glutamic acid)-*block*-poly(L-lysine) (PGA-*b*-PLys) has been demonstrated (Fig. 11B). They also described the mechanism by neutralisation of the polypeptide block, which then changes from a random coil conformation into a neutral and compact α -helical structure.

Another recent example in the category of polypeptides is cationic poly(L-arginine) for constructing double hydrophilic block copolypeptides. The cationic segment can penetrate cells, and was already used in supra-amphiphile-based polymers. Furthermore, Praveen *et al.*¹⁸⁵ described the synthesis of a pH-responsive supra-amphiphilic DHBC based on PEG-*b*-PLys) (Fig. 11C). Encapsulation of the hydrophobic model dye Nile red, and subsequent co-localisation studies, showed the successful uptake of encapsulation of the dye.

Light-responsive DHCs

Light-responsive materials are receiving more and more attention, mainly because the “activation” can be controlled both spatially and temporally.²¹⁰ Consequently, light-responsive polymers have been the subject of several recent reviews.^{125,210–212}

While temperature- and pH-responsive DHCs have been reported frequently, the world of light-responsive DHCs is rather unexplored compared to that. One reason for this, presumably, is that many of the chromophores employed are rather hydrophobic.

In general, photochromic dyes are used to construct light-responsive polymers. These dyes usually undergo absorption or excitation and a reversible or irreversible isomerisation upon irradiation. This behaviour is typically associated with a change in polarity, as well as a corresponding colour change. Such processes are observed in hydrophobic compounds like azobenzene, spiropyran, salicylideneaniline, spirooxazine, coumarin, *etc.*^{125,213–217} Although these moieties are rather hydrophobic, some light-responsive DHCs have appeared recently (Table 5). They can be divided into two main categories: (i) the light-responsive units are comonomers and chromophores simultaneously, or (ii) the chromophore is introduced as an end-group (label).

Table 4 Examples of pH-responsive DHCs, showing their structure and potential features and applications. In addition to their pH-response, the materials are responsive towards: temperature and metal ions

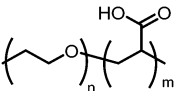
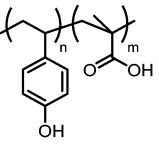
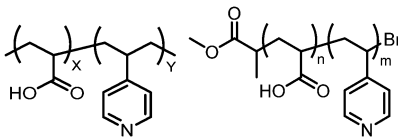
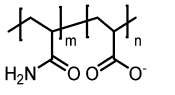
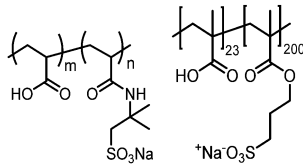
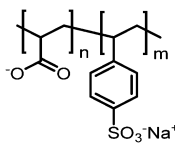
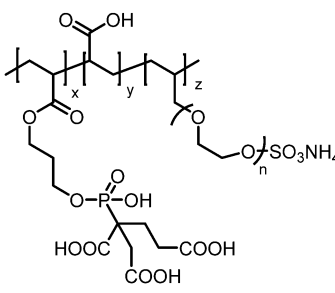
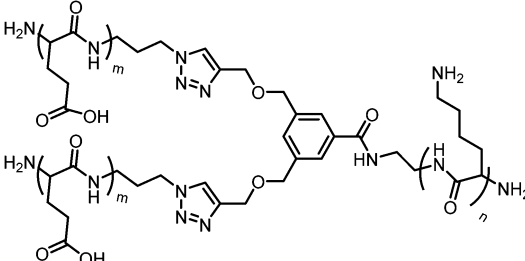
(Co)polymer structures	Special feature/application	Ref.
<p>pH-Responsive DHCs carrying carboxylic acid units</p> 	<p>Self-assembly/disassembly of giant vesicles at biologically-relevant pH, ion complexation, templates Photocontrolled self-assembly of supramolecular polymer nanocontainers Oxidation-responsive micelles based on a selenium-containing polymeric superamphiphiles</p>	23, 176 and 186–188
	<p>pH- and metal ion-responsive Tunable self-assembly pH-Responsive</p>	189
	<p>Encapsulation and release of metalloporphyrins Dispersion of TiO₂ Dual pH-responsive</p>	27 and 168
	<p>Hydration-dependent hierarchical structures pH-Responsive</p>	190
	<p>Coating of iron oxide NPs to provide colloidal stability Template for Zinc Oxide/Magnetite iron oxide nanoparticles pH-Responsive</p>	191 and 192
	<p>Dispersant for coal Template for magnetite iron oxide nanoparticles pH-Responsive</p>	193 and 194
	<p>Application in oil recovery Multi-acidic pH-Responsive</p>	195
	<p>Well-defined AB₂ Y-shaped miktoarm star polypeptide Dual pH-Responsive superamphiphiles pH-Responsive</p>	96

Table 4 (continued)

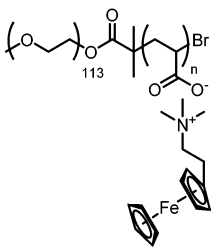
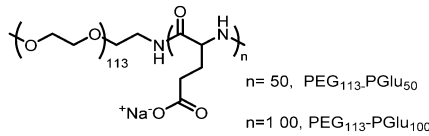
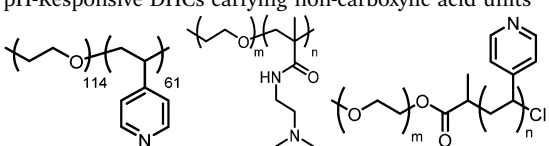
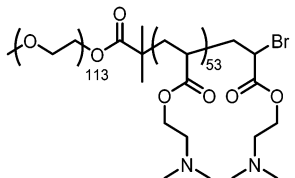
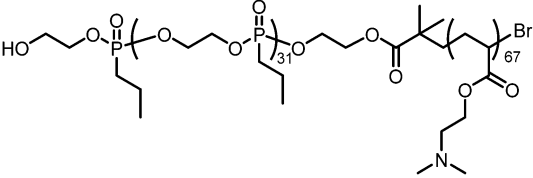
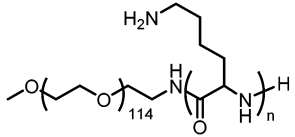
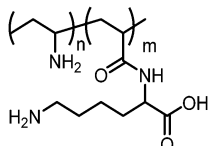
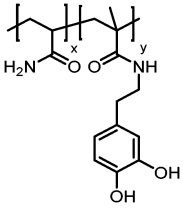
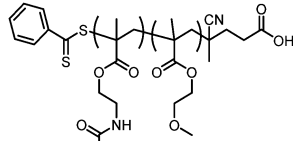
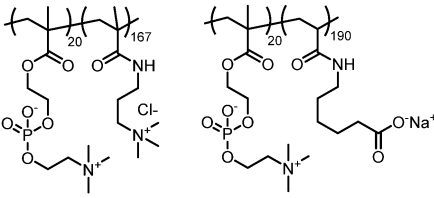
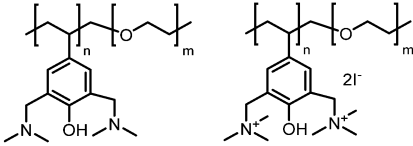
(Co)polymer structures	Special feature/application	Ref.
	Voltage-responsive superamphiphiles pH-Responsive	196
	Platform to construct tunable and functional super-amphiphilic aggregates pH-Responsive	197
	Micellisation induced by porphyrin Template pH-Responsive	198–202
	Template for superparamagnetic iron oxide nanoparticles pH-Responsive	201 and 202
	Polyphosphoester-based responsive DHBC pH-Responsive	203
	Iminoboronate-based dual-responsive micelles pH-Responsive	204
	Mixed polyplex micelles Dual pH-responsive	137
	Multi-responsive hydrogels Glucose and pH-responsive	205

Table 4 (continued)

(Co)polymer structures	Special feature/application	Ref.
	Spectrophotometric determination of fluoride pH-Responsive	206
	Formation of polyion complex vesicles pH-Responsive	207
	Polyelectrolyte–surfactant complexes Solubilisation of hydrophobic compounds (pyrene) pH-Responsive	208 and 209

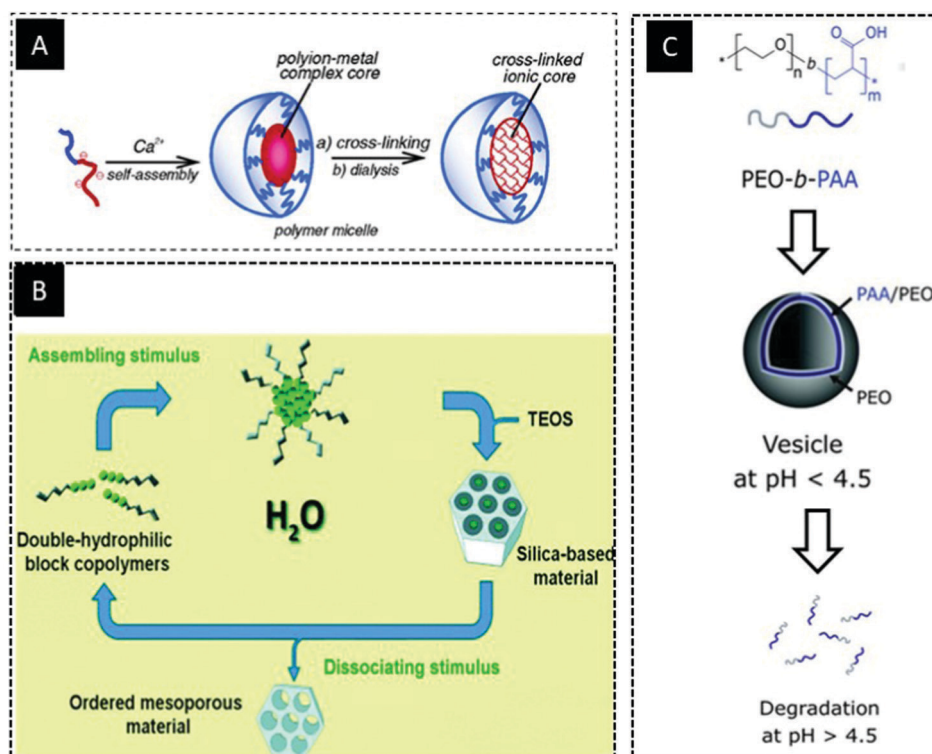


Fig. 10 (A) Polymeric micelle with crosslinked ionic core. Reprinted with permission from ref. 113. Copyright © 2005 American Chemical Society. (B) Schematic formation and degradation of vesicles formed from PEO-*b*-PAA. Adapted with permission from ref. 23. Copyright 2018, Royal Society of Chemistry, and (C) schematic illustration for structuring silica using induced micelles of DHCs. Reprinted with permission from ref. 175. Copyright © 2008 John Wiley & Sons, Inc.

As an example for the attachment of a hydrophilic chromophore to a DHC backbone, we must highlight the work of Boussiron *et al.*²¹⁸ and Gota *et al.*²¹⁹ The former reported

light-responsive core-shell particles were accessed by RAFT polymerisation of acrylic acid with 2-Rose Bengal ethyl acrylate. Self-assembly occurs once the hydrophilic macromolecular

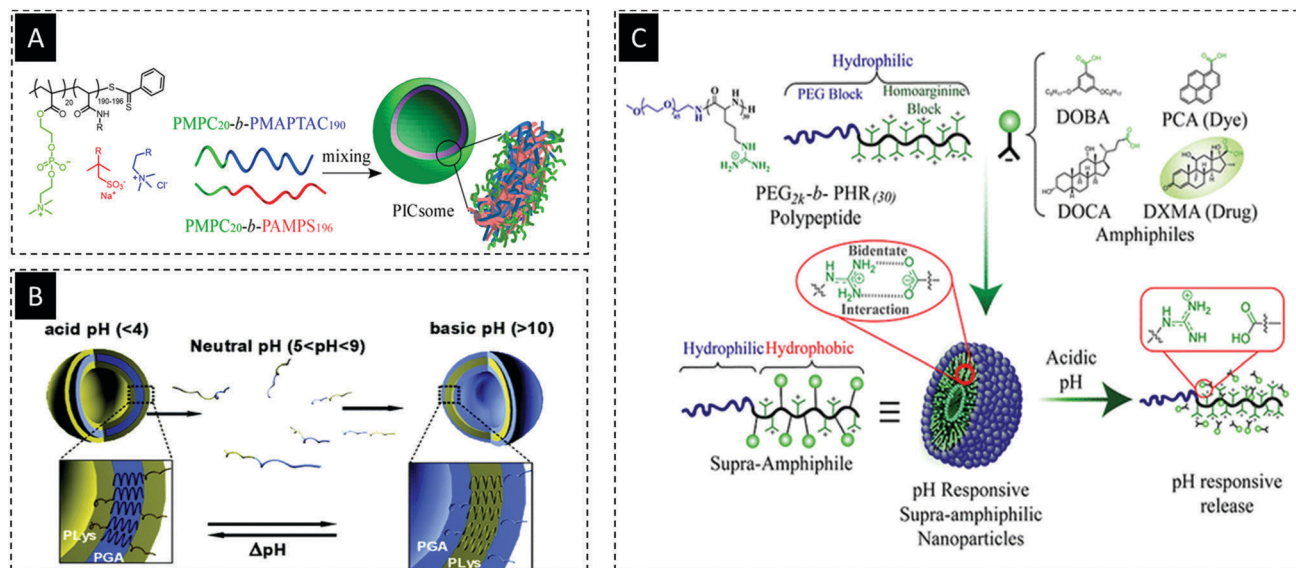


Fig. 11 (A) Schematic illustration of polyion complex vesicle formation from charged diblock copolymers. Adapted with permission from ref. 178. Copyright 2017, Molecular Diversity Preservation International, (B) schematic representation of the self-assembly into vesicles of the diblock copolymer PGA-*b*-PLys.¹⁷⁷ Reprinted with permission from ref. 177. Copyright © 2005 American Chemical Society, and (C) supramolecular self-assembly between double hydrophilic PEG-*b*-poly(L-homoarginine) and carboxylate-containing amphiphiles leading to nanoparticle formation.¹⁸⁵ Reprinted with permission from ref. 185. Copyright © 2019 American Chemical Society.

chain transfer agent is extended with hydrophobic *n*-butyl acrylate leading to PISA. (Fig. 12). This then allowed the preparation of light-responsive polymeric films.

In this direction, Hu *et al.*²²⁰ also reported the fabrication of highly sensitive fluorescent probes for pH value and temperature based on a DHC of NIPAAm and oligo(ethylene glycol) monomethyl ether methacrylate (OEGMA). In this case, both blocks were copolymerised with rhodamine B-ethylene diamine (RhBAM) and fluorescein isothiocyanate (FITC) to prepare P(NIPAAm-*co*-FITC)-*b*-P(OEGMA-*co*-RhBAM). Upon heating, the collapse of the PNIPAAm leads to micelles enabling effective fluorescence resonance energy transfer between the FITC and RhBAM units.

Regarding the aforementioned labelling approach, most DHC examples were prepared by attachment of one or several chromophores to a polymer backbone (Table 5). Notably, even one light-responsive unit can be sufficient to induce significant property changes or to enable tracking of the resulting DHC, allowing the use of these samples as fluorescence probes,²²⁰ labelling reagents for drug delivery,^{221,226,227} in fluorometric techniques,²²⁸ as polymeric pH sensors, chemosensors and biosensors,^{229–231} or as temperature probes.²³² As another interesting case, Romão *et al.*²²¹ labelled poly(*N,N*-dimethyl acrylamide)-*block*-poly(*N,N*-diethyl acrylamide) with rhodamine B and used the resulting DHC to monitor phase separation and interactions in mixed monolayers of dipalmitoyl phosphatidylglycerol.

Stimuli-responsive MHCs

Nowadays, a relatively new trend in stimuli-responsive polymeric materials is the combination of several functional

moieties within one polymer that can respond to different stimuli. As a result, multi-stimuli responsive polymers appeared (response to > 2 triggers), which can be regarded as a starting point for complex sensing or versatile theranostic approaches.¹³⁰ These materials are often synthetically more challenging, but in return offer broad applicability.^{233,234} Ideally, the combination of different and orthogonal stimuli can enhance the degree of precision of a given sensor and in addition changes the conditions necessary for a certain response.¹³⁰

DHCs have also been developed in that direction, with the predominant focus on sensing applications.^{15,229,235,236} We have already presented different examples regarding the synthesis of DHCs, including the introduction of different stimuli-responsive units. Often, also here one building block represents a temperature-responsive polymer segment, and prominent examples are listed in Table 6. Hereby, additional thermo-, pH-, or light-responsive building blocks were introduced. As already mentioned, variation of the pH value can directly influence the LCST of a given system. For instance, Jinag *et al.*²³⁷ reported the preparation of multi-responsive DHCs that combine pH-responsive segments with thermo-responsive poly(*N*-isopropyl acrylamide) (Fig. 13A).

As an example, an ABC triblock terpolymer, poly(2-(diethyl amino)ethyl methacrylate)-*block*-poly(2-(dimethyl amino)ethyl methacrylate)-*block*-poly(*N*-isopropylacrylamide) (PDEA-*b*-PDMA-*b*-PNIPAM) was synthesised by RAFT polymerisation. They reported on “schizophrenic” micellisation in aqueous solution. However, three-layered micelles were also observed.

In another approach to construct multi-responsive DHCs, thermo-responsive blocks can be combined with light-responsive segments. He *et al.*²³⁸ reported on the preparation of nanogels

Table 5 Examples of light-responsive DHCs, showing their structure and potential features and applications. In addition to their light-response the materials are responsive towards: temperature, pH, and metal ions

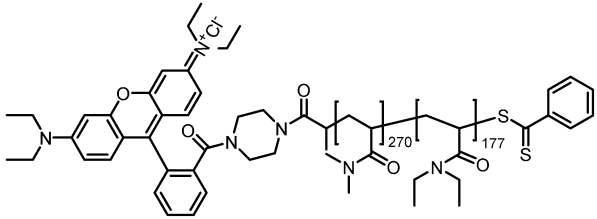
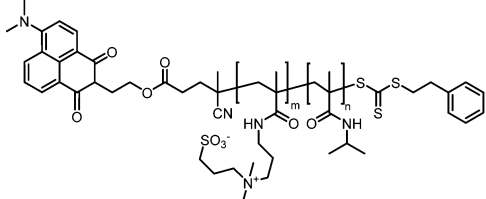
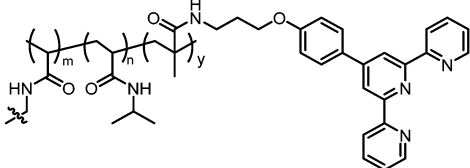
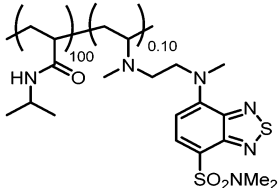
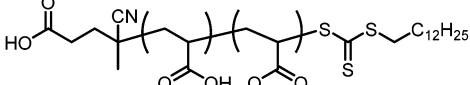
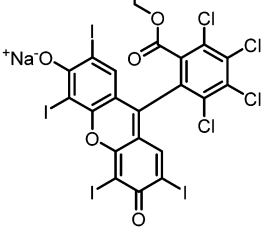
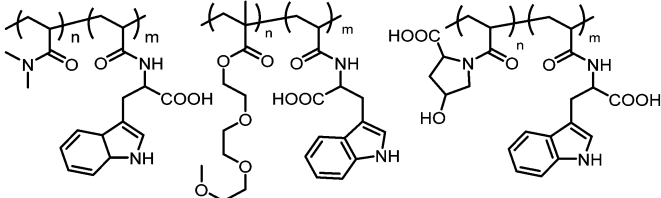
Copolymer	Special feature/application	Ref.
<p>Light-responsive DHCs with chromophores as end-group</p> 	Schizophrenic behaviour Dye end-group Light signal and thermo-responsive	221 and 222
	Dye end-group Light- and thermo-responsive	223
	Multi-responsive microgels Light-, metal ion- and thermo-responsive	164
<p>Light-responsive DHCs with chromophores as separate comonomer</p> 	Temperature-dependent fluorescence lifetime Light- and thermo-responsive	219
	Shell material for photoactive latex particles through polymerisation-induced self-assembly Production of singlet oxygen Light- and pH-Responsive	218
	Probes for ratiometric fluorescent and chiroptical F ⁻ sensors Light-responsive	224
	Sensor for sensitive detection and bioimaging of Zn ²⁺ and Pb ²⁺ Light-, metal ion- and thermo-responsive	225



Fig. 12 Schematic illustration for the synthesis of photoactive latex particles and films.²¹⁸ Reprinted with permission from ref. 218. © 2018 Wiley-VCH Verlag GmbH & Co.

from poly[*N,N*-dimethyl acrylamide-*co*-4-methyl-[7-(methacryloyl)oxyethoxy] coumarin]-*block*-poly[*N*-isopropylacrylamide-*co*-4-methyl-[7-(methacryloyl)oxyethoxy]coumarin] (P(DMA-*co*-CMA)-*b*-P(NIPAM-*co*-CMA)) by RAFT polymerisation (Fig. 13B). In this work, they incorporated coumarin as photo-crosslinkers randomly into the two constituting blocks, after crosslinking, the prepared nanostructures were both light- and temperature-responsive.

In another DHC system reported by Yu *et al.*,²³⁹ a thermo- and pH-responsive block was prepared by the copolymerisation of *N*-hydroxymethyl acrylamide (NHMA) and NIPAAm, which was then grafted with 2-diazo-1,2-naphthoquinone to generate a triple-responsive DHC, albeit the light response was irreversible in this case.

In case of PEG, a non-ionic segment, in combination with another responsive block often enables self-assembly on demand (trigger), whereby PEG grants the overall solubility of the formed nanostructure. As one example, Wei *et al.*²⁴⁰ reported triple hydrophilic block copolymers with dual LCST from PEG-*b*-PNIPAAm-*b*-P(NIPAAm-*co*-HEAAm) by ATRP (Fig. 13C). This led to a two-stage morphological transition, starting from unimers to micelles, and finally to vesicles.

In another interesting example, Banerjee *et al.*²⁴¹ investigated a series of triblock terpolymers from poly(ethylene glycol)-*block*-poly(*N*-isopropyl acrylamide)-*block*-poly(*tert*-butyl acrylate) and poly(ethylene glycol)-*block*-poly(*N*-isopropyl acrylamide)-*block*-poly(glycidyl methacrylate). In addition, different morphological transitions in water could be demonstrated here.

As outlined above, the properties and functions of DHCs can not only be tuned by the choice of the topology but also the smart combination of stimuli-responses. This adds more functionality, and the interplay of different responses gives interesting solution properties, *e.g.*, schizophrenic micellisation, the possibility of crosslinking or different readout signals. Considering these design aspects, certain applications may be targeted, as described in the following section.

Applications

Water-soluble polymers are very attractive materials, and they find applications in various fields from cosmetics, detergents, water treatment, or coatings.^{5,221–225} This is mostly due to favourable interactions with other materials, *e.g.*, complex formation or even stabilising effects to improve solubility.^{48,170,251–254} Examples would be the coating,²⁹ stabilisation,^{12,48} or functionalization of inorganic nanoparticles in aqueous media.^{15,33,249} DHCs play a significant role here, and are employed in drug and gene delivery, as surfactants, or to support crystallisation. Their application has already been addressed in several review articles.^{11,44,49,255} However, during the last twenty years, new applications for DHCs have appeared.^{11,44,49,255} These will be outlined here and discussed for different DHCs in the following sections. First, we will focus on hybrid materials based on DHCs, which currently represent one of the most vibrant areas of nanoscience research. We will also show that DHCs offer intriguing properties for the design of hybrid materials and how additional functionality can be implemented. We will then discuss some of their interesting applications in catalysis and sensing, which address some of the current society demands, *e.g.* the efficient hydrogen production or the sensing of heavy metal ions.^{15,61}

Hybrid materials based on DHCs

Organic–inorganic hybrid materials have been widely utilised – even in industrial applications.^{52,256–258} The integration of both organic and inorganic components into one material is desired to improve the overall features, to tune the physical and chemical properties and obtain additional functionalities in the resulting hybrid materials.²⁵⁷

More specific, hybrid materials based on polymers have attracted great attention, and show outstanding potential to combine different properties in one material and open new windows towards catalysis, sensing, adsorption, separation, gas storage, or optical devices.^{258–261}

DHCs, typically the organic component of such a hybrid material, generally act as templates, stabilisers and matrices for the inorganic building blocks. Multifunctional stimuli-responsive polymers have become an indispensable component of organic–inorganic hybrid materials, and many reviews have addressed both stimuli-responsive polymers^{129,130,227} and hybrid materials.^{52,256–258} Yet, a comprehensive review summarising the current progress in hybrid materials based on stimuli-responsive DHCs is not available. Consequently, this part of the review will elucidate hybrid materials based solely on DHCs as the organic component, focusing on new applications for these hybrid systems.

Commonly, DHCs are used as modifiers, shell coating, templates, stabilisers, embedding environment and synthetic reactors for inorganic materials such as metal ions, noble metal nanoparticles, (semiconducting) metal oxides and silicon oxide nanoparticles. The tunability of DHCs and their functional groups allows almost perfect control over the properties of the hybrid system. This can be observed *e.g.* for control over the size distribution of semiconducting, magnetic, and noble metal NPs.^{12,61}

Table 6 Examples of stimuli-responsive MHCs, being responsive to light, temperature, pH, and metal ions

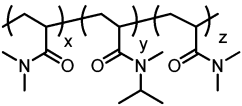
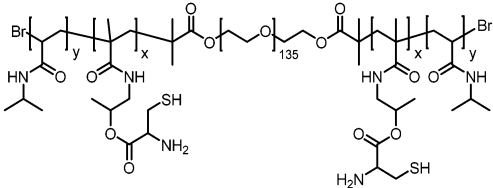
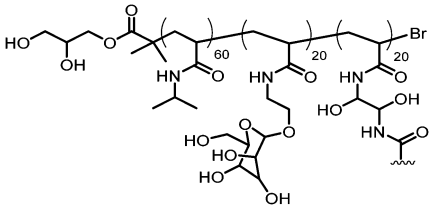
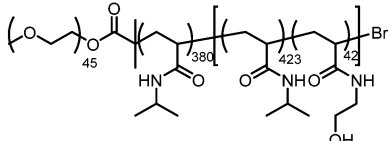
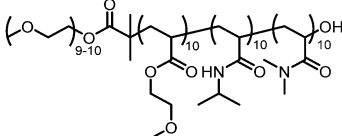
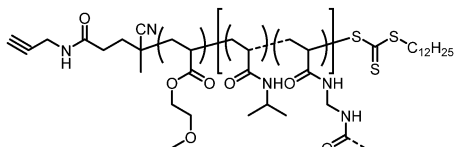
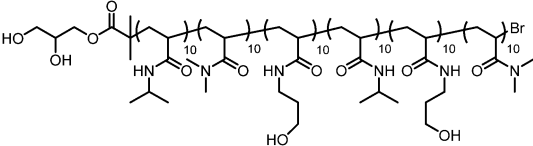
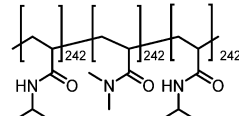
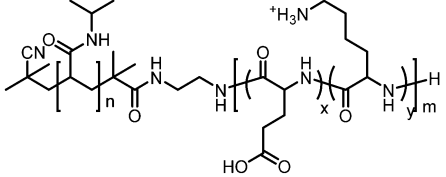
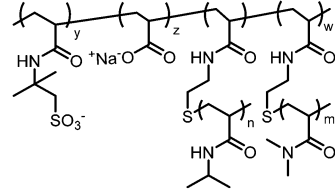
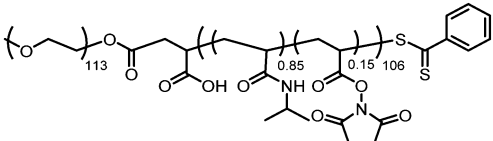
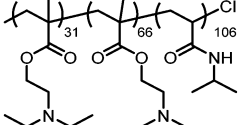
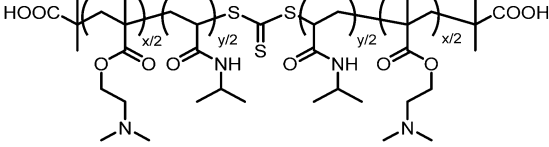
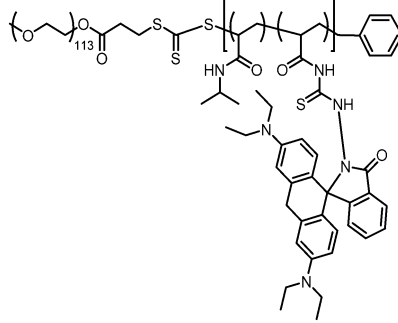
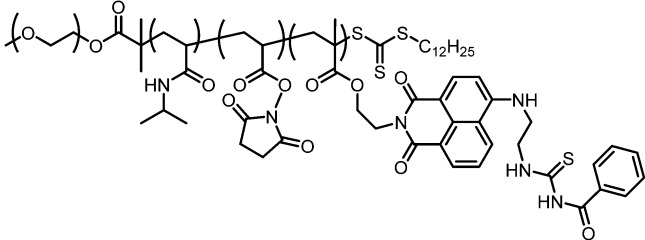
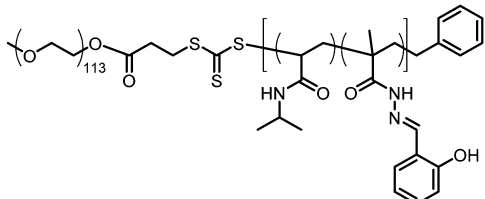
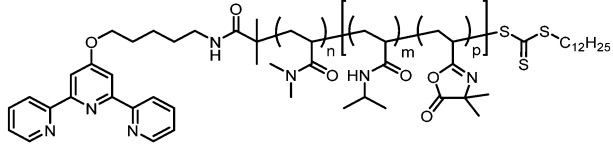
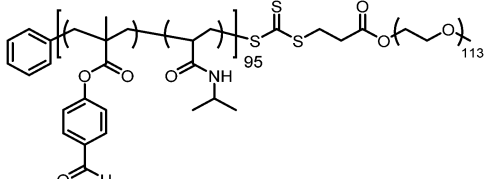
Copolymers	Stimuli-response/feature	Ref.
	Thermo-responsive Statistical, diblock and triblock copolymers Tunable aggregation behavior	242
	Temperature-dependent self-assembly Crosslinking possible Thermo-responsive	243
	Multi-arm star-shaped glycopolymers Sugars as binding sites Thermo-responsive	244
	Triple hydrophilic block copolymer with dual LCST and temperature-induced self-assembly Thermo-responsive	240
	Tunable self-assembly Thermo-responsive	241
	Sono-RAFT polymerisation-induced self-assembly thermo-responsive	245
	Sequence-controlled multi-block copolymerization Dual thermo-responsive	35
	BAB triblock copolymer Tunable aggregation behavior Thermo-responsive	171
	Dual pH- and thermo-responsive	246
	Complexation of a cationic surfactant pH- and thermo-responsive	85

Table 6 (continued)

Copolymers	Stimuli-response/feature	Ref.
	pH- and thermo-responsive	247
	pH- and thermo-responsive	237
	pH- and thermo-responsive	248
	Hg ²⁺ -Reactive probes Light-, metal ion- and thermo-responsive	229
	Ratiometric fluorescent detection of Hg ²⁺ ions Crosslinking possible Light-, metal ion- and thermo-responsive	235
	Fluorescence chemosensor Metal ion and thermo-responsive	249
	Dynamic hydrogel Metal ion- and thermo-responsive	140
	Detection of Hg ²⁺ ions modulated by morphological changes Metal ion- and thermo-responsive	250

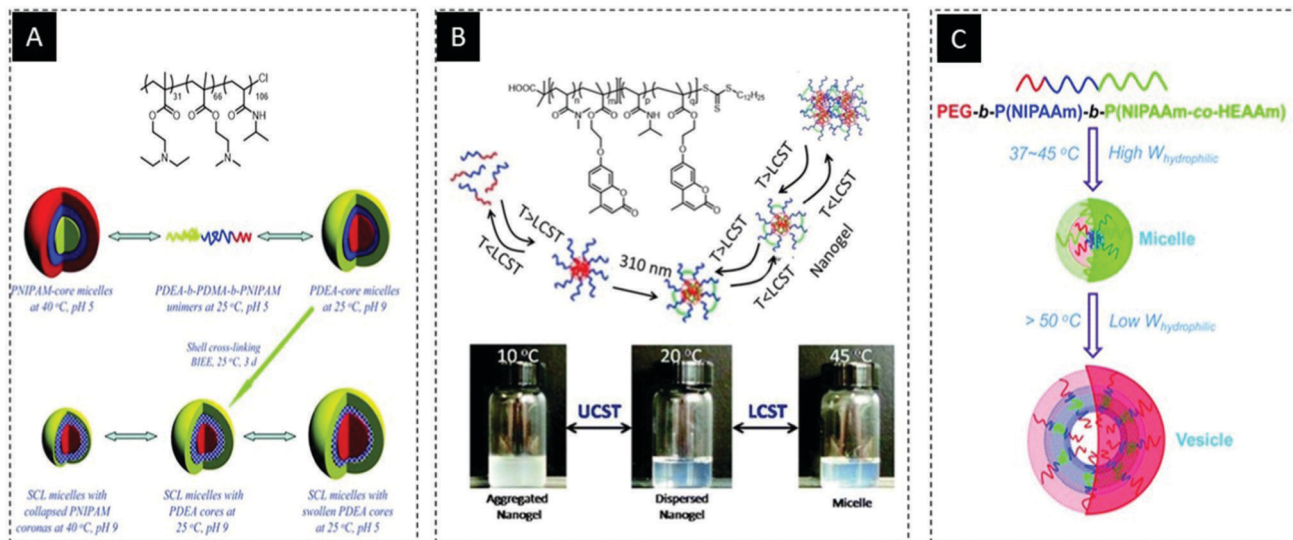


Fig. 13 (A) Schizophrenic micellisation of a PDEA-*b*-PDMA-*b*-PNIPAM triblock terpolymer in aqueous solution.²³⁷ Adapted with permission from ref. 237. Copyright © 2007 American Chemical Society. (B) Schematic illustration of the preparation of both core- and shell-crosslinked nanogel particles and their thermal transitions in aqueous solution.²³⁸ Adapted with permission from ref. 238. Copyright © 2011 American Chemical Society, and (C) schematic illustration of micelles and vesicles formed from PEG-*b*-PNIPAAm-*b*-P(NIPAAm-co-HEAAm) triblock copolymer,²⁴⁰ reprinted from ref. 240 with permission of Royal Society of Chemistry.

DHCs with functional segments bearing ligand groups in each monomer unit enable the interaction with metal ions, inducing the formation of polyion complexes. In that regard carboxylic acids, amino moieties, dopamine, and phosphonic acid were found to be suitable binding sites.^{46,48,61,262} The second block may either be ionic (positively or negatively charged) or non-ionic in nature. These materials exhibit well-defined micellar structures, stabilised by the second, solubility-promoting block.³³ For this, the choice of the DHC composition and architecture determines the strength and type of interaction.

Mostly the interaction of the DHCs and the corresponding component (metal ion, surface or NP) is physically, but also the chemical linkage between the building blocks was observed.^{61,263}

The hybrid materials introduced are either based on metal cations (I), noble metal NPs (II), or semiconducting or metal oxide NPs (III). In addition to the more common physical interactions between components, a covalent approach will be detailed as well (IV). These nanocomposites are high-performing materials, and after elucidating the underlying role of the DHCs and potential uses, we focus on their application in catalysis and sensing.

Chelation of metal cations – concept and applications

Loading micellar structures with metal ions draws great attention because of their ability to use them as reservoirs of inorganic ions in nanoreactors and catalytic reactions such as inorganic polycondensation.^{264–266} Metal ions by themselves often reveal interesting characteristics and may be incorporated in DHC nanocontainers to increase their stability, or to deliver them to a certain target. Here, the complexation of Mn^{2+} , Gd^{2+} and Pt^{2+} is particularly relevant for biomedical applications.

Mn^{2+} has attracted particular attention due to its paramagnetic properties arising from its 5 unpaired electrons and its

high coordination number.^{267,268} Mn^{2+} ions were also introduced to DHC to induce self-assembly and to form magnetic nano-objects by several research groups.²⁶ Notably, complexation of Mn^{2+} ions does not always lead to self-assembly due to the relatively high aqueous solubility of coordinated Mn^{2+} ions. In this context, Shin *et al.*²⁶⁹ reported a more successful system based on poly(ethylene glycol)-*block*-poly(acrylic acid) (PEG-*b*-PAA) for direct conjugation of Mn^{2+} ions inside sterically stabilised polymer assemblies (Fig. 14A). Moreover, PEG-*b*-PAA was end-functionalised with the fluorophore pyrene. Their observation indicates the ability of the hybrid system to form a crosslinked gel-like scaffold with moderate hydrophilicity at the Mn^{2+} ions-chelated interior, allowing efficient water permeation for an enhanced magnetic resonance contrasting effect.

Magnetic Resonance Imaging (MRI) is a valuable medical imaging technique that can be used for imaging and analysis of biological tissue.²⁷⁰ In this technique, gadolinium ions are employed as agents to provide contrast between different tissue types.^{268,271} Immobilisation of Gd-complexes within macromolecules is one way to slow down the rotational motion and provide more efficient relaxation.^{268,271,272} Recently, DHCs were also utilised to immobilise Gd-complexes through the formation of hybrid polymeric NPs. In this area, Frangville *et al.*¹⁹ reported a PEO-*b*-PAA DHBC complexing gadolinium ions (Fig. 14B). The polymeric NPs formed through the chelation of the gadolinium ions by the PAA units are stable against dilution, pH, and ionic strength, and had an average diameter near 20 nm. However, their observations regarding the magnetic properties of Gd ions proposed high magnetic relaxivities and *in vivo* magnetic resonance potential for polymeric NPs.

Cisplatin, a platinum(II)-based anticancer drug, is a well-known metal complex that exhibits high antitumor activity.^{273,274} However, its clinical toxicity can cause major problems.^{274,275}

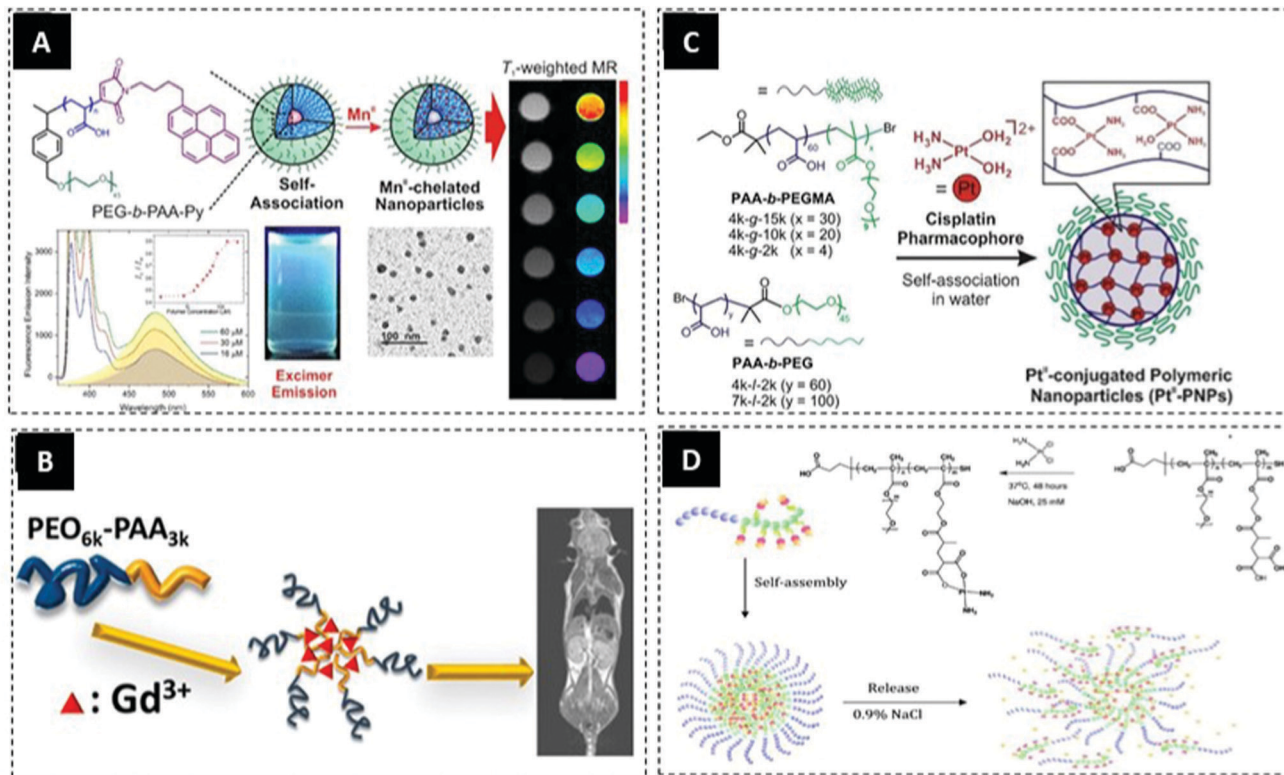


Fig. 14 (A) Construction of paramagnetic manganese-chelated polymeric nanoparticles using a pyrene-end-modified double hydrophilic block copolymer. Reprinted with permission from ref. 269. Copyright © 2019 American Chemical Society.²⁶⁹ (B) Self-assembly of double hydrophilic block copolymers triggered by the presence of gadolinium ions. Reprinted with permission from ref. 19. Copyright © 2016 American Chemical Society.¹⁹ (C) Schematic illustration of the self-assembly process for the formation of Pt^{II}-polymeric NPs. Reprinted with permission from ref. 51. Copyright © 2018 American Chemical Society.⁵¹ and (D) conjugation of Pt drugs and the formation of micelles, and the release of platinum from polymeric platinum micelles. Reprinted with permission from ref. 263. Copyright © 2011 American Chemical Society.²⁶³

To moderate this, many strategies to encapsulate this cytotoxic drug inside versatile delivery pockets such as lipid vesicles and polymeric micelles have been carried out. A straightforward strategy to enhance the delivery efficiency whilst alleviating its toxicity is through encapsulation by DHCs containing a metal-coordinating ligand block. So far, numerous attempts have been made to encapsulate this cytotoxic agent inside different DHC architectures.^{51,263,276,277} For instance, Jeong *et al.*⁵¹ reported a facile regulation strategy for the drug-release of a Pt^{II}-encapsulated delivery system based a PAA block and a solubilising mPEG-grafted poly(methacrylate) segment (poly(PEGMA)) (Fig. 14C). In addition to the relative ratio between the Pt^{II}-binding residues (PAA) and the hydrophilic block (mPEG/PEGMA), their results indicated that the different copolymers exhibited significantly different kinetic regimes for the Pt^{II}-mediated unimer association.

Another interesting DHC system for loading cisplatin was reported by Huynh *et al.* in 2011 (Fig. 14D).²⁶³ They first synthesised a polymerisable monomer to coordinate with the Pt complex (*i.e.*, 1,1-di-*tert*-butyl 3-(2-(methacryloyloxy)ethyl)butane-1,1,3-tricarboxylate) by Michael addition. The obtained monomer was used for block extension of poly[oligo(ethylene glycol)methyl ether methacrylate] (POEGMEMA), a macro-RAFT agent, to form block copolymers carrying bidentate carboxylate

ligands with varying block lengths (Fig. 14B). The length of the core block significantly contributed to micellar size and the overall toxicity of the platinum drug. Their observations for toxicity with A549, a lung cancer cell, indicates that while a shorter PMAETC block led to higher platinum drug loading, it also can provide a better and faster drug release.

Polyelectrolyte-based DHCs were also used to form micellar structures loaded with metal ions.^{264–266} In this context, Schacher *et al.*^{12,26,33} reported different compositions of DHCs based on poly(2-acrylamidoglycolic acid) (PAGA) for chelating metal ions and forming a variety of nanostructures. For instance, in one study they described the chain-extension of a poly(2-iso-propyl-2-oxazoline) macroinitiator with PAGA to obtain poly(2-iso-propyl-2-oxazoline)-*block*-poly(2-acrylamidoglycolic acid) PiPrOx-*b*-PAGA (Fig. 15). Their observations indicate that PiPrOx-*b*-PAGA can encapsulate metal ions due to chelation by the PAGA segment (*i.e.*, Cu²⁺, Co²⁺, or Ni²⁺). Their investigation also revealed that the DHC formed different micellar nanostructures, and their morphology was influenced both by the type of metal ion, as well as the weight fraction of PAGA within the block copolymer. This was also reported for other block copolymer compositions containing PAGA segments such as poly(*N*-acryloylmorpholine)-*block*-PAGA (PNAM-*b*-PAGA) or poly(ethylene oxide)-*block*-PAGA (PEO-*b*-PAGA).²⁶

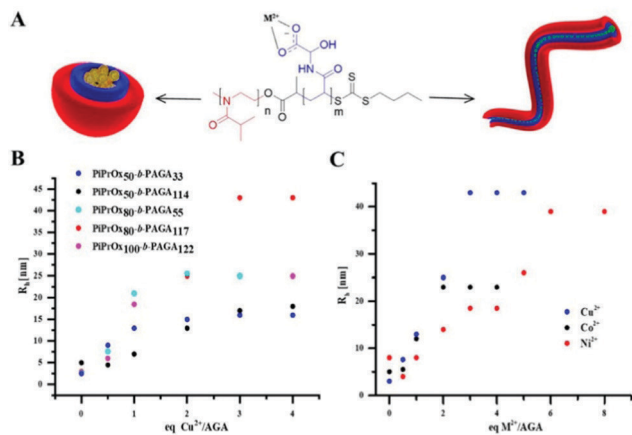


Fig. 15 Schematic depiction of the aggregation of PiPrOx-*b*-PAGA by the addition of metal ions (A), hydrodynamic radii for different PiPrOx-*b*-PAGA (1.0 mg mL⁻¹) block copolymers after the addition of varying amounts of Cu²⁺ (B), and R_h and R_n for the aggregates formed by PiPrOx₈₀-*b*-PAGA₁₁₇ (1.0 mg mL⁻¹) and various metal ions at different ratios (C).³³ Reprinted with permission from ref. 33. Copyright © 2020 American Chemical Society.

Layrac *et al.*²⁶⁵ also reported that a system containing neutral poly(acrylamide) and ionisable poly(vinylphosphonic acid) (PAM-*b*-PVPA) was synthesised by quantitative chain extension of a polyacrylamide macroxanthate with vinylphosphonic acid. They also indicated the formation of micellar structures in the presence of metal ions such as Ni²⁺, Co²⁺, Mn²⁺, Cu²⁺, and Zn²⁺. Similar approaches were also reported for polyion complex micelles by Sanson *et al.*²⁶⁶ In this study, block copolymers are designed based on poly(acrylic acid)-*block*-poly(acrylamide) (PAA-*b*-PAM) or poly(acrylic acid)-*block*-poly(2-hydroxyethylacrylate) (PAA-*b*-PHEA). These DHCs also consist of an ionisable complexing block (PAA, PAM) and a neutral stabilising block (PHEA), and they were mixed with solutions of metal ions such as Al³⁺ and La³⁺.²⁶⁶

Templates for the preparation of noble metal NPs – DHC-assisted complexation and reduction of metal ions

Noble metal NPs, especially Au and Ag, are currently receiving tremendous research interest due to their physicochemical properties, chemical stability, and their wide range of applications.^{278–280} Therefore, it is not surprising that tailor-made DHCs were developed for their synthesis and stabilisation – being advantageous compared to low-molecular weight compounds, especially by granting enhanced stability.²⁸¹ The template-assisted synthesis gives control over the physical and chemical properties of crystals determining their shape and composition. A common strategy to synthesise crystals using DHCs is utilising the polyelectrolyte segment *via* a complexation/reduction approach.^{15,46,158} In this strategy, the DHC acts as a reducing/stabilising agent. For instance, Max *et al.*⁴⁶ introduced a pH-responsive polyampholytic graft copolymer templates as a simple way to control the formation, size, and shape of Au and AgNPs by tuning the overall charge of the DHC. To achieve this, they used poly(dehydroalanine)-*graft*-poly(ethylene glycol) (PDha-*g*-PEG), which is based on a

polyampholytic backbone with varying net charge and charge density depending on pH (Fig. 16A). They indicate that the PDha backbone with both amino and carboxylic acid groups in each repeat unit can selectively interact with [AuCl₄]⁻ and Ag⁺ salts in solution, and this permits a straightforward synthesis of Ag, Au, and AgAu alloy NPs, where the composition of the alloys was even determined by the environmental pH.

Another key example of synthesising noble metal NPs and utilizing them as antimicrobial coating was reported by Falentin-Daudré *et al.*^{282,283} Here, AgNPs were prepared using polyelectrolyte micelles, which were exploited as an antimicrobial coating on stainless steel. This interesting polyelectrolyte micelle was constructed by electrostatic interactions between the polycation based on a DHC from 3,4-dihydroxyphenylalanine (DOPA) and polyanion based (poly(styrene sulfonate), PSS) (Fig. 16B). Their observations indicated that the DOPA units anchor to the stainless steel and form and stabilize biocidal AgNP. In a similar manner, Liu *et al.*²⁸⁴ reported a micellar nanoreactor consisting of poly[(ethylene oxide)-*block*-glycerol monomethacrylate-*block*-2-(diethyl amino)ethyl methacrylate] (PEO-MA-DEA) and poly[(ethylene oxide)-*block*-2-hydroxyethyl methacrylate-*block*-2-(diethylamino)ethyl methacrylate] (PEO-EMA-DEA) triblock terpolymers for the synthesis of AuNPs within the core. In this report, the basic DEA residues in the core of the crosslinked shell micelles were first protonated using HAuCl₄, and then the electrostatically bound AuCl₄⁻ anions were reduced to NPs of elemental gold using NaBH₄ at neutral pH. The gold-loaded crosslinked micellar structures exhibited excellent long-term colloidal stability.

The stability of AuNPs is often limited in various biological environments, that may be improved using DHCs. In this context, Seo *et al.*²⁸¹ reported a highly stable system based on DHCs to stabilize the AuNPs against cyanide etching. They introduced PEO-*b*-PAA as a template to form AuNPs from etching (Fig. 16D). They observed that the stability of the NPs in the solution can be tuned by adjusting the molecular weight of the different copolymer blocks.

Silica nanostructures decorated with metal NP are of interest in the context of catalysis or diagnostics.^{285–288} Especially here, multifunctional DHCs can fulfill several roles, *e.g.* by connecting both towards the SiO₂ and potential noble metal NPs.

As an interesting representative work, Bastakoti *et al.*²⁸⁵ reported a simple approach to synthesise Ag@SiO₂ core-shell NPs using poly[3-(methacryloyl amino)propyl trimethyl ammonium chloride]-*block* poly[2-(dimethyl amino)ethyl methacrylate] (PMAP-TAC-*b*-PDMAEMA) as a structure-directing template (Fig. 16D). However, after synthesising the core-shell hybrid structures, and tuning the size by adjusting the block copolymer length, the Ag@SiO₂ core-shell NPs were used as a nano-catalyst to reduce *p*-nitrophenol. These core-shell hybrids prepared using DHC materials exhibited excellent catalytic properties.

Preparation and stabilisation of semiconducting and metal oxide NPs

Semiconducting and metal oxide NPs are important inorganic compounds found in many applications such as catalysis and

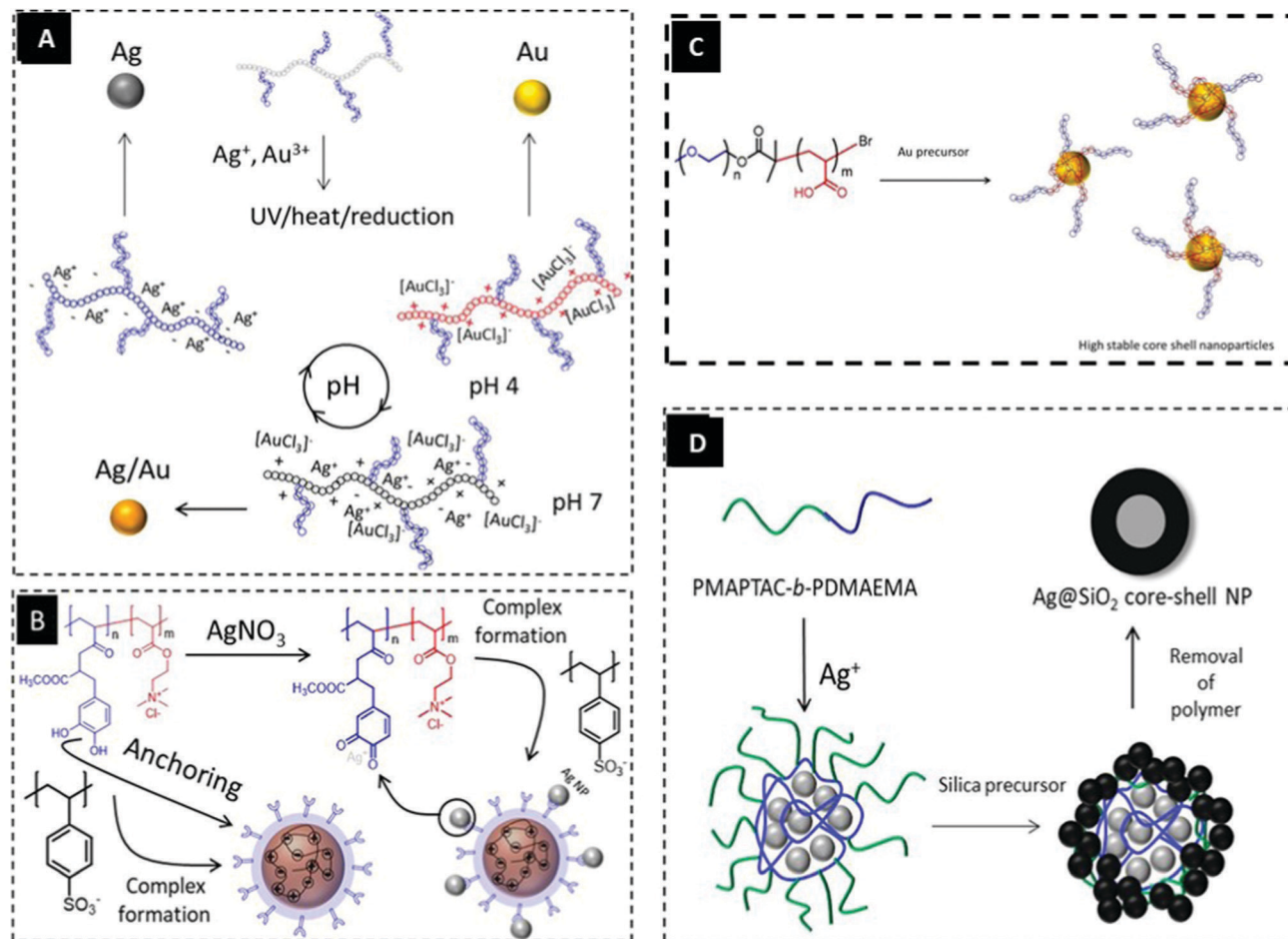


Fig. 16 (A) Preparation of NPs and bimetallic alloys in the presence of PDha-*g*-PEG graft copolymers by the reduction of metal-containing salts using a reducing agent, heat, or UV-light. Adapted with permission from ref. 46. Copyright © 2020 American Chemical Society. (B) Strategy for the formation of positively charged micelles (PSS/P(mDOPA)-*co*-P(DMAEMA⁺)) and positively charged silver-loaded micelles (PSS/P(mDOPA)-*co*-P(DMAEMA⁺)/Ag⁰/AgCl).²⁸² Adopted with permission from ref. 282. Copyright © 2012 American Chemical Society. (C) Schematic representation of AuNP formation via DHBC templates.²⁸¹ Adapted from ref. 281 with permission from Royal Society of Chemistry, and (D) schematic diagram of the synthesis of Ag@SiO₂ core-shell nanoparticles.²⁸⁵ Adapted from ref. 285 with permission from Royal Society of Chemistry.

waste-water treatment.^{289,290} Similarly to the above described metal chelation and noble metal NP preparation, DHCs were designed as suitable nanoreactors and stabilisers.^{12,291–293}

Semiconducting NPs have drawn much interest during the past decades owing to their application in catalysis,^{12,61} sensors,¹⁵ light emitting diodes and transistors.²⁹⁴ They have unique size-dependent chemical and physical properties, which may be tuned by the DHCs.^{60,295–298}

For instance, Cölfen *et al.*⁶⁰ synthesised stable CdS NPs using a poly(ethylene glycol)-*block*-poly(ethylene imine) double hydrophilic BCP. In another case, Nabiyan *et al.*¹² demonstrated the use of a DHC based on poly(2-iso-propyl-2-oxazoline)-*block*-poly(2-acrylamido glycolic acid) (PiPrOx-*b*-PAGA) for the preparation of photocatalytically-active organic/inorganic hybrid micelles.

ZnS, a wide-bandgap semiconductor, is also highly interesting owing to its light-emitting, UV sensing and photocatalytic properties.^{299–301} Furthermore, ZnS is used exhaustively as a capping material for quantum dots based on toxic CdS and

CdSe due to its low toxicity, as these materials are designed for biomedical applications.²⁹⁹ Recently, DHCs were also used to prepare Zn NPs, as shown by Tarasov *et al.*³⁰¹ (Fig. 17A). They exploited poly(acrylic acid)-*block*-polyacrylamide (PAA-*b*-PAM) of various molecular weights for the formation of polyion micelles loaded with precursor hybrid. In this micellar structure, the anionic PAA core was composed of Zn²⁺ ions, while the PAM corona stabilised the core-corona system. Their observation indicated the formation of ZnS NP with a diameter of 3–4 nm. In this respect, their investigation revealed that the size of ZnS NP is weakly dependent on the copolymer block length, while the size distribution correlates with the copolymer asymmetry degree in such a way that a higher $M_{\text{PAM}}/M_{\text{PAA}}$ ratio yields particles with a narrower size distribution.

On the other hand, closely related ZnO is an environmentally friendly and inexpensive luminescent semiconductor, which renders this material very attractive for biological applications. Many studies have been performed to control the size and shape of the ZnO inorganic core and/or to choose the

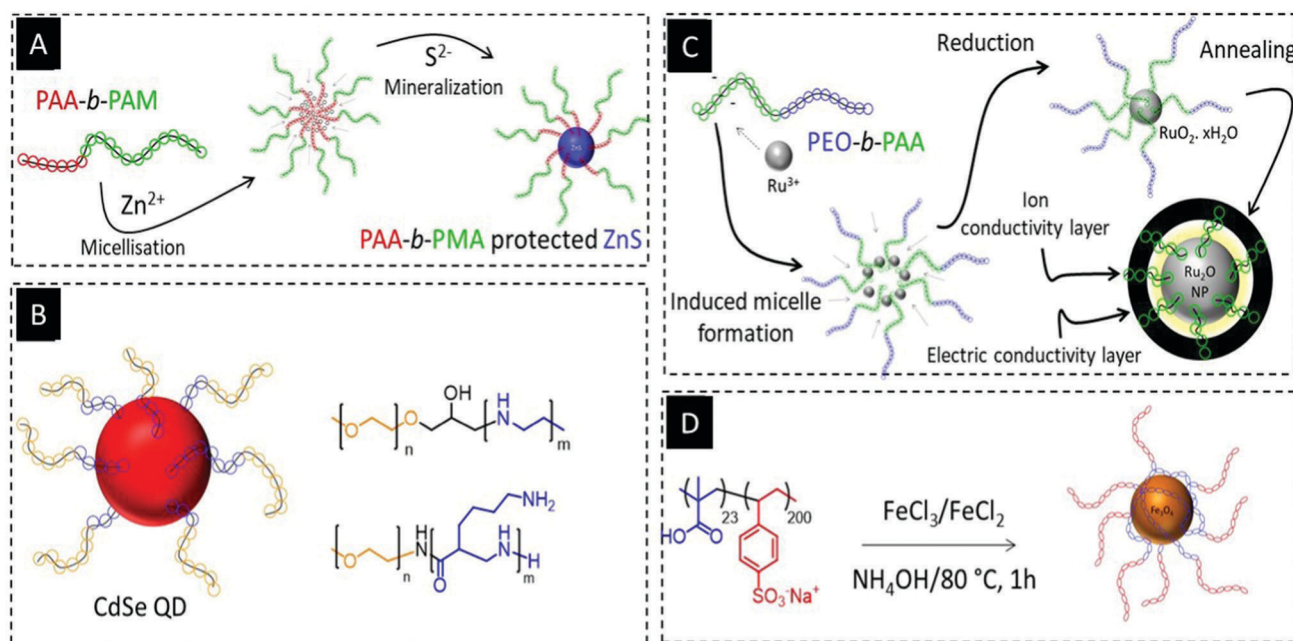


Fig. 17 (A) Scheme showing the formation of ZnS nanoparticles with the use of a copolymer PAA-*b*-PAM.³⁰¹ Adapted from ref. 301 with permission of Royal Society of Chemistry. (B) Scheme of CdSe quantum dots stabilised by a DHBC.³⁰⁸ (C) Schematic illustration of the synthesis of RuO₂ nanoparticles using a double hydrophilic block copolymer as a template.³⁰⁹ Adapted from ref. 309 with permission of Royal Society of Chemistry, and (D) schematic representation of the synthesis of magnetite nanoparticles stabilised with the diblock copolymer PMAA₂₃-*b*-PStSNa₂₀₀, and their occlusion within calcite single crystals.¹⁹⁴ Adapted from ref. 194. with permission of Royal Society of Chemistry.

chemical structure of the stabilising ligand shell.^{302–305} Different families of polymeric ligands with different architectures (branched, block, *etc.*) and compositions have been shown to favour ligand exchange on preformed ZnONPs. As we are focussing on DHCs, we direct you to the work by Zheng *et al.*,³⁰² who introduced low molar mass poly(ethylene glycol)-*block*-poly(acrylic acid) (PEG-*b*-PAA) and poly(ethylene glycol)-*block*-poly(vinylphosphonic acid) (PEG-*b*-PVPA) to form a stable colloidal solution of ZnO NPs in both organic solvents and water. In general, amine and carboxyl groups promote the luminescent properties and ensure good anchoring to the surface of the ZnO NPs.³⁰⁶ However, phosphonic acid groups also demonstrate a high affinity to metal oxide-based NPs.³⁰⁷ Nevertheless, they selected PAA as a first interacting block to promote the replacement of amine ligands present on the surface of ZnO NPs. Their optical observations indicate, that while luminescence remains constant for pristine ZnO NPs, an increase in luminescence is observed for ZnO NPs modified by the two types of polymers. They also discussed the advantages and drawbacks of phosphonic acid groups over carboxylic acid groups.

CdSe semiconductors reveal a tunable band gap between 1.7 eV for the bulk material to 2.4 eV by decreasing the particle size to 2 nm.^{297,308} Therefore, CdSe quantum dots can cover a wide domain of the visible spectrum, which is suitable for applications in sensing and solar cells.^{308,310,311} Notably, for any application employing CdSe quantum dots, it is essential that no cadmium is released to the environment. This is particularly important if applying these quantum dots for cell labelling due to their cytotoxicity. Therefore, such quantum

dots are ideally highly photostable, synthesised directly in water, and protected by ideal capping agents. As an example, Cölfen *et al.*³⁰⁸ reported a DHC consisting of a PEG block and a poly(ethylene imine) segment *via* a straightforward approach to obtain CdSe quantum dots in an aqueous solution with a controllable size (Fig. 17B). They determined that the particle size can be controlled simply by adjusting the polymer concentration during synthesis.

Nowadays, supercapacitors are important in the field of electrochemical energy storage and conversion devices due to their satisfactory performance with respect to secondary batteries and fuel cells.^{312,313} Among the various electrode materials used to fabricate supercapacitors, materials based on ruthenium oxide (RuO₂) are particularly noteworthy. The main reason is that RuO₂ features a high theoretical specific capacitance (1400–2000 F g⁻¹), but high production costs and agglomeration effects currently prevent market usage.^{314–316} However, the relatively low electronic conductivity of hydrous RuO₂·*x*H₂O (89 S cm⁻¹) is still a problem, which prevents the balancing of the electronic and proton conduction channels needed to achieve a high power supercapacitor electrode.³⁰⁹ Furthermore, the high capacitance of RuO₂ remains, with good proton permeation and electronic conduction simultaneously. In order to address these issues, Seo *et al.*³⁰⁹ suggest using a DHC as a nanoreactor, which then also acts as an ionic and electronic conduction layer for ruthenium oxide NPs. In their reports, they used a DHC based on PEO-*b*-PAA to form micellar nanostructures. Upon the addition of the ruthenium precursor, RuCl₃·*x*H₂O, and a reducing agent, RuO₂ NPs were successfully formed within the DHC micelles (Fig. 17C).

NPs with strong magnetic properties may be exploited for a wide range of applications: the magnetic separation of biochemical materials^{289,317} and cells,³¹⁸ magnetic guidance of particle systems for site-specific drug delivery,^{317–320} contrast agents for magnetic resonance imaging (MRI),^{321,322} diagnosis,³²³ or tissue repair.³²⁴ The size and charge of magnetic particles strongly affects their biodistribution.^{319,325} Another crucial point is that the magnetic properties and solution behaviour rely significantly on the surface chemistry of the particles.^{319,326} Indeed, in this context, due to the fact that the bare iron oxide particles are likely to agglomerate, it is necessary to tailor the NP surface chemistry appropriately.

Usually, surface tailoring should establish a high colloidal stability, biocompatibility, and specific bio-recognition of the particle surface.³²⁷ Polymers can play a significant role in stabilising magnetic NPs, and can offer enhanced colloidal stability. For example, in our previous review, we described polyzwitterions as a subclass of polyelectrolytes and their use as coating materials for magnetic particles.³²⁷ Focusing on DHCs, we will also discuss the synthesis of this class of polymer-based hybrid materials and the use of DHCs in stabilising magnetic particles. Graft and block copolymers containing acidic groups were found to be strong ligands, but also catechol (dopamine) moieties can attach to metal oxide surfaces.^{262,328} In 2014, Nguyen *et al.*³²⁹ summarised some conventional DHBCs, that were used as templates to prepare iron oxide NPs. The iron oxide particles were typically prepared by a coprecipitation approach in the presence of the DHBCs. Some examples are highlighted in Table 7, including selected cases reported by Nguyen *et al.*

As an interesting example, Kulak *et al.*¹⁹⁴ report a facile strategy for the crystal growth of Fe₃O₄ with the assistance of a DHBC, poly(sodium 4-styrenesulphonate)-*block*-poly(methacrylic acid) [PNaStS-*b*-PMAA] (Fig. 17D).

Kulak *et al.*¹⁹⁴ they observed that the PMAA acted as the anchoring block and physically adsorbed onto the inorganic NP. Moreover, they noted that the PNaStS units behaved as electrostatic stabilisers, guaranteeing the colloidal stability of the formed nanoparticles in solution. Furthermore, these strong acidic units enhanced the binding ability towards both the NP and the host crystal. In a similar approach, Sondjaja *et al.*^{176,330} also used a double hydrophilic block copolymer, PEO-*b*-PAA, to prepare magnetic NPs. They showed that PEO-*b*-PAA can control the particle growth, as well as act as a stabiliser and clustering agent. They also indicated that the iron-to-polymer ratio can be used to tune the particle size up to 100 nm. Graft copolymers have also been used to prepare and stabilise iron oxide NPs. In one example, Gu *et al.*⁷⁹ synthesised a well-defined densely grafted double hydrophilic copolymer by ATRP, poly[poly(ethylene glycol)methyl ether acrylate]-*graft*-poly(methoxymethyl methacrylate), which was used in the preparation and stabilisation of iron oxide NPs with a narrow size distribution (Fig. 18A).

The nature of the anchoring groups is a crucial parameter for the strong attachment of the polymer to the iron oxide NP surface. Alkoxysilyl, dopamine, and carboxylic groups are

among the most commonly used surface anchoring moieties.³²⁹ However, some restrictions of the mentioned anchoring groups have been described in a review and publications by Boyer and coworkers.^{272,331–333} In this context, while dopamine and carboxylic acid groups form mostly unstable bonds, phosphonates are strong binding groups due to the formation of Fe–O–P bonds.^{331,334–336}

DHCs were also developed for anchoring through the phosphonate functional group. To achieve this, Markiewicz *et al.*³⁰⁷ prepared poly(vinyl phosphonic acid)-based double hydrophilic block copolymers for a one-step *in situ* preparation of water-dispersible iron oxide NPs with well-defined and controllable size and high colloidal stability (Fig. 18B-2).

Poly(ethylene glycol)-*block*-poly(vinylphosphonic acid) block copolymers (PEG-*b*-PVPA, Fig. 18B-1) were obtained using RAFT polymerisation. Hemocompatibility tests demonstrated that the haemolysis rates with phosphonated copolymers were much lower than for their carboxylated analogues. In another key example, Linot *et al.*³⁴⁶ reported a high-density core-shell magnetofluorescent hybrid material. The DHC shell was tailored by varying the composition and architecture of the PEG, PMAA, and (2-methylacryloyl) oxy methyl phosphonic acid (MAPA) units. The ability of DHCs for constructing the hybrid materials provides a great opportunity to construct magnetofluorescent architectures of superparamagnetic iron oxide NPs.³⁴⁶ In a similar approach, Armes *et al.*³⁴⁷ reported the use of poly[2-(methacryloyloxy)ethyl phosphoryl choline]-*block*-(glycerol monomethacrylate) in the synthesis of colloidally stable ultrafine magnetite sols (Fig. 18B-1). In this work, paramagnetic sols were synthesised in the aqueous solution by chemical coprecipitation of ferric and ferrous salts in the presence of the block copolymer. They claim that the sol strategy implemented improves the colloidal stability with respect to long-term storage and pH variation.

Covalent attachment of DHCs on surfaces

The above-described examples mainly describe the physical interactions between the polymer and the inorganic material, *e.g.*, *via* electrostatic attraction. Although this approach is quite straightforward and already leads to highly stable composites, the covalent linking of hydrophilic copolymers by chemical linkage was investigated and will be outlined in this section.

The most common strategy to chemically link the organic and inorganic components in a nanocomposite is through grafting. This can be further divided into “grafting-from”, “grafting-to”, and a one-pot “grafting-through” approach. Here, we focus on recent developments of DHCs within the mentioned categories, highlighting some of these concepts with selected literature reports.

In the “grafting-to” method, as-synthesised polymers are grafted onto the surface through a chemical reaction or a ligand exchange. Polymers used for this purpose must contain one or more functional groups that can be immobilised either directly to the surface or to the original capping ligands on the surface. Double hydrophilic block copolymers were also used for the “grafting-to” approach. In this context, Luo *et al.*³⁴⁸ reported

Table 7 Double hydrophilic block copolymers used for preparation of magnetic iron oxide particles by coprecipitation

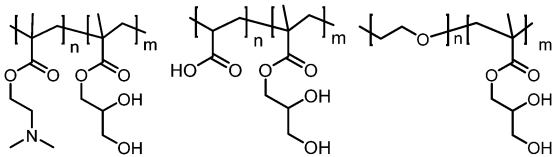
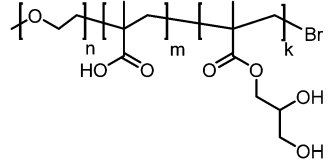
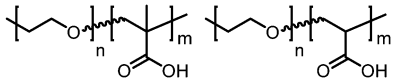
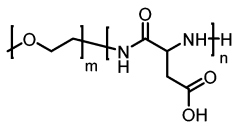
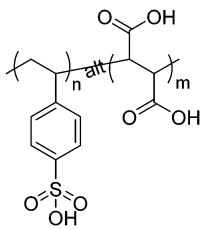
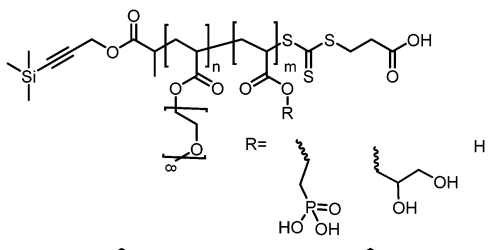
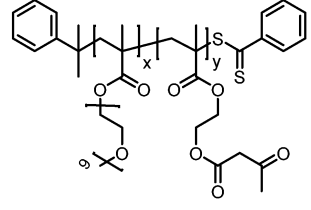
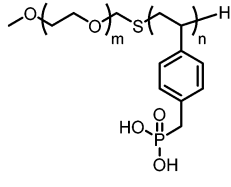
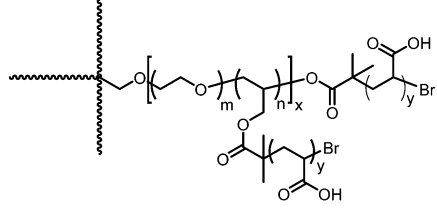
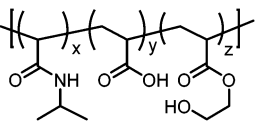
DHC composition	Ref.
	337
	338
	330 and 339
	340
	341
	333
	342
	343
	344

Table 7 (continued)

DHC composition	Ref.
	345

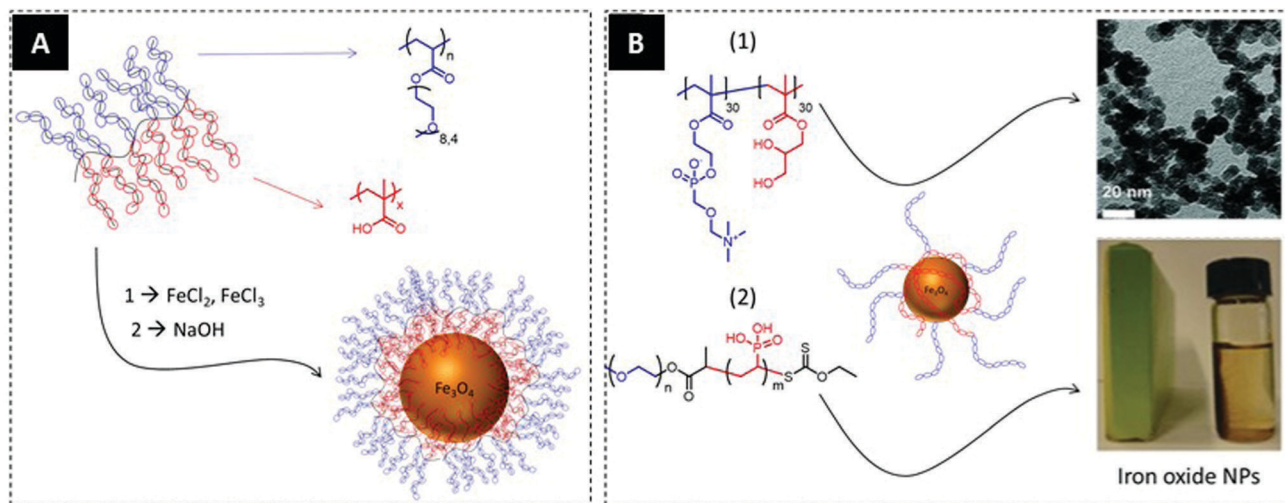


Fig. 18 (A) Superparamagnetic Fe_3O_4 /polymer nanocomposites with PEGMEA-*g*-PMAA densely grafted double hydrophilic copolymers via the grafting-through strategy. Adapted from ref. 79. with permission of Royal Society of Chemistry and (B) (1) poly(vinyl phosphonic acid)-based double hydrophilic block copolymers for the stabilisation of iron oxide nanoparticles. Adapted with permission from ref. 347. Copyright © 2019 American Chemical Society.³⁴⁷ (2) Synthesis of biocompatible poly[2-(methacryloyloxy)ethyl phosphorylcholine]-coated magnetite NPs.³⁰⁷ Adapted from ref. 307 with permission of Royal Society of Chemistry.

the synthesis of a three-layer microstructure with a gold core, poly(2-(dimethyl amino)ethyl methacrylate) (PDMA) inner shell, and poly(ethylene oxide) (PEO) outer corona (Fig. 19A-1). PEO-*b*-PDMA, a double hydrophilic block copolymer, was prepared by RAFT polymerisation and grafted to the AuNPs *via* the thiol end-groups. The inner shell was afterwards crosslinked by 1,2-bis(2-iodoethoxy)ethane and their results indicate that core-shell AuNPs before and after shell crosslinking both exhibit reversible swelling upon varying the solution pH. Compared to the non-crosslinked core-shell AuNPs, the shell crosslinking of the hybrid gold NPs leads to a permanent core-shell nanostructure with increased colloidal stability.

In another example of “grafting-to”, Eckardt *et al.*³⁴⁹ introduced a method to tune the charge of SiO_2 NPs by well-defined poly(2-ethyl-2-oxazoline-*stat*-ethylene imine) P(EtOx-*stat*-EI) (Fig. 19B). In this study, PETox was first polymerised by cationic ring-opening polymerisation before being grafted onto the surface of the SiO_2 NPs by the triethoxysilyl linker. They further introduced positive charges onto the SiO_2 NPs by the acidic hydrolysis of PETox to produce P(EtOx-*stat*-EI).

The “grafting-from” method usually uses surface-initiated controlled/“living” polymerization to grow polymers from the NP surface. The resulting hybrid polymers feature high grafting densities due to the lower steric hindrance and the higher

diffusivity of the initiators/monomers if compared to the polymers. However, to obtain high-quality hybrid polymers, several possible problems need to be solved, including NP stability during polymerisation and crosslinking of the growing polymers. Li *et al.*³⁵⁰ reported a binary thermo-responsive DHC of poly(*N*-isopropylacrylamide) and poly(methoxy-oligo(ethylene glycol)methacrylate) that are grafted from AuNPs through a consecutive ATRP strategy (Fig. 19A-2). They proposed from their observations that the core-shell hybrid NPs are well-defined with cloud points at around 33 and 55 °C in water. They attribute the two cloud points to the inner PNIPAAm homopolymer layer and the outer PMOEGMA-containing copolymer layer, respectively.

In the “grafting-through” approach, usually, the polymerisable groups are anchored onto the surface of the NP. Accordingly, the polymerization can be started in a solution that often contains initiator, monomers, and modified NP. However, the NP can act as a crosslinking agent during polymerization. Hereby, by entering to the propagation stage, the pre-attached polymerisable moiety will be integrated into the growing polymer chains.^{352,353} So far, quite a few examples of the “grafting-through” approach have been reported for NPs such as Fe_3O_4 , silica and gold NPs.^{352,354,355} For example, in the case of silica, Biggs *et al.*³⁵⁵ reported a two-step route to prepare anionic ATRP

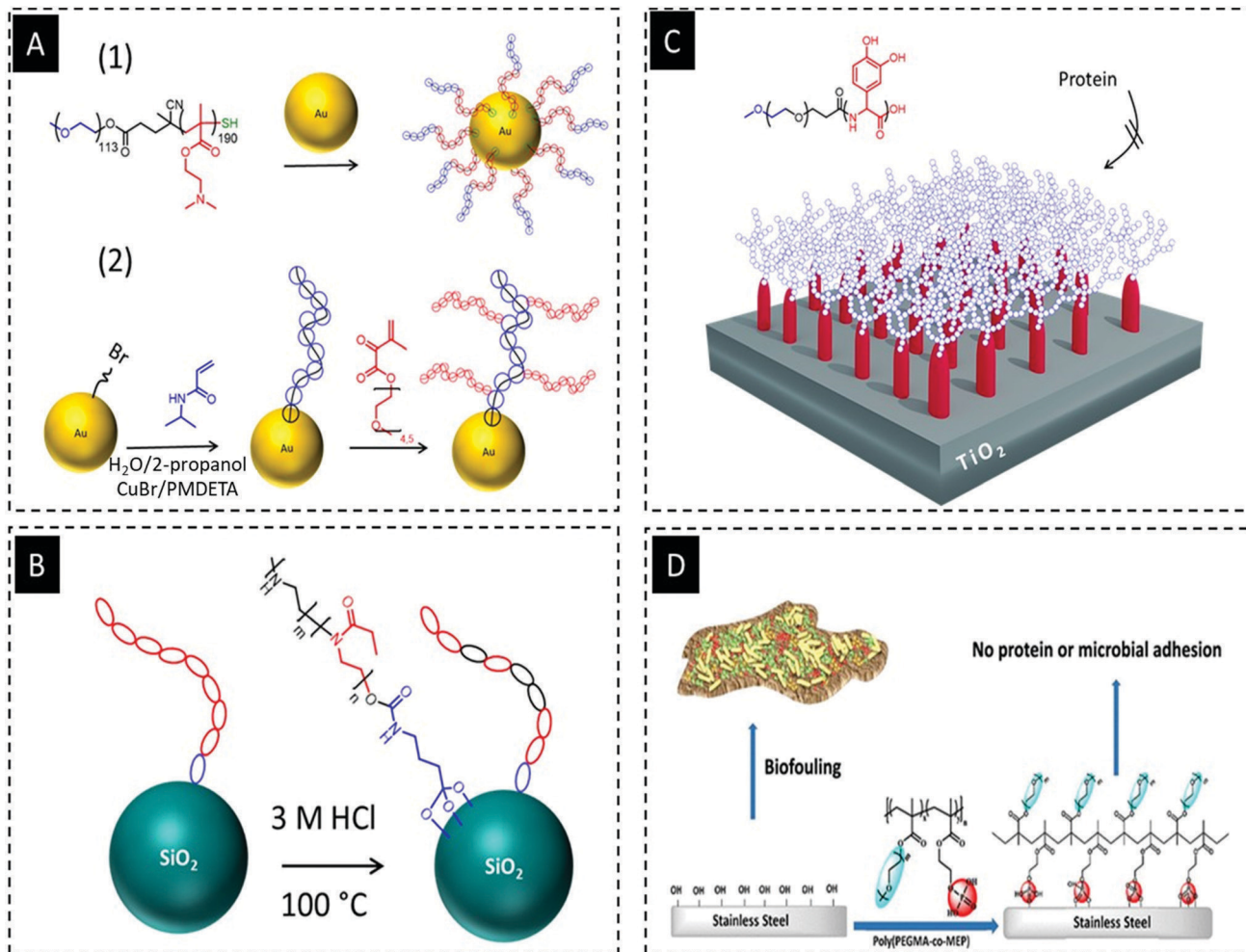


Fig. 19 (A) (1) Synthesis of shell crosslinked core-shell gold nanoparticles with a gold core, a crosslinked PDMA inner shell, and a PEO outer corona.³⁴⁸ Adopted with permission from ref. 348. Copyright © 2005 American Chemical Society. (2) Schematic illustration for the fabrication of Au@copolymer nanostructures.³⁵⁰ (B) SiO₂@P(EtOx-stat-EI) core-shell hybrid NPs and (B) cryo-TEM image of SiO₂@P(EtOx-stat-EI)₂₀ after the *in situ* generation of AuNPs.³⁴⁹ Adopted with permission from ref. 349. Copyright 2015. Wiley-VCH. (C) Chemical structure of the ethylene glycol dendrons covalently coupled to surface-active oligo-catechol anchors.^{262,328} Adopted with permission from ref. 328 and 262. Copyright © 2005 and 2011 American Chemical Society. (D) Schematic illustration of protein-resistant behaviour of poly(ethylene glycol)-containing phosphonate/phosphate units on stainless steel surfaces.³⁵¹ Reprinted with permission from ref. 351. Copyright © 2021 American Chemical Society.

macroinitiators from poly(2-hydroxyethyl methacrylate) precursors. The macroinitiator was electrostatically adsorbed onto ultrafine cationic Ludox CL silica sols. The obtained hybrid was surface polymerised with various hydrophilic monomers in aqueous solution. Their results indicate a range of polymer-grafted ultrafine silica sols.

Beyond core-shell materials based on NPs, modification of rather flat surfaces using polymer coatings can provide and protect functionality, durability, and reliability of a wide range of compounds that have been utilised in corrosion and wear protection, medical implants, drug delivery systems, and biosensors.³²⁸ Compared to other polymers, DHCs exhibit excellent performance within this field. This type of modification also follows the “grafting-from” and “grafting-to” techniques. For instance, Textor *et al.*^{262,328} reported a DHC with dendritic architecture and copolymers based on ethylene glycol and a catechol segment (Fig. 19C). This dendron was molecularly

assembled in an aqueous buffer onto titanium oxide surfaces. In this study, they evaluated the resistance of the monomolecular layers against nonspecific protein adsorption in contact with full blood serum. They also reported the adsorption kinetics and resulting surface coverage.

Stainless steel is utilised in a wide variety of applications from the food industry to medical care. The surface of steel has great potential to adsorb different compounds such as proteins and bacteria, eventually leading to biofouling. One main strategy used to overcome these issues and establish antifouling surfaces is the introduction of polymers.^{356–359}

Among the different polymers examined for this purpose, DHCs showed excellent antifouling effects.^{357,360–362} As one example, Kousar *et al.*³⁵¹ reported a nano-coating for a stainless steel substrate. In this work, they used copolymers based on poly(ethylene glycol) methyl ether methacrylate and 2-(methacryloyloxy)ethyl phosphate (poly(PEGMA-co-MEP)), that was

used also as an antifouling coating for covering steel surface (Fig. 19D). Their observations indicated that the copolymer barrier exhibited a resistance to protein absorption of over 99% compared to a bare surface. In another key report by Giambianco *et al.*,³⁶¹ they compared the protein adsorption on iron oxide NPs (sub-10 nm) and flat substrates functionalised using a grafting-to approach. The polymer coating was constructed of an alternating polymer from poly(ethylene glycol methacrylate-*co*-dimethyl(methacryloyloxy) methyl phosphonic acid) and poly(poly(ethylene glycol) methacrylate-*co*-methacrylic acid) (poly(PEGMA-*co*-MAA)). Here, they achieved different protein resistance values ranging typically from 65 to 99% depending on polymer composition, acid–base conditions, the molecular weight of copolymers, and nature of the grafting agent and layer extension.

Stimuli-responsive copolymers have also been grafted onto various surfaces to form brushes. These smart polymeric surfaces have been used for various applications such as drug delivery systems and antireflection coatings. Kumar *et al.*³⁶³ introduced a general approach to graft stimuli-responsive DHC brushes onto the surface of silicon wafers and quartz glass by ATRP. The polymer brush was obtained by grafting poly(*N,N'*-dimethylacrylamide)-*block*-poly(*N*-isopropylacrylamide) (PDMA-*b*-PNIPAM) onto the surface. They achieved a thermosensitive release of dyes and switched between swollen and collapsed PNIPAM chains. However, this switching was used to control the release kinetics of the entrapped guest molecules such as model dye molecules.

DHCs for catalysis and sensing

The above-described strategies towards DHC-based hybrid materials can be carefully chosen for each individual inorganic compound to determine the resulting properties. Now we want to highlight the transfer of these materials to catalysis and sensing, as two emerging applications. While catalysts often rely on hybrid materials, sensors rely on the function of the polymer itself. Depending on the application, the distribution of the hydrophilic monomer units may be segmented or even random, since sometimes only the effect of both distinct entities in the resulting materials is important. In the case of micellar structures, segmented DHCs are beneficial, while molecular catalysts may also be carried by random or graft copolymers.^{15,364,365}

Catalysis

Catalysis is one of the most important processes in nature. These types of reactions typically occur in aqueous environments. To prevent the deactivation of catalysts in water or protection of the main reaction from unwanted cross-reactions, catalysts are often separately protected by specific compartments. These concepts have inspired the design of a range of synthetic nanoreactors. Polymers with the capability of forming nanoreactors were already introduced as successful and prominent examples,^{366–371} and in this context different advantages were found, including control over-reactivity and composition of active sites, enhanced stability, and defined 3D environments

for catalysis (Fig. 20).^{367,370,371} This development was supported by milestones in controlled/“living” polymerisation techniques, and in the meantime, the self-assembly of (co)polymers was found to be a versatile strategy to prepare a broad range of functional materials in a controlled manner with different ordered structures.³⁷² In that regard, many examples for polymer-supported catalysis have been developed, and their structure and properties have been discussed in multiple reviews.^{366,370–372}

Regarding DHCs, the catalytically active moieties are typically embedded, and the examples can be divided into three categories: (i) incorporation in the DHC as a separate organic segment; (ii) covalent grafting/complexation of metals or organic functional groups to the DHC segments; (iii) catalytically active molecules or NPs were attached to the core or the shell of DHC micellar structures.

We will first highlight some examples where catalytically active moieties were incorporated into DHCs as a separate segment. In this regard, Liu *et al.*³⁷³ first reported DHC micelles containing a catalytic segment that was able to catalyse the hydrolysis of esters. They reported that poly(*N*-isopropylacrylamide)-*block*-poly(*N*-vinyl imidazole) (PNIPAAm-*b*-PVim) was successfully prepared by RAFT polymerisation (Fig. 20A). Herein, the PVim segment was able to catalyse ester hydrolysis and above the phase transition temperature of PNIPAM or in a suitable mixture of methanol/water (cononsolvency), the PNIPAAm block becomes hydrophobic and stable micelles were formed with a dense core consisting of a hydrophobic PNIPAAm block and a polar PVim shell. The catalytic activity of the PNIPAAm-*b*-PVim toward the hydrolysis of *p*-nitrophenyl acetate (NPA) could be tuned by the external temperature or solvent composition.

Micellar structures could become more attractive when they are switchable. Yu *et al.*^{375,376} reported a thermo-responsive block containing azlactone moieties used for the post-polymerisation attachment of an amino-functionalised organocatalyst based on *L*-prolinamide. For this, they synthesised a thermo-responsive DHC based on poly(*N*-isopropylacrylamide-*co*-vinyl-4,4-dimethylazlactone) attached to different blocks such as poly(ethylene glycol), poly(*N,N*-dimethylacrylamide), and poly(2,3-dihydroxypropyl acrylate). They showed by dynamic light scattering that temperature-induced self-assembly of the functionalised block copolymers led to the formation of nanoreactors with the hydrophobic substrates in the core and the immobilised organocatalyst at the hydrophilic/hydrophobic interface. The functionalised DHCs were subjected to an aldol reaction between *p*-nitro benzaldehyde and cyclohexanone in water. Upon temperature-induced aggregation, an increase in conversion was observed. The enantioselectivity of the polymer-bound organocatalyst hereby improved with an increasing hydrophilic/hydrophobic interface as a result of the different stability of the polymer aggregates.

Mimicking enzymes that contain the catalytically active site has always inspired polymer chemists to create functional chains able to “fold” into unimolecular or single-chain polymer nanoparticles. Over the years, many researchers have introduced the catalytic site within a single-chain polymer.³⁷⁷ In this

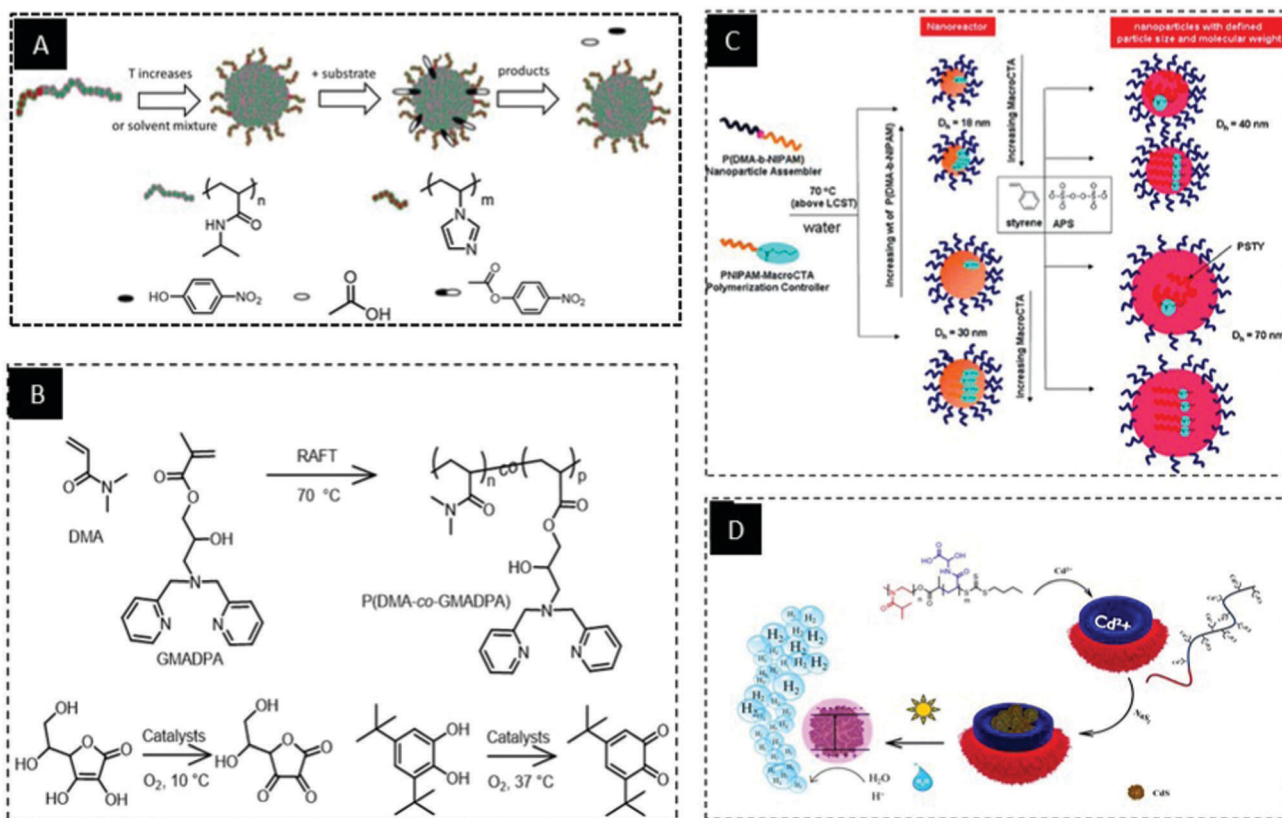


Fig. 20 (A) Schematic illustration of the catalysis mechanism using PNIPAM-*b*-PVim micelles as catalytic nanoreactors.³⁷³ Reprinted from ref. 373. Copyright © 2007, American Chemical Society. (B) Synthesis illustration of P(DMA-co-GMADPA) and the corresponding oxidation reactions used in catalysis.³⁶⁴ (C) Designer thermo-responsive nanoreactors for the templated control radical polymerization of styrene to obtain monodisperse nanoparticles with independent control over particle size and molecular weight.³⁷⁴ Reprinted from ref. 374. Copyright © 2010, American Chemical Society, and (D) photocatalytically-active block copolymer hybrid micelles from PiPrOx-*b*-PAGA.¹² Reprinted with permission from ref. 12, © 2020 Elsevier.

context, the catalytic sites are distributed randomly within a segment or as an entire block, while water-soluble segments stabilise the single chain polymer nanoparticles in aqueous environments.^{366,377} Accordingly, DHCs that contain catalytic sites in a random or ordered fashion within a segment, were reported to enhance the catalytic efficiency.

For example, Thanneeru *et al.*³⁶⁴ reported the use of synthetic polymers to assist Cu-based dioxygen activation. In their work, a series of linear random copolymers of poly(*N,N'*-dimethylacrylamide)-*co*-2-hydroxy-3-(dipicolylamino) propyl methacrylate (P(DMA-*co*-GMADPA)) were introduced to incorporate type-3 Cu sites through Cu-dipicolylamine (DPA) coordination (Fig. 20B). The random copolymers of P(DMA-*co*-GMADPA) were synthesised using RAFT polymerisation and a small library of copolymers with different mole fractions of GMADPA was prepared by varying the feed ratios of DMA and GMADPA monomers. These bioinspired catalytic hybrids were used to enhance the catalytic activity in oxygen activation. For this purpose, the enzyme-like activity of these Cu-based polymers using O₂ for the oxidation of ascorbic acid (AA) and 3,5-di-*tert*-butylcatechol (DTBC) was studied. Their investigation indicates that a 6–8-fold activity enhancement may be reached, compared to the molecular complex of Cu with an identical coordination site.

A single DHC chain can also directly host the organocatalysts, as shown by Moore *et al.*³⁷⁸ for the incorporation of the MacMillan catalyst. This organocatalyst is capable of catalysing a variety of organic reactions such as Diels–Alder reactions,³⁷⁹ 1,3-dipolar cycloadditions,³⁸⁰ and Friedel–Crafts alkylations.³⁸¹ They successfully³⁷⁸ synthesised a monomer containing the MacMillan catalytic functionality and afterwards a variety of copolymers with the comonomer diethylene glycol methyl ether methacrylate (DEGMA) by RAFT polymerisation. These polymers showed lower critical solution temperature (LCST) behaviour where the cloud point was found to be dependent on the degree of catalyst incorporation. The catalytic activity of the functional copolymers was demonstrated by the Diels–Alder reaction between cyclopentadiene and trans-hexen-1-ol and shows enantioselectivity close to those previously reported by MacMillan. Catalytic activity of the copolymers could be demonstrated with high yields and selectivities. Interestingly, a DHC system was also used as a nanoreactor for polymerisation. As a representative example, Sebakhy *et al.*³⁷⁴ successfully polymerised styrene by RAFT using poly(*N*-isopropylacrylamide-*block*-dimethyl acrylamide) as a nanoreactor (Fig. 20C).³⁷⁴

Whereas, the previously discussed DHCs typically rely on the covalent attachment of organic or inorganic catalysts to the

polymers, it is effectively possible to load the catalytic compounds into DHC nanoreactors by co-assembly or encapsulation. The corresponding nanocontainers may even be loaded with more than one catalytic moiety. In this regard, Costabel *et al.*⁴⁸ presented a new self-assembly strategy based on DHCs to activate the fourfold-substituted perylene monoimide (PMI) photosensitisers for visible light-driven hydrogen evolution. They showed that PDha-*g*-PEG can solubilise PMI and $[\text{Mo}_3\text{S}_{13}]^{2-}$ clusters simultaneously, and this solubilization resulted in hybrid materials for enhanced visible light-driven hydrogen evolution reaction (HER).

Metal and metal oxide NPs are already well-known as unique catalytically active materials.³⁸² However, due to their high specific surface area, they commonly need efficient immobilisation and stabilisation while maintaining their catalytic activity.³⁶⁶ Dealing with this issue, DHCs are often used as templates to form and immobilise the catalytically active metal NPs. Here, we will highlight several such examples involving DHCs.

Nabiyan *et al.*¹² prepared photocatalytically active DHCs by immobilising CdS nanoparticles for photocatalytic water splitting within well-defined poly(2-iso-propyl-2-oxazoline)-*block*-poly(2-acrylamido glycolic acid) (PiPrOx-*b*-PAGA) block copolymers (Fig. 20D). A spherical inorganic-organic micellar system was attained containing ultra-small CdS nanoparticles within

the core. These particles maintained their photoactivity, and were applied in photocatalytic H_2 production with an 18-fold increase in H_2 production compared to bare CdS nanoparticles under similar conditions. They attributed this enhancement in photocatalytic activity to several factors: the 3D confinement within the DHC micellar nanostructures, the presence of ultra-small CdS nanoparticles, and the improved stability of the CdS nanoparticles within the micellar core.

In another example, Duan *et al.*³⁸³ reported a nanohybrid catalytic system consisting of ultrafine palladium NPs supported on reduced graphene oxide modified with a thermo-responsive polymer for heterogeneous catalysis. The polymer system was grafted by a catechol-terminated thermo-responsive double-hydrophilic diblock copolymer, poly(poly(ethylene glycol)-methyl ether methacrylate-*co*-2,3-epithiopropyl methacrylate)-*block*-poly(*N*-isopropylacrylamide) (P(PEGMA-*co*-ETMA)-*b*-PNIPAM) using RAFT polymerisation from a catechol-containing chain transfer agent (Fig. 21A).

In this system, the PETMA segments behaved as ligands in the block copolymer, which can interact with the Pd atoms and stabilise the PdNPs in aqueous solution. Besides, the obtained block copolymer can be easily adhered to graphene oxide *via* mussel-inspired chemistry, as a powerful way of surface adhesion. The catalytic activity of the nanohybrid system was

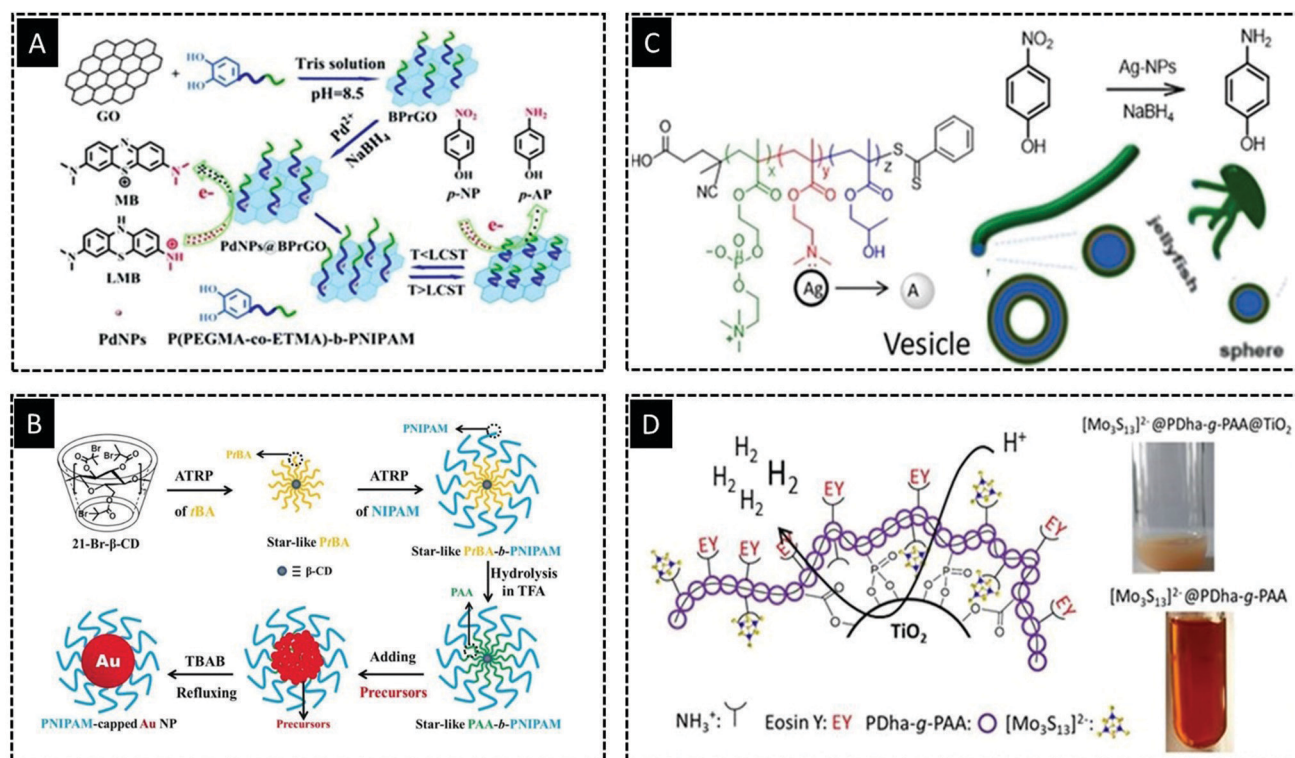


Fig. 21 (A) Schematic depiction of the preparation and catalytic application of the PdNPs@BPrGO nanocatalyst.³⁸³ Reprinted from ref. 383 with permission from Royal Society of Chemistry. (B) *In situ* synthesis and thermo-responsiveness of PNIPAM-capped AuNPs in the absence of free linear PNIPAM chains.⁹⁰ Reprinted with permission from ref. 90. Copyright 2019. Wiley-VCH, (C) structure depiction of PMPC-*b*-PDMA-*b*-PHPMA and corresponding worm, jellyfish, and vesicles that can be directly prepared, depending on either the total solids concentration or the mean degree of polymerisation of the PHPMA block and reduction of *p*-NP to *p*-AP. Adapted with permission from ref. 384. Copyright © 2018 American Chemical Society and (D) schematic illustration of polyampholytic graft copolymer@TiO₂ as matrix for hydrogen production. Adopted with permission from ref. 61. Copyright 2020. Wiley-VCH.

studied in detail using the model reduction reaction of methylene blue (MB) and nitrophenols in the presence of NaBH_4 with high catalytic activity. In a similar approach, Chen *et al.*⁹⁰ reported a hybrid nanoreactor based on star-like thermo-responsive PAA-*b*-PNIPAAm (Fig. 21B). The unimolecular star-like DHCs were used as a nanoreactor to form Au-NPs and the resulting hybrid material was able to tune the optical properties by its thermo-response and the hydrogenation of 4-nitrophenol, a model reaction, was evaluated with respect to the temperature-dependent catalytic activation.

Towards the hybrid nanoreactor, a biomimetic template based on DHCs was also introduced by Sugihara *et al.*³⁸⁴ with a triple-hydrophilic ABC triblock copolymers of poly[2-(methacryloyloxy) ethyl phosphoryl choline]-*block*-poly[2-(dimethyl amino) ethyl methacrylate]-*block*-poly(2-hydroxy propyl methacrylate) (PMPC-*b*-PDMA-*b*-PHPMA) (Fig. 21C). The polymer template was used to embed Ag^+ ions to form Ag-NPs *in situ*. The final morphology could be tuned by the degree of polymerisation of HPMA and the solid concentration in the polymerisation mixture. The resulting Ag-NPs loaded in the assemblies exhibited excellent stability, dispersibility, and catalytic activity for the reduction of *p*-nitrophenol. The order of rate constants for the reduction using Ag-NPs loaded in the assemblies is worms > vesicles > spheres.

Tailored core-shell hybrid NPs have attracted extensive attention as a result of their tunable properties.^{385,386} With a special emphasis on this material class, Nabiyan *et al.*⁶¹ reported a core-shell hybrid system based on polyampholytic graft copolymers to enhance the performance of TiO_2 NPs for hydrogen evolution. Here, they coated the TiO_2 core with a polyampholytic (poly(dehydroalanine)-*graft*-(*n*-propyl phosphonic acid acrylamide) shell (PDha-*g*-PAA@ TiO_2 , Fig. 21D). The multifunctional PDha-*g*-PAA shell facilitates the efficient immobilisation of the negatively charged photosensitiser Eosin Y (EY) and enables electronic interactions between EY, the TiO_2 core, and $[\text{Mo}_3\text{S}_{13}]^{2-}$ clusters as cocatalyst. This is an important example showing how DHCs can be systematically designed and act as versatile matrices to combine various compounds in close proximity.

Sensors

Over the past two decades, also polymeric sensors have received growing attention. In this area, stimuli-responsive (co)polymers that can respond to specific analytes or environmental parameters have found many uses in the development of sensory devices. There are several reviews that highlight polymers as important materials for the construction of sensors with various applications such as the sensing of heavy metals, analysts or environmental conditions.³⁸⁷⁻³⁹⁰

In polymer-based sensing systems, a wide range of stimuli, such as pH, temperature, ionic strength, light, specific analytes or external additives (ions, bioactive molecules, *etc.*), have been exploited, inducing changes in chain conformation, solubility, and the self-assembly of responsive polymers.³⁸⁷

As we outlined above, a tremendous amount of (multi)-stimuli-responsive DHCs have been prepared. Hence, DHC-based

sensors have shown great success, based on the function of the DHC itself. They have been designed mostly in two research directions: (i) the integration of molecules and functional groups with sensing ability directly into the DHC structure; and (ii) the introduction of novel detection mechanisms and concepts into responsive polymer-based sensors, *e.g.*, through hybridisation. Here, we focus on the recent developments in DHC-based sensors, highlighting some of these concepts and mechanisms.

The intrinsic properties of DHCs (such as pH- or temperature-response) can be combined with a fluorescence signal, which emanates from covalently incorporated sensitive fluorescent moieties. In this approach, DHCs can undergo chain collapse or aggregation in an aqueous solution upon changing the pH or temperature, accompanied by changes in chain conformations and the formation of hydrophobic/hydrophilic domains. In the meantime, pH and temperature variations can be converted into considerable changes in fluorescence output intensities by changes in the microenvironment hydrophilicity/hydrophobicity which the respective chromophore experiences.^{30,49}

Thermo-responsive DHCs in aqueous solution commonly generate aggregates with reduced polarity above their LCST temperature, and in combination with fluorescent dyes, the DHCs become promising thermometers. Uchiyama *et al.* reported several DHC systems based on a thermo-responsive polymer and fluorescent comonomers.^{219,228,365,391,392} In a typical example,²²⁸ they copolymerised 4-*N*-(2-acryloyl oxyethyl)-*N*-methylamino-7-(*N,N*-dimethylamino)sulfonyl-2,1,3-benzoxadiazole (DBD-AE) with *N,N*-dimethyl aminopropyl acrylamide (DMAPAM) and *N*-*tert*-butylacrylamide (NTBAM) (poly(DBD-AE-*co*-DMAPAM-*co*-NTBAM)). They observed a dramatic increase in fluorescence emission intensity at temperatures above the LCST (Fig. 22A). They also determined that the thermal phase transition leads to the collapse and aggregation of polymer chains, and this renders the microenvironment of DBD dyes to transform from being hydrophilic to hydrophobic, accompanied by a considerable increase in quantum yields of the covalently embedded DBDAE dyes. Other fluorescent dyes such as rhodamine,^{25,222,229,232,393,394} and Eosin³⁹⁵ were also covalently attached to thermo-responsive units to construct polymer-based thermometers.

Measuring and exploiting variations in pH value is crucial in the diagnosis of different types of cancer.^{128,398} pH sensors based on DHCs have been constructed, using similar principles for temperature sensing. In this respect, pH changes above or below the pK_a resulted in either protonation or deprotonation, which is typically accompanied by a significant variation in aqueous solubility.^{128,399,400}

Sun *et al.*⁴⁰¹ reported the copolymerisation of acrylamide and methylenebis(acrylamide) with a pH-sensitive dye comonomer (a fluoresceinamine derivative) and a pH-insensitive reference dye (a rhodamine B derivative). Their approach by micro-emulsion led to NPs with a mean diameter of 50 nm. These sensors were capable of detecting the pH in the physiologically relevant range from pH 5.8 to 7.2. In another interesting study, Wu *et al.*³⁹⁹ incorporated Calcon dye covalently into a

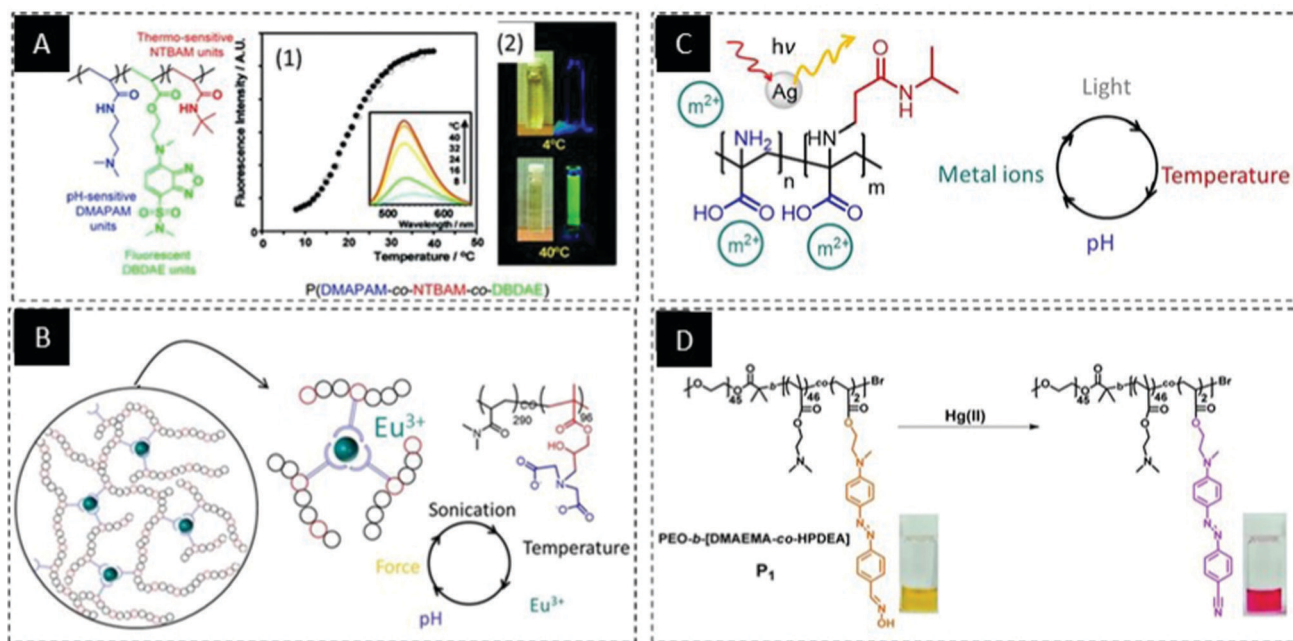


Fig. 22 (A) Thermo-responsive P(DMAPAM-co-NTBAM-co-DBDAE) copolymer in aqueous solution serves as a fluorescent molecular thermometer. (1) Fluorescence intensity changes upon heating and cooling cycles. Inset: Fluorescence spectra. (2) Visual and fluorescent images at temperatures below and above the LCST. Adapted from ref. 228. Copyright © 2004, American Chemical Society. (B) Scheme showing the chemical structures of P(DMA₂₉₀-co-IDHPMA₉₆) and Eu³⁺ ions, and the corresponding illustration of fluorescence ON/OFF and sol-gel transition driven by dynamic metal-ligand coordination.^{169,396} (C) Triple-responsive graft copolymer based on PDha-*g*-NIPAAm,¹⁵ and (D) colorimetric detection of mercury(II) ions via the formation of the strongly electron-withdrawing cyanide groups promoted by mercury(II) ions.³⁹⁷ Reprinted from ref. 397 with permission of Royal Society of Chemistry.

semisoft pH-sensitive polymer matrix microgel of poly(*N*-isopropylacrylamide-co-acrylic acid-co-acrylamide) (P(NIPAM-co-AA-co-AM)) to fabricate nanoparticle-based pH sensors.

Sensors for heavy metal ions (chemosensors) have attracted great interest in recent years because of their environmental and biological relevance. The mechanism of these types of sensors mostly relies on the communication between the supramolecular recognition and fluorescent reporter units. The combination of specific supramolecular recognition with fluorescent systems has allowed the construction of on/off switchable molecular logic gates. In this category, Weng *et al.*^{169,396} reported Eu-containing DHC hydrogels that exhibit fast self-healing and tuneable fluorochromic properties in response to several different stimuli: pH, temperature, metal ions, sonication, moisture and force (Fig. 22B). The DHC hydrogels are constructed using Eu-iminodiacetate (IDA) coordination in a hydrophilic poly(*N,N*-dimethyl acrylamide) matrix. Dynamic metal-ligand coordination allows reversible formation and disruption of hydrogel networks under various stimuli.

In another recent example of sensors for heavy metal ions, polyampholytic graft copolymers have been utilised to construct a detection system with tuneable sensitivity.¹⁵ In this research a metal-chelating and pH-responsive polymer was combined with thermo-responsive monomers and Ag NPs due to their optical properties. Max *et al.*¹⁵ showed that three triggers result in two measurable outputs from polymeric sensors (Fig. 22C). They first designed a multi-responsive

polyampholytic graft copolymer of poly(dehydroalanine)-*graft*-NIPAAm, (PDha-*g*-NIPAAm). They then investigated its response to changes in pH and temperature, as well as the type and concentration of metal cations. The interplay of these responses allowed these changes to be detected by the transformation of external triggers into simple measurable outputs, *e.g.*, the cloud point temperature. In the case of Ag-NP-based hybrid materials, changes in the surface plasmon resonance (SPR) of the encapsulated NPs was also detected as an additional output.

Another notable example is the sensing of mercury(II) ions, which was carried out using an oxime-containing polymeric probe. Kim *et al.*³⁹⁷ reported a DHC of 2-(dimethylamino)ethyl methacrylate (DMAEMA) and (*E*)-2-((4-((4-formylphenyl)diazenyl)phenyl)(methyl-amino)ethyl acrylate (FPDEA), which were copolymerised from a poly(ethylene oxide) (PEO) macro-initiator using ATRP (Fig. 22D). The synthesised DHC detected mercury(II) ions by a temperature-dependent morphological transition between unimers and micellar aggregates.

A key example of sensors based on supramolecular recognition and DHCs, microgels and nanogels were utilised by many research groups to construct detection systems with tuneable sensitivity.^{236,402-406} For instance, Liu *et al.* reported several DHC microgel sensor systems based on NIPAAm.^{236,402-404} In most of the cases, a metal-chelating and fluorescence reporting comonomer was copolymerised with a thermo-responsive monomer such as NIPAAm. Liu *et al.*⁴⁰² in their investigation

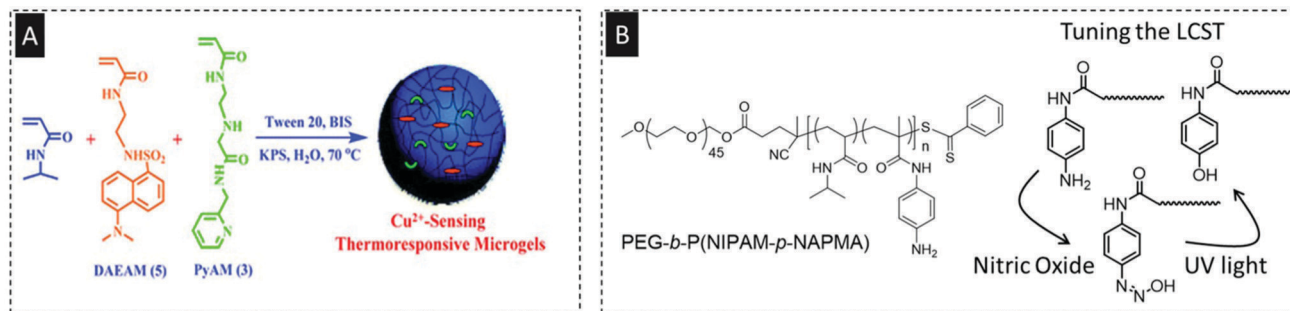


Fig. 23 (A) Synthetic scheme depicting the preparation of Cu^{2+} -sensing P(NIPAM-*co*-PyAM-*co*-DAEAM) microgels. Adapted with permission from ref. 402. Copyright © 2009 American Chemical Society. (B) Schematic representation of the chemical structure transitions of a thermo-responsive PEG-*b*-P(NIPAM-*co*-*p*-NAPMA) diblock copolymer in the presence of NO followed by UV irradiation.⁴⁰⁷

also indicate the microgel system based on dansyl aminoethyl-acrylamide (DAEAM): fluorescence reporter, *N*-(2-(2-oxo-2-(pyridine-2-ylmethylamino)ethylamino)ethyl) acrylamide (PyAM): metal-chelating, and NIPAAm: thermo-responsive monomer (P(NIPAAm-*co*-PyAM-*co*-DAEAM), (Fig. 23A).

They utilised the thermo-responsive collapse/swelling of microgels to construct detection systems with tuneable sensitivity in the detection of Cu^{2+} ions. Their data revealed that the binding of metal ions to metal-chelating units leads to the fluorescence quenching of the fluorescence reporter. However, they also confirmed that the detection sensitivity of P(NIPAAm-*co*-PyAM-*co*-DAEAM) microgels can be dramatically enhanced *via* thermo-induced microgel collapse at elevated temperatures.

Systems that are responsive to endogenous gas transmitter molecules (*i.e.*, nitric oxide, hydrogen sulfide, and carbon monoxide) are becoming an interesting research topic within the sensor community. Here, DHCs are also used for detecting nitric oxide. In the exemplary research by Hu *et al.*,⁴⁰⁷ and for the first time, *N*-(4-aminophenyl) methacryl amide (*p*-NAPMA), which is responsive to nitric oxide, was polymerised with poly(ethylene glycol)-*b*-(*N*-isopropylacrylamide-*co*-*p*-NAPMA) (PEG-*b*-P(NIPAM-*co*-NAPMA)) (Fig. 23B). Indeed, PEG-*b*-P(NIPAM-*co*-*p*-NAPMA) was rendered with unique NO- and UV-responsive characteristics. They also observed a relationship between UV irradiation and the LCST transition.

Conclusions

The field of DHCs has seen huge progress during the last decade, both with respect to synthetic approaches, architectural variety as well as design and application – rendering these materials an important class of water-soluble polymers. As outlined above, DHCs profit from a high tunability considering topology and, with that, the density of functional groups, self-assembly in different environments, solubility, viscosity, and (backbone) conformation. Besides, the combination of different (stimuli-responsive) monomers and their sequence, *e.g.*, block *vs.* random copolymers gives access to truly tailor-made materials. Hereby, modern synthetic tools including end-group functionalization, the use of multi-functional initiators, or

post-polymerization modifications also gave access to multi-hydrophilic copolymers (MHCs).

Self-assembly of DHCs has been thoroughly studied relying both on inter- and intrachain interactions. In this regard, crosslinking of micelles, worms, and nanogels has led to an increased stability in water. In general, micelle formation often is controlled by the response to a suitable external stimulus and novel DHCs might allow the use of several such triggers, leading to programmable materials, *e.g.*, through ‘schizophrenic’ behaviour. We herein described the combination of the most important and frequently used stimuli (pH, temperature, light, or the presence of metal ions), including several examples for triple-responsive polymers. Understanding their structure–property relationship and functions in water enables the DHCs to be exploited in various application fields, one of the most promising being hybrid materials. DHCs mainly act as nanoreactors, nanocarriers, templates, matrices, stabilizers, and dispersants *via* both attractive physical and chemical interactions.

Within this review different hybrid materials have been highlighted and divided into the combination of DHCs with metal ions, NPs, or other surfaces. It is noteworthy that in many cases the individual building blocks might be exchanged and due to this, the number of such examples is expected to grow further. For example, DHCs were exploited for the efficient complexation of metal cations such as Mn^{2+} or Gd^{3+} , leading to the formation of micellar structures. Similar assemblies were also used as templates for the preparation of stable and well-defined noble metal, semiconducting, and magnetic NPs. Moreover, DHCs may be used as coatings for a wide range of surfaces such as stainless steel. It can be said that whereas earlier utilisation of DHCs took place predominantly in biomedicine and biomineralization, the field in our opinion is moving more towards efficient platforms for sensing or the combination/immobilization of different compounds in close proximity, *e.g.*, in (photo)catalysis. Regarding the latter, photocatalytic hydrogen evolution can be seen as a key example, and several cases report on a significant boost of catalytic activity in DHC-based hybrid materials.

In summary, the field of DHCs shows tremendous further potential and room for synthetic innovations. We are quite sure that this will lead to more examples of high-performance

polymeric materials to be applied in interdisciplinary research fields, in so far unexplored organic/inorganic hybrid materials, or sensing and/or separation approaches in water. However, DHCs in our opinion can also build bridges between hydrophilic and hydrophobic materials, thereby promising greener approaches for the transfer of different systems to aqueous media or for the use of surface-active compounds in general. We expect that such materials also have a bright future in terms of heterogeneous catalysis, allowing hierarchical structuring of functional materials and hybrid materials, or assisting in structure formation in general. Likewise, constructing eco-friendly DHCs will undoubtedly continue to be an attractive research topic. In addition, although we described a variety of applications for DHCs, the exploration of them in other areas, such as photonics, energy storage, or solar energy conversion is still in its infancy. We hope that this review will promote the further integration of DHCs in other related disciplines.

Author contributions

A. Nabiyan and J. B. Max equally conceived, researched, wrote, and edited this contribution. All authors jointly wrote the manuscript and discussed the content.

Conflicts of interest

There are no conflicts to declare.

Acknowledgements

This research was supported by the Deutsche Forschungsgemeinschaft (DFG, project no. SCHA1640/18-1) and within the framework of TRR234 ‘‘CataLight’’ (Project No. 364549901, project B5).

Notes and references

- 1 F. S. Bates and G. H. Fredrickson, *Phys. Today*, 1999, **52**(2), 32.
- 2 F. H. Schacher, P. A. Rugar and I. Manners, *Angew. Chem., Int. Ed.*, 2012, **51**, 7898–7921.
- 3 T. Rudolph, M. von der L uhe, M. Hartlieb, S. Norsic, U. S. Schubert, C. Boisson, F. D’Agosto and F. H. Schacher, *ACS Nano*, 2015, **9**, 10085–10098.
- 4 V. G. Kadajji and G. V. Betageri, *Polymers*, 2011, **3**, 1972–2009.
- 5 C. Feng, Z. Shen, Y. Li, L. Gu, Y. Zhang, G. Lu and X. Huang, *J. Polym. Sci., Part A: Polym. Chem.*, 2009, **47**, 1811–1824.
- 6 C. Feng, Y. Li, D. Yang, Y. Li, J. Hu, S. Zhai, G. Lu and X. Huang, *J. Polym. Sci., Part A: Polym. Chem.*, 2010, **48**, 15–23.
- 7 C. Feng, Z. Shen, L. Gu, S. Zhang, L. Li, G. Lu and X. Huang, *J. Polym. Sci., Part A: Polym. Chem.*, 2008, **46**, 5638–5651.
- 8 Z. Ge, Y. Zhou, J. Xu, H. Liu, D. Chen and S. Liu, *J. Am. Chem. Soc.*, 2009, **131**, 1628–1629.
- 9 M. Kamachi, M. Kurihara and J. K. Stille, *Macromolecules*, 1972, **5**, 161–167.
- 10 Z. Ge and S. Liu, *Chem. Soc. Rev.*, 2013, **42**, 7289–7325.
- 11 H. C olfen, *Macromol. Rapid Commun.*, 2001, **22**, 219–252.
- 12 A. Nabiyan, M. Schulz, C. Neumann, B. Dietzek, A. Turchanin and F. H. Schacher, *Eur. Polym. J.*, 2020, **140**, 110037.
- 13 Y. Nakagawa, S. Ohta, M. Nakamura and T. Ito, *RSC Adv.*, 2017, **7**, 55571–55576.
- 14 C. Kilic Bektas, T. Dursun Usal, N. Hasirci and V. Hasirci, *Biol. Soft Matter Fundam. Prop. Appl.*, 2021, 89–114.
- 15 J. B. Max, A. Nabiyan, J. Eichhorn and F. H. Schacher, *Macromol. Rapid Commun.*, 2021, 2000671.
- 16 N. V. Semagina, A. V. Bykov, E. M. Sulman, V. G. Matveeva, S. N. Sidorov, L. V. Dubrovina, P. M. Valetsky, O. I. Kiselyova, A. R. Khokhlov and B. Stein, *J. Mol. Catal. A: Chem.*, 2004, **208**, 273–284.
- 17 S. Lee, K. Saito, H.-R. Lee, M. J. Lee, Y. Shibasaki, Y. Oishi and B.-S. Kim, *Biomacromolecules*, 2012, **13**, 1190–1196.
- 18 N. T. T. Le, T. N. Q. Nguyen, V. Du Cao, D. T. Hoang, V. C. Ngo and T. T. Hoang Thi, *Pharmaceutics*, 2019, **11**, 591.
- 19 C. Frangville, Y. Li, C. Billotey, D. R. Talham, J. Taleb, P. Roux, J.-D. Marty and C. Mingotaud, *Nano Lett.*, 2016, **16**, 4069–4073.
- 20 B. Mahltig, J.-F. Gohy, S. Antoun, R. J er ome and M. Stamm, *Colloid Polym. Sci.*, 2002, **280**, 495–502.
- 21 J. B. Max, P. J. Mons, J. C. Tom and F. H. Schacher, *Macromol. Chem. Phys.*, 2020, **221**, 1900383.
- 22 K. Vijayakrishna, S. K. Jewrajka, A. Ruiz, R. Marcilla, J. A. Pomposo, D. Mecerreyes, D. Taton and Y. Gnanou, *Macromolecules*, 2008, **41**, 6299–6308.
- 23 S. H. R. Shin, P. T. McAninch, I. M. Henderson, A. Gomez, A. C. Greene, E. C. Carnes and W. F. Paxton, *Chem. Commun.*, 2018, **54**, 9043–9046.
- 24 M. Arot ar ena, B. Heise, S. Ishaya and A. Laschewsky, *J. Am. Chem. Soc.*, 2002, **124**, 3787–3793.
- 25 Y. Wu, H. Hu, J. Hu, T. Liu, G. Zhang and S. Liu, *Langmuir*, 2013, **29**, 3711–3720.
- 26 L. Volkmann, M. K ohler, F. H. Sobotta, M. T. Enke, J. C. Brendel and F. H. Schacher, *Macromolecules*, 2018, **51**, 7284–7294.
- 27 Q. Bo and Y. Zhao, *J. Polym. Sci., Part A: Polym. Chem.*, 2006, **44**, 1734–1744.
- 28 E. Seo, J. Kim, Y. Hong, Y. S. Kim, D. Lee and B.-S. Kim, *J. Phys. Chem. C*, 2013, **117**, 11686–11693.
- 29 K. Lipponen, S. T ahk a, M. Kostianen and M. Riekkola, *Electrophoresis*, 2014, **35**, 1106–1113.
- 30 B. V. K. J. Schmidt, *Macromol. Chem. Phys.*, 2018, **219**, 1700494.
- 31 Y. Cai, Y. Tang and S. P. Armes, *Macromolecules*, 2004, **37**, 9728–9737.
- 32 M. Khimani, S. Yusa, V. K. Aswal and P. Bahadur, *J. Mol. Liq.*, 2019, **276**, 47–56.

- 33 A. Nabiyan, P. Biehl and F. H. Schacher, *Macromolecules*, 2020, **53**, 5056–5067.
- 34 S. Khan, J. McCabe, K. Hill and P. A. Beales, *J. Colloid Interface Sci.*, 2020, **562**, 418–428.
- 35 F. Alsubaie, A. Anastasaki, P. Wilson and D. M. Haddleton, *Polym. Chem.*, 2014, **6**, 406–417.
- 36 Y. Tezuka and H. Oike, *J. Am. Chem. Soc.*, 2001, **123**, 11570–11576.
- 37 A. Skandalis and S. Pispas, *J. Polym. Sci., Part A: Polym. Chem.*, 2019, **57**, 1771–1783.
- 38 F. Wurm, J. Nieberle and H. Frey, *Macromolecules*, 2008, **41**, 1184–1188.
- 39 T. Rudolph, S. Crotty, M. Von der Lühe, D. Pretzel, U. S. Schubert and F. H. Schacher, *Polymers*, 2013, **5**, 1081–1101.
- 40 Y. Qiu, W. Zhang, Y. Yan, J. Zhu, Z. Zhang and X. Zhu, *J. Polym. Sci., Part A: Polym. Chem.*, 2010, **48**, 5180–5188.
- 41 Y. Cai and S. P. Armes, *Macromolecules*, 2005, **38**, 271–279.
- 42 Y.-W. Harn, Y. He, Z. Wang, Y. Chen, S. Liang, Z. Li, Q. Li, L. Zhu and Z. Lin, *Macromolecules*, 2020, **53**, 8286–8295.
- 43 F. Sun, C. Feng, H. Liu and X. Huang, *Polym. Chem.*, 2016, **7**, 6973–6979.
- 44 A. Harada and K. Kataoka, *Polym. J.*, 2018, **50**, 95–100.
- 45 Y. Cui, X. Jiang, C. Feng, G. Gu, J. Xu and X. Huang, *Polym. Chem.*, 2016, **7**, 3156–3164.
- 46 J. B. Max, K. Kowalczyk, M. Köhler, C. Neumann, F. Pielenz, L. V. Sigolaeva, D. V. Pergushov, A. Turchanin, F. Langenhorst and F. H. Schacher, *Macromolecules*, 2020, 1900383.
- 47 Z. Ge and S. Liu, *Macromol. Rapid Commun.*, 2009, **30**, 1523–1532.
- 48 D. Costabel, A. Skabeev, A. Nabiyan, Y. Luo, J. Max, A. Rajagopal, D. Kowalczyk, B. Dietzek, M. Wächtler, H. Görls, D. Ziegenbalg, Y. Zagranyski, C. Streb, F. H. Schacher and K. Peneva, *Chem. – Eur. J.*, 2020, 4511–4523.
- 49 A. El Jundi, S. J. Buwalda, Y. Bakkour, X. Garric and B. Nottelet, *Adv. Colloid Interface Sci.*, 2020, 102213.
- 50 M. Khimani, H. Patel, V. Patel, P. Parekh and R. L. Vekariya, *Polym. Bull.*, 2019, 1–28.
- 51 Y.-H. Jeong, H.-W. Shin, J.-Y. Kwon and S.-M. Lee, *ACS Appl. Mater. Interfaces*, 2018, **10**, 23617–23629.
- 52 M. S. Saveleva, K. Eftekhari, A. Abalymov, T. E. L. Douglas, D. Volodkin, B. V. Parakhonskiy and A. G. Skirtach, *Front. Chem.*, 2019, **7**, 179.
- 53 M. J. MacLachlan, I. Manners and G. A. Ozin, *Adv. Mater.*, 2000, **12**, 675–681.
- 54 K. J. C. Van Bommel, A. Friggeri and S. Shinkai, *Angew. Chem., Int. Ed.*, 2003, **42**, 980–999.
- 55 Y. Mai and A. Eisenberg, *Chem. Soc. Rev.*, 2012, **41**, 5969–5985.
- 56 J. C. Brendel and F. H. Schacher, *Chem. – Asian J.*, 2018, **13**, 230–239.
- 57 H. Feng, X. Lu, W. Wang, N.-G. Kang and J. W. Mays, *Polymers*, 2017, **9**, 494.
- 58 J. Xu, Z. Ge, Z. Zhu, S. Luo, H. Liu and S. Liu, *Macromolecules*, 2006, **39**, 8178–8185.
- 59 Z. Ge, Y. Cai, J. Yin, Z. Zhu, J. Rao and S. Liu, *Langmuir*, 2007, **23**, 1114–1122.
- 60 L. Qi, H. Cölfen and M. Antonietti, *Nano Lett.*, 2001, **1**, 61–65.
- 61 A. Nabiyan, J. B. Max, C. Neumann, M. Heiland, A. Turchanin, C. Streb and F. H. Schacher, *Chem. – Eur. J.*, 2021, DOI: 10.1002/chem.202100091.
- 62 C. Li, Z. Ge, J. Fang and S. Liu, *Macromolecules*, 2009, **42**, 2916–2924.
- 63 J. B. Max, D. V. Pergushov, L. V. Sigolaeva and F. H. Schacher, *Polym. Chem.*, 2019, **10**, 3006–3019.
- 64 J. Willersinn, M. Drechsler, M. Antonietti and B. V. K. J. Schmidt, *Macromolecules*, 2016, **49**, 5331–5341.
- 65 J. Willersinn and B. V. K. J. Schmidt, *Polym. Chem.*, 2018, **9**, 1626–1637.
- 66 J. Sarkar, K. B. J. Chan and A. Goto, *Polym. Chem.*, 2021, **12**, 1060–1067.
- 67 W. Zhang, W. Zhang, Z. Cheng, N. Zhou, J. Zhu, Z. Zhang, G. Chen and X. Zhu, *Macromolecules*, 2011, **44**, 3366–3373.
- 68 C. Feng, Y. Li, D. Yang, J. Hu, X. Zhang and X. Huang, *Chem. Soc. Rev.*, 2011, **40**, 1282–1295.
- 69 J. He, W. Zhang, C. Lv, R. Chen, L. Wang, Y. Wang and X. Pan, *Polymer*, 2021, **215**, 123345.
- 70 M. H. Stenzel, C. Barner-Kowollik, T. P. Davis and H. M. Dalton, *Macromol. Biosci.*, 2004, **4**, 445–453.
- 71 L. Zhang, T. L. U. Nguyen, J. Bernard, T. P. Davis, C. Barner-Kowollik and M. H. Stenzel, *Biomacromolecules*, 2007, **8**, 2890–2901.
- 72 W. Wu, W. Wang and J. Li, *Prog. Polym. Sci.*, 2015, **46**, 55–85.
- 73 T. Higashihara, M. Hayashi and A. Hirao, *Prog. Polym. Sci.*, 2011, **36**, 323–375.
- 74 C. Feng, L. Gu, D. Yang, J. Hu, G. Lu and X. Huang, *Polymer*, 2009, **50**, 3990–3996.
- 75 T. Jiang, V. Aseyev, J. Niskanen, S. Hietala, Q. Zhang and H. Tenhu, *Macromolecules*, 2020, **53**, 8267–8275.
- 76 M. Baško and P. Kubisa, *Macromolecules*, 2002, **35**, 8948–8953.
- 77 J. Virtanen, C. Baron and H. Tenhu, *Macromolecules*, 2000, **33**, 336–341.
- 78 J. Virtanen and H. Tenhu, *Macromolecules*, 2000, **33**, 5970–5975.
- 79 L. Gu, Z. Shen, C. Feng, Y. Li, G. Lu, X. Huang, G. Wang and J. Huang, *J. Mater. Chem.*, 2008, **18**, 4332–4340.
- 80 L. Gu, C. Feng, D. Yang, Y. Li, J. Hu, G. Lu and X. Huang, *J. Polym. Sci., Part A: Polym. Chem.*, 2009, **47**, 3142–3153.
- 81 H. Chen, J. Li, Y. Ding, G. Zhang, Q. Zhang and C. Wu, *Macromolecules*, 2005, **38**, 4403–4408.
- 82 D. Zhao, R. Rajan and K. Matsumura, *ACS Appl. Mater. Interfaces*, 2019, **11**, 39459–39469.
- 83 K. Sui, X. Zhao, Z. Wu, Y. Xia, H. Liang and Y. Li, *Langmuir*, 2012, **28**, 153–160.
- 84 J. Hao, G. Yuan, W. He, H. Cheng, C. C. Han and C. Wu, *Macromolecules*, 2010, **43**, 2002–2008.
- 85 A. Daktiloudis, A. Chronaios, N. Mavriki, Z. Iatridi and G. Bokias, *J. Colloid Interface Sci.*, 2014, **430**, 293–301.

- 86 L. Tan, J. Xing, F. Cao, L. Chen, C. Zhang, R. Shi and Y. Wang, *Chinese J. Polym. Sci.*, 2013, **31**, 691–701.
- 87 L. Wang, Z. Li, P. Huang, Z. He and W. Ding, *Colloid Polym. Sci.*, 2018, **296**, 1787–1794.
- 88 A. Fanova, I. Davidovich, Y. Talmon, A. Skandalis, S. Pispas and M. Štěpánek, *ACS Appl. Polym. Mater.*, 2021, 1956–1963.
- 89 A. Taghavi-Kahagh, S. A. Safavi-Mirmahalleh, R. Pashaei-Sarnaghi, M. Salami-Kalajahi and H. Roghani-Mamaqani, *J. Mol. Liq.*, 2021, 116247.
- 90 Y. Chen, Z. Wang, Y. W. Harn, S. Pan, Z. Li, S. Lin, J. Peng, G. Zhang and Z. Lin, *Angew. Chem., Int. Ed.*, 2019, **58**, 11910–11917.
- 91 Y. Nakagawa, Y. Amano, S. Nakasako, S. Ohta and T. Ito, *ACS Biomater. Sci. Eng.*, 2015, **1**, 914–918.
- 92 R. Aksakal, M. Resmini and C. R. Becer, *Polym. Chem.*, 2016, **7**, 171–175.
- 93 S. Sun, S. Xu, W. Zhang, P. Wu, W. Zhang and X. Zhu, *Polym. Chem.*, 2013, **4**, 5800–5809.
- 94 S. Sun, W. Zhang, W. Zhang, P. Wu and X. Zhu, *Soft Matter*, 2012, **8**, 3980–3987.
- 95 S. Sun, P. Wu, W. Zhang, W. Zhang and X. Zhu, *Soft Matter*, 2013, **9**, 1807–1816.
- 96 J. Rao, Y. Zhang, J. Zhang and S. Liu, *Biomacromolecules*, 2008, **9**, 2586–2593.
- 97 Y. Zhang, H. Liu, J. Hu, C. Li and S. Liu, *Macromol. Rapid Commun.*, 2009, **30**, 941–947.
- 98 H. Liu, C. Li, H. Liu and S. Liu, *Langmuir*, 2009, **25**, 4724–4734.
- 99 V. Bütün, S. Liu, J. V. M. Weaver, X. Bories-Azeau, Y. Cai and S. P. Armes, *React. Funct. Polym.*, 2006, **66**, 157–165.
- 100 S. Pispas, N. Hadjichristidis, I. Potemkin and A. Khokhlov, *Macromolecules*, 2000, **33**, 1741–1746.
- 101 S. Pispas, Y. Poulos and N. Hadjichristidis, *Macromolecules*, 1998, **31**, 4177–4181.
- 102 L. Sun, Y. Zhou, X. Zhou, Q. Fu, S. Zhao, X. Tu, X. Zhang, L. Ma, M. Liu and H. Wei, *Polym. Chem.*, 2017, **8**, 500–504.
- 103 O. Koshkina, T. Lang, R. Thiermann, D. Docter, R. H. Stauber, C. Secker, H. Schlaad, S. Weidner, B. Mohr and M. Maskos, *Langmuir*, 2015, **31**, 8873–8881.
- 104 Y. Sun, Y. Jiao, Y. Wang, D. Lu and W. Yang, *Int. J. Pharm.*, 2014, **465**, 112–119.
- 105 H. He, Y. Li, X.-R. Jia, J. Du, X. Ying, W.-L. Lu, J.-N. Lou and Y. Wei, *Biomaterials*, 2011, **32**, 478–487.
- 106 H. Yu, Y. Nie, C. Dohmen, Y. Li and E. Wagner, *Biomacromolecules*, 2011, **12**, 2039–2047.
- 107 S. Pan, C. Wang, X. Zeng, Y. Wen, H. Wu and M. Feng, *Int. J. Pharm.*, 2011, **420**, 206–215.
- 108 S. N. Sidorov, L. M. Bronstein, P. M. Valetsky, J. Hartmann, H. Cölfen, H. Schnablegger and M. Antonietti, *J. Colloid Interface Sci.*, 1999, **212**, 197–211.
- 109 F. M. Haque and S. M. Grayson, *Nat. Chem.*, 2020, **12**, 433–444.
- 110 R. Liénard, J. De Winter and O. Coulembier, *J. Polym. Sci.*, 2020, **58**, 1481–1502.
- 111 J. O. Kim, A. V. Kabanov and T. K. Bronich, *J. Controlled Release*, 2009, **138**, 197–204.
- 112 S. Bontha, A. V. Kabanov and T. K. Bronich, *J. Controlled Release*, 2006, **114**, 163–174.
- 113 T. K. Bronich, P. A. Keifer, L. S. Shlyakhtenko and A. V. Kabanov, *J. Am. Chem. Soc.*, 2005, **127**, 8236–8237.
- 114 J.-B. Qu, R. Chapman, F. Chen, H. Lu and M. H. Stenzel, *ACS Appl. Mater. Interfaces*, 2017, **9**, 13865–13874.
- 115 T. K. Bronich, S. Bontha, L. S. Shlyakhtenko, L. Bromberg, T. Alan Hatton and A. V. Kabanov, *J. Drug Target*, 2006, **14**, 357–366.
- 116 N. J. W. Penfold, J. Yeow, C. Boyer and S. P. Armes, *ACS Macro Lett.*, 2019, **8**, 1029–1054.
- 117 C. Liu, C.-Y. Hong and C.-Y. Pan, *Polym. Chem.*, 2020, **11**, 3673–3689.
- 118 J. He, X. Tong and Y. Zhao, *Macromolecules*, 2009, **42**, 4845–4852.
- 119 M. Mishra, *Handbook of encapsulation and controlled release*, CRC Press, 2015.
- 120 S. Yusa, M. Sugahara, T. Endo and Y. Morishima, *Langmuir*, 2009, **25**, 5258–5265.
- 121 R. Rajan and K. Matsumura, *Macromol. Rapid Commun.*, 2017, **38**, 1700478.
- 122 S. Vinogradov, E. Batrakova and A. Kabanov, *Colloids Surf., B*, 1999, **16**, 291–304.
- 123 C. Ganta, A. Shi, S. K. Battina, M. Pyle, S. Rana, D. H. Hua, M. Tamura and D. Troyer, *J. Nanosci. Nanotechnol.*, 2008, **8**, 2334–2340.
- 124 F. Pinelli, F. Pizzetti, Ó. F. Ortolà, A. Marchetti, A. Rossetti, A. Sacchetti and F. Rossi, *Int. J. Mol. Sci.*, 2020, **21**, 6621.
- 125 F. D. Jochum and P. Theato, *Chem. Soc. Rev.*, 2013, **42**, 7468–7483.
- 126 K. Bauri, M. Nandi and P. De, *Polym. Chem.*, 2018, **9**, 1257–1287.
- 127 L. Johnson, D. M. Gray, E. Niezabitowska and T. O. McDonald, *Nanoscale*, 2021, **13**, 7879–7896.
- 128 L. Hu, Q. Zhang, X. Li and M. J. Serpe, *Mater. Horiz.*, 2019, **6**, 1774–1793.
- 129 M. Wei, Y. Gao, X. Li and M. J. Serpe, *Polym. Chem.*, 2017, **8**, 127–143.
- 130 P. Schattling, F. D. Jochum and P. Theato, *Polym. Chem.*, 2014, **5**, 25–36.
- 131 T. Manouras and M. Vamvakaki, *Polym. Chem.*, 2017, **8**, 74–96.
- 132 H. Che and J. C. M. van Hest, *J. Mater. Chem. B*, 2016, **4**, 4632–4647.
- 133 L. K. Rivera-Tarazona, Z. T. Campbell and T. H. Ware, *Soft Matter*, 2021, **17**, 785–809.
- 134 A. B. Lowe and C. L. McCormick, *Stimuli responsive water-soluble and amphiphilic (co) polymers*, ACS Publications, 2001.
- 135 A. Schmalz, M. Hanisch, H. Schmalz and A. H. E. Müller, *Polymer*, 2010, **51**, 1213–1217.
- 136 Z. A. Jiménez and R. Yoshida, *Macromolecules*, 2015, **48**, 4599–4606.
- 137 R. Kanto, R. Yonenuma, M. Yamamoto, H. Furusawa, S. Yano, M. Haruki and H. Mori, *Langmuir*, 2021, **37**, 3001–3014.

- 138 Z. An, Q. Shi, W. Tang, C.-K. Tsung, C. J. Hawker and G. D. Stucky, *J. Am. Chem. Soc.*, 2007, **129**, 14493–14499.
- 139 T. Li, B. Kumru, N. Al Nakeeb, J. Willersinn and B. V. K. J. Schmidt, *Polymers*, 2018, **10**, 576.
- 140 M. Le Bohec, M. Banère, S. Piogé, S. Pascual, L. Benyahia and L. Fontaine, *Polym. Chem.*, 2016, **7**, 6834–6842.
- 141 L. Mäkinen, D. Varadharajan, H. Tenhu and S. Hietala, *Macromolecules*, 2016, **49**, 986–993.
- 142 H. Yoshimitsu, E. Korchagina, A. Kanazawa, S. Kanaoka, F. M. Winnik and S. Aoshima, *Polym. Chem.*, 2016, **7**, 2062–2068.
- 143 C. M. Papadakis, P. Müller-Buschbaum and A. Laschewsky, *Langmuir*, 2019, **35**, 9660–9676.
- 144 C. M. Schilli, M. Zhang, E. Rizzardo, S. H. Thang, Y. K. Chong, K. Edwards, G. Karlsson and A. H. E. Müller, *Macromolecules*, 2004, **37**, 7861–7866.
- 145 W. Zhang, L. Shi, K. Wu and Y. An, *Macromolecules*, 2005, **38**, 5743–5747.
- 146 R. Hoogenboom, *Angew. Chem., Int. Ed.*, 2009, **48**, 7978–7994.
- 147 R. Hoogenboom and H. Schlaad, *Polym. Chem.*, 2017, **8**, 24–40.
- 148 R. Takahashi, X.-P. Qiu, N. Xue, T. Sato, K. Terao and F. M. Winnik, *Macromolecules*, 2014, **47**, 6900–6910.
- 149 G. Delecourt, L. Plet, V. Bennevault and P. Guégan, *ACS Appl. Polym. Mater.*, 2020, **2**, 2696–2705.
- 150 J. E. Sayed, C. Lorthioir, P. Perrin and N. Sanson, *Soft Matter*, 2019, **15**, 963–972.
- 151 A. Alexander, J. Khan, S. Saraf and S. Saraf, *Eur. J. Pharm. Biopharm.*, 2014, **88**, 575–585.
- 152 N. Morimoto, R. Obeid, S. Yamane, F. M. Winnik and K. Akiyoshi, *Soft Matter*, 2009, **5**, 1597–1600.
- 153 P. De, S. R. Gondi and B. S. Sumerlin, *Biomacromolecules*, 2008, **9**, 1064–1070.
- 154 A. J. Convertine, B. S. Lokitz, Y. Vasileva, L. J. Myrick, C. W. Scales, A. B. Lowe and C. L. McCormick, *Macromolecules*, 2006, **39**, 1724–1730.
- 155 Y. Maki, H. Mori and T. Endo, *Macromol. Chem. Phys.*, 2010, **211**, 45–56.
- 156 C. Zhao, X. Zhuang, C. He, X. Chen and X. Jing, *Macromol. Rapid Commun.*, 2008, **29**, 1810–1816.
- 157 J. Rao, Z. Luo, Z. Ge, H. Liu and S. Liu, *Biomacromolecules*, 2007, **8**, 3871–3878.
- 158 Y. Zhou, K. Jiang, Y. Chen and S. Liu, *J. Polym. Sci., Part A: Polym. Chem.*, 2008, **46**, 6518–6531.
- 159 A. E. Smith, X. Xu, S. E. Kirkland-York, D. A. Savin and C. L. McCormick, *Macromolecules*, 2010, **43**, 1210–1217.
- 160 W. Pan, H. Chen, G. Wen, D. Giaouzi, S. Pispas and J. Zuo, *J. Phys. Chem. C*, 2020, **124**, 17150–17157.
- 161 X. Zhang, J. Li, W. Li and A. Zhang, *Biomacromolecules*, 2007, **8**, 3557–3567.
- 162 R. P. Johnson, Y. Il Jeong, J. V. John, C.-W. Chung, D. H. Kang, M. Selvaraj, H. Suh and I. Kim, *Biomacromolecules*, 2013, **14**, 1434–1443.
- 163 M. Nuopponen and H. Tenhu, *Langmuir*, 2007, **23**, 5352–5357.
- 164 J. Lee, E. J. Choi, I. Varga, P. M. Claesson, S.-H. Yun and C. Song, *Polym. Chem.*, 2018, **9**, 1032–1039.
- 165 J. Shen, C. Chen, W. Fu, L. Shi and Z. Li, *Langmuir*, 2013, **29**, 6271–6278.
- 166 A. Viswanath, Y. Shen, A. N. Green, R. Tan, A. B. Greytak and B. C. Benicewicz, *Macromolecules*, 2014, **47**, 8137–8144.
- 167 G. Kocak, C. Tuncer and V. Bütün, *Polym. Chem.*, 2017, **8**, 144–176.
- 168 J. R. C. Costa, C. Correia, J. R. Gois, S. M. C. Silva, F. E. Antunes, J. Moniz, A. C. Serra and J. F. J. Coelho, *Prog. Org. Coat.*, 2017, **104**, 34–42.
- 169 G. Weng, S. Thanneeru and J. He, *Adv. Mater.*, 2018, **30**, 1706526.
- 170 H. Sai, A. Erbas, A. Dannenhoffer, D. Huang, A. Weingarten, E. Siismets, K. Jang, K. Qu, L. C. Palmer and M. O. De La Cruz, *J. Mater. Chem. A*, 2020, **8**, 158–168.
- 171 K. Skrabania, W. Li and A. Laschewsky, *Macromol. Chem. Phys.*, 2008, **209**, 1389–1403.
- 172 N. S. Vishnevetskaya, V. Hildebrand, B.-J. Niebuur, I. Grillo, S. K. Filippov, A. Laschewsky, P. Müller-Buschbaum and C. M. Papadakis, *Macromolecules*, 2017, **50**, 3985–3999.
- 173 Y. Li, Y.-K. Gong, K. Nakashima and Y. Murata, *Langmuir*, 2002, **18**, 6727–6729.
- 174 W. Tjandra, J. Yao, P. Ravi, K. C. Tam and A. Alamsjah, *Chem. Mater.*, 2005, **17**, 4865–4872.
- 175 N. Baccile, J. Reboul, B. Blanc, B. Coq, P. Lacroix-Desmazes, M. In and C. Gérardin, *Angew. Chem.*, 2008, **120**, 8561–8565.
- 176 H. R. Sondjaja, T. A. Hatton and K. C. Tam, *Langmuir*, 2008, **24**, 8501–8506.
- 177 J. Rodríguez-Hernández and S. Lecommandoux, *J. Am. Chem. Soc.*, 2005, **127**, 2026–2027.
- 178 K. Nakai, K. Ishihara, M. Kappl, S. Fujii, Y. Nakamura and S. Yusa, *Polymers*, 2017, **9**, 49.
- 179 R. P. Johnson, S. Uthaman, J. V. John, H. R. Lee, S. J. Lee, H. Park, I.-K. Park, H. Suh and I. Kim, *ACS Appl. Mater. Interfaces*, 2015, **7**, 21770–21779.
- 180 H. Huang, J. Li, L. Liao, J. Li, L. Wu, C. Dong, P. Lai and D. Liu, *Eur. Polym. J.*, 2012, **48**, 696–704.
- 181 W. Agut, A. Brület, D. Taton and S. Lecommandoux, *Langmuir*, 2007, **23**, 11526–11533.
- 182 A. Kishimura, S. Liamsuwan, H. Matsuda, W.-F. Dong, K. Osada, Y. Yamasaki and K. Kataoka, *Soft Matter*, 2009, **5**, 529–532.
- 183 S. Katayose and K. Kataoka, *Bioconjugate Chem.*, 1997, **8**, 702–707.
- 184 M. Yokoyama, M. Miyauchi, N. Yamada, T. Okano, Y. Sakurai, K. Kataoka and S. Inoue, *Cancer Res.*, 1990, **50**, 1693–1700.
- 185 K. Praveen, S. Das, V. Dhaware, B. Pandey, B. Mondal and S. Sen Gupta, *ACS Appl. Bio Mater.*, 2019, **2**, 4162–4172.
- 186 J. Reboul, T. Nugay, N. Anik, H. Cottet, V. Ponsinet, M. In, P. Lacroix-Desmazes and C. Gérardin, *Soft Matter*, 2011, **7**, 5836–5846.
- 187 P. Han, N. Ma, H. Ren, H. Xu, Z. Li, Z. Wang and X. Zhang, *Langmuir*, 2010, **26**, 14414–14418.
- 188 Y. Wang, P. Han, H. Xu, Z. Wang, X. Zhang and A. V. Kabanov, *Langmuir*, 2010, **26**, 709–715.

- 189 G. Mountrichas and S. Pispas, *Macromolecules*, 2006, **39**, 4767–4774.
- 190 G. A. Ferreira, L. Piculell and W. Loh, *Macromolecules*, 2018, **51**, 9915–9924.
- 191 Z. Xue, E. Foster, Y. Wang, S. Nayak, V. Cheng, V. W. Ngo, K. D. Pennell, C. W. Bielawski and K. P. Johnston, *Energy Fuels*, 2014, **28**, 3655–3665.
- 192 A. N. Kulak, R. Grimes, Y.-Y. Kim, M. Semsarilar, C. Anduix-Canto, O. Cespedes, S. P. Armes and F. C. Meldrum, *Chem. Mater.*, 2016, **28**, 7528–7536.
- 193 T. Kakui and H. Kamiya, *Energy Fuels*, 2004, **18**, 652–658.
- 194 A. N. Kulak, M. Semsarilar, Y.-Y. Kim, J. Ihli, L. A. Fielding, O. Cespedes, S. P. Armes and F. C. Meldrum, *Chem. Sci.*, 2014, **5**, 738–743.
- 195 X. Liu, X. Sheng, Q. Yao, L. Zhao, Z. Xu and Y. Zhou, *Energy Fuels*, 2021, 6136–6143.
- 196 X. Chang, Z. Cheng, B. Ren, R. Dong, J. Peng, S. Fu and Z. Tong, *Soft Matter*, 2015, **11**, 7494–7501.
- 197 Y. Han, L. Xia, L. Zhu, S. Zhang, Z. Li and Y. Wang, *Langmuir*, 2012, **28**, 15134–15140.
- 198 L. Zhao, R. Ma, J. Li, Y. Li, Y. An and L. Shi, *Biomacromolecules*, 2008, **9**, 2601–2608.
- 199 L. Zhao, X. Wang, Y. Li, R. Ma, Y. An and L. Shi, *Macromolecules*, 2009, **42**, 6253–6260.
- 200 L. Zhao, A. Li, R. Xiang, L. Shen and L. Shi, *Langmuir*, 2013, **29**, 8936–8943.
- 201 N. Rocha, J. Mendes, L. Durães, H. Maleki, A. Portugal, C. F. G. C. Geraldes, A. Serra and J. Coelho, *J. Mater. Chem. B*, 2014, **2**, 1565–1575.
- 202 N. Rocha, D. P. Rodrigues, A. Gaspar, L. Durães, A. C. Serra and J. F. J. Coelho, *RSC Adv.*, 2014, **4**, 24428–24432.
- 203 X. Liu, P. Ni, J. He and M. Zhang, *Macromolecules*, 2010, **43**, 4771–4781.
- 204 R. Ma, C. Zhang, Y. Liu, C. Li, Y. Xu, B. Li, Y. Zhang, Y. An and L. Shi, *RSC Adv.*, 2017, **7**, 21328–21335.
- 205 R. Guo, Q. Su, J. Zhang, A. Dong, C. Lin and J. Zhang, *Biomacromolecules*, 2017, **18**, 1356–1364.
- 206 J. Hu, M. R. Whittaker, T. P. Davis and J. F. Quinn, *ACS Macro Lett.*, 2015, **4**, 236–241.
- 207 Y. Ohara, K. Nakai, S. Ahmed, K. Matsumura, K. Ishihara and S. Yusa, *Langmuir*, 2018, **35**, 1249–1256.
- 208 M. Stepanek, P. Matejicek, K. Procházka, S. K. Filippov, B. Angelov, M. Slouf, G. Mountrichas and S. Pispas, *Langmuir*, 2011, **27**, 5275–5281.
- 209 G. Mountrichas and S. Pispas, *J. Polym. Sci., Part A: Polym. Chem.*, 2007, **45**, 5790–5799.
- 210 J. Schumers, C. Fustin and J. Gohy, *Macromol. Rapid Commun.*, 2010, **31**, 1588–1607.
- 211 Y. Zhao, *J. Mater. Chem.*, 2009, **19**, 4887–4895.
- 212 Y. Zhao, *Macromolecules*, 2012, **45**, 3647–3657.
- 213 F. D. Jochum and P. Theato, *Chem. Commun.*, 2010, **46**, 6717–6719.
- 214 Y. Wang, N. Ma, Z. Wang and X. Zhang, *Angew. Chem., Int. Ed.*, 2007, **46**, 2823–2826.
- 215 O. Grimm, S. C. Maßmann and F. H. Schacher, *Polym. Chem.*, 2019, **10**, 2674–2685.
- 216 F. Ercole, T. P. Davis and R. A. Evans, *Polym. Chem.*, 2010, **1**, 37–54.
- 217 A. Ben-Miled, A. Nabiyan, K. Wondraczek, F. H. Schacher and L. Wondraczek, *Polymers*, 2021, **13**, 1633.
- 218 C. Boussiron, M. Le Behec, L. Petrizza, J. Sabalot, S. Lacombe and M. Save, *Macromol. Rapid Commun.*, 2019, **40**, 1800329.
- 219 C. Gota, S. Uchiyama, T. Yoshihara, S. Tobita and T. Ohwada, *J. Phys. Chem. B*, 2008, **112**, 2829–2836.
- 220 J. Hu, X. Zhang, D. Wang, X. Hu, T. Liu, G. Zhang and S. Liu, *J. Mater. Chem.*, 2011, **21**, 19030–19038.
- 221 R. I. S. Romao, Q. Ferreira, J. Morgado, J. M. G. Martinho and A. M. P. S. Goncalves da Silva, *Langmuir*, 2010, **26**, 17165–17177.
- 222 R. I. S. Romao, M. Beija, M.-T. Charreyre, J. P. S. Farinha, A. M. P. S. Goncalves da Silva and J. M. G. Martinho, *Langmuir*, 2010, **26**, 1807–1815.
- 223 L. P. Kreuzer, T. Widmann, N. Aldosari, L. Bießmann, G. Mangiapia, V. Hildebrand, A. Laschewsky, C. M. Papadakis and P. Müller-Buschbaum, *Macromolecules*, 2020, **53**, 9108–9121.
- 224 H. Mori, E. Takahashi, A. Ishizuki and K. Nakabayashi, *Macromolecules*, 2013, **46**, 6451–6465.
- 225 G. Wei, G. Zhao, N. Lin, S. Guang and H. Xu, *Org. Electron.*, 2020, **82**, 105711.
- 226 S. Ganta, H. Devalapally, A. Shahiwala and M. Amiji, *J. Controlled Release*, 2008, **126**, 187–204.
- 227 A. Klaikherd, C. Nagamani and S. Thayumanavan, *J. Am. Chem. Soc.*, 2009, **131**, 4830–4838.
- 228 S. Uchiyama, N. Kawai, A. P. de Silva and K. Iwai, *J. Am. Chem. Soc.*, 2004, **126**, 3032–3033.
- 229 J. Hu, C. Li and S. Liu, *Langmuir*, 2010, **26**, 724–729.
- 230 T. Liu and S. Liu, *Anal. Chem.*, 2011, **83**, 2775–2785.
- 231 H. N. Kim, Z. Guo, W. Zhu, J. Yoon and H. Tian, *Chem. Soc. Rev.*, 2011, **40**, 79–93.
- 232 K. Zhou, Y. Wang, X. Huang, K. Luby-Phelps, B. D. Sumer and J. Gao, *Angew. Chem., Int. Ed.*, 2011, **50**, 6109–6114.
- 233 S. Guragain, B. P. Bastakoti, V. Malgras, K. Nakashima and Y. Yamauchi, *Chem. – Eur. J.*, 2015, **21**, 13164–13174.
- 234 J. Zhuang, M. R. Gordon, J. Ventura, L. Li and S. Thayumanavan, *Chem. Soc. Rev.*, 2013, **42**, 7421–7435.
- 235 X. Wan, T. Liu and S. Liu, *Langmuir*, 2011, **27**, 4082–4090.
- 236 C. Li and S. Liu, *J. Mater. Chem.*, 2010, **20**, 10716–10723.
- 237 X. Jiang, Z. Ge, J. Xu, H. Liu and S. Liu, *Biomacromolecules*, 2007, **8**, 3184–3192.
- 238 J. He, B. Yan, L. Tremblay and Y. Zhao, *Langmuir*, 2011, **27**, 436–444.
- 239 Y. Yu, F. Tian, C. Wei and C. Wang, *J. Polym. Sci., Part A: Polym. Chem.*, 2009, **47**, 2763–2773.
- 240 H. Wei, S. Perrier, S. Dehn, R. Ravarian and F. Dehghani, *Soft Matter*, 2012, **8**, 9526–9528.
- 241 R. Banerjee and D. Dhara, *Langmuir*, 2014, **30**, 4137–4146.
- 242 J. Li, S. Mizutani, S. Sato, A. Narumi, O. Haba, S. Kawaguchi, M. Kikuchi, T. Kakuchi and X. Shen, *Polym. Chem.*, 2020, **11**, 2346–2359.

- 243 M. Najafi, M. Habibi, R. Fokkink, W. E. Hennink and T. Vermonden, *Soft Matter*, 2021, **17**, 2132–2141.
- 244 A. Monaco, V. P. Beyer, R. Napier and C. R. Becer, *Biomacromolecules*, 2020, **21**, 3736–3744.
- 245 S. Piogé, T. N. Tran, T. G. McKenzie, S. Pascual, M. Ashokkumar, L. Fontaine and G. Qiao, *Macromolecules*, 2018, **51**, 8862–8869.
- 246 J. Li, T. Wang, D. Wu, X. Zhang, J. Yan, S. Du, Y. Guo, J. Wang and A. Zhang, *Biomacromolecules*, 2008, **9**, 2670–2676.
- 247 J. Zhang, X. Jiang, Y. Zhang, Y. Li and S. Liu, *Macromolecules*, 2007, **40**, 9125–9132.
- 248 G. Yang, Z. Yang, C. Mu, X. Fan, W. Tian and Q. Wang, *Polym. Chem.*, 2015, **6**, 3382–3386.
- 249 J. Han, B. An, Y. Wang, X. Bao, L. Ni, C. Li, L. Wang and X. Xie, *Sens. Actuators, B*, 2017, **250**, 436–445.
- 250 L. Wang, Y. Wang, W. Li, W. Zhi, Y. Liu, L. Ni and Y. Wang, *ACS Appl. Mater. Interfaces*, 2019, **11**, 40575–40584.
- 251 D. Nakayama, Y. Nishio and M. Watanabe, *Langmuir*, 2003, **19**, 8542–8549.
- 252 J.-X. Jian, Q. Liu, Z.-J. Li, F. Wang, X.-B. Li, C.-B. Li, B. Liu, Q.-Y. Meng, B. Chen and K. Feng, *Nat. Commun.*, 2013, **4**, 1–9.
- 253 L. Xie, J. Tian, Y. Ouyang, X. Guo, W. Zhang, U.-P. Apfel, W. Zhang and R. Cao, *Angew. Chem.*, 2020, 15978–15982.
- 254 F. Schué, *Water soluble polymers: solution properties and applications*, ed. Z. Amjad, Plenum Press, New York, 1998, pp. 259, ISBN 0-306-45931-0.
- 255 B. L. Rivas, E. D. Pereira, M. Palencia and J. Sánchez, *Prog. Polym. Sci.*, 2011, **36**, 294–322.
- 256 L. Nicole, C. Laberty-Robert, L. Rozes and C. Sanchez, *Nanoscale*, 2014, **6**, 6267–6292.
- 257 C. Sanchez, P. Belleville, M. Popall and L. Nicole, *Chem. Soc. Rev.*, 2011, **40**, 696–753.
- 258 G. Schottner, *Chem. Mater.*, 2001, **13**, 3422–3435.
- 259 J. Pyun and K. Matyjaszewski, *Chem. Mater.*, 2001, **13**, 3436–3448.
- 260 C. Sanchez, C. Boissiere, S. Cassaignon, C. Chanéac, O. Durupthy, M. Faustini, D. Grosso, C. Laberty-Robert, L. Nicole and D. Portehault, *Chem. Mater.*, 2014, **26**, 221–238.
- 261 S. H. Mir, L. A. Nagahara, T. Thundat, P. Mokarian-Tabari, H. Furukawa and A. Khosla, *J. Electrochem. Soc.*, 2018, **165**, B3137.
- 262 J. L. Dalsin, L. Lin, S. Tosatti, J. Vörös, M. Textor and P. B. Messersmith, *Langmuir*, 2005, **21**, 640–646.
- 263 V. T. Huynh, P. de Souza and M. H. Stenzel, *Macromolecules*, 2011, **44**, 7888–7900.
- 264 C. Gérardin, N. Sanson, F. Bouyer, F. Fajula, J. Putaux, M. Joanicot and T. Chopin, *Angew. Chem.*, 2003, **115**, 3809–3813.
- 265 G. Layrac, C. Gérardin, D. Tichit, S. Harriison and M. Destarac, *Polymer*, 2015, **72**, 292–300.
- 266 N. Sanson, F. Bouyer, M. Destarac, M. In and C. Gérardin, *Langmuir*, 2012, **28**, 3773–3782.
- 267 M. Tan, Z. Ye, E.-K. Jeong, X. Wu, D. L. Parker and Z.-R. Lu, *Bioconjugate Chem.*, 2011, **22**, 931–937.
- 268 A. J. L. Villaraza, A. Bumb and M. W. Brechbiel, *Chem. Rev.*, 2010, **110**, 2921–2959.
- 269 H.-W. Shin, H. Sohn, Y.-H. Jeong and S.-M. Lee, *Langmuir*, 2019, **35**, 6421–6428.
- 270 V. C. Pierre, M. J. Allen and P. Caravan, *JBIC, J. Biol. Inorg. Chem.*, 2014, **19**, 127–131.
- 271 C. S. Winalski, S. Shortkroff, R. V. Mulkern, E. Schneider and G. M. Rosen, *Magn. Reson. Med.*, 2002, **48**, 965–972.
- 272 Y. Li, S. Laurent, L. Esser, L. Vander Elst, R. N. Muller, A. B. Lowe, C. Boyer and T. P. Davis, *Polym. Chem.*, 2014, **5**, 2592–2601.
- 273 T. C. Johnstone, K. Suntharalingam and S. J. Lippard, *Chem. Rev.*, 2016, **116**, 3436–3486.
- 274 L. Kelland, *Nat. Rev. Cancer*, 2007, **7**, 573–584.
- 275 S. van Zutphen and J. Reedijk, *Coord. Chem. Rev.*, 2005, **249**, 2845–2853.
- 276 N. Nishiyama, M. Yokoyama, T. Aoyagi, T. Okano, Y. Sakurai and K. Kataoka, *Langmuir*, 1999, **15**, 377–383.
- 277 Y.-H. Jeong, T. Ahn, W. Yu and S.-M. Lee, *ACS Macro Lett.*, 2021, **10**, 492–497.
- 278 V. Amendola, R. Pilot, M. Frascioni, O. M. Maragò and M. A. Iati, *J. Phys.: Condens. Matter*, 2017, **29**, 203002.
- 279 Y.-C. Yeh, B. Creran and V. M. Rotello, *Nanoscale*, 2012, **4**, 1871–1880.
- 280 N. Tarannum and Y. K. Gautam, *RSC Adv.*, 2019, **9**, 34926–34948.
- 281 E. Seo, S.-H. Lee, S. Lee, S.-H. Choi, C. J. Hawker and B.-S. Kim, *Polym. Chem.*, 2017, **8**, 4528–4537.
- 282 C. Falentin-Daudré, E. Faure, T. Svaldo-Lanero, F. Farina, C. Jérôme, C. Van De Weerd, J. Martial, A.-S. Duwez and C. Detrembleur, *Langmuir*, 2012, **28**, 7233–7241.
- 283 A. Charlot, V. Sciannaméa, S. Lenoir, E. Faure, R. Jérôme, C. Jérôme, C. Van De Weerd, J. Martial, C. Archambeau and N. Willet, *J. Mater. Chem.*, 2009, **19**, 4117–4125.
- 284 S. Liu, J. V. M. Weaver, M. Save and S. P. Armes, *Langmuir*, 2002, **18**, 8350–8357.
- 285 B. P. Bastakoti, S. Guragain, S. Yusa and K. Nakashima, *RSC Adv.*, 2012, **2**, 5938–5940.
- 286 Y. Lu, Y. Yin, Z.-Y. Li and Y. Xia, *Nano Lett.*, 2002, **2**, 785–788.
- 287 S. Cavaliere-Jaricot, M. Darbandi and T. Nann, *Chem. Commun.*, 2007, 2031–2033.
- 288 C. Xue, X. Chen, S. J. Hurst and C. A. Mirkin, *Adv. Mater.*, 2007, **19**, 4071–4074.
- 289 M. Iranmanesh and J. Hulliger, *Chem. Soc. Rev.*, 2017, **46**, 5925–5934.
- 290 T. Shao, N. Falcone and H.-B. Kraatz, *ACS Omega*, 2020, **5**, 1312–1317.
- 291 A. A. Ensafi, M. Jafari-Asl, A. Nabiyan and B. Rezaei, *J. Electrochem. Soc.*, 2016, **163**, H610–H617.
- 292 J. Wang, P. Wang, J. Hou, J. Qian, C. Wang and Y. Ao, *Catal. Sci. Technol.*, 2018, **8**, 5406–5415.
- 293 J. Aldana, Y. A. Wang and X. Peng, *J. Am. Chem. Soc.*, 2001, **123**, 8844–8850.
- 294 A. L. Rogach, N. Gaponik, J. M. Lupton, C. Bertoni, D. E. Gallardo, S. Dunn, N. Li Pira, M. Paderi, P. Repetto and S. G. Romanov, *Angew. Chem., Int. Ed.*, 2008, **47**, 6538–6549.
- 295 A. Eychmüller, *J. Phys. Chem. B*, 2000, **104**, 6514–6528.

- 296 A. Mills and S. Le Hunte, *J. Photochem. Photobiol., A: Chem.*, 1997, **108**, 1–35.
- 297 A. P. Alivisatos, *Science*, 1996, **271**, 933–937.
- 298 S. Zhong, Y. Xi, S. Wu, Q. Liu, L. Zhao and S. Bai, *J. Mater. Chem. A*, 2020, **8**, 14863–14894.
- 299 X. Fang, T. Zhai, U. K. Gautam, L. Li, L. Wu, Y. Bando and D. Golberg, *Prog. Mater. Sci.*, 2011, **56**, 175–287.
- 300 W. W. Yu, E. Chang, J. C. Falkner, J. Zhang, A. M. Al-Somali, C. M. Sayes, J. Johns, R. Drezek and V. L. Colvin, *J. Am. Chem. Soc.*, 2007, **129**, 2871–2879.
- 301 K. Tarasov, D. Houssein, M. Destarac, N. Marcotte, C. Gérardin and D. Tichit, *New J. Chem.*, 2013, **37**, 508–514.
- 302 Z. Zheng, M. Mounsamy, N. Lauth-de Viguierie, Y. Coppel, S. Harrisson, M. Destarac, C. Mingotaud, M. L. Kahn and J.-D. Marty, *Polym. Chem.*, 2019, **10**, 145–154.
- 303 Y. L. Wu, C. S. Lim, S. Fu, A. I. Y. Tok, H. M. Lau, F. Y. C. Boey and X. T. Zeng, *Nanotechnology*, 2007, **18**, 215604.
- 304 M. Beija, R. Salvayre, N. Lauth-de Viguierie and J.-D. Marty, *Trends Biotechnol.*, 2012, **30**, 485–496.
- 305 A. A. Ensafi, E. Khoddami, A. Nabiyan and B. Rezaei, *React. Funct. Polym.*, 2017, **116**, 1–8.
- 306 R. Quiñones, K. Rodriguez and R. J. Iuliucci, *Thin Solid Films*, 2014, **565**, 155–164.
- 307 K. H. Markiewicz, L. Seiler, I. Misztalewska, K. Winkler, S. Harrisson, A. Z. Wilczewska, M. Destarac and J.-D. Marty, *Polym. Chem.*, 2016, **7**, 6391–6399.
- 308 D. Runge and H. Cölfen, *Z. Phys. Chem.*, 2018, **232**, 1281–1293.
- 309 E. Seo, T. Lee, K. T. Lee, H.-K. Song and B.-S. Kim, *J. Mater. Chem.*, 2012, **22**, 11598–11604.
- 310 Y. Tang, Q. Yang, T. Wu, L. Liu, Y. Ding and B. Yu, *Langmuir*, 2014, **30**, 6324–6330.
- 311 M. M. Rahman, M. R. Karim, H. F. Alharbi, B. Aldokhayel, T. Uzzaman and H. Zahir, *Chem. – Asian J.*, 2021, **16**, 902–921.
- 312 C. Yuan, L. Yang, L. Hou, L. Shen, X. Zhang and X. W. D. Lou, *Energy Environ. Sci.*, 2012, **5**, 7883–7887.
- 313 P. Simon and Y. Gogotsi, *Nanosci. Technol.*, 2010, 320–329.
- 314 C.-C. Hu, K.-H. Chang, M.-C. Lin and Y.-T. Wu, *Nano Lett.*, 2006, **6**, 2690–2695.
- 315 R. Liu, J. Duay, T. Lane and S. B. Lee, *Phys. Chem. Chem. Phys.*, 2010, **12**, 4309–4316.
- 316 D. Majumdar, T. Maiyalagan and Z. Jiang, *ChemElectroChem*, 2019, **6**, 4343–4372.
- 317 M. Zborowski and J. J. Chalmers, *Magnetic cell separation*, Elsevier, 2011.
- 318 Y. Haik, V. Pai and C.-J. Chen, *J. Magn. Magn. Mater.*, 1999, **194**, 254–261.
- 319 P. A. Dresco, V. S. Zaitsev, R. J. Gambino and B. Chu, *Langmuir*, 1999, **15**, 1945–1951.
- 320 B. Polyak and G. Friedman, *Expert Opin. Drug Delivery*, 2009, **6**, 53–70.
- 321 X. Huang, I. H. El-Sayed, W. Qian and M. A. El-Sayed, *J. Am. Chem. Soc.*, 2006, **128**, 2115–2120.
- 322 Y. Jun, Y.-M. Huh, J. Choi, J.-H. Lee, H.-T. Song, S. Kim, S. Yoon, K.-S. Kim, J.-S. Shin and J.-S. Suh, *J. Am. Chem. Soc.*, 2005, **127**, 5732–5733.
- 323 M. Fuentes, C. Mateo, A. Rodriguez, M. Casqueiro, J. C. Tercero, H. H. Riese, R. Fernández-Lafuente and J. M. Guisán, *Biosens. Bioelectron.*, 2006, **21**, 1574–1580.
- 324 D. L. Kraitchman, A. W. Heldman, E. Atalar, L. C. Amado, B. J. Martin, M. F. Pittenger, J. M. Hare and J. W. M. Bulte, *Circulation*, 2003, **107**, 2290–2293.
- 325 M. I. Papisov, A. Bogdanov Jr, B. Schaffer, N. Nossiff, T. Shen, R. Weissleder and T. J. Brady, *J. Magn. Magn. Mater.*, 1993, **122**, 383–386.
- 326 D. Pouliquen, H. Perroud, F. Calza, P. Jallet and J. J. Le Jeune, *Magn. Reson. Med.*, 1992, **24**, 75–84.
- 327 P. Biehl, M. Von der Lühe, S. Dutz and F. H. Schacher, *Polymers*, 2018, **10**, 91.
- 328 T. Gillich, E. M. Benetti, E. Rakhmatullina, R. Konradi, W. Li, A. Zhang, A. D. Schlüter and M. Textor, *J. Am. Chem. Soc.*, 2011, **133**, 10940–10950.
- 329 V. T. A. Nguyen, M. Gauthier and O. Sandre, *Nanomaterials*, 2014, **4**, 628–685.
- 330 R. Sondjaja, T. A. Hatton and M. K. C. Tam, *J. Magn. Magn. Mater.*, 2009, **321**, 2393–2397.
- 331 C. Boyer, M. R. Whittaker, V. Bulmus, J. Liu and T. P. Davis, *NPG Asia Mater.*, 2010, **2**, 23–30.
- 332 N. Zaquen, J. Yeow, T. Junkers, C. Boyer and P. B. Zetterlund, *Macromolecules*, 2018, **51**, 5165–5172.
- 333 J. S. Basuki, A. Jacquemin, L. Esser, Y. Li, C. Boyer and T. P. Davis, *Polym. Chem.*, 2014, **5**, 2611–2620.
- 334 L. Sandiford, A. Phinikaridou, A. Protti, L. K. Meszaros, X. Cui, Y. Yan, G. Frodsham, P. A. Williamson, N. Gaddum and R. M. Botnar, *ACS Nano*, 2013, **7**, 500–512.
- 335 C. Boyer, V. Bulmus, P. Priyanto, W. Y. Teoh, R. Amal and T. P. Davis, *J. Mater. Chem.*, 2009, **19**, 111–123.
- 336 J. S. Basuki, H. T. T. Duong, A. Macmillan, R. B. Erlich, L. Esser, M. C. Akerfeldt, R. M. Whan, M. Kavallaris, C. Boyer and T. P. Davis, *ACS Nano*, 2013, **7**, 10175–10189.
- 337 S. Wan, Y. Zheng, Y. Liu, H. Yan and K. Liu, *J. Mater. Chem.*, 2005, **15**, 3424–3430.
- 338 M. Guo, Y. Yan, H. Zhang, H. Yan, Y. Cao, K. Liu, S. Wan, J. Huang and W. Yue, *J. Mater. Chem.*, 2008, **18**, 5104–5112.
- 339 K. Wormuth, *J. Colloid Interface Sci.*, 2001, **241**, 366–377.
- 340 M. Kumagai, Y. Imai, T. Nakamura, Y. Yamasaki, M. Sekino, S. Ueno, K. Hanaoka, K. Kikuchi, T. Nagano and E. Kaneko, *Colloids Surf., B*, 2007, **56**, 174–181.
- 341 K. Y. Yoon, C. Kotsmar, D. R. Ingram, C. Huh, S. L. Bryant, T. E. Milner and K. P. Johnston, *Langmuir*, 2011, **27**, 10962–10969.
- 342 P. Papaphilippou, L. Loizou, N. C. Popa, A. Han, L. Vekas, A. Odysseos and T. Krasia-Christoforou, *Biomacromolecules*, 2009, **10**, 2662–2671.
- 343 K. Ujiie, N. Kanayama, K. Asai, M. Kishimoto, Y. Ohara, Y. Akashi, K. Yamada, S. Hashimoto, T. Oda and N. Ohkohchi, *Colloids Surf., B*, 2011, **88**, 771–778.
- 344 P. Li and J. Huang, *J. Appl. Polym. Sci.*, 2008, **109**, 501–507.
- 345 J. Zhang, S. Xu and E. Kumacheva, *J. Am. Chem. Soc.*, 2004, **126**, 7908–7914.

- 346 C. Linot, J. Poly, J. Boucard, D. Pouliquen, S. Nedellec, P. Hulin, N. Marec, P. Arosio, A. Lascialfari and A. Guerrini, *ACS Appl. Mater. Interfaces*, 2017, **9**, 14242–14257.
- 347 J.-J. Yuan, S. P. Armes, Y. Takabayashi, K. Prassides, C. A. P. Leite, F. Galembeck and A. L. Lewis, *Langmuir*, 2006, **22**, 10989–10993.
- 348 S. Luo, J. Xu, Y. Zhang, S. Liu and C. Wu, *J. Phys. Chem. B*, 2005, **109**, 22159–22166.
- 349 O. Eckardt, C. Pietsch, O. Zumann, M. von der Lühe, D. S. Brauer and F. H. Schacher, *Macromol. Rapid Commun.*, 2016, **37**, 337–342.
- 350 D. Li, Y. Cui, K. Wang, Q. He, X. Yan and J. Li, *Adv. Funct. Mater.*, 2007, **17**, 3134–3140.
- 351 F. Kousar, J. Malmström, S. Swift, J. Ross, J. Perera and S. C. Moratti, *ACS Appl. Polym. Mater.*, 2021, 2785–2801.
- 352 L. Wu, U. Glebe and A. Böker, *Polym. Chem.*, 2015, **6**, 5143–5184.
- 353 M. A. Macchione, C. Biglione and M. Strumia, *Polymers*, 2018, **10**, 527.
- 354 S. Z. Khaled, A. Cevenini, I. K. Yazdi, A. Parodi, M. Evangelopoulos, C. Corbo, S. Scaria, Y. Hu, S. G. Haddix and B. Corradetti, *Biomaterials*, 2016, **87**, 57–68.
- 355 C.-D. Vo, A. Schmid, S. P. Armes, K. Sakai and S. Biggs, *Langmuir*, 2007, **23**, 408–413.
- 356 I. Banerjee, R. C. Pangule and R. S. Kane, *Adv. Mater.*, 2011, **23**, 690–718.
- 357 J. Wei, D. B. Ravn, L. Gram and P. Kingshott, *Colloids Surf., B*, 2003, **32**, 275–291.
- 358 A. R. Statz, R. J. Meagher, A. E. Barron and P. B. Messersmith, *J. Am. Chem. Soc.*, 2005, **127**, 7972–7973.
- 359 J. L. Dalsin and P. B. Messersmith, *Mater. Today*, 2005, **8**, 38–46.
- 360 S. Jiang and Z. Cao, *Adv. Mater.*, 2010, **22**, 920–932.
- 361 N. Giambianco, G. Marletta, A. Graillot, N. Bia, C. Loubat and J.-F. Berret, *ACS Omega*, 2017, **2**, 1309–1320.
- 362 V. Torrisi, A. Graillot, L. Vitorazi, Q. Crouzet, G. Marletta, C. Loubat and J.-F. Berret, *Biomacromolecules*, 2014, **15**, 3171–3179.
- 363 S. Kumar, Y. L. Dory, M. Lepage and Y. Zhao, *Macromolecules*, 2011, **44**, 7385–7393.
- 364 S. Thanneeru, N. Milazzo, A. Lopes, Z. Wei, A. M. Angeles-Boza and J. He, *J. Am. Chem. Soc.*, 2019, **141**, 4252–4256.
- 365 S. Uchiyama, Y. Matsumura, A. P. de Silva and K. Iwai, *Anal. Chem.*, 2004, **76**, 1793–1798.
- 366 T.-L. Nghiem, D. Coban, S. Tjaberings and A. H. Gröschel, *Polymers*, 2020, **12**, 2190.
- 367 D. E. Bergbreiter, J. Tian and C. Hongfa, *Chem. Rev.*, 2009, **109**, 530–582.
- 368 G. I. Dzhardimalieva, A. K. Zharmagambetova, S. E. Kudaibergenov and I. E. Uflyand, *Kinet. Catal.*, 2020, **61**, 198–223.
- 369 V. S. Vyas, V. W. Lau and B. V. Lotsch, *Chem. Mater.*, 2016, **28**, 5191–5204.
- 370 Z. B. Shifrina, V. G. Matveeva and L. M. Bronstein, *Chem. Rev.*, 2020, 1350–1396.
- 371 B. L. Wadsworth, D. Khusnutdinova and G. F. Moore, *J. Mater. Chem. A*, 2018, **6**, 21654–21665.
- 372 C. Li, Q. Li, Y. V. Kaneti, D. Hou, Y. Yamauchi and Y. Mai, *Chem. Soc. Rev.*, 2020, **49**, 4681–4736.
- 373 Z. Ge, D. Xie, D. Chen, X. Jiang, Y. Zhang, H. Liu and S. Liu, *Macromolecules*, 2007, **40**, 3538–3546.
- 374 K. O. Sebakhy, S. Kessel and M. J. Monteiro, *Macromolecules*, 2010, **43**, 9598.
- 375 X. Yu, A. Herberg and D. Kuckling, *Eur. Polym. J.*, 2019, **120**, 109207.
- 376 X. Yu, A. Herberg and D. Kuckling, *Polymers*, 2020, **12**, 2265.
- 377 I. Perez-Baena, F. Barroso-Bujans, U. Gasser, A. Arbe, A. J. Moreno, J. Colmenero and J. A. Pomposo, *ACS Macro Lett.*, 2013, **2**, 775–779.
- 378 B. L. Moore, A. Lu, D. A. Longbottom and R. K. O'Reilly, *Polym. Chem.*, 2013, **4**, 2304–2312.
- 379 K. A. Ahrendt, C. J. Borths and D. W. C. MacMillan, *J. Am. Chem. Soc.*, 2000, **122**, 4243–4244.
- 380 W. S. Jen, J. J. M. Wiener and D. W. C. MacMillan, *J. Am. Chem. Soc.*, 2000, **122**, 9874–9875.
- 381 J. F. Austin and D. W. C. MacMillan, *J. Am. Chem. Soc.*, 2002, **124**, 1172–1173.
- 382 L. Liu and A. Corma, *Chem. Rev.*, 2018, **118**, 4981–5079.
- 383 H. Duan, Y. Yang, J. Lü and C. Lü, *Nanoscale*, 2018, **10**, 12487–12496.
- 384 S. Sugihara, M. Sudo and Y. Maeda, *Langmuir*, 2018, **35**, 1346–1356.
- 385 M. B. Gawande, A. Goswami, T. Asefa, H. Guo, A. V. Biradar, D.-L. Peng, R. Zboril and R. S. Varma, *Chem. Soc. Rev.*, 2015, **44**, 7540–7590.
- 386 C. Gao, F. Lyu and Y. Yin, *Chem. Rev.*, 2021, **121**, 834–881.
- 387 J. Hu and S. Liu, *Macromolecules*, 2010, **43**, 8315–8330.
- 388 S. Cichosz, A. Masek and M. Zaborski, *Polym. Test.*, 2018, **67**, 342–348.
- 389 D. T. McQuade, A. E. Pullen and T. M. Swager, *Chem. Rev.*, 2000, **100**, 2537–2574.
- 390 K. Peters, *Smart Mater. Struct.*, 2010, **20**, 13002.
- 391 S. Uchiyama, Y. Matsumura, A. P. de Silva and K. Iwai, *Anal. Chem.*, 2003, **75**, 5926–5935.
- 392 M. Onoda, S. Uchiyama and T. Ohwada, *Macromolecules*, 2007, **40**, 9651–9657.
- 393 Y. Shiraishi, R. Miyamoto and T. Hirai, *J. Photochem. Photobiol., A: Chem.*, 2008, **200**, 432–437.
- 394 Y. Shiraishi, R. Miyamoto, X. Zhang and T. Hirai, *Org. Lett.*, 2007, **9**, 3921–3924.
- 395 G. Liu, J. Hu, G. Zhang and S. Liu, *Bioconjugate Chem.*, 2015, **26**, 1328–1338.
- 396 X. Zhou, L. Wang, Z. Wei, G. Weng and J. He, *Adv. Funct. Mater.*, 2019, **29**, 1903543.
- 397 H.-J. Kim and H. Lee, *Polym. Chem.*, 2019, **10**, 4017–4024.
- 398 L. Li, Z. Yang and X. Chen, *Acc. Chem. Res.*, 2020, **53**, 2044–2054.
- 399 W. Wu, T. Zhou, M. Aiello and S. Zhou, *Chem. Mater.*, 2009, **21**, 4905–4913.
- 400 S. Li, Z. T. Bennett, B. D. Sumer and J. Gao, *Acc. Chem. Res.*, 2020, **53**, 2546–2557.
- 401 H. Sun, A. M. Scharff-Poulsen, H. Gu and K. Almdal, *Chem. Mater.*, 2006, **18**, 3381–3384.

- 402 J. Yin, X. Guan, D. Wang and S. Liu, *Langmuir*, 2009, **25**, 11367–11374.
- 403 T. Liu, J. Hu, J. Yin, Y. Zhang, C. Li and S. Liu, *Chem. Mater.*, 2009, **21**, 3439–3446.
- 404 J. Yin, C. Li, D. Wang and S. Liu, *J. Phys. Chem. B*, 2010, **114**, 12213–12220.
- 405 W. Wu, T. Zhou, J. Shen and S. Zhou, *Chem. Commun.*, 2009, 4390–4392.
- 406 C. Gota, K. Okabe, T. Funatsu, Y. Harada and S. Uchiyama, *J. Am. Chem. Soc.*, 2009, **131**, 2766–2767.
- 407 J. Hu, M. R. Whittaker, J. F. Quinn and T. P. Davis, *Macromolecules*, 2016, **49**, 2741–2749.